Synthetic and Structural Studies of Compounds Based Upon Icosahedral Carbaboranes

David J. Donohoe

Thesis Presented for the Degree of
Doctor of Philosophy
University of Edinburgh
1996

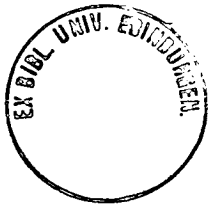

Declaration

Except where specific reference is made to other sources, the work presented in this Thesis is the original work of the author. It has not been submitted, in whole or in part, for any other degree. Certain of the results have been published.

For my Parents

"There is nothing better in life, than writing on the sole of your slipper with a Biro."

"The Best Things in Life," from the album "Back Again in The DHSS,"
by Half-Man, Half-Biscuit.

Acknowledgements

I would firstly like to thank my supervisor, Professor Alan Welch, for enthusiasm and support, above and beyond the call of duty. Thanks too to Dr. Lesley Yellowlees for all of her help.

As always, a thesis is a team effort and so I would like to take this opportunity to thank Drs. Dave Reed and Alan Boyd, as well as John Millar, Heather Grant and Wesley Kerr for nmr spectroscopy, Lorna Eades for microanalysis and Dr. Rod Ferguson for mass spectrometry.

I would also like to thank Rhona Knox, who synthesised and characterised compounds **3** and **3a** and Natalia Douek, who supervised me during my fourth year project. Dr. Andrew Weller deserves a special mention for 'interesting conversations and useful suggestions,' the loan of his computer and donation of his sympathy - "which was nice." Thanks too to Dr. Georgina Rosair, who solved several of the later crystal structures and Rhodri Thomas, who helped with my 'formatting fiasco!' A big thanks also goes to Dr. Colin Pulham for his preparation of some $[Me_2GaCl]_2$ and help and high-vacuum line in the synthesis of compound **5**. Profs. Michel Hospital, Daniel Chasseau, Georges Bravic and Dr. Bob Gould are very gratefully acknowledged for their help in arranging my trip to Bordeaux.

The supporting cast of thousands include Dr. Eric McInnes, (barbecues in Manchester not-withstanding), Allan "Pints?" Young, Ally Thomson, Aida Gioe and Philippe Guionneau in Bordeaux (*superbon!*), Alan "de la bière?" Brown in Paris and the Chemsoc. Football Team for not complaining about my distinct lack of pace...too much. The final special mentions go to "the lovely" Lynn Bryson, who, as well as synthesising and characterising compound **18**, has provided me with some of the most exciting chemistry of this Thesis! and my family for support, both emotional and financial... I love each and everyone of you!!

Finally, my thanks to the EPSRC for funding, ERASMUS for a bursary to study crystallography in Bordeaux for three months, the University of Edinburgh and Heriot-Watt University for use of facilities and the Callery Chemical Company for the generous gift of decaborane!

Abbreviations

amu	atomic mass unit
AO	atomic orbital
btma	benzyltrimethylammonium
^{t}Bu	*tert*-butyl
1,5-cod	1,5-*cyclo*-octadiene
Cp	cyclopentadienyl
Cp*	pentamethylcyclopentadienyl
Cy	cyclohexyl
COSY	correlation spectroscopy
dppe	bis(diphenylphosphino)ethane
EHMO	extended Hückel molecular orbital
Et	ethyl
Et_2O	diethyl ether
FAB	fast atom bombardment
FTIR	Fourier transform infra-red
HOMO	highest occupied molecular orbital
Indy	indenyl
Indy*	heptamethylindenyl
IR	infra-red
LUMO	lowest unoccupied molecular orbital
Me	methyl
mes	mesityl
MO	molecular orbital
nmr	nuclear magnetic resonance
o-tol	*ortho*-tolyl
Ph	phenyl
ppm	parts per million
pr	propyl
PSEP	polyhedral skeletal electron pair
ROPM	relative overlap population matrix
thf	tetrahydrofuran
tlc	thin layer chromatography
TOCSY	total correlation spectroscopy

Abbreviations for Specific Compounds

1 1-Ph-1,2-*closo*-$C_2B_{10}H_{11}$

2 1-CO_2H-1,2-*closo*-$C_2B_{10}H_{11}$

2a [$HNEt_3$][1-CO_2-1,2-*closo*-$C_2B_{10}H_{11}$]

2b [$HNEtMe_2$][1-CO_2-1,2-*closo*-$C_2B_{10}H_{11}$]

3 1-CO_2H-2-CH_3-1,2-*closo*-$C_2B_{10}H_{10}$

3a [$HNEt_3$][1-CO_2-2-CH_3-1,2-*closo*-$C_2B_{10}H_{10}$]

4 1-CO_2H-2-CH_2OCH_3-1,2-*closo*-$C_2B_{10}H_{10}$

4a [$HNEt_3$][1-CO_2-2-CH_2OCH_3-1,2-*closo*-$C_2B_{10}H_{10}$]

5 1-CH_2OCH_3-2-{Me_2Ga}-1,2-*closo*-$C_2B_{10}H_{10}$

6 1-Ph-2-{P(*o*-tol)$_3$Au}-1,2-*closo*-$C_2B_{10}H_{10}$

6a P(*o*-tol)$_3$AuMe

7 1-Ph-2-{PCy_3Au}-1,2-*closo*-$C_2B_{10}H_{10}$

7a PCy_3AuMe

8 1-Ph-2-{PEt_3Au}-1,2-*closo*-$C_2B_{10}H_{10}$

8a PEt_3AuMe

9 1-Ph-2-{$Pmes_3Au$}-1,2-*closo*-$C_2B_{10}H_{10}$

10 1-Ph-2-{P(C_6F_5)$_3$Au}-1,2-*closo*-$C_2B_{10}H_{10}$

11 1-H-2-{P(*o*-tol)$_3$Au}-1,2-*closo*-$C_2B_{10}H_{10}$

12 1-Me-2-{P(*o*-tol)$_3$Au}-1,2-*closo*-$C_2B_{10}H_{10}$

13 1-^{t}Bu-2-{P(*o*-tol)$_3$Au}-1,2-*closo*-$C_2B_{10}H_{10}$

14 P(C_6F_5)$_3$AuCl

15 $C_6F_5AuP(C_6F_5)Me_2$

16 [$HNEt_3$][7,8-Ph_2-7,8-*nido*-$C_2B_9H_{10}$]

16a [$HNEt_3$][7-Ph-7,8-*nido*-$C_2B_9H_{11}$]

17 $\mu_{(4,9)}$-*exo*-{(PPh_3)$_2$Rh}-7,8-Ph_2-7,8-*nido*-$C_2B_9H_{10}$

17a μ_2-*exo*-{(PPh_3)$_2$Rh}-7,9-Ph_2-7,9-*nido*-$C_2B_9H_{10}$

18 [(dppe)$_2$Rh][7,8-Ph_2-7,8-*nido*-$C_2B_9H_{10}$]

19 1,2-Ph_2-3-(η^3-C_8H_{13})-*pseudocloso*-3,1,2-$RhC_2B_9H_9$

19a 1-Ph-3-(η^3-C_8H_{13})-*closo*-3,1,2-$RhC_2B_9H_{10}$

Abstract

Chapter 1 begins with a brief history of heteroborane chemistry, from the pioneering work of Alfred Stock to some of the most recent advances and their applications. A discussion of the unique bonding within these molecules follows and leads to the development of heteroboranes and carbaboranes in particular. The development of carbametallaboranes is detailed, with emphasis on those which are sterically crowded. The chapter ends by listing the scope of work presented.

Chapter 2 describes the (improved) synthesis, characterisation and crystallographic study of the parent carbaborane 1-Ph-1,2-*closo*-$C_2B_{10}H_{11}$, **1**. The synthesis and characterisation of a series of carbaborane carboxylic acids and carboxylate salts of the general types 1-CO_2H-2-R-1,2-*closo*-$C_2B_{10}H_{10}$ and [1-CO_2-2-R-1,2-*closo*-$C_2B_{10}H_{10}$][$HNEt_3$], respectively (R = H (**2**, **2a**), Me (**3**, **3a**) and CH_2OCH_3 (**4**, **4a**)), is presented. X-ray diffraction studies on the carboxylate salts are also presented, which agree with EHMO predictions, regarding the conformation of the carboxylate moiety. Finally, the synthesis and characterisation of the first example of a σ-bonded carbagallaborane, 1-CH_2OCH_3-2-{Me_2Ga}-1,2-*closo*-$C_2B_{10}H_{10}$, **5**, is discussed.

Chapter 3 argues the hypothesis that carbaboranes can act as efficient σ-donors. The synthesis and characterisation of a series of carbaauraboranes of the general type 1-R-2-{PR'_3Au}-1,2-*closo*-$C_2B_{10}H_{10}$ (R = Ph, R′ = *o*-tol, **6**, Cy, **7**, Et, **8**, mes, **9**, C_6F_5, **10**; R′ = *o*-tol; R = Ph, H, **11**, Me, **12**, ^{t}Bu, **13**) is discussed and the crystallographically determined structures of compounds **6** and **7** are compared with those of P(*o*-tol)$_3$AuMe, **6a**, and PCy_3AuMe, **7a**, respectively. Further spectroscopic and structural studies (on compounds **6**, **11**, **12**, **13**) and EHMO calculations show that variation of the (R) substituent group does not significantly affect the electronic properties of the carbaborane cage. Finally the synthesis, characterisation and X-ray diffraction study of the product of the reaction between MeLi and the new compound $P(C_6F_5)_3AuCl$, **14**, to afford $C_6F_5AuP(C_6F_5)Me_2$, **15**, is discussed.

Chapter 4 details the synthesis, characterisation and structural studies of a series of carbarhodaboranes involving the sterically crowded

7,8-Ph_2-7,8-*nido*-C_2B_9 ligand. The (mono-)anionic ligand, **16**, is initially presented as the $[HNEt_3]^+$ salt followed by two isomers of μ_2-*exo*-{$(PPh_3)_2Rh$}-7,8-Ph_2-7,8-*nido*-$C_2B_9H_{10}$, **17** and **17a**, the product of the reaction of **16** with $(PPh_3)_3RhCl$. Attempts to synthesise the dppe analogue of **17** are described and the X-ray diffraction study of the actual product [$(dppe)_2Rh$][7,8-Ph_2-7,8-*nido*-$C_2B_9H_{10}$], **18**, is discussed. Finally, the characterisation and crystallographic study of 1,2-Ph_2-3-{η^3-C_8H_{13}}-3,1,2-*pseudocloso*-$RhC_2B_9H_9$, **19**, synthesised by reaction of **16** with [Rh(1,5-cod)Cl]$_2$, is discussed. The synthesis and characterisation of the monophenyl analogue, **19a**, is also discussed.

Chapter 5 details the synthesis of compounds **1** to **19a**, as well as their characterisation by microanalysis, IR and nmr (^1H, ^{11}B-{^1H}, ^{19}F-{^1H} and ^{31}P-{^1H}) spectroscopies, mass spectrometry and X-ray crystallography.

Appendix A contains details of courses and lectures attended, whilst reprints of published work are given in **Appendix B**.

Contents

Chapter 1

Background

1.1 Introduction

Alfred Stock embarked upon his fundamental research of boranes in 1910,[1] at a time when very little was known of these compounds. His initial research involved the synthesis and characterisation of several boron hydrides (boranes). Since many of these compounds were volatile, poisonous and highly air- and moisture-sensitive, he had to design and develop high vacuum lines to allow their safe manipulation. Indeed, these early designs are the basis of modern vacuum lines. Perhaps the most amazing aspect of Stock's research is that he characterised the compounds without the aid of IR or nmr spectroscopy, mass spectrometry or X-ray crystallography.[2]

The American government initiated and funded a multi-million dollar research program in the 1950's in the belief that boranes would prove to be useful as high energy rocket fuels. This research, although ultimately fruitless, did result in the development of the carbaboranes and anionic boron hydrides and led to a renaissance in boron chemistry that has now developed into a varied and important branch of chemistry, with many applications such as boron neutron capture therapy (BNCT)[3] and thermally and oxidatively stable polymers.[4]

It was initially thought that the boranes adopted hydrocarbon-like structures. However, they do not possess enough valence electrons for these structures, which are based upon classical two-centre, two-electron bonding. For example, diborane (B_2H_6) possesses 12 valence electrons ((2 x B) + (6 x H) = 6 + 6 = 12), yet for an ethane-like structure, 7 two-centre, two-electron bonds (6 x B-H and 1 x B-B) requiring 14 valence electrons, are necessary. Obviously, this structure is not possible in terms of 'classical' electron-counting. Diborane, was eventually shown, after much argument,[5] to have the bridged structure below (**Fig. 1.1**).[6]

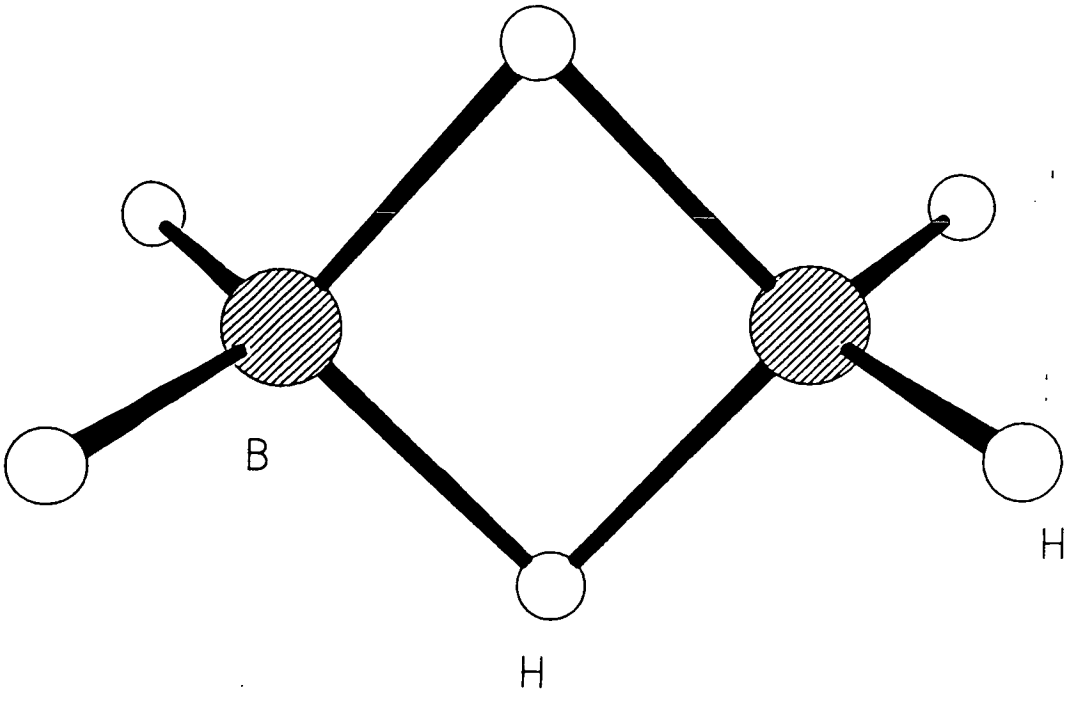

Figure 1.1 Molecular Structure of Diborane (B_2H_6)

It is now accepted, primarily as a result of X-ray[7] and electron diffraction studies[8] on further boranes and hydroborate anions ($[B_nH_n]^{2-}$), that boranes are molecular polyhedra and that their rather unusual geometries are a direct result of the 'non-classical,' multi-centre bonding which they adopt in order to overcome their 'classical' electron-deficiency.

As the number of polyhedral boranes structurally characterised increased, it was observed that they could be organised in a systematic way according to their geometry. Lipscomb developed the idea of multi-centre bonding using a topological approach to describe boranes in terms of **three**-centre, two-electron bonding, using localised molecular orbitals.[1] This approach, however, quickly becomes very complicated for large, symmetric molecules. Later approaches centred around a full molecular orbital treatment of the polyhedra, although the immense size of the calculations required meant that this method was unsuitable for (carba)metallaboranes.

It was not until 1971 that a theory was developed which could account for all of the above species types (and also certain metal clusters). Wade's Polyhedral Skeletal Electron Pair (PSEP) Theory[9] explained the observed

geometries with respect to the number of electron pairs available for cluster bonding. **Section 1.2** gives a more detailed account of these theories, with reference to pertinent examples (and exceptions!).

The possibility of heteroboranes, and specifically carbaboranes, was first suggested by EHMO calculations performed by Lipscomb and Hoffmann.[10] The calculations showed that a $\{BH\}^-$ fragment is isolobal and isoelectronic with {CH}, hence a double substitution of $\{BH\}^-$ by {CH} in a hydroborate anion $[B_nH_n]^{2-}$ should afford the neutral carbaborane $C_2B_{n-2}H_n$. The first carbaborane, $C_2B_3H_5$, was synthesised in 1962 and was shown to be considerably more stable than its borane precursor.[11] Since then, further examples of heteroboranes, which contain most of the main group non-metals, have been synthesised,[12] although carbaboranes dominate the literature. An overview of the syntheses, chemistry and structures of the carbaboranes, as well as a short discussion of other heteroboranes, is given in **Section 1.3**.

In 1965, Hawthorne reacted $FeCl_2$ with [7,8-*nido*-$C_2B_9H_{11}]^{2-}$ (the open C_2B_3 face of which is isolobal to Cp^-) to afford the ferrocene analogue $[Fe(C_2B_9H_{11})_2]^{2-}$ **(Fig. 1.2)**.[13]

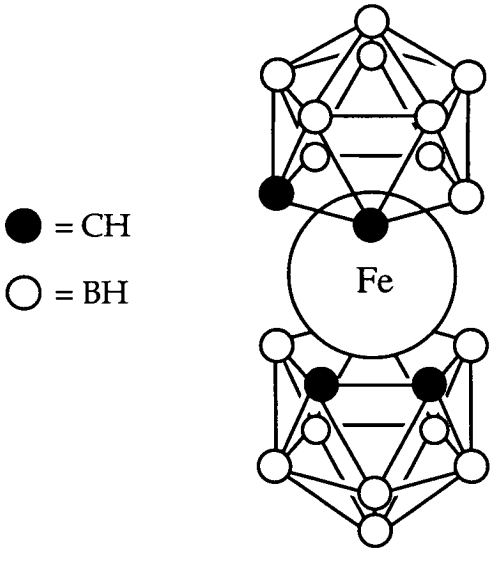

Figure 1.2 Representation of $[Fe(C_2B_9H_{11})_2]^{2-}$

Hawthorne's compound was the first reported carbametallaborane, of which there are now several hundred in the literature. Examples include

carbametallaboranes with main group[14] and transition metals as well as lanthanide[15] and actinide[16] species. Metallaboranes and carbametallaboranes were recently classified into three types.[17] The examples given above, where "the metal occupies a polyhedral vertex" are termed **Class 1** and are by far the most prevalent in the literature, accounting for over 90% of all reported examples. **Class 2** (carba)metallaboranes are defined as those where "the metal fragment bridges a polyhedral edge." This type is the least common. One example of these species is $\mu_{(10,11)}$-{PPh_3Au}-9-SMe_2-7,8-*nido*-$C_2B_9H_{10}$ (**Fig. 1.3**).[18]

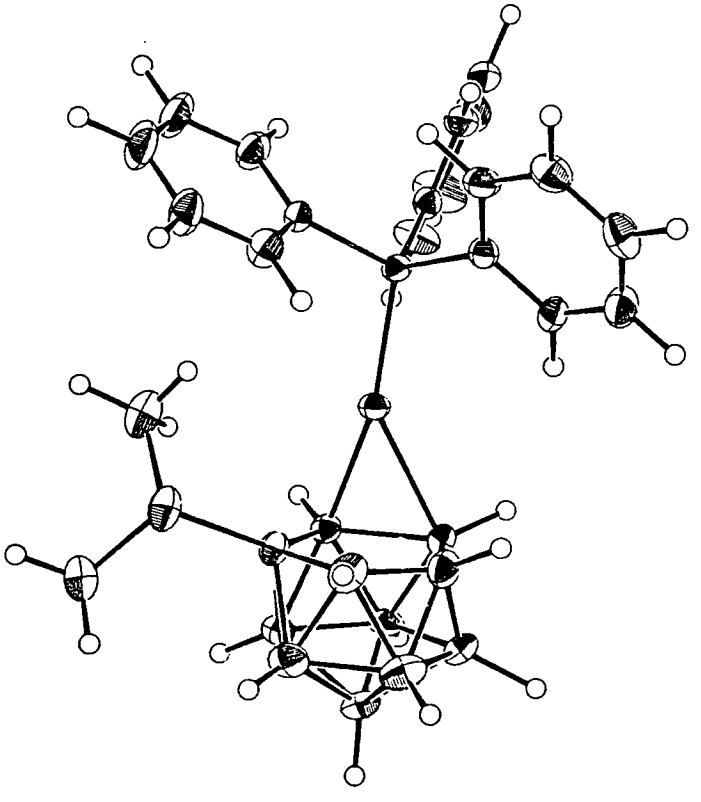

Figure 1.3 Perspective View of $\mu_{(10,11)}$-{PPh_3Au}-9-SMe_2-7,8-*nido*-$C_2B_9H_{10}$

Class 3 (carba)metallaboranes are defined as those where "the metal fragment is bonded to the cage by a single (two-centre, two-electron) σ-bond, usually to a cage carbon atom." One example of a Class 3 carbametallaborane is 1-Ph-2-{$CpFe(CO)_2$}-1,2-*closo*-$C_2B_{10}H_{10}$ (**Fig. 1.4**, below).[19]

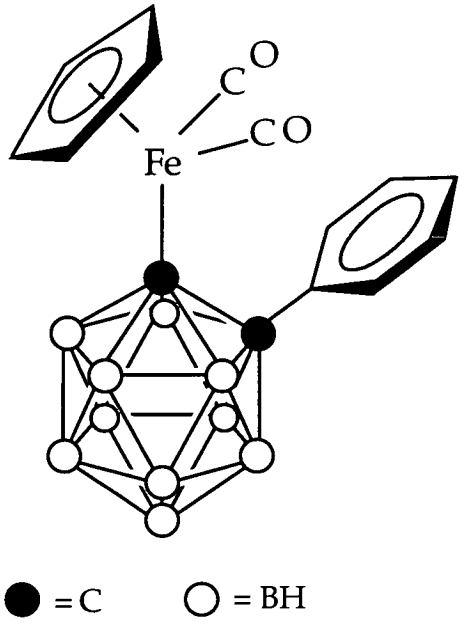

Figure 1.4 Representation of a Class 3 Carbametallaborane

Section 1.4 presents a general discussion of (carba)metallaboranes, with particular emphasis on **Class 1** and **Class 3** carbametallaboranes.

Sections of **Chapter 4** deal with the consequences of deliberate intramolecular steric crowding within carbametallaboranes and so **Section 1.5** is a brief overview of the three ways in which this steric congestion is relieved, namely **Vertex Extrusion** (e.g $\mu_{(10,11)}$-*exo*-{$(PPh_3)_2Rh$}-7-Me-8-Ph-7,8-*nido*-$C_2B_9H_{10}$ - **Fig. 1.5a**),[20] **Polyhedral Isomerisation** (e.g. 1,11-Ph_2-3,3-$(PMe_2Ph)_2$-3,1,11-*closo*-$PtC_2B_9H_9$ - **Fig. 1.5b**)[21] and **Polyhedral Deformation** (e.g. 1,2-Ph_2-3-(η^5-C_9Me_7)-3,1,2-*pseudocloso*-$RhC_2B_9H_9$ - **Fig. 1.5c**).[22]

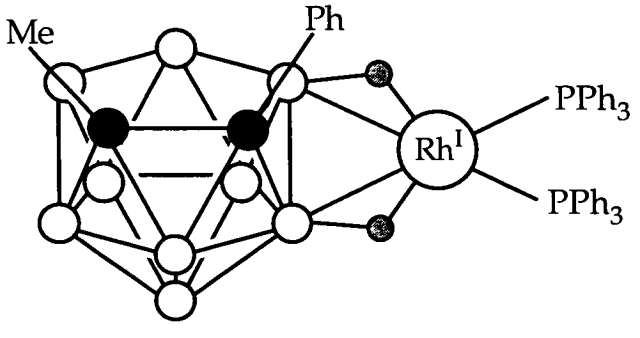

Figure 1.5a $\mu_{(10,11)}$-*exo*-{$(PPh_3)_2Rh$}-7-Me-8-Ph-7,8-*nido*-$C_2B_9H_{10}$

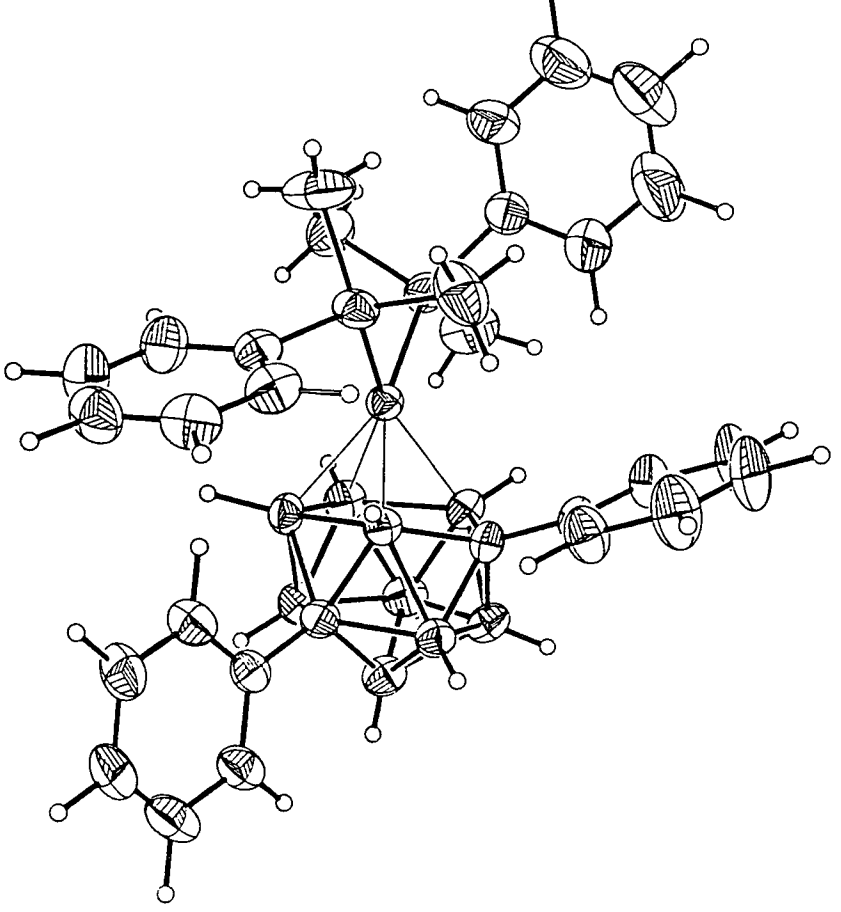

Figure 1.5b 1,11-Ph_2-3,3-$(PMe_2Ph)_2$-3,1,11-*closo*-$PtC_2B_9H_9$

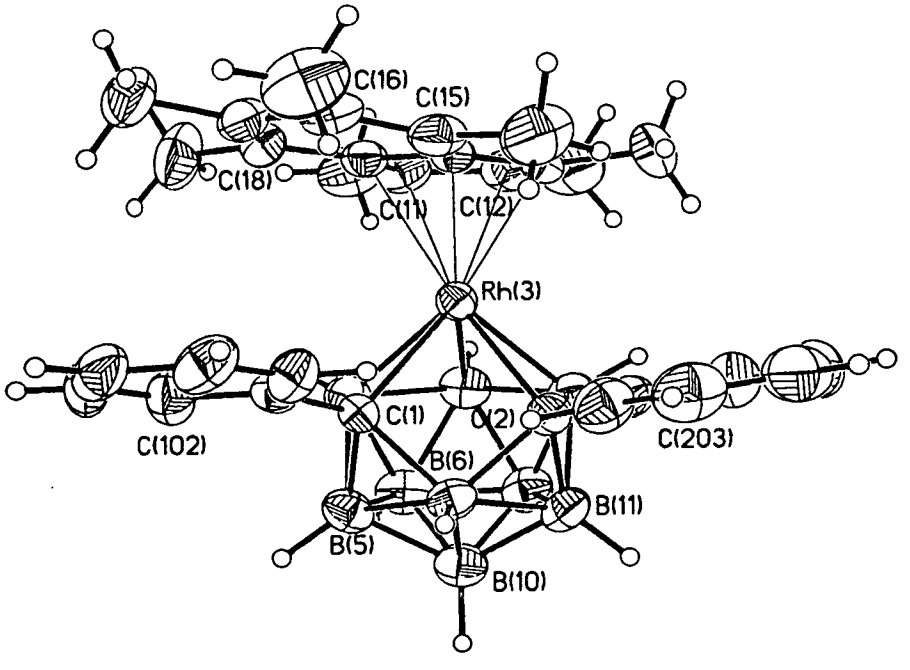

Figure 1.5c 1,2-Ph_2-3-(η^5-C_9Me_7)-3,1,2-*pseudocloso*-$RhC_2B_9H_9$

Figure 1.5 Examples of Vertex Extrusion, Polyhedral Isomerisation and Polyhedral Deformation

Finally, the scope of the research presented in this Thesis is outlined in **Section 1.7**.

1.2 Bonding and Structure

As noted in **Section 1.1**, boranes, hydroborates and heteroboranes are 'classically' electron deficient. As we shall see later, however, this is a misrepresentation as it is only the constituent **fragments** that are electron-deficient.

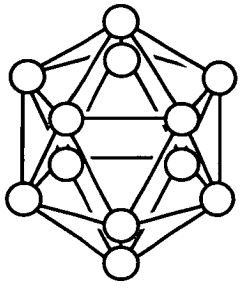

1.6a [*closo*-$B_{12}H_{12}$]$^{2-}$

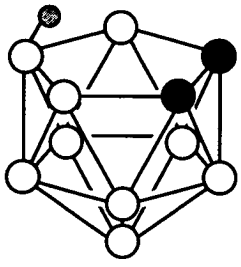

1.6b [*nido*-$C_2B_9H_{12}$]$^-$

○ = BH ● = CH ◍ = H

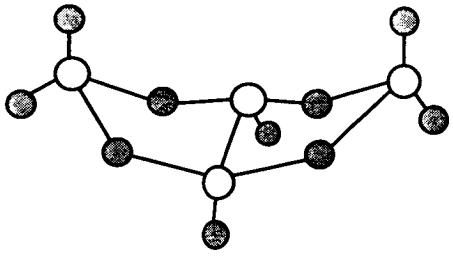

1.6c *arachno*-B_4H_{10}

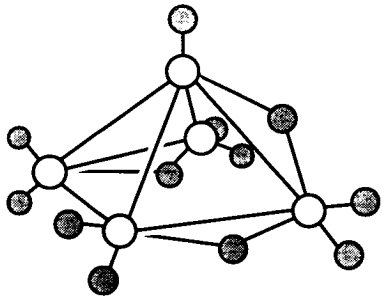

1.6d [*hypho*-B_5H_{12}]$^-$

○ = B ◍ = H

Figure 1.6 Representations of the Four Main Geometry Types

Boranes, hydroborate anions and heteroboranes were observed to form distinct structural patterns, based upon regular polyhedra (i.e. those containing only triangular faces). The term '*closo*' is used to describe these regular polyhedra (*closo* is Greek for 'closed'). Removal of a single vertex from one of these *closo* species affords the *nido* (nest) geometry. Sequential removal of two further vertices affords species with *arachno* (spider's web) and *hypho* (net) geometries respectively. **Figure 1.6** illustrates these four main geometry types with examples of borane, hydroborate and heteroborane compounds.

The boron atom in the {BH} fragment below (**Fig. 1.7**) is *sp* hybridised and has three valence electrons ($2s^1\ 2p^2$). One orbital and one valence electron are used to form a σ-bond between the boron and hydrogen atoms, and hence the boron atom is now a two-electron, three-orbital donor and has insufficient electrons to form classical two-centre, two-electron bonds.

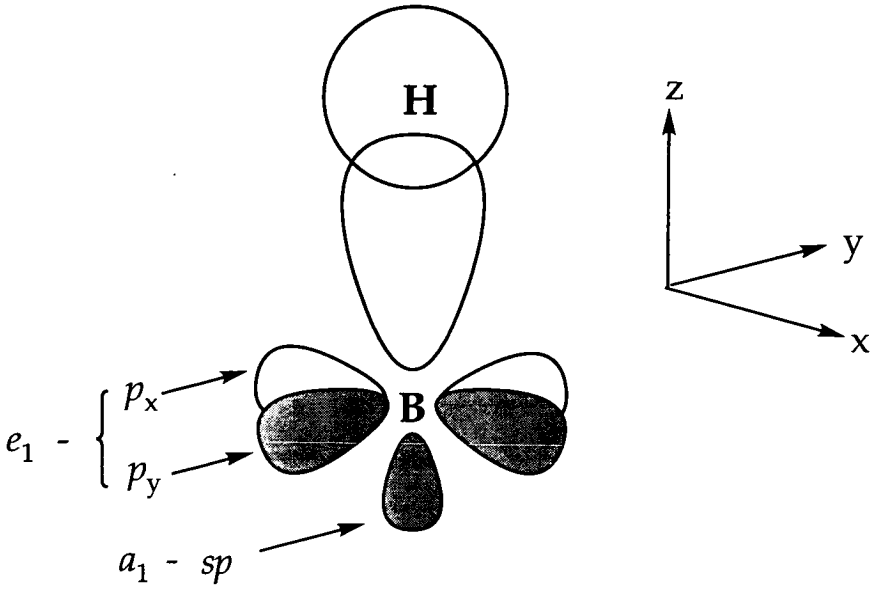

Figure 1.7 Representation of a {BH} Fragment

Similarly, {CH} fragments are three-electron, three-orbital donors. Group 15 elements are also three-electron, three-orbital donors, with the fourth orbital being a non-bonding lone pair, which is *exo* to (i.e. points away from) the cage. Group 16 elements are four-electron, three-orbital donors. Again, the fourth orbital is a non-bonding lone pair.

This 'classical' electron-deficiency is obviated by the 'non-classical,' multi-centre bonding that these species adopt. This was first modelled by Lipscomb, who described these molecular polyhedra in terms of a series of localised molecular orbitals for the constituent BBB (open), BBB (closed) and BHB three-centre, two-electron bonds (**Fig. 1.8**).[1]

This topological approach, however, proved to be too unwieldy to be useful for large, symmetrical molecules.

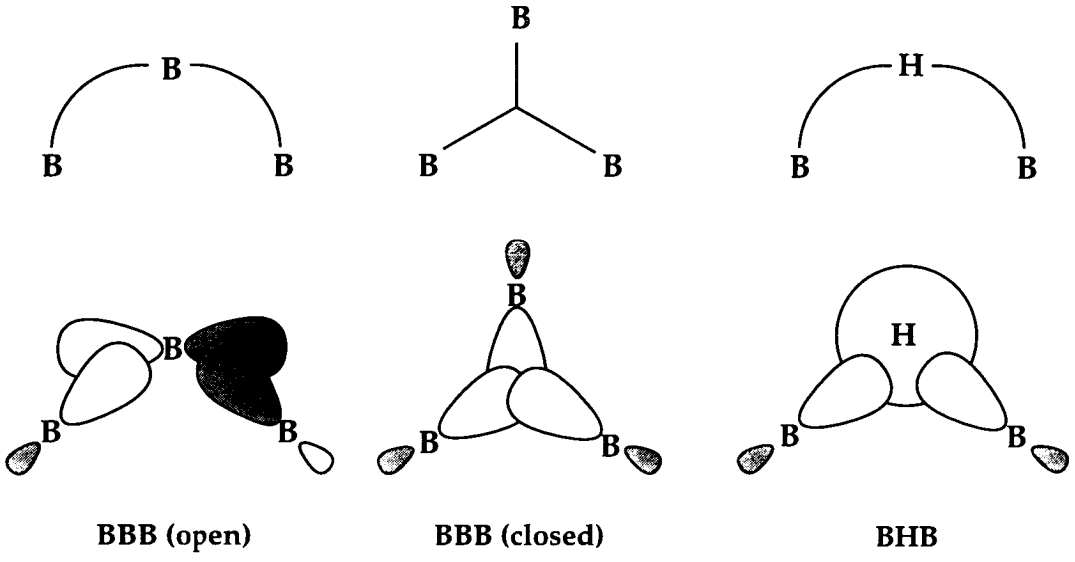

Figure 1.8 Representation of Some Three-Centre, Two-Electron Bonds

The reason for the observed patterns in polyhedral structures is found in MO theory. Consider $[B_6H_6]^{2-}$, which can be thought of as being composed of $(BH)_6$. As described above, each {BH} fragment possesses three atomic orbitals for the purposes of cluster bonding. One *sp* AO (σ) is directed to the centre of the cluster leaving p_x and p_y AOs (π) tangential to the cage.

The σ-MOs that can arise are shown below and are a_{1g} (fully bonding), t_{1u}* (weakly anti-bonding) and e_g* (strongly anti-bonding) (**Fig. 1.9**).

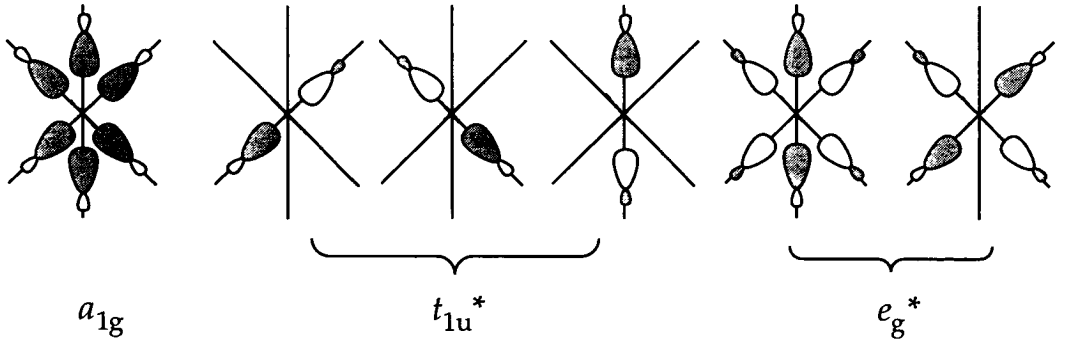

Figure 1.9 Representation of the Radial MOs of $[B_6H_6]^{2-}$

There are twelve possible bonding and anti-bonding combinations of the tangential MOs. These are accounted for as four triply degenerate sets, the t_{2g} and t_{1u}, bonding and the t_{2u}^* and t_{1g}^* anti-bonding sets (**Fig. 1.10**).

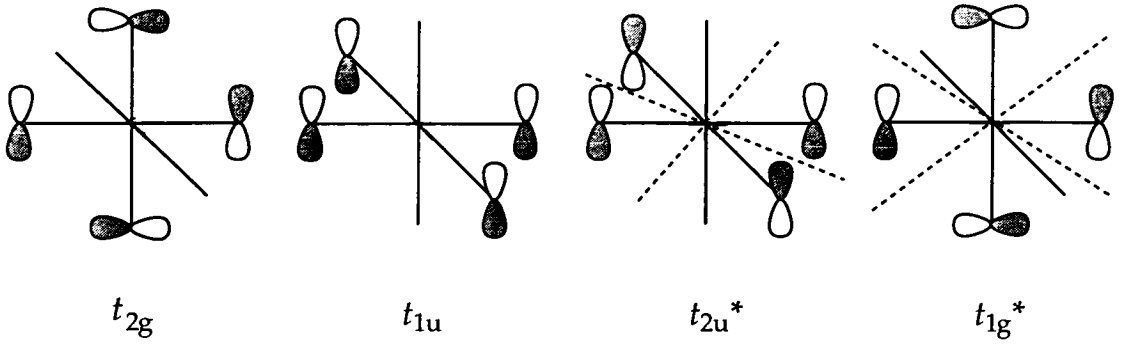

Figure 1.10 Representation of the Tangential MOs of $[B_6H_6]^{2-}$

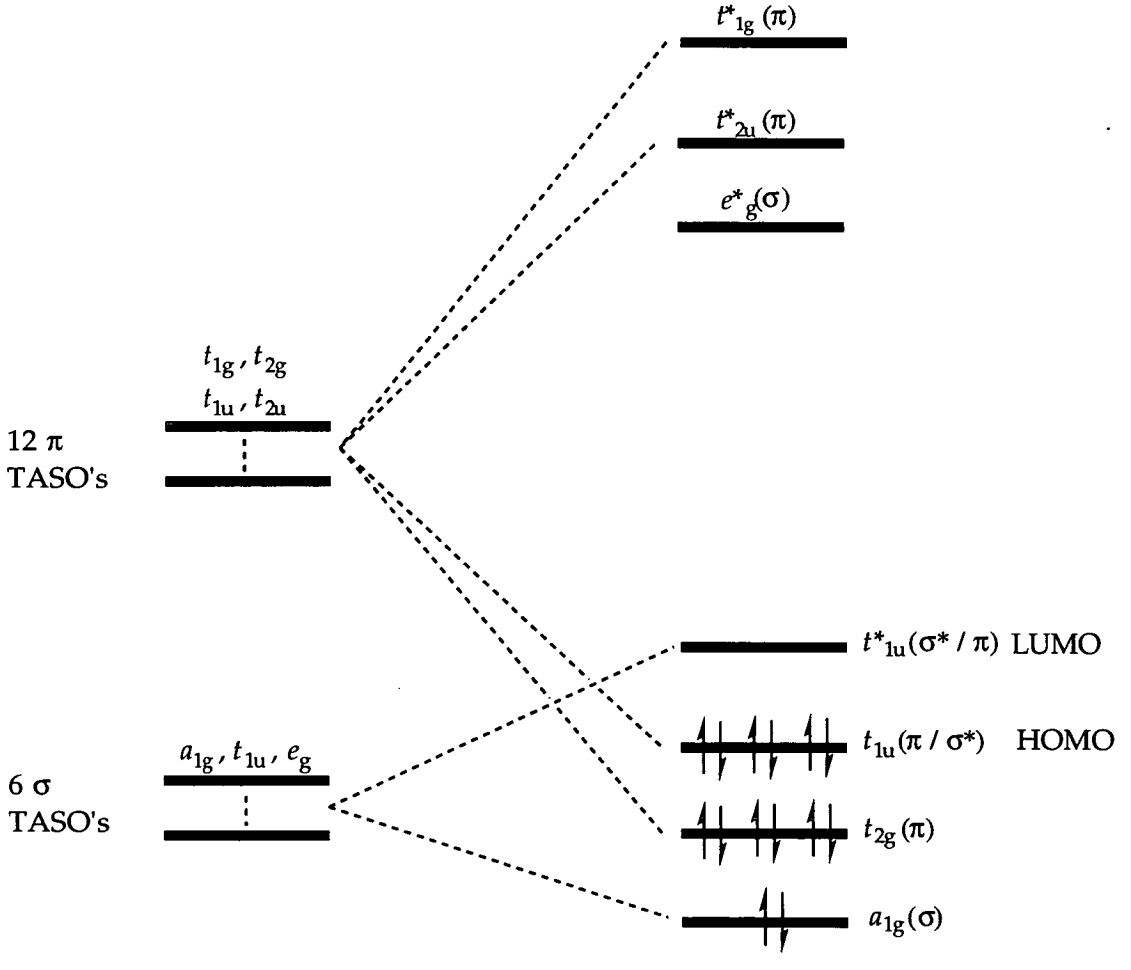

Figure 1.11 Qualitative MO Diagram for $[B_6H_6]^{2-}$

A qualitative MO diagram for $[B_6H_6]^{2-}$ is shown above (**Fig. 1.11**) with its fourteen valence electrons. Note that there is mixing of the σ- and π-MOs of t_{1u} symmetry (bonding and anti-bonding). Although suitable for small molecules, the computational power required for larger systems meant that this approach was deemed too complicated to be useful for larger clusters.

In 1971, Wade proposed his Polyhedral Skeletal Electron (PSEP) Theory,[9] which successfully rationalised the observed geometries of most boranes and their derivatives. He related the number of skeletal electron pairs (**x**) to the number of polyhedral vertices (**n**). The number of SEP's is calculated by considering the number of electrons available for cluster bonding from the constituent fragments, any bridging or *endo*-H atoms and the overall charge. Comparison of **x** with **n**, allows the polyhedral geometry to be predicted (**Table 1.1**).

Table 1.1 Relationship of **x** and **n** to Polyhedral Geometry

Number of SEP's (x)	Geometry
n + 1	*closo*
n + 2	*nido*
n + 3	*arachno*
n + 4	*hypho*

For example, consider the structure of $[C_2B_9H_{12}]^-$. The molecule, when broken up into its constituent parts, can be thought of as two {CH} and nine {BH} fragments, one *endo*-H atom and a single negative charge.

Table 1.2 Calculation of Polyhedral Geometry for $[C_2B_9H_{12}]^-$

Skeletal Electron Source	Number of Skeletal Electrons
2 x {CH}	2 x 3 = 6
9 x {BH}	9 x 2 = 18
endo-H	1
overall charge (-1)	1
	Total = 26

Hence, there are 13 SEP's and 11 vertices and thus the compound has a *nido* geometry (**x** = **n** + **2**). The structure of this compound has been

determined by X-ray crystallography and was indeed shown to have the predicted *nido* structure (**Fig. 1.12**).[23]

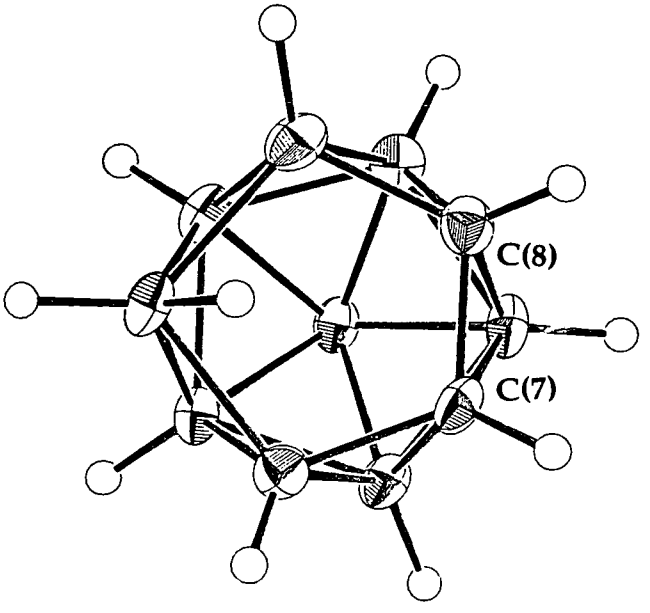

Figure 1.12 Plan View of $[C_2B_9H_{12}]^-$

One of the main strengths of PSEP Theory is its applicability to all types of boron-containing clusters such as heteroboranes and carbametallaboranes as well as metal clusters.

For example, the compound formed by the reaction of $Cs[C_2B_9H_{12}]$ with Wilkinson's catalyst, $(PPh_3)_3RhCl$, which will be discussed later in **Section 1.6**, was formulated as $(PPh_3)_2Rh(H)C_2B_9H_{11}$.[24]

Table 1.3 Calculation of Polyhedral Geometry for $(PPh_3)_2Rh(H)C_2B_9H_{11}$

Skeletal Electron Source	**Number of Skeletal Electrons**
2 x {CH}	2 x 3 = 6
9 x {BH}	9 x 2 = 18
$\{(PPh_3)_2Rh(H)\}$	2 *
	Total = 26

(* N.B. For a transition metal fragment such as $\{(PPh_3)_2Rh(H)\}$, the metal possesses nine valence orbitals (5 x *d*, 3 x *p* and 1 x *s*). Six of these are

involved in *exo*-polyhedral bonding or are non-bonding, leaving three orbitals for cluster bonding. Since the six bonding and non-bonding orbitals are usually filled, the number of electrons available for bonding from such a fragment is given by **e = v + x' - 12**, where **v** is the number of valence electrons of the neutral metal and **x'** is the number of electrons donated to the metal by the *exo*-polyhedral ligands (counted as neutral). Hence, **e = 9 + 5 - 12 = 2.**)

Hence, there are 13 SEP's and 12 vertices and the compound therefore has a *closo* geometry. This was later confirmed by an X-ray crystallographic study (**Fig. 1.13**).[25]

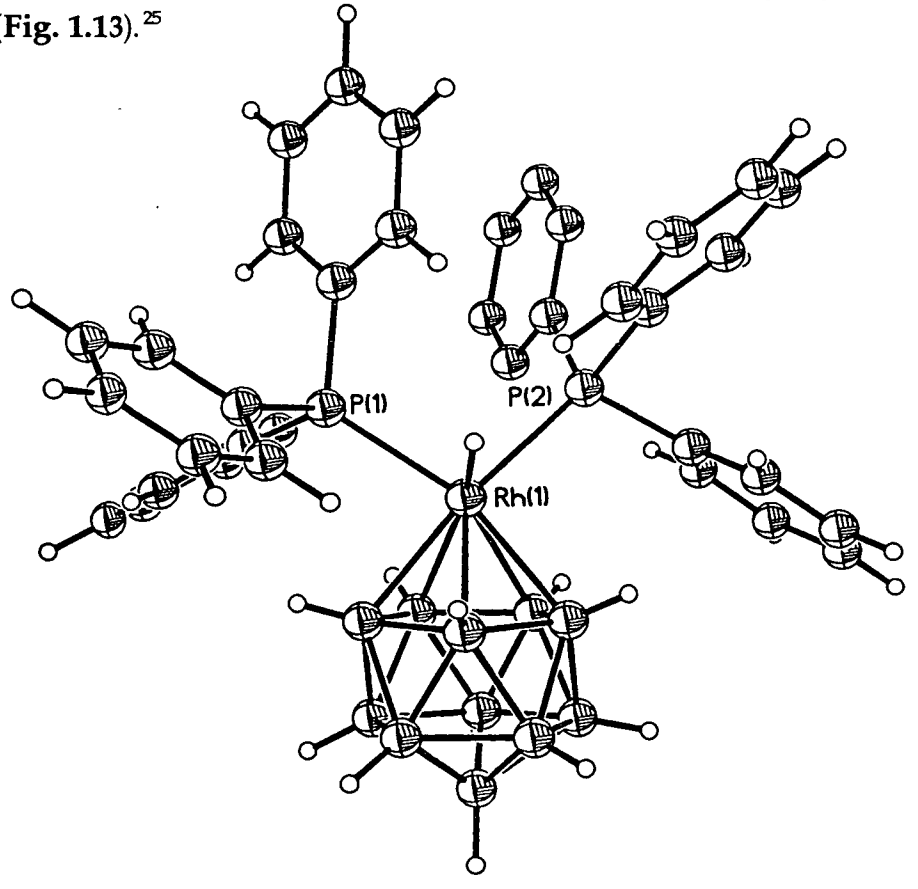

Figure 1.13 Perspective View of 3,3-$(PPh_3)_2$-3-H-*closo*-3,1,2-$RhC_2B_9H_{11}$

Although PSEP theory correctly rationalises the vast majority of polyhedral clusters, there are exceptions to the rule. One of the main reasons for this non-conformation is the closeness in energy of the different geometries. One of the most notable examples is B_8H_{12}, which has a *nido* electron-count (10 SEP's) but an *arachno* geometry. EHMO calculations[26] have shown that *arachno*-B_8H_{12} is more stable than the PSEP precise anion,

[*arachno*-B_8H_{12}]$^{2-}$, although currently there has still been no full explanation as to why this is so.

Non-conformation to the predicted geometry of large clusters often occurs due kinetic stabilisation, as rearrangement to the thermodynamically favoured geometry is not possible under mild conditions. For example, the fourteen-vertex cluster $Cp_2Fe_2Me_4C_4B_8H_8$ and its isomers contain open faces at room temperature, in contradiction of PSEP theory, which predicts a *closo* geometry. Strictly speaking, however, this molecule does not violate Wade's rules since at high temperature there is cluster isomerisation to afford the *closo* species.[27]

Eight-vertex polyhedra such as $Cp_4M_4B_4H_4$ (M = Co, Ni)[28] exhibit a tendency to adopt *closo* geometries, regardless of their electron counts (n and n + 2, respectively). Neutral, halogenated boranes of the type B_nX_n possess n SEP's, yet adopt *closo* geometries. Theoretical[29] and experimental[30] studies have suggested that there is significant back-bonding from the X substituents, which donate sufficient electron density to the cluster such that the electron count is greater than n SEP's. Wade and O'Neill[31] rationalised this anomalous behaviour of 8-, 9- and 11-vertex polyhedra, showing that n, (n + 1) and (n + 2) SEP's could be accommodated with stretching or contracting of polyhedral edges, but without shape altering Jahn-Teller distortions. A further example of non-conformity of a highly halogenated species is $C_4H_4B_2F_2$,[32] which is a cyclic, planar system (as opposed to the isoelectronic $C_4B_2H_6$, which is a pentagonal pyramid).

1.3 Carbaboranes and Other Heteroboranes

1.3.1 *Closo* Carbaboranes

One of the first reported carbaboranes, $C_2B_3H_5$, was synthesised by the reaction of pentaborane(9) (B_5H_9) and acetylene (C_2H_2) in a silent discharge apparatus and was given the name 'carborane-*n*.'[11] It was considerably more stable than the highly flammable, air- and shock-sensitive B_5H_9 precursor (it could be stored at room temperature for several weeks without decomposition and was inert to air, CO_2, acetone, water and triethylamine) and was successfully characterised by IR and nmr spectroscopies and mass spectrometry.

The first carbaborane isomers, which had the general formula $C_2B_4H_6$, were synthesised in 1963.[33] The ^{11}B nmr spectrum of what was termed the *sym*-isomer was a single doublet due to coupling with the *exo*-hydrogen atom. This indicated that all of the ^{11}B nuclei were equivalent. In contrast, the ^{11}B nmr spectrum of the *unsym*-isomer indicated two separate boron environments, of equal intensity. The compounds were thus assigned the geometries below (**Fig. 1.14**).

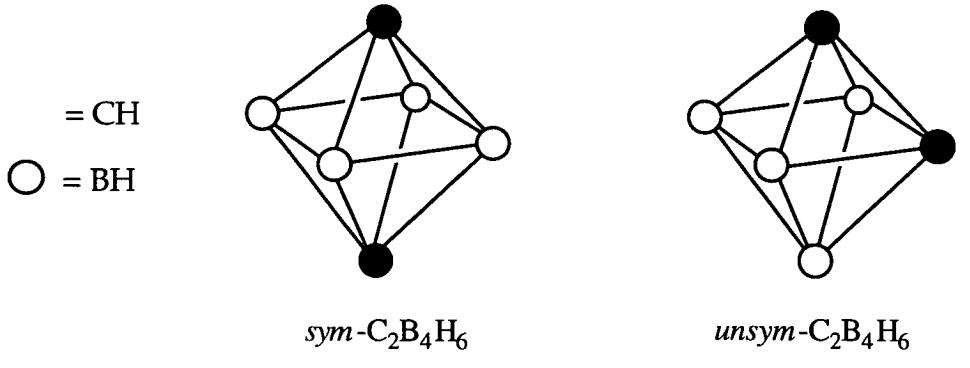

Figure 1.14 The *Sym* and *Unsym* Isomers of $C_2B_4H_6$

After these early examples, the numbers of reported carbaboranes increased rapidly, especially after the synthesis and characterisation of the first icosahedral carbaborane, *ortho*-$C_2B_{10}H_{12}$,[34] and it became necessary to devise a systematic nomenclature/numbering scheme. An early system[35] was soon overtaken by the more rigorous one described here.[36]

As the research in this Thesis involves only icosahedral carbaboranes, the numbering rules listed here will be illustrated with examples of these types of carbaboranes.

There are several rules to determine atom precedence. Firstly, the carbon (or other hetero) atoms take the lowest possible number. Secondly, the boron atoms must be numbered sequentially (low to high), after the heteroatoms, in a clockwise direction (when viewed along the axis through C(1) and its antipodal atom) around the upper pentagon. Moving from this upper to the lower pentagon causes a connectivity to be crossed. Thirdly, if one of the cage carbon atoms is substituted, it takes the lowest number, e.g. 1-Me-1,2-*closo*-$C_2B_{10}H_{11}$. The formula is written so as to give information on the cage carbon atom positions (usually 1 and 2), any substituents and the position of substitution and the geometry of the cluster. These rules are slightly modified for non-*closo* geometries and for carbametallaboranes (see later).

Figure 1.15 shows representations of *ortho*-$C_2B_{10}H_{12}$ and its two geometrical isomers, *meta*- and *para*-$C_2B_{10}H_{12}$,[37,38,39] (more correctly referred to as 1,2-, 1,7- and 1,12-*closo*-$C_2B_{10}H_{12}$, respectively - see below) which are obtained by extended heating of *o*-$C_2B_{10}H_{12}$ to 450 and 625°C, respectively.

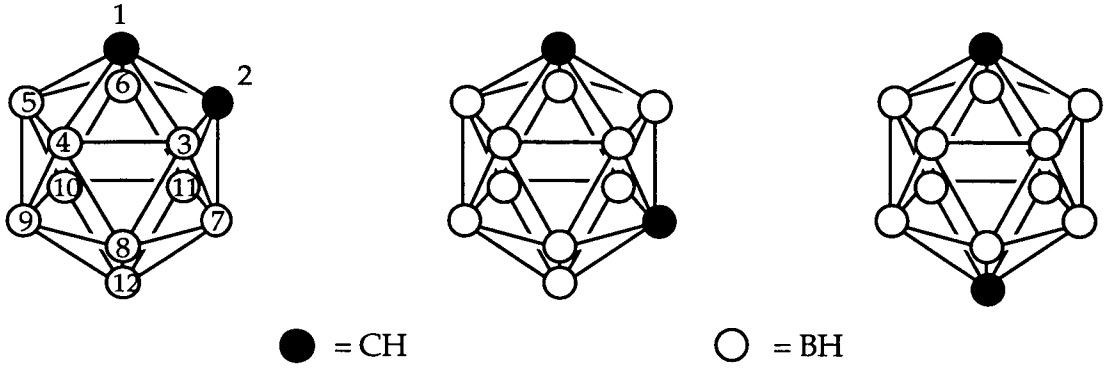

Figure 1.15 Representations of *o*- *m*- and *p*-$C_2B_{10}H_{12}$

Interestingly, it was noted that the *sym* isomer of $C_2B_4H_6$ (the 1,6-isomer using the IUPAC nomenclature described above) was much more stable than the *unsym* isomer (1,2-*closo*-$C_2B_4H_6$). A similar order of stability is observed for the icosahedral carbaboranes, namely 1,12- > 1,7- > 1,2-*closo*-$C_2B_{10}H_{12}$, as, in both cases, the most stable isomer is afforded when the cage

carbon atoms are the furthest possible distance apart. Stability also increases with increasing size of the cluster. For example, 1,2-*closo*-$C_2B_{10}H_{12}$ is an indefinitely air-stable solid, which is thermally resistant up to temperatures of 450°C. In contrast, 1,2-*closo*-$C_2B_4H_6$ is highly reactive, so much so that its colligative properties are not reported. Even the more stable 1,6-isomer is a liquid above -32.6°C.

1.3.2 Synthesis

As described previously, the first carbaborane was synthesised in minimal yields (0.1 - 0.2%) by reaction of B_5H_9 and C_2H_2 in a silent discharge apparatus. 1,2-*closo*-$C_2B_{10}H_{12}$ was afforded in much higher yields (65-77%) using a totally different methodology. Decaborane(14) ($B_{10}H_{14}$), which is a *nido* fragment of a *closo* octadecahedron (an 11-vertex, regular polyhedron), is reacted with two equivalents of a Lewis Base, L (an electron-pair donor), such as Et_2S[40] or CH_3CN.[41] The two molecules of Lewis base substitute two of the four bridging hydrogen atoms, adopting *exo*-positions on the apical B(6) and B(9) atoms, with the remaining hydrogen atoms rearranging so that they bridge the B(8)-B(7) and B(5)-B(10) connectivities with concomitant evolution of hydrogen (**Fig. 1.16**).

The cluster now has two more skeletal electrons (L is a two skeletal-electron donor, whereas H is a single skeletal-electron donor), but the same number of vertices and adopts a more open, *arachno* geometry. C_2H_2 then inserts into the cluster with further loss of a molecule of H_2 and two of Lewis base. The icosahedral species formed is isoelectronic and isostructural with $[B_{12}H_{12}]^{2-}$.[42]

Use of suitable, substituted acetylenes (i.e. those that are resistant to the above reaction conditions) dramatically increases the number of carbaboranes that can be synthesised. **Table 1.4** lists several examples of compounds that have been synthesised by this route.

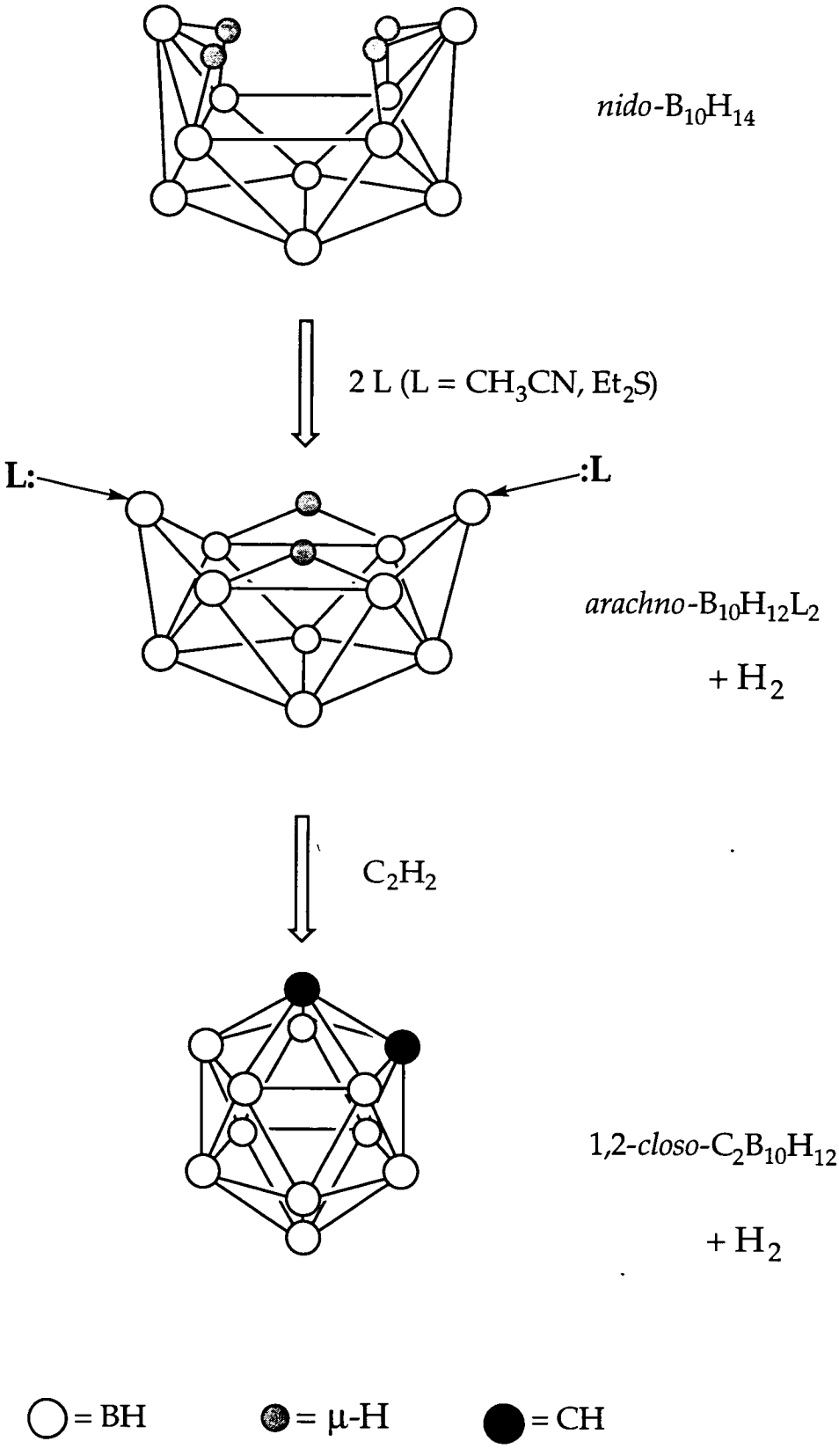

Figure 1.16 Synthesis of 1,2-*closo*-$C_2B_{10}H_{12}$

Table 1.4 Examples of 1-R-2-R'-1,2-*closo*-$C_2B_{10}H_{10}$ Synthesised by Direct Reaction of RCCR' and $B_{10}H_{12}L_2$

R	R'	Reference
Me	H	**38**
$CH{=}CH_2$	H	**38**
CH_2OCH_3	CH_2OCH_3	**43**
Ph	Me	**44**

The two C_{cage} H atoms in *o*-$C_2B_{10}H_{12}$ are relatively acidic, due to carbon being more electronegative than boron. As such, they can be selectively removed using two equivalents of a strong base such as $[Me]^-$ (from MeLi) in a suitable solvent such as thf or Et_2O. The resulting di-lithium salt may then be reacted further with a variety of electrophiles to produced a di-sustituted derivative (**Table 1.5**). It is impossible, however, to **singly** deprotonate *o*-$C_2B_{10}H_{12}$ in these polar solvents since an equilibrium between the mono-deprotonated species and the fully protonated and fully deprotonated species is established (**Fig. 1.17**).

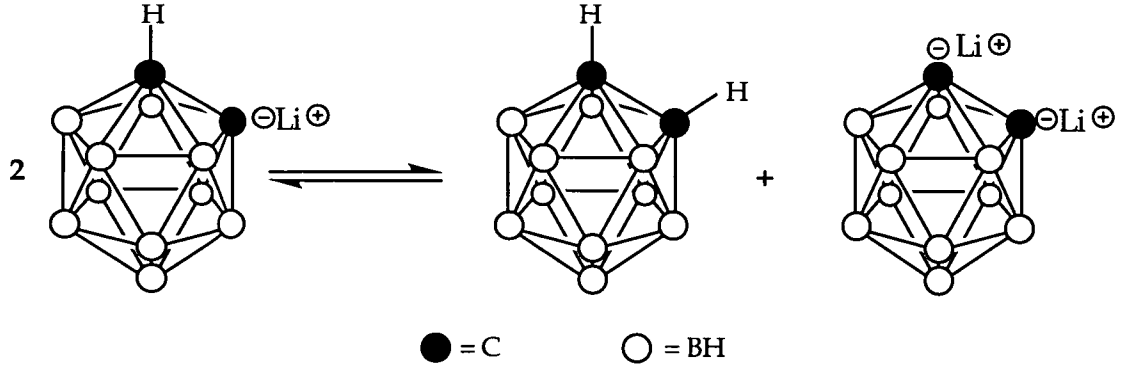

Figure 1.17 Equilibrium established for Li[1,2-*closo*-$C_2B_{10}H_{11}$] in Polar Solvents

This equilibrium is not established, however, if the deprotonation is effected using *n*-BuLi in C_6H_6 at 75°C.[45] Under these conditions, the mono-lithium salt is the exclusive product and this may be reacted further with one equivalent of a suitable electrophile to afford mono-substituted carbaboranes.

It is not possible for this equilibrium to become established for parent carbaboranes which already bear a C-bound substituent and hence removal of the remaining proton is easily effected with one equivalent of MeLi at 0°C. **Table 1.5** lists examples of several carbaboranes that have been synthesised by these three methods.

Table 1.5 Examples of 1-R-2-R′-1,2-*closo*-$C_2B_{10}H_{10}$ Synthesised by Electrophilic Addition

R	R′	Source of E^+	Reference
CO_2H	H	CO_2	**45**
PPh_2	PPh_2	PPh_2Cl	**46**
Me	Ph	MeI	**47**
$CpFe(CO)_2$	Me	$CpFe(CO)_2I$	**48**
C_6F_4Br	Me	C_6F_5Br	**49**
Br	Ph	Br_2	**50**

This range of compounds is yet further increased by isomerisation of the 1,2-isomers, e.g. 1-Ph-1,2-*closo*-$C_2B_{10}H_{11}$ and 1,2-Ph_2-1,2-*closo*-$C_2B_{10}H_{10}$ have been isomerised to give the respective 1,7-isomers.[51,52]

1.3.3 *Nido* Carbaboranes

Nido carbaborane salts are readily derived from the parent *closo* carbaboranes by degrading the cluster by heating to reflux with an excess of KOH in ethanol.[47] By altering the reaction conditions, the mono- (2 equivalents of KOH) or di-anionic (6 equivalents) potassium salt is afforded. For substituted *closo* carbaboranes the reaction is sterically hindered and so the reaction time is extended accordingly. The open C_2B_3 face of the di-anion is approximately isolobal to cyclopentadienyl, a common organometallic ligand, and can be used to coordinate metal fragments (**Section 1.4**).

The numbering of *nido* carbaboranes is slightly different to that of the parent *closo* carbaboranes. This difference is that for *nido* (and other open) polyhedra the (most connected) vertex opposite the open face takes the lowest number. Therefore, the $[C_2B_9H_{12}]^-$ anion described previously is numbered thus (**Fig. 1.18**):

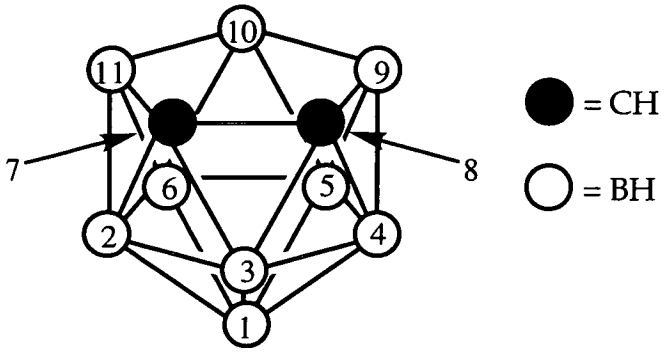

Figure 1.18 Numbering Scheme Adopted for 7,8-*nido* Carbaboranes

Hence, most eleven-vertex, *nido* carbaborane derivatives are of the type 7-R-8-R'-7,8-*nido*-C_2B_9. Note that the carbons have the lowest numbers of the five open face atoms and that the 7-substituent is of a higher precedence than the 8-substituent.

The corresponding 7,9-isomer is afforded by either deboronation of 1,7-*closo*-$C_2B_{10}H_{12}$ or by thermal rearrangement of the respective 7,8-*nido* salt.[47]

1.3.4 Characterisation

The compounds in this Thesis have been characterised by a wide variety of techniques, including microanalysis, IR and nmr (^1H, ^{11}B-{^1H}, ^{19}F-{^1H} and ^{31}P-{^1H}) spectroscopies, mass spectrometry and ultimately X-ray crystallography. Experimental details and machine specifications are given in **Section 5.2.1**.

IR spectroscopy can be used to monitor reactions or to determine if eluted bands are boron containing, by virtue of the presence of a broad, strong absorption band at 2500-2600 cm^{-1}, due to $B\text{-}H_{exo}$ stretches. Microanalysis is also used and generally gives figures which are in good accordance with calculated values.

Information on the C_{cage}-substituents can be gleaned from analysis of the ^1H nmr spectrum, but ^{11}B-{^1H} nmr spectroscopy generally affords the greatest amount of information of any spectroscopic technique.[53] The number of boron environments (and sometimes the time-averaged symmetry of the molecule) can be obtained from the proton-decoupled spectrum, whilst the

proton-coupled spectrum can afford information upon any extra, facial protons that might be present. The shielding pattern and chemical shifts can be related to the geometry of the molecule. For example, the appearance of two high-field signals of relative integral-one indicates that the compound has a *nido* 11-vertex geometry, whereas a *closo* 12 vertex geometry is often denoted by two resonances of relative integral-one, occurring at much lower-field than the other resonances. Moreover, the range of shifts for comparable *closo* species is much narrower than for those of a *nido* geometry.

Individual resonances can be assigned to specific nuclei (or sets of equivalent nuclei), by means of two-dimensional ^{11}B-$\{^1H\}$/^{11}B-$\{^1H\}$ correlated spectroscopy (COSY) experiments, which provide correlations between resonances due to adjacent nuclei within a cluster,[54] whereas total correlation spectroscopy (TOCSY) experiments show correlations between **all** of the boron resonances within a given spin system. This is advantageous where there are different cluster types within a compound such as, 1-Ph-3,3-$(CO)_2$-3-(1'-Ph-2'-PPh_2-1,2-*closo*-$C_2B_{10}H_{10}$)-3,1,2-*closo*-$RuC_2B_9H_{10}$,[55] or where the resolution from a COSY experiment is poor (**Section 2.2.2**). The normally broad, overlapping H_{exo} resonances can be observed by ^1H-$\{^{11}B\}$ experiments (See **Section 2.2.2**)

Ultimately, characterisation is by X-ray crystallography, provided suitable crystals can be grown. This method affords complete structural information (with the occasional exception of some hydrogen atoms) on a compound, in terms of both the gross structure (connectivities, bonds etc.), and the geometry (bond lengths and angles etc.) of the molecule.

1.3.5 Heteroboranes

Although carbaboranes dominate the heteroborane literature (where hetero- refers to main group non-metals), many other hetero atoms have been incorporated into borane clusters.[56]

The first example was a phosphacarbaborane, 1,2-*closo*-$PCB_{10}H_{11}$, which possesses an icosahedral structure, isoelectronic with 1,2-*closo*-$C_2B_{10}H_{12}$.[12a] The phosphorous atom projects a non-bonding, lone pair of electrons out from the cage, instead of a hydrogen atom.

Reaction of $R_2Be.OEt_2$ (R = Me, Et) with 7,8-*nido*-$C_2B_9H_{13}$ affords the twelve-vertex compound, 3-Et_2O-3,1,2-*closo*-$BeC_2B_9H_{11}$. The Et_2O moiety, which is datively coordinated to the beryllium atom, is readily substituted by NMe_3 to afford 3-NMe_3-3,1,2-*closo*-$BeC_2B_9H_{11}$.[57]

Several other heteroatoms, including boron (to regenerate 1,2-*closo*-$C_2B_{10}H_{12}$),[58] nitrogen,[59] sulphur,[60] silicon,[61] selenium[62] and arsenic,[12c] have been incorporated into borane clusters to form relatively stable compounds with significant chemistry of their own, including isomerisation and deboronation[12c] as well as the formation of transition metal complexes.[63]

1.4. Carbametallaboranes

1.4.1 Class 1 Carbametallaboranes

As described earlier, borane and metallic clusters share several structural features in addition to their conformation (usually) to PSEP Theory. It is not surprising, therefore, that there exist intermediate species, whereby one or more metal atoms occupy polyhedral vertices within (hetero)borane clusters. Although the author acknowledges that a significant body of research concerned with metallaboranes exists,[64] the following discussion will limit itself to carbametallaborane examples, to reflect the scope of the Thesis.

In 1965 Hawthorne realised that the open C_2B_3 face of [7,8-*nido*-$C_2B_9H_{11}]^{2-}$ and $[Cp]^-$ were approximately isolobal (**Fig. 1.19**) and as such it should be possible to synthesise carbaborane analogues of metallocenes and other cyclopentadienyl-containing complexes.

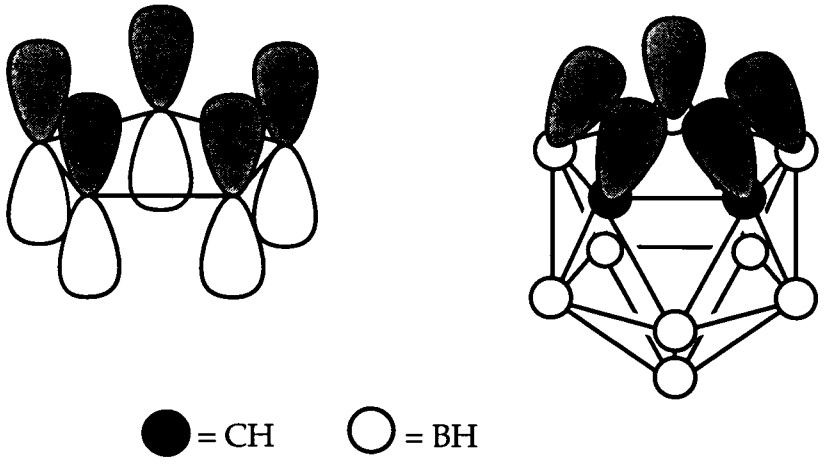

Figure 1.19 Representation of the Open Faces of Cp^- and [7,8-*nido*-$C_2B_9H_{11}]^{2-}$

He successfully synthesised the first carbametallaborane, the ferrocene analogue $[Fe^{II}(C_2B_9H_{11})_2]^{2-}$ (**Fig. 1.20**) by reacting $FeCl_2$ with two equivalents of Na_2[7,8-*nido*-$C_2B_9H_{11}$].[13] The Fe(III) species was easily generated by polarography giving the maroon, ferricinium analogue, $[Fe^{III}(C_2B_9H_{11})_2]^-$. The Fe^{II} species was easily regenerated on reduction of the ferricinium-type complex with sodium amalgam. The compound was characterised as being a sandwich complex by nmr spectroscopy. The open C_2B_3 face (assuming η^5

coordination) contributes six electrons to Fe^{2+} (d^6), which, thus, has a full shell [Kr] configuration.

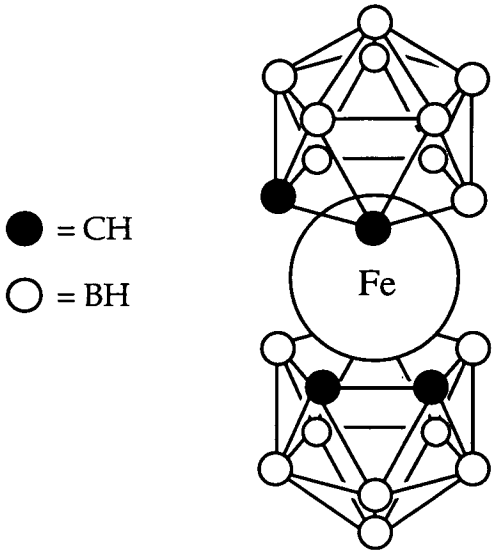

Figure 1.20 Representation of $[Fe^{II}(C_2B_9H_{11})_2]^{2-}$

Since this initial report, there have been several hundred examples of carbametallaboranes reported in the literature.[64, 65] Most of these are sandwich species, similar to that described above, of which there are several types; full sandwich, e.g. $[Fe^{II}(C_2B_9H_{11})_2]^{2-}$, half sandwich, e.g. [3,3,3-$(CO)_3$-3,1,2-*closo*-$ReC_2B_9H_{11}]^-$,[66] bent sandwich, e.g. $[Cl_2U(C_2B_9H_{11})_2]^{2-}$ [16] and slipped[67] sandwich, e.g. $[Au^{III}(C_2B_9H_{11})_2]^-$.[68]

Slipped sandwich complexes occur when full η^5 coordination of the metal centre by the carbaborane cages would cause the metal to possess more than an eighteen electron (full-shell) configuration. Hence, there is slippage, which is always away from the cage carbons, of the metal to an η^3 position, with the cage now donating four electrons to the metal centre.

The analogy between the cyclopentadienyl and [7,8-*nido*-$C_2B_9H_{11}]^{2-}$ ligands is not a true one, however, since there is a difference in the overall charge of the ligands of one electron. The charge compensated species [9-SMe_2-7,8-*nido*-$C_2B_9H_{11}$] (carb'H) and its mono- (supercarb'H) and di-phenyl- (super^{2}carb'H) substituted analogues are easily deprotonated and can be used to synthesise metallocene analogues, e.g. [Fe(carb')$_2$] (**Fig. 1.21**), which shows very similar redox behaviour to $FeCp_2$.[69]

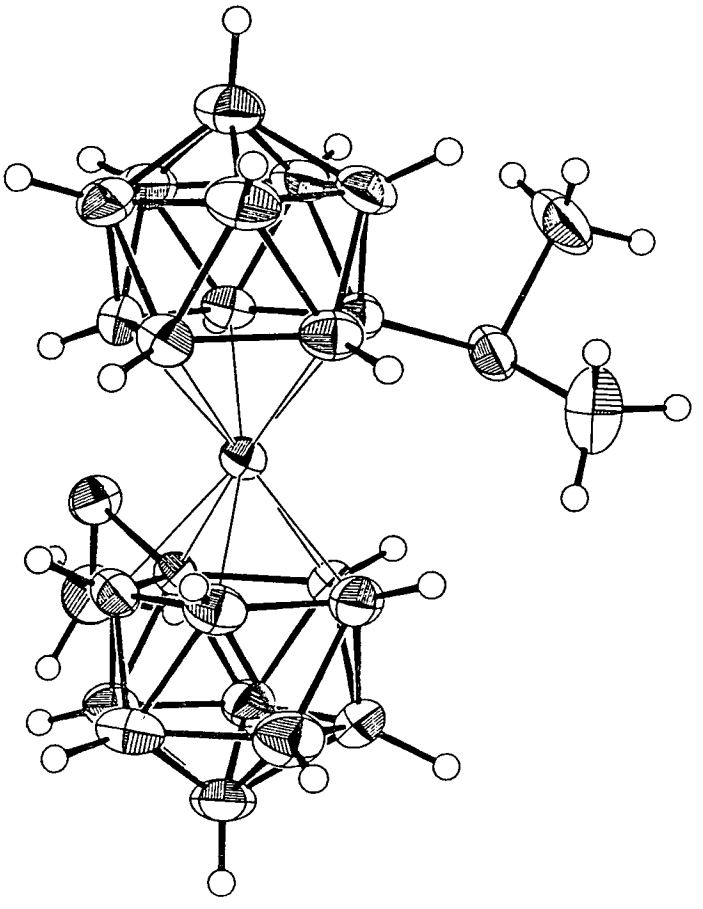

Fig. 1.21 Perspective view of [Fe(carb')$_2$]

All of the above examples are Class 1 carbametallaboranes, which are defined as those in which, "the metal fragment occupies a polyhedral vertex." The reason that there is such a prodigious number of these species, which include main group,[70] actinide[16] and lanthanide[15] examples, as well as the more common transition-metal carbametallaboranes,[71] is due to the stabilising effect of the carbaborane ligand. The stabilisation afforded by this ligand is such that high oxidation states of the late *d*-block elements (e.g. Co ^{IV}, Ni^{IV}), as well as low oxidation states of early *d*-block elements (Ti^{II}, Zr^{II}), are regularly observed.[71] Moreover, there are several sandwich complexes that have no known metallocene analogue, e.g. Pd(II).[4]

There are other types of Class 1 carbametallaboranes, such as mixed metal species and *pseudocloso* species. Mixed metal species are outwith the purview of this thesis and, as such, will not be discussed. *Pseudocloso* species will be discussed in **Section 1.5**.

1.4.2 Class 2 Carbametallaboranes

Class 2 carbametallaboranes are defined as those in which, "the metal fragment bridges a polyhedral edge," and are by far the least common type of carbametallaborane.

The reaction of the zerovalent platinum complex $[(PEt_3)_4Pt_2(1,5\text{-cod})]$ with the small carbaboranes 2,3-*nido*-$C_2B_4H_8$, 2,3-Me_2-2,3-*nido*-$C_2B_4H_8$ and 2-*nido*-CB_5H_9 afforded a series of class 2 carbametallaboranes. The product of the reaction with 2,3-*nido*-$C_2B_4H_8$ was characterised by X-ray crystallography and shown to be $\mu_{(4,5)}$-*exo*-{*trans*-$(PEt_3)_2Pt(H)$}-$\mu_{(5,6)}$-H-2,3-*nido*-$C_2B_4H_6$, with the platinum fragment bridging the B(4)-B(5) connectivity (**Fig. 1.22**).[72]

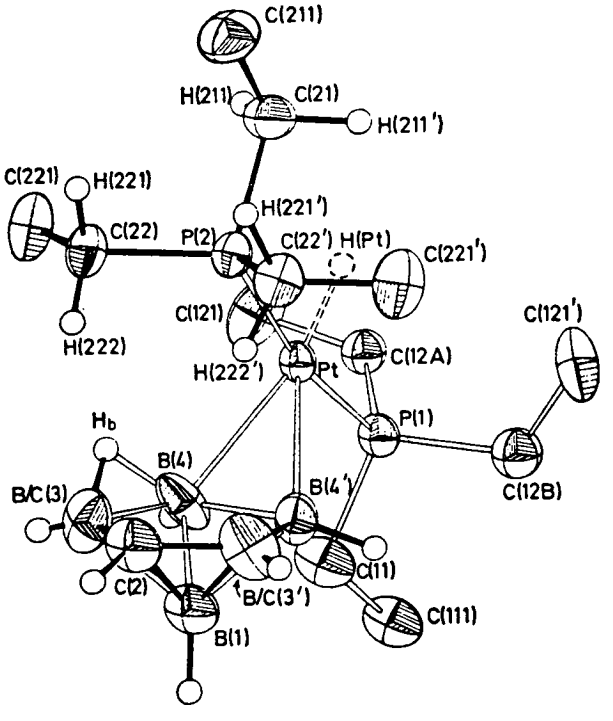

Figure 1.22 Perspective view of $\mu_{(4,5)}$-{*trans*-$(PEt_3)_2Pt(H)$}-$\mu_{(5,6)}$-H-2,3-*nido*-$C_2B_4H_6$

Other transition metal examples of class 2 carbametallaboranes include $\mu_{(4,5)}$-*exo*-{$CpFe(CO)_2$}-$\mu_{(5,6)}$-H-2,3-*nido*-$C_2B_4H_6$.[73] Examples of this mode of bonding occuring for *p*-block metal fragments include $\mu_{(9,10)}$-*exo*-{Me_2Al}-7,8-*nido*-$C_2B_9H_{12}$ (**Fig. 1.23**),[74] which is afforded by the reaction in benzene of 7,8-*nido*-$C_2B_9H_{13}$ with $AlMe_3$ at room temperature. The compound was shown by ^{11}B-{^1H} nmr spectroscopy to be highly fluxional in solution, exhibiting a time-averaged mirror plane through B(8), B(6) and B(10).[75]

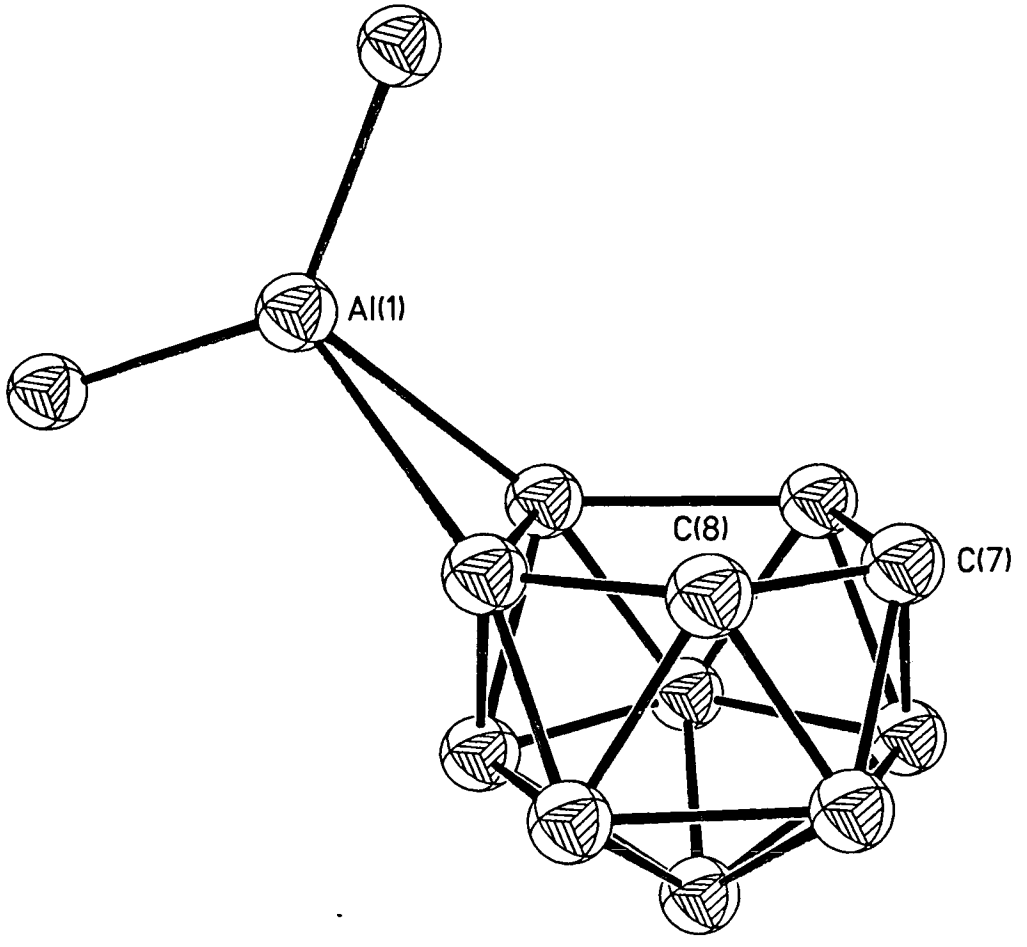

Figure 1.23 Perspective view of $\mu_{(9,10)}$-{Me_2Al}-7,8-*nido*-$C_2B_9H_{12}$

Heating this solution to reflux for 25 hours causes evolution of methane and the formation of the class 1 species, 3-Me-3,1,2-*closo*-$AlC_2B_9H_{11}$.[70b] The former species (i.e $\mu_{(9,10)}$-{Me_2Al}-7,8-*nido*-$C_2B_9H_{12}$) is also termed *exo-nido*, as the metal fragment is *exo* to the *nido* cage. This particular type of carbametallaborane geometry will be dicussed in more detail in **Section 1.5.2**, with particular reference to rhodium compounds.

1.4.3 Class 3 Carbametallaboranes

Class 3 carbametallaboranes are defined as those in which, "the metal fragment is bound to the cluster by a single, two-centre, two-electron bond, usually to a cage carbon atom." The first examples were of the main group elements germanium, tin and lead.[76] The first transition metal complexes were of platinum, and were synthesised by the reaction of *trans*-$PtCl_2(PEt_3)_2$ and *trans*-$PtCl_2(P(n\text{-}Pr)_3)_2$ with one equivalent of either Li[1-R-1,2-*closo*-$C_2B_{10}H_{10}$] (R = Me, Ph) or Li[1-Me-1,7-*closo*-$C_2B_{10}H_{10}$].[77] The products were shown to be monomeric, four-coordinate, Pt^{II} species, which no longer contained a C_{cage}-H. The suggested structure is shown below in **Figure 1.24**. There is loss of a proton from one of the alkyl groups of the coordinated phosphine groups with concomitant formation of a second Pt-C bond. The platinum centre adopts a distorted square planar geometry, with the two phosphine ligands mutually *cis*. The proton is lost as HCl immediately following the replacement of the first chlorine atom, which then reacts with unreacted lithium carbaborane salt regenerating parent carbaborane.

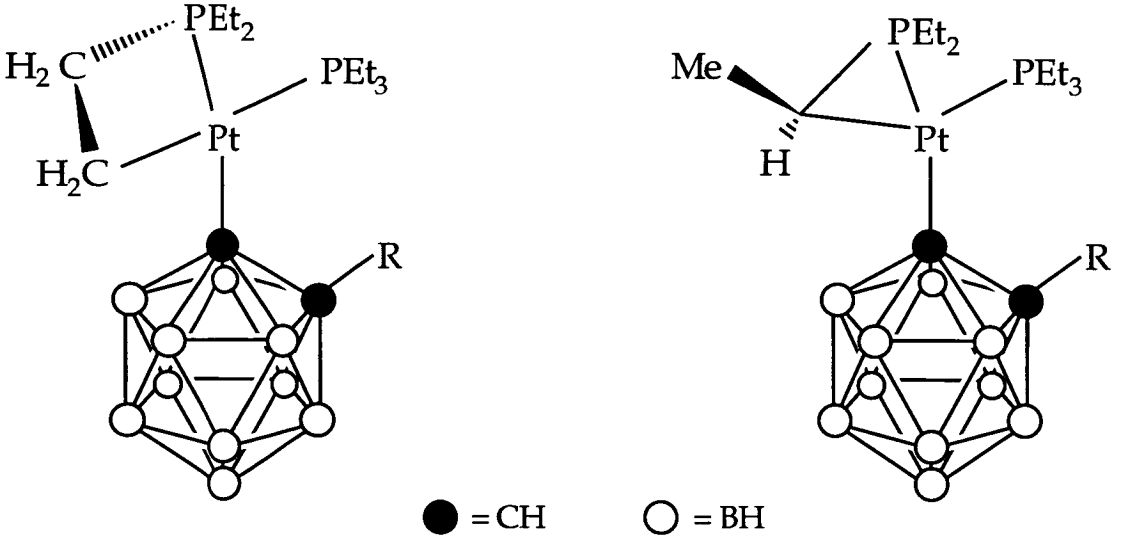

Figure 1.24 Proposed and Actual Structures of (R-carb)Pt$(PEt_3)_2$

This mode of bonding was shown to be correct by X-ray crystallographic studies,[78] although cyclometallation was observed as occurring via the α-carbon and not the β-carbon atom as initially thought. This bonding mode is typical for this system, since further structural determinations of the $PMePh_2$ and $P(CH_2Ph)_3$ analogues have all displayed the same bonding mode. [79]

In addition, Hawthorne synthesised several examples where the metal fragments {$CpFe(CO)_2$} and {$Mn(CO)_5$} were bound to various C_2B_8 and C_2B_{10} clusters, although none were structurally characterised.[48, 19]

All of these examples were synthesised by reaction of the appropriate lithium salt with the desired metal-halide fragment. Other routes *via* Grignard[4] and copper[80] reagents have also been reported. The reaction between the carbaborane acid chloride 1-COCl-1,7-*closo*-$C_2B_{10}H_{11}$ and $Na[CpFe(CO)_2]$ affords 1-{$CpFe(CO)_2OC$}-1,7-*closo*-$C_2B_{10}H_{11}$, which loses a molecule of CO on being heated to reflux in *p*-xylene, to afford a class 2 carbametallaborane similar to those synthesised above by Hawthorne.[81]

At this time, examples of most main-block carbametallaboranes have been synthesised,[82] as well as further examples containing transition elements.[83] There have also been reports of lanthanide and actinide derivatives.[84] Until recently,[85] all of the transition metal examples have contained metals with electronic configurations of d^6 or greater. The reason that research has focussed upon the late transition metal series is most likely due to the misconception that the carbaborane cage is electron-deficient and thus incapable of stabilising high oxidation state metal centres. Indeed, this was the opinion expressed by Stone, who ascribed the "unusual" stability of the Au-C_{cage} σ-bond in a series of carbaauraboranes to "the electron-withdrawing influence of...the car(ba)borane group," (the Au-C_{cage} bond in 1-Me-2-{PPh_3Au}-1,2-*closo*-$C_2B_{10}H_{10}$ is inert to CF_3CO_2H in benzene, whereas the Au-C_{Me} bond of PPh_3AuMe is readily cleaved, giving $PPh_3AuO_2CCF_3$). Whilst the carbaborane moiety **is** electron deficient in **classical** terms, one must remember that carbaboranes and similar clusters adopt **non-classical**, multi-centre bonding. Moreover, the corollary to Stone's argument is that the {PPh_3Au} fragment is an electron-donor, even though it has been shown that the valence *d*-orbitals of this fragment are low-lying and therefore unsuitable.[86]

Following recent work by Reid,[85] it was felt that *closo* carbaborane cages are best described as efficient σ-donors that are at least as good as methyl, itself a well known, good σ-donor. He synthesised a series of class 3 carbaauraboranes of the general type 1-R-2-{ER'_3Au}-1,2-*closo*-$C_2B_{10}H_{10}$ (R = Ph, CH_2OCH_3; R' = Ph, Cy, Et, *o*-tol; E = P, As).[87] Nmr studies revealed that

for E = P, the $^{31}P-\{^{1}H\}$ resonances lay between those of the related PR'_3AuX species (X = Cl, Me, where, as for the carbaauraboranes, the ligand is necessarily *trans* to the phosphine). The resonance was at high field relative to the related PR'_3AuMe species and low field to the chloride species. Since the ^{31}P chemical shift moves to higher frequency with increasing basicity of the phosphine, these results showed that the carbaborane was a better σ-donor than methyl (purely a σ-donor), but not as good as chloride (a σ- and π-donor). The ^{11}B nmr data also suggested that the carbaborane moiety was acting as a σ-donor, since substitution of a C_{cage}-H with an isolobal $\{PR'_3Au\}$ fragment causes deshielding of the ^{11}B nuclei, consistent with a loss of electron density from the cage.

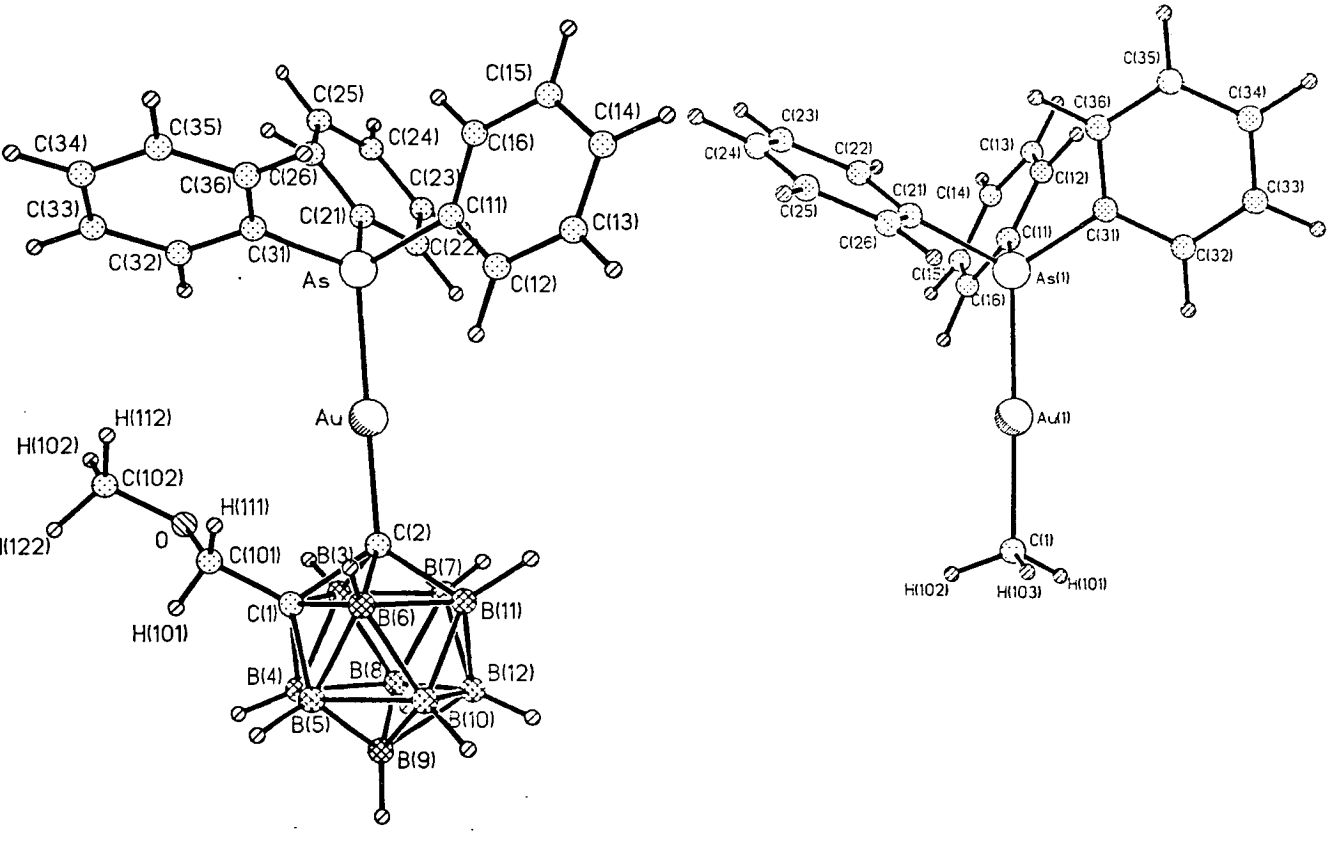

Figure 1.25 Perspective Views of 1-CH_2OCH_3-2-$\{AsPh_3Au\}$-1,2-*closo*-$C_2B_{10}H_{10}$ and $AsPh_3AuMe$

The crystallographically determined structures of 1-CH_2OCH_3-2-$\{AsPh_3Au\}$-1,2-*closo*-$C_2B_{10}H_{10}$ and $AsPh_3AuMe$ (**Fig. 1.25**) were compared and it was found that the Au-C_{cage} bond length in the carbaborane (2.039(8) Å) was significantly shorter than the Au-C_{Me} bond length in the methyl

species (2.124(9) Å), suggesting that the Au-C_{cage} bond was the stronger of the two, a hypothesis supported by EHMO calculations on model compounds. Taken together this work provided a great deal of strong evidence to support the hypothesis that the carbaborane ligand is indeed acting as an efficient σ-donor.

This work suggested that it would be possible to synthesise class 3 carbametallaboranes with low d^n configurations, since the donor properties of the carbaborane could help stabilise any high oxidation states. This was indeed the case and Reid successfully synthesised two carbatitanaboranes by reaction of Li[1-CH_2OCH_3-1,2-*closo*-$C_2B_{10}H_{10}$] with either $CpTiCl_3$ or $TiCl_4$ (the product of this latter reaction was further reacted with 2,2′-bipyridyl (bipy) in an attempt to render it less unstable). The compounds, for which the titanium centre has a d^0 configuration, are relatively air- and moisture-sensitive, although this is typical of Ti^{IV} chemistry. One of the compounds was characterised by X-ray crystallography (**Fig. 1.26**).

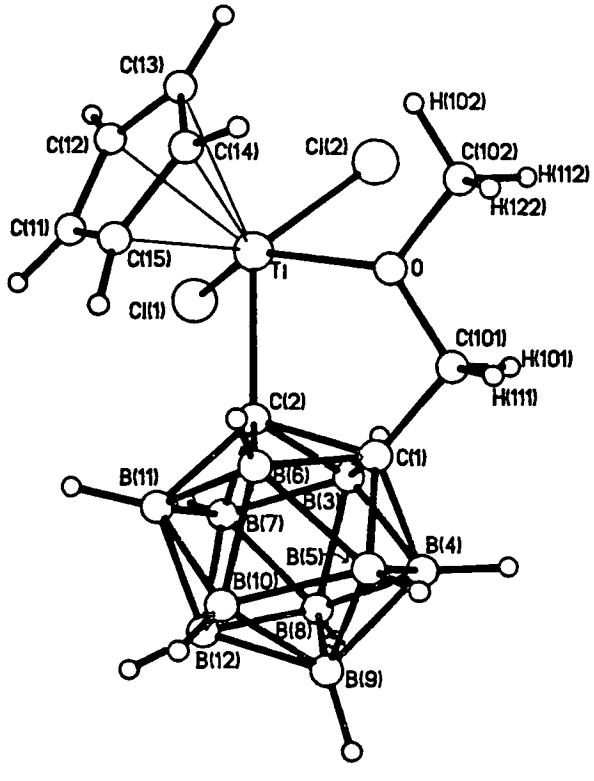

Figure 1.26 Perspective view of 1-CH_2OCH_3-2-{$CpTiCl_2$}-1,2-*closo*-$C_2B_{10}H_{10}$

There is intramolecular coordination of the ether-oxygen to the titanium centre, to form a distorted five-membered ring. This causes the titanium atom to be pulled away from the ideal Ti-C_{cage} bonding vector, although any destabilisation that this causes must be more than compensated for by the coordination of the ether-oxygen. This type of intramolecular coordination has been observed before with both oxygen[88] and nitrogen.[89] **(Fig. 1.27)**.

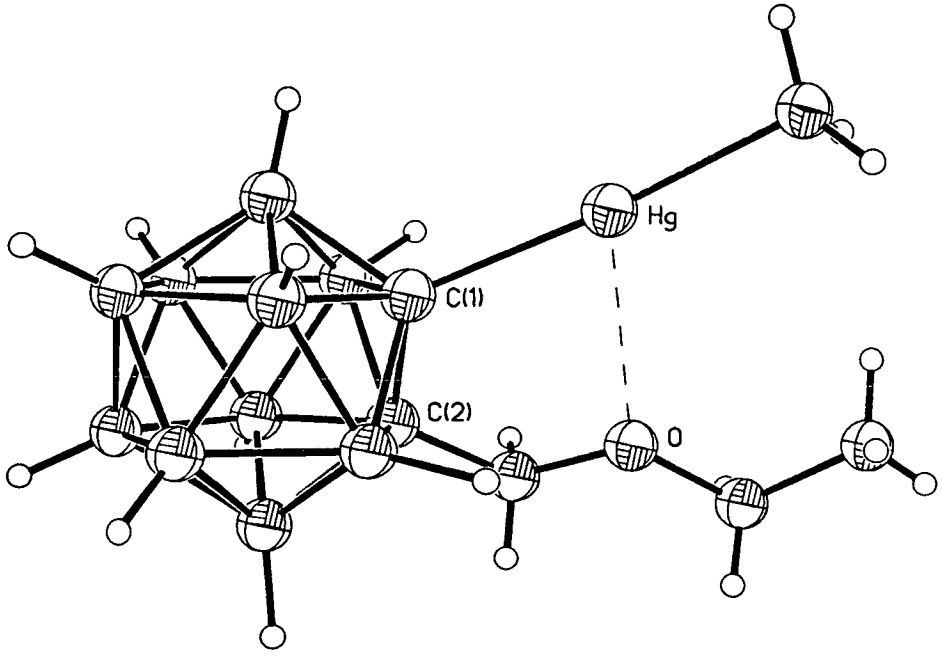

Figure 1.27 Perspective view of 1-$CH_2OCH_2CH_3$-2-{HgMe}-1,2-*closo*-$C_2B_{10}H_{10}$

In addition, there are several examples of ethercarbaboranes that complex metal atoms or metal-ligand fragments. One such example is $[(7,8\text{-}(CH_2OCH_3)_2\text{-}7,8\text{-}nido\text{-}C_2B_9H_9)_2Li(thf)_2]$[90] (**Fig. 1.28**). Here, the lithium atom is coordinated to the four oxygen atoms; two each from the ether groups and thf molecules.

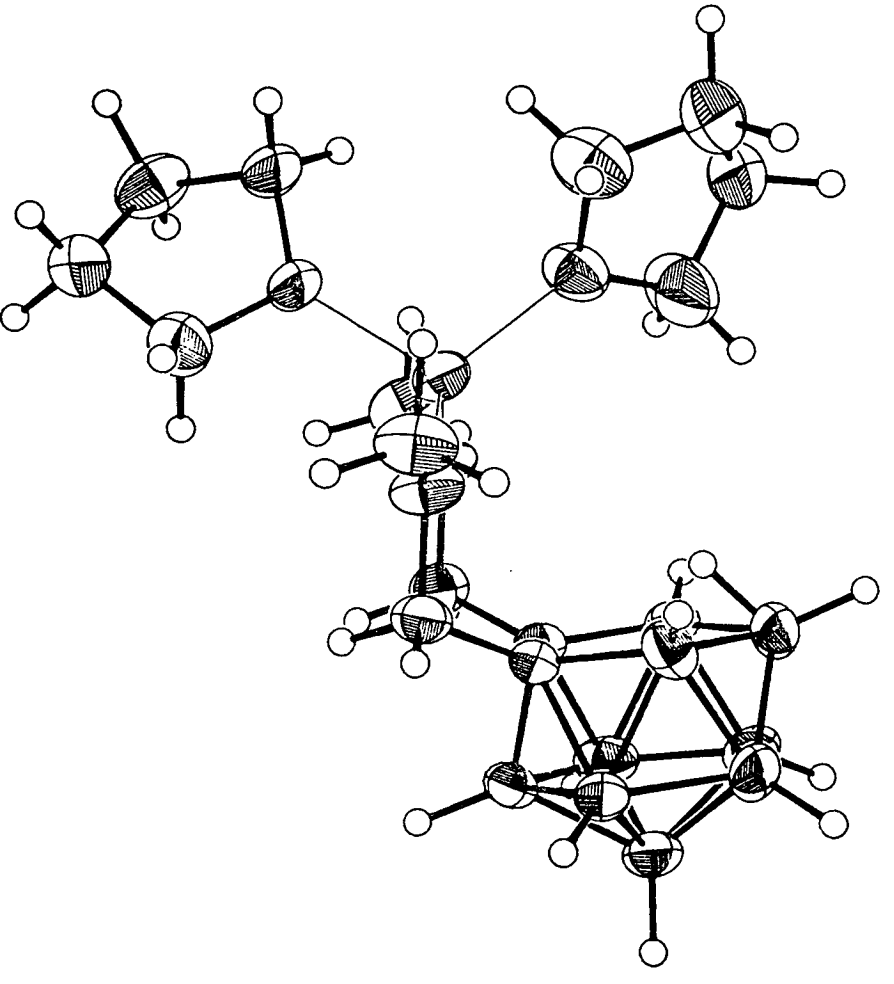

Figure 1.28 Perspective view of $[(7,8\text{-}(CH_2OCH_3)_2\text{-}7,8\text{-}nido\text{-}C_2B_9H_9)_2Li(thf)_2]$

The substituted carbaborane $1,2\text{-}(PPh_2)_2\text{-}1,2\text{-}closo\text{-}C_2B_{10}H_{10}$ has been used to coordinate nickel,[91] gold[92] and iron[93] ligand fragments, for example $Fe(CO)_3$. Teixidor *et al* have synthesised several carbaboranes which incorporate a macrocyclic ring.[94] The coordinated metal, usually an alkali earth metal, is held away from the two cage carbon atoms (**Fig. 1.29**).

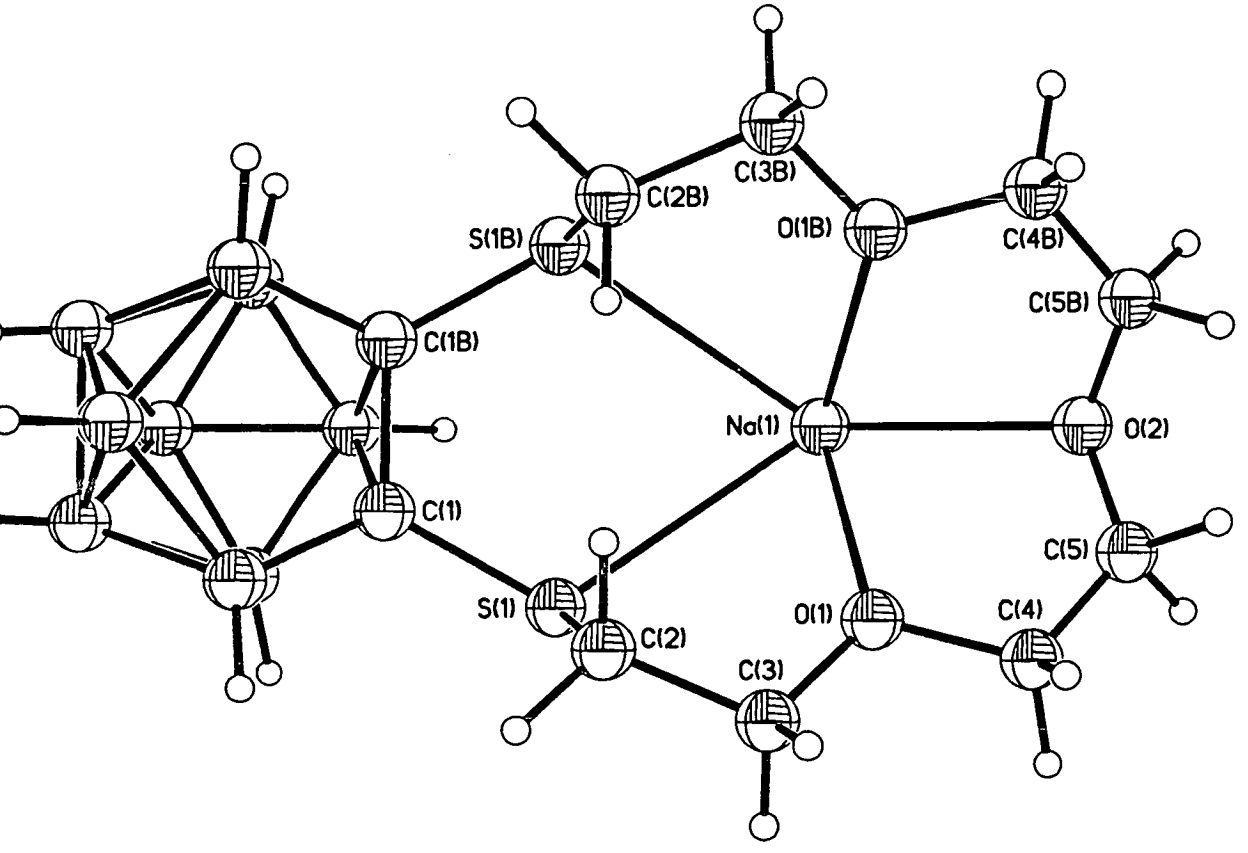

Figure 1.29 Perspective view of 7,8-[$SCH_2CH_2(OCH_2CH_2)_3Na$]-7,8-*nido*-$C_2B_9H_{10}$

1.5 Sterically Crowded Carbametallaboranes.

1.5.1 Introduction

Recently, this research group has undertaken a systematic study of the effects of deliberately crowding carbametallaboranes. **Figure 1.30** is a representation of the surface of a typical class 1 carbametallaborane, 1-X-2-Y-3-{Z}-3,1,2-*closo*-$MC_2B_9H_9$, where X and Y are the cage carbon substituents and Z is the ligand set for a transition metal, M.

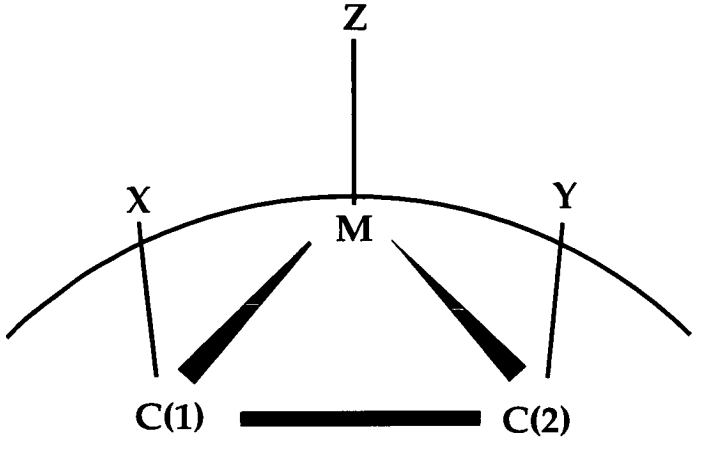

Figure 1.30 Representation of 1-X-2-Y-3-{Z}-3,1,2-*closo*-$MC_2B_9H_9$

As the steric requirements of the X, Y and Z groups increase, the degree of mutual repulsion of the three ligands increases, and, in such a situation, the cluster may relieve the steric strain by a variety of subtle changes to the cage geometry. These include lengthening the C(1)-C(2) connectivity, slippage of the metal-ligand fragment to the back of the open face or back-bending or twisting of the cage carbon substituents.

However, when the steric requirements of the substituents become sufficiently high, the distortions described above do not provide enough relief and radical geometry changes, which fall into three main types, are forced upon the molecule. The first of these is **Vertex Extrusion**, where a metal-ligand fragment vertex flips from a position at a polyhedral vertex to one outside the cage. The second type of geometry change is **Polyhedral Isomerisation**, where one of the cage carbon atoms migrates to the lower pentagonal ring of the icosahedron, either spontaneously or upon gentle heating. Not only does this provide relief from the steric strain, but it is also

more thermodynamically favourable for the cage carbon atoms to be as far apart as possible. The third process is **Polyhedral Deformation**, where the C(1)-C(2) connectivity is broken to afford a more open, less crowded *pseudocloso* geometry.

1.5.2 Vertex Extrusion

In 1974, Hawthorne synthesised the carbarhodaborane 3,3-$(PPh_3)_2$-3-H-3,1,2-*closo*-$RhC_2B_9H_{11}$, which was initially characterised by IR and nmr (^1H, ^{11}B-{^1H}, ^{31}P-{^1H}) spectroscopies[24] and later by an X-ray crystallographic study (**Fig. 1.31**).[25]

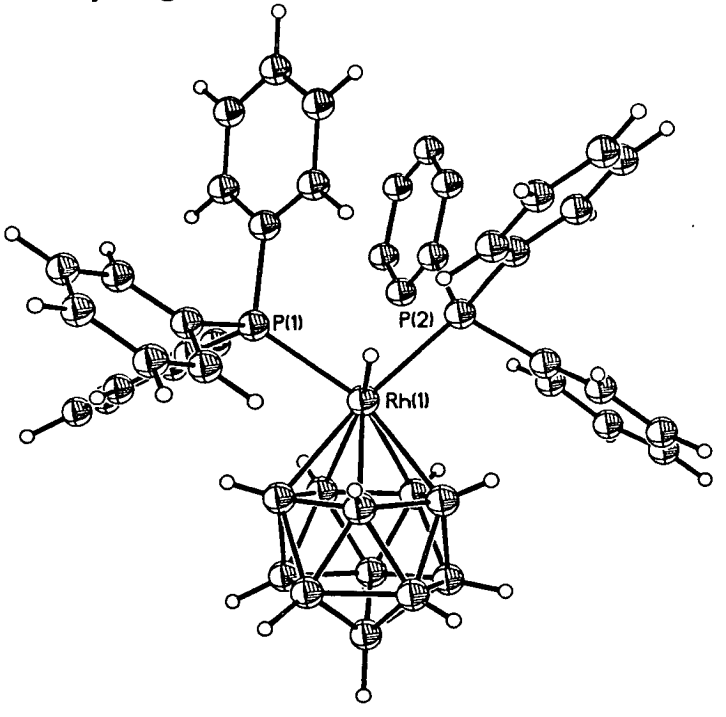

Figure 1.31 Perspective view of 3,3-$(PPh_3)_2$-3-H-3,1,2-*closo*-$RhC_2B_9H_{11}$

The compound was shown to possess catalytic activity,[24] which was rather surprising in view of the fact that the metal centre was both coordinatively (*pseudo*-octahedral geometry) and electronically (d^6 Rh^{III}, 18-electron) saturated. Hawthorne hypothesised that there was a tautomeric form responsible for this catalytic activity, in which an *exo*-{$(PPh_3)_2Rh$} fragment bridges a B-B connectivity of a *nido* cage *via* two B-H-Rh bridges. This tautomer, which he termed *'exo-nido'*, accounted for the observed catalytic activity, since the metal centre was now both coordinatively (square planar geometry) and electronically (d^8 Rh^I, 16-electron) unsaturated (**Fig. 1.32**).[25]

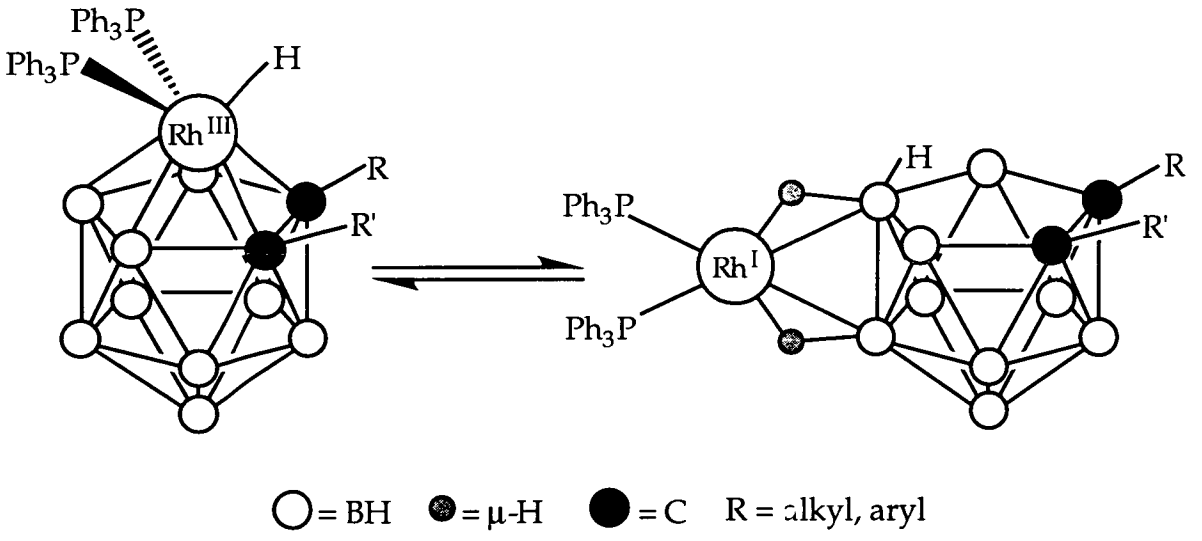

Figure 1.32 Representations of 1-R'-2-R-3,3-$(PPh_3)_2$-3-H-3,1,2-*closo*-$RhC_2B_9H_9$ and its *Exo-Nido* Tautomer

This hypothesis was proved to be correct by several studies on a series of carbarhodaboranes synthesised with increasingly more sterically demanding C_{cage} substituents,[95, 20] which were also shown to possess catalytic activity.[96] **Table 1.6** gives some examples of these substituents and the resulting geometries.

Table 1.6 Geometries of Bisphosphine Carbarhodaboranes

R	R'	Geometry
H	H	*closo*
Ph	H	*closo*
o-phenylene		*closo / exo-nido*
Me	Me	*closo / exo-nido*
μ-$(CH_2)_3$		*exo-nido*
Ph	Me	*exo-nido*

This tautomerism is sterically driven by mutual repulsion of the PPh_3 groups and the C_{cage} substituents, and hence the equilibrium moves further to the right the greater the steric requirements of these substituents become. Interestingly, for R = R' = Me or R, R' = *o*-phenylene, **both** tautomers were observed by $^{31}P-\{^1H\}$ nmr spectroscopy (for R = R' = Me, the $^{31}P-\{^1H\}$ nmr spectrum shows doublets at 44.4 ppm ($^1J_{Rh-P}$ = 186 Hz - *exo-nido*) and 43.3 ppm ($^1J_{Rh-P}$ = 146 Hz - *closo*), although for R = R' = Me, only the *exo-nido*

species was crystallised).[20] For R, R′ = *o*-phenylene, reaction with PCy_3 afforded a mixed phosphine species, where the metal ligand fragment was {$(PCy_3)(PPh_3)Rh$}. Due to the larger cone angle, θ, of PCy_3 relative to PPh_3 (θ = 170 and 145°, respectively[97]), the equilibrium is forced even further to the right, to afford the *exo-nido* species as the exclusive product.

Hawthorne also synthesised analogous carbarhodaboranes where the phosphine was PEt_3. For sterically demanding C_{cage} substituents (R = Me, R′ = Me, Ph; R = H, R′ =1,2-*closo*-$C_2B_{10}H_{11}$) , the compound did not adopt the expected *exo-nido* geometry. Instead, there was migration of the cage carbon atom bearing the bulkiest substituent to the lower pentagonal ring to afford the 2,1,8-isomer (**Fig. 1.33**).[20b]

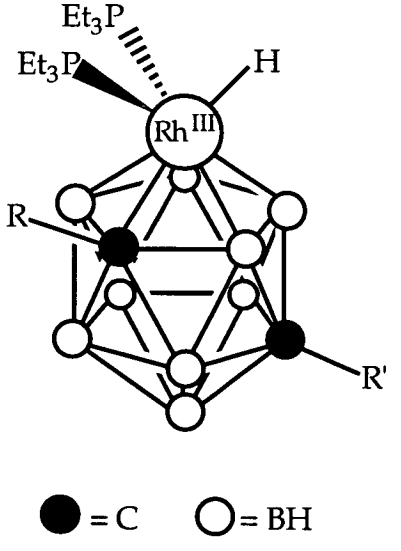

Figure 1.33 Representation of 1-R-8-R′-2,2-$(PEt_3)_2$-2-H-*closo*-2,1,8-$RhC_2B_9H_9$

This is an example of **polyhedral isomerisation** and will be discussed in greater detail in **Section 1.5.3**.

These *exo-nido* compounds are similar the class 2 carbametallaboranes (M = Al, Ga), where {R_2M} fragments (R = Me, Et) were shown to bridge a B-B connectivity on the open face of a *nido*-C_2B_9 cage.[74, 75] These products, however, were not afforded as a direct result of intramolecular steric crowding, as was the case for the carbarhodaboranes described above, although heating the complexes caused the metal fragment to adopt a position at a polyhedral vertex, with concomitant loss of either methane or

ethane. The *exo-nido* compounds were also shown to be highly fluxional with the $\{R_2M\}$ fragment migrating about the sides of the cage giving time-averaged mirror (C_s) symmetry,[74,75] typical of other *exo-nido* species. The first transition metal carbametallaboranes to display an *exo-nido* geometry were *exo*-$\{(H)_2(PPh_3)_2Ir\}$-7,8-*nido*-$C_2B_9H_{12}$, in which the $\{(H)_2(PPh_3)_2Ir\}$ fragment is bound to the cage by two three-centre, two-electron B-H-Ir bridges, and the related eleven-vertex ruthenium, iridium and rhodium species.[98] As for the above main group *exo-nido* carbametallaboranes, these examples, are not afforded as a result of intramolecular steric crowding although some degree of tautomerism is observed.

More recent examples of vertex extrusion have been described by Cowie, who synthesised examples of *exo-nido* carbametallaboranes with both ruthenium[99] and copper.[100] In the carbaruthenaborane, the metal-ligand fragment, $\{(PPh_3)_2RuCl\}$, is attached to a triangular face *via* three Ru-H-B bridges, as opposed to a single B-B connectivity (**Fig. 1.34**).

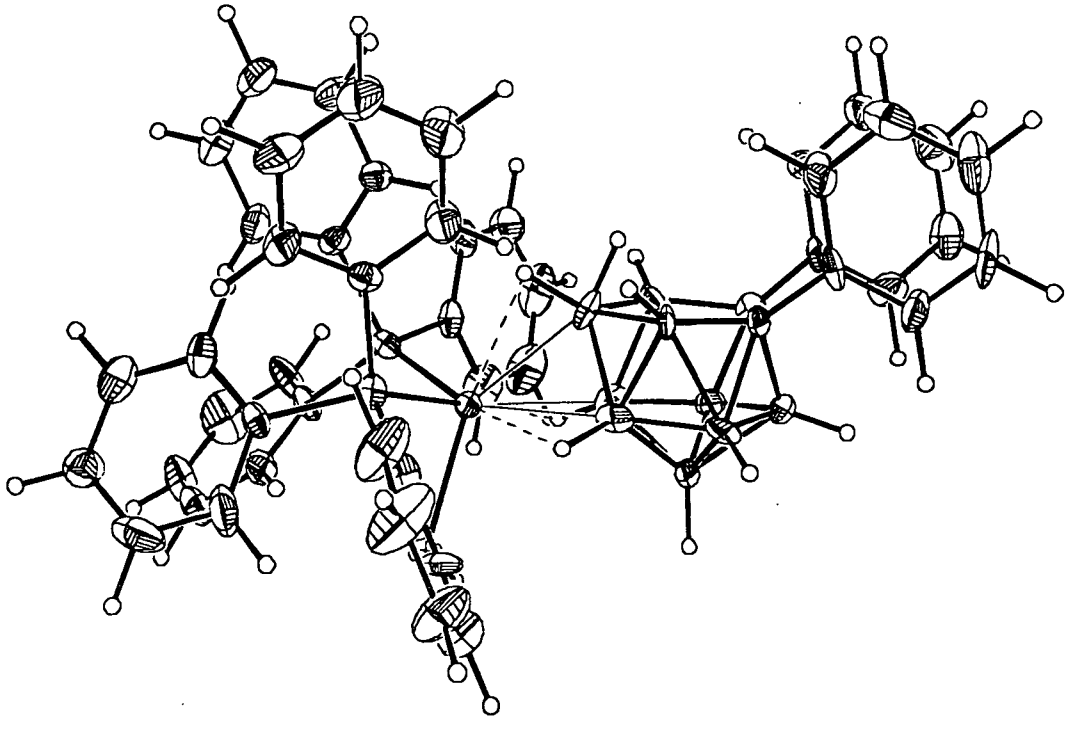

Figure 1.34 Perspective View of $\mu_{(5,6,10)}$-*exo*-$\{(PPh_3)_2RuCl\}$-7,8-Ph_2-7,8-*nido*-$C_2B_9H_9$

The metal-ligand fragment, {PPh_3Cu}, of the carbacupraborane is also attached to a triangular face, with a second {PPh_3Cu} fragment η-bonded to the open C_2B_3 face, slipped away from the cage carbon atoms (**Fig. 1.35**).

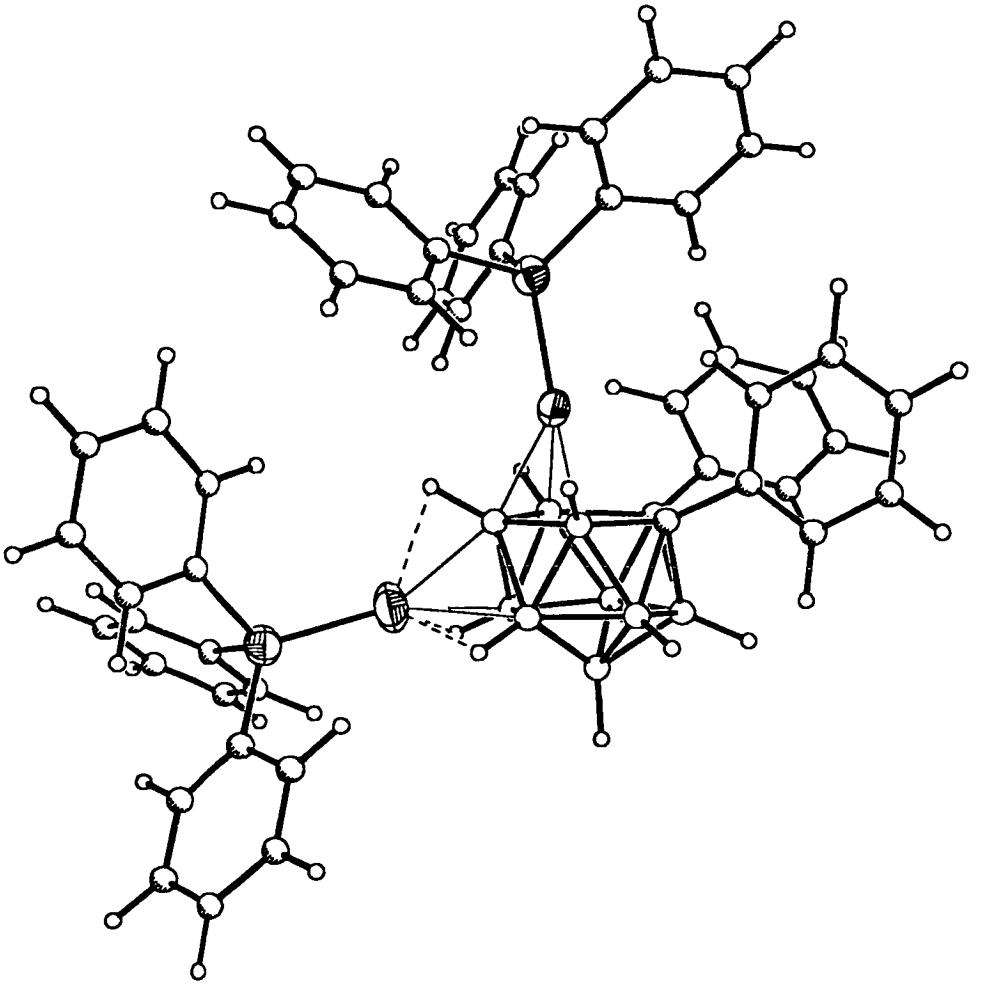

Figure 1.35 Perspective View of $\mu_{(8,9,12)}$-*exo*-{PPh_3Cu}-1,2-Ph_2-3-{PPh_3Cu}-3,1,2-*closo*-$C_2B_9H_9$

1.5.3 Polyhedral Isomerisation

The second type of process undergone by sterically crowded carbametallaboranes is migration of cage carbon atoms to afford less sterically strained geometries. Isomerisation of carbaboranes has been a recognised aspect of their chemistry since early in their development.[33] For example, the reaction between C_2H_2 and B_5H_9 affords two isomers, 1,2- and 1,6-*closo*-$C_2B_4H_6$. The 1,2-isomer is unstable and it is likely that, under the reaction conditions, the more stable 1,6-isomer is produced by relatively facile isomerisation of 1,2-*closo*-$C_2B_4H_6$. The 1,6-isomer is more stable due a reduction in the electrostatic repulsion of the cage carbon atoms by being the furthest possible distance apart. It has also been observed that *o*-$C_2B_{10}H_{12}$ can be isomerised to *m*- and *p*-$C_2B_{10}H_{12}$ at elevated temperatures (450 and 625°C, respectively). The 1,2 → 1,6 and 1,2 → 1,7 isomerisations described above are believed to occur *via* a diamond-square-diamond (dsd) process (**Fig. 1.36**), which involves the cooperative stretching and squeezing of the opposite corners of a diamond-shaped group of atoms into a bent square and back into a diamond.[4]

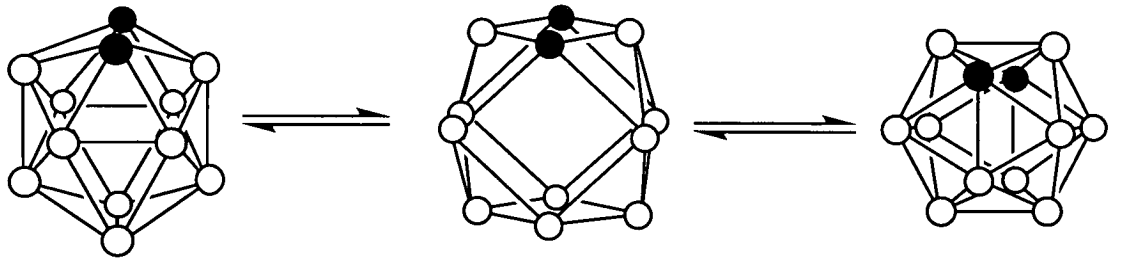

Figure 1.36 The Diamond-Square-Diamond Process

This process, however, does not account for the formation of the 1,12-isomer from 1,7-*closo*-$C_2B_{10}H_{12}$, which has been suggested as occuring *via* a combination of triangular face rotations and dsd isomerisations.

Such isomerisations can be easily effected at more ambient temperatures within sterically crowded carbametallaborane systems. For example, 1-Ph-3,3-$(PMe_2Ph)_2$-3,1,2-*closo*-$PtC_2B_9H_{10}$ is easily thermolysed at 55°C to its two 3,1,11-isomers, 11-Ph-3,3-$(PMe_2Ph)_2$-3,1,11-*closo*-$PtC_2B_9H_{10}$ and 1-Ph-3,3-$(PMe_2Ph)_2$-3,1,11-*closo*-$PtC_2B_9H_{10}$ (**Fig. 1.37**).[101]

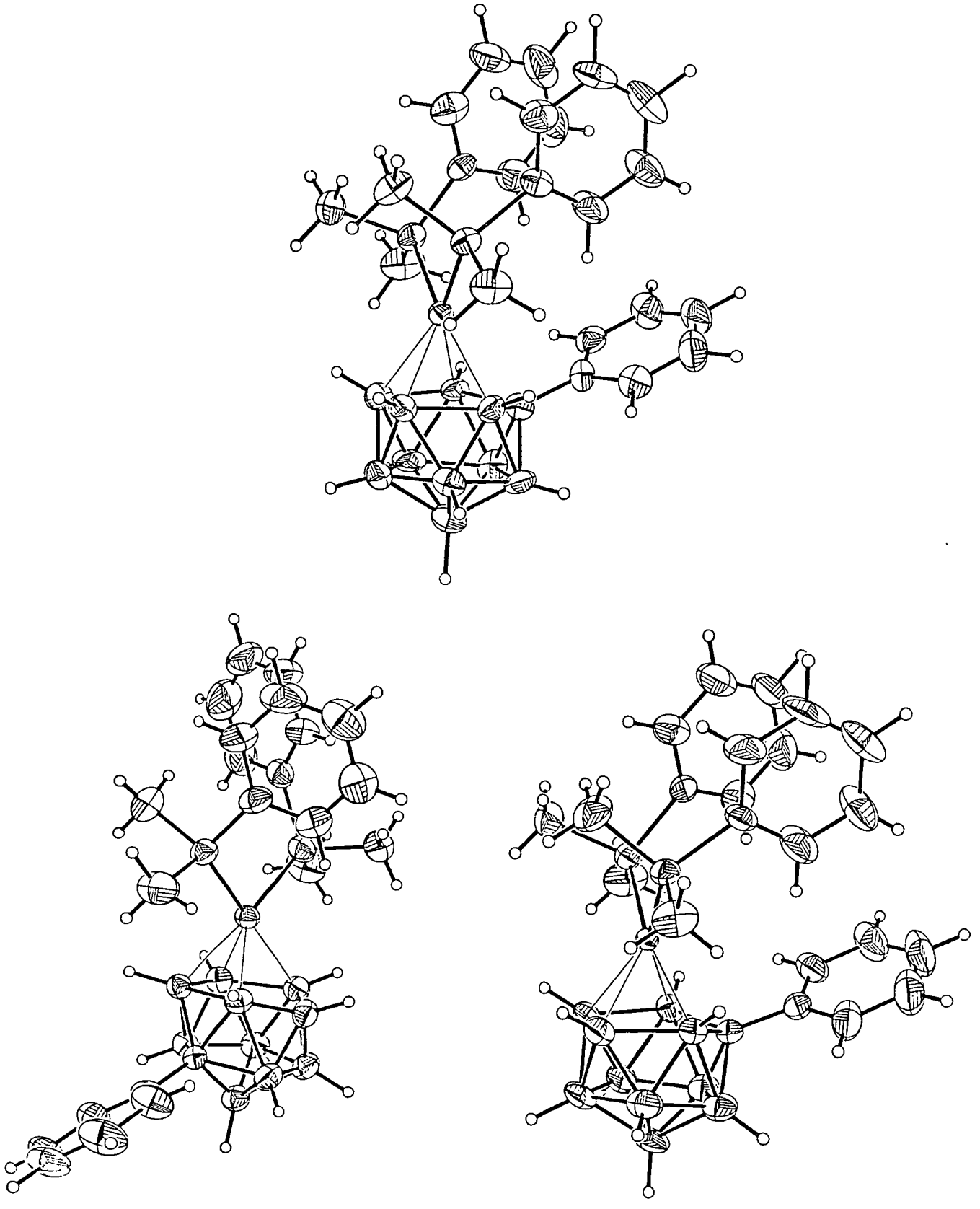

Figure 1.37 Perspective Views of 1-Ph-3,3-$(PMe_2Ph)_2$-3,1,2-*closo*-$PtC_2B_9H_{10}$ and its Thermolysis Products (55°C)

The more crowded diphenyl-substituted analogue spontaneously isomerises at room temperature and the only isolable product is 1,11-Ph_2-3,3-$(PMe_2Ph)_2$-3,1,11-*closo*-$PtC_2B_9H_9$ (**Fig. 1.38**). However, these isomerisation products could **not** have been afforded by a simple dsd process and recent work within this research group has focussed upon trying to determine the mechanism of this reaction.[102,103]

As described in the **Section 1.5.2**, polyhedral isomerisation has been observed for bis(phosphine)hydridocarbarhodaboranes. Gently heating the salt $[(PEt_3)_4Rh][7\text{-R-}8\text{-R}'\text{-}7,8\text{-}nido\text{-}C_2B_9H_{10}]$ (R = Me, R′ = Ph; R = H, R′ = 1,2-*closo*-$C_2B_{10}H_{11}$) at 60°C for several hours affords the species 1-R-7-R′-2,2-$(PEt_3)_2$-2-H-2,1,8-*closo*-$RhC_2B_9H_9$. Again, one of the cage carbon atoms has migrated to the lower pentagonal belt under relatively mild conditions. Similar products were afforded by heating the unrearranged compounds 1-R-2-R′-3,3-$(PEt_3)_2$-3-H-3,1,2-*closo*-$RhC_2B_9H_9$ (R = R′ = Me; R, R′ = $\mu(CH_2)_3$).

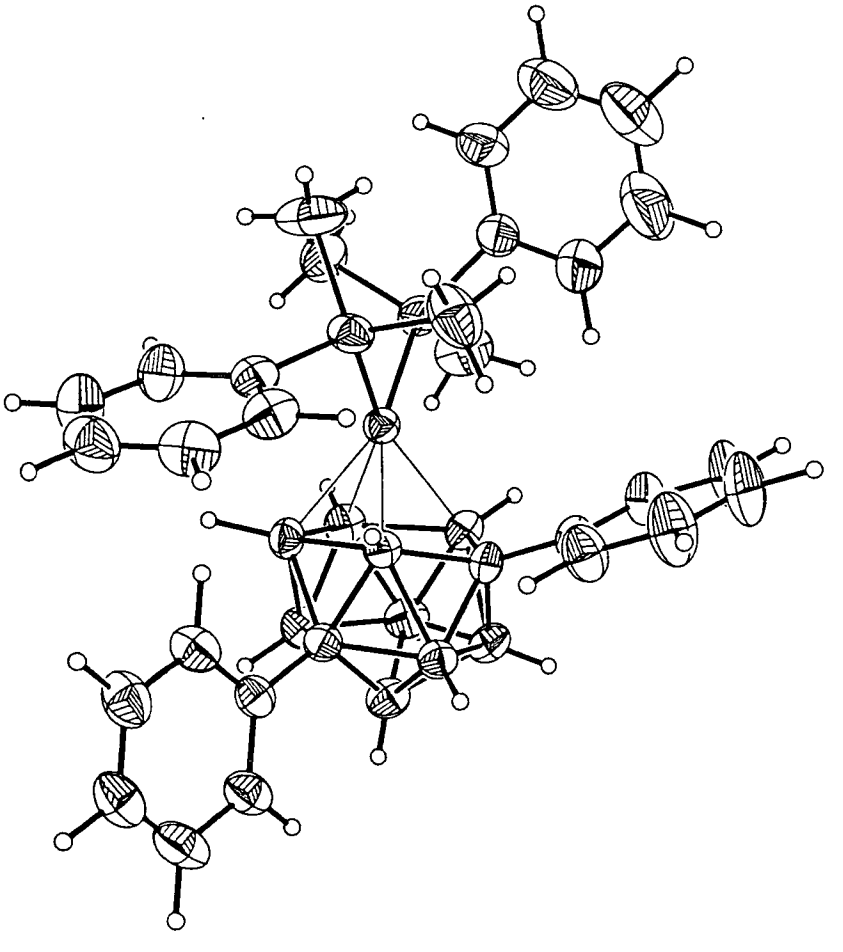

Figure 1.38 Perspective View of 1,11-Ph_2-3,3-$(PMe_2Ph)_2$-3,1,11-*closo*-$PtC_2B_9H_9$

1.5.4 Polyhedral Deformation

The third process whereby a carbametallaborane may relieve intramolecular strain is polyhedral deformation. X-ray diffraction studies on compounds of the type 1,2-Ph_2-3-{η-L}-3,1,2-*pseudocloso*-$MC_2B_9H_9$ (L = C_6H_6, C_6Me_6, *p*-cym, M = Ru; L = Cp*, Indy*, [9]aneS_3, M = Rh, Ir)[104] have shown that the C(1)-C(2) connectivity is extended from 1.727(6) Å in 1,2-Ph_2-1,2-*closo*-$C_2B_{10}H_{10}$,[105] to approximately 2.5 Å in the corresponding *pseudocloso* carbametallaborane (**Fig. 1.39**).

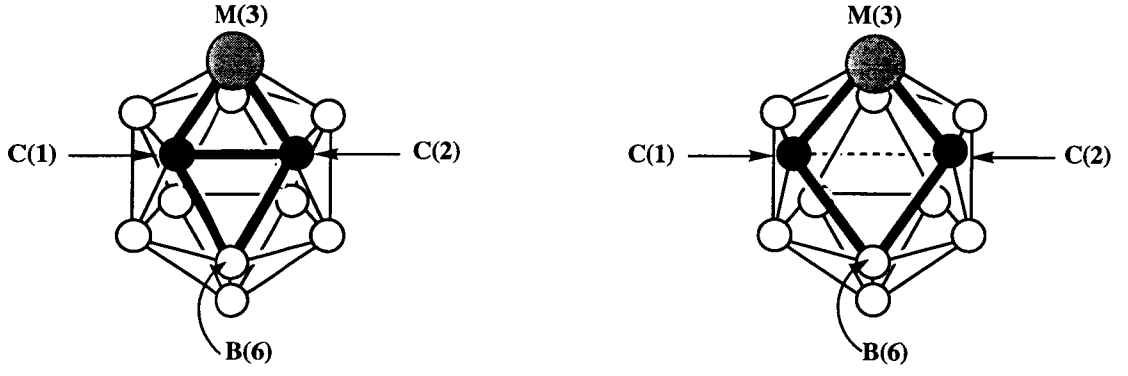

Figure 1.39 Representations of *Closo* and *Pseudocloso* Geometries

This dramatic change in cage geometry is reflected by the ^{11}B-{^1H} nmr spectrum, which indicates deshielding of the ^{11}B nuclei (by several ppm) relative to the mono-phenyl-substituted, *closo* carbametallaborane. The lowest-field (relative integral-one) resonance generally occurs between 25 and 35 ppm, with the next lowest-field resonance occuring at between 12 and 16 ppm. **Table 1.7** (below) gives details of *pseudocloso* species characterised thus far.

The first example of this type of compound to be synthesised was 1,2-Ph_2-3-{Cp*}-3,1,2-*pseudocloso*-$RhC_2B_9H_9$ (**Fig. 1.40**). In addition to the breaking of the C(1)-C(2) connectivity, the molecule also displayed several other features, which are typical of *pseudocloso* species. The most noticeable of these is that the phenyl rings are lying almost coplanar. This is in contrast to the *closo* parent and *nido* salt from which it is derived. In both of these cases, the phenyl rings are almost perpendicular to the plane through the atomic sequence C_{phenyl}-C_{cage}-C_{cage}-C_{phenyl}. This orientation is necessary to reduce

steric repulsion between the two bulky phenyl rings, which are in close proximity to each other (C_{cage}-C_{cage} = 1.727(6) and 1.590(5) Å, respectively). All of the ligands used to bind the metal, however, contain delocalised π-systems, and are necessarily flat in order to maximise interaction. Were the phenyl rings of the carbametallaborane to retain the conformation observed for the *closo* and *nido* parents, it would cause extreme intramolecular crowding and hence the phenyl rings flatten and push against each other, causing the C(1)-C(2) connectivity to lengthen and eventually break.

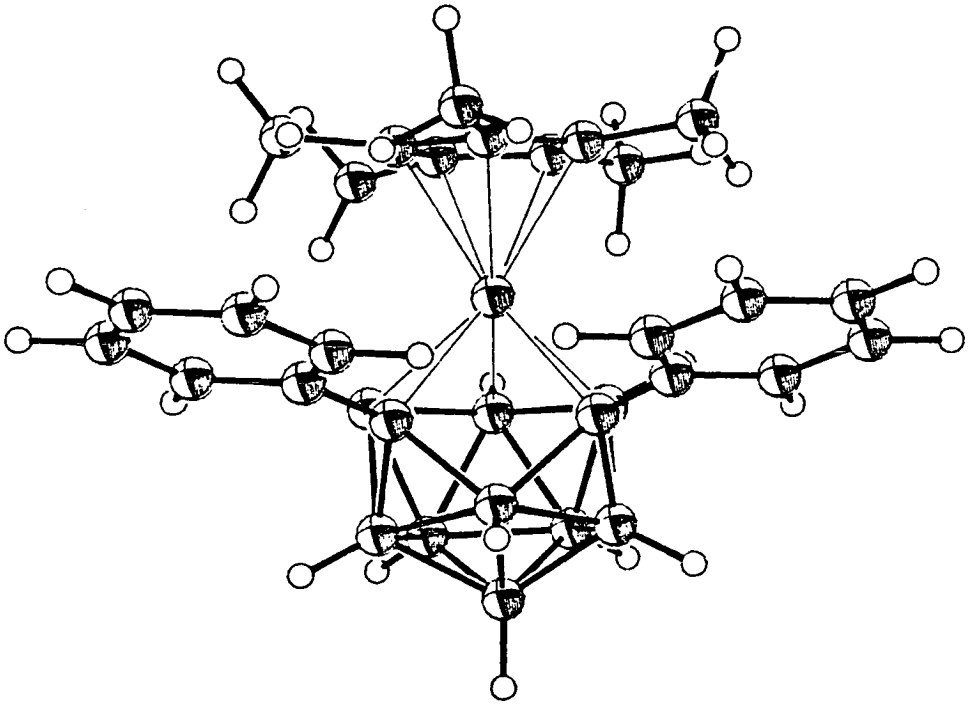

Figure 1.40 Perspective View of 1,2-Ph_2-3-{C_5Me_5}-3,1,2-*pseudocloso*-$RhC_2B_9H_9$

Table 1.7 Examples of *Pseudocloso* Carbametallaboranes

η-L	M	C(1)···C(2)/ (Å)	mean ^{11}B δ/(ppm)	Reference
C_5Me_5	Rh	2.51(3)	5.42	**104a**
C_5Me_5	Ir	*	2.94	**104b**
C_6H_6	Ru	2.485(8)	5.36	**104b**
p-cym	Ru	2.453(5)	5.58	**104b**
C_6Me_6	Ru	*	6.40	**104b**
C_9Me_7	Rh	2.491(6)	5.43	**22**
[9]aneS_3	Ru	2.504(7)	8.18	**104d**

(* crystals suitable for X-ray diffraction could not be grown)

1.6 Scope of Thesis

Chapter 2 is concerned with how planar, σ-bonded sustituents orientate themselves with respect to the carbaborane cage. As such X-ray crystallography has been used to determine the structures of 1-R-1,2-*closo*-$C_2B_{10}H_{11}$ (R = C_6H_5, $[CO_2]^-$) and the results of these studies are compared with the predicted orientations, determined by EHMO calculations. The structures of two substituted carbaborane carboxylate salts are also described. This work led to attempts to synthesise carbaboranes σ-bonded to {$GaMe_2$} fragments, which, in the case of mono-ethercarbaborane were successful.

Chapter 3 is an extension of the work of Reid, whereby a series of carbaauraboranes were studied spectroscopically and crystallographically and by EHMO calculations. Compounds of the type PR'_3AuMe (R' = Cy, *o*-tol, Et) were also studied and compared to the respective carbaborane analogues. The (unexpected) product of the reaction between $P(C_6F_5)_3AuCl$ and MeLi was characterised as being $C_6F_5AuP(C_6F_5)Me_2$ by an X-ray crystallographic study.

Chapter 4 describes the synthesis and characterisation of several carbarhodaboranes using the $[7,8\text{-}Ph_2\text{-}7,8\text{-}nido\text{-}C_2B_9H_{10}]^-$ ligand. The ligand was used to design compounds which were sterically very crowded with a view to studying the molecular distortion that this afforded.

Chapter 1 References

1 E.g. (**a**) W.N. Lipscomb, "*Boron Hydrides*," Benjamin, New York, 1963; (**b**) E.L. Muetterties, "*Boron Hydrides*," Academic Press, New York, 1975.

2 E.g. (**a**) A. Stock, "*Hydrides of Boron and Silicon*," Cornell University Press, Ithaca, New York, 1936; (**b**) V. Bartow, *Adv. Chem. Ser.*, 1961, **32**, 5.

3 J. Plesek, *Chem. Rev.*, 1992, **92**, 269.

4 K.F. Purcell and J.C. Kotz, "*Inorganic Chemistry*," Chapter 18, W.B. Saunders Company, Philadelphia, 1977, and references therein.

5 E.g. (**a**) S.H. Bauer, *J. Am. Chem. Soc.*, 1937, **59**, 1096; (**b**) R.S. Mulliken, *Chem. Rev.*, 1947, **41**, 207.

6 W.C. Price, *J. Chem. Phys.*, 1947, **15**, 614.

7 E.g. (**a**) J.S. Kasper, C.M. Lucht and D. Harker, *Acta Cryst.*, 1950, **3**, 436; (**b**) W.J. Dulmage and W.N. Lipscomb, *Acta Cryst.*, 1952, **5**, 260; (**c**) C.E. Nordman and W.N. Lipscomb, *J. Chem. Phys.*, 1953, **21**, 1856; (**d**) C.R. Peters and C.E. Nordman, *J. Am. Chem. Soc.*, 1960, **82**, 5758; (**e**) R.D. Dobrott and W.N. Lipscomb, *J. Chem. Phys.*, 1962, **37**, 1779.

8 (**a**) K. Hedberg and V. Schomaker, *J. Am. Chem. Soc.*, 1951, **73**, 1482; (**b**) K. Hedberg, M.E. Jones and V. Schomaker, *Proc. Natl. Acad. Sci. U.S.*, 1952, **38**, 679.

9 K. Wade, *J. Chem. Soc., Chem. Commun.*, 1971, 792.

10 (**a**) W.N. Lipscomb, *Proc. Natl. Acad. Sci. U.S..*, 1961, **36**, 1791; (**b**) R. Hoffmann and W.N. Lipscomb, *J. Chem. Phys.*, 1962, **36**, 3489.

11 C.D. Good, I. Shapiro and R.E. Williams, *J. Am. Chem. Soc.*, 1962, **84**, 3837.

12 E.g. (**a**) J. Little, J.T. Moran and L.J. Todd, *J. Am. Chem. Soc.*, 1967, **89**, 5495; (**b**) L.J. Todd, A.R. Burke, H.T. Silverstein, J.L. Little and G.S. Wilkholm, *J. Am. Chem. Soc.*, 1969, **91**, 3376; (**c**) L.J. Todd, A.R Burke, A.R. Garber, H.T. Silverstein and B.N. Storhoff, *Inorg. Chem.*, 1970, **9**, 2175; (**d**) V.A. Brattsev, S.P. Knyazev, G.N. Danilova and V.I. Stanko, *Zh. Obshch. Khim.*, 1975, **45**, 1393.

13 D.C. Young, P.A. Wegner and M.F. Hawthorne, *J. Am. Chem. Soc.*, 1965, **87**, 1818.

14 E.g. (**a**) R.L. Voorhees and R.W. Rudolph, *J. Am. Chem. Soc.*, 1969, **91**, 2173; (**b**) R.N. Grimes and W.J. Rademaker, *J. Am. Chem. Soc.*, 1969, **91**, 6498.

15 M.J. Manning, C.B. Knobler, R. Khattar and M.F. Hawthorne, *Inorg.*

Chem., 1991, **30**, 2009.

16 F.R. Fronczek, G.W. Halstead and K.N. Raymond, *J. Am. Chem. Soc.*, 1977, **99**, 1769.

17 A.J. Wynd, A.J. McLennan, D. Reed and A.J. Welch, *J. Chem. Soc., Dalton Trans.*, 1987, 2761.

18 E.J.M. Hamilton and A.J. Welch, *Acta Cryst.*, 1990, **C46**, 1228.

19 D.A. Owen, D.C. Smart, P.M. Garrett and M.F. Hawthorne, *J. Am. Chem. Soc.*, 1971, **93**, 1362.

20 C.B. Knobler, T.B. Marder, E.A. Misuzawa, R.G. Teller, J.A. Long, P.E. Behnken and M.F. Hawthorne, *J. Am. Chem. Soc.*, 1984, **106**, 2990.

21 E.g. D.R. Baghurst, R.C.B. Copley, H. Fleischer, G.O. Kyd, D.M.P. Mingos, D. O'Connell, T.R. Spalding, A.J. Welch and L.J. Yellowlees, *J. Organomet. Chem.*, 1993, **447**, C14.

22 U. Grädler, D. Reed, A.S. Weller and A.J. Welch, *J. Chem. Soc., Dalton Trans.*, 1996, 335.

23 J. Buchanan, E.J.M. Hamilton, D. Reed and A.J. Welch, *J. Chem. Soc., Dalton Trans.*, 1990, 667.

24 T.E. Paxson and M.F. Hawthorne, *J. Am. Chem. Soc.*, 1974, **96**, 4674.

25 R.T. Baker, M.S. Delaney, R.E. King, C.B. Knobler, J.A. Long, T.B. Marder, T.E. Paxson, R.G. Teller and M.F. Hawthorne, *J. Am. Chem. Soc.*, 1984, **106**, 2965.

26 A.J. Wynd and A.J. Welch, *J. Chem. Soc., Dalton Trans.*, 1990, 2803.

27 W.M. Maxwell, R. Weiss, E. Sinn and R.N. Grimes, *J. Am. Chem. Soc.*, 1977, **99**, 4016.

28 (**a**) J.R. Pipal and R.N. Grimes, *Inorg. Chem.*, 1979, **18**, 257; (**b**) J.R. Bowser, A. Bonny, J.R. Pipal and R.N. Grimes, *J. Am. Chem. Soc.*, 1979, **101**, 6220.

29 (**a**) R.W. Rudolph, *Acc. Chem. Res.*, 1976, **9**, 446; (**b**) R.N. Camp, D.S. Marynick, G.D. Graham and W.N. Lipscomb, *J. Am. Chem. Soc.*, 1978, **100**, 6781.

30 E.H. Wong and R.M. Kabbani, *Inorg. Chem.*, 1979, **18**, 2165.

31 M.E. O'Neill and K. Wade, *Inorg. Chem.*, 1982, **21**, 461.

32 P.L. Timms, *J. Am. Chem. Soc.*, 1968, **90**, 4585.

33 C.D. Good, B. Keilin, I. Shapiro and R.E. Williams, *J. Am. Chem. Soc.*, 1963, **85**, 3167.

34 T.L. Heying, J.W. Ager, S.L. Clark, D.J. Mangold, H.L. Goldstein, M. Hillman, R.J. Polak and J.W. Szymanski, *Inorg. Chem.*, 1963, **2**, 1089.

35 R. Adams, *Inorg. Chem.*, 1963, **2**, 1087.

36 J.B. Casey, W.J. Evans and W.H. Powell, *Inorg. Chem.*, 1983, **22**, 2228.
37 D. Grafstein and J. Dvorak, *Inorg. Chem.*, 1963, **2**, 1128.
38 S. Papetti and T.L. Heying, *J. Am. Chem. Soc.*, 1964, **86**, 2295.
39 R.K. Bohn and M.D. Bohn, *Inorg. Chem.*,1971, **10**, 350.
40 D.E. Sands and A. Zalkin, *Acta Cryst.*, 1962, **15**, 410.
41 (**a**) J. Reddy, and W.N. Lipscomb, *J. Am. Chem. Soc.*, 1959, **84**, 754; (**b**) J. Reddy, and W.N. Lipscomb, *J. Chem. Phys.*, 1959, **31**, 610.
42 A.R. Pitochelli and M.F. Hawthorne, *J. Am. Chem. Soc.*, 1960, **82**, 3228.
43 K.F. Shaw and A.J. Welch, *Polyhedron*, 1992, **11**, 157.
44 T.D. McGrath and A.J. Welch, *Acta Cryst.*, 1995, **C51**, 647.
45 L.I. Zakharkin and A.V Grebennikov, *Isz. Akad. Nauk. SSR Ser. Khim.*, 1967, **6**, 1376.
46 R.P. Alexander and H.A. Schroeder, *Inorg. Chem.*, 1963, **2**, 1107.
47 M.F. Hawthorne, D.C. Young, P.M. Garrett, D.A. Owen, S.G. Schwerin, F.N. Tebbe and P.A. Wegner, *J. Am. Chem. Soc.*, 1968, **90**, 862.
48 J.C. Smart, P.M. Garrett and M.F. Hawthorne, *J. Am. Chem. Soc.*, 1969, **91**, 1031.
49 R.L. Thomas, Unpublished Results.
50 L.I. Zakharkin and L.S. Podvisotskaya, *Isz. Akad. Nauk. SSR Ser. Khim.*, 1965, **8**, 1464.
51 M.M. Fein, J. Bobinski, N. Mayes, N. Schwartz and M.S. Cohen, *Inorg. Chem.*, 1963, **2**, 1111.
52 (**a**) A.V. Astakhin, V.V. Romanov, A.I. Gusev, V.N. Kalinin, L.I. Zakharkin and M.G. Los, *Zh. Strukt. Khim.*, 1977, **18**, 406; (**b**) A.S. Weller, G.M. Rosair and A.J. Welch, *Acta Cryst.*, In Press.
53 S. Hermanek, *Chem. Rev.*, 1992, **92**, 325.
54 X.L.R. Fontaine and J.D. Kennedy, *J. Chem. Soc., Chem. Commun.*, 1986, 779.
55 D.M.C. Smit, Personal Communication.
56 L.J. Todd in "*Comprehensive Organometallic Chemistry*," Eds. G. Wilkinson, F.G.A. Stone and E.W. Abel, Pergamon Press, 1981, Sec. 5.6.
57 (**a**) G. Popp and M.F. Hawthorne, *J. Am. Chem. Soc.*, 1968, **90**, 6553; (**b**) G. Popp and M.F. Hawthorne, *Inorg. Chem.*, 1971,**10**, 391.
58 P.A. Wegner and M.F. Hawthorne, *J. Am. Chem. Soc.*, 1968, **90**, 896.
59 J. Plesek, B Stibr and S. Hermanek, *Chem. Ind. (London)*, 1974, 662.
60 V.A. Brattsev, S.P. Knyazev, G.N. Danilova and V.N. Stanko, *Zh. Obshch. Khim.*, 1975, **45**, 1393.

61 M.L. Thompson and R.N. Grimes, *Inorg. Chem.*, 1972, **11**, 1925.

62 K. Base, J. Plesek, S. Hermanek, J. Huffman, P. Ragatz and R. Schaeffer, *J. Chem. Soc., Chem. Commun.*, 1975, 934.

63 L.J. Todd, I.C. Paul, J.L. Little, P.S. Welcker and C.R. Peterson, *J. Am. Chem. Soc.*, 1968, **90**, 4489.

64 E.g. R.N. Grimes in "*Comprehensive Organometallic Chemistry*," Eds. G. Wilkinson, F.G.A. Stone and E.W. Abel, Pergamon Press, 1981, Sec. 5.5.

65 E.g. (**a**) M.F. Hawthorne, *J. Organomet. Chem.*, 1975, **100**, 97; (**b**) R.N. Grimes, *Coord. Chem. Rev.*, 1979, **28**, 47.

66 A. Zalkin, T.E. Hopkins and D.H. Templeton, *Inorg. Chem.*, 1966, **5**, 1189.

67 D.M.P. Mingos, M.I. Forsyth and A.J. Welch, *J. Chem. Soc., Chem. Commun.*, 1977, 605.

68 L.F. Warren and M.F. Hawthorne, *J. Am. Chem. Soc.*, 1968, **90**, 4823.

69 E.J.M. Hamilton, Ph.D. Thesis, University of Edinburgh, 1990.

70 E.g. (**a**) R.W. Rudolph, R.L. Voorhees and R.E. Cochoy, *J. Am. Chem. Soc.*, 1970, **92**, 3351; (**b**) D.A.T. Young, G.R. Willey, M.F. Hawthorne M.R. Churchill and A.H. Reis, *J. Am. Chem. Soc.*, 1970, **92**, 6663; (**c**) K. Wong and R.N. Grimes, *Inorg. Chem.*, 1977, **16**, 2053;

71 E.g. D.C. Young, T.D. Andrews, D.V. Howe, R.L. Pilling, A.D. Pitts, M. Reintjes, L.F. Warren, P.A. Wegner and M.F. Hawthorne, *J. Am. Chem. Soc.*, 1968, **90**, 879.

72 G.K. Barker, M. Green, F.G.A. Stone, A.J. Welch, T.P. Onak and G. Siwapanyoyos, *J. Chem. Soc., Dalton Trans.*, 1979, 1687.

73 (**a**) L.G. Sneddon and R.N. Grimes, *J. Am. Chem. Soc.*, 1972, **94**, 7161; (**b**) L.G. Sneddon, D.C. Beer and R.N. Grimes, *J. Am. Chem. Soc.*, 1973, **95**, 6623.

74 M.R. Churchill, A.H. Reis, D.A.T. Young, G.R. Willey and M.F. Hawthorne, *J. Chem. Soc., Chem. Commun.*, 1971, 298.

75 D.A.T. Young, R.J. Wiersema and M.F. Hawthorne, *J. Am. Chem. Soc.*, 1971, **93**, 5687.

76 E.g. (**a**) L.I. Zakharkin, V.I. Bregadze and O.Y. Okhlobystin, *J. Organomet. Chem.*, 1965, **4**, 211; (**b**) A.Y. Aleksandrov, V.I. Brgadze, V.I. Gol'danskii, L.I. Zakharkin and O.Y. Okhlobystin, *Doklady Akad. Nauk SSSR.*, 1965, **165**, 593.

77 (**a**) S. Bresadola, P. Rigo and A. Turco, *J. Chem. Soc., Chem. Commun.*, 1968, 1205; (**b**) S. Bresadola, A. Frigo, B. Longato and G. Rigatti, *Inorg. Chem.*, 1973, **12**, 2788.

78 (a) N. Bresciani, M. Calligaris, P. Delise, G. Nardin and L. Randaccio, *J. Am. Chem. Soc.*, 1974, **96**, 5642; (b) N. Bresciani-Pahor, *Acta Cryst.*, 1977, **B33**, 3214.

79 (a) S. Bresadola, B. Longato and F. Morandini, *J. Organomet. Chem.*, 1977, **128**, C5; (b) S. Bresadola and N. Bresciani-Pahor, *J. Organomet. Chem.*, 1979, **179**, 73.

80 L.I. Zakharkin, A.I. Kovredov, M.G. Meiramov and A.V. Kazantsev, *Izv. Akad. Nauk. SSSR, Ser. Khim.*, 1977, 1673.

81 L.I. Zakharkin, L.V. Orlova and L.I. Denisovich, *Zh. Obshch. Khim.*, 1972, **42**, 2217.

82 E.g. (a) L.J. Todd, A.R. Burke, H.T. Silverstein, J.L. Little and G.S. Wilkholm, *J. Am. Chem. Soc.*, 1969, **91**, 3376; (b) Reference **14a**; (c) Reference **14b**.

83 E.g. (a) C.M. Mitchell and F.G.A. Stone, *J. Chem. Soc., Chem. Commun.*, 1970, 1263; (b) V.N. Kalinin, Y.T. Struchkov, A.T. Yanovskii, L.I. Zakharkin and O.M. Turlova, *Zh. Struct. Khim.*, 1981, **22**, 120; (c) S. Bresadola, "*Metal Interactions in Boron Clusters*," Ed. R.N. Grimes, Plenum Press, New York, 1982.

84 G.Z. Suleimanov, V.I. Bregadze, N.A. Koval'chuk and I.P. Beletskaya, *J. Organomet. Chem.*, 1982, **235**, C17.

85 B.D. Reid, Ph.D. Thesis, University of Edinburgh, 1992.

86 D.G. Evans and D.M.P. Mingos, *J. Organomet. Chem.*, 1982, **232**, 171.

87 B.D. Reid and A.J. Welch, *J. Organomet. Chem.*, 1992, **438**, 371.

88 V.N. Kalinin, Y.T. Struchkov, A.T. Yanovskii, L.I. Zakharkin and O.M. Turlova, *Zh. Struct. Khim.*, 1981, **22**, 120.

89 I.S. Savel'eva and L.I. Zakharkin, *Zh. Obshch. Khim.*, 1974, **44**, 1832.

90 K.F. Shaw, Ph.D. Thesis, University of Edinburgh, 1992.

91 H.D. Smith, *J. Am. Chem. Soc.*, 1965, **87**, 1817.

92 O. Crespo, M.C. Gimeno, P.G. Jones and A. Laguna, *J. Chem. Soc., Dalton Trans.*, 1992, 1601.

93 L.I. Zakharkin and G.G. Zhigareva, *Izv. Akad. Nauk SSSR, Ser. Khim.*, 1965, 932.

94 J. Casabo, C. Miravitlles, J. Ruis, F. Teixidor and C. Vinas, *Inorg. Chem.*, 1990, **29**, 149.

95 J.A. Long, T.B. Marder and M.F. Hawthorne, *J. Am. Chem. Soc.*, 1984, **106**, 3004.

96 (a) P.E. Behnken, J.A. Belmont, D.C. Busby, M.S. Delaney, R.E. King,

C.W. Kreimendahl, T.B. Marder, J.J. Wilczynski and M.F. Hawthorne, *J. Am. Chem. Soc.*, 1984, **106**, 3011; (**b**) P.E. Behnken, D.C. Busby, M.S. Delaney, R.E. King, C.W. Kreimendahl, T.B. Marder, J.J. Wilczynski and M.F. Hawthorne, *J. Am. Chem. Soc.*, 1984, **106**, 7444.

97 C.A. Tolman, *Chem. Rev.*, 1977, 313.

98 (**a**) J.A. Doi, R.G. Teller and M.F. Hawthorne, *J. Chem. Soc., Chem. Commun.*, 1980, 80; (**b**) C.W. Jung and M.F. Hawthorne, *J. Am. Chem. Soc.*, 1980, **102**, 3024.

99 J. Cowie, Ph.D. Thesis, University of Edinburgh, 1996.

100 K.J. Adams, J. Cowie, S.G.D. Henderson, G.J. McCormick and A.J. Welch, *J. Organomet. Chem.*, 1994, **481**, C9.

101 D.R. Baghurst, R.B. Copley, H. Fleischer, G.O. Kyd, D.M.P. Mingos, D. O'Connell, T.R. Spalding, L.J. Yellowlees and A.J. Welch, *J. Organomet. Chem.*, 1993, **447**, C14.

102 T.D. McGrath, Ph.D. Thesis, University of Edinburgh, 1995.

103 G.O. Kyd, Ph.D. Thesis, University of Edinburgh, 1994.

104 (**a**) Z.G. Lewis and A.J. Welch, *J. Organomet. Chem.*, 1992, **430**, C45; (**b**) P.T. Brain, M.Bühl, J. Cowie, Z.G. Lewis and A.J. Welch, *J. Chem. Soc., Dalton Trans.*, 1996, 231; (**c**) Reference **22**; (**d**) A.S. Weller and A.J. Welch, *Inorg. Chem.*, In Press.

105 Z.G. Lewis, *Acta Cryst.*, 1993, **C49**, 705.

Chapter 2

Carbaboranes with σ-Bonded Planar Substituents

2.1 Introduction

1-Ph-1,2-*closo*-$C_2B_{10}H_{11}$ (mono-phenylcarbaborane) was one of the first C-substituted analogues of 1,2-*closo*-$C_2B_{10}H_{12}$ (*ortho*-carborane), reported more than thirty years ago.[1] Ostensibly it is the fusion of a phenyl group and a carbaborane C_2B_{10} cage, with the former attached to one of the cage carbon atoms by a single, two-centre, two-electron bond. It is synthesised, in relatively low yield, by the extended heating to reflux of decaborane ($B_{10}H_{14}$) and mono-phenylacetylene (PhC_2H) in toluene in the presence of two equivalents of a Lewis base, L (L = SMe_2, CH_3CN). The Lewis base forms an adduct with decaborane to afford $B_{10}H_{12}L_2$ ($B_{10}H_{14}$, a *nido* fragment of an eleven-vertex, *closo* borane, has two of its bridging, facial hydrogen atoms (each a one-electron donor) substituted by two molecules of Lewis base (two-electron donors), which adopt positions *exo*s to the cluster, with rearrangement of the two remaining facial hydrogen atoms).[2] The adduct now has two more cluster electrons than *nido*-$B_{10}H_{14}$, but still has the same number of vertices and hence, as predicted by PSEP theory,[3] adopts the more open *arachno* geometry, which is characterised by the white/yellow to orange colour change. The acetylene now inserts into the cage framework, with loss of the two molecules of Lewis base and two further bridging hydrogen atoms, to afford the twelve-vertex, *closo* carbaborane in a similar manner to that described for *ortho*-carborane (**Section 1.3.2**).

The other cage carbon bears a hydrogen atom, which is relatively acidic due to carbon being more electronegative than boron. In a suitable solvent, such as Et_2O or thf, this proton can be easily removed by strong bases such as $[Me]^-$ (in MeLi) to afford the mono-anionic lithium salt, which can then be reacted further with a suitable electrophile to produce di-substituted carbaboranes, both substituents being attached to the cage by σ-bonds.[4] This deprotonation reaction works for all mono-substituted, *closo* carbaboranes and, unlike for 1,2-*closo*-$C_2B_{10}H_{12}$ (in Et_2O), it is not possible for an equilibrium between the desired mono-deprotonated species and fully protonated and fully deprotonated forms to become established[5]

As described previously in **Section 1.5**, co-workers from this group have recently shown that when carbametallaboranes become sufficiently crowded, they relieve local steric congestion in one of three ways: **vertex extrusion** of metal-ligand fragment to a position *exo* to the cage, **polyhedral deformation** by the breaking of cage connectivities and **polyhedral isomerisation**, where the cage undergoes a sudden and facile rearrangement of the cage carbon atoms. This latter example can afford rearrangement products which cannot be produced by simple diamond-square-diamond processes.[6] Welch *et al* have synthesised a series of di-substituted carbaboranes, for which both of the cage carbon substituents are sterically demanding.[7] The C(1) substituent is a phenyl ring, with the substituent on C(2) varying from a relatively small group such as Me to the very sterically demanding Si^{t}BuMe$_2$ group and beyond. This approach, whereby the steric requirements of the system are gradually increased to a point where isomerisation occurs, provided that there are a sufficient number of crystallographically determined structures, could give an indication of the mechanism of isomerisation by analysis of the geometries of the most sterically crowded, but, as yet, non-isomerised, compounds.

Although mono-phenylcarbaborane has been known for many years, there has never been an X-ray diffraction study undertaken. Such a study would provide an origin for this deformation continuum and allow comparison of structural parameters (e.g. the lengths of the C(1)-C(11) bond and the C(1)-C(2) connectivity and the twist and possible back-bend of the phenyl ring) in the mono-substituted and di-substituted carbaboranes.

Previous reports have indicated that there is a preferred conformation of the phenyl ring in mono-phenylcarbaborane.[8] EHMO calculations showed that the minimum energy conformation is when the phenyl ring is orientated with a θ value of 90° (θ is defined as the modulus of the average of the C(2)-C(1)-C(11)-C(12) and C(2)-C(1)-C(11)-C(16) torsion angles; i.e. for θ = 90°, the phenyl ring and two cage carbon atoms are coplanar; for θ = 0°, the ring is twisted about C(1)-C(11) such that C(2) is the furthest distance from it). Moreover, these calculations also showed that both the C(1)-C(11) and C(1)-C(2) interactions were strongest at θ = 90° (**Fig. 2.1**). Furthermore, the C(1)-C(2) overlap is stronger at θ = 90° (and weaker at θ = 0°) than the C(1)-C(2) overlap in *o*-$C_2B_{10}H_{12}$.

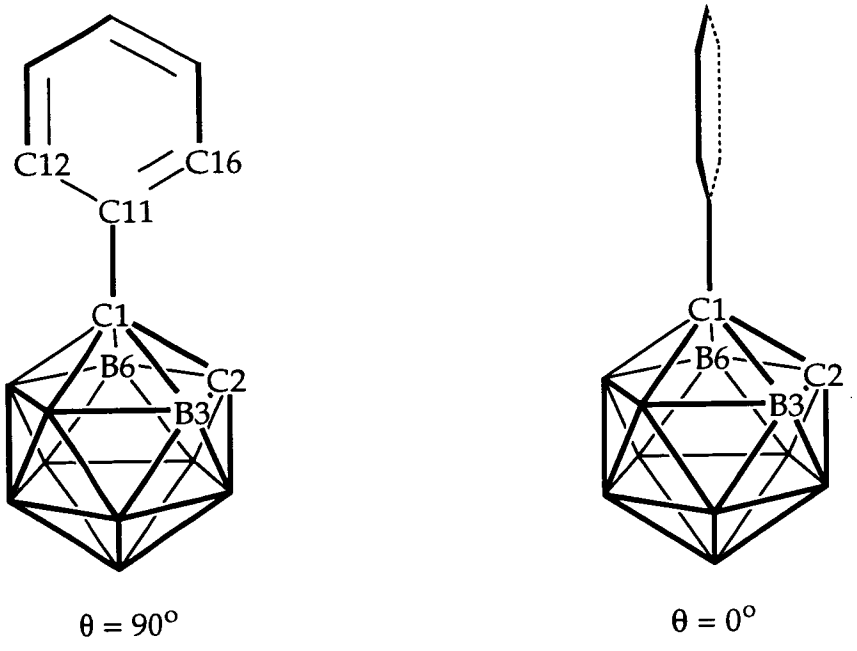

Figure 2.1 Conformations of Mono-phenylcarbaborane (θ = 90 and 0°)

These results imply that there is some degree of conjugation between the cage and the phenyl ring and that this, perhaps, is responsible for the preferred orientation of the phenyl ring that has been calculated. Undertaking the X-ray diffraction study of mono-phenylcarbaborane would allow comparison of this calculated preferred orientation with the exerimentally observed orientation (a recent electron diffraction experiment[9] to ascertain the gas-phase structure could not differentiate between the unsubstituted C(2) carbon atom and the four boron atoms adjacent to C(1)).

Carboxylic acid derivatives of carbaboranes have been known since 1963,[10] when they were synthesised by bubbling CO_2 through an ethereal solution of the appropriate carbaborane lithium salt, followed by acid hydrolysis. These compounds may be reacted with base, which removes the carboxylic acid proton to form the corresponding carboxylate species.[11] Since the carboxylate functionality, with its extended π-system, can be thought of as a gross approximation to the first three carbon atoms of a phenyl ring, it is likely that the $[CO_2]^-$ moiety will also have a preferred orientation with respect to the cage. This could be investigated by EHMO calculations and compared with solid-state structures from X-ray diffraction studies.

Although there are several examples of both class 1 and class 2 carbagallaboranes reported in the literature,[12] there have been no class 3 species reported. It would be interesting, therefore, to synthesise such compounds and determine the orientation of the $\{GaR_2\}$ fragment with respect to the cage, since this fragment is isoelectronic with $[CH_2]^+$ (as opposed to $[CO_2]^-$, which is effectively isoelectronic with $[CH_2]^-$).

This chapter describes the preparation and modified, higher-yield work-up, of 1-Ph-1,2-*closo*-$C_2B_{10}H_{11}$, **1**, (**Section 2.2**). The results of $^{11}B\{^1H\}/^{11}B\{^1H\}$ (COSY), $^1H\{^{11}B\}$, $^1H\{^{11}B_{selective}\}$ and $^1H\{^{11}B\}/^1H\{^{11}B\}$ (COSY) experiments are reported, and the full assignment of its $^{11}B\{^1H\}$ nmr spectrum explained and compared with the nmr spectrum calculated by IGLO methods. The results of an $^{11}B\{^1H\}/^{11}B\{^1H\}$ (TOCSY; **TO**tal Correlation Spectroscop**Y**) experiment are also reported and discussed. A low-temperature crystallographic study of 1-Ph-1,2-*closo*-$C_2B_{10}H_{11}$, is also reported and the results compared to those from EHMO and high level, *'ab initio'* calculations. **Section 2.4** reports EHMO calculations on the [1-CO_2-1,2-*closo*-$C_2B_{10}H_{11}$]$^-$, [1-CH_2-1,2-*closo*-$C_2B_{10}H_{11}$]$^+$ and [1-CH_2-1,2-*closo*-$C_2B_{10}H_{11}$]$^-$ ions, which were performed in order to determine the preferred conformations of the pendant groups. The results of the first calculation are compared with those of a crystallographic study of [HNEtMe_2][1-CO_2-1,2-*closo*-$C_2B_{10}H_{11}$], **2b**. The X-ray diffraction studies of two further carboxylate compounds [$HNEt_3$][1-CO_2-2-R-1,2-*closo*-$C_2B_{10}H_{10}$] (R = Me, **3a**, CH_2OCH_3, **4a**) are also reported and discussed. The ^1H and $^{11}B\{^1H\}$ nmr spectra of these species are also reported, as are those of the carbaborane carboxylic acids from which they are derived, 1-R-2-CO_2H-1,2-*closo*-$C_2B_{10}H_{10}$; R =H, **2**, CH_3, **3**, CH_2OCH_3, **4**, (**Section 2.3**). The synthesis and characterisation of the first σ-bonded carbagallaborane, 1-CH_2OCH_3-2-{Me_2Ga}-1,2-*closo*-$C_2B_{10}H_{10}$, **5**, is reported and discussed (**Section 2.5**). Finally, the conclusions for this chapter are presented (**Section 2.6**).

2.2 1-Ph-1,2-*closo*-$C_2B_{10}H_{11}$ (1)

2.2.1 Preparation of 1

The title compound was prepared in high yield (62.5%) according to the method of Reid[13] by the extended heating to reflux of $B_{10}H_{14}$ and PhC_2H with 0.1 equivalents of CH_3CN in toluene for 72 hours. The improvement in yield (previous syntheses gave maximum yields of 55%) was due to a more careful recrystallisation step from methanol/water.

Upon overlaying the methanolic solution on the water, a significant proportion of the product immediately precipitates as a very fine 'milk' (mono-phenylcarbaborane is highly insoluble in water). Since this precipitate is extremely fine, it is lost when the crystals are filtered off. The formation of this milk was almost completely avoided, as well as affording purer product, by using the following method: (**1**) The methanol solution was made as dilute as possible to slow the rate of crystallisation; (**2**) The water layer was overlayed with a thin layer of methanol, before addition of the methanolic solution. This means that when the solution of **1** is added, it does not come into immediate contact with a solvent in which it is totally insoluble. This method also applies to recrystallisation of other parent carbaboranes. The crystals obtained were then dissolved in Et_2O and stirred over $MgSO_4$ for 18 hours. After filtration, the filtrate was reduced *in vacuo* to afford the product as a dry, white solid. This last step was introduced to remove any residual water would have reacted preferentially with the alkyl lithium reagents used to remove the acidic C_{cage} proton (**Section 5.2.5**).

Colourless, diffraction quality *blocks* were grown by the slow cooling to room temperature of a hot-filtered, ethanolic solution. The solution was insulated in a sealed boiling tube, which was suspended in a Thermos flask of boiling water.

2.2.2 Characterisation of 1

The compound was initially characterised by IR spectroscopy. There was a broad band at 2595 cm^{-1} due to B-H_{exo} stretches. Microanalysis figures for the recrystallised needles were in excellent accordance with the calculated values.

In the ^1H nmr spectrum of 1-Ph-1,2-*closo*-$C_2B_{10}H_{11}$, the phenyl protons resonate between 7.58 and 7.38 ppm, appearing as a doublet (*ortho*-protons), doublet of doublets (*meta*) and a triplet (*para*) in the ratio 2:2:1, indicating that the phenyl ring is either rotating rapidly on the nmr time-scale or has a static conformation of $\theta = 0^o$, i.e. the *ortho* protons are magnetically equivalent to each other (as are the *meta* protons to each other), since there is a mirror plane through the phenyl ring. The C_{cage} hydrogen atom, C(2)-H, resonates at 3.97 ppm and occurs as a broad singlet, typical of such protons in mono-substituted carbaboranes.[14]

The $^{11}B-\{^1H\}$ nmr spectrum (**Fig. 2.2**) indicates that mono-phenylcarbaborane has C_s (mirror) symmetry on the nmr timescale. Thus, the boron environments comprise 2 unique boron atoms, B(9) and B(12), which lie on the mirror plane and four pairs of equivalent boron atoms, B(3,6), B(4,5), B(7,11) and B(8,10), which are related to each other by reflection in the mirror plane (where the mirror plane is defined as bisecting C(1), C(2), B(9) and B(12). The shielding pattern from low- to high-field shows resonances occuring at -1.19, -3.49, -8.06, -9.88, -10.32 and -11.85 ppm, respectively, with relative integrals in the ratio 1:1:2:2:2:2. Each resonance in the ^{11}B nmr spectrum is split by the associated *exo* proton ($^1J_{B\text{-}Hexo}$ = 148-170 Hz) to give a doublet. This shielding pattern, i.e. the two integral-one boron resonances occuring at highest frequency, is typical of mono-substituted, *closo* carbaboranes. The B(9) and B(12) resonances occur at higher frequency relative to other resonances due to their position in the cage, opposite the more electronegative cage carbon atoms.

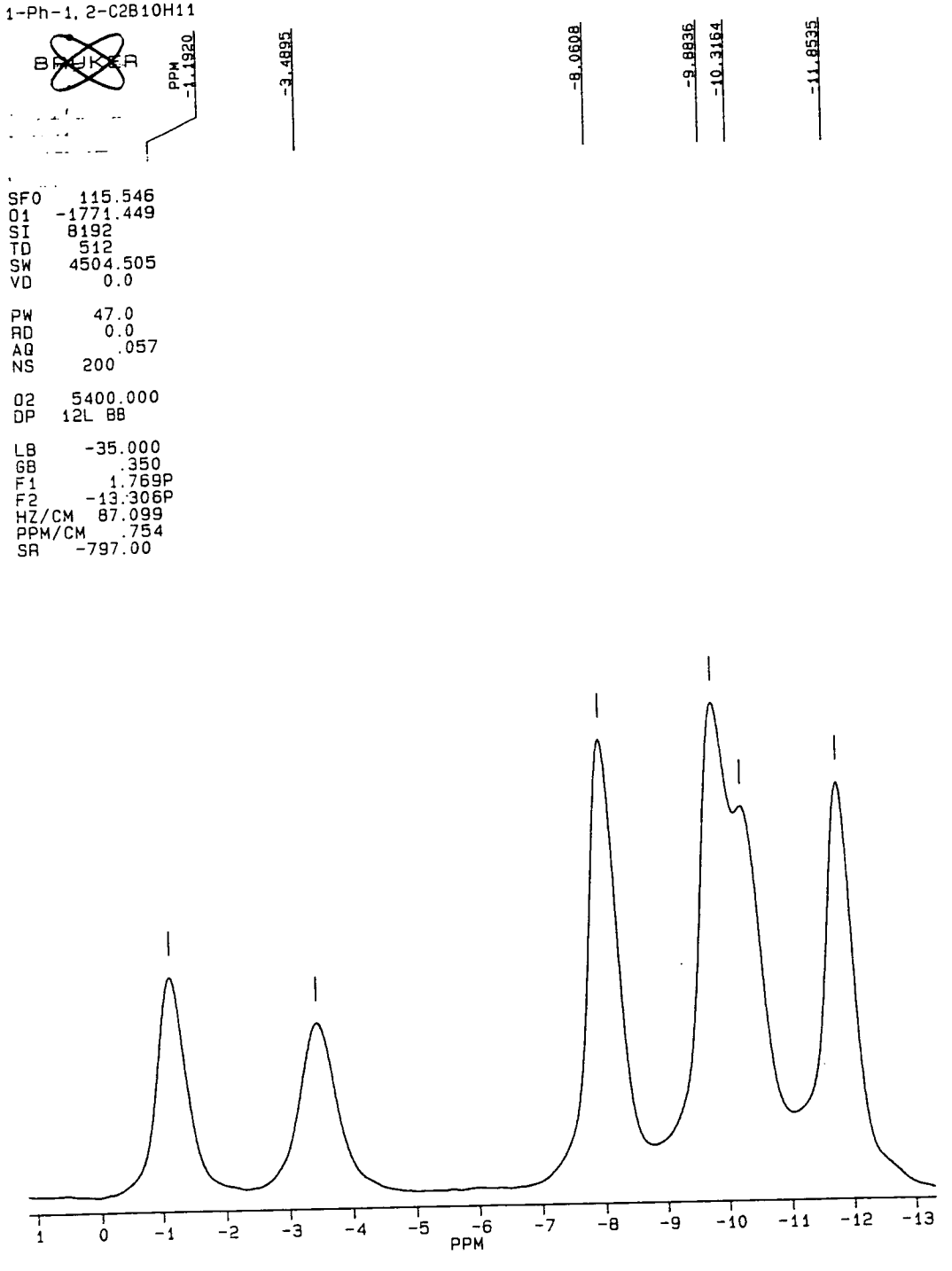

Figure 2.2 ^{11}B-{^{1}H} Nmr Spectrum of **1** (192.6 MHz)

The boron resonances in the ^{11}B-{^{1}H} nmr spectrum of **1** were fully assigned by a series of ^{11}B-{^{1}H}/^{11}B-{^{1}H} (COSY), ^{1}H-{^{11}B}, ^{1}H-{$^{11}B_{selective}$} and ^{1}H-{^{11}B}/^{1}H-{^{11}B} (COSY) experiments. Partial assignment was made initially on the basis of the ^{11}B-{^{1}H}/^{11}B-{^{1}H} (COSY) spectrum (**Fig. 2.3**). The two high frequency resonances, both of relative integral one, are accorded to B(9) and B(12), as these are the two unique boron atoms. It can be seen that there is only one resonance which couples to all other resonances (in COSY, there are only correlations (cross-peaks) between adjacent boron nuclei).[15] Hence, this resonance, which occurs at -8.06 ppm is due to B(8,10) as this is the only boron pair adjacent to all other boron atoms. The resonance at -10.32 ppm can be assigned to B(3,6) as there are no cross-peaks between it and the two integral-one resonances (due to B(9) and B(12)). The remaining assignments are still ambiguous.

The ^{1}H-{^{11}B} spectrum (**Fig. 2.4**) shows five resonances in the B-H_{exo} region, with relative integrals, from low- to high-field, in the ratio 2:3:1:2:2 (the resonance of relative integral-three being a 2+1 coincidence). A ^{1}H-{$^{11}B_{selective}$} experiment enhanced the following proton resonances (ppm): 2.46 (from decoupling of the ^{11}B resonance at -1.19 (ppm)), 2.35 (-3.49), 2.35 (-8.06), 2.35 (-9.88), 2.62 (-10.32), 2.30 (-11.85). Hence the H_{exo} protons bonded to B(3,6) and B(8,10) resonate at 2.62 and 2.35 ppm, respectively.

Full assignment was accomplished by analysis of the ^{1}H-{^{11}B}/^{1}H-{^{11}B} (COSY) spectrum (**Fig. 2.5**). The C(2)-proton couples to two other resonances; that at 2.62 ppm, due to H(3,6), and at 2.30 ppm, which must be due to H(7,11). From the previous ^{1}H-{$^{11}B_{selective}$} experiment, one can assign B(7,11) to the resonance at -11.85 ppm. All other ^{11}B and ^{1}H resonances can now be assigned. In the ^{11}B-{^{1}H}/^{11}B-{^{1}H} (COSY) spectrum, the resonance at -11.85 ppm couples to a single integral-one resonance. This resonance occurs at -3.49 ppm, and must be due to B(12). Consequently, the other integral-one resonance at -1.19 ppm is assigned to B(9). The remaining resonance, which occurs at -9.88 ppm, is assigned to B(4,5) by elimination. Moreover, as one would expect, in the ^{11}B-{^{1}H}/^{11}B-{^{1}H} (COSY) spectrum, there are cross peaks between B(4,5) and B(3,6), B(8,10) and B(9).

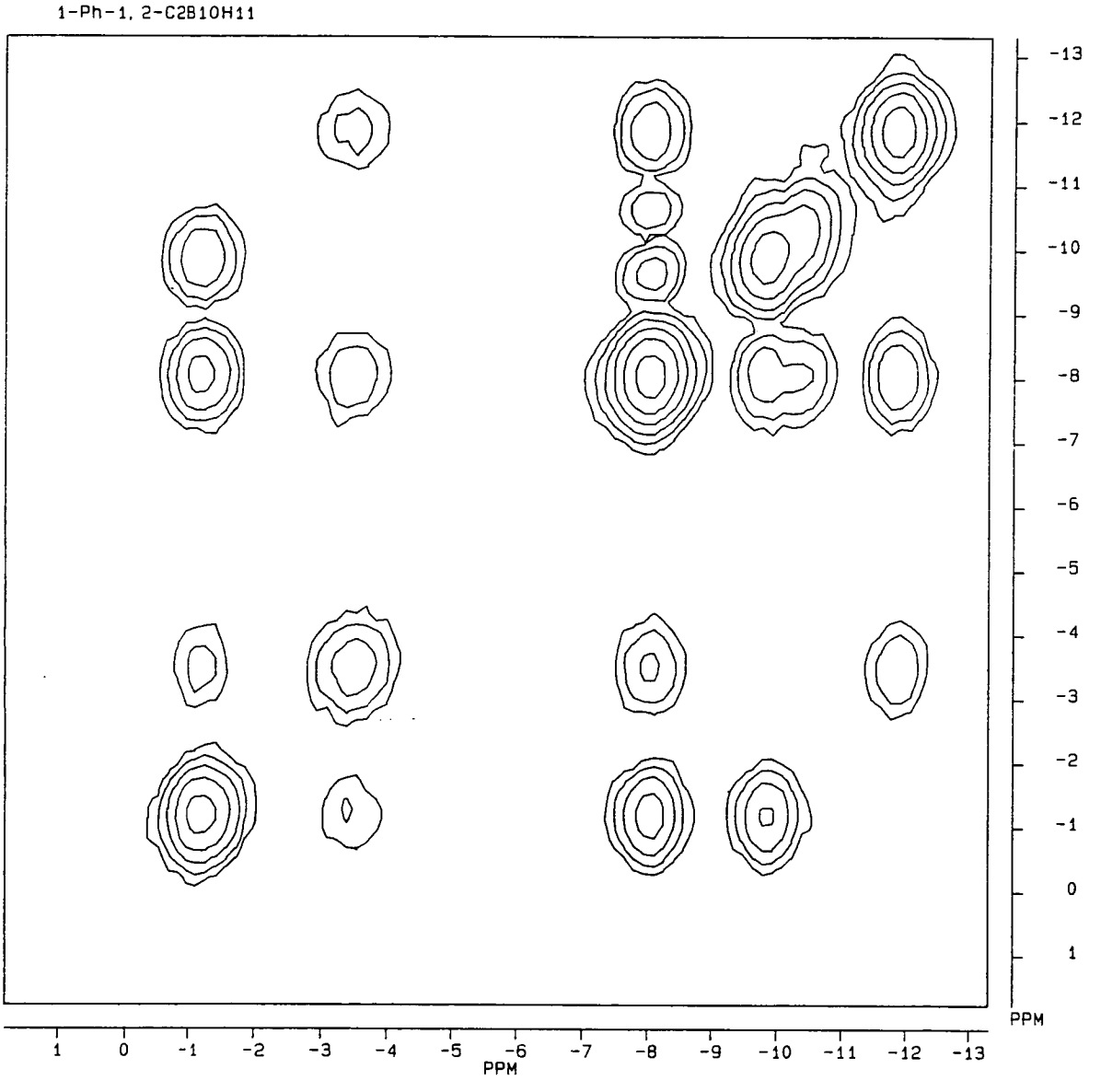

Figure 2.3 ^{11}B-{^{1}H}/^{11}B-{^{1}H} (COSY) Nmr Spectrum of **1** (192.6 MHz)

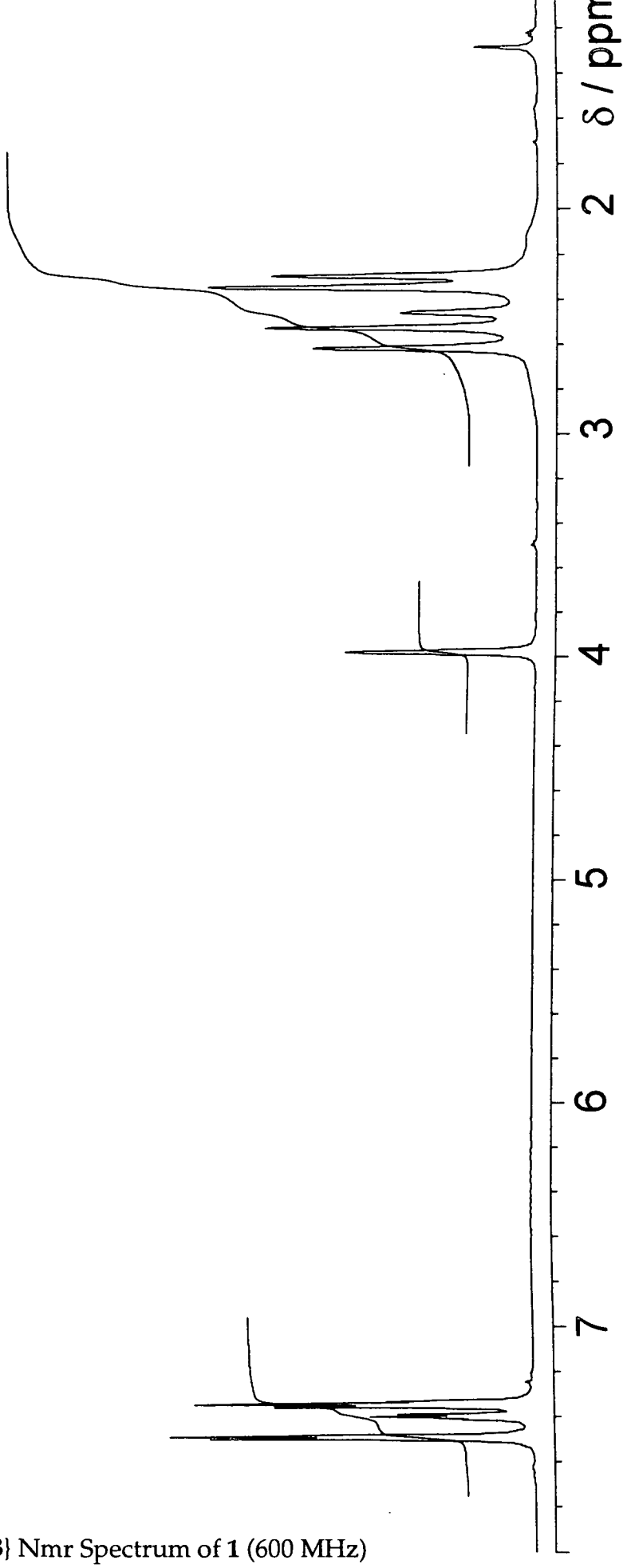

Figure 2.4 ^{1}H-{^{11}B} Nmr Spectrum of **1** (600 MHz)

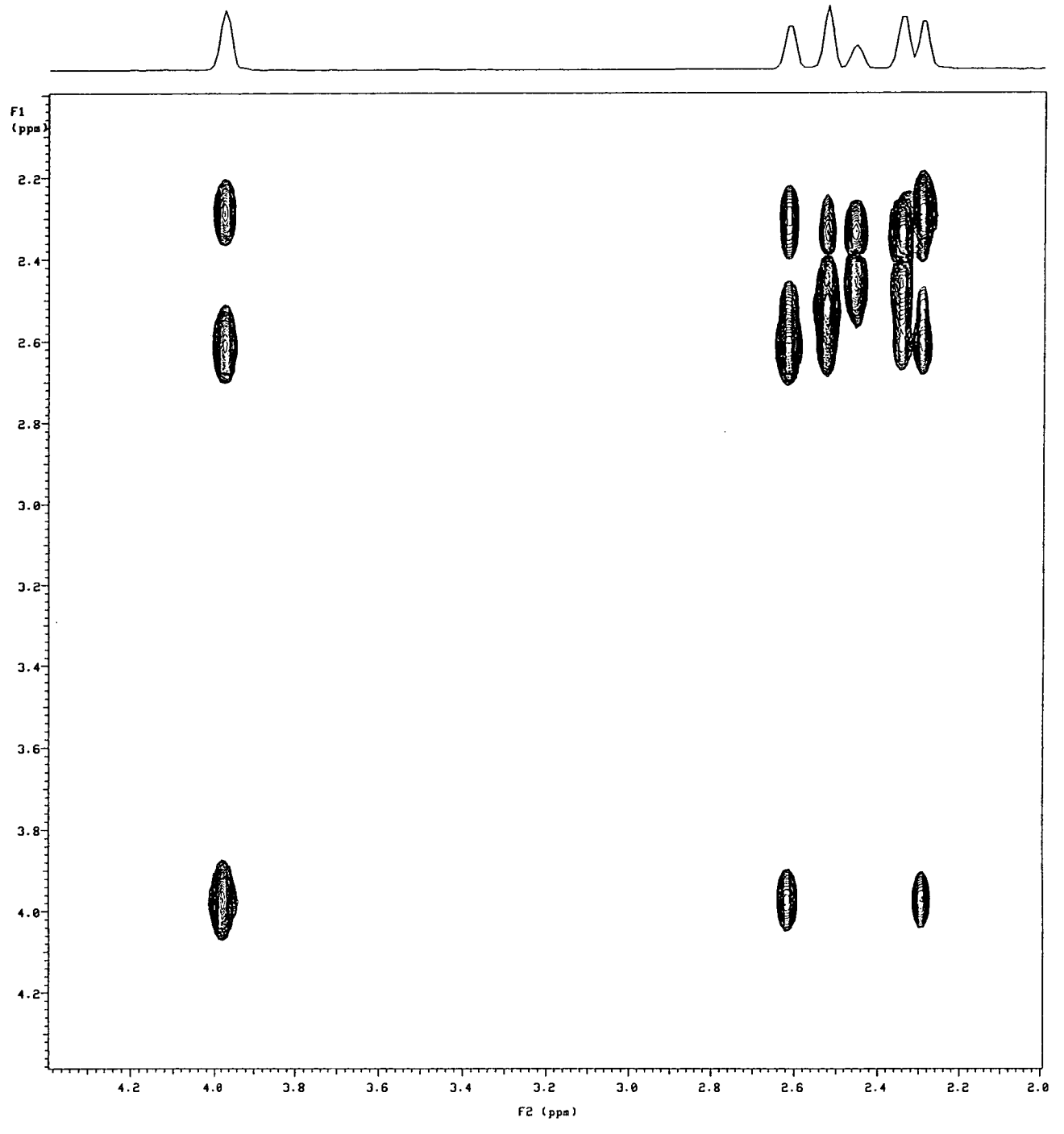

Figure 2.5 $^{1}H\{^{11}B\}/^{1}H\{^{11}B\}$ (COSY) Nmr Spectrum of **1** (600 MHz)

The H_{exo} resonances can also be fully assigned by referring back to the $^1H\{^{11}B_{selective}\}$ experiment. All $^{11}B\{^1H\}$ and ^1H resonances are summarised in **Table 2.1**. The $^{11}B\{^1H\}$ nmr shielding pattern and shifts are extremely close to those recently reported for 1-CH_2OCH_3-1,2-*closo*-$C_2B_{10}H_{11}$.[14a]

Table 2.1 Assignment of the ^1H and ^{11}B Nmr Chemical Shifts in **1**

Position	δ (^1H)/(ppm)	δ (^{11}B)/(ppm)
9	2.46	-1.19
12	2.35	-3.49
8, 10	2.35	-8.06
4, 5	2.53	-9.88
3, 6	2.62	-10.32
7, 11	2.30	-11.85

Table 2.2 ^{11}B Nmr Chemical Shifts of 1,2-*closo*-$C_2B_{10}H_{12}$, 1-Ph-1,2-*closo*-$C_2B_{10}H_{11}$ and 1,2-Ph_2-1,2-*closo*-$C_2B_{10}H_{10}$

	δ (^{11}B) Shifts of 1-R-2-R′-1,2-*closo*-$C_2B_{10}H_{10}$ /(ppm)		
Position	**R′ = R = H**	**R′ = H; R = Ph**	**R′ = R = Ph**
9	-1.78	-1.19	-1.72
12	-1.78	-3.49	-1.72
8, 10	-8.59	-8.06	-8.41
4, 5	-12.99	-9.88	-8.41
3, 6	-14.10	-10.32	-9.71
7, 11	-12.99	-11.85	-9.90
mean δ	**-10.08**	**-8.49**	**-6.83**

Comparison of the $^{11}B\{^1H\}$ shifts with those of 1,2-*closo*-$C_2B_{10}H_{12}$[14a] and 1,2-Ph_2-1,2-*closo*-$C_2B_{10}H_{10}$[16] (**Table 2.2**) shows the ^{11}B nuclei becoming increasingly deshielded as the number of phenyl rings increase from zero to two. As electron density is removed from the C_2B_{10} cage, one would expect them to become easier to deboronate as the B(3,6) atoms become more δ+ (as evinced by a shift to higher frequency) and hence more prone to nucleophilic attack. This, however, is not the case, since the steric bulk of the phenyl rings, which hinder attack, and thus deboronation, far outweigh their positive, electronic effect (**Section 4.2.1**). Substitution of one of the C_{cage} protons of 1,2-*closo*-$C_2B_{10}H_{12}$ by a phenyl ring also causes deshielding of the remaining

C_{cage} proton. In 1,2-*closo*-$C_2B_{10}H_{12}$, the C_{cage} protons resonate at 3.55 ppm, compared to 3.97 ppm in compound **1**.

As alluded to earlier, COSY experiments only show cross-peaks between adjacent boron nuclei. Moreover, one does not always observe the predicted number of cross-peaks[17] (although not in this case). TOCSY has already been widely used in ^1H nmr analyses, particularly in the study of polypeptides and proteins,[18] and is designed to show cross-peaks linking **all** members of a given spin system. Extension of this to ^{11}B nuclei should afford cross-peaks between all ^{11}B-{^1H} resonances within a (hetero)borane cluster.

The TOCSY experiment was carried out (experimental details are reported in greater depth elsewhere)[19] and the spectrum obtained shown below (**Fig. 2.6**).

As predicted, there are cross-peaks between all of the boron resonances. This is in contrast to the COSY experiment, where cross-peaks occur only between resonances due to **adjacent** nuclei. Moreover, the cross-peaks in the TOCSY spectrum are much more compact than those of the corresponding COSY. This is the main advantage of TOCSY over COSY techniques for single-spin systems, especially in cases where the resonances are poorly resolved. For species which contain two or more spin systems, however, another advantage of TOCSY is that it may be possible to differentiate which ^{11}B-{^1H} resonance arises from which spin system. One such example of this type of compound is 1-Ph-3,3-$(CO)_2$-3-(1′-Ph-2′-PPh_2-1,2-*closo*-$C_2B_{10}H_{10}$)-3,1,2-*closo*-$RuC_2B_9H_{10}$,[20] synthesised by Smit (**Fig. 2.7**).

Several IGLO ^{11}B chemical shift calculations have been performed[9] for a variety of optimised structures of mono-phenylcarbaborane, the main difference being the orientation of the phenyl ring relative to the cage, i.e. θ. The calculated shifts are in close accordance for both the DZ and II'' basis sets when employing the GED model. The ^{11}B shifts of the boron atoms antipodal to the cage carbon atoms, B(9) and B(12), were slightly overestimated.

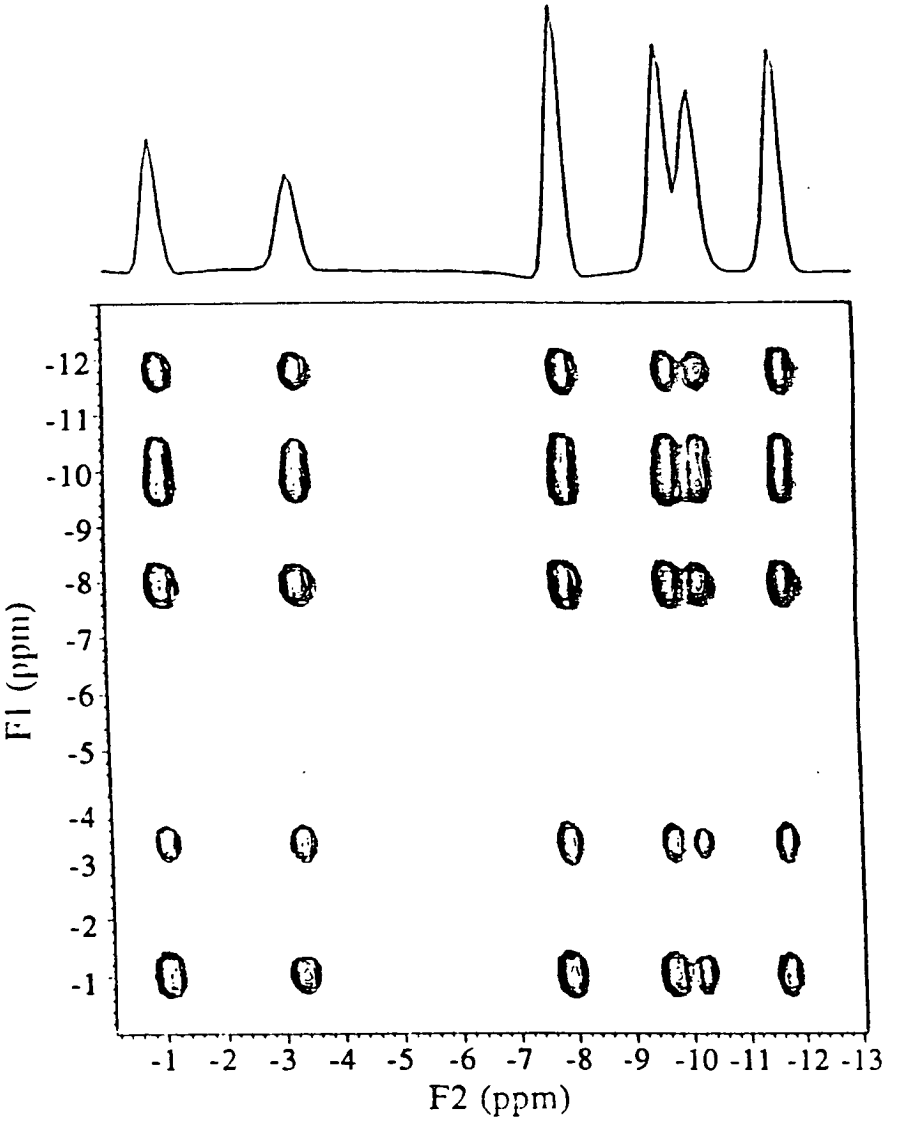

Figure 2.6 ^{11}B-{^{1}H}/^{11}B-{^{1}H} (TOCSY) Nmr Spectrum of **1** (192.6 MHz)

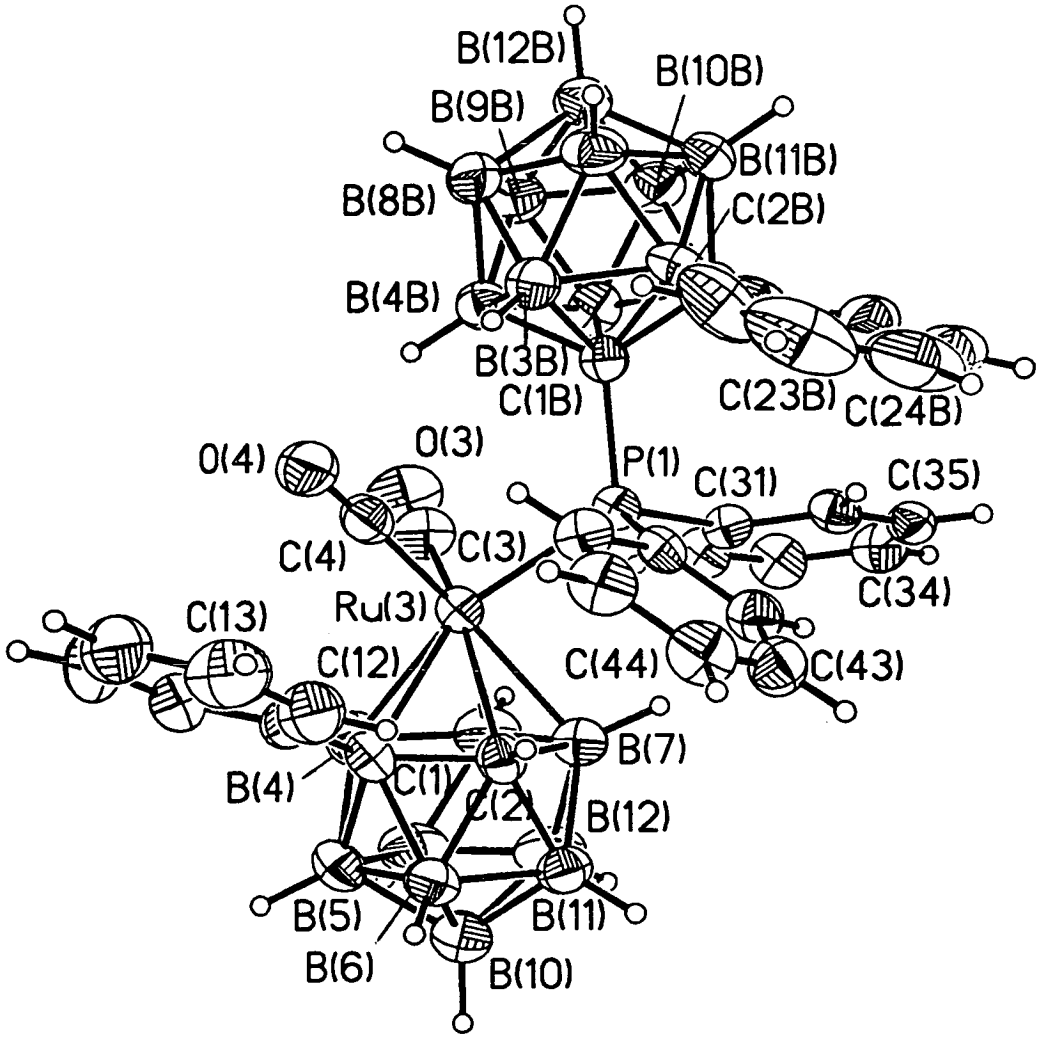

Figure 2.7 Perspective View of 1-Ph-3,3-$(CO)_2$-3-(1′-Ph-2′-PPh_2-1,2-*closo*-$C_2B_{10}H_{10}$)-3,1,2-*closo*-$RuC_2B_9H_{10}$

2.2.3 Crystallographic Study of 1

Colourless, diffraction quality *blocks* of **1** were afforded by the very slow cooling to room temperature of a warm, concentrated, ethanolic solution. Intensity data were measured on an Enraf-Nonius CAD4 diffractometer operating with Mo-K_α *X*-radiation (λ_{bar} = 0.71073 Å). The single crystal was placed in a glass capillary, which was held in a stream of nitrogen gas at 199(2) K.

Crystal data

$C_8H_{16}B_{10}$, M = 220.23, monoclinic, $P2_1/a$, a = 12.047(3) Å, b = 18.627(4) Å, c = 12.332(5) Å, β = 110.09(4)°, V = 2595.3(14) Å^3, from least squares refinement of 25 reflections ($8 \leq \theta \leq 11°$) at 199(2) K, Z = 8 (2 independent molecules), D_c = 1.128 gcm^{-3}, μ(Mo-K_α) = 0.05 mm^{-1}, F(0,0,0) = 912e.

Data collection and reduction

Intensity data collected in the range $2<2\theta<50°$ by the ω-2θ scan method; ω-scan width (0.8+0.34tanθ), ω-scan speeds in the range 0.235 to 0.782°min^{-1}. The intensities of 4572 unique reflections (h -14 to 14, k 0 to 22, l 0 to 14) were measured (DATCOL).

Structure solution and refinement

The structure was solved using direct methods (SHELX86) and developed by iterative, full-matrix least-squares refinement and difference Fourier syntheses (SHELXTL). The asymmetric fraction of the unit cell contains two crystallographically independent molecules. In molecule A, the C(2A) carbon atom was disordered over the five cage atoms adjacent to C(1A) and could not be identified. Consequently, these atoms were refined as boron atoms in subsequent ΔF syntheses and given a site occupancy of 1.04.

The C(2B) atom was, however, identifiable. The five cage atoms adjacent to C(1B) were initially refined as boron atoms. Analysis of the results of this refinement allowed the assignment of the C(2B) atom as the atom with the smallest U_{ij} value and the shortest C(1B)-B/C connectivity. Consequently, the discussion of the molecular structure of compound **1** will

be limited to molecule B. Phenyl rings were treated as planar hexagons (C-C = 1.39 Å), with phenyl protons set in idealised positions (C-H = 0.93 Å). Cage-H atoms were set 1.10 Å from C or B on a radial extension from the centre of the icosahedron. All hydrogens were given isotropic displacement parameters riding at 1.2 times the equivalent isotropic parameter of their attached atom. In the final stages of refinement, all non-H atoms were refined anisotropically. Data were weighted such that $w^{-1} = [\sigma^2(F_o^2) + (0.1189P)^2 + 1.05P]$ where $P = [\text{max. } (F_o^2 \text{ or } 0) + 2F_c^2]/3$. Using 2592 observed data, R = 0.0831 and S = 1.073 for 301 variable parameters. The maximum residue and minimum trough in a final Fourier synthesis were 0.34 and -0.26 $eÅ^{-3}$, respectively. Atomic scattering factors were those inlaid in SHELXTL. Selected bond lengths (Å) and angles (°), fractional coordinates and equivalent isotropic thermal parameters of non-hydrogen atoms are in **Tables 1A** and **1B**, respectively.

As described above, there are two crystallographically independent molecules of **1** (molecules A and B) in the asymmetric fraction of the unit cell, and these are shown in **Figures 2.8a** and **2.8b** (in this Thesis, non-hydrogen atoms are shown with 30% thermal ellipsoids, with H atoms given an artificial radius of 0.1 Å for clarity). There are no significant contacts between molecules. The two most pertinent parameters, θ and the C(1B)-C(2B) distance, were measured as 67.7(3)° and 1.640(5) Å, respectively and compare well with a recent X-ray crystallographic study of a second polymorph of 1-Ph-1,2-*closo*-$C_2B_{10}H_{11}$ (θ = 71.2(2)°, C(1)-C(2) = 1.649(2) Å).[21] As for all other structural determinations of carbaboranes, the C(1B)-B connectivities, which are in the range 1.705(5) to 1.743(5) Å, are longer than C(1B)-C(2B) (1.640(5) Å). The B-B connectivities are longer still, between 1.756(6) and 1.795(6) Å.

These experimental values also compare well with the values afforded by *ab initio* calculations. The C(1)-C(2) distance and θ were calculated as being 1.627(8) Å and 65°, respectively (the molecule was modelled with C_1 symmetry at the HF/6-31G* level). A unique solution could not be gained from the electron diffraction data, due principally to the low energy barrier to rotation (calculated as being 2.1 $kJmol^{-1}$ at the HF/6-31G* level). Models were adopted where the molecules had either C_s or C_1 symmetry. The refinement, for which the molecule had C_s symmetry, gave a better fit of the data at θ = 90° than at θ = 0°, but the optimum refinement was achieved with

the molecule modelled as having C_1 symmetry ($\theta = 54^o$). This more complex model was simplified by giving the C_2B_{10} cage and hexagonal C_6 rings local C_{2v} and D_{6h} symmetry, respectively. The EHMO calculations are in relatively poor agreement with this result, due mainly to the molecule being poorly modelled (C-C = C-B = B-B) and with no account being taken of any possible steric interactions between C(2)-H and the *ortho*-H atoms of the phenyl ring.

As expected, the value of θ is far greater and the C(1)-C(2) distance shorter than for other reported derivatives of the type 1-Ph-2-X-1,2-*closo*-$C_2B_{10}H_{10}$ (X = Me[22] ($\theta = 16.7^o$, C(1)-C(2) = 1.696(5) Å), Br[7a] (2.2°, 1.692(8) Å), $SiMe_3$[23] (7.6°, 1.742(5) Å)), since the C(2) substituent in **1** (a hydrogen atom) is much smaller than either of those given above. The C(1B)-C(11B) bond length is 1.503(4) Å, similar to other C_{cage}-C_{Ph} distances in di-substitued, *closo* carbaboranes. The phenyl ring is not able to adopt the conformation with $\theta = 90^o$ due to steric interaction between C(2)-H and the *ortho*-H atoms of the phenyl ring, as alluded to earlier. This interaction can be clearly seen in the space filling diagram below in **Figure 2.9** (Atoms in the space-filling diagram have been given the following van der Waal's radii; C (non-aryl) - 1.70 Å, C (aryl) - 1.85 Å, B - 1.70 Å, H - 1.20 Å[24]).

The shortest distances between the cage-H atoms and phenyl *ortho*-H atoms H(2B)···H(16B) and H(12B)···H(6B) are 2.21 and 2.30 Å, respectively. This is consistent with what one would expect, i.e. the phenyl ring is trying to adopt a conformation as close to $\theta = 90^o$ as is sterically possible.

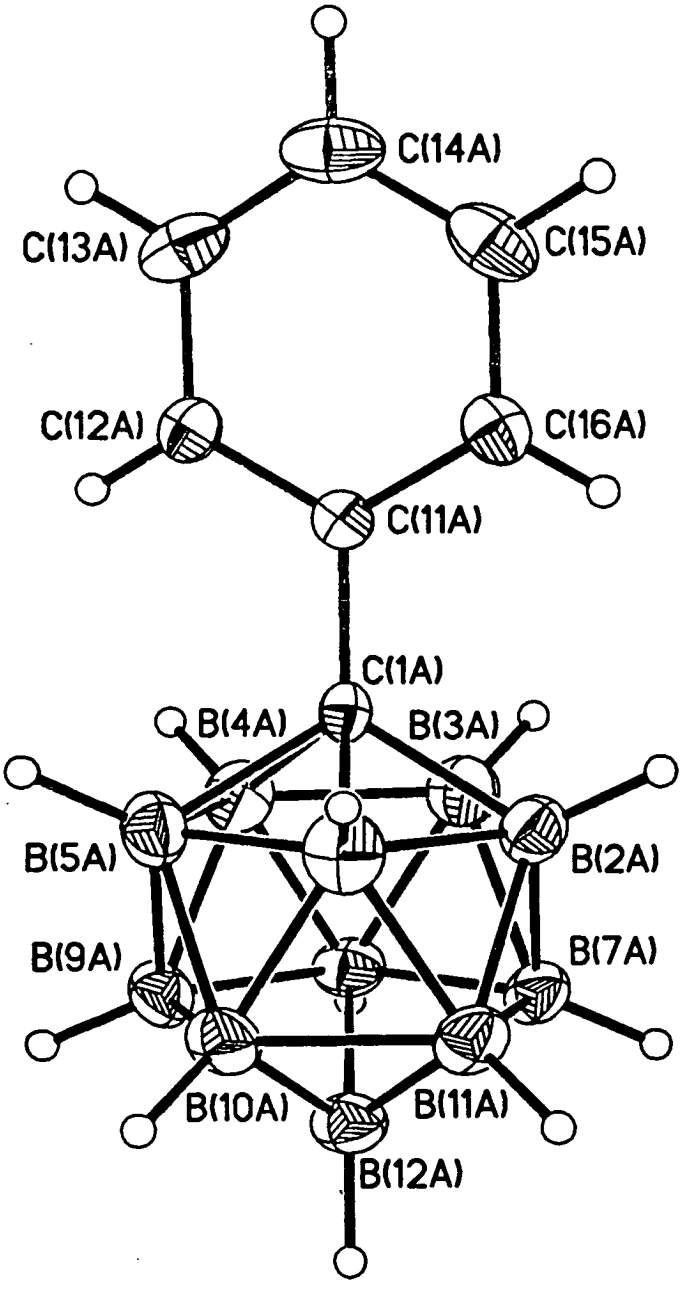

Molecule A

Figure 2.8a Perspective View of **1** (Molecule A)

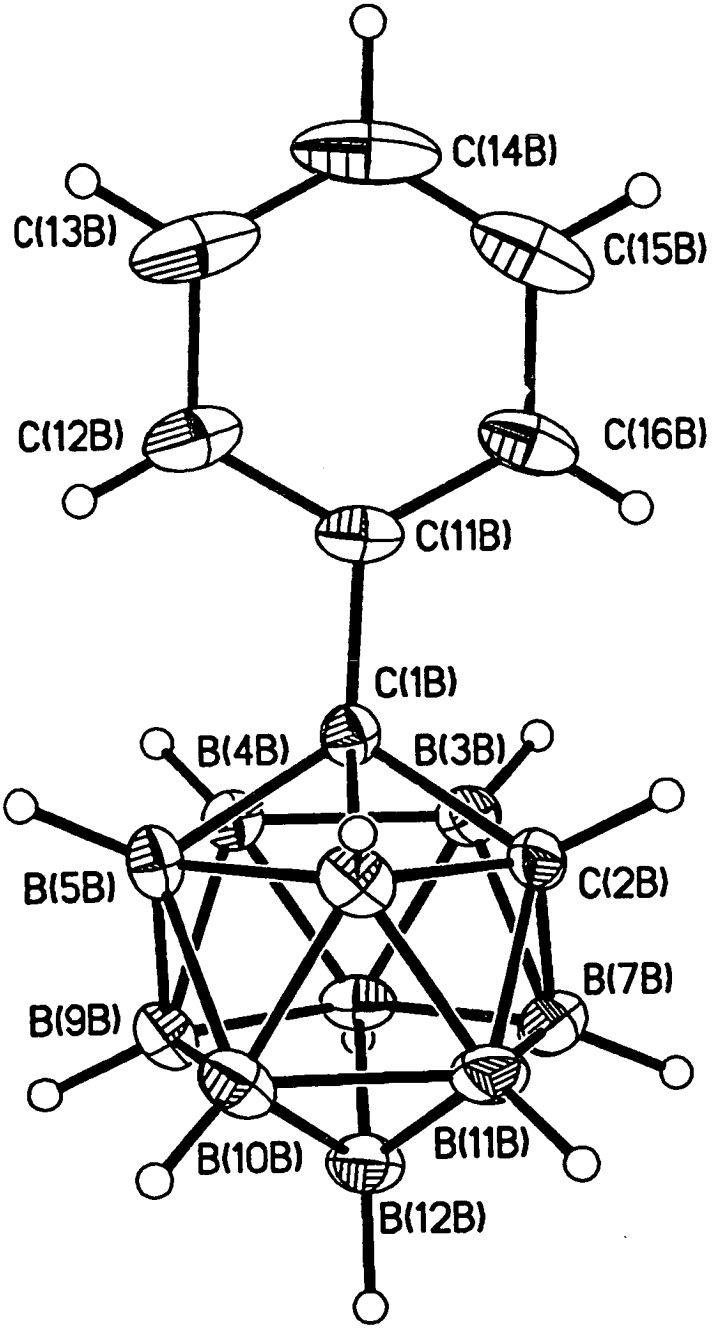

Molecule B

Figure 2.8b Perspective View of **1** (Molecule B)

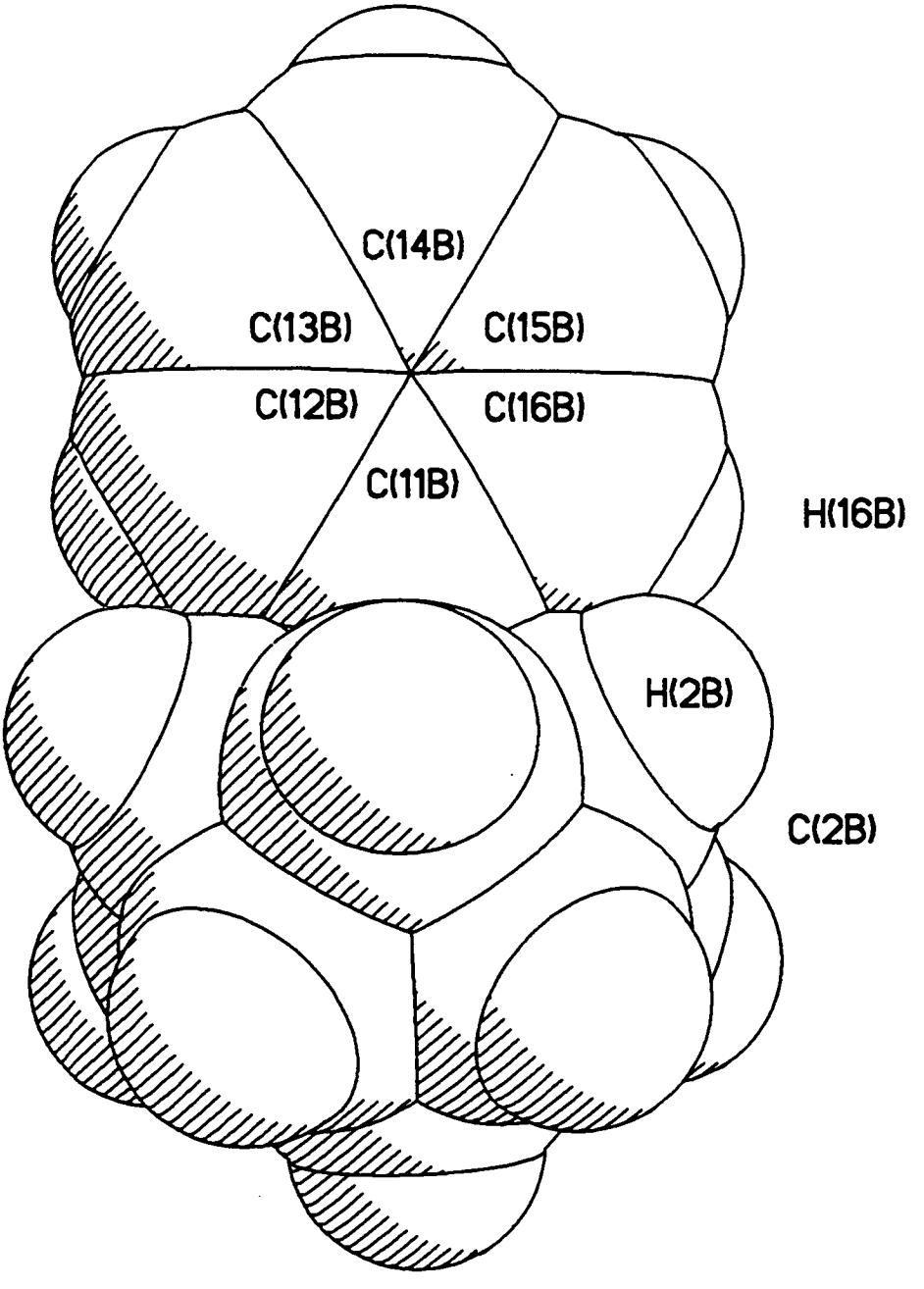

Figure 2.9 Space-filling Diagram of **1**

Further evidence of conjugation between pendant groups and carbaboranes cages has been presented by Wade *et al*, who recently synthesised 1-(PhC≡C)-2-Ph-1,2-*closo*-$C_2B_{10}H_{11}$ (**Fig. 2.10**).[25]

The C(15)-C(20) phenyl ring is attached to the C(1) cage carbon atom *via* an ethynyl unit, which relieves the steric strain between the two phenyl groups. As such, the ring is able to adopt a conformation, for which $\theta = 76.2^{o}$, close to that for **1**, when one would perhaps expect it to adopt a similar conformation to that observed for the C(2)-bound phenyl ring, so as to minimise mutual steric repulsions. Wade also states that there is "Evidence of some delocalisation of pi-electronic charge in the phenylethynyl ligand towards the car(ba)borane cage is provided by the carbon-carbon distances [1.431(2), 1.194(2) and 1.433(2) Å, respectively from benzene ring to car(ba)borane icosahedron]."

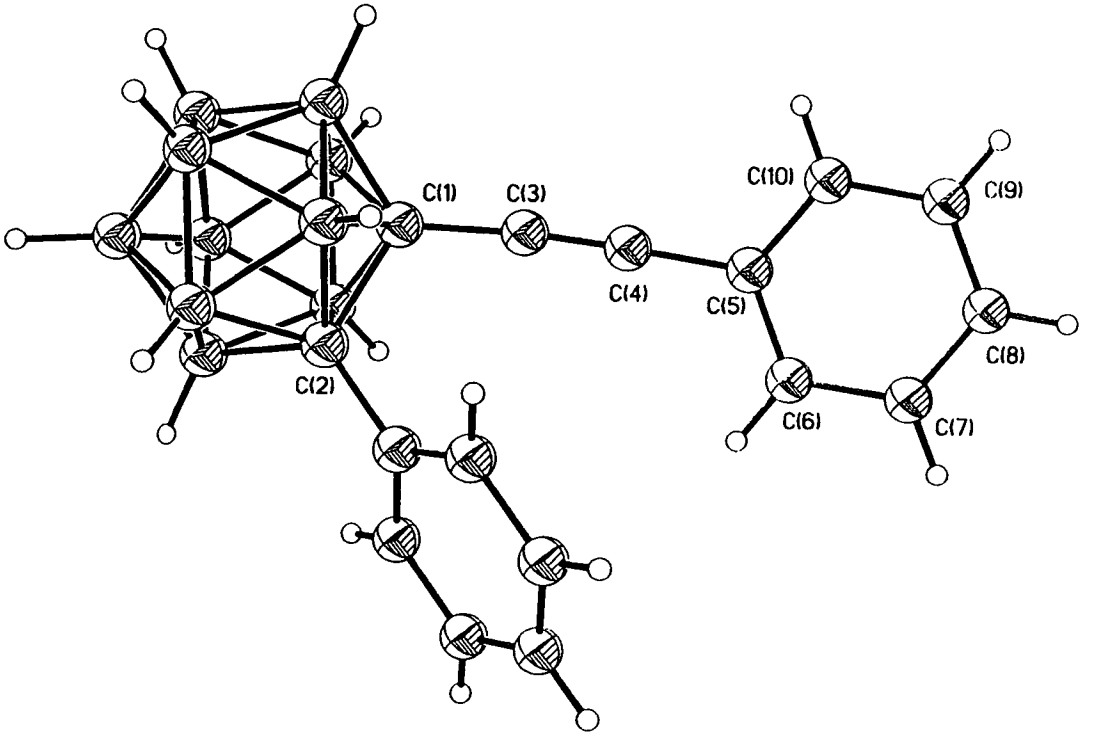

Figure 2.10 Perspective View of 1-(PhC≡C)-2-Ph-1,2-*closo*-$C_2B_{10}H_{10}$

Further evidence of conjugated systems interacting with carbaborane cages, relating to carbaborane carboxylates is presented in **Section 2.4**.

Table 1A Selected Bond Lengths (Å) and Angles (°) for **1**

C(1A)-C(11A)	1.501(4)	C(1A)-B(4A)	1.674(5)
C(1A)-B(2A)	1.687(5)	C(1A)-B(5A)	1.713(5)
C(1A)-B(6A)	1.718(5)	C(1A)-B(3A)	1.728(5)
B(2A)-B(11A)	1.735(6)	B(2A)-B(3A)	1.736(6)
B(2A)-B(7A)	1.737(6)	B(2A)-B(6A)	1.739(6)
B(3A)-B(4A)	1.736(6)	B(3A)-B(7A)	1.774(6)
B(3A)-B(8A)	1.778(6)	B(4A)-B(9A)	1.735(6)
B(4A)-B(5A)	1.735(6)	B(4A)-B(8A)	1.743(6)
B(5A)-B(6A)	1.749(6)	B(5A)-B(10A)	1.752(6)
B(5A)-B(9A)	1.762(6)	B(6A)-B(10A)	1.761(6)
B(6A)-B(11A)	1.762(6)	B(7A)-B(8A)	1.767(7)
B(7A)-B(11A)	1.773(6)	B(7A)-B(12A)	1.781(6)
B(8A)-B(9A)	1.771(6)	B(8A)-B(12A)	1.772(7)
B(9A)-B(10A)	1.768(7)	B(9A)-B(12A)	1.772(7)
B(10A)-B(12A)	1.778(6)	B(10A)-B(11A)	1.790(7)
B(11A)-B(12A)	1.785(7)	C(1B)-C(11B)	1.503(4)
C(1B)-C(2B)	1.640(5)	C(1B)-B(4B)	1.705(5)
C(1B)-B(5B)	1.716(5)	C(1B)-B(3B)	1.719(5)
C(1B)-B(6B)	1.743(5)	C(2B)-B(7B)	1.681(6)
C(2B)-B(11B)	1.683(5)	C(2B)-B(6B)	1.709(6)
C(2B)-B(3B)	1.711(6)	B(3B)-B(8B)	1.761(6)
B(3B)-B(4B)	1.761(6)	B(3B)-B(7B)	1.768(6)
B(4B)-B(12B)	1.778(6)	B(4B)-B(5B)	1.784(5)
B(4B)-B(8B)	1.795(6)	B(5B)-B(6B)	1.758(6)
B(5B)-B(12B)	1.769(6)	B(5B)-B(10B)	1.771(6)
B(6B)-B(10B)	1.756(6)	B(6B)-B(11B)	1.766(7)
B(7B)-B(9B)	1.761(7)	B(7B)-B(11B)	1.767(7)
B(7B)-B(8B)	1.770(7)	B(8B)-B(9B)	1.767(6)
B(8B)-B(12B)	1.780(6)	B(9B)-B(11B)	1.766(6)
B(9B)-B(12B)	1.769(6)	B(9B)-B(10B)	1.787(7)
B(10B)-B(11B)	1.764(7)	B(10B)-B(12B)	1.783(6)

C(11A)-C(1A)-B(4A)	119.8(3)	C(11A)-C(1A)-B(2A)	121.5(3)
C(11A)-C(1A)-B(5A)	119.0(3)	B(4A)-C(1A)-B(5A)	61.6(2)
C(11A)-C(1A)-B(6A)	120.1(3)	B(2A)-C(1A)-B(6A)	61.4(2)
B(5A)-C(1A)-B(6A)	61.3(2)	C(11A)-C(1A)-B(3A)	118.4(3)
B(4A)-C(1A)-B(3A)	61.4(2)	B(2A)-C(1A)-B(3A)	61.1(2)
C(1A)-B(2A)-B(3A)	60.6(2)	B(11A)-B(2A)-B(7A)	61.4(3)
B(3A)-B(2A)-B(7A)	61.4(2)	C(1A)-B(2A)-B(6A)	60.2(2)
B(11A)-B(2A)-B(6A)	61.0(2)	C(1A)-B(3A)-B(2A)	58.3(2)
C(1A)-B(3A)-B(4A)	57.8(2)	B(2A)-B(3A)-B(7A)	59.3(2)
B(4A)-B(3A)-B(8A)	59.5(2)	B(7A)-B(3A)-B(8A)	59.7(3)
C(1A)-B(4A)-B(5A)	60.3(2)	B(9A)-B(4A)-B(5A)	61.0(3)
C(1A)-B(4A)-B(3A)	60.8(2)	B(9A)-B(4A)-B(8A)	61.2(3)
B(3A)-B(4A)-B(8A)	61.4(2)	C(1A)-B(5A)-B(4A)	58.1(2)
C(1A)-B(5A)-B(6A)	59.5(2)	B(6A)-B(5A)-B(10A)	60.4(3)
B(4A)-B(5A)-B(9A)	59.5(2)	B(10A)-B(5A)-B(9A)	60.4(3)

C(1A)-B(6A)-B(2A)	58.4(2)	C(1A)-B(6A)-B(5A)	59.2(2)
B(5A)-B(6A)-B(10A)	59.9(3)	B(2A)-B(6A)-B(11A)	59.4(2)
B(10A)-B(6A)-B(11A)	61.1(3)	B(2A)-B(7A)-B(11A)	59.2(3)
B(2A)-B(7A)-B(3A)	59.2(2)	B(8A)-B(7A)-B(3A)	60.3(2)
B(8A)-B(7A)-B(12A)	59.9(3)	B(11A)-B(7A)-B(12A)	60.3(3)
B(4A)-B(8A)-B(9A)	59.2(3)	B(7A)-B(8A)-B(12A)	60.4(3)
B(9A)-B(8A)-B(12A)	60.0(3)	B(4A)-B(8A)-B(3A)	59.1(2)
B(7A)-B(8A)-B(3A)	60.0(2)	B(4A)-B(9A)-B(5A)	59.5(2)
B(5A)-B(9A)-B(10A)	59.5(3)	B(4A)-B(9A)-B(8A)	59.6(2)
B(10A)-B(9A)-B(12A)	60.3(3)	B(8A)-B(9A)-B(12A)	60.0(3)
B(5A)-B(10A)-B(6A)	59.7(2)	B(5A)-B(10A)-B(9A)	60.1(3)
B(9A)-B(10A)-B(12A)	60.0(3)	B(6A)-B(10A)-B(11A)	59.5(3)
B(12A)-B(10A)-B(11A)	60.0(3)	B(2A)-B(11A)-B(6A)	59.6(2)
B(2A)-B(11A)-B(7A)	59.3(2)	B(7A)-B(11A)-B(12A)	60.1(3)
B(6A)-B(11A)-B(10A)	59.4(3)	B(12A)-B(11A)-B(10A)	59.6(3)
B(8A)-B(12A)-B(9A)	60.0(3)	B(9A)-B(12A)-B(10A)	59.7(3)
B(8A)-B(12A)-B(7A)	59.7(3)	B(10A)-B(12A)-B(11A)	60.3(3)
B(7A)-B(12A)-B(11A)	59.6(3)	C(16A)-C(11A)-C(1A)	120.2(2)
C(12A)-C(11A)-C(1A)	119.8(2)	C(11B)-C(1B)-C(2B)	119.2(3)
C(11B)-C(1B)-B(4B)	120.9(3)	C(11B)-C(1B)-B(5B)	122.7(3)
B(4B)-C(1B)-B(5B)	62.9(2)	C(11B)-C(1B)-B(3B)	116.4(3)
C(2B)-C(1B)-B(3B)	61.2(2)	B(4B)-C(1B)-B(3B)	61.9(2)
C(11B)-C(1B)-B(6B)	118.3(3)	C(2B)-C(1B)-B(6B)	60.6(2)
B(5B)-C(1B)-B(6B)	61.1(2)	B(7B)-C(2B)-B(11B)	63.4(3)
C(1B)-C(2B)-B(6B)	62.7(2)	B(11B)-C(2B)-B(6B)	62.7(3)
C(1B)-C(2B)-B(3B)	61.7(2)	B(7B)-C(2B)-B(3B)	62.8(3)
C(2B)-B(3B)-C(1B)	57.1(2)	C(1B)-B(3B)-B(4B)	58.6(2)
B(8B)-B(3B)-B(4B)	61.3(2)	C(2B)-B(3B)-B(7B)	57.8(2)
B(8B)-B(3B)-B(7B)	60.2(3)	C(1B)-B(4B)-B(3B)	59.4(2)
C(1B)-B(4B)-B(5B)	58.9(2)	B(12B)-B(4B)-B(5B)	59.6(2)
B(3B)-B(4B)-B(8B)	59.4(2)	B(12B)-B(4B)-B(8B)	59.7(2)
C(1B)-B(5B)-B(6B)	60.2(2)	B(6B)-B(5B)-B(10B)	59.7(2)
B(12B)-B(5B)-B(10B)	60.5(2)	C(1B)-B(5B)-B(4B)	58.3(2)
B(12B)-B(5B)-B(4B)	60.0(2)	C(2B)-B(6B)-C(1B)	56.7(2)
C(1B)-B(6B)-B(5B)	58.7(2)	B(10B)-B(6B)-B(5B)	60.5(2)
C(2B)-B(6B)-B(11B)	57.9(2)	B(10B)-B(6B)-B(11B)	60.1(3)
C(2B)-B(7B)-B(11B)	58.4(3)	B(9B)-B(7B)-B(11B)	60.1(3)
C(2B)-B(7B)-B(3B)	59.4(2)	B(9B)-B(7B)-B(8B)	60.0(2)
B(3B)-B(7B)-B(8B)	59.7(2)	B(3B)-B(8B)-B(7B)	60.1(2)
B(9B)-B(8B)-B(7B)	59.7(3)	B(9B)-B(8B)-B(12B)	59.8(2)
B(3B)-B(8B)-B(4B)	59.4(2)	B(12B)-B(8B)-B(4B)	59.7(2)
B(7B)-B(9B)-B(11B)	60.1(3)	B(7B)-B(9B)-B(8B)	60.2(3)
B(8B)-B(9B)-B(12B)	60.4(2)	B(11B)-B(9B)-B(10B)	59.5(3)
B(12B)-B(9B)-B(10B)	60.2(3)	B(6B)-B(10B)-B(11B)	60.2(3)
B(6B)-B(10B)-B(5B)	59.8(2)	B(5B)-B(10B)-B(12B)	59.7(2)
B(11B)-B(10B)-B(9B)	59.6(3)	B(12B)-B(10B)-B(9B)	59.4(2)
B(10B)-B(11B)-B(9B)	60.8(3)	C(2B)-B(11B)-B(6B)	59.4(2)
B(10B)-B(11B)-B(6B)	59.7(3)	C(2B)-B(11B)-B(7B)	58.3(3)
B(9B)-B(11B)-B(7B)	59.8(3)	B(5B)-B(12B)-B(4B)	60.4(2)

B(9B)-B(12B)-B(8B)	59.7(2)	B(4B)-B(12B)-B(8B)	60.6(2)
B(9B)-B(12B)-B(10B)	60.4(3)	B(5B)-B(12B)-B(10B)	59.8(2)
C(16B)-C(11B)-C(1B)	121.5(2)	C(12B)-C(11B)-C(1B)	118.4(2)

Table 1B Atomic Coordinates (x 10^4) and Equivalent Isotropic Thermal Parameters ($Å^2$ x 10^3) for **1**

	x	y	z	U(eq)
C(1A)	-197(3)	1083(2)	7610(3)	30(1)
B(2A)	-160(3)	1985(2)	7745(3)	48(1)
B(3A)	560(4)	1458(2)	8944(3)	53(1)
B(4A)	-348(4)	712(2)	8787(3)	51(1)
B(5A)	-1557(3)	754(2)	7511(4)	53(1)
B(6A)	-1437(4)	1566(2)	6846(4)	56(1)
B(7A)	-298(4)	2209(2)	9059(4)	47(1)
B(8A)	-422(4)	1390(3)	9734(4)	46(1)
B(9A)	-1720(4)	947(3)	8846(4)	49(1)
B(10A)	-2412(4)	1492(3)	7623(4)	51(1)
B(11A)	-1524(4)	2279(2)	7752(4)	50(1)
B(12A)	-1713(4)	1893(3)	9001(4)	51(1)
C(12A)	462(2)	-45(1)	6913(2)	43(1)
C(13A)	1091(2)	-401(1)	6321(2)	58(1)
C(14A)	1758(2)	-13(2)	5803(2)	62(1)
C(15A)	1795(2)	732(2)	5877(2)	59(1)
C(16A)	1166(2)	1089(1)	6468(2)	43(1)
C(11A)	499(2)	700(1)	6986(2)	31(1)
C(1B)	-406(3)	3872(2)	2669(3)	32(1)
C(2B)	175(3)	3067(2)	2949(3)	42(1)
B(3B)	-1073(4)	3177(2)	1757(3)	38(1)
B(4B)	-1911(3)	3813(2)	2199(3)	34(1)
B(5B)	-1081(3)	4069(2)	3650(3)	37(1)
B(6B)	274(4)	3605(2)	4102(3)	42(1)
B(7B)	-852(5)	2415(3)	2662(4)	53(1)
B(8B)	-2225(4)	2872(2)	2210(4)	42(1)
B(9B)	-1586(4)	2567(2)	3651(4)	47(1)
B(10B)	-879(4)	3305(3)	4553(4)	46(1)
B(11B)	-36(4)	2678(3)	4094(4)	50(1)
B(12B)	-2234(4)	3431(2)	3377(4)	41(1)
C(12B)	-63(2)	5150(1)	2294(2)	60(1)
C(13B)	445(3)	5680(1)	1825(3)	85(2)
C(14B)	1213(3)	5493(2)	1252(3)	86(2)
C(15B)	1473(2)	4775(2)	1148(2)	79(2)
C(16B)	965(2)	4244(1)	1617(2)	59(1)
C(11B)	197(2)	4431(1)	2190(2)	41(1)

2.3 Carbaborane Carboxylic Acids

2.3.1 Synthesis

A series of carboxylic acids of the general type 1-CO_2H-2-R-1,2-*closo*-$C_2B_{10}H_{10}$ were synthesised according to the methods of Zakharkin *et al* (R = H)[26] and Grafstein *et al* (R = CH_3, CH_2OCH_3).[10] Full characterisation of compounds **2, 3** and **4** are reported (although two of these compounds have been synthesised previously (R = H, CH_3), full characterisation by microanalysis, ^1H and ^{11}B-{^1H} nmr and IR spectroscopies has not been reported).

Compounds **2, 3** and **4** were synthesised by one of two methods. For carboxylic acid derivatives of both mono-substituted parent carbaboranes, the carababorane was dissolved in Et_2O and deprotonated using 1.1 equivalents of 1.4M MeLi, added dropwise as an Et_2O solution. After being allowed to warm to room temperature, CO_2 gas was bubbled through the cloudy solution for approximately 30 minutes, after which time the lithium carboxylate, Li[1-CO_2-2-R-1,2-*closo*-$C_2B_{10}H_{10}$] was hydrolysed by the addition of an excess of 2M HCl. The carboxylic acid, which is much more soluble in Et_2O, was separated, the aqueous phase extracted twice more and the combined extractions stirred over $MgSO_4$ overnight. Filtration, followed by removal of the solvent *in vacuo* afforded the carbaborane carboxylic acids **3** and **4** as white solids in relatively high yields (67 and 74%, respectively).

It is not possible, however, to synthesise the unsubstituted carboxylic acid, **2**, *via* a similar method (i.e. in Et_2O) since the mono-anion would be in equilibrium with the fully protonated and fully deprotonated species (**Section 1.3**). Hence the deprotonation was performed in C_6H_6 at 75°C, using *n*-BuLi to remove the C_{cage} proton.[26] Addition of *n*-BuLi in C_6H_6 to a stirring solution of the parent carbaborane afforded an immediate white precipitate of the mono-lithium salt. The solution was allowed to cool to room temperature and a small amount of Et_2O added to dissolve this precipitate, before CO_2 was bubbled through the solution for approximately 30 minutes. After this time, the solvents were removed and the resulting white solid redissolved in Et_2O. The carboxylate solution was then hydrolysed, dried and filtered as described above. The filtrate was removed *in vacuo* to afford the compound as a white solid in good yield (73%).

All compounds were readily soluble in chlorinated solvents, thf, Et_2O and acetone. Solubility in *n*-pentane and hexanes was slight.

2.3.2 Characterisation

Compounds **2**, **3** and **4** were initially characterised by IR spectroscopy as CH_2Cl_2 solutions. Absorption bands due to terminal B-H stretches were observed between 2580 and 2600 cm^{-1}. Carbonyl stretching frequencies were observed at approximately 1730 and 1765 cm^{-1}. These two absorption bands correspond to the H-bonded dimer and free monomer, respectively.[27]

The ^1H nmr spectra all showed the expected resonances due to the C(2) substituents and carboxylic acid protons, although it was not possible to rationalise the differing shifts of the latter. The $^{11}B-\{^1H\}$ nmr spectra were all consistent with the expected C_s symmetry, despite several of the resonances being coincidental. Microanalysis figures were generally in close accordance with the calculated figures, although high purity was not especially important, since the acids would be reacted on before the final products were recrystallised.

The ^1H nmr spectrum of compound **2** shows two signals, both broad singlets, in the ratio 1:1. The C(2)-H resonance occurs at 4.00 ppm, which is a typical chemical shift for a C_{cage} proton,[9,14] and the carboxylic acid resonance is observed at 10.40 ppm. The $^{11}B-\{^1H\}$ nmr spectrum shows resonances in the ratio 2:2:2:2:2 (low- to high-field). Without $^1H-\{^{11}B_{selective}\}$ experiments, it was not possible to determine which of the integral-two resonances was the 1+1 coincidence, although the two integral-one resonances generally occur at much higher frequency (several ppm) than the other resonances. Microanalysis figures were in fair accordance with the calculated figures.

The ^1H nmr spectrum of **3** shows two peaks at 8.81 and 2.22 ppm, in the ratio 1:3, which are due to the carboxylic acid and C(2)-methyl protons, respectively. Again, the carboxylic acid resonance is a broad singlet, whereas the methyl resonance is the expected sharp singlet. The $^{11}B-\{^1H\}$ nmr spectrum is again consistent with C_s symmetry with very closely spaced resonances, in the ratio 1:1:8, at 2.66, -2.36 and -6.34 ppm, respectively. The

integral-eight ratio is a 2+2+2+2 coincidence. Microanalysis figures are in good agreement with the calculated values for C and H.

The ^{1}H nmr spectrum of **4** exhibits three resonances, which are due to the carboxylic acid and the methylene and methyl groups of the C(2)-ether substituent. Respectively, these occur at 6.55, 4.14 and 3.34 ppm, in the ratio 1:2:3. The carboxylic proton is a broad singlet, the other two sharp singlets. As for compound **3**, the resonances in the $^{11}B-\{^{1}H\}$ nmr spectrum are in the ratio 1:1:8 (2+2+2+2 coincidence) and occur at -1.35, -3.54 and -10.00 ppm, respectively.

The weighted ^{11}B shifts for compounds **2, 3** and **4** are -7.23, -5.04 and -8.49 ppm, respectively. Although these shifts are typical for a *closo* C_2B_{10} cage, they do not appear to be influenced by the C(2) substituents. The mean shifts of compounds **2, 3** and **4** are, however, deshielded relative to the parent carbaboranes, which strongly suggests that the carboxylic acid moiety is removing electron density from the cage, the corollary to which is that the cage is acting as an electron donor.

Comparison of the weighted ^{11}B chemical shifts of the acids and the parent carbaboranes from which they are derived (**Table 2.3, Section 2.4.2**), indicates that the substitution of the C_{cage} proton by a carboxylic acid functionality causes deshielding of the ^{11}B nuclei, i.e. electron density is being removed from the cage.

2.4 Carbaborane Carboxylate Salts

2.4.1 Synthesis

A series of carbaborane carboxylates of the general type $[HNEt_3][1\text{-}CO_2\text{-}2\text{-}R\text{-}1,2\text{-}closo\text{-}C_2B_{10}H_{10}]$ (R = H, **2a**, CH_3, **3a**, CH_2OCH_3, **4a**) were synthesised by dropwise addition of an excess of NEt_3 to a stirring solution of the appropriate carbaborane carboxylic acids **2**, **3** and **4** (**Section 2.3**). The carboxylic acid proton is removed by the NEt_3 to form an ether-insoluble carboxylate salt, which can be isolated by filtration as a fine white precipitate. Since the precipitate was often very fine, yields were greatly improved if the Et_2O was removed *in vacuo* to afford an oily white/yellow solid, which was then recrystallised from CH_2Cl_2/hexanes (*i*-, *n*- or petroleum ether (60-80)) to afford the salts as white microcrystalline solids.

The compounds were readily soluble in chlorinated solvents, thf, and acetone and insoluble in Et_2O and hexanes. As such, diffraction quality, colourless needles of **3a** and **4a** were grown by slow diffusion of *n*-hexane and a CH_2Cl_2 solution (4:1) at -30°C. These needles were relatively air-stable, but did degrade after several weeks in the atmosphere affording sticky, brown solids. Although compound **2a** was synthesised by the method described above, all attempts to grow diffraction quality crystals with $[HNEt_3]^+$ as the cation were unsuccesful and hence several cations were used, including $[Li]^+$, $[HN(Me_2CH)_2Et]^+$ and $[btma]^+$. The $[btma]^+$ salt was synthesised by direct metathesis of the lithium carboxylate with [btma][Cl]. Crystals were grown, but were very fine needles and unsuitable for an X-ray diffraction study. Diffraction quality blocks were eventually grown of $[HNMe_2Et][1\text{-}H\text{-}2\text{-}CO_2\text{-}1,2\text{-}closo\text{-}C_2B_{10}H_{10}]$, **2b**, by slow diffusion of *n*-hexane and a thf solution at -30°C. The crystallisation tube contained only one crystal (!), a large, colourless block, which was cut and covered in grease to prevent any possible loss of solvent, before it was mounted. Hence, it was not possible to characterise **2b** by usual analytical methods and all data (except crystallographic) relate to **2a**.

2.4.2 Characterisation

The compounds were all characterised initially by IR spectroscopy. There were broad B-H stretching bands at approximately the same frequencies as the parent carboxylic acids, between 2580 and 2600 cm^{-1}. There are two carbonyl stretching frequencies at approximately 1655 cm^{-1} (*anti*-symmetric stretch) and at 1330 cm^{-1} (symmetric stretch).[27] As one would expect, the CO stretching frequencies are shifted to lower frequency with respect to the carboxylic acids, since the bond order has decreased from 2 to 1.5.

The ^{1}H nmr spectrum of **2a** confirmed that it is a 1:1 salt, with resonances due to C_{cage}-H, N-H, methylene and methyl protons in the ratio 1:1:6:9. As expected, there is no longer a resonance due to the carboxylic acid proton. The C_{cage}-H resonance occurs at 4.07 ppm and is the expected broad singlet. The N-H proton is also a broad singlet and occurs at 3.65 ppm, the methylene and methyl signals are a quartet and triplet centred at 2.99 and 1.23 ppm, respectively. The ^{11}B-{^{1}H} nmr spectrum shows six resonances, with integrals in the ratio 1:1:2:2:2:2 (from low- to high-field), indicative of the expected C_s symmetry. Microanalysis figures are in fair accordance with the calculated values.

Compound **3a** was also shown to be a 1:1 salt from its ^{1}H nmr spectrum. The C(2)-Me signal is a singlet at 2.15 ppm of relative integral-three. The N-H, methylene and methyl protons of the cation are at similar shifts as for **2a** (3.71, 3.06 and 1.28 ppm, respectively) in the ratio 1:6:9. The shielding pattern in the ^{11}B-{^{1}H} nmr spectrum is of three resonances at 2.66, -2.36 and -6.34 ppm, in the ratio 1:1:8, from low- to high-field, similar to that for compound **3**. Microanalysis figures are in very good accordance with the calculated values.

Compound **4a** is similarly a 1:1 salt. The methylene and methyl protons of the ether substituent occur in the ratio 2:3 as singlets at 3.96 and 3.39 ppm, respectively. The N-H, methylene and methyl protons of the counter-ion occur in the ratio 1:6:9 at 4.67 (broad singlet), 2.05 (quartet) and 0.97 ppm (triplet), respectively. The ^{11}B-{^{1}H} nmr spectrum has a shielding pattern of resonances in the ratio 1:1:2:2:2:2 (low- to high-field), typical of a

C_2B_{10} cage with C_s symmetry. Again, microanalysis figures are in excellent accordance with the calculated values.

There are substantial downfield shifts of the mean ^{11}B resonances of between 1.07 and 3.86 ppm upon substitution of C_{cage}-H by $\{CO_2H\}$ and between 0.72 and 3.52 ppm by $\{CO_2\}^-$ relative to the parent carbaboranes, indicating that the these moieties are electron-withdrawing (CO_2H more so than $[CO_2]^-$) (**Table 2.3**).

Table 2.3 Mean ^{11}B Chemical Shifts of 1-R-2-R′-1,2-*closo*-$C_2B_{10}H_{10}$

	Mean δ ^{11}B of 1-R-2-R′-1,2-*closo*-$C_2B_{10}H_{10}$ /(ppm)		
R′	**R = H**	**R = CO_2H**	**R = $[CO_2]^-$**
H	-10.08	-7.23	-7.61
CH_3	-8.90	-5.04	-6.38
CH_2OCH_3	-9.56	-8.49	-8.84

There is also a marked deshielding effect of the ^1H nmr chemical shifts of the C(2)-bound substituents of the substituted species relative to the parent carbaboranes (NB: for comparison only, the parent carbaboranes are numbered so that the non-H substituent is C(2)-bound; this is so as to be consistent with the numbering scheme adopted for compounds **2-4a** (see also **Section 3.4.2**)). Again, the difference between the chemical shifts of the CO_2H and $[CO_2]^-$ species are slight (**Table 2.4**).

Table 2.4 ^1H Chemical Shifts of 1-R-2-R′-1,2-*closo*-$C_2B_{10}H_{10}$

	δ ^1H of 1-R-2-R′-1,2-*closo*-$C_2B_{10}H_{10}$ /(ppm)		
R′	**R = H**	**R = CO_2H**	**R = $[CO_2]^-$**
H	3.35	4.00	4.07
CH_3	2.01	2.22	2.15
CH_2OCH_3	3.79, 3.55	4.05, 3.37	4.10, 3.32

2.4.3 EHMO Calculations on Carbaborane Carboxylates and Related Species

A series of extended Hückel molecular orbital (EHMO) calculations were performed to determine the preferred conformation of a $[CX_2]^{n+}$ fragment (X = H, O; n = ±1) bound to a 1,2-*closo*-C_2B_{10} cage by a single σ-bond. The carbaborane cage was modelled more realistically (pertinent bond lengths used in the calculations are given in **Table 2.5**) than in the calculations to determine the preferred orientation of the phenyl ring in **1** (where C-C = B-C = B-B = 1.75 Å). The C_{cage}-CO_2 bond length is an average value from two previous structures (**3a** (1.550(5) Å) and **4a** (1.562(3) Å), close to that determined for the related 1,7-analogue (1.55(2) Å).[11b] The actual value of the C_{cage}-CO_2 bond length was later found from an X-ray diffraction study (i.e. upon **2b**) to be 1.541(4) Å.

Table 2.5 Model Parameters for [1-CX_2-1,2-*closo*-$C_2B_{10}H_{11}]^{n+}$

Connectivity/Bond	Length/ (Å)
C_{cage}-C_{cage}	1.65
C_{cage}-CH_2	1.50
C_{cage}-CO_2	1.56
C_{cage}-B	1.7575
B-B	1.85
C-O	1.20
C-H	1.08
C_{cage}/B-H	1.15

The reduced overlap population matrices (ROPM) for the C_{cage}-C_{cage} and C_{cage}-CX_2 distances as well as the total energy of the molecule were calculated for orientations of the CX_2 group between θ = 90 and 0° at intervals of 9°, using a locally modified version of ICON8.[28] Initial calculations were with $[CH_2]^-$ and $[CH_2]^+$ as the pendant groups, and were later extended to include the anion [1-CO_2-1,2-*closo*-$C_2B_{10}H_{11}]^-$, which was synthesised some time later. The results of these calculations are given in **Tables 2.6**, **2.7** and **2.8**, respectively.

Table 2.6 Total Energy (eV) and C_{cage}-C_{cage} and C_{cage}-C_{exo} Overlaps for Conformations of [1-CH_2-1,2-*closo*-$C_2B_{10}H_{11}$]$^-$ (θ = 90 - 0°)

θ / (°)	Total Energy / (eV)	C_{cage}-C_{cage} Overlap	C_{cage}-C_{exo} Overlap
90	-882.344848	0.5426	0.9869
81	-882.341575	0.5421	0.9859
72	-882.331969	0.5408	0.9832
63	-882.316909	0.5387	0.9788
54	-882.297863	0.5361	0.9727
45	-882.276530	0.5332	0.9654
36	-882.255115	0.5304	0.9573
27	-882.235602	0.5279	0.9492
18	-882.220069	0.5259	0.9422
9	-882.210040	0.5246	0.9375
0	-882.206549	0.5242	0.9359

Table 2.7 Total Energy (eV) and C_{cage}-C_{cage} and C_{cage}-C_{exo} Overlaps for Conformations of [1-CH_2-1,2-*closo*-$C_2B_{10}H_{11}$]$^+$ (θ = 90 - 0°)

θ / (°)	Total Energy / (eV)	C_{cage}-C_{cage} Overlap	C_{cage}-C_{exo} Overlap
90	-861.194602	0.5391	0.8095
81	-861.210040	0.5383	0.8101
72	-861.220069	0.5357	0.8117
63	-861.235602	0.5316	0.8142
54	-861.255115	0.5262	0.8174
45	-861.276530	0.5198	0.8209
36	-861.297863	0.5130	0.8243
27	-861.316909	0.5068	0.8273
18	-861.331969	0.5020	0.8298
9	-861.341575	0.4989	0.8313
0	-861.344848	0.4979	0.8318

Table 2.8 Total Energy (eV) and C_{cage}-C_{cage} and C_{cage}-C_{exo} Overlaps for Conformations of [1-CO_2-1,2-*closo*-$C_2B_{10}H_{11}$]$^-$ (θ = 90 - 0°)

θ / (°)	Total Energy / (eV)	C_{cage}-C_{cage} Overlap	C_{cage}-C_{exo} Overlap
90	-1105.768438	0.5369	0.8380
81	-1105.764580	0.5366	0.8376
72	-1105.753341	0.5358	0.8362
63	-1105.735781	0.5346	0.8340
54	-1105.713582	0.5330	0.8313
45	-1105.688860	0.5313	0.8281
36	-1105.663972	0.5296	0.8250
27	-1105.641399	0.5281	0.8220
18	-1105.623437	0.5269	0.8197
9	-1105.611906	0.5262	0.8181
0	-1105.607932	0.5259	0.8176

The calculations on [1-CH_2-1,2-*closo*-$C_2B_{10}H_{11}$]$^-$ revealed that for conformation of θ = 90°, the overlap is greatest for both C_{cage}-C_{cage} **and** C_{cage}-C_{exo} . This is also refected in the lower total energy of the molecule at this conformation compared that for θ = 0°.

The calculations on [1-CH_2-1,2-*closo*-$C_2B_{10}H_{11}$]$^+$ (**Table 2.9**) indicate that the most stable conformation for the CH_2 group is one for which θ = 0°. At this conformation the C_{cage}-C_{exo} overlap is maximised although maximum C_{cage}-C_{cage} overlap is achieved for a conformation of θ = 90°.

The calculations on [1-CO_2-1,2-*closo*-$C_2B_{10}H_{11}$]$^-$ indicate that the carboxylate moiety has a preferred conformation (θ = 90°), since it is this conformation which affords the largest C_{cage}-C_{cage} and C_{cage}-C_{exo} overlaps. Indeed, a subsequent X-ray diffraction study determined that this group adopted a conformation for which θ = 87.5° (**Section 2.4.4**).

2.4.4 Crystallographic Study of 2b

A single diffraction quality, colourless block of **2b** was grown by the slow diffusion of *n*-hexane and a thf solution at -30°C. Intensity data were measured on an Siemens P4 diffractometer operating with Mo-K_α X-radiation (λ_{bar} = 0.71073 Å). The single crystal was mounted in a glass capillary and the experiment performed at 293(2) K.

Crystal data

$C_7H_{23}B_{10}NO_2$, M = 261.36, monoclinic, $P2_1/c$, a = 6.9276(6) Å, b = 21.4920(15) Å, c = 11.0747(7) Å, β = 92.941(5)°, V = 1646.7(2) Å^3, from the random search of a single hemisphere at 293(2) K, Z = 4 ion-pairs, D_c = 1.054 gcm^{-3}, μ(Mo-K_α) = 0.06 mm^{-1}, F(0,0,0) = 552e.

Data collection and reduction

Intensity data collected in the range $2<2\theta<50°$ by the ω scan method; ω-scan width of 0.86°, ω-scan speeds in the range 1.5 to 60.0°min^{-1}. The intensities of 2891 unique reflections (h -1 to 8, k -1 to 25, l -13 to 13) were measured (XSCANS).

Structure solution and refinement

The structure was solved using direct methods and developed by iterative, full-matrix least-squares refinement and difference Fourier syntheses (SHELXTL). There are four ion-pairs per unit cell. The cation is partially disordered, with the methylene carbon atom (C(31)) of the ethyl group occupying two sites (C(31A) and C(31B)). The anion was, in contrast, fully ordered and the C(2) carbon atom readily identified in a similar manner to that described for 1-Ph-1,2-*closo*-$C_2B_{10}H_{11}$ (**Section 2.2.3**). Cage-H atoms were set 1.10 Å from C or B on a radial extension from the centre of the icosahedron, with all other C-H atoms fixed in idealised positions (C-H = 0.93 Å). All hydrogens were given isotropic displacement parameters riding at 1.5 (Me) or 1.2 times of the equivalent isotropic parameter of their attached atom. In the final stages of refinement, all non-H atoms were refined anisotropically.

Data were absorption corrected (ψ-scans) and weighted such that $w^{-1} = [\sigma^2(F_o^2) + (0.1318P)^2 + 0.7727P]$ where $P = [\text{max.}\ (F_o^2) + 2F_c^2]/3$. Using 1690 observed data ($F_o > 4.0\sigma(F_o)$), $R = 0.0855$, $wR_2 = 0.2621$ and $S = 1.118$ for 233 variable parameters. The maximum residue and minimum trough in a final difference Fourier synthesis were 0.36 and -0.34 eÅ^{-3}, respectively. Atomic scattering factors were those inlaid in SHELXTL. Selected bond lengths (Å) and angles (°), fractional coordinates and equivalent isotropic thermal parameters of non-hydrogen atoms are in **Tables 2bA** and **2bB**, respectively.

A perspective view of a single anion is shown in **Figure 2.11**, which confirms that the carbaborane cage has the expected icosahedral geometry, consistent with its $^{11}B\text{-}\{^1H\}$ nmr spectrum. The C(1)-C(2) distance is 1.633(4) Å, with B-C and B-B connectivities in the range 1.687(5) to 1.717(6) and 1.753(6) to 1.780(7) Å, respectively.

The carboxylate moiety is oriented such that $\theta = 87.5°$, presumably so as to maximise the interaction between itself and the carbaborane cage. The observed value of θ is much greater than that for compounds **3a** and **4a** (34.0 and 36.5°, respectively), with a concomitant shortening of the C(1)-C(101) and C(1)-C(2) distances of **2b** relative to **3a** and **4a**. These observations are in very good agreement with the EHMO calculations described previously, which predict that the preferred conformation of $\theta = 90°$would afford the greatest orbital overlap between C(1) and C(2) and C(1) and C(101). There is also the possibility of an interaction between one of the the lone pairs of O(102) and the C_{cage} H atom (O(102)···H(2) = 2.56 Å), which may be a contributing factor (if only slightly so) to the observed conformation.

The carboxylate moiety, (C(1), C(101), O(101), O(102), is essentially planar ($\sigma = 0.0004$ Å, where $\sigma = (\Sigma z_i^2)$ and z_i is the the displacement of the *i*th atom from the least squares plane), with an O(101)-C(101)-O(102) bond angle of 128.1(3)°. The C(101)-O(101) bond length is slightly, yet significantly, longer than C(101)-O(102) (1.235(4) and 1.213(4) Å, respectively). This is possibly due to the inter-ionic H-bonding observed between O(101) and H(001) (N-H) (O(101)···H(001) = 1.610 Å), removing electron density from the C(101)-O(101) bond and thus reducing the bond order relative to C(101)-O(102) (**Fig. 2.12**).

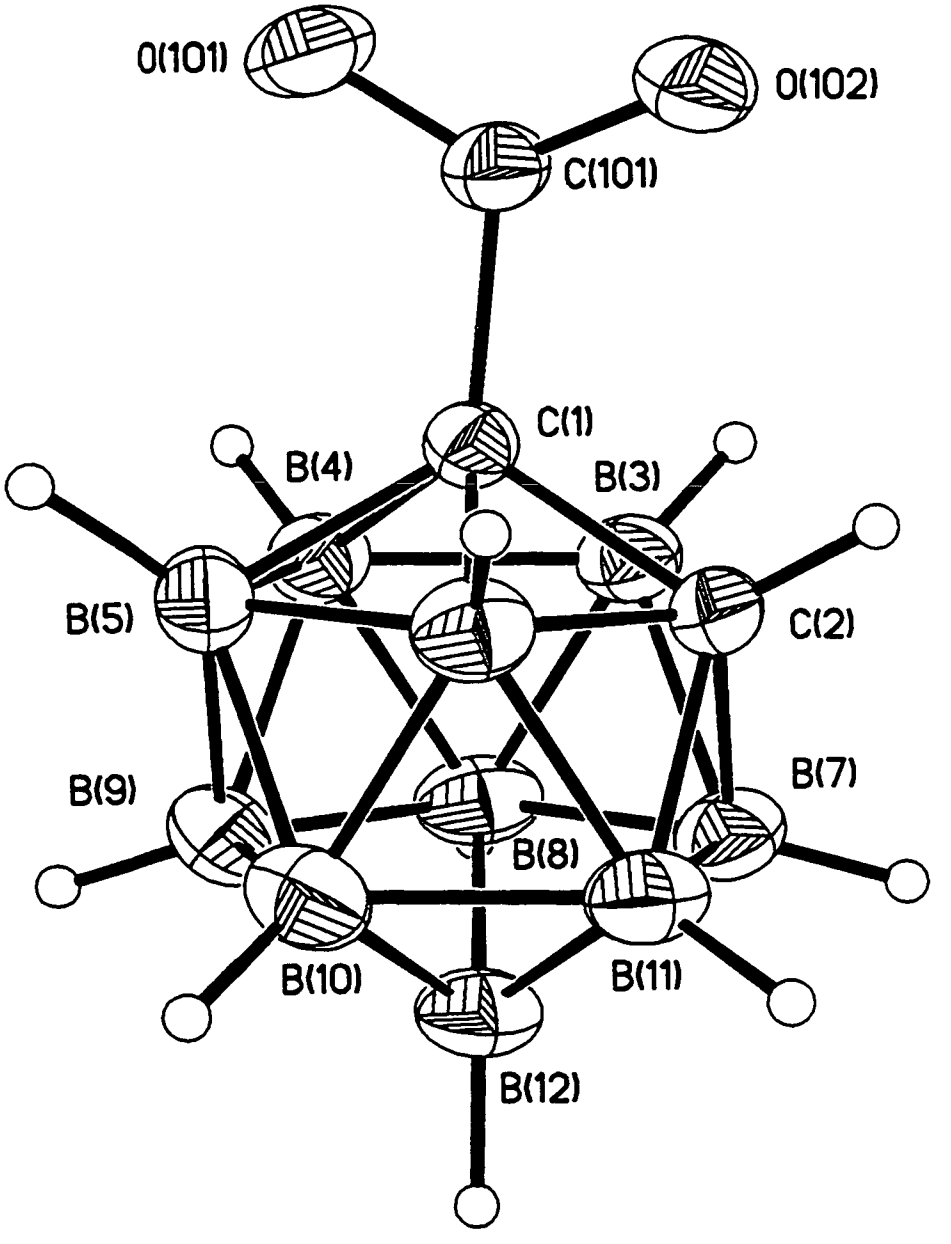

Figure 2.11 Perspective View of [1-CO_2-1,2-*closo*-$C_2B_{10}H_{11}$]$^-$

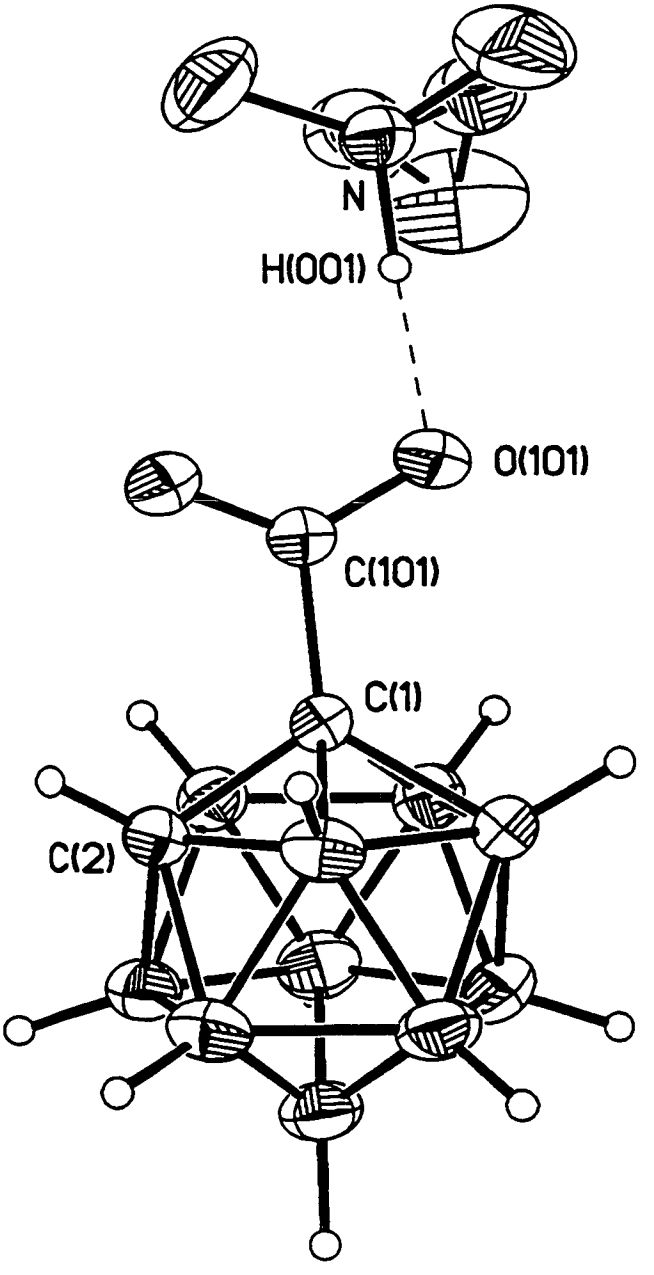

Figure 2.12 Hydrogen Bonding for **2b**

Unlike compound **1**, the possibility of steric repulsion between the C(1)-bound moiety and the C(2) H atom does not exist, more so since the C(1)-C(101) bond length is much longer than the corresponding distance for compound **1** (1.541(4) and 1.503(4) Å, respectively). This is very well emphasised by the space-filling diagram for **2b** shown in **Figure 2.13** (van der Waal's radii are as for **Figure 2.9** plus O - 1.5 Å[24]).

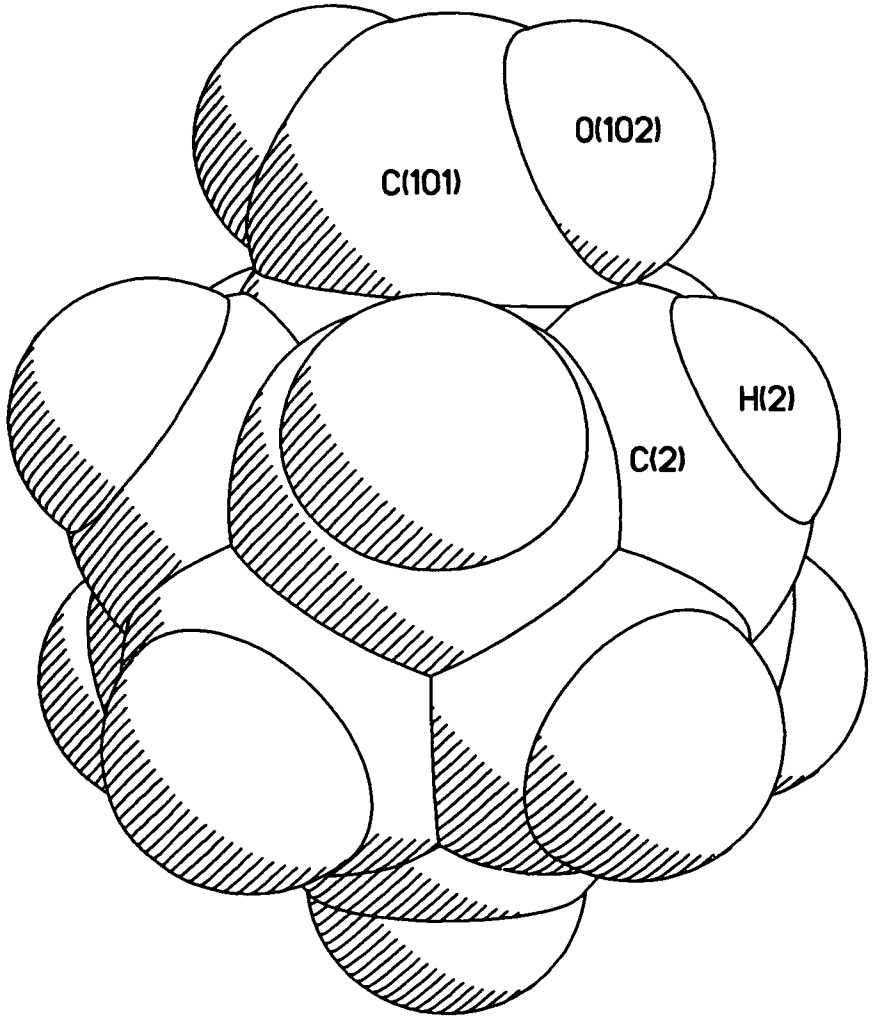

Figure 2.13 Space-filling Diagram of [1-CO_2-1,2-*closo*-$C_2B_{10}H_{11}$]$^-$

Table 2bA Selected Bond Lengths (Å) and Angles (°) for **2b**

C(1)-C(101)	1.541(4)	C(1)-C(2)	1.633(4)
C(1)-B(4)	1.696(5)	C(1)-B(5)	1.701(5)
C(1)-B(3)	1.712(5)	C(1)-B(6)	1.717(6)
C(2)-B(11)	1.687(5)	C(2)-B(7)	1.689(5)
C(2)-B(6)	1.694(6)	C(2)-B(3)	1.705(6)
B(3)-B(8)	1.753(6)	B(3)-B(7)	1.765(6)
B(3)-B(4)	1.772(6)	B(4)-B(9)	1.759(6)
B(4)-B(5)	1.761(7)	B(4)-B(8)	1.773(6)
B(5)-B(9)	1.766(6)	B(5)-B(6)	1.778(6)
B(5)-B(10)	1.778(7)	B(6)-B(10)	1.754(6)
B(6)-B(11)	1.771(6)	B(7)-B(8)	1.758(7)
B(7)-B(12)	1.760(7)	B(7)-B(11)	1.768(7)
B(8)-B(9)	1.765(8)	B(8)-B(12)	1.780(7)
B(9)-B(12)	1.765(7)	B(9)-B(10)	1.775(7)
B(10)-B(12)	1.767(7)	B(10)-B(11)	1.774(7)
B(11)-B(12)	1.766(6)	C(101)-O(102)	1.213(4)
C(101)-O(101)	1.235(4)	N-C(21)	1.429(6)
N-C(31B)	1.44(2)	N-C(11)	1.455(7)
N-C(31A)	1.537(14)	C(31A)-C(32)	1.292(14)
C(31B)-C(32)	1.46(2)		

C(101)-C(1)-C(2)	116.7(3)	C(101)-C(1)-B(4)	122.9(3)
C(101)-C(1)-B(5)	122.4(3)	B(4)-C(1)-B(5)	62.5(2)
C(101)-C(1)-B(3)	116.4(3)	C(2)-C(1)-B(3)	61.3(2)
B(4)-C(1)-B(3)	62.6(2)	C(101)-C(1)-B(6)	116.0(3)
C(2)-C(1)-B(6)	60.7(2)	B(5)-C(1)-B(6)	62.7(2)
B(11)-C(2)-B(7)	63.2(3)	C(1)-C(2)-B(6)	62.1(2)
B(11)-C(2)-B(6)	63.2(3)	C(1)-C(2)-B(3)	61.7(2)
B(7)-C(2)-B(3)	62.7(2)	C(2)-B(3)-C(1)	57.1(2)
C(2)-B(3)-B(7)	58.2(2)	B(8)-B(3)-B(7)	60.0(3)
C(1)-B(3)-B(4)	58.2(2)	B(8)-B(3)-B(4)	60.4(3)
C(1)-B(4)-B(5)	58.9(2)	B(9)-B(4)-B(5)	60.2(3)
C(1)-B(4)-B(3)	59.1(2)	B(9)-B(4)-B(8)	60.0(3)
B(3)-B(4)-B(8)	59.3(2)	C(1)-B(5)-B(4)	58.6(2)
B(4)-B(5)-B(9)	59.8(3)	C(1)-B(5)-B(6)	59.1(2)
B(9)-B(5)-B(10)	60.1(3)	B(6)-B(5)-B(10)	59.1(2)
C(2)-B(6)-C(1)	57.2(2)	C(2)-B(6)-B(11)	58.2(2)
B(10)-B(6)-B(11)	60.4(3)	C(1)-B(6)-B(5)	58.2(2)
B(10)-B(6)-B(5)	60.5(3)	B(8)-B(7)-B(12)	60.8(3)
C(2)-B(7)-B(3)	59.1(2)	B(8)-B(7)-B(3)	59.7(3)
C(2)-B(7)-B(11)	58.4(2)	B(12)-B(7)-B(11)	60.1(3)
B(3)-B(8)-B(7)	60.3(3)	B(3)-B(8)-B(4)	60.3(2)
B(9)-B(8)-B(4)	59.6(3)	B(7)-B(8)-B(12)	59.6(3)
B(9)-B(8)-B(12)	59.7(3)	B(4)-B(9)-B(8)	60.4(3)
B(12)-B(9)-B(8)	60.6(3)	B(4)-B(9)-B(5)	60.0(3)
B(12)-B(9)-B(10)	59.9(3)	B(5)-B(9)-B(10)	60.3(3)
B(6)-B(10)-B(11)	60.3(3)	B(12)-B(10)-B(11)	59.8(3)

B(12)-B(10)-B(9)	59.8(3)	B(6)-B(10)-B(5)	60.4(2)
B(9)-B(10)-B(5)	59.6(3)	C(2)-B(11)-B(7)	58.5(2)
B(12)-B(11)-B(7)	59.7(3)	C(2)-B(11)-B(6)	58.6(2)
B(12)-B(11)-B(10)	59.9(3)	B(6)-B(11)-B(10)	59.3(3)
B(7)-B(12)-B(11)	60.2(3)	B(9)-B(12)-B(10)	60.4(3)
B(11)-B(12)-B(10)	60.3(3)	B(7)-B(12)-B(8)	59.6(3)
B(9)-B(12)-B(8)	59.7(3)	O(102)-C(101)-O(101)	128.1(3)
O(102)-C(101)-C(1)	117.8(3)	O(101)-C(101)-C(1)	114.1(3)
C(21)-N-C(31B)	129.1(8)	C(21)-N-C(11)	113.9(7)
C(31B)-N-C(11)	82.4(8)	C(21)-N-C(31A)	96.5(8)
C(31B)-N-C(31A)	42.8(7)	C(11)-N-C(31A)	123.2(8)
C(32)-C(31A)-N	118.6(10)	N-C(31B)-C(32)	114.4(11)
C(31A)-C(32)-C(31B)	46.3(7)		

Table 2bB Atomic Coordinates (x 10^4) and Equivalent Isotropic Thermal Parameters ($Å^2$ x 10^3) for **2b**

	x	y	z	U(eq)
C(1)	3363(5)	4134(1)	8141(3)	46(1)
C(2)	4660(5)	4025(2)	9396(3)	53(1)
B(3)	5692(6)	3877(2)	8060(4)	56(1)
B(4)	3776(7)	3561(2)	7132(4)	56(1)
B(5)	1664(7)	3565(2)	7952(4)	59(1)
B(6)	2254(7)	3884(2)	9406(4)	58(1)
B(7)	6071(7)	3386(2)	9327(4)	62(1)
B(8)	5497(8)	3068(2)	7890(4)	67(1)
B(9)	3017(8)	2874(2)	7830(5)	68(1)
B(10)	2059(7)	3075(2)	9235(5)	68(1)
B(11)	3969(7)	3393(2)	10168(4)	62(1)
B(12)	4417(8)	2765(2)	9191(4)	67(1)
C(101)	2971(6)	4814(2)	7763(3)	59(1)
O(101)	2045(5)	4871(1)	6786(3)	89(1)
O(102)	3590(6)	5221(1)	8435(3)	92(1)
N	782(6)	6026(2)	6391(3)	76(1)
C(11)	1217(20)	6176(3)	5153(6)	216(6)
C(21)	1533(17)	6464(3)	7264(8)	237(7)
C(31A)	-1283(21)	6007(5)	6834(12)	110(3)
C(31B)	-1155(24)	5969(6)	5860(16)	110(3)
C(32)	-2395(11)	5549(4)	6500(9)	164(3)

2.4.5 Crystallographic Study of 3a

Diffraction quality, colourless *needles* of **3a** were grown by the slow diffusion of *n*-hexane and a CH_2Cl_2 solution at -30°C. Intensity data were measured on an Enraf-Nonius CAD4 diffractometer operating with Mo-K_α X-radiation (λ_{bar} = 0.71073 Å). The single crystal was mounted in a glass capillary and the experiment performed at 291(2) K.

Crystal data

$C_{10}H_{29}B_{10}NO_2$, M = 606.89, orthorhombic, $P2_12_12_1$, a = 7.429(3) Å, b = 12.055(4) Å, c = 20.800(4) Å, V = 1862.7(9) Å^3, from least squares refinement of 25 reflections ($9 \leq \theta \leq 13°$) at 291(2) K, Z = 4 ion-pairs, D_c = 1.082 gcm^{-3}, μ(Mo-K_α) = 0.06 mm^{-1}, F(0,0,0) = 648e.

Data collection and reduction

Intensity data collected in the range $4 < 2\theta < 50°$ by the ω-2θ scan method; ω-scan width (0.8+0.34tanθ), ω-scan speeds in the range 0.92 to 2.35°min^{-1}. The intensities of 3265 unique reflections (h -8 to 8, k 0 to 14, l 0 to 24) were measured (DATCOL).

Structure solution and refinement

The structure was solved using direct methods (SHELX86) and developed by iterative, full-matrix least-squares refinement and difference Fourier syntheses (SHELX76, SHELXTL). The unit cell contains four ion-pairs and the cation is fully ordered. In the final model, all non-H atoms were refined anisotropically. The N-H and cage-H atoms were allowed free positional refinement. All other H-atoms were set in idealised positions with all H-atoms given a group isotropic thermal parameter, 0.093(3) Å^2 at convergence.

Data were absorption corrected (DIFABS) and weighted according to $w^{-1} = [\sigma^2(F_o^2) + (0.09P)^2 + 0.5P]$. Using 1826 observed data ($F_o > 4.0\sigma(F_o)$), R = 0.0689, wR_2 = 0.1753 and S = 0.924 for 233 variables. The maximum and minimum residues in the final Fourier synthesis were 0.21 and -0.16 eÅ^{-3}, respectively. Atomic scattering factors were those inlaid in SHELXTL.

Selected bond lengths (Å) and angles (°), fractional coordinates and equivalent isotropic thermal parameters of non-hydrogen atoms are in **Tables 3aA** and **3aB**, respectively.

A perspective view of a single anion is shown in **Figure 2.14**, which confirms that the carbaborane cage has the expected icosahedral geometry. The C(1)-C(2) distance is 1.672(5) Å, with B-C and B-B connectivities in the range 1.688(6) to 1.737(6) and 1.745(7) to 1.780(7) Å, respectively.

The carboxylate moiety is twisted to a θ value of 34°, away from the electronically favourable conformation of θ = 87.5° observed for **2b** ($\theta_{predicted}$ = 90°), due to the steric bulk of the C(2) bound methyl group. As one would expect, there is an increase in the length of the C(1)-C(2) connectivity, relative to **2b** (1.672(5) *vs.* 1.633(4) Å, respectively) as well as a slight increase in the C(1)-C(101) bond length (1.550(5) *vs.* 1.541(4) Å, respectively). These increases are undoubtedly due to the reduction in orbital overlap between C(1) and C(101), reducing the effectiveness of the π-delocalisation into the cage thus increasing the length of the relatively weakened C(1)-C(2) connectivity. These observations are, moreover, mirrored by **4a** (**Section 2.4.6**) indicating the C(2)-bound methyl group has similar steric requirements to those of the pendant ether group.

Again, the carboxylate group is essentially planar (σ = 0.0046 Å). The internal angles of the carboxylate moiety total 360°, the largest of which is, again, O(101)-C(101)-O(102) (125.0(7)°). There is a hydrogen bond between the N-H, H(001), proton and the nearest carboxylate oxygen atom, (O(101)(H(001)···O(101) = 1.494 Å). As a result of this, the C(101)-O(101) bond length is increased relative to C(101)-O(102) (1.177(5) *vs.* 1.156(5) Å, respectively). There is a slight, forward bending towards each other of both the carboxylate and methyl groups. Although the methyl protons are arranged so as to be as close as possible to the carboxylate oxygen atoms, the distances (O(101)···H(012) = 2.583 Å, O(102)···H(013) = 3.619 Å) are too large to be significant.

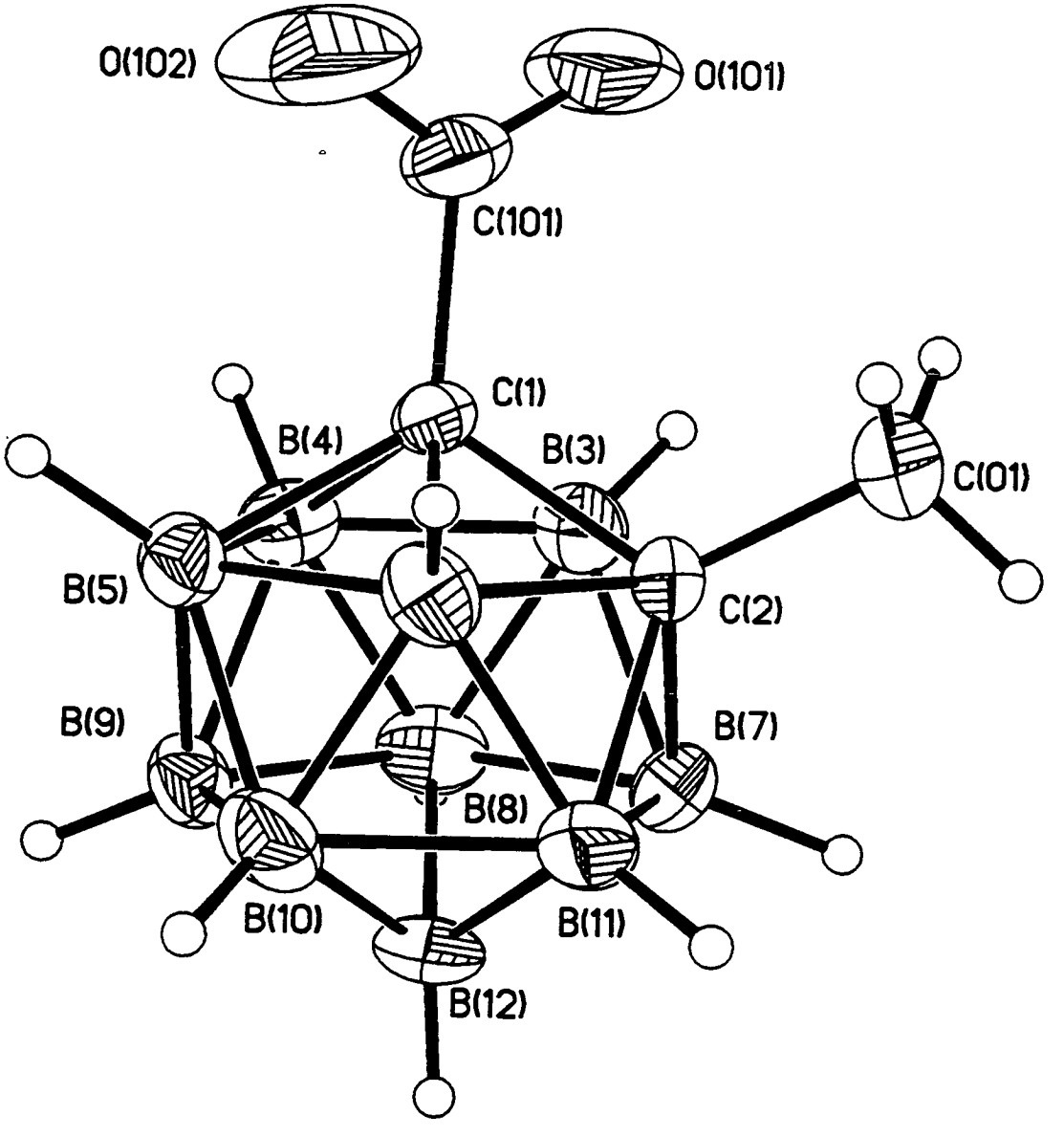

Figure 2.14 Perspective View of [1-CO_2-2-CH_3-1,2-*closo*-$C_2B_{10}H_{10}$]$^-$

Comparison of the the structure of the anion with that of 1-Ph-2-Me-1,2-*closo*-$C_2B_{10}H_{10}$ (**Fig. 2.15**),[7a] shows several similarities. The carboxylate group, like the phenyl ring is twisted from its preferred conformation with the overall change in θ being similar when the C(1) substituent is either a phenyl or a carboxylate group (Δ = 51.1 and 53.5°, respectively). The phenyl ring does, however, twist to a lower θ value (16.6°) than the carboxylate (34.0°), as a result of its larger effective steric bulk, due to the *ortho*-protons and the shorter C(1)-C(Ph) bond length, relative to C(1)-C(CO_2). The C(2)-C(Me) bond lengths for the carboxylate and phenyl species are the same (1.518(4) and 1.518(6) Å, respectively).

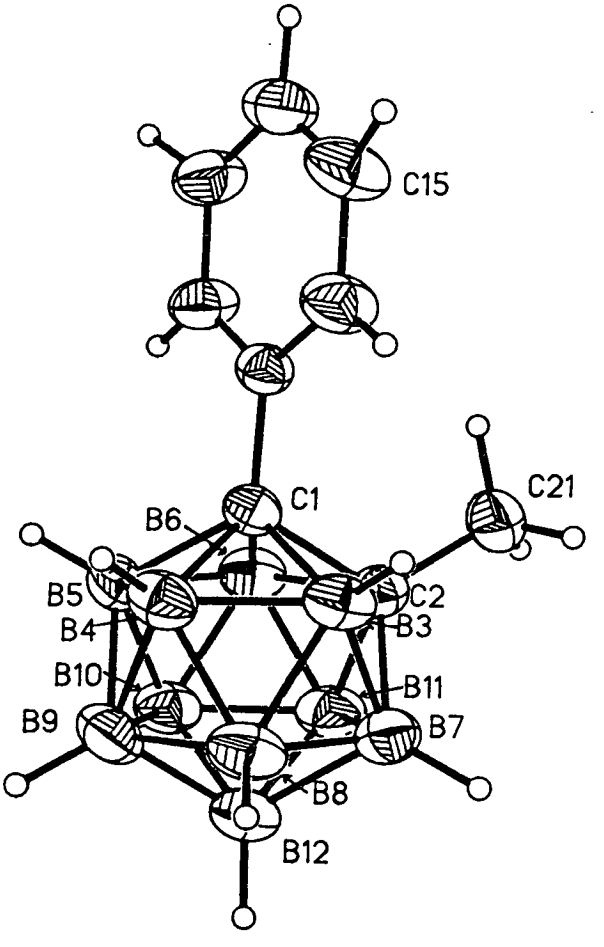

Fig. 2.15 Perspective View of 1-Ph-2-Me-1,2-*closo*-$C_2B_{10}H_{10}$

Table 3aA Selected Bond Lengths (Å) and Angles (°) for **3a**

C(1)-C(101)	1.550(5)	C(1)-C(2)	1.672(5)
C(1)-B(3)	1.699(6)	C(1)-B(4)	1.701(6)
C(1)-B(5)	1.706(6)	C(1)-B(6)	1.737(6)
C(2)-C(01)	1.518(4)	C(2)-B(7)	1.688(6)
C(2)-B(11)	1.695(6)	C(2)-B(3)	1.699(6)
C(2)-B(6)	1.736(6)	B(3)-B(8)	1.749(7)
B(3)-B(7)	1.759(7)	B(3)-B(4)	1.763(7)
B(4)-B(8)	1.745(7)	B(4)-B(9)	1.771(7)
B(4)-B(5)	1.780(7)	B(5)-B(10)	1.765(7)
B(5)-B(6)	1.767(7)	B(5)-B(9)	1.771(6)
B(6)-B(10)	1.752(7)	B(6)-B(11)	1.770(7)
B(7)-B(11)	1.761(8)	B(7)-B(8)	1.771(7)
B(7)-B(12)	1.780(7)	B(8)-B(12)	1.752(7)
B(8)-B(9)	1.759(7)	B(9)-B(12)	1.763(8)
B(9)-B(10)	1.770(7)	B(10)-B(11)	1.765(7)
B(10)-B(12)	1.774(8)	B(11)-B(12)	1.764(8)
C(101)-O(102)	1.156(5)	C(101)-O(101)	1.177(5)
N-C(11)	1.481(7)	N-C(21)	1.494(5)
N-C(31)	1.497(5)	C(11)-C(12)	1.510(5)
C(21)-C(022)	1.494(6)	C(31)-C(32)	1.485(5)

C(101)-C(1)-C(2)	117.6(3)	C(101)-C(1)-B(3)	117.8(3)
C(2)-C(1)-B(3)	60.5(2)	C(101)-C(1)-B(4)	122.4(3)
B(3)-C(1)-B(4)	62.5(3)	C(101)-C(1)-B(5)	121.4(3)
B(4)-C(1)-B(5)	63.0(3)	C(101)-C(1)-B(6)	116.4(3)
C(2)-C(1)-B(6)	61.2(2)	B(5)-C(1)-B(6)	61.7(3)
C(01)-C(2)-C(1)	118.6(3)	C(01)-C(2)-B(7)	120.8(3)
C(01)-C(2)-B(11)	121.0(3)	B(7)-C(2)-B(11)	62.7(3)
C(01)-C(2)-B(3)	117.9(3)	C(1)-C(2)-B(3)	60.5(2)
B(7)-C(2)-B(3)	62.6(3)	C(01)-C(2)-B(6)	116.9(3)
C(1)-C(2)-B(6)	61.3(2)	B(11)-C(2)-B(6)	62.1(3)
C(2)-B(3)-C(1)	58.9(2)	C(2)-B(3)-B(7)	58.4(3)
B(8)-B(3)-B(7)	60.6(3)	C(1)-B(3)-B(4)	58.8(2)
B(8)-B(3)-B(4)	59.6(3)	C(1)-B(4)-B(3)	58.7(2)
B(8)-B(4)-B(3)	59.8(3)	B(8)-B(4)-B(9)	60.1(3)
C(1)-B(4)-B(5)	58.6(2)	B(9)-B(4)-B(5)	59.8(3)
C(1)-B(5)-B(6)	60.0(2)	B(10)-B(5)-B(6)	59.5(3)
B(10)-B(5)-B(9)	60.1(3)	C(1)-B(5)-B(4)	58.4(2)
B(9)-B(5)-B(4)	59.8(3)	C(2)-B(6)-C(1)	57.5(2)
C(1)-B(6)-B(5)	58.3(2)	B(10)-B(6)-B(5)	60.2(3)
C(2)-B(6)-B(11)	57.8(3)	B(10)-B(6)-B(11)	60.1(3)
C(2)-B(7)-B(3)	59.0(3)	C(2)-B(7)-B(11)	58.8(3)
B(3)-B(7)-B(8)	59.4(3)	B(11)-B(7)-B(12)	59.7(3)
B(8)-B(7)-B(12)	59.1(3)	B(4)-B(8)-B(3)	60.6(3)
B(4)-B(8)-B(9)	60.7(3)	B(12)-B(8)-B(9)	60.3(3)
B(3)-B(8)-B(7)	60.0(3)	B(12)-B(8)-B(7)	60.7(3)
B(8)-B(9)-B(12)	59.7(3)	B(12)-B(9)-B(10)	60.3(3)

B(8)-B(9)-B(4)	59.2(3)	B(10)-B(9)-B(5)	59.8(3)
B(4)-B(9)-B(5)	60.4(3)	B(6)-B(10)-B(11)	60.4(3)
B(6)-B(10)-B(5)	60.3(3)	B(5)-B(10)-B(9)	60.1(3)
B(11)-B(10)-B(12)	59.8(3)	B(9)-B(10)-B(12)	59.6(3)
C(2)-B(11)-B(7)	58.5(3)	B(7)-B(11)-B(12)	60.7(3)
B(12)-B(11)-B(10)	60.4(3)	C(2)-B(11)-B(6)	60.1(3)
B(10)-B(11)-B(6)	59.4(3)	B(8)-B(12)-B(9)	60.1(3)
B(9)-B(12)-B(10)	60.0(3)	B(11)-B(12)-B(10)	59.8(3)
B(8)-B(12)-B(7)	60.2(3)	B(11)-B(12)-B(7)	59.6(3)
O(102)-C(101)-O(101)	125.0(5)	O(102)-C(101)-C(1)	118.7(5)
O(101)-C(101)-C(1)	116.2(4)	C(11)-N-C(21)	113.8(2)
C(11)-N-C(31)	112.0(2)	C(21)-N-C(31)	110.3(3)
N-C(11)-C(12)	113.8(2)	N-C(21)-C(022)	115.6(4)
C(32)-C(31)-N	114.4(3)		

Table 3aB Atomic Coordinates (x 10^4) and Equivalent Isotropic Thermal Parameters ($Å^2$ x 10^3) for **3a**

	x	y	z	U(eq)
C(1)	-298(5)	-10713(3)	-4050(2)	42(1)
C(2)	1857(4)	-11107(3)	-4015(2)	48(1)
B(3)	318(7)	-11960(4)	-4362(2)	54(1)
B(4)	-1678(6)	-11814(4)	-3911(3)	54(1)
B(5)	-1266(7)	-10796(4)	-3308(2)	52(1)
B(6)	978(6)	-10330(4)	-3387(2)	53(1)
B(7)	2025(7)	-12477(4)	-3858(3)	66(2)
B(8)	-230(7)	-12925(4)	-3765(2)	63(1)
B(9)	-1209(7)	-12224(4)	-3111(2)	54(1)
B(10)	435(7)	-11310(5)	-2796(2)	63(1)
B(11)	2415(7)	-11479(5)	-3255(2)	62(1)
B(12)	1063(8)	-12644(4)	-3080(3)	64(2)
C(101)	-796(6)	-9774(4)	-4527(2)	71(1)
O(101)	-429(8)	-9930(4)	-5070(2)	172(3)
O(102)	-1519(9)	-8994(3)	-4332(2)	162(2)
C(01)	3210(3)	-10534(2)	-4450(1)	78(1)
N	-1225(3)	-8655(2)	-6042(1)	50(1)
C(11)	-1337(3)	-9433(2)	-6589(1)	66(1)
C(12)	304(7)	-10161(4)	-6664(3)	94(2)
C(21)	346(6)	-7882(4)	-6076(2)	72(1)
C(022)	398(7)	-7136(4)	-6649(2)	87(2)
C(31)	-2933(5)	-8015(3)	-5953(2)	68(1)
C(32)	-4469(6)	-8684(4)	-5711(2)	80(1)

2.4.6 Crystallographic Study of 4a

Diffraction quality, colourless *needles* of **4a** were grown by the slow diffusion of *n*-hexane and a CH_2Cl_2 solution at -30°C. Intensity data were measured on an Enraf-Nonius CAD4 diffractometer operating with Mo-K_α *X*-radiation (λ_{bar} = 0.71073 Å). The single crystal was mounted in a glass capillary, which was held in a stream of nitrogen gas at 199(2) K.

Crystal data

$C_{11}H_{31}B_{10}NO_3$, M = 636.03, monoclinic, $P2_1/c$, a = 10.2159(11) Å, b = 13.5374(14) Å, c = 14.1497(14) Å, β = 91.050(9)°, V = 1956.5(4) Å^3, from least squares refinement of 25 reflections ($9 \leq \theta \leq 13°$) at 199(2) K, Z = 4 ion-pairs, D_c = 1.132 gcm^{-3}, μ(Mo-K_α) = 0.07 mm^{-1}, F(0,0,0) = 712e.

Data collection and reduction

Intensity data collected in the range $0<2\theta<50°$ by the ω-2θ scan method; ω-scan width (0.8+0.34tanθ), ω-scan speeds in the range 0.9 to 2.35°min^{-1}. The intensities of 3437 unique reflections (h -12 to 12, k 0 to 16, l 0 to 16) were measured (DATCOL).

Structure solution and refinement

The structure was solved using direct methods (SHELX86) and developed by iterative, full-matrix least-squares refinement and difference Fourier syntheses (SHELX76, SHELXTL). The unit cell contains four ion pairs and the cation is fully ordered. In the final model, all non-H atoms were refined anisotropically. The N-H and cage-H atoms were allowed free positional refinement. Methyl protons were set in idealised positions and allowed to ride on their respective carbon atoms with U(H) = 1.5 U(C_{Me}), whilst methylene protons were similarly fixed with U(H) = 1.2 U(C/B). The cage H-atoms were given a group isotropic thermal parameter, 0.0308(5) Å^2 at convergence.

Data were absorption corrected (DIFABS) and weighted according to $w^{-1} = [\sigma^2(F_o^2) + (0.0882P)^2 + 0.62P]$. Using 2450 observed data ($F_o > 4.0\sigma(F_o)$) R = 0.0586, wR_2 = 0.1559 and S = 1.041 for 254 variables. The maximum and

minimum residues in the final Fourier synthesis were 0.28 and -0.28 eÅ^{-3}, respectively. Atomic scattering factors were those inlaid in SHELXTL. Selected bond lengths (Å) and angles (°), fractional coordinates and equivalent isotropic thermal parameters of non-hydrogen atoms are in **Tables 4aA** and **4aB**, respectively.

A perspective view of a single anion is shown in **Figure 2.16**, which confirms that the carbaborane cage has the expected icosahedral geometry. The C(1)-C(2) distance is 1.672(3) Å, with B-C and B-B connectivities in the range 1.705(5) to 1.739(3) and 1.763(3) to 1.788(4) Å, respectively.

As observed for **3a**, the carboxylate moiety is twisted (θ = 36.5°) away from the preferred orientation determined for **2b** (θ = 87.5°). The carboxylate group is unable to adopt this more electronically favoured conformation due to the steric bulk of the C(2)-bound ether group. Consequently, the C(1)-C(2) connectivity is lengthened relative to **2b** (1.633(4) *vs* 1.672(3) Å), due to reduced conjugation between the cage and the carboxylate group. There is also an increase in the C(1)-C(101) bond length (1.541(4) *vs*. 1.562(3) Å). These increases in connectivity and bond lengths are similar to those observed for compound **3a**, indicating a similar steric size of the ether group (in this conformation) to the methyl group. The ether group bends back, at the C(01) atom, to minimise steric interaction between itself and the carboxylate group on C(1) (the torsion angles C(1)-C(2)-C(01)-O(11) and C(2)-C(01)-O(11)-C(02) are 81.9 and 168.3°, respectively). The C(2)-C(01), C(01)-O(11) and O(11)-C(02) bond lengths are 1.518(3), 1.392(3) and 1.421(3) Å, respectively. This conformation of the ether group is similar to that observed in the structural determination of the parent carbaborane, 1-CH_2OCH_3-1,2-*closo*-$C_2B_{10}H_{11}$.[14a]

As for **3a**, the carboxylate moiety is almost planar (σ = 0.0030 Å), with an O(101)-C(101)-O(102) bond angle of 128.47(20)°. There is also hydrogen bonding between the ion pair (H(001)···O(101) = 1.669 Å) causing slight lengthening of the C(101)-O(101) bond, relative to C(101)-O(102) (1.251(3) *vs*. 1.215(3) Å, respectively). Again, the carboxylate function bends slightly towards the ether group, although, unlike for **3a**, the C(2) substituent does not bend towards the carboxylate group. The θ value of the carboxylate group is much less than that for the unsubstituted species, **2b**, and similar to

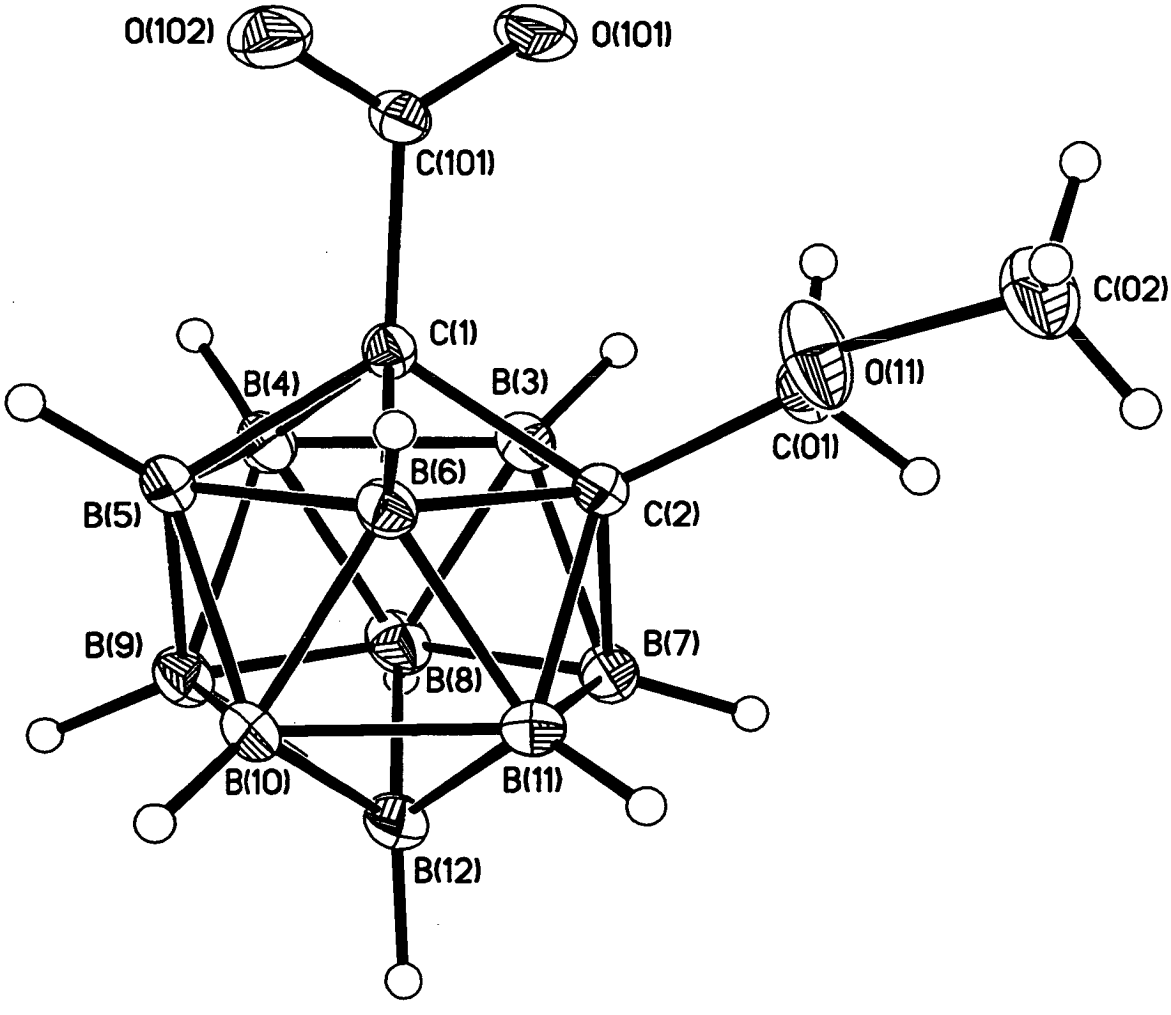

Figure 2.16 Perspective View of [1-CO_2-2-CH_2OCH_3-1,2-*closo*-$C_2B_{10}H_{10}$]$^-$

Table 4aA Selected Bond Lengths (Å) and Angles (°) for **4a**

C(1)-C(101)	1.562(3)	C(1)-C(2)	1.672(3)
C(1)-B(4)	1.705(3)	C(1)-B(5)	1.711(3)
C(1)-B(6)	1.716(3)	C(1)-B(3)	1.734(3)
C(2)-C(01)	1.518(3)	C(2)-B(11)	1.706(3)
C(2)-B(7)	1.708(3)	C(2)-B(3)	1.720(3)
C(2)-B(6)	1.739(3)	B(3)-B(8)	1.764(4)
B(3)-B(7)	1.772(4)	B(3)-B(4)	1.776(4)
B(4)-B(8)	1.778(4)	B(4)-B(5)	1.788(4)
B(4)-B(9)	1.785(4)	B(5)-B(6)	1.763(4)
B(5)-B(10)	1.769(4)	B(5)-B(9)	1.776(4)
B(6)-B(10)	1.773(4)	B(6)-B(11)	1.783(4)
B(7)-B(12)	1.763(4)	B(7)-B(8)	1.763(4)
B(7)-B(11)	1.785(4)	B(8)-B(9)	1.781(4)
B(8)-B(12)	1.785(5)	B(9)-B(12)	1.768(4)
B(9)-B(10)	1.776(4)	B(10)-B(12)	1.779(4)
B(10)-B(11)	1.781(4)	B(11)-B(12)	1.772(4)
C(101)-O(102)	1.215(3)	C(101)-O(101)	1.251(3)
C(01)-O(11)	1.392(3)	O(11)-C(02)	1.421(3)
N-C(31)	1.494(3)	N-C(11)	1.496(3)
N-C(21)	1.505(3)	C(11)-C(12)	1.507(3)
C(21)-C(22)	1.498(3)	C(31)-C(32)	1.501(3)

C(101)-C(1)-C(2)	118.2(2)	C(101)-C(1)-B(4)	121.8(2)
C(101)-C(1)-B(5)	120.8(2)	B(4)-C(1)-B(5)	63.13(14)
C(101)-C(1)-B(6)	115.9(2)	C(2)-C(1)-B(6)	61.73(13)
B(5)-C(1)-B(6)	61.91(14)	C(101)-C(1)-B(3)	118.0(2)
C(2)-C(1)-B(3)	60.62(13)	B(4)-C(1)-B(3)	62.18(14)
C(01)-C(2)-C(1)	120.2(2)	C(01)-C(2)-B(11)	120.3(2)
C(01)-C(2)-B(7)	119.1(2)	B(11)-C(2)-B(7)	63.0(2)
C(01)-C(2)-B(3)	116.4(2)	C(1)-C(2)-B(3)	61.48(13)
B(7)-C(2)-B(3)	62.3(2)	C(01)-C(2)-B(6)	119.1(2)
C(1)-C(2)-B(6)	60.39(13)	B(11)-C(2)-B(6)	62.34(14)
C(2)-B(3)-C(1)	57.90(12)	C(2)-B(3)-B(7)	58.56(14)
B(8)-B(3)-B(7)	59.8(2)	C(1)-B(3)-B(4)	58.11(13)
B(8)-B(3)-B(4)	60.3(2)	C(1)-B(4)-B(3)	59.71(13)
B(3)-B(4)-B(8)	59.5(2)	C(1)-B(4)-B(5)	58.60(13)
B(8)-B(4)-B(9)	60.0(2)	B(5)-B(4)-B(9)	59.61(14)
C(1)-B(5)-B(6)	59.19(13)	B(6)-B(5)-B(10)	60.25(14)
B(10)-B(5)-B(9)	60.1(2)	C(1)-B(5)-B(4)	58.28(13)
B(9)-B(5)-B(4)	60.1(2)	C(1)-B(6)-C(2)	57.88(12)
C(1)-B(6)-B(5)	58.90(13)	B(5)-B(6)-B(10)	60.0(2)
C(2)-B(6)-B(11)	57.95(13)	B(10)-B(6)-B(11)	60.12(14)
B(12)-B(7)-B(8)	60.8(2)	C(2)-B(7)-B(3)	59.20(14)
B(8)-B(7)-B(3)	59.9(2)	C(2)-B(7)-B(11)	58.44(14)
B(12)-B(7)-B(11)	59.9(2)	B(3)-B(8)-B(7)	60.3(2)
B(3)-B(8)-B(4)	60.20(14)	B(4)-B(8)-B(9)	60.2(2)
B(7)-B(8)-B(12)	59.6(2)	B(9)-B(8)-B(12)	59.4(2)

B(12)-B(9)-B(10)	60.2(2)	B(5)-B(9)-B(10)	59.8(2)
B(12)-B(9)-B(8)	60.4(2)	B(5)-B(9)-B(4)	60.28(14)
B(8)-B(9)-B(4)	59.8(2)	B(5)-B(10)-B(6)	59.70(14)
B(5)-B(10)-B(9)	60.1(2)	B(9)-B(10)-B(12)	59.7(2)
B(6)-B(10)-B(11)	60.23(14)	B(12)-B(10)-B(11)	59.7(2)
B(12)-B(11)-B(10)	60.1(2)	C(2)-B(11)-B(7)	58.53(14)
B(12)-B(11)-B(7)	59.4(2)	C(2)-B(11)-B(6)	59.71(13)
B(10)-B(11)-B(6)	59.64(14)	B(7)-B(12)-B(11)	60.7(2)
B(9)-B(12)-B(10)	60.1(2)	B(11)-B(12)-B(10)	60.2(2)
B(7)-B(12)-B(8)	59.6(2)	B(9)-B(12)-B(8)	60.2(2)
O(102)-C(101)-O(101)	128.5(2)	O(102)-C(101)-C(1)	116.6(2)
O(101)-C(101)-C(1)	114.9(2)	O(11)-C(01)-C(2)	110.0(2)
C(01)-O(11)-C(02)	111.8(2)	C(31)-N-C(11)	112.0(2)
C(31)-N-C(21)	110.9(2)	C(11)-N-C(21)	113.7(2)
N-C(11)-C(12)	112.3(2)	C(22)-C(21)-N	115.4(2)
N-C(31)-C(32)	112.27(10)		

Table 4aB Atomic Coordinates (x 10^4) and Equivalent Isotropic Thermal Parameters ($Å^2$ x 10^3) for **4a**

	x	y	z	U(eq)
C(1)	-2259(2)	2690(2)	3682(1)	23(1)
C(2)	-3163(2)	3511(2)	4264(1)	24(1)
B(3)	-3659(2)	2297(2)	4246(2)	29(1)
B(4)	-3241(3)	1858(2)	3107(2)	30(1)
B(5)	-2458(2)	2839(2)	2487(2)	27(1)
B(6)	-2366(2)	3871(2)	3245(2)	26(1)
B(7)	-4793(2)	3277(2)	4093(2)	33(1)
B(8)	-4869(3)	2238(2)	3342(2)	37(1)
B(9)	-4137(3)	2575(2)	2257(2)	34(1)
B(10)	-3591(3)	3818(2)	2343(2)	33(1)
B(11)	-3994(3)	4257(2)	3488(2)	33(1)
B(12)	-5080(3)	3452(2)	2872(2)	39(1)
C(101)	-903(2)	2388(2)	4121(2)	28(1)
O(101)	-949(2)	2015(2)	4928(1)	53(1)
O(102)	50(2)	2530(1)	3637(1)	43(1)
C(01)	-2689(2)	3912(2)	5212(2)	30(1)
0(11)	-1799(2)	4675(1)	5075(1)	49(1)
C(02)	-1529(3)	5200(2)	5926(2)	50(1)
N	1410(2)	1675(1)	5767(1)	31(1)
C(11)	1132(2)	1111(2)	6650(2)	29(1)
C(12)	192(2)	270(2)	6475(2)	41(1)
C(21)	2138(2)	1086(2)	5043(2)	45(1)
C(22)	3487(2)	762(2)	5338(2)	41(1)
C(31)	2089(2)	2630(2)	5971(2)	48(1)
C(32)	1223(2)	3353(2)	6461(2)	79(1)

that observed for **3a**, again indicating the similar steric bulk of Me and CH_2OCH_3.

2.4.7 Overview

X-ray diffraction studies on a series of carbaborane carboxylate salts, the anions of which are of the general type [1-CO_2-2-R-1,2-*closo*-$C_2B_{10}H_{10}$]$^-$ (R = H, **2b**, CH_3, **3a**, CH_2OCH_3, **4a**) have revealed that the carboxylate group has a preferred conformation, which is realised if R = H. The conformation predicted from EHMO considerations (θ = 90°) is extremely close to that observed by an X-ray diffraction study (θ = 87.5°) of the anion [1-CO_2-1,2-*closo*-$C_2B_{10}H_{11}$]$^-$ When the C(2)-bound proton is substituted by a larger group, such as CH_3 or CH_2OCH_3, the carboxylate cannot adopt the preferred conformation due to steric repulsion between the two C_{cage}-bound substituents and is forced to adopt conformations defined by θ = 34.0 and 36.5°, respectively. This deviation from the most stable conformation, reduces conjugation between the cage and the carboxylate moiety, causing lengthening of the C(1)-C(2) and C(1)-C(101) distances (**Table 2.4**).

Table 2.4 C(1)-C(2), C(1)-C(101) (Å) and θ(°) for compounds **2b**, **3a** and **4a**

Compound	C(1)-C(2)/(Å)	C(1)-C(101)/(Å)	θ/(°)
2b	1.633(4)	1.541(4)	87.5
3a	1.674(6)	1.552(8)	34.0
4a	1.667(4)	1.571(4)	36.5

Moreover, these increases in the C(1)-C(2) and C(1)-C(101) distances and decreases in θ in **3a** and **4a**, relative to **2b**, are remarkably similar indicating that the methyl and ether group (in this 'bent-back' conformation) have a similar steric bulk.

There are many examples of compounds where the π-systems of a carboxylate and another delocalised system overlap, leading to the mean planes of the two π-systems lying almost coplanar. For example the dihedral angles between the phenyl and carboxylate groups in the metal dimer $Cr_2(O_2CPh)_4(PhCO_2H)_2$ (**Fig. 2.17**) are 8 and 12°, which correspond to θ values of 82 and 78°, respectively (when the phenyl group is substituted by

anthracene, however, steric crowding increases the dihedral angles to 45 and 69°; θ = 45 and 21°, respectively).

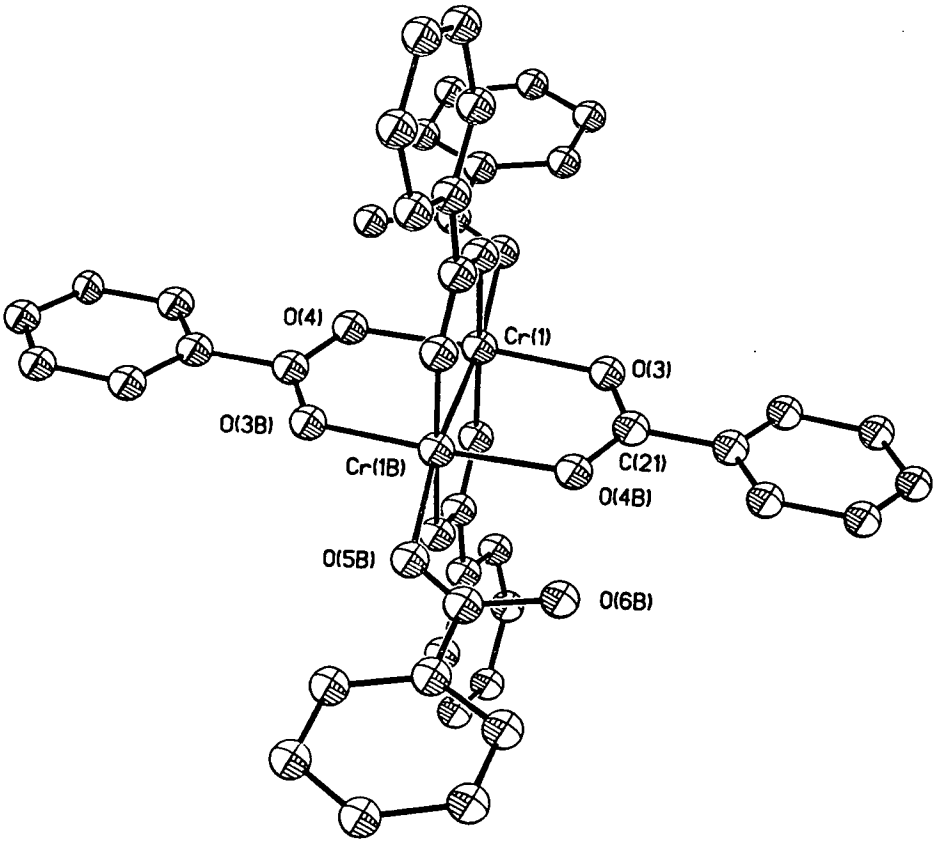

Figure 2.17 Perspective View of $Cr_2(PhCO_2)_4(PhCO_2H)_2$

There are many examples of other carboxylate-type ligands adopting this conformation, including *o*-Br-$C_6H_4CO_2$ and *o*-CO_2-C_5H_4N.

Recently, the first examples of structurally characterised carbaborane carboxylates have been reported.[11] Two of these are derived from 1,2-*closo*-C_2B_{10} cages and are shown below (**Fig. 2.18**).[11a] However, due to the extreme steric requirements of these clusters, none of the carboxylate moieties can adopt a conformation for which θ = 90°. There has also been a structural study of a 1,7-C_2B_{10} derivative, $\{[(1\text{-}CO_2\text{-}1,7\text{-}C_2B_{10}H_{11})Bu_2Sn]_2O\}_2$, which has been shown to possess anti-tumour activity.[11b] The C-O bond lengths are between 1.17(2) and 1.26(1) Å, similar to those for **2b**. The C-CO_2 bond length is 1.55(2) Å, longer than for **2b** (1.541(4) Å). This could possibly reflect a slight reduction in orbital overlap between the cage and the carboxylate moiety, which can no longer align itself with a C-C connectivity as is the case

for **2b**, although due to the relatively large errors in the atomic positions of the 1,7- species, the two bond distance are not considered to be significantly different.

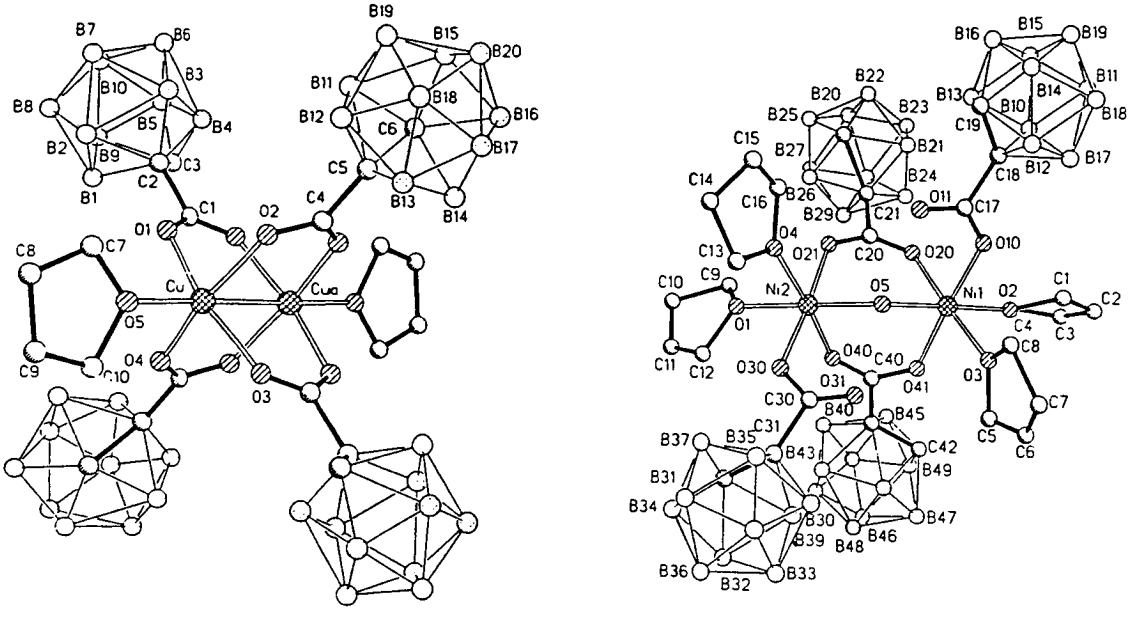

Figure 2.18 Perspective Views of $Cu_2(1\text{-}CO_2\text{-}1,2\text{-}closo\text{-}C_2B_{10}H_{11})_4(thf)_2$ and $Ni_2(1\text{-}CO_2\text{-}1,2\text{-}closo\text{-}C_2B_{10}H_{11})_4(thf)_2(H_2O).2$ thf

All three compounds showed hydrogen bonding between the two ions, specifically between the H(001) atom of the cation and the O(101) atom of the carboxylate group. The hydrogen bonds caused a slight increase in the C(101)-O(101) bond length relative to C(101)-O(102) due to loss of electron density and a reduction in the bond order. **Table 2.5** summarises the results of this hydrogen bonding.

Table 2.5 Summary of Hydrogen Bonding and its Effect Upon C-O bond Lengths (Å) in Compounds **2b**, **3a** and **4a**

Compound	H(001)···O(101)/(Å)	C(101)-O(101)/(Å)	C(101)-O(102)/(Å)
2b	1.610	1.235(4)	1.213(4)
3a	1.494	1.177(5)	1.156(5)
4a	1.669	1.251(3)	1.25(3)

2.5 σ-Bonded Carbagallaboranes

2.5.1 Synthesis of 5

The first Class 3 carbagallaborane, 1-CH_2OCH_3-2-{Me_2Ga}-1,2-*closo*-$C_2B_{10}H_{10}$, **5**, was synthesised in good yield by the reaction of $[Me_2GaCl]_2$ with 0.5 equivalents of Li[1-CH_2OCH_3-1,2-*closo*-$C_2B_{10}H_{10}$].

Distilled, degassed toluene was added to solid Li[1-CH_2OCH_3-1,2-*closo*-$C_2B_{10}H_{10}$] to afford an off-white suspension. To this was added half an equivalent of $[Me_2GaCl]_2$, which, due to its extreme air-sensitivity, was weighed and transferred within a glove-box to a Schlenk tube. The colourless crystals were then dissolved in distilled, degassed toluene and slowly added to the stirring suspension *via* a cannula. After several minutes it appeared that a fine white precipitate was forming, and so stirring was continued for 18 hours to allow the reaction to go to completion. After that time, stirring was discontinued and the very fine precipitate allowed to settle. Due to the extreme fineness of the precipitate, the supernatant was decanted off into another Schlenk tube, using a cannula to avoid any contact with air, instead of filtration. The solid was washed twice with small amounts of toluene, which were subsequently added to the first decantation. The toluene was removed *in vacuo* to afford a dry, off-white solid. The compound was seen to be slightly volatile and so vacuum sublimation was used to further purify it (the compound was found at this point not to be air-sensitive). Although successful, the yield of sublimed **5** was just a few milligrams of pure, white solid, sufficient only for a FAB mass spectrum. The compound was only readily soluble in toluene and benzene, and *d*-8 toluene was used to make up an nmr sample as a sealed tube.

Attempts to synthesise the analogous compounds 1-R-2-{Me_2Ga}-1,2-*closo*-$C_2B_{10}H_{10}$ (R = H, Ph), were unsuccessful, affording only (regenerated) carbaborane after work-up. We believe the main reason for this is the inability of either Ph or H to stabilise the gallium atom (see also **Section 2.5.2**).

2.5.2 Characterisation of 5

Since the air-stable product, **5**, was insoluble in chlorinated solvents, it was initially characterised by IR spectroscopy as a KBr disc. Terminal B-H stretches appeared as a broad band centred on 2565 cm^{-1}. The IR spectrum of the parent mono-ethercarbaborane has peaks attributable to the pendant ether group at 1483, 1407 and 1119 cm^{-1}. The spectrum of **5** showed several peaks in that region including ones at 1476, 1460, 1451, 1387, 1261, 1198 and 1126 cm^{-1}, making it impossible to ascertain whether or not the oxygen had coordinated to the gallium on the basis of the IR spectrum alone .

The ^1H nmr spectrum of **5** (**Fig. 2.19**), run in *d*-8 toluene, showed no evidence of the broad singlet at 2.98 ppm, indicating that substitution of the C_{cage} proton had occurred. There are three other singlets due to the OCH_2, OCH_3 and methyl protons in the ratio 2:3:6. The methylene and methyl resonances of the pendant ether group occur at 2.84 and 2.17 ppm, respectively, compared to similar resonances at 2.91 and 2.53 ppm for the parent carbaborane (also in *d*-8 toluene). The Ga-Me protons occur as a singlet at -0.39 ppm, which compares to a chemical shift of -0.1 ppm for the starting material, $[Me_2Ga(\mu\text{-}Cl)]_2$ and 0.01 ppm for the related compound $[Me_2Ga(\mu\text{-}H)]_2$.

There are several examples of gallium coordinated by an oxygen (or other donor) atom to stabilise the gallium atom and give it a full-shell ([Ar] $4s^2\ 3d^{10}\ 4p^6$) configuration, including the dimeric species $[Me_2Ga(\mu\text{-}OC_6H_4\text{-}2\text{-}OMe)]_2$,[29] (**Fig. 2.20**) where each of the $\{Me_2Ga\}$ fragments are bridged by two oxygen atoms and datively coordinated by the oxygen atom of a methoxy group. The chemical shift of the methoxy protons in this dimer is 3.13 ppm compared a typical shift for an uncoordinated, aryl-bound methoxy group of 3.8 to 3.9 ppm (that for 'parent,' 2-methoxyphenol, is 3.8 ppm).[30] These shifts to lower frequency of the methoxy protons upon coordination to a $\{GaMe_2\}$ fragment, suggest that there is a significant change in environment of the methoxy groups, which in the case of $[Me_2Ga(\mu\text{-}OC_6H_4\text{-}2\text{-}OMe)]_2$ was confirmed as being coordination of the methoxy oxygen to gallium and formation of a five membered ring

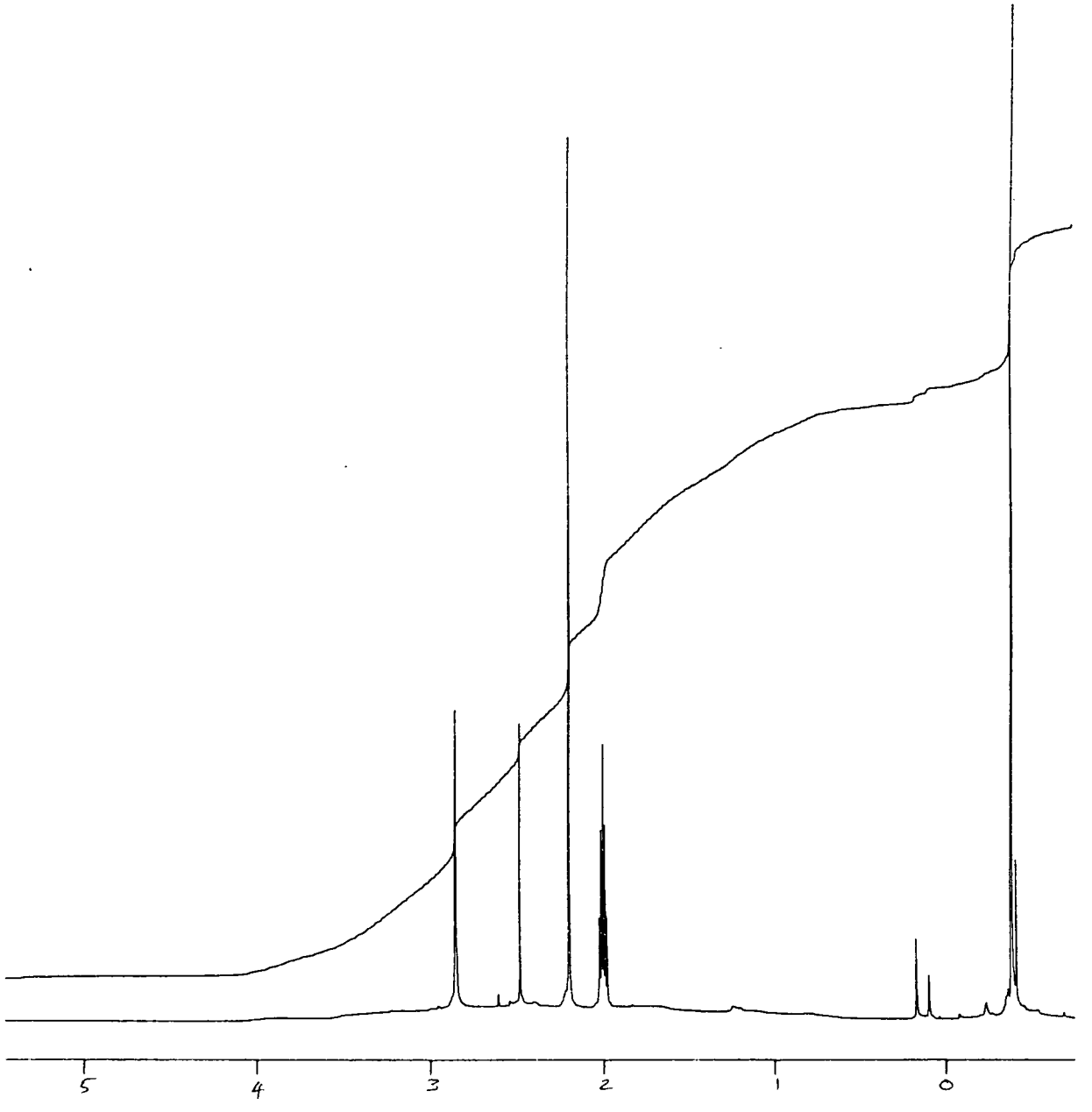

Figure 2.19 ^{1}H nmr spectrum of **5** (*d*-8 toluene) (360 MHz)

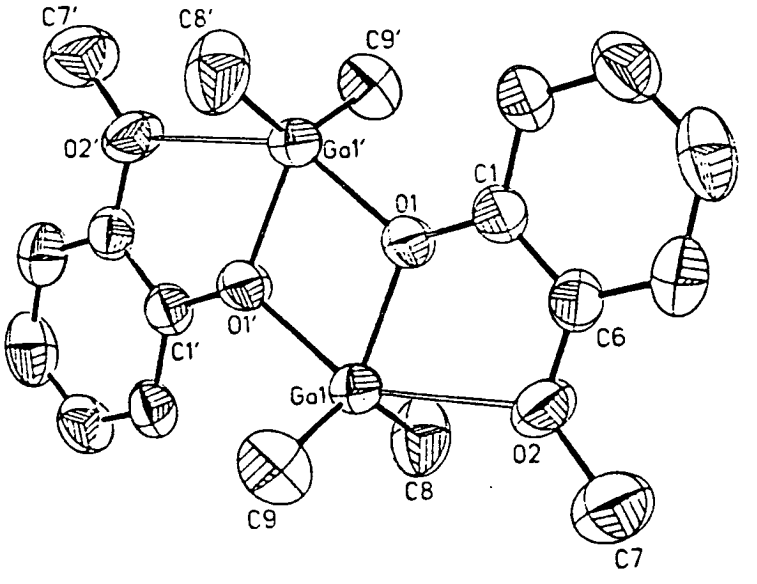

Figure 2.20 Perspective View of $[Me_2Ga(\mu\text{-}OC_6H_4\text{-}2\text{-}OMe)]_2$

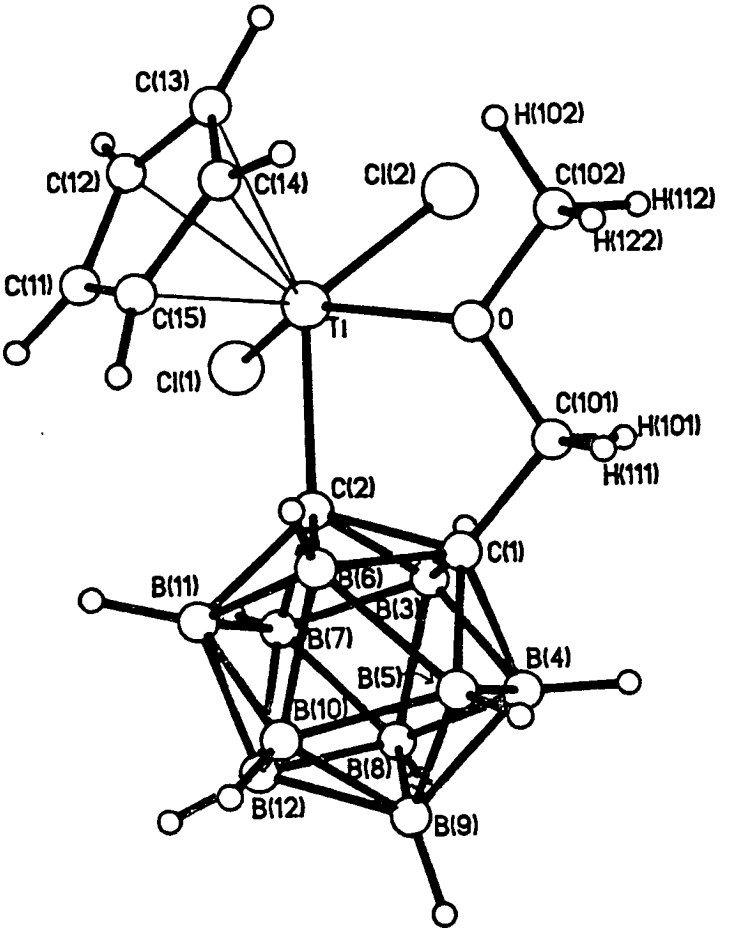

Figure 2.21 Perspective View of 1-CH_2OCH_3-{$CpTiCl_2$}-1,2-*closo*-$C_2B_{10}H_{10}$

There are several examples of carbametallaboranes, where a hetero atom coordinates to a metal centre σ-bonded to the adjacent cage carbon atom, including 1-CH_2OCH_3-{$CpTiCl_2$}-1,2-*closo*-$C_2B_{10}H_{10}$ (**Fig. 2.21**, above), where the ether oxygen atom coordinates a Ti(IV) (d^0) metal centre.[13] In the case of the carbatitanaborane, however, the shift of the methyl (3.71 ppm) and methylene (4.23 ppm) resonances are at higher frequency relative to the parent carbaborane (by 0.44 and 0.35 ppm, respectively), which was interpreted as a **reduction** in electron density at the ether substituent. Apart from the fact that one is comparing *d*-block and *p*-block metals, one must also consider the difference in the attached ligands; the titanium atom is bonded to three electron-withdrawing groups (Cp and two Cl), whereas the gallium atom is bonded to two electron-donating methyl groups.

The ^{11}B-{^1H} nmr spectrum of **5** shows five resonances consistent with the expected C_s symmetry. These are, from low- to high-field, in the ratio 1:1:2:2:4 and occur at -0.72, -1.16, -4.27, -8.74 and 9.57 ppm, respectively, the integral-four resonance being a 2+2 coincidence. This was compared with the ^{11}B-{^1H} nmr spectrum for the parent compound (*d*-8 toluene), which showed a similar shielding pattern with ^{11}B-{^1H} resonances at slightly higher frequencies (substitution of the C_{cage} proton caused the mean ^{11}B chemical shift to increase from -6.99 to -6.62 ppm), consistent with a loss of electron density from the carbaborane cage.

A FAB mass spectrum was recorded and the molecular ion peak was observed at 287 amu, which was fully consistent with the proposed structure.

In the absence of crystals suitable for an X-ray diffraction study, it is not possible to unambiguously determine whether or not the ether oxygen atom is coordinated to the gallium atom on the basis of IR and nmr data alone. We do hypothesise, however, that there **is** coordination of the ether oxygen atom to the gallium centre, given that compound **5** is highly air-stable. We feel that such stability could only be realised by coordination of the ether oxygen atom to the metal affording the gallium atom a desirable, full shell ([Kr]) configuration. There are, moreover, several precedents for intramolecular coordination in carbametallaboranes containg a CH_2OCH_3 substituent. The proposed structure, which is not inconsistent with the IR and nmr spectroscopic data, is given below in **Figure 2.22**.

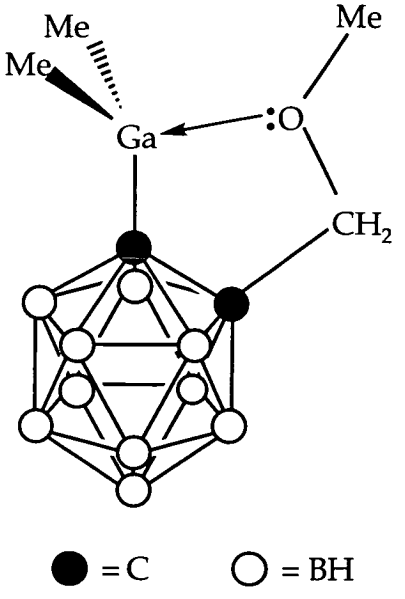

Figure 2.22 Proposed Structure of **5**

2.6 Conclusions

1-Ph-1,2-*closo*-$C_2B_{10}H_{11}$, **1**, has been obtained in high yield by improvement of the recrystallisation step. Diffraction quality crystals were grown and the molecular structure determined by an X-ray diffraction study. The orientation of the phenyl ring with respect to the cage (θ = 67.7(3)°) was similar to that calculated to be the most stable orientation by Hofmann and Schleyer (θ = 65°). The phenyl ring was not able to adopt the conformation predicted from EHMO calculations by Lewis and Welch (θ = 90°), due to the steric interaction between the C_{cage} proton and the phenyl *ortho*-protons. The C(1B)-C(2B) distance is 1.640(5) Å, similar to that of of 1,2-*closo*-$C_2B_{10}H_{12}$ (1.65(5) Å - electron-diffraction study), but significantly less than that of 1,2-Ph_2-1,2-*closo*-$C_2B_{10}H_{10}$ (1.726 Å - mean value). These parameters for **1** compare well with a subsequent structural determination of a second polymorph (θ = 71.2(2)°, C(1)-C(2) = 1.649(2) Å).

The ^{11}B-{^1H} nmr spectrum of compound **1** was fully assigned using ^{11}B-{^1H}/^{11}B-{^1H} (COSY), ^1H-{^{11}B}, ^1H-{$^{11}B_{selective}$} and ^1H-{^{11}B}/^1H-{^{11}B} (COSY) experiments. These results compared well with the IGLO calculations performed by Hofmann and Schleyer and were also similar to those obtained by the full assignment of 1-CH_2OCH_3-1,2-*closo*-$C_2B_{10}H_{11}$. A TOCSY experiment was carried out and cross peaks were observed between all resonances.

A series of carbaborane carboxylic acids (**2-4**) were synthesised by the reaction of CO_2 with the appropriate mono-lithium salt, followed by hydrolysis with dilute HCl, and fully characterised by microanalysis and IR and nmr (^1H, ^{11}B-{^1H}) spectroscopies. The carboxylate salt derivatives (**2a**, **2b**, **3a** and **4a**), were synthesised by reaction of the appropriate carbaborane carboxylic acid with NEt_3 or $NEtMe_2$ in Et_2O, recrystallised from CH_2Cl_2/hexanes and similarly characterised. Diffraction quality crystals of **2b**, **3a** and **4a** were grown by solvent diffusion and the molecular structures determined from X-ray diffraction studies, the main purpose of which was to ascertain the conformation of the carboxylate function with respect to the carbaborane cage. For the unsubstituted carboxylate **2b**, the conformation was similar to that predicted by EHMO calculations (θ_{calc} = 90°, $\theta_{obs.}$ = 87.5°). Moreover, EHMO calculations showed this conformation gave the strongest overlap between C(1) and C(2) (and between the carboxylate group and the

cage), suggesting conjugation of the π-system of the carboxylate to the carbaborane. The conformations of the carboxylate functions in compounds **3a** and **4a** were 34.0° and 36.5°, respectively. This deviation from the preferred conformation observed for the unsubstituted species, **2b**, is due to the (similar) steric bulk of the methyl and ether groups on the adjacent C(1) carbon atoms. This causes lengthening of the C(1)-C(2) and C(1)-C(101) connectivities (as predicted by EHMO calculations), which are similar for both **3a** and **4a**, and consistent with a reduction in orbital overlap.

The carboxylate group of compound **2b** was shown to have a preferred conformation similar to that observed for the phenyl ring in compound **1**. Unlike **1** there were no repulsive interactions between the carboxylate group and the C_{cage} protons due to the greater C(1)-C(CO_2) distance compared to C(1)-C(Ph) (1.541(4) and 1.503(4) Å, respectively).

The ^{11}B-{^1H} nmr spectra showed that substitution of the C_{cage} proton by either CO_2H or $[CO_2]^-$ resulted in the removal of electron density from the carbaborane cage, as evinced by the deshielding of the ^{11}B nuclei. The carboxylic acid group was slightly more electron-withdrawing than the carboxylate moiety, although the difference in charge of the two species makes it difficult to draw any worthwhile conclusions from this.

The first example of a class 3 carbagallaborane, 1-CH_2OCH_3-2-{Me_2Ga}-1,2-*closo*-$C_2B_{10}H_{10}$, **5**, has been synthesised and fully characterised by microanalysis IR and nmr (^1H, ^{11}B-{^1H}) spectroscopies and by FAB mass spectrometry. The identity of the compound was confirmed by the ^1H nmr spectrum, which showed relative integrals of the methylene and methyl resonances of the ether group and the methyl resonances of the {Me_2Ga} fragment to be in the ratio 2:3:6. The broad singlet due to the C_{cage} proton had disappeared.

Although neither IR nor nmr spectroscopy afforded unequivocal evidence as to whether the oxygen atom was coordinated to the gallium atom or not, we hypothesise that it does in fact coordinate as the compound is highly air stable. Moreover, unsuccessful attempts to synthesise analogues of **5**, where it was not possible for a heteroatom to stabilise the gallium atom are also consistent with the above hypothesis.

Chapter 2 References

1 J. Bobinski, M.S. Cohen, M. Fein, N. Mayers and N.N. Schwartz, *Inorg. Chem.* , 1963, **2**, 1111.

2 R. Schaeffer, *J. Am. Chem. Soc.*, 1957, **79**, 1006.

3 K. Wade, *J. Chem. Soc., Chem. Commun.*, 1971, 792.

4 E.g. R.N. Grimes, "Carboranes," Academic Press, New York, 1970; and references therein.

5 (**a**) V.A. Brattsev, Yu.A. Chapovski, A.I. Klimova, O.Yu. Okhoblobystin, A.A. Ponomanenko, V.I. Stanko and L.I. Zakharkin, *Dokl. Akad. Nauk.SSR.*, 1964, **155**, 1119; (**b**) A.V. Grebennikov, A.V. Kazuntsev and L.I. Zakharkin, *Izv. Akad. Nauk. SSR Ser. Khim.*, 1967, 2079.

6 E.g. (**a**) W.N. Lipscomb, "Boron Hydrides," Benjamin, New York, 1963; (**b**) E. L. Muetterties and W.H. Knoth, "Polyhedral Boranes," Dekker, New York, 1968.

7 E.g. (**a**) T.D. McGrath and A.J. Welch, *Acta Cryst.*, 1995, **C51**, 649; (**b**) T.D. McGrath and A.J. Welch, *Acta Cryst.*, 1995, **C51**, 654.

8 Z.G. Lewis and A.J. Welch, *Acta Cryst.*, 1993, **C49**, 705.

9 P.T. Brain, J. Cowie, D.J. Donohoe, M. Hofmann, D. Hnyk, D.W.H. Rankin, D. Reed, B.D. Reid, H.E. Robertson, P.v.R. Schleyer and A.J. Welch, *Inorg. Chem.*, 1996, **35**, 1701.

10 D. Grafstein, J. Bobinski, J. Dvôrak, H. Smith, N. Schwartz, M.S. Cohen and M.M. Fein, *Inorg. Chem.*, 1963, **2**, 1089.

11 E.g. (**a**) O. Kriz, A.L. Rheingold, M. Shang and T.P. Fehlner, *Inorg. Chem.*, 1994, **33**, 3777; (**b**) M.Gielen, A Bouhdid, R. Willem, V.I. Brgadze, L.V. Ermanson and E.R.T. Tiekink, *J. Organometal. Chem.*, 1995, **501**, 277.

12 E.g. (**a**) D.A.T. Young, R.J. Wiersema and M.F. Hawthorne, *J. Am. Chem. Soc.*, 1971, **93**, 5687; (**b**) R.N. Grimes, W.J. Rademaker, M.L. Denniston, R.F. Bryan and P.T. Greene, *J. Am. Chem. Soc.*, 1972, **94**, 1865; (**c**) C.P. Magee, L.G. Sneddon, D.C Beer and R.N. Grimes, *J. Organomet. Chem.*, 1975, **86**, 159.

13 B.D. Reid, Ph.D. Thesis, University of Edinburgh, 1992.

14 E.g. (**a**) K.F. Shaw and A.J. Welch, *Polyhedron*, 1992, **11**, 157; (**b**) Reference 13; (**c**) T.D. McGrath, Ph.D. Thesis, University of Edinburgh, 1995.

15 R.N. Grimes, W.C. Hutton and T.L. Venable, *J. Am. Chem. Soc.*, 1982, **104**, 4716.

16 Z.G. Lewis, Ph.D. Thesis, University of Edinburgh, 1991.

17 (a) O. Ni Dhubhghaill, D. Reed and T.R. Spalding, *Polyhedron*, 1993, **12**, 1977; (**b**) D. Reed, G. Ferguson, B.L. Rühl, O. Ni Dhubhghaill and T.R. Spalding, *Polyhedron*, 1988, **7**, 117; (**c**) S. Hermanek, *Chem. Rev.* 1992, **92**, 325; (**d**) D. Reed, *Chem. Soc. Rev.*, 1993, **22**, 109.

18 (a) L. Braunschweiler and R.R. Ernst, *J. Magn. Reson.*, 1983, **53**, 521; (**b**) A. Bax and D.G. Davis, *J. Magn. Reson.*, 1985, **65**, 355.

19 D.J. Donohoe, D. Reed and A.J. Welch, *Polyhedron*, 1995, **14**, 961.

20 D.M.C. Smit, Personal Communication.

21 R.L. Thomas, G.M. Rosair and A.J. Welch, *Acta Cryst.*, 1996, **C52**, 1024.

22 T.D. McGrath and A.J. Welch, *Acta Cryst.*, 1995, **C51**, 646.

23 T.D. McGrath and A.J. Welch, *Acta Cryst.*, 1995, **C51**, 651.

24 A. Bondi, *J. Phys. Chem.*, 1964, **68**, 441.

25 W. Clegg, R. Coult, M.A. Fox, W.R. Gill, J.A.H. MacBride and K. Wade, *Polyhedron*, 1993, **12**, 2711.

26 L.I. Zakharkin and A.V. Grebennikov, Isz. Akad. Nauk. SSSR Ser. Khim., 1967, 1376.

27 D.H. Williams and I. Fleming, "*Spectroscopic Methods in Organic Chemistry*" (Third Edition), McGraw-Hill Book Company (UK) Limited, 1980, pp 45-55.

28 ICON8: J. Howell, A. Rossi, D. Wallace, K. Haraki and R. Hoffmann, *Quantum Chemistry Program Exchange*, University of Indiana, No. 344.

29 D.G. Hendershot, M. Barber, R. Kumar and J.P. Oliver, *Organometallics*, 1991, **10**, 3302.

30 "Aldrich Library of ^{13}C and ^{1}H FT Nmr Spectra," First Edition, C.J. Pouchert and J. Behnke, Aldrich Chemical Co., Inc., Milwaukee, 1992.

Chapter 3

σ-Bonded Carbaauraboranes

3.1 Introduction

Research into class 3 carbametallaboranes has been relatively neglected compared to the attention given those in class 1, which account for more than 90% of all reported carbametallaboranes. This is due, no doubt, to the misconception that carbaborane (and borane) clusters are electron-deficient.[1] This thinking is reflected by the literature, which, prior to 1992, included examples of *closo* carbametallaboranes attached only to transition metals with an electronic configuration of d^6 or greater. The rationale for this is presumably that the metal centre needs to be in a low oxidation state (e.g. Fe(II),[2] Rh(I)[3]), with the associated high number of valence electrons necessary to stabilise the 'weak' metal-carbon σ-bond.

This approach, however, does not take into account the 'non-classical' nature of the bonding in carbaborane (and borane) clusters. The geometries that these clusters adopt are a direct result of the overcoming of their 'classical' electron deficiency by their multi-centre, 'non-classical' bonding, so that they may no longer be considered as being electron deficient.

One such example of this misconception was the rationalisation of "unusual stability," of the gold-carbon σ-bond in the carbaauraborane 1-Me-2-{PPh_3Au}-1,2-*closo*-$C_2B_{10}H_{10}$, synthesised by Mitchell and Stone.[4] They reported that the above complex was stable to CF_3CO_2H in benzene, but that the related compound PPh_3AuMe degraded *via* cleavage of the Au-C_{Me} bond to afford $PPh_3AuO_2CCF_3$ (the former two compounds can be thought of being the same $\{PPh_3Au\}^+$ fragment bonded to the [1-Me-1,2-*closo*-$C_2B_{10}H_{10}$]$^-$ and $[CH_3]^-$ ligands, respectively). They ascribed this stability to "the electron-withdrawing effect of the car(ba)borane cage." However, this would require the $\{PPh_3Au\}^+$ fragment to act as an electron-donor, which runs counter to EHMO calculations that show such a fragment has low-lying *d*-orbitals, that are are not readily available for bonding.[5] An alternative explanation for the observed stability is that the Au-C_{cage} bond is being stabilised by the carbaborane cage, which is acting as

a σ-donor, pushing electrons towards the gold. Since the methyl ligand, itself a well-known, good σ-donor, can not equally stabilise the Au-C_{Me} bond, this suggests that the σ-donation from the carbaborane moiety is significant.

Moreover, nmr and single-crystal X-ray diffraction studies, as well as EHMO calculations, by Reid of similar class 3 carbaauraboranes[6] has provided further evidence which supports the hypothesis that the carbaborane cage is acting as an efficient σ-donor. They synthesised a series of compounds of the general type 1-R-2-{ER'$_3$Au}-1,2-*closo*-$C_2B_{10}H_{10}$ (R = CH_2OCH_3, Ph; R' = Ph, Et, Cy, *o*-tol; E = P or As) as well as the analogous ER'$_3$AuMe species.

Previous nmr studies had shown that for compounds of the type PR'$_3$AuX (X = Cl or Me), the ^{31}P nmr shift of the chloride species, to which the phosphine is necessarily *trans*, occurs at lower frequency than that of the analogous methyl species (between 13 (PEt_3) and 29 (P(*o*-tol)$_3$) ppm). Reid observed that for X = 1-R-1,2-*closo*-$C_2B_{10}H_{10}$ (R = CH_2OCH_3 or Ph) the ^{31}P resonance occurs between the two extremes, at between 1 and 8 ppm to higher frequency than PR'$_3$AuCl and at between 6 and 28 ppm to lower frequency than PR'$_3$AuMe (**Table 3.1**). Overall, this implies that the carbaborane is at least as good a σ-donor than methyl (exclusively a σ-donor), but not as good a donor as chloride, which can act both as a σ-donor and a π-donor).

Table 3.1 Comparison of the ^{31}P-{^{1}H} Chemical Shifts of Some PR'$_3$AuX Species

		δ ^{31}P/(ppm)	
R	**X = CH_3**	**X = carb***	**X = Cl**
Cy	60.0	55.6	54.3
Et	45.3	37.2	32.0
Ph	47.4	38.6	33.5
(*o*-tol)	37.4	16.6	8.62

(* carb = 1-CH_2OCH_3-1,2-*closo*-$C_2B_{10}H_{10}$)

Similar conclusions are drawn from the ^{11}B-{^{1}H} nmr spectra. When the C_{cage} H atom attached to the second cage-carbon is replaced by

an isolobal {PR_3Au} fragment in a mono-substituted carbaborane, there is a general shift to higher frequency, consistent with a loss of electron-density from the boron atoms i.e. deshielding, suggesting again that the cage is acting as a donor.

The most emphatic evidence that the carbaborane cage acts an electron donor, however, was the result of two single crystal X-ray diffraction studies on 1-CH_2OCH_3-2-{$AsPh_3Au$}-1,2-*closo*-$C_2B_{10}H_{10}$ and $AsPh_3AuMe$ (**Section 1.4.3**). Comparisons of the Au-C_{cage} and Au-C_{Me} bond lengths show the former to be the shorter of the two (2.039(8) Å and 2.124(28) Å, respectively), suggestive of the Au-C_{cage} bond being stronger than the corresponding Au-C_{Me} bond. This result was further investigated by EHMO calculations performed on two, related model compounds 1-{AsH_3Au}-1,2-*closo*-$C_2B_{10}H_{11}$ (**I**) and AsH_3AuMe (**II**). These were consistent with the crystallographic studies, in that, for the same Au-C bond length, the reduced overlap population matrix (ROPM) element, (essentially a measure of relative bond strengths) was greater for **I** than for **II**. Moreover, there was also a greater net charge localised on the gold atom for **I**. By looking at the individual atomic orbital contributions, it was found that a substantial proportion of this extra charge was localised in the 6*s* and $6p_z$ orbitals (the model defined the Au-C vector as being along the *z*-axis).

This chapter reports the extension of this work and offers yet more evidence of 1,2-*closo* carbaboranes acting as efficient σ-donors. The synthesis and characterisation of a series of carbaauraboranes (**6-13**) of the general type 1-R-2-{PR'_3Au}-1,2-*closo*-$C_2B_{10}H_{10}$ (R = Ph, R' = *o*-tol, **6**, Cy, **7**, Et, **8**, mes, **9**, C_6F_5, **10**; R' = *o*-tol, R = Ph, **6**, H, **11**, Me, **12**, ^{t}Bu, **13**) is reported (**Section 3.2**). **Section 3.3** details the synthesis and characterisation of some of the methyl analogues, PR_3AuMe (R = *o*-tol, **6a**, Cy, **7a**, Et, **8a**) as well as the novel phosphine gold chloride species $P(C_6F_5)AuCl$, **14**, and the product of the reaction of **14** with MeLi, $C_6F_5Au(C_6F_5)Me_2$, **15**. **Section 3.4** is a discussion of nmr studies of the two series of compounds 1-Ph-2-{PR'_3Au}-1,2-*closo*-$C_2B_{10}H_{10}$ (Compounds **6** to **10**) and 1-R-2-{$P(o\text{-tol})_3Au$}-1,2-*closo*-$C_2B_{10}H_{10}$ (Compounds **6** and **11** to **13**) and is related to EHMO calculations on a range of mono-anions, [1-R-1,2-*closo*-$C_2B_{10}H_{10}]^-$ (R = Ph, Me, H, CF_3), which examines the electronic influence (if any) of the σ bonded C(1) substituents on the C_2B_{10} cage (**Section 3.5**). The solid-state

structures of compounds **6-15** as determined by X-ray crystallography are presented and discussed in **Section 3.6**. Finally, the conclusions are reported (**Section 3.7**).

3.2 1-R-2-{PR′$_3$Au}-1,2-*closo*-$C_2B_{10}H_{10}$

3.2.1 Synthesis

Class 3, σ-bonded carbaauraboranes of the general type 1-R-2-{PR′$_3$Au}-1,2-*closo*-$C_2B_{10}H_{10}$ (R = Ph, R′ = *o*-tol, Cy, Et, mes, C_6F_5; R′ = *o*-tol, R = Ph, H, Me,^{t}Bu) were synthesised in varying yields (15 - 60%) by the addition of an ethereal solution of Li[1-R-1,2-*closo*-1,2-$C_2B_{10}H_{10}$] to a stirring ethereal suspension of PR′$_3$AuCl. After being stirred for two hours, the Et_2O was removed *in vacuo* and the resulting off-white solid extracted into CH_2Cl_2. The main by-product of the reaction, LiCl, was removed as a precipitate by filtration and the filtrate analysed by spot tlc to ascertain if the compound was impure and required further work-up before crystallisation (either in bulk or by solvent diffusion to afford diffraction quality crystals). If further purification was necessary, preparative tlc was used and the colourless mobile bands detected using a UV lamp. The bands were characterised by IR spectroscopy (to ascertain if the band was boron-containing) and, if necessary, by ^{1}H nmr spectroscopy. Parent carbaboranes were removed by triturating the reduced CH_2Cl_2 filtrate with *n*-pentane or hexanes. Synthesis of several of the compounds (**6**, **9** and **10**) caused the deposition of a dark purple precipitate (colloidal gold), which could not be removed by filtration. This colouration was easily removed by preparative tlc or by column chromatography. Full characterisation of all compounds was accomplished using IR and nmr (^{1}H, ^{11}B-{^{1}H} and ^{31}P-{^{1}H}) spectroscopies, microanalysis and ultimately X-ray diffraction studies.

The compounds were generally air-stable, both as solutions and indefinitely as crystalline solids. Solubility was high in chlorinated solvents, acetone and thf. Solubility was low, but significant in both *n*-pentane and hexanes (*i*- and *n*-hexane and petroleum ether (60-80)). As such, bulk recrystallisations were carried out by removal *in vacuo* of CH_2Cl_2 from a CH_2Cl_2/hexane solution to afford pure products as either colourless microcrystals or white solids.

All compounds, **6-13**, were recrystallised to give colourless, diffraction quality crystals in the form of needles, blocks or plates. These crystals were grown by slow diffusion of *i*-hexane (**11**, **13**), *n*-hexane (**6**, **7**,

10, 12) or petroleum ether (60-80) (**8, 9**) and CH_2Cl_2 solutions at either -30°C or room temperature, **9**. Needles of **13** were found to contain solvent (CH_2Cl_2), which was lost after several hours out of the mother liquor, making them unsuitable for an X-ray diffraction study. As a result of this, diffraction quality plates of **13** were also grown by slow evaporation of an *i*-hexane solution at room temperature. These contained no solvent (^1H nmr) and as such were suitable for an X-ray diffraction study.

3.2.2 Characterisation

This section describes the characterisation of compounds **6 - 13**, which are of the general type 1-R-2-{PR'_3Au}-1,2-*closo*-$C_2B_{10}H_{10}$, where R' = *o*-tol, **6**, Cy, **7** ,Et, **8**, mes, **9**, and C_6F_5, **10**, for R = Ph and where R = Ph, **6**, H, **11**, Me, **12**, and ^{t}Bu, **13**, for R' = *o*-tol. The IR spectra and microanalysis data are discussed in general, whilst the nmr (^1H, ^{11}B-{^1H}, and ^{31}P-{^1H}) spectra are discussed for each compound. Shielding patterns are always quoted from low- to high-field. A more detailed discussion of the nmr studies of the two series of compounds follows in **Sections 3.4.1** (**6 - 10**) and **3.4.2** (**6, 11 - 13**).

Initial characterisation was by IR spectroscopy, with spectra being run as CH_2Cl_2 solutions. This was particularly useful in ascertaining if compounds that had been isolated by preparative tlc were boron containing, by examining the 2500-2700 cm^{-1} region for the strong, broad absorption band indicative of B-H_{exo} stretches. All compounds were submitted for microanalysis in crystalline form and were in excellent agreement with the calculated figures.

The ^1H nmr spectrum of compound **6** consists of overlapping multiplets in the aromatic region between 7.65 and 6.69 ppm, due to the five protons on the C(1)-phenyl ring and the twelve protons of the three *ortho*-tolyl rings. The 2-Me resonance is a sharp singlet occuring at 2.35 ppm and integrates against the aromatic protons in the expected ratio 9:17. The range of resonances in the ^{11}B-{^1H} nmr spectrum is very narrow (1.63 to -5.98 ppm), which seems to be typical for these types of compounds. Consequently, there are several multiple coincidences, with the shielding pattern showing resonance integrals in the ratio 2:2:6. The lowest field resonance is probably a 1+1 coincidence, since the two unique boron nuclei

in 1,2-*closo*-C_2B_{10} systems, B(9) and B(12), generally occur at a much higher frequency (several ppm) than the other nuclei.[7] The highest field resonance is a 2+2+2 coincidence. The spectrum is consistent with the molecule possessing C_s symmetry. A sharp singlet at 17.50 ppm is observed in the $^{31}P-\{^1H\}$ nmr spectrum.

The ^1H nmr spectrum of compound **7** shows several proton environments within the two *exo* substituents. Again, there are five phenyl protons, which integrate against the methylene (30) and methylidene (3) protons in the ratio 5:33. The phenyl protons appear as two distinct signals; a doublet at 7.73 ppm (*ortho*-protons, 2H) and overlapping multiplets at 7.16 ppm (*meta*- and *para*-protons, 3H). The cyclohexyl protons appear as unresolved multiplets between 1.96 and 0.99 ppm. The $^{11}B-\{^1H\}$ nmr spectrum is consistent with the expected C_s symmetry, having resonance integrals in the ratio 1:1:4:4 (the integral-four resonances being two, 2+2 coincidences). Again the $^{31}P-\{^1H\}$ nmr spectrum shows a singlet, which occurs at 56.11 ppm.

Similar resonances, slightly shifted relative to those for compound **7**, are observed in the aromatic region of the ^1H nmr spectrum of compound **8**. The methylene and methyl signals from the PEt_3 ligand are observed as multiplets at 1.57 and 1.17 ppm, respectively. These three resonances are in the ratio 5:6:9. The methylene resonance is split by the methyl protons ($^3J_{H-H}$ = 7.4Hz) to give a quartet before being further split by the phosphorous atom ($^2J_{P-H}$ = 10.0Hz) to give the observed (overlapping) doublet of quartets. Similarly, the methyl resonance is split by the methylene protons and the phosphorous atom ($^3J_{P-H}$ = 18.4 Hz) to give a doublet of triplets. Clearly, $^3J_{P-H}$ is greater than $^2J_{P-H}$, which is typically the case.[8] Again, there are multiple coincidences in the $^{11}B-\{^1H\}$ nmr spectrum, the resonance integrals being in the ratio 2:2:6. The highest field resonance is not a full coincidence, merely very broad due to overlapping. That at lowest field is probably a 1+1 coincidence for similar reasons to those given above. The $^{31}P-\{^1H\}$ nmr spectrum shows a singlet at 37.37 ppm.

The ^1H nmr spectrum of compound **9** shows three main resonances. The aromatic region contains several multiplets, which correspond to the five C(1)-phenyl protons and the two ring protons of

each of the three mesityl groups (11H in total). The other two resonances are due to the 2,6-Me and 4-Me protons, which appear as singlets at 2.32 (18H) and 1.58 (9H) ppm, respectively. The $^{11}B-\{^1H\}$ nmr spectrum again contains coincidental resonances, the integrals of which are in the ratio 2:2:6, the lowest and highest field resonances probably being 1+1 and 2+2+2 coincidences, respectively. The $^{31}P-\{^1H\}$ nmr spectrum shows a singlet at 5.54 ppm.

In the case of **10**, only C(1)-phenyl protons are readily visible, occuring as multiplets in the ^1H nmr spectrum. It was not possible therefore, to accurately integrate these against other protons in the compound, although as described previously, there are two distinct signals due to *ortho-* (7.68 ppm) and *meta-* and *para*-protons (7.06 ppm), which are in the relative ratio 2:3. Integration of the $B-H_{exo}$ region, although not very accurate, did afford a ratio of $B-H_{exo}$ to C_6H_5 of approximately 10:5. The $^{11}B-\{^1H\}$ nmr spectrum affords resonances with integrals in the ratio 1:1:4:4 (the integral-four resonances being two, 2+2 coincidences). The $^{31}P-\{^1H\}$ nmr spectrum consists of an unresolved multiplet centred at -19.35 ppm.

The ^1H nmr spectrum of **11** was run using crystals which did not contain any solvent of crystallisation (CH_2Cl_2) and, as such, contains three distinct signals, the integrals of which are in the ratio 12:1:9. The highest frequency resonance is due to the twelve *ortho*-tolyl protons, whilst the broad resonance at 3.97 ppm is due to the C_{cage} proton. The 2-Me protons resonate as a singlet at 2.50 ppm. The integrals of the the $^{11}B-\{^1H\}$ resonances are in the ratio 2:2:2:2:2. Again, the high frequency resonance at 0.26 ppm is likely to be a 1+1 coincidence, especially since it is more than 5 ppm higher than the next highest frequency resonance. The $^{31}P-\{^1H\}$ nmr spectrum consisists of a singlet at 16.51 ppm.

Compound **12** shows the *ortho*-tolyl protons resonating at a slightly lower frequency than that for compound **11**. The two resonances at 2.69 and 1.98 ppm are in the ratio 3:1 and are assigned to the 2-Me and C(1)-Me protons, respectively. From low- to high-field, the protons are in the ratio 12:9:3. There are several coincidences in the $^{11}B-\{^1H\}$ spectrum, with resonances at 1.12, -4.45 and -5.58 ppm in the ratio 1:5:4. The integral-five

resonance is a 2+2+1 coincidence. The ^{31}P-{^{1}H} nmr spectrum consisists of a singlet at 17.47 ppm.

The ^{1}H nmr spectrum of compound **13**, which did not contain solvent of crystallisation (CH_2Cl_2), shows three types of protons. Again, there are twelve aromatic protons due to the *ortho*-tolyl groups. The other two resonances at 2.60 and 1.28 ppm are due to the 2-Me and ^{t}Bu protons, which can not be assigned solely on the basis of relative integral heights. The resonance at 2.60 ppm was assigned as being due to the 2-Me protons, however, by comparison of the shifts of the analogous protons in compounds **6**, **11** and **12** (2.35, 2.50 and 2.69 ppm, respectively). Hence, the remaining integral-nine resonance was assigned as being due to the ^{t}Bu protons. The resonance integrals of the ^{11}B-{^{1}H} spectrum are in the ratio 1:1:8, with the integral-eight resonance being a 2+2+2+2 coincidence. The ^{31}P-{^{1}H} nmr spectrum is a singlet at 17.21 ppm.

3.3 PR'_3AuMe, $P(C_6F_5)_3AuCl$ and $C_6F_5AuP(C_6F_5)Me_2$

3.3.1 Synthesis of PR'_3AuMe

Compounds **6a**, **7a** and **8a**, PR'_3AuMe (R = *o*-tol, Cy, Et) were successfully synthesised by methylation of appropriate phosphine gold chlorides, PR'_3AuCl, and characterised by $^{31}P-\{^1H\}$ nmr spectroscopy. These compounds can be thought of as analogues to compounds **6**, **7** and **8**, with the [1-Ph-1,2-*closo*-$C_2B_{10}H_{10}$]$^-$ anion being replaced by the isolobal $[CH_3]^-$ moiety.

Typically, 1.1 equivalents of MeLi in Et_2O was added dropwise to a stirring ethereal suspension of phosphine gold chloride. The potent nucleophile $[Me]^-$ attacks the gold centre with concomitant displacement of the labile chloride ligand. Excess MeLi was destroyed by the dropwise addition of distilled, degassed water, which also acts to dissolve the formed LiCl. The product was extracted into Et_2O and the ethereal layer dried by stirring over $MgSO_4$ for 18 hours, before being filtered and the filtrate reduced *in vacuo* to afford the compounds as a white solids. These solids were then recrystallised from CH_2Cl_2/hexanes.

Compounds **6a** and **7a** were air stable, both as solution for several hours and indefinitely as colourless, crystalline solids. Compound **8a**, however, was highly air-sensitive, turning purple in a matter of seconds upon exposure to air. As for compounds **6-13**, solubility was high in chlorinated solvents, thf and acetone and low, but appreciable in pentane and hexanes.

Diffraction quality, colourless crystals of **6a** and **7a** were grown by slow diffusion of *i*-hexane and CH_2Cl_2 (4:1) solutions at -30°C. Attempts to grow diffraction quality crystals of **8a** were unsuccessful.

Attempts to synthesise similar analogues of compounds **9** and **10** were unsuccessful. Upon addition of distilled water to the MeLi/$Pmes_3AuCl/Et_2O$ reaction mixture, it immediately turned dark purple. After a work-up, which included preparative tlc, ^1H nmr spectroscopy revealed that the starting material, $Pmes_3$ had been recovered.

3.3.2 Synthesis of $P(C_6F_5)_3AuCl$ (14)

The novel phosphine gold chloride species was synthesised by reacting two equivalents of $P(C_6F_5)_3$ with $HAuCl_4.3H_2O$ in EtOH. The orange solution gradually turned colourless over a period of ten minutes, with slight warming of the solution to speed the reaction. Reduction of the solvent *in vacuo* to approximately half volume precipitated the product as a white solid. Following removal of all of the solvent, the product was recrystallised in bulk from CH_2Cl_2/*i*-hexane to afford pure **14**. Diffraction quality, colourless blocks were grown by the slow diffusion of *i*-hexane and a CH_2Cl_2 solution at -30°C. Intensity data were collected from a single crystal, but no solution to the data was found in a number of different space groups.

3.3.3 Synthesis of $C_6F_5AuP(C_6F_5)Me_2$ (15)

The same methylation reaction as described in **Section 3.3.1** was also attempted with compound **14**. Upon addition of the MeLi to an ethereal suspension of **14**, the reaction mixture turned dark purple. The reaction mixture was worked up as described above to remove the purple/black precipitate, and fine, diffraction quality, colourless needles were grown, in relatively low yield (34%), by slow diffusion of *i*-hexane and a CH_2Cl_2 solution (4:1) at -30°C. The product was characterised by ^1H, ^{19}F-{^1H} and ^{31}P {^1H} nmr spectroscopies, microanalysis and ultimately by an X-ray diffraction study, the latter confirming it to be $C_6F_5AuP(C_6F_5)Me_2$.

3.3.4 Characterisation of PR'_3AuMe

Compounds **6a**, **7a** and **8a** were characterised by microanalysis (except **8a**, see **Section 3.3.1**) and ^{31}P-{^1H} nmr spectroscopy (comparison with literature values).

Microanalysis of the crystalline compounds **6a** and **7a** was in very good accordance with the calculated values.

All the compounds were observed as sharp singlets in the ^{31}P-{^1H} nmr spectra at 37.02 (**6a**), 60.02 (**7a**) and 46.52 ppm (**8a**), respectively, reflecting their relative basicities (Cy > Et > *o*-tol). These resonances are at

higher frequency relative to both the mono-phenylcarbaborane and chloride analogues, which also mirror this order of basicity. As the basicity of the phosphine increases, the electron density on the phosphorous atom is reduced and the resonances shift accordingly to higher frequency (**Table 3.2, Section 3.4.1**).

3.3.5 Characterisation of $P(C_6F_5)_3AuCl$

The $^{31}P-\{^1H\}$ nmr spectrum of **14** consists of a broad, unresolved multiplet centred at -32.02 ppm. The phosphorous atom can be assumed to be coupling to fluorine atoms in at least two, and possibly three, different environments, leading to the observed broad resonance.

The $^{19}F-\{^1H\}$ nmr spectrum shows three different environments at -128.00, -141.20 and -156.47 ppm with integrals in the ratio 2:1:2, respectively. The resonance at -141.20 ppm is assigned to the *para*-fluorine atoms, as there is only one of these *per* C_6F_5 ring. The resonance at -128.00 ppm is a broad doublet of doublets (apparent triplet; $^3J_{F-F}$ = 20.4Hz) and is tentatively assigned as being due to the *meta*-fluorine atoms, which couples to the *ortho*- and *para*-fluorines. The resonance at -156.47 ppm is also very broad and an apparent triplet similar to that at -128.00 ppm (although not as broad). It is not possible to measure the coupling constants for this multiplet, possibly due to the extra (smaller) coupling to the phosphorous atom, which places the resonances much closer together.

3.3.6 Characterisation of $C_6F_5AuP(C_6F_5)Me_2$

The ^1H nmr spectrum of **15** consists of a doublet of triplets centred at 2.05 ppm. The methyl proton resonance is split by the phosphorous atom ($^2J_{P-H}$ = 9.2Hz) to give a doublet, which is split further by coupling to the *ortho*-fluorine atoms on the C_6F_5 ring bonded directly to the phosphorous atom ($^5J_{F-H}$ = 1.5Hz).

The $^{31}P-\{^1H\}$ nmr spectrum of **15**, is an apparent quintet centered at 10.98 ppm. The quintet is actually two overlapping triplets due to coupling to the two types of *ortho*-fluorine atoms. The coupling constant is approximately 10 Hz, with the multiplet exhibiting fine structure due to the phosphorous atom coupling to the other fluorine atoms.

The ^{19}F-{^{1}H} nmr spectrum of **15** exhibits six different fluorine environments corresponding to the two inequivalent C_6F_5 rings. The resonances occur at -116.50, -129.38, -146.23, -158.19, -158.35 and -162.58 ppm, with integrals in the ratio 2:2:1:1:2:2, respectively. The integral-one resonances are assigned as being due to the *para*-fluorine atoms, and are triplets due to coupling to the *meta*-flourine atoms ($^{3}J_{F-F}$ = 21.5 and 20.0 Hz for the resonances at -146.23 and -158.19 ppm, respectively). The resonance at -158.35 ppm is a doublet of apparent triplets with splittings of 8Hz (doublet) and 20Hz (apparent triplet). Comparison of the ^{19}F chemical shifts of **15** with those of **15** allows tentative assignment of the resonances at -129.38, -146.23 and -158.35 (*meta*, *para* and *ortho*, respectively) as being due to the phosphorous bound C_6F_5 ring. The remaining, unassigned resonances are those at -116.46 (overlapping doublet of doublets (apparent quartet), $^{3}J_{F-F}$ = 20Hz) and -162.58 ppm (overlapping doublet of doublet of doublets), $^{3}J_{F-F}$ = 20Hz, J_{F-X} = 8Hz) are assigned as the *meta* and *ortho* fluorine resonances, respectively. The 8Hz coupling to the *ortho* fluorines is not assigned, but could possibly be long range couplings to either phosphorous or the non-adjacent *meta* fluorine.

3.4 Nmr Studies

3.4.1 1-Ph-2-{PR'_3Au}-1,2-*closo*-$C_2B_{10}H_{10}$

The broad singlet at 3.97 ppm due to the C_{cage} H atom is not observed in the ^1H nmr spectra of compounds **6-10**, indicating it has been substituted by the isolobal {PR'_3Au} fragment. The shifts of the phenyl proton resonances of compounds **7**, **8** and **10** are very similar to those of the parent carbaboranes.

Comparison of the ^{31}P-{^1H} nmr shifts of compounds **6-10** reveal a shift to low-field with increasing basicity, as described by Tolman[9] (Cy > Et > *o*-tol > mes > C_6F_5). **Table 3.2** gives the ^{31}P chemical shifts of compounds **6-10** and the electronic parameters (ν) of the corresponding free phosphine, L (ν is the A_1 CO stretching frequency (cm^{-1}) of $Ni(CO)_3L$ in CH_2Cl_2).

Table 3.2 Variation of δ ^{31}P-{^1H} for Compounds **6-10** and of ν for the Free Phosphine (PR'_3)

R'	δ ^{31}P-{^1H}/(ppm)	ν/(cm^{-1})
Cy	56.11	2056.4
Et	37.37	2061.7
***o*-tol**	17.50	2066.6
mes	5.54	*
C_6F_5	-19.35	2090.9

(* the value of ν for L = $Pmes_3$ was not reported)

The more basic the phosphine, the higher the frequency of the ^{31}P-{^1H} resonance for 1-Ph-2-{PR'_3Au}-1,2-*closo*-$C_2B_{10}H_{10}$ and the lower the value of ν. As the basicity of the phosphine increases, so too does the degree of back-bonding into the π* orbitals of the *trans* carbonyl ligand. This reduces the bond order and hence the stretching frequency is reduced.

Previous reports have placed the ^{31}P-{^1H} chemical shifts of σ-bonded carbaauraboranes between those of the corresponding PR'_3AuX species (X = Cl, Me) and this is also observed for compounds **6-10**. Moreover, the shift of the carbaauraborane is much closer to that of the

corresponding phosphine gold chloride species than to that of the phosphine gold methyl (the shift to low field is approximately $^1/_3$ of the difference in shifts for PR'_3AuMe and PR'_3AuCl (**Table 3.3**).

Table 3.3 Comparison of the ^{31}P-{^1H} Chemical Shifts of PR'_3AuX with Respect to X

			δ ^{31}P/(ppm)		
R'	**(X =Me)**	Δ_1	**(X = carb)***	Δ_2	**(X = Cl)**
Cy	60.02	3.89	56.11	1.81	54.3
Et	46.52	9.15	37.37	5.37	32.00
***o*-tol**	37.02	19.52	17.50	8.88	8.62

(* **carb** = 1-Ph-1,2-*closo*-$C_2B_{10}H_{10}$; where Δ_1 is δ ^{31}P (X =Me) - δ ^{31}P (X = carb) and Δ_2 is δ ^{31}P (X = carb) - δ ^{31}P (X = Cl), respectively)

Moreover, the basicity of the phosphine decreases much more rapidly when the group *trans* to the phosphine is a carbaborane, again suggesting that the carbaborane moiety is an efficient σ-donor. This is best illustrated by comparing the differences in shifts of the PR'_3AuX species with decreasing phosphine basicity (**Table 3.4**).

Table 3.4 Comparison of the ^{31}P-{^1H} Chemical Shifts of PR'_3AuX with Respect to R

			δ ^{31}P/(ppm)			
		(R' = Cy)	Δ_a	**(R' = Et)**	Δ_b	**(R' = *o*-tol)**
	Me	60.0	13.48	46.52	9.50	37.02
X	**carb***	56.11	18.74	37.37	19.87	17.50
	Cl	54.30	22.30	32.00	23.28	8.62

(* carb = 1-Ph-1,2-*closo*-$C_2B_{10}H_{10}$; where Δ_a is δ ^{31}P (R' = Cy) - δ ^{31}P (R' = Et) and Δ_b is δ ^{31}P (R' = Et) - δ ^{31}P (R' = *o*-tol), respectively)

Comparison of the mean ^{11}B-{^1H} nmr shifts with the parent carbaborane reveals that substitution of the C_{cage} H atom with an isolobal {PR'_3Au} fragment causes deshielding of the the boron nuclei. **Table 3.5** shows that compounds **6-10** have all shifted to higher frequency with respect to the parent, indicating that the cage is donating electrons to the

the gold phosphine fragment. There is no correlation, however, between the basicity of the phosphine and the mean ^{11}B-{^1H} nmr shift.

Table 3.5 Mean ^{11}B-{^1H} Shifts and Chemical Shift Ranges for 1-Ph-2-R-1,2-*closo*-$C_2B_{10}H_{10}$

R	Mean Shift /(ppm)	Shift Range/(ppm)
H	-8.49	10.66
{PCy_3Au}	-3.82	7.31
{PEt_3Au}	-2.56	7.54
{P(*o*-tol)$_3$Au}	-3.06	7.61
{$Pmes_3Au$}	-2.83	6.10
{$P(C_6F_5)_3Au$}	-3.73	8.29

Moreover, the range is also consistently narrower for the carbaauraboranes relative to the parent carbaborane.

3.4.2 1-R-2-{P(*o*-tol)$_3$Au}-1,2-*closo*-$C_2B_{10}H_{10}$

As in **Section 3.4.1**, the broad resonance due to the C_{cage} H atom is not observed in the ^1H nmr spectra of compounds **6**, **12** and **13** due its substitution by the isolobal {P(*o*-tol)$_3$Au} fragment. This has a minimal effect on the shifts of the ^1H resonances of the C(1) substituents (it is not possible to compare the shifts of the phenyl protons, due to overlap of the aromatic *ortho*-tolyl proton resonances). The C_{cage} proton (**11**) and C_{cage} methyl (**12**) resonances are slightly shifted to higher field (Δ = 0.18 and 0.03 ppm, respectively), whilst those of the C_{cage} *tert*-butyl (**13**) (methyl) resonances are shifted very slightly to low-field (Δ = 0.06 ppm) (**Table 3.5**).

Table 3.6 Comparison of the ^{1}H and Mean ^{11}B Nmr Shifts of 1-R-2-X-1,2-*closo*-$C_2B_{10}H_{10}$

	δ ^{1}H/(ppm)		mean δ ^{11}B/(ppm)	
R	**(X = H)**	**(X = {P(*o*-tol)$_3$Au})**	**(X = H)**	**(X = {P(*o*-tol)$_3$Au})**
Ph	7.58-7.33	*	-8.49	-3.06
H	3.55	3.37	-10.08	-4.35
Me	2.01	1.98	-8.90	-5.93
^{t}Bu	1.22	1.28	-7.40	-4.50

(* not observable)

Similarly, the ^{11}B-{^{1}H} nmr shifts of both the parent carbaboranes (X = H) and the carbabauraboranes (X = {P(*o*-tol)$_3$Au}) are all similar with varying R (within 3 ppm of each other) again suggesting that the C(1) substituent has no effect on the electronic properties of the cage. Variation of X from H to {P(*o*-tol)$_3$Au}, however, causes deshielding of the boron nuclei. The mean shifts of the carbaauraboranes are between 5.73 and 2.90 ppm to lower field than those of the parent carbaboranes. The corollary to this deshielding of the boron nuclei is that the carbaborane cage is donating electron density to the gold phosphine fragment.

This lack of effect upon the donor properties of the carbaborane cage by the C(1) substituents is best emphasised by the ^{31}P-{^{1}H} nmr data (**Table 3.7**)

Table 3.7 ^{31}P-{^{1}H} Shifts for 1-R-2-{P(*o*-tol)$_3$Au}-1,2-*closo*-$C_2B_{10}H_{10}$

R	**Ph**	**H**	**Me**	**^{t}Bu**
δ ^{31}P/(ppm)	17.50	16.51	17.47	17.21

There is even less variation in the chemical shifts for the ^{31}P-{^{1}H} nmr data than that for the ^{11}B-{^{1}H} data. These results are fully consistent with X-ray crystallographic determinations of these compounds (**Section 3.6.2**) as well as EHMO calculations to calculate the HOMO energies of [1-R-1,2-*closo*-$C_2B_{10}H_{10}$]$^{-}$ (**Section 3.5**), both of which strongly suggested that the C(1)-bound substituents have no effect on the electronic properties of the carbaborane cage.

3.5 EHMO Calculations

Extended Hückel molecular orbital calculations were performed to determine the energy of the HOMO of anions of the general type [1-R-1,2-*closo*-$C_2B_{10}H_{10}]^-$, and thus an indication of the donor properties of the cage (the higher the energy, the better the donor), using a locally modified version of ICON8. Model parameters are given in **Table 3.8** below.

Tbale 3.8 Model Parameters used in EHMO Calculations on [1-R-1,2-*closo*-$C_2B_{10}H_{10}]^-$

Connectivity/Bond	Length/(Å)
C_{cage}-C_{cage}	1.65
C_{cage}-C	1.50
C_{cage}-B	1.7575
B-B	1.85
C-F	1.45
C_{aryl}-C_{aryl}	1.395
C-H	1.08
B-H	1.15

The calculations indicated that the energies of the anion HOMO's were almost identical, regardless of the electronic nature of the C(1) bound substituent (**Table 3.9**). In all cases, the HOMO's were localised at the C(2) carbon atom.

Table 3.9 HOMO Energies of [1-R-1,2-*closo*-$C_2B_{10}H_{10}]^-$

R	HOMO Energy/(eV)
Me	-10.531
H	-10.571
Ph ($\theta = 90^o$)	-10.534
Ph ($\theta = 0^o$)	-10.547
CF_3	-10.546

This result is entirely consistent with crystallographic studies on compounds **6**, **11**, **12** and **13**, which show that changing the C(1) bound substituent, R, in carbaauraboranes of the general type 1-R-2-{P(*o*-tol)$_3$Au}-1,2-*closo*-$C_2B_{10}H_{10}$ has no significant effect upon the Au-C(2) bond length (**Section 3.6.3**) and ^{31}P-{^1H} nmr studies which show the chemical shifts of the phosphorous nuclei to be within 1 ppm of each other.

3.6 Crystallographic Studies

A series of compounds of the type 1-R-2-{PR'_3Au}-1,2-*closo*-$C_2B_{10}H_{10}$ (R = Ph, R' = *o*-tol, **6**, Cy, **7**, Et, **8**, mes, **9**, C_6F_5, **10**; R' = *o*-tol, R = Ph, **6**, H, **11**, Me, **12**, ^{t}Bu, **13**) and PR'_3AuMe (R' = *o*-tol, **6a**, Cy, **7a**) have been structurally characterised by X-ray diffraction experiments. This section details the individual experimental and structural details, as well as any general trends observed within the series 1-Ph-2-{PR'_3Au}-1,2-*closo*-$C_2B_{10}H_{10}$ and 1-R-2-{$P(o\text{-tol})'_3Au$}-1,2-*closo*-$C_2B_{10}H_{10}$ (**Sections 3.6.1** and **3.6.3**, respectively). The crystallographic studies on $P(o\text{-tol})_3AuMe$ and PCy_3AuMe are discussed in **Section 3.6.2**, whilst that of $C_6F_5AuP(C_6F_5)Me_2$ is detailed in **Section 3.6.4**.

3.6.1 Crystallographic Studies of 1-Ph-2-{PR'_3Au}-1,2-*closo*-$C_2B_{10}H_{10}$

Crystallographic Study of 1-Ph-2-{$P(o\text{-tol})_3Au$}-1,2-*closo*-$C_2B_{10}H_{10}$ (6)

Colourless, diffraction quality *blocks* of **6** were grown by diffusion of *n*-hexane and a CH_2Cl_2 solution at -30°C. Intensity data were measured on an Enraf-Nonius CAD4 diffractometer operating with Mo-K_α *X*-radiation (λ_{bar} = 0.71073 Å). The single crystal was mounted in a glass capillary and the experiment performed at 291(2) K.

Crystal data

$C_{29}H_{36}B_{10}AuP$, M = 720.62, triclinic, *P*bar1, a = 10.529(7) Å, b = 10.658(3) Å, c = 15.104(6) Å, α = 104.70(3)°, β = 108.30(4)°, γ = 93.35(4)°, V = 1538.8(13) Å^3, from least squares refinement of 25 reflections ($9 \leq \theta \leq 12°$) at 291(2) K, Z = 2, D_c = 1.555 gcm^{-3}, μ(Mo-K_α) = 4.85 mm^{-1}, F(0,0,0) = 708e.

Data collection and reduction

Intensity data collected in the range $0<2\theta<50°$ by the ω-2θ scan method; ω-scan width (0.8+0.34tanθ), ω-scan speeds in the range 0.92 to 2.35°min^{-1}. The intensities of 5409 unique reflections (h -12 to 11, k -12 to 12, l 0 to 17) were measured (DATCOL).

Structure solution and refinement

The structure was solved using Patterson methods (Au) (SHELX76) and ΔF syntheses (P, C, B) and developed by iterative, least-squares refinement and further difference Fourier syntheses (SHELXTL). There are 2 molecules *per* unit cell. In the final model all non-H atoms were refined anisotropically. The *o*-tolyl rings were treated as planar hexagons (C-C = 1.39 Å) with the 2-Me groups modelled as being rigid. The phenyl and *o*-tolyl H atoms were all set in idealised positions (C-H = 0.93 Å). Cage H atoms were also set in idealised positions, 1.10 Å from the boron atoms on a radial extension from the centre of the icosahedron. Methyl protons were allowed to ride on their respective carbon atoms with U(H) = 1.5 $U(C_{Me})$. All other fixed protons were similarly fixed with U(H) = 1.2 U(C/B).

Data were absorption corrected (DIFABS) and weighted such that $w^{-1} = [\sigma^2(F_o^2) + (0.0186P)^2 + 14.14P]$ where $P = [\text{max. } (F_o^2) + 2F_c^2]/3$. Using 4979 observed data ($F_o > 4.0\sigma(F_o)$), $R = 0.0370$, $wR_2 = 0.1346$ and $S = 1.518$ for 332 variable parameters. The maximum residue and minimum trough in a final Fourier synthesis were 1.99 and -1.49 eÅ^{-3}, respectively. Atomic scattering factors were those inlaid in SHELXTL. Selected bond lengths (Å) and angles (°), fractional coordinates and equivalent isotropic thermal parameters of non-hydrogen atoms are in **Tables 6A** and **6B**, respectively.

Figure 3.1 (below) shows a perspective view of **6**, which was shown by the structural study to possess the expected icosahedral, *closo* geometry. The C(1)-C(2) distance is 1.709(12) Å, significantly longer than for the unhindered carbaborane 1-Ph-1,2-*closo*-$C_2B_{10}H_{11}$, **1**, (1.640(5) Å) and carbaauraborane 1-H-2-{P(*o*-tol)$_3$Au}-1,2-*closo*-$C_2B_{10}H_{11}$, **11**, (1.656(7) Å). This reflects the steric crowding between the gold atom and the phenyl group, which are bonded to the two adjacent cage carbon atoms, C(2) and C(1), respectively. This steric crowding causes the phenyl ring to twist away from the preferred conformation (θ = 67.7°), observed for **1**, to one for which θ = 5.9°. The C(1)-C(01) distance is not, however significantly lengthened. The B-C and B-B connectivities are in the range 1.706(11) to 1.729(12) Å and 1.756(13) to 1.786(14) Å, respectively.

The geometry of the gold atom is significantly, deviated from linear (173.97(18)°), probably due to steric repulsion between the two C_{cage}-bound substituents, especially since the analogous angles in the uncrowded compounds P(*o*-tol)$_3$AuMe, **6a**, and P(*o*-tol)$_3$AuCl[10] are 180.0 (Au, P and C lie along a crystallographically imposed three-fold axis) and 179.4(1)°, respectively. Aurophilic interactions, similar to those observed for 1,1′-{PPh_3Au}$_2$-[2-(1′,2′-*closo*-$C_2B_{10}H_{10}$)-1,2-*closo*-$C_2B_{10}H_{10}$],[11] where the C-Au-P bond angles are 166.2(8) and 161.4(8)° and for which the intramolecular Au···Au distance is 3.119(1) Å, or PMe_3AuCl,[12] which packs in a helical fashion with Au...Au distances between 3.271(1) and 3.386(1) Å, are not responsible for this deviation. Indeed the nearest Au···Au contacts are > 10.5 Å.

The Au-C(2) bond length is 2.046(8) Å, shorter, though not significantly so, than in **6a**, (2.083(14) Å). This also the case for compounds **7** and **7a** (see below) and 1-CH_2OCH_3-2-{$AsPh_3Au$}-1,2-*closo*-$C_2B_{10}H_{10}$ and $AsPh_3AuMe$,[6] suggesting that the carbaborane moiety may be acting as an efficient σ-donor. The Au-P bond length is 2.289(2) Å, significantly different to those observed for P(*o*-tol)$_3$AuCl (2.243(2) Å) and P(*o* tol)$_3$AuMe (2.306(3) Å). All of the above distances are typical for Au(I) bound to C and P atoms.[13]

The geometry about the phosphorous atom is approximately tetrahedral with Au-P-C bond angles of 116.03(19), 112.25(18) and 111.34(18)°. These compare with angles of 113.99(22)° in **6a** and 108.7(5), 111.7(5) and 112.8(4)° for P(*o*-tol)$_3$AuCl.[10] In all three cases, the *ortho*-methyl groups point towards the gold atom, with the nearest Au···H_{Me} distances being 2.612, 2.726 and 2.513 Å, respectively. This conformation, which possibly allows more efficient packing, is also observed for 1-Ph-2-{$Pmes_3Au$}-1,2-*closo*-$C_2B_{10}H_{10}$, **9** (**Figure 3.5**, below), and $Pmes_3AuCl$.[14]

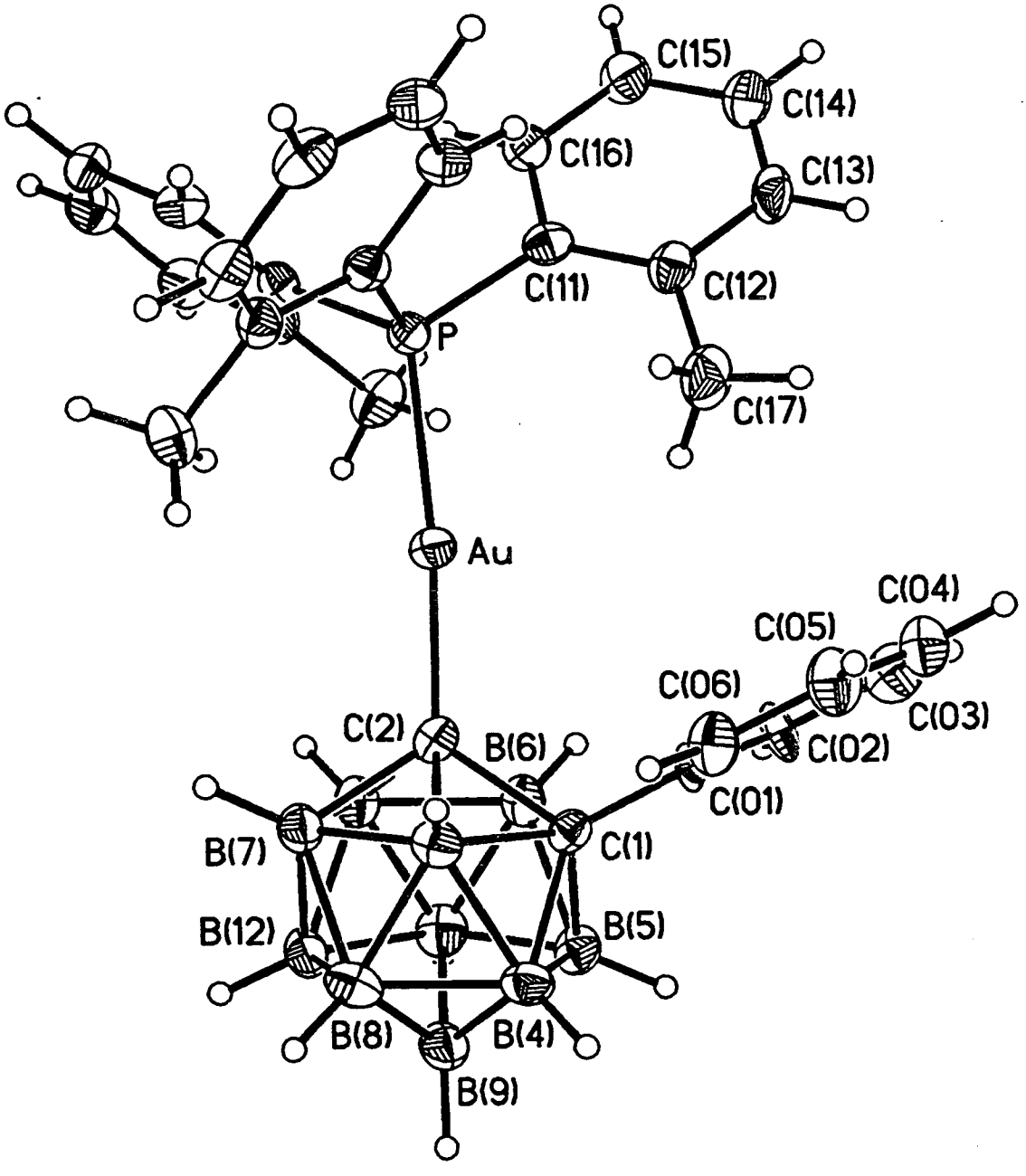

Figure 3.1 Perspective View of **6**

Table 6A Selected Bond Lengths (Å) and Angles (°) for **6**

Au-C(2)	2.046(8)	Au-P	2.289(2)
C(1)-C(01)	1.492(8)	C(1)-B(3)	1.706(11)
C(1)-C(2)	1.709(10)	C(1)-B(4)	1.715(11)
C(1)-B(5)	1.715(11)	C(1)-B(6)	1.720(11)
C(2)-B(7)	1.707(12)	C(2)-B(11)	1.725(12)
C(2)-B(3)	1.725(12)	C(2)-B(6)	1.729(12)
B(3)-B(7)	1.758(13)	B(3)-B(8)	1.772(13)
B(3)-B(4)	1.780(13)	B(4)-B(8)	1.76(2)
B(4)-B(5)	1.772(13)	B(4)-B(9)	1.775(14)
B(5)-B(9)	1.765(14)	B(5)-B(6)	1.766(14)
B(5)-B(10)	1.786(14)	B(6)-B(10)	1.769(14)
B(6)-B(11)	1.772(13)	B(7)-B(11)	1.756(13)
B(7)-B(12)	1.776(13)	B(7)-B(8)	1.783(14)
B(8)-B(12)	1.774(14)	B(8)-B(9)	1.778(14)
B(9)-B(10)	1.78(2)	B(9)-B(12)	1.776(14)
B(10)-B(12)	1.757(14)	B(10)-B(11)	1.761(14)
B(11)-B(12)	1.774(14)	P-C(11)	1.827(4)
P-C(21)	1.835(4)	P-C(31)	1.837(4)
C(12)-C(17)	1.515(10)	C(22)-C(27)	1.528(9)
C(32)-C(37)	1.525(9)		

C(2)-Au-P	174.2(2)	C(01)-C(1)-B(3)	116.9(6)
C(01)-C(1)-C(2)	118.1(6)	B(3)-C(1)-C(2)	60.7(5)
C(01)-C(1)-B(4)	120.4(6)	B(3)-C(1)-B(4)	62.7(5)
C(01)-C(1)-B(5)	122.0(6)	B(4)-C(1)-B(5)	62.2(5)
C(01)-C(1)-B(6)	119.3(6)	C(2)-C(1)-B(6)	60.6(5)
B(5)-C(1)-B(6)	61.9(5)	B(7)-C(2)-B(11)	61.6(5)
B(7)-C(2)-B(3)	61.6(5)	C(1)-C(2)-B(3)	59.6(5)
C(1)-C(2)-B(6)	60.0(5)	B(11)-C(2)-B(6)	61.7(5)
B(7)-C(2)-Au	120.8(5)	C(1)-C(2)-Au	122.9(5)
B(11)-C(2)-Au	118.5(5)	B(3)-C(2)-Au	121.6(5)
B(6)-C(2)-Au	118.4(5)	C(1)-B(3)-C(2)	59.7(5)
C(2)-B(3)-B(7)	58.7(5)	B(7)-B(3)-B(8)	60.7(6)
C(1)-B(3)-B(4)	58.9(5)	B(8)-B(3)-B(4)	59.5(6)
C(1)-B(4)-B(5)	58.9(5)	B(8)-B(4)-B(9)	60.3(6)
B(5)-B(4)-B(9)	59.7(6)	C(1)-B(4)-B(3)	58.4(5)
B(8)-B(4)-B(3)	60.0(5)	C(1)-B(5)-B(6)	59.2(5)
C(1)-B(5)-B(4)	58.9(5)	B(9)-B(5)-B(4)	60.2(6)
B(9)-B(5)-B(10)	60.0(6)	B(6)-B(5)-B(10)	59.7(6)
C(1)-B(6)-C(2)	59.4(4)	C(1)-B(6)-B(5)	58.9(5)
B(5)-B(6)-B(10)	60.7(6)	C(2)-B(6)-B(11)	59.0(5)
B(10)-B(6)-B(11)	59.7(6)	C(2)-B(7)-B(11)	59.7(5)
C(2)-B(7)-B(3)	59.7(5)	B(11)-B(7)-B(12)	60.3(6)
B(3)-B(7)-B(8)	60.0(5)	B(12)-B(7)-B(8)	59.8(6)
B(4)-B(8)-B(3)	60.5(5)	B(4)-B(8)-B(9)	60.2(6)
B(12)-B(8)-B(9)	60.0(6)	B(3)-B(8)-B(7)	59.3(5)
B(12)-B(8)-B(7)	59.9(5)	B(5)-B(9)-B(4)	60.1(5)

B(5)-B(9)-B(10)	60.6(6)	B(10)-B(9)-B(12)	59.3(6)
B(4)-B(9)-B(8)	59.5(6)	B(12)-B(9)-B(8)	59.9(6)
B(12)-B(10)-B(11)	60.6(6)	B(11)-B(10)-B(6)	60.3(5)
B(12)-B(10)-B(9)	60.3(6)	B(6)-B(10)-B(5)	59.6(5)
B(9)-B(10)-B(5)	59.4(6)	C(2)-B(11)-B(7)	58.7(5)
C(2)-B(11)-B(6)	59.2(5)	B(10)-B(11)-B(6)	60.1(6)
B(7)-B(11)-B(12)	60.4(5)	B(10)-B(11)-B(12)	59.6(6)
B(10)-B(12)-B(11)	59.8(6)	B(11)-B(12)-B(7)	59.3(5)
B(8)-B(12)-B(7)	60.3(6)	B(10)-B(12)-B(9)	60.3(6)
B(8)-B(12)-B(9)	60.1(6)	C(06)-C(01)-C(1)	122.5(4)
C(02)-C(01)-C(1)	117.4(4)	C(11)-P-C(21)	104.7(2)
C(11)-P-C(31)	105.7(2)	C(21)-P-C(31)	106.1(2)
C(11)-P-Au	116.0(2)	C(21)-P-Au	112.3(2)
C(31)-P-Au	111.3(2)	C(12)-C(11)-P	121.5(3)
C(16)-C(11)-P	118.5(3)	C(11)-C(12)-C(17)	122.9(5)
C(13)-C(12)-C(17)	117.1(5)	C(22)-C(21)-P	121.4(3)
C(26)-C(21)-P	118.6(3)	C(23)-C(22)-C(27)	117.4(5)
C(21)-C(22)-C(27)	122.5(5)	C(32)-C(31)-P	121.4(3)
C(36)-C(31)-P	118.6(3)	C(33)-C(32)-C(37)	116.6(5)
C(31)-C(32)-C(37)	123.4(5)		

Table 6B Atomic Coordinates (x 10^4) and Equivalent Isotropic Thermal Parameters ($Å^2$ x 10^3) for **6**

	x	y	z	U(eq)
Au	2012(1)	1236(1)	2786(1)	38(1)
C(1)	3331(7)	-213(7)	1147(5)	34(2)
C(2)	2812(8)	-262(8)	2103(6)	39(2)
B(3)	4509(9)	-121(9)	2245(7)	40(2)
B(4)	4656(9)	-1072(9)	1138(7)	43(2)
B(5)	2991(10)	-1739(9)	327(7)	43(2)
B(6)	1855(9)	-1201(10)	938(7)	42(2)
B(7)	3790(10)	-1178(9)	2741(7)	44(2)
B(8)	4952(10)	-1717(10)	2137(8)	50(2)
B(9)	3997(11)	-2728(10)	946(7)	49(2)
B(10)	2264(11)	-2805(10)	839(7)	49(2)
B(11)	2143(10)	-1855(9)	1940(7)	44(2)
B(12)	3481(10)	-2795(9)	1947(7)	45(2)
C(02)	2131(4)	1041(5)	63(4)	46(2)
C(03)	2023(5)	2146(6)	-269(4)	62(3)
C(04)	3045(6)	3220(5)	170(4)	59(2)
C(05)	4177(5)	3190(5)	942(4)	59(2)
C(06)	4286(4)	2084(5)	1275(3)	50(2)
C(01)	3263(5)	1010(4)	835(4)	33(2)
P	1105(2)	2788(2)	3654(1)	33(1)
C(11)	-59(4)	3674(5)	2955(4)	39(2)
C(12)	256(4)	4195(5)	2281(4)	43(2)
C(13)	-632(6)	4903(5)	1786(3)	51(2)
C(14)	-1833(5)	5091(6)	1965(4)	58(2)
C(15)	-2148(4)	4571(6)	2640(4)	53(2)
C(16)	-1260(5)	3863(5)	3135(3)	42(2)
C(17)	1529(10)	4000(11)	2029(8)	65(3)
C(21)	137(5)	2087(5)	4281(3)	34(2)
C(22)	-899(5)	1033(5)	3780(3)	39(2)
C(23)	-1615(5)	526(4)	4275(4)	50(2)
C(24)	-1294(5)	1072(5)	5272(4)	53(2)
C(25)	-258(5)	2127(5)	5773(3)	47(2)
C(26)	458(5)	2634(4)	5277(3)	42(2)
C(27)	-1320(9)	407(10)	2681(6)	58(2)
C(31)	2432(4)	4053(4)	4608(3)	34(2)
C(32)	3529(5)	3724(4)	5258(4)	39(2)
C(33)	4528(4)	4704(5)	5960(3)	48(2)
C(34)	4430(4)	6014(4)	6013(3)	50(2)
C(35)	3333(5)	6344(3)	5362(4)	46(2)
C(36)	2334(4)	5363(4)	4660(3)	41(2)
C(37)	3717(9)	2313(9)	5249(7)	53(2)

Compounds **7** to **10** are structurally very similar to compound **6**, above. As such, these structures will be not be described fully. Instead, the pertinent bond lengths and angles are presented in **Table 3.8**, below, although any notable features are discussed in more detail.

Table 3.8 Pertinent Bond Lengths (Å) and Angles (°) for Compounds **6** to **10**

Compound	**6**	**7**	**8**	**9**	**10**
C(1)-C(2)/(Å)	1.709(12)	1.687(6)	1.699(11)	1.688(8)	1.687(7)
C(1)-C(01)/(Å)	1.492(8)	1.505(5)	1.514(14)	1.518(8)	1.512(7)
Au-C(2)/(Å)	2.046(8)	2.057(4)	2.065(7)	2.050(5)	2.044(5)
Au-P/(Å)	2.289(2)	2.277(1)	2.271(3)	2.310(1)	2.262(1)
C(2)-Au-P/(°)	173.97(18)	172.48(13)	176.31(31)	178.96(16)	175.74(13)
Au-P-C(11)/(°)	116.03(19)	109.18(16)	*	109.61(17)	113.92(14)
Au-P-C(12)/(°)	112.25(18)	111.66(15)	*	104.41(18)	110.22(14)
Au-P-C(13)/(°)	111.34(18)	111.66(14)	*	107.18(17)	113.70(14)
θ/(°)	5.9	16.7	18.0	11.9	4.0
C-B min/(Å)	1.706(11)	1.706(7)	1.696(15)	1.696(8)	1.698(7)
C-B max/(Å)	1.729(12)	1.717(6)	1.720(13)	1.734(8)	1.718(8)
B-B min/(Å)	1.756(13)	1.746(10)	1.741(20)	1.744(9)	1.744(12)
B-B max/(Å)	1.786(14)	1.784(9)	1.803(19)	1.797(11)	1.786(9)

(* not calculable due to disorder)

All of the carbaborane cages possess an approximately icosahedral, *closo* geometry, with two adjacent cage carbons, C(1) and C(2), attached to a phenyl group and a gold(I) phosphine fragment, respectively. The order of lengths of connectivities is C(1)-C(2) < C-B < B-B, which is typical of 1,2-*closo*-C_2B_{10} species.[7] The C(1)-C(2) connectivities are in the range 1.687(6) to 1.709(12) Å, and are thus not significantly different from each other. This C(1)-C(2) connectivity is significantly shorter than for the parent carbaborane, **1**, which was found to be 1.640(5) Å. The increase in this distance for compounds **6** to **10** relative to **1** is no doubt due to the steric repulsion between the gold atom and the phenyl ring on the adjacent cage carbon atom. Indeed, this steric strain causes the phenyl rings to adopt conformations with θ values in the range 18.0 to 4.0° compared to 67.7° in

the unhindered carbaborane. The C(1)-C(01) distance is not significantly affected by the twist of the phenyl group.

The gold atoms all display an approximately linear geometry, with C(2)-Au-P bond angles in the range 172.48(13) to 178.96(16)°. These (significant) deviations from linearity do not appear to be related to the size of the attached phosphine as compound **9** contains the phosphine ($Pmes_3$) with the largest cone angle (212°),[9] yet affords the least deviation away from a linear geometry of the gold atom.

The Au-C bond lengths are not significantly different from each other and are similar to the corresponding bond lengths in the four σ bonded carbaauraboranes structurally characterised thus far (1-CH_2OCH_3-2-{$AsPh_3Au$}-1,2-*closo*-$C_2B_{10}H_{10}$ - 2.039(8) Å,[6] 1-{PPh_3Au}-1,2-*closo*-$C_2B_{10}H_{11}$ - 2.039(8) Å,[15] 1,2-{PPh_3Au}$_2$-1,2-*closo*-$C_2B_{10}H_{10}$ - 2.055(14) and 2.033(15) Å[11] and 1,1′-{PPh_3Au}$_2$-[2-(1′,2′-*closo*-$C_2B_{10}H_{10}$)-1,2-*closo*-$C_2B_{10}H_{10}$] - 2.09(3) and 2.13(3) Å.[11] The Au-P bonds lengths for compounds **6** to **10** are in the range 2.262(1) to 2.310(1) Å and are thus significantly different. There appears to be no correlation between the Au-P distance and the basicity of the phosphine (as indicated by υ or δ $^{31}P\{^1H\}$). These bond lengths are similar to the the Au-P or Au-As bond lengths of the four σ-bonded carbaauraboranes structurally characterised thus far (see above) (2.3740(8), 2.271(2), 2.270(4), 2.273(5), 2.293(8) and 2.281(9) Å, respectively), for which the C(1) substituent is not a phenyl group.

The geometry of the phosphorous atoms are approximately tetrahedral with Au-P-C bond angles in the range 104.41(18) to 116.03(19)°. Those phosphines containing aromatic rings are arranged in a propeller-type arrangement, similar to those observed for the corresponding PR'_3AuCl species (except $P(C_6F_5)_3AuCl$, which has not been structurally characterised).[16]

Crystallographic Study of 1-Ph-2-{PCy_3Au}-1,2-*closo*-$C_2B_{10}H_{10}$ (7)

Colourless, diffraction quality *blocks* and *needles* of **7** were grown by diffusion of *n*-hexane and a CH_2Cl_2 (4:1) solution at -30°C. Intensity data were measured on an Enraf-Nonius CAD4 diffractometer operating with Mo-K_α *X*-radiation (λ_{bar} = 0.71073 Å). The single crystal (block) was mounted in a glass capillary and the experiment performed at 291(2) K.

Crystal data

$C_{26}H_{48}B_{10}AuP$, M = 348.34, triclinic, *P*bar1, a = 11.167(4) Å, b = 12.338(5) Å, c = 12.416(3) Å, α = 86.02(3)°, β = 76.09(2)°, γ = 75.70(3)°, V = 1608.9(9) Å^3, from least squares refinement of 25 reflections (11≤θ≤12°) at 291(2) K, Z = 2, D_c = 1.438 gcm^{-3}, μ(Mo-K_α) = 4.64 mm^{-1}, F(0,0,0) = 696e.

Data collection and reduction

Intensity data collected in the range 0<2θ<50° by the ω-2θ scan method; ω-scan width (0.8+0.34tanθ), ω-scan speeds in the range 0.92 to 2.35°min^{-1}. The intensities of 5634 unique reflections (*h* -12 to 13, *k* -14 to 14, *l* 0 to 14) were measured (DATCOL).

Structure solution and refinement

The structure was solved using Patterson methods (Au) (SHELX76) and ΔF syntheses (P, C, B) and developed by iterative full matrix, least-squares refinement and further difference Fourier syntheses (SHELXTL). There are 2 molecules *per* unit cell. In the final model all non-H atoms were refined anisotropically. The phenyl ring was treated as a regular hexagon (C-C = 1.39 Å), with phenyl and cyclohexyl H atoms set in idealised positions (C-H = 0.93 Å). The cage H atoms were also fixed in idealised positions, 1.10 Å from the boron atoms on a radial extension from the centre of the icosahedron. The fixed H atoms were allowed to ride on their respective carbon atoms with U(H) = 1.2 U(B/C).

Data were absorption corrected (DIFABS) and weighted such that $w^{-1} = [\sigma^2(F_o^2) + (0.413P)^2 + 2.5241P]$ where P = [max. (F_o^2) + $2F_c^2]/3$. Using 5127 observed data ($F_o > 4.0\sigma(F_o)$), R = 0.0273, wR_2 = 0.072 and S = 1.053 for

332 variable parameters. The maximum residue and minimum trough in a final Fourier synthesis were 1.16 and -1.12 eÅ^{-3}, respectively. Atomic scattering factors were those inlaid in SHELXTL. Selected bond lengths (Å) and angles (°), fractional coordinates and equivalent isotropic thermal parameters of non-hydrogen atoms are in **Tables 7A** and **7B**, respectively.

Figure 3.2 is a perspective view of compound **7**, which confirms the structure to be similar to that of **6**. The C(2)-Au-P bond angle affords the greatest deviation from linearity (172.48(13)°) of the five compounds. A packing diagram (**Fig. 3.3**) reveals that the molecules are arranged in zig-zagging chains in mutually anti positions, with Au···Au distances of 9.241 Å. Hence the possibilty of the distortion from linearity being a result of aurophilic interactions can be discounted.

The Au-P bond length (2.277(1) Å) is similar to those in PCy_3AuMe, **7a** (2.292(2) Å), and PCy_3AuCl (2.279(5) Å),[16a] for which the conformation of the cyclohexyl groups is also extremely similar. As for compounds **6** and **6a**, the Au-C distance in **7** (2.057(4) Å) is shorter, although not significantly so, than for the corresponding methyl species, **7a** (2.065(6) Å), suggesting that the carbaborane cage is acting as a σ-donor.

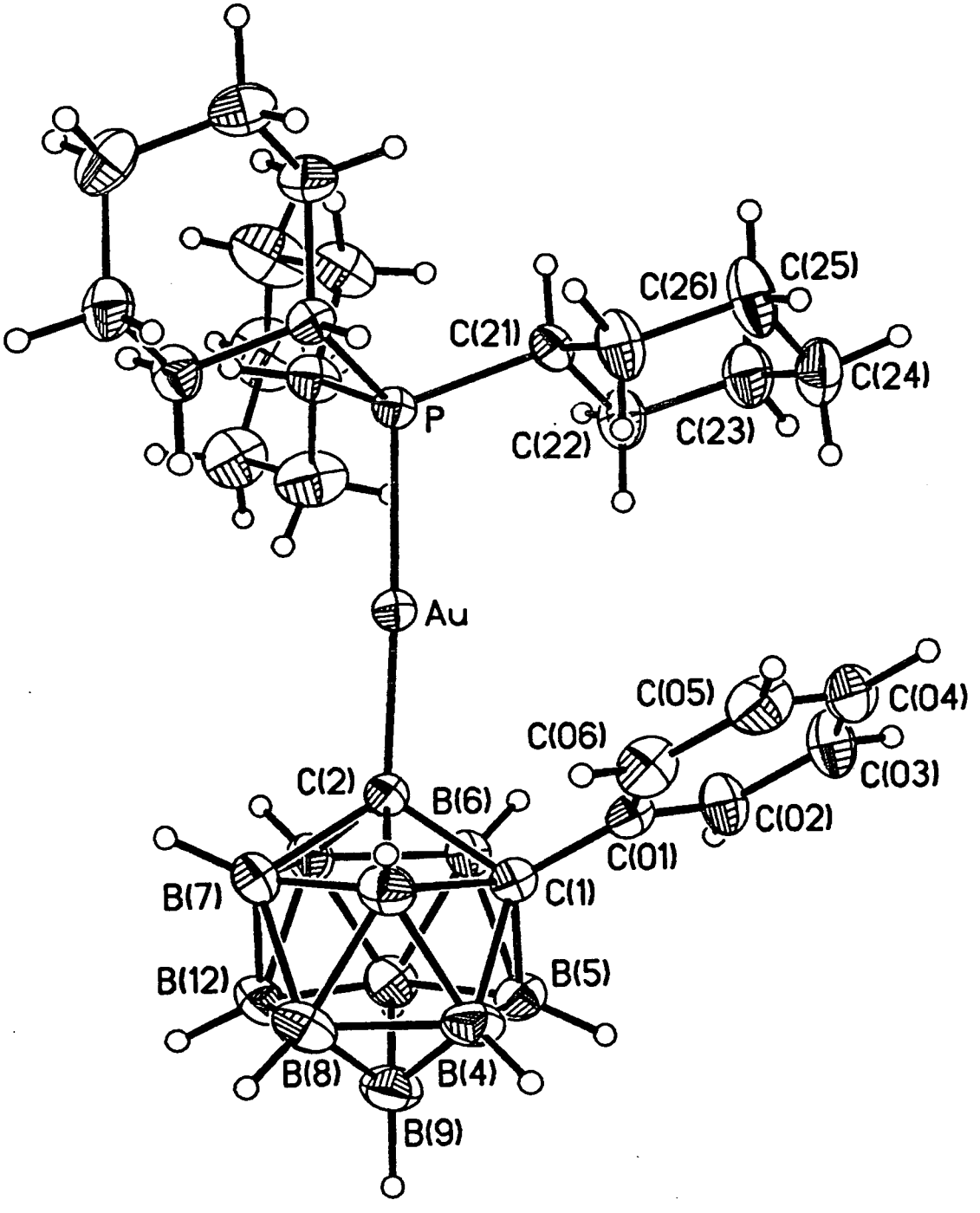

Figure 3.2 Perspective View of 7

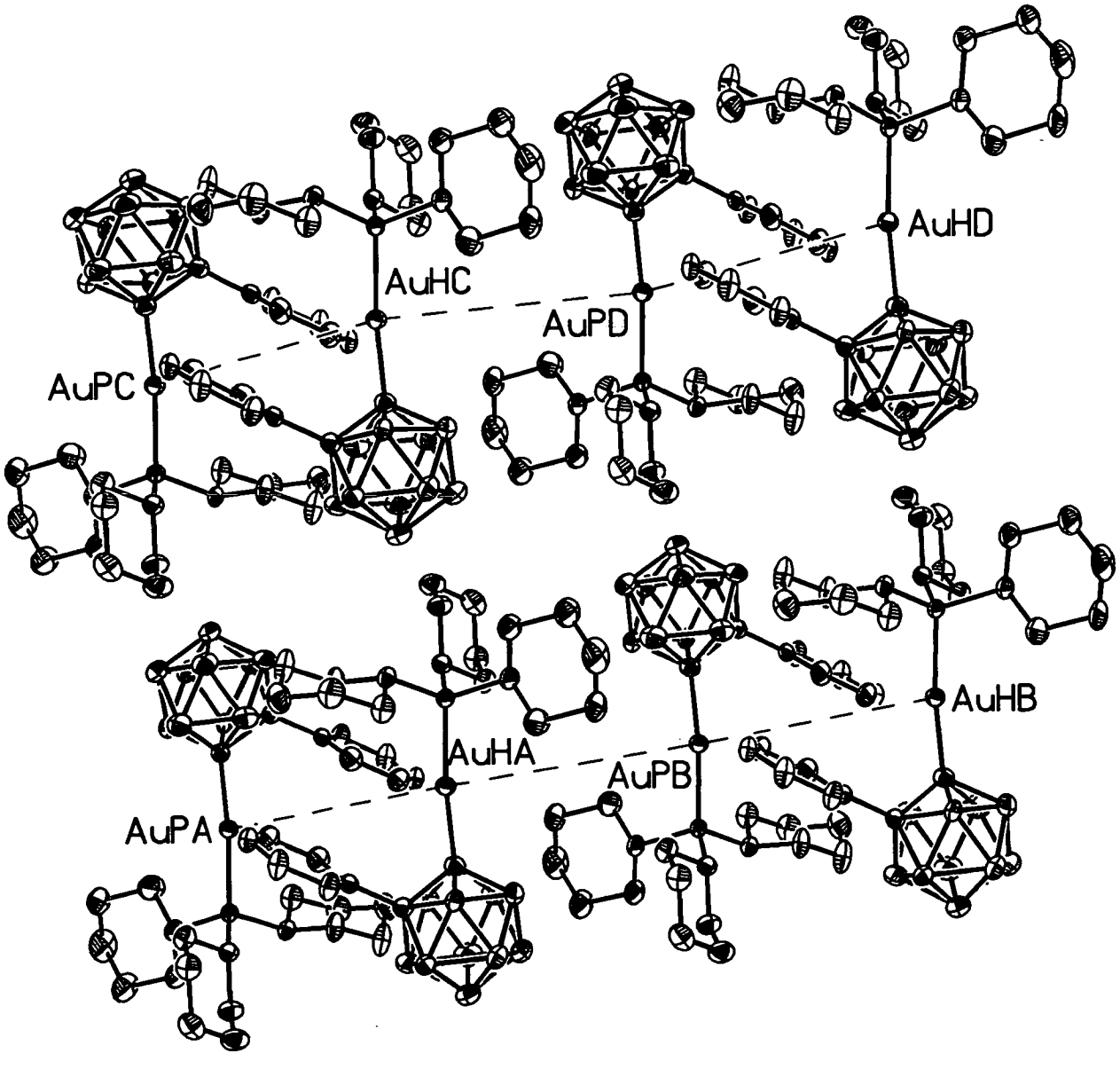

Figure 3.3 Packing Diagram of 7

Table 7A Selected Bond Lengths (Å) and Angles (°) for **7**

Au-C(2)	2.056(4)	Au-P	2.2768(13)
C(1)-C(01)	1.499(6)	C(1)-C(2)	1.686(6)
C(1)-B(4)	1.706(7)	C(1)-B(3)	1.708(7)
C(1)-B(5)	1.710(7)	C(1)-B(6)	1.717(6)
C(2)-B(6)	1.711(7)	C(2)-B(7)	1.711(7)
C(2)-B(11)	1.712(7)	C(2)-B(3)	1.716(7)
B(3)-B(7)	1.747(10)	B(3)-B(4)	1.775(9)
B(3)-B(8)	1.783(9)	B(4)-B(5)	1.759(9)
B(4)-B(9)	1.765(9)	B(4)-B(8)	1.774(10)
B(5)-B(9)	1.762(9)	B(5)-B(10)	1.771(8)
B(5)-B(6)	1.785(8)	B(6)-B(11)	1.756(8)
B(6)-B(10)	1.770(8)	B(7)-B(11)	1.762(10)
B(7)-B(8)	1.769(9)	B(7)-B(12)	1.773(10)
B(8)-B(12)	1.750(11)	B(8)-B(9)	1.765(11)
B(9)-B(12)	1.756(10)	B(9)-B(10)	1.776(10)
B(10)-B(11)	1.762(9)	B(10)-B(12)	1.770(10)
B(11)-B(12)	1.771(8)	C(01)-C(06)	1.380(7)
C(01)-C(02)	1.395(6)	C(02)-C(03)	1.375(8)
C(03)-C(04)	1.363(9)	C(04)-C(05)	1.359(9)
C(05)-C(06)	1.388(7)	P-C(21)	1.838(4)
P-C(31)	1.839(4)	P-C(11)	1.844(5)
C(11)-C(12)	1.484(7)	C(11)-C(16)	1.503(7)
C(12)-C(13)	1.544(8)	C(13)-C(14)	1.489(10)
C(14)-C(15)	1.463(11)	C(15)-C(16)	1.518(8)
C(21)-C(26)	1.519(6)	C(21)-C(22)	1.524(7)
C(22)-C(23)	1.525(7)	C(23)-C(24)	1.516(9)
C(24)-C(25)	1.513(9)	C(25)-C(26)	1.522(7)
C(31)-C(36)	1.527(6)	C(31)-C(32)	1.530(6)
C(32)-C(33)	1.529(7)	C(33)-C(34)	1.505(8)
C(34)-C(35)	1.507(9)	C(35)-C(36)	1.522(7)

C(2)-Au-P	172.49(13)	C(01)-C(1)-C(2)	117.5(3)
C(01)-C(1)-B(4)	122.2(4)	C(01)-C(1)-B(3)	118.3(4)
C(2)-C(1)-B(3)	60.7(3)	B(4)-C(1)-B(3)	62.7(3)
C(01)-C(1)-B(5)	121.3(4)	B(4)-C(1)-B(5)	62.0(3)
C(01)-C(1)-B(6)	116.8(4)	C(2)-C(1)-B(6)	60.3(3)
B(5)-C(1)-B(6)	62.7(3)	C(1)-C(2)-B(6)	60.7(3)
B(6)-C(2)-B(11)	61.7(3)	B(7)-C(2)-B(11)	62.0(4)
C(1)-C(2)-B(3)	60.3(3)	B(7)-C(2)-B(3)	61.3(4)
C(1)-C(2)-Au	120.6(3)	B(6)-C(2)-Au	114.0(3)
B(7)-C(2)-Au	123.8(3)	B(11)-C(2)-Au	118.1(3)
B(3)-C(2)-Au	123.4(3)	C(1)-B(3)-C(2)	59.0(3)
C(2)-B(3)-B(7)	59.2(3)	C(1)-B(3)-B(4)	58.6(3)
B(7)-B(3)-B(8)	60.1(4)	B(4)-B(3)-B(8)	59.8(4)
C(1)-B(4)-B(5)	59.1(3)	B(5)-B(4)-B(9)	60.0(4)
B(9)-B(4)-B(8)	59.8(4)	C(1)-B(4)-B(3)	58.7(3)
B(8)-B(4)-B(3)	60.3(4)	C(1)-B(5)-B(4)	58.9(3)

B(4)-B(5)-B(9)	60.2(4)	B(9)-B(5)-B(10)	60.3(4)
C(1)-B(5)-B(6)	58.8(3)	B(10)-B(5)-B(6)	59.7(3)
C(2)-B(6)-C(1)	58.9(3)	C(2)-B(6)-B(11)	59.2(3)
B(11)-B(6)-B(10)	60.0(3)	C(1)-B(6)-B(5)	58.4(3)
B(10)-B(6)-B(5)	59.8(3)	C(2)-B(7)-B(3)	59.5(3)
C(2)-B(7)-B(11)	59.0(3)	B(3)-B(7)-B(8)	60.9(4)
B(11)-B(7)-B(12)	60.1(4)	B(8)-B(7)-B(12)	59.2(4)
B(12)-B(8)-B(9)	60.0(4)	B(12)-B(8)-B(7)	60.5(4)
B(9)-B(8)-B(4)	59.8(4)	B(7)-B(8)-B(3)	58.9(4)
B(4)-B(8)-B(3)	59.9(4)	B(12)-B(9)-B(8)	59.6(4)
B(5)-B(9)-B(4)	59.9(3)	B(8)-B(9)-B(4)	60.3(4)
B(12)-B(9)-B(10)	60.2(4)	B(5)-B(9)-B(10)	60.1(4)
B(11)-B(10)-B(6)	59.6(3)	B(11)-B(10)-B(12)	60.2(4)
B(6)-B(10)-B(5)	60.5(3)	B(12)-B(10)-B(9)	59.4(4)
B(5)-B(10)-B(9)	59.6(4)	C(2)-B(11)-B(6)	59.1(3)
C(2)-B(11)-B(7)	59.0(3)	B(6)-B(11)-B(10)	60.4(3)
B(7)-B(11)-B(12)	60.2(4)	B(10)-B(11)-B(12)	60.1(4)
B(8)-B(12)-B(9)	60.5(4)	B(9)-B(12)-B(10)	60.5(4)
B(10)-B(12)-B(11)	59.7(4)	B(8)-B(12)-B(7)	60.3(4)
B(11)-B(12)-B(7)	59.6(4)	C(06)-C(01)-C(02)	118.1(5)
C(06)-C(01)-C(1)	119.5(4)	C(02)-C(01)-C(1)	122.4(4)
C(01)-C(02)-C(03)	120.5(5)	C(04)-C(03)-C(02)	120.5(5)
C(03)-C(04)-C(05)	120.1(5)	C(06)-C(05)-C(04)	120.3(6)
C(05)-C(06)-C(01)	120.5(5)	C(21)-P-C(31)	107.3(2)
C(21)-P-C(11)	110.1(2)	C(31)-P-C(11)	106.8(2)
C(21)-P-Au	111.7(2)	C(31)-P-Au	111.66(14)
C(11)-P-Au	109.2(2)	C(12)-C(11)-C(16)	112.2(5)
C(12)-C(11)-P	113.2(4)	C(16)-C(11)-P	117.2(3)
C(11)-C(12)-C(13)	112.3(5)	C(14)-C(13)-C(12)	111.0(6)
C(15)-C(14)-C(13)	112.5(6)	C(14)-C(15)-C(16)	113.8(7)
C(11)-C(16)-C(15)	111.7(5)	C(26)-C(21)-C(22)	110.8(4)
C(26)-C(21)-P	111.1(3)	C(22)-C(21)-P	110.7(3)
C(21)-C(22)-C(23)	111.8(5)	C(24)-C(23)-C(22)	111.7(5)
C(25)-C(24)-C(23)	111.2(5)	C(24)-C(25)-C(26)	111.6(5)
C(21)-C(26)-C(25)	111.5(4)	C(36)-C(31)-C(32)	110.6(4)
C(36)-C(31)-P	116.5(3)	C(32)-C(31)-P	111.3(3)
C(33)-C(32)-C(31)	110.3(4)	C(34)-C(33)-C(32)	111.8(4)
C(33)-C(34)-C(35)	111.4(4)	C(34)-C(35)-C(36)	111.9(5)
C(35)-C(36)-C(31)	110.4(4)		

Table 7B Atomic Coordinates (x 10^4) and Equivalent Isotropic Thermal Parameters ($Å^2$ x 10^3) for **7**

	x	y	z	U(eq)
Au	3570(1)	776(1)	2709(1)	39(1)
C(1)	2367(4)	-1050(4)	1832(3)	39(1)
C(2)	3064(4)	-726(4)	2790(4)	42(1)
B(3)	3855(6)	-1803(5)	1892(5)	54(1)
B(4)	2690(7)	-2463(5)	1674(5)	61(2)
B(5)	1203(6)	-1726(5)	2435(5)	51(1)
B(6)	1459(5)	-607(4)	3120(4)	42(1)
B(7)	3878(7)	-1937(5)	3297(6)	66(2)
B(8)	3631(8)	-3057(5)	2630(7)	74(2)
B(9)	1987(8)	-2993(5)	2965(6)	69(2)
B(10)	1215(7)	-1842(6)	3862(5)	60(2)
B(11)	2390(6)	-1201(5)	4064(5)	56(1)
B(12)	2722(8)	-2675(5)	3964(6)	69(2)
C(01)	2229(4)	-247(4)	882(3)	40(1)
C(02)	3256(5)	-146(5)	17(4)	61(1)
C(03)	3088(6)	607(6)	-835(4)	72(2)
C(04)	1913(7)	1258(5)	-852(4)	72(2)
C(05)	894(6)	1164(5)	-26(5)	72(2)
C(06)	1045(5)	411(5)	843(4)	57(1)
P	3978(1)	2473(1)	2852(1)	35(1)
C(11)	3448(5)	2909(4)	4315(4)	52(1)
C(12)	2459(7)	2363(6)	4975(5)	86(2)
C(13)	2169(7)	2607(6)	6226(4)	83(2)
C(14)	1854(8)	3832(7)	6427(6)	105(3)
C(15)	2823(10)	4375(6)	5771(5)	106(3)
C(16)	3140(7)	4141(4)	4538(4)	69(2)
C(21)	3187(4)	3537(4)	1975(3)	40(1)
C(22)	1774(5)	3574(5)	2208(5)	61(1)
C(23)	1103(5)	4421(5)	1461(5)	71(2)
C(24)	1738(6)	4216(6)	245(5)	76(2)
C(25)	3138(6)	4188(6)	19(5)	83(2)
C(26)	3808(5)	3329(5)	753(4)	61(1)
C(31)	5688(4)	2412(4)	2429(4)	40(1)
C(32)	6444(4)	1488(4)	3058(4)	54(1)
C(33)	7869(5)	1348(5)	2580(5)	60(1)
C(34)	8263(5)	2429(5)	2588(5)	68(2)
C(35)	7500(5)	3350(5)	1992(5)	65(1)
C(36)	6078(5)	3509(4)	2462(5)	56(1)

Crystallographic Study of 1-Ph-2-{PEt_3Au}-1,2-*closo*-$C_2B_{10}H_{10}$ (8)

Colourless, diffraction quality *blocks* of **8** were grown by diffusion of petroleum ether (60-80) and a CH_2Cl_2 solution (4:1) at -30°C. Intensity data were measured on a Siemens P4 diffractometer operating with Mo-K_α *X*-radiation (λ_{bar} = 0.71073 Å). The single crystal was mounted in a glass capillary and the experiment performed at 293(2) K.

Crystal data

$C_{14}H_{36}B_{10}AuP$, M = 534.42, monoclinic, $P2_1/n$, a = 11.847(1) Å, b = 15.852(2) Å, c = 11.985(1) Å, β = 101.681(4)°, V = 2204.1(4) Å^3, from least squares refinement of 44 reflections ($5 \leq \theta \leq 25°$) at 293(2) K, Z = 4, D_c = 1.611 gcm^{-3}, μ(Mo-K_α) = 6.74 mm^{-1}, F(0,0,0) = 1032e.

Data collection and reduction

Intensity data collected in the range $2<2\theta<50°$ by the ω-scan method; ω-scan width 0.8°, ω-scan speeds in the range 1.5 to 60.0°min^{-1}. The intensities of 3833 unique reflections (h -1 to 14, k -1 to 18, l -14 to 14) were measured (XSCANS).

Structure solution and refinement

The structure was solved using Patterson methods (Au) and ΔF syntheses (P, C, B) and developed by iterative, least-squares refinement and further difference Fourier syntheses (SHELXTL). There are 4 molecules *per* unit cell. In the final model all non-H atoms were refined anisotropically. The phenyl H atoms were set in idealised positions (C-H = 0.93 Å), as were the Cage H atoms, 1.10 Å from the boron atoms on a radial extension from the centre of the icosahedron. The α-carbons of each of the three ethyl groups were disordered over two sites, which were consequently modelled with 50% occupancy. The methylene protons were fixed in idealised positions (C-H = 1.08 Å), whilst the methyl protons were not included in the model. All of the fixed H atoms were allowed to ride on their respective carbon atoms with U(H) = 1.2 U(B/C).

Data were absorption corrected (ψ-scans) and weighted such that $w^{-1} = [\sigma^2(F_o^2) + (0.416P)^2]$ where $P = [\text{max. } (F_o^2) + 2F_c^2]/3$. Using 2483 observed data ($F_o > 4.0\sigma(F_o)$), $R = 0.0445$, $wR_2 = 0.1066$ and $S = 1.044$ for 265 variable parameters. The maximum residue and minimum trough in a final Fourier synthesis were 0.49 and -0.93 $eÅ^{-3}$, respectively. Atomic scattering factors were those inlaid in SHELXTL. Interatomic distances (Å) and selected interbond angles (°), fractional coordinates and anisotropic thermal parameters of non-hydrogen atoms are in tables **8A** and **8B**, respectively.

A crystallographic study confirmed compound **8** to possess a structure very similar to that observed for compound **6** above (**Fig. 3.4**). The most noticeable feature of the structure is the disorder of the PEt_3 group. Each of the three α-carbon atoms of the ethyl groups are disordered over two sites, whilst the β-carbons are fully ordered and point toward the gold atom. This is in contrast to PEt_3AuCl, where one of the ethyl groups points away from the gold.[16b] The Au-Cl and Au-P bond lengths are 2.305(6) and 2.31(9) Å, respectively, similar to those of previously determined phosphine gold chlorides. The Au-P-C bond angle is almost linear (176.31(31)°), and close to that for PEt_3AuCl (178.5(3)°). The small size of the phosphine is also reflected in the twist of the C(1)-bound phenyl ring, which has a θ value of 18.0°.

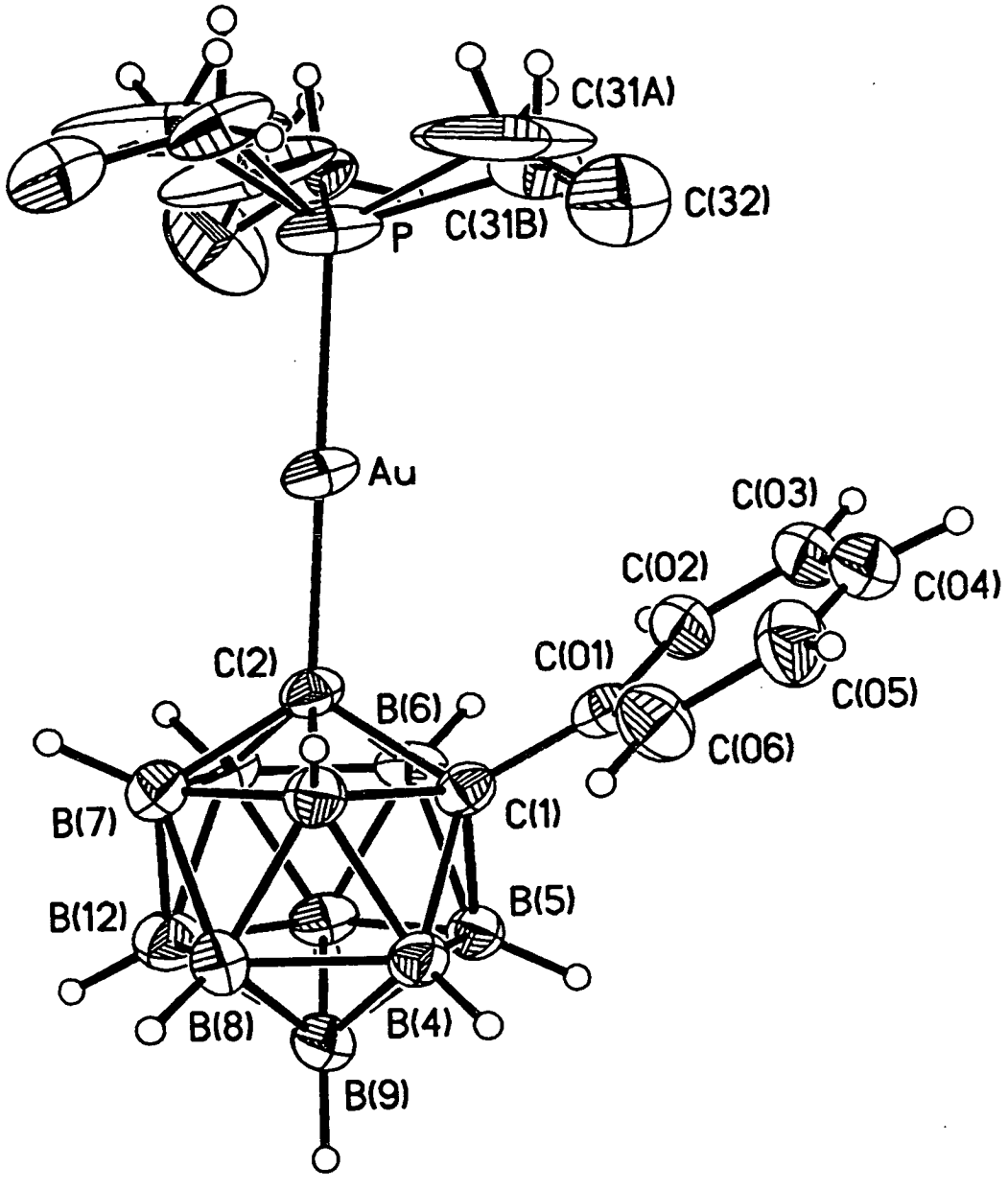

Figure 3.4 Perspective View of 8

Table 8A Selected Bond Lengths (Å) and Angles (°) for **8**

Au-C(2)	2.064(9)	Au-P	2.271(3)
C(1)-C(01)	1.514(14)	C(1)-C(2)	1.699(11)
C(1)-B(6)	1.706(14)	C(1)-B(3)	1.714(14)
C(1)-B(5)	1.715(13)	C(1)-B(4)	1.720(13)
C(2)-B(11)	1.70(2)	C(2)-B(7)	1.71(2)
C(2)-B(6)	1.71(2)	C(2)-B(3)	1.72(2)
B(3)-B(8)	1.78(2)	B(3)-B(7)	1.78(2)
B(3)-B(4)	1.786(14)	B(4)-B(5)	1.77(2)
B(4)-B(8)	1.78(2)	B(4)-B(9)	1.78(2)
B(5)-B(9)	1.77(2)	B(5)-B(10)	1.78(2)
B(5)-B(6)	1.786(14)	B(6)-B(11)	1.76(2)
B(6)-B(10)	1.78(2)	B(7)-B(11)	1.74(2)
B(7)-B(12)	1.78(2)	B(7)-B(8)	1.78(2)
B(8)-B(12)	1.80(2)	B(8)-B(9)	1.80(2)
B(9)-B(12)	1.76(2)	B(9)-B(10)	1.80(2)
B(10)-B(11)	1.768(14)	B(10)-B(12)	1.78(2)
B(11)-B(12)	1.78(2)	C(01)-C(02)	1.36(2)
C(01)-C(06)	1.38(2)	C(02)-C(03)	1.37(2)
C(03)-C(04)	1.37(2)	C(04)-C(05)	1.33(2)
C(05)-C(06)	1.43(2)	P-C(21B)	1.83(4)
P-C(11A)	1.84(4)	P-C(21A)	1.85(2)
P-C(31A)	1.88(4)	P-C(11B)	1.86(2)
P-C(31B)	1.95(3)	C(11B)-C(12)	1.50(4)
C(11A)-C(12)	1.26(4)	C(21B)-C(22)	1.24(4)
C(21A)-C(22)	1.45(3)	C(31B)-C(32)	1.39(4)
C(31A)-C(32)	1.30(4)		

C(2)-Au-P	176.3(3)	C(01)-C(1)-C(2)	118.9(7)
C(01)-C(1)-B(6)	119.0(8)	C(2)-C(1)-B(6)	60.4(6)
C(01)-C(1)-B(3)	116.4(8)	C(2)-C(1)-B(3)	60.5(6)
C(01)-C(1)-B(5)	122.0(7)	B(6)-C(1)-B(5)	62.9(6)
C(01)-C(1)-B(4)	120.2(7)	B(3)-C(1)-B(4)	62.7(6)
B(5)-C(1)-B(4)	61.9(6)	B(11)-C(2)-B(7)	61.5(8)
B(11)-C(2)-B(6)	62.3(7)	C(1)-C(2)-B(6)	60.0(6)
C(1)-C(2)-B(3)	60.2(6)	B(7)-C(2)-B(3)	62.6(7)
B(11)-C(2)-Au	121.7(6)	C(1)-C(2)-Au	118.5(6)
B(7)-C(2)-Au	123.3(6)	B(6)-C(2)-Au	116.4(7)
B(3)-C(2)-Au	118.9(6)	C(1)-B(3)-C(2)	59.3(6)
C(2)-B(3)-B(7)	58.4(7)	B(8)-B(3)-B(7)	60.0(7)
C(1)-B(3)-B(4)	58.8(6)	B(8)-B(3)-B(4)	59.7(6)
C(1)-B(4)-B(5)	58.9(6)	B(5)-B(4)-B(9)	59.9(7)
B(8)-B(4)-B(9)	60.9(7)	C(1)-B(4)-B(3)	58.5(6)
B(8)-B(4)-B(3)	60.0(6)	C(1)-B(5)-B(4)	59.2(6)
B(4)-B(5)-B(9)	60.4(7)	B(9)-B(5)-B(10)	60.8(7)
C(1)-B(5)-B(6)	58.3(5)	B(10)-B(5)-B(6)	59.8(6)
C(1)-B(6)-C(2)	59.6(6)	C(2)-B(6)-B(11)	58.4(6)
B(11)-B(6)-B(10)	59.9(7)	C(1)-B(6)-B(5)	58.8(6)

B(10)-B(6)-B(5)	60.0(6)	C(2)-B(7)-B(11)	58.9(7)
B(11)-B(7)-B(12)	60.7(8)	C(2)-B(7)-B(3)	58.9(7)
B(12)-B(7)-B(8)	60.6(7)	B(3)-B(7)-B(8)	60.0(7)
B(4)-B(8)-B(3)	60.2(6)	B(3)-B(8)-B(7)	60.0(7)
B(7)-B(8)-B(12)	59.6(7)	B(4)-B(8)-B(9)	59.7(7)
B(12)-B(8)-B(9)	58.4(7)	B(5)-B(9)-B(4)	59.6(7)
B(12)-B(9)-B(10)	60.1(8)	B(5)-B(9)-B(10)	59.8(7)
B(12)-B(9)-B(8)	60.7(7)	B(4)-B(9)-B(8)	59.4(7)
B(11)-B(10)-B(6)	59.7(7)	B(6)-B(10)-B(5)	60.2(7)
B(11)-B(10)-B(12)	60.2(7)	B(5)-B(10)-B(9)	59.4(7)
B(12)-B(10)-B(9)	58.7(7)	C(2)-B(11)-B(7)	59.7(7)
C(2)-B(11)-B(6)	59.3(7)	B(6)-B(11)-B(10)	60.4(7)
B(7)-B(11)-B(12)	60.7(7)	B(10)-B(11)-B(12)	60.3(7)
B(9)-B(12)-B(10)	61.1(7)	B(11)-B(12)-B(10)	59.5(7)
B(11)-B(12)-B(7)	58.6(7)	B(9)-B(12)-B(8)	60.9(7)
B(7)-B(12)-B(8)	59.8(7)	C(02)-C(01)-C(06)	118.2(12)
C(02)-C(01)-C(1)	122.0(10)	C(06)-C(01)-C(1)	119.7(10)
C(01)-C(02)-C(03)	122.8(13)	C(04)-C(03)-C(02)	118.3(13)
C(05)-C(04)-C(03)	121.6(14)	C(04)-C(05)-C(06)	120.(2)
C(01)-C(06)-C(05)	119.4(14)	C(21B)-P-C(11A)	83(3)
C(21B)-P-C(21A)	23(3)	C(11A)-P-C(21A)	103(2)
C(21B)-P-C(31A)	121(3)	C(11A)-P-C(31A)	106(3)
C(21A)-P-C(31A)	104(3)	C(21B)-P-C(11B)	103(2)
C(11A)-P-C(11B)	21(3)	C(21A)-P-C(11B)	120.5(11)
C(31A)-P-C(11B)	88(3)	C(21B)-P-C(31B)	111(4)
C(11A)-P-C(31B)	125(2)	C(21A)-P-C(31B)	90.3(12)
C(31A)-P-C(31B)	20(3)	C(11B)-P-C(31B)	108.6(13)
C(21B)-P-Au	112(2)	C(11A)-P-Au	114.1(12)
C(21A)-P-Au	112.4(9)	C(31A)-P-Au	116.2(12)
C(11B)-P-Au	113.1(11)	C(31B)-P-Au	109.0(10)
C(12)-C(11B)-P	115(2)	C(12)-C(11A)-P	131(3)
C(11A)-C(12)-C(11B)	27(4)	C(22)-C(21B)-P	128(3)
C(22)-C(21A)-P	114(2)	C(21B)-C(22)-C(21A)	31(5)
C(32)-C(31B)-P	116(2)	C(32)-C(31A)-P	127(3)
C(31A)-C(32)-C(31B)	29(5)		

Table 8B Atomic Coordinates (x 10^4) and Equivalent Isotropic Thermal Parameters ($Å^2$ x 10^3) for **8**

	x	y	z	U(eq)
Au	5705(1)	9082(1)	7700(1)	63(1)
C(1)	7710(8)	9380(6)	6262(7)	45(2)
C(2)	7231(7)	9615(8)	7469(8)	52(2)
B(3)	7189(10)	10370(8)	6433(11)	56(3)
B(4)	8450(10)	10221(7)	5854(9)	51(3)
B(5)	9186(9)	9332(7)	6535(10)	48(3)
B(6)	8372(9)	8941(8)	7526(10)	56(3)
B(7)	7657(11)	10613(9)	7906(11)	64(3)
B(8)	8424(11)	11020(9)	6889(11)	65(3)
B(9)	9678(11)	10359(9)	6974(11)	61(3)
B(10)	9633(10)	9551(10)	8017(11)	62(3)
B(11)	8376(10)	9731(9)	8564(10)	60(3)
B(12)	9191(11)	10603(10)	8225(11)	65(3)
C(01)	6973(8)	8827(6)	5372(8)	52(3)
C(02)	6846(11)	7985(8)	5537(10)	67(3)
C(03)	6194(12)	7472(9)	4733(11)	80(4)
C(04)	5662(11)	7825(10)	3718(12)	82(4)
C(05)	5713(13)	8651(10)	3527(12)	86(4)
C(06)	6403(10)	9177(10)	4364(10)	75(3)
P	4094(3)	8442(3)	8042(3)	93(1)
C(11B)	2846(24)	9173(23)	7926(22)	81(15)
C(11A)	3063(41)	9167(25)	8503(69)	312(57)
C(12)	3085(21)	9960(16)	8626(25)	151(10)
C(21B)	4290(36)	8060(61)	9509(48)	231(54)
C(21A)	4420(24)	7670(16)	9222(21)	70(9)
C(22)	5201(23)	7983(17)	10227(16)	154(10)
C(31B)	3666(25)	7525(17)	6951(28)	80(13)
C(31A)	3234(54)	7817(64)	6831(43)	304(54)
C(32)	3434(21)	7752(18)	5809(22)	147(8)

Crystallographic Study of 1-Ph-2-{$Pmes_3Au$}-1,2-*closo*-$C_2B_{10}H_{10}$ (9)

Colourless, diffraction quality *blocks* of **9** were grown by diffusion of petroleum ether (60-80) into a CH_2Cl_2 solution (4:1) at room temperature. Intensity data were measured on an Enraf-Nonius FAST diffractometer operating with Mo-K_α *X*-radiation (λ_{bar} = 0.71073 Å). The single crystal was mounted in a glass capillary and the experiment performed at 199(2) K.

Crystal data

$C_{35}H_{48}B_{10}AuP$, M = 804.77, orthorhombic, *Pbca*, a = 15.381(3) Å, b = 20.801(4) Å, c = 23.460(5) Å, V = 7505.8(26) Å^3, from the random search of a single hemisphere at 199(2) K, Z = 8, D_c = 1.424 gcm^{-3}, μ(Mo-K_α) = 3.99 mm^{-1}, F(0,0,0) = 3216e.

Data collection and reduction

Intensity data collected assuming a triclinic cell, with a detector-to-crystal setting of 50.28mm. The cell dimensions and orientation matrix were determined using MADNES, from 50 strong reflections. Intensity data corresponding to slightly more than one hemisphere of reciprocal space were recorded using two ω-scan regions of 99.8°. The intensities of 5822 unique reflections (h -18 to 17, k -20 to 22, l -25 to 26) were measured.

Structure solution and refinement

The structure was solved using Patterson methods (Au) and ΔF syntheses (P, C, B) and developed by iterative, least-squares refinement and further difference Fourier syntheses (SHELXTL). There are 8 molecules *per* unit cell. In the final model all non-H atoms were refined anisotropically. The phenyl and mesityl H atoms were set in idealised positions (C-H = 0.93 Å), as were cage H atoms, 1.10 Å from the boron atoms on a radial extension from the centre of the icosahedron. Methyl protons were allowed to ride on their respective carbon atoms with U(H) = 1.5 U(C_{Me}). All other fixed protons were similarly treated with U(H) = 1.2 U(C/B).

Data were absorption corrected (DIFABS) and weighted such that $w^{-1} = [\sigma^2(F_o^2) + (0.0478P)^2]$ where $P = [\text{max.}\ (F_o^2) + 2F_c^2]/3$. Using 4247 observed data ($F_o > 4.0\sigma(F_o)$), $R = 0.0378$, $wR_2 = 0.0871$ and $S = 0.945$ for 424 variable parameters. The maximum residue and minimum trough in a final difference Fourier synthesis were 3.59 and -0.72 eÅ^{-3}, respectively. Atomic scattering factors were those inlaid in SHELXTL. Selected bond lengths (Å) and angles (°), fractional coordinates and equivalent isotropic thermal parameters of non-hydrogen atoms are given in **Tables 9A** and **9B**, respectively.

The compound was confirmed as having a similar structure to **6** by the crystallographic study. **Figure 3.5** shows a perspective view of the molecule. In a similar manner to compound **6**, one *ortho*-methyl group from each of the mesityl groups points towards the gold atom, with the nearest Au···H_{Me} distance being 2.60 Å, respectively. This conformation is also observed for $Pmes_3AuCl$[14] (the closest Au···H_{Me} approach is 2.40 Å. Surprisingly, given the large cone angle of $Pmes_3$, the C(2) Au-P sequence is almost linear (178.96(16)°), although the phenyl ring does adopt a conformation for which $\theta = 11.9°$.

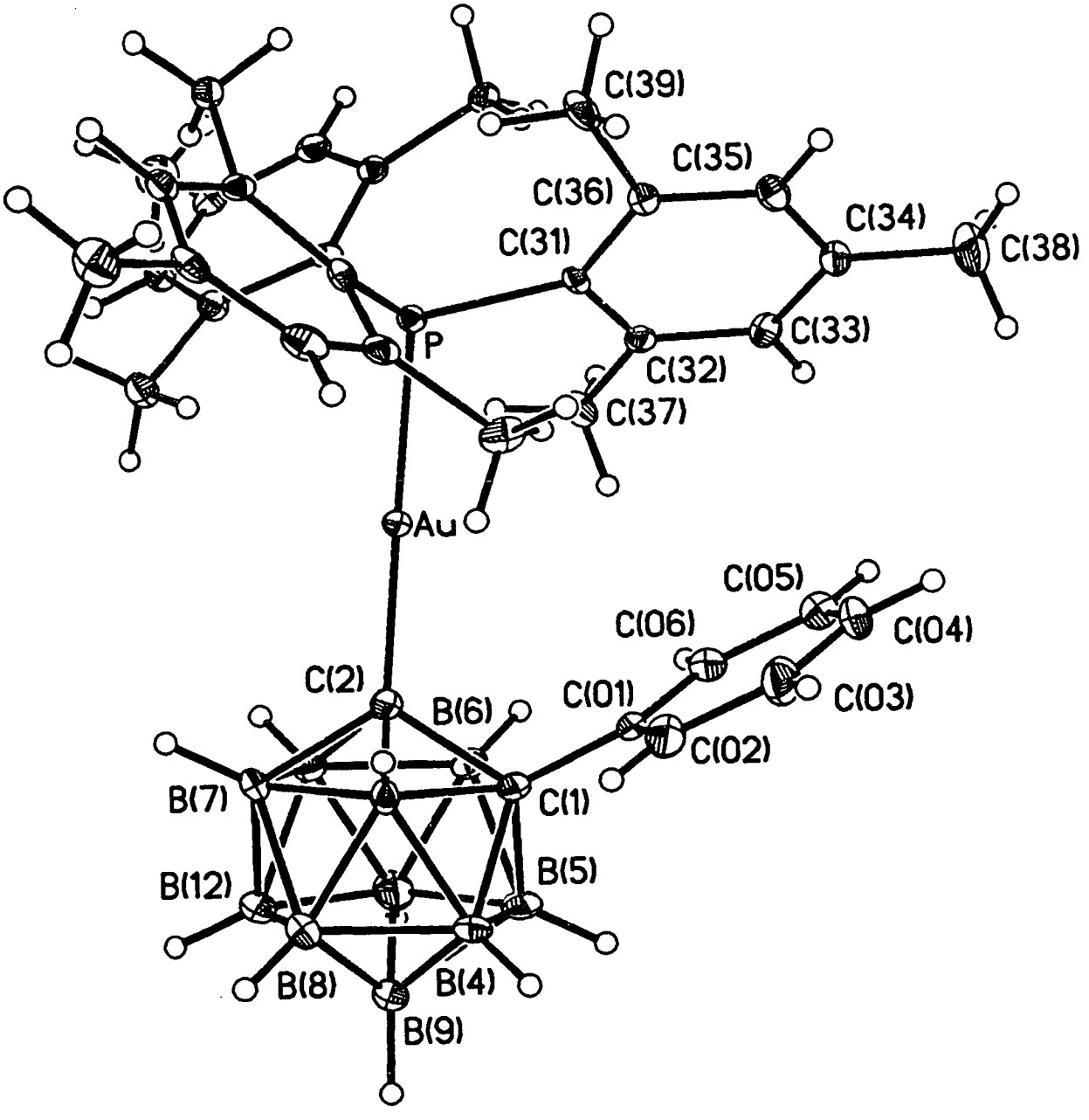

Figure 3.5 Perspective View of **9**

Table 9A Selected Bond Lengths (Å) and Angles (°) for **9**

Au-C(2)	2.050(5)	Au-P	2.3100(14)
C(1)-C(01)	1.518(8)	C(1)-C(2)	1.688(8)
C(1)-B(6)	1.716(9)	C(1)-B(3)	1.716(8)
C(1)-B(4)	1.718(9)	C(1)-B(5)	1.734(9)
C(2)-B(7)	1.696(8)	C(2)-B(11)	1.714(8)
C(2)-B(6)	1.716(8)	C(2)-B(3)	1.713(8)
B(3)-B(7)	1.745(9)	B(3)-B(8)	1.759(10)
B(3)-B(4)	1.773(9)	B(4)-B(5)	1.770(11)
B(4)-B(8)	1.784(10)	B(4)-B(9)	1.797(11)
B(5)-B(9)	1.769(10)	B(5)-B(10)	1.767(11)
B(5)-B(6)	1.797(9)	B(6)-B(11)	1.767(9)
B(6)-B(10)	1.776(10)	B(7)-B(11)	1.746(9)
B(7)-B(12)	1.784(10)	B(7)-B(8)	1.781(9)
B(8)-B(12)	1.783(11)	B(8)-B(9)	1.796(11)
B(9)-B(10)	1.764(11)	B(9)-B(12)	1.770(10)
B(10)-B(11)	1.787(10)	B(10)-B(12)	1.791(11)
B(11)-B(12)	1.776(10)	C(01)-C(06)	1.370(8)
C(01)-C(02)	1.382(8)	C(02)-C(03)	1.397(9)
C(03)-C(04)	1.375(9)	C(04)-C(05)	1.353(9)
C(05)-C(06)	1.414(9)	P-C(31)	1.828(5)
P-C(21)	1.841(5)	P-C(11)	1.839(5)
C(11)-C(16)	1.404(7)	C(11)-C(12)	1.417(8)
C(12)-C(13)	1.399(8)	C(12)-C(17)	1.512(8)
C(13)-C(14)	1.378(8)	C(14)-C(15)	1.386(8)
C(14)-C(18)	1.500(8)	C(15)-C(16)	1.393(7)
C(16)-C(19)	1.515(8)	C(21)-C(22)	1.412(8)
C(21)-C(26)	1.415(7)	C(22)-C(23)	1.403(7)
C(22)-C(27)	1.498(7)	C(23)-C(24)	1.397(7)
C(24)-C(25)	1.363(8)	C(24)-C(28)	1.511(7)
C(25)-C(26)	1.388(8)	C(26)-C(29)	1.518(8)
C(31)-C(32)	1.409(7)	C(31)-C(36)	1.423(7)
C(32)-C(33)	1.391(8)	C(32)-C(37)	1.525(7)
C(33)-C(34)	1.383(8)	C(34)-C(35)	1.385(8)
C(34)-C(38)	1.493(8)	C(35)-C(36)	1.383(8)
C(36)-C(39)	1.520(7)		

C(2)-Au-P	179.0(2)	C(01)-C(1)-C(2)	119.7(4)
C(01)-C(1)-B(6)	120.1(5)	C(2)-C(1)-B(6)	60.5(3)
C(01)-C(1)-B(3)	117.4(5)	C(2)-C(1)-B(3)	60.4(3)
C(01)-C(1)-B(4)	119.1(5)	B(3)-C(1)-B(4)	62.2(4)
C(01)-C(1)-B(5)	121.4(5)	B(6)-C(1)-B(5)	62.7(4)
B(4)-C(1)-B(5)	61.7(4)	B(7)-C(2)-B(11)	61.6(4)
C(1)-C(2)-B(6)	60.5(3)	B(11)-C(2)-B(6)	62.0(4)
C(1)-C(2)-B(3)	60.6(3)	B(7)-C(2)-B(3)	61.6(4)
C(1)-C(2)-Au	118.4(4)	B(7)-C(2)-Au	122.9(4)
B(11)-C(2)-Au	121.6(4)	B(6)-C(2)-Au	116.9(4)
B(3)-C(2)-Au	119.7(4)	C(2)-B(3)-C(1)	59.0(3)

C(2)-B(3)-B(7)	58.8(4)	B(7)-B(3)-B(8)	61.1(4)
C(1)-B(3)-B(4)	59.0(4)	B(8)-B(3)-B(4)	60.7(4)
C(1)-B(4)-B(5)	59.6(4)	C(1)-B(4)-B(3)	58.9(4)
B(3)-B(4)-B(8)	59.3(4)	B(5)-B(4)-B(9)	59.5(4)
B(8)-B(4)-B(9)	60.2(4)	C(1)-B(5)-B(4)	58.7(4)
B(9)-B(5)-B(4)	61.0(4)	B(9)-B(5)-B(10)	59.8(4)
C(1)-B(5)-B(6)	58.1(4)	B(10)-B(5)-B(6)	59.8(4)
C(2)-B(6)-C(1)	58.9(3)	C(2)-B(6)-B(11)	58.9(3)
B(11)-B(6)-B(10)	60.6(4)	C(1)-B(6)-B(5)	59.1(4)
B(10)-B(6)-B(5)	59.3(4)	C(2)-B(7)-B(3)	59.7(4)
C(2)-B(7)-B(11)	59.7(4)	B(11)-B(7)-B(12)	60.4(4)
B(3)-B(7)-B(8)	59.9(4)	B(12)-B(7)-B(8)	60.0(4)
B(3)-B(8)-B(7)	59.0(4)	B(7)-B(8)-B(12)	60.1(4)
B(3)-B(8)-B(4)	60.0(4)	B(12)-B(8)-B(9)	59.3(4)
B(4)-B(8)-B(9)	60.2(4)	B(10)-B(9)-B(5)	60.0(4)
B(10)-B(9)-B(12)	60.9(4)	B(5)-B(9)-B(4)	59.5(4)
B(12)-B(9)-B(8)	60.0(4)	B(4)-B(9)-B(8)	59.6(4)
B(9)-B(10)-B(5)	60.1(4)	B(5)-B(10)-B(6)	60.9(4)
B(6)-B(10)-B(11)	59.4(4)	B(9)-B(10)-B(12)	59.7(4)
B(11)-B(10)-B(12)	59.5(4)	C(2)-B(11)-B(7)	58.7(3)
C(2)-B(11)-B(6)	59.1(3)	B(7)-B(11)-B(12)	60.9(4)
B(6)-B(11)-B(10)	60.0(4)	B(12)-B(11)-B(10)	60.3(4)
B(11)-B(12)-B(7)	58.7(4)	B(9)-B(12)-B(8)	60.7(4)
B(7)-B(12)-B(8)	59.9(4)	B(9)-B(12)-B(10)	59.4(4)
B(11)-B(12)-B(10)	60.1(4)	C(06)-C(01)-C(02)	119.1(6)
C(06)-C(01)-C(1)	121.7(6)	C(02)-C(01)-C(1)	119.2(5)
C(01)-C(02)-C(03)	120.6(6)	C(04)-C(03)-C(02)	119.4(7)
C(05)-C(04)-C(03)	121.0(7)	C(04)-C(05)-C(06)	119.5(7)
C(01)-C(06)-C(05)	120.4(6)	C(31)-P-C(21)	112.2(2)
C(31)-P-C(11)	110.6(2)	C(21)-P-C(11)	112.5(2)
C(31)-P-Au	107.2(2)	C(21)-P-Au	104.4(2)
C(11)-P-Au	109.6(2)	C(16)-C(11)-C(12)	119.4(5)
C(16)-C(11)-P	123.5(4)	C(12)-C(11)-P	117.0(4)
C(13)-C(12)-C(11)	118.7(5)	C(13)-C(12)-C(17)	116.8(5)
C(11)-C(12)-C(17)	124.5(5)	C(14)-C(13)-C(12)	122.7(6)
C(13)-C(14)-C(15)	117.0(5)	C(13)-C(14)-C(18)	121.7(6)
C(15)-C(14)-C(18)	121.3(5)	C(14)-C(15)-C(16)	123.5(5)
C(15)-C(16)-C(11)	118.3(5)	C(15)-C(16)-C(19)	116.3(5)
C(11)-C(16)-C(19)	125.4(5)	C(22)-C(21)-C(26)	119.9(5)
C(22)-C(21)-P	123.2(4)	C(26)-C(21)-P	116.1(4)
C(21)-C(22)-C(23)	117.2(5)	C(21)-C(22)-C(27)	124.8(5)
C(23)-C(22)-C(27)	117.9(5)	C(24)-C(23)-C(22)	123.6(5)
C(25)-C(24)-C(23)	116.5(5)	C(25)-C(24)-C(28)	122.7(5)
C(23)-C(24)-C(28)	120.8(5)	C(24)-C(25)-C(26)	123.9(5)
C(25)-C(26)-C(21)	118.4(5)	C(25)-C(26)-C(29)	117.3(5)
C(21)-C(26)-C(29)	124.3(5)	C(32)-C(31)-C(36)	118.1(5)
C(32)-C(31)-P	117.2(4)	C(36)-C(31)-P	124.6(4)
C(33)-C(32)-C(31)	120.0(5)	C(33)-C(32)-C(37)	116.7(5)
C(31)-C(32)-C(37)	123.2(5)	C(34)-C(33)-C(32)	122.3(5)

C(33)-C(34)-C(35)	116.9(5)	C(33)-C(34)-C(38)	121.1(5)
C(35)-C(34)-C(38)	122.1(5)	C(36)-C(35)-C(34)	123.7(5)
C(35)-C(36)-C(31)	118.6(5)	C(35)-C(36)-C(39)	117.3(5)
C(31)-C(36)-C(39)	124.1(5)		

Table 9B Atomic Coordinates (x 10^4) and Equivalent Isotropic Displacement Parameters ($Å^2$ x 10^3) for **9**

	x	y	z	U(eq)
Au	4164(1)	1417(1)	4089(1)	16(1)
C(1)	3617(4)	1275(3)	2771(2)	26(2)
C(2)	3585(3)	938(3)	3426(2)	21(1)
B(3)	4218(4)	596(3)	2907(3)	24(2)
B(4)	3655(5)	693(4)	2253(3)	33(2)
B(5)	2673(5)	1106(4)	2396(3)	37(2)
B(6)	2659(4)	1274(3)	3147(3)	26(2)
B(7)	3593(4)	126(3)	3366(3)	24(2)
B(8)	3628(5)	-55(4)	2625(3)	37(2)
B(9)	2649(5)	260(4)	2316(3)	42(2)
B(10)	2037(5)	630(4)	2861(3)	39(2)
B(11)	2626(4)	532(3)	3513(3)	25(2)
B(12)	2622(5)	-97(4)	3001(3)	35(2)
C(01)	4110(4)	1899(3)	2681(2)	24(1)
C(02)	4918(4)	1881(3)	2424(3)	34(2)
C(03)	5378(4)	2448(3)	2320(3)	42(2)
C(04)	5020(5)	3027(3)	2478(3)	45(2)
C(05)	4230(5)	3056(3)	2730(3)	47(2)
C(06)	3765(4)	2481(3)	2833(3)	34(2)
P	4831(1)	1967(1)	4824(1)	16(1)
C(11)	4189(3)	1876(3)	5480(2)	17(1)
C(12)	3851(3)	1256(3)	5598(2)	19(1)
C(13)	3247(3)	1187(3)	6040(2)	25(2)
C(14)	2972(3)	1696(3)	6369(2)	24(1)
C(15)	3359(3)	2287(3)	6267(2)	24(1)
C(16)	3975(3)	2391(3)	5841(2)	18(1)
C(17)	4121(4)	649(3)	5290(2)	25(1)
C(18)	2296(4)	1615(3)	6823(3)	38(2)
C(19)	4371(4)	3057(3)	5815(2)	23(1)
C(21)	5914(3)	1597(3)	4881(2)	18(1)
C(22)	6247(3)	1342(3)	5393(2)	17(1)
C(23)	6949(3)	914(3)	5350(2)	21(1)
C(24)	7360(3)	762(3)	4837(2)	22(1)
C(25)	7064(4)	1072(3)	4363(3)	27(1)
C(26)	6354(3)	1484(3)	4361(2)	20(1)
C(27)	5939(3)	1522(3)	5978(2)	20(1)
C(28)	8098(4)	284(3)	4819(3)	34(2)
C(29)	6122(3)	1804(3)	3799(2)	28(2)
C(31)	4887(3)	2812(3)	4613(2)	15(1)
C(32)	4127(3)	3090(3)	4385(2)	19(1)
C(33)	4164(4)	3691(3)	4126(2)	22(1)
C(34)	4917(4)	4054(3)	4114(2)	25(1)
C(35)	5645(4)	3791(3)	4372(3)	26(2)
C(36)	5655(3)	3193(3)	4629(2)	20(1)

C(37)	3239(3)	2766(3)	4409(3)	26(2)
C(38)	4934(4)	4700(3)	3837(3)	44(2)
C(39)	6490(3)	2992(3)	4926(3)	29(2)

Crystallographic Study of 1-Ph-2-{$P(C_6F_5)_3Au$}-1,2-*closo*-$C_2B_{10}H_{10}$ (10)

Colourless, diffraction quality *plates* of **10** were grown by diffusion of *n*-hexane and a CH_2Cl_2 solution (4:1) at -30°C. Intensity data were measured on an Enraf-Nonius CAD4 diffractometer operating with Mo-K_α *X*-radiation (λ_{bar} = 0.71073 Å). The single crystal was mounted in a glass capillary and the experiment performed at 291(2) K.

Crystal data

$C_{26}H_{15}B_{10}F_{15}AuP$, M = 948.42, triclinic, *P*bar1, a = 11.159(8) Å, b = 12.050(9) Å, c = 13.380(10) Å, α = 91.23(6)°, β = 89.73(6)°, γ = 116.07(4)°, V = 1615.7(6) Å^3, from least squares refinement of 25 reflections ($11 \leq \theta \leq 13°$) at 291(2) K, Z = 2, D_c = 1.949 gcm^{-3}, μ(Mo-K_α) = 4.71 mm^{-1}, F(0,0,0) = 900e.

Data collection and reduction

Intensity data collected in the range $4<2\theta<60°$ by the ω-2θ scan method; ω-scan width (1.4+0.35tanθ), ω-scan speeds in the range 1.21 to 1.89°min^{-1}. The intensities of 6433 unique reflections (h -1 to 15, k -16 to 16, l -18 to 18) were measured (DATCOL).

Structure solution and refinement

The structure was solved using Patterson methods (Au) (SHELX76) and ΔF syntheses (P, C, B, F) and developed by iterative, least-squares refinement and further difference Fourier syntheses (SHELXTL). There are 2 molecules *per* unit cell. In the final model all non-H atoms were refined anisotropically. The phenyl H atoms were set in idealised positions (C-H = 0.93 Å), as were cage H atoms, 1.10 Å from the boron atoms on a radial extension from the centre of the icosahedron. Idealised protons were allowed to refine on their respective atoms with U(H) = 1.2 U(C/B).

Data were absorption corrected (ψ-scans) and weighted such that $w^{-1} = [\sigma^2(F_o^2) + (0.0193P)^2 + 3.26P]$ where $P = [\text{max.}\ (F_o^2) + 2F_c^2]/3$. Using 5628 observed data ($F_o > 4.0\sigma(F_o)$), R = 0.0288, wR_2 = 0.0664 and S = 1.155 for 478 variable parameters. The maximum residue and minimum trough in a

final difference Fourier synthesis were 1.87 and -1.34 eÅ^{-3}, respectively. Atomic scattering factors were those inlaid in SHELXTL. Selected bond lengths (Å) and angles (°), fractional coordinates and equivalent isotropic thermal parameters of non-hydrogen atoms are given in **Tables 10A** and **10B**, respectively.

The crystallographic study confirmed compound **10** as having the expected structure, a perspective view of which is shown in **Figure 3.6**, below.

The C_6F_5 rings are arranged in a propeller-type arrangement with the closest Au···F distances being 2.919(6) and 3.124(7) Å. The C_6F_5 rings are essentially planar (σ = 0.0122, 0.0140 and 0.0133 Å for C(11)-F(16), C(21)-F(26) and C(31)-F(36), respectively), with angles of less than the expected 120° at the *ipso* carbons, similar to that observed for **14** (**Section 3.6.4**) and other C_6F_5 rings.[17] The size of the phosphine causes the phenyl ring to twist to a θ value of 4.1° and the C(2)-Au-P sequence to deviate significantly from linearity (175.74(31)°).

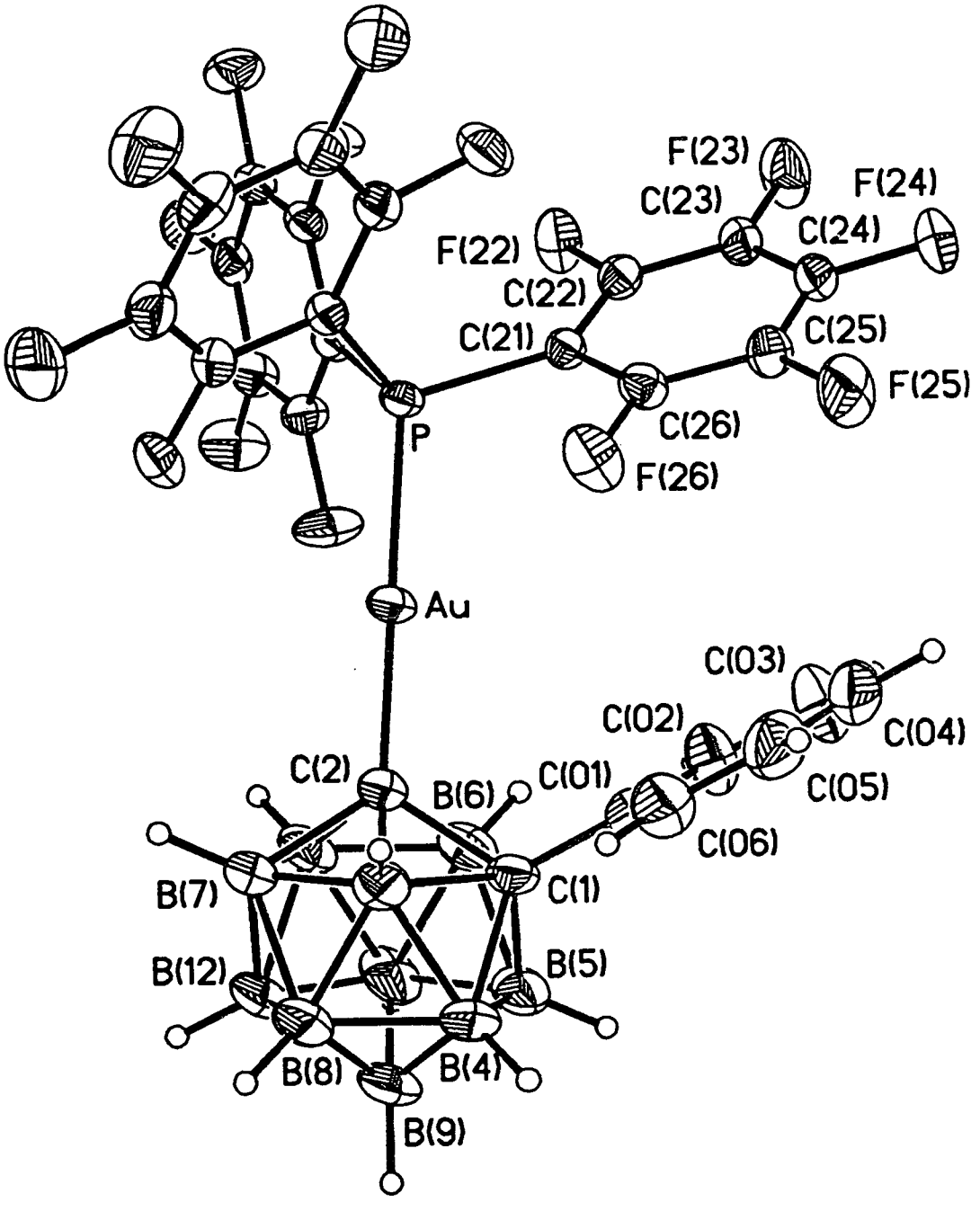

Figure 3.6 Perspective View of **10**

Table 10A Selected Bond Lengths (Å) and Angles (°) for **10**

Au-C(2)	2.044(5)	Au-P	2.2620(11)
P-C(11)	1.820(4)	P-C(21)	1.821(4)
P-C(31)	1.832(5)	C(1)-C(01)	1.512(7)
C(1)-C(2)	1.687(7)	C(1)-B(6)	1.700(8)
C(1)-B(5)	1.706(8)	C(1)-B(4)	1.710(7)
C(1)-B(3)	1.718(8)	C(2)-B(3)	1.698(7)
C(2)-B(6)	1.712(8)	C(2)-B(11)	1.713(8)
C(2)-B(7)	1.716(8)	B(3)-B(7)	1.754(10)
B(3)-B(8)	1.757(10)	B(3)-B(4)	1.777(10)
B(4)-B(8)	1.757(11)	B(4)-B(5)	1.768(12)
B(4)-B(9)	1.768(13)	B(5)-B(10)	1.752(12)
B(5)-B(9)	1.764(10)	B(5)-B(6)	1.768(10)
B(6)-B(10)	1.766(9)	B(6)-B(11)	1.771(10)
B(7)-B(11)	1.759(10)	B(7)-B(12)	1.762(10)
B(7)-B(8)	1.770(10)	B(8)-B(12)	1.756(12)
B(8)-B(9)	1.782(12)	B(9)-B(12)	1.744(12)
B(9)-B(10)	1.760(13)	B(10)-B(12)	1.762(11)
B(10)-B(11)	1.775(11)	B(11)-B(12)	1.786(9)
C(01)-C(02)	1.377(8)	C(01)-C(06)	1.380(8)
C(02)-C(03)	1.383(9)	C(03)-C(04)	1.355(11)
C(04)-C(05)	1.366(10)	C(05)-C(06)	1.370(9)
C(11)-C(12)	1.379(6)	C(11)-C(16)	1.389(6)
C(12)-F(12)	1.334(5)	C(12)-C(13)	1.387(6)
C(13)-F(13)	1.334(5)	C(13)-C(14)	1.363(7)
C(14)-F(14)	1.334(5)	C(14)-C(15)	1.361(7)
C(15)-F(15)	1.331(5)	C(15)-C(16)	1.380(6)
C(16)-F(16)	1.327(5)	C(21)-C(22)	1.381(6)
C(21)-C(26)	1.387(6)	C(22)-F(22)	1.331(5)
C(22)-C(23)	1.384(6)	C(23)-F(23)	1.331(5)
C(23)-C(24)	1.365(7)	C(24)-F(24)	1.326(5)
C(24)-C(25)	1.364(7)	C(25)-F(25)	1.329(5)
C(25)-C(26)	1.379(6)	C(26)-F(26)	1.336(5)
C(31)-C(36)	1.381(6)	C(31)-C(32)	1.392(6)
C(32)-F(32)	1.334(5)	C(32)-C(33)	1.370(7)
C(33)-F(33)	1.335(6)	C(33)-C(34)	1.378(8)
C(34)-F(34)	1.322(6)	C(34)-C(35)	1.365(8)
C(35)-F(35)	1.336(6)	C(35)-C(36)	1.378(7)
C(36)-F(36)	1.334(5)		

C(2)-Au-P	175.74(13)	C(11)-P-C(21)	108.0(2)
C(11)-P-C(31)	105.7(2)	C(21)-P-C(31)	104.7(2)
C(11)-P-Au	113.92(14)	C(21)-P-Au	110.22(14)
C(31)-P-Au	113.70(14)	C(01)-C(1)-C(2)	118.7(4)
C(01)-C(1)-B(6)	118.8(4)	C(2)-C(1)-B(6)	60.7(3)
C(01)-C(1)-B(5)	121.8(5)	B(6)-C(1)-B(5)	62.5(4)
C(01)-C(1)-B(4)	120.6(5)	B(5)-C(1)-B(4)	62.3(4)
C(01)-C(1)-B(3)	117.3(5)	C(2)-C(1)-B(3)	59.8(3)

B(4)-C(1)-B(3)	62.4(4)	C(1)-C(2)-B(3)	61.0(3)
C(1)-C(2)-B(6)	60.0(3)	B(6)-C(2)-B(11)	62.3(4)
B(3)-C(2)-B(7)	61.8(4)	B(11)-C(2)-B(7)	61.7(4)
C(1)-C(2)-Au	119.3(3)	B(3)-C(2)-Au	122.0(4)
B(6)-C(2)-Au	114.5(3)	B(11)-C(2)-Au	118.8(3)
B(7)-C(2)-Au	123.9(3)	C(2)-B(3)-C(1)	59.2(3)
C(2)-B(3)-B(7)	59.6(3)	B(7)-B(3)-B(8)	60.6(4)
C(1)-B(3)-B(4)	58.6(3)	B(8)-B(3)-B(4)	59.6(4)
C(1)-B(4)-B(5)	58.7(4)	B(8)-B(4)-B(9)	60.8(5)
B(5)-B(4)-B(9)	59.9(5)	C(1)-B(4)-B(3)	59.0(3)
B(8)-B(4)-B(3)	59.6(4)	B(10)-B(5)-B(9)	60.1(5)
C(1)-B(5)-B(6)	58.6(3)	B(10)-B(5)-B(6)	60.2(4)
C(1)-B(5)-B(4)	58.9(4)	B(9)-B(5)-B(4)	60.1(5)
C(1)-B(6)-C(2)	59.3(3)	C(1)-B(6)-B(5)	58.9(4)
B(10)-B(6)-B(5)	59.4(5)	C(2)-B(6)-B(11)	58.9(3)
B(10)-B(6)-B(11)	60.3(4)	C(2)-B(7)-B(3)	58.6(3)
C(2)-B(7)-B(11)	59.0(3)	B(11)-B(7)-B(12)	60.9(4)
B(3)-B(7)-B(8)	59.8(4)	B(12)-B(7)-B(8)	59.6(5)
B(3)-B(8)-B(4)	60.8(4)	B(12)-B(8)-B(7)	60.0(4)
B(3)-B(8)-B(7)	59.6(4)	B(12)-B(8)-B(9)	59.0(5)
B(4)-B(8)-B(9)	59.9(5)	B(12)-B(9)-B(10)	60.4(5)
B(10)-B(9)-B(5)	59.6(5)	B(5)-B(9)-B(4)	60.1(4)
B(12)-B(9)-B(8)	59.7(5)	B(4)-B(9)-B(8)	59.3(5)
B(5)-B(10)-B(9)	60.3(5)	B(9)-B(10)-B(12)	59.4(5)
B(5)-B(10)-B(6)	60.3(4)	B(12)-B(10)-B(11)	60.6(4)
B(6)-B(10)-B(11)	60.0(4)	C(2)-B(11)-B(7)	59.2(3)
C(2)-B(11)-B(6)	58.9(3)	B(6)-B(11)-B(10)	59.7(4)
B(7)-B(11)-B(12)	59.6(4)	B(10)-B(11)-B(12)	59.3(4)
B(9)-B(12)-B(8)	61.2(5)	B(9)-B(12)-B(10)	60.3(5)
B(8)-B(12)-B(7)	60.4(4)	B(10)-B(12)-B(11)	60.1(4)
B(7)-B(12)-B(11)	59.4(4)	C(02)-C(01)-C(06)	117.8(5)
C(02)-C(01)-C(1)	120.5(5)	C(06)-C(01)-C(1)	121.6(5)
C(01)-C(02)-C(03)	119.9(7)	C(04)-C(03)-C(02)	121.8(7)
C(03)-C(04)-C(05)	118.6(7)	C(04)-C(05)-C(06)	120.6(7)
C(05)-C(06)-C(01)	121.4(7)	C(12)-C(11)-C(16)	116.1(4)
C(12)-C(11)-P	121.4(3)	C(16)-C(11)-P	122.5(3)
F(12)-C(12)-C(11)	121.3(4)	F(12)-C(12)-C(13)	116.1(4)
C(11)-C(12)-C(13)	122.6(4)	F(13)-C(13)-C(14)	120.9(4)
F(13)-C(13)-C(12)	120.0(4)	C(14)-C(13)-C(12)	119.1(4)
F(14)-C(14)-C(15)	119.9(5)	F(14)-C(14)-C(13)	119.6(5)
C(15)-C(14)-C(13)	120.5(4)	F(15)-C(15)-C(14)	119.9(4)
F(15)-C(15)-C(16)	120.3(4)	C(14)-C(15)-C(16)	119.7(4)
F(16)-C(16)-C(15)	118.2(4)	F(16)-C(16)-C(11)	119.7(4)
C(15)-C(16)-C(11)	122.0(4)	C(22)-C(21)-C(26)	116.0(4)
C(22)-C(21)-P	127.1(3)	C(26)-C(21)-P	116.9(3)
F(22)-C(22)-C(21)	121.6(4)	F(22)-C(22)-C(23)	116.7(4)
C(21)-C(22)-C(23)	121.7(4)	F(23)-C(23)-C(24)	119.3(4)
F(23)-C(23)-C(22)	120.4(4)	C(24)-C(23)-C(22)	120.3(4)
F(24)-C(24)-C(25)	120.4(5)	F(24)-C(24)-C(23)	119.7(5)

C(25)-C(24)-C(23)	119.9(4)	F(25)-C(25)-C(24)	120.5(4)
F(25)-C(25)-C(26)	120.3(5)	C(24)-C(25)-C(26)	119.2(4)
F(26)-C(26)-C(25)	118.5(4)	F(26)-C(26)-C(21)	118.6(4)
C(25)-C(26)-C(21)	122.9(4)	C(36)-C(31)-C(32)	115.9(4)
C(36)-C(31)-P	118.3(3)	C(32)-C(31)-P	125.4(3)
F(32)-C(32)-C(33)	116.8(4)	F(32)-C(32)-C(31)	121.2(4)
C(33)-C(32)-C(31)	122.0(4)	F(33)-C(33)-C(32)	120.2(5)
F(33)-C(33)-C(34)	119.5(5)	C(32)-C(33)-C(34)	120.3(5)
F(34)-C(34)-C(35)	121.1(5)	F(34)-C(34)-C(33)	119.9(5)
C(35)-C(34)-C(33)	119.0(5)	F(35)-C(35)-C(34)	119.8(5)
F(35)-C(35)-C(36)	120.1(5)	C(34)-C(35)-C(36)	120.1(5)
F(36)-C(36)-C(35)	117.8(4)	F(36)-C(36)-C(31)	119.6(4)
C(35)-C(36)-C(31)	122.6(5)		

Table 10B Atomic Coordinates (x 10^4) and Equivalent Isotropic Thermal Parameters ($Å^2$ x 10^3) for **10**

	x	y	z	U(eq)
Au	3220(1)	1745(1)	4225(1)	40(1)
P	3109(1)	1702(1)	2536(1)	34(1)
C(1)	4780(5)	2348(5)	6338(3)	48(1)
C(2)	3294(5)	1648(4)	5745(3)	43(1)
B(3)	3600(7)	2888(6)	6510(5)	58(2)
B(4)	4574(8)	2795(9)	7523(5)	78(2)
B(5)	4854(8)	1476(9)	7303(5)	77(2)
B(6)	4065(7)	789(6)	6158(5)	58(2)
B(7)	2047(7)	1586(7)	6530(4)	60(2)
B(8)	2852(8)	2311(8)	7663(5)	76(2)
B(9)	3614(9)	1412(10)	8155(5)	94(3)
B(10)	3302(8)	176(8)	7307(6)	83(3)
B(11)	2325(7)	276(7)	6301(5)	66(2)
B(12)	2074(8)	692(9)	7547(5)	80(2)
C(01)	6002(5)	3133(5)	5738(4)	51(1)
C(02)	6724(6)	2606(6)	5255(5)	79(2)
C(03)	7862(7)	3341(8)	4734(6)	99(3)
C(04)	8277(7)	4575(8)	4659(6)	90(2)
C(05)	7570(7)	5103(7)	5142(6)	86(2)
C(06)	6455(7)	4395(6)	5680(5)	75(2)
C(11)	2046(4)	186(4)	1996(3)	37(1)
C(12)	1612(5)	-867(4)	2555(3)	44(1)
C(13)	787(5)	-2030(4)	2166(4)	47(1)
C(14)	397(4)	-2146(4)	1190(4)	47(1)
C(15)	790(5)	-1133(5)	611(3)	47(1)
C(16)	1607(4)	19(4)	1010(3)	41(1)
F(12)	1990(4)	-821(3)	3506(2)	69(1)
F(13)	417(4)	-3020(3)	2737(3)	78(1)
F(14)	-382(3)	-3262(3)	804(2)	68(1)
F(15)	418(3)	-1261(3)	-345(2)	68(1)
F(16)	2006(3)	984(3)	417(2)	59(1)
C(21)	4770(4)	2215(4)	2007(3)	33(1)
C(22)	5169(4)	1603(4)	1294(3)	41(1)
C(23)	6458(5)	2108(5)	926(4)	48(1)
C(24)	7382(5)	3228(5)	1279(4)	49(1)
C(25)	7035(5)	3855(4)	1994(4)	50(1)
C(26)	5741(5)	3352(4)	2340(3)	43(1)
F(22)	4333(3)	498(3)	925(2)	66(1)
F(23)	6809(3)	1506(4)	228(3)	82(1)
F(24)	8610(3)	3708(3)	914(3)	76(1)
F(25)	7921(3)	4954(3)	2336(3)	82(1)
F(26)	5401(3)	4002(3)	3008(2)	69(1)
C(31)	2488(4)	2754(4)	2032(3)	37(1)
C(32)	3033(5)	3529(4)	1228(4)	45(1)

C(33)	2631(5)	4410(5)	978(4)	52(1)
C(34)	1656(5)	4554(5)	1523(4)	58(1)
C(35)	1077(5)	3787(5)	2300(4)	57(1)
C(36)	1491(5)	2905(5)	2545(4)	47(1)
F(32)	3979(3)	3445(3)	663(2)	65(1)
F(33)	3189(3)	5144(3)	206(3)	79(1)
F(34)	1301(4)	5430(3)	1292(3)	86(1)
F(35)	111(4)	3896(4)	2824(3)	92(1)
F(36)	892(3)	2176(3)	3310(2)	66(1)

3.6.2 Crystallographic Studies of PR'_3AuMe

Crystallographic Study of P(*o*-tol)$_3$AuMe (6a)

Colourless, diffraction quality *blocks* and *octahedra* of **6a** were grown by diffusion of *i*-hexane and a CH_2Cl_2 solution at -30°C. Intensity data were measured on a Siemens P4 diffractometer operating with Mo-K_α *X*-radiation (λ_{bar} = 0.71073 Å). The single crystal (block) was mounted in a glass capillary and the experiment performed at 291(2) K.

Crystal data

$C_{22}H_{24}AuP$, M = 516.35, cubic, *Pa*bar3, a = 15.7166(12) Å, V = 3882.2(5) Å^3, from least squares refinement of 25 reflections ($10 \leq \theta \leq 13°$) at 291(2) K, Z = 8, D_c = 1.767 gcm^{-3}, μ(Mo-K_α) = 7.66 mm^{-1}, F(0,0,0) = 2000e.

Data collection and reduction

Intensity data collected in the range $0 < 2\theta < 50°$ by the ω-scan method; ω-scan width 0.9°, ω-scan speeds in the range 1.5 to 60°min^{-1}. The intensities of 1147 unique reflections (h -1 to 18, k -1 to 18, l -1 to 18) were measured (XSCANS).

Structure solution and refinement

The structure was solved using Patterson methods (Au) and ΔF syntheses (P, C) and developed by iterative, full-matrix least-squares refinement and further difference Fourier syntheses (SHELXTL). The unit cell contains 8 molecules, the Au-P-C_{Me} vector of which lies on a three-fold axis. In the final model all non-H atoms were refined anisotropically. The *o*-tolyl and methyl H atoms were all set in idealised positions (C-H = 0.93 Å). Methyl protons were allowed to ride on their respective carbon atoms with U(H) = 1.5 U(C_{Me}). All other fixed protons were similarly fixed with U(H) = 1.2 U(C/B).

Data were absorption corrected (ψ-scans) and weighted such that $w^{-1} = [\sigma^2(F_o^2) + (0.032P)^2]$ where P = [max. (F_o^2) + $2F_c^2]/3$. Using 791 observed data ($F_o > 4.0\sigma(F_o)$), R = 0.0345, wR_2 = 0.0790 and S = 1.033 for 73

variable parameters. The maximum residue and minimum trough in a final difference Fourier synthesis were 0.46 and -0.54 eÅ^{-3}, respectively. Atomic scattering factors were those inlaid in SHELXTL. Selected bond lengths (Å) and angles (°), fractional coordinates and equivalent isotropic thermal parameters of non-hydrogen atoms are in **Tables 6aA** and **6aB**, respectively.

The crystallographic study confirmed the compound as being the P(*o*-tol)$_3$AuMe (**Fig. 3.7**). The molecule lies along a crystallographically imposed three-fold axis and, as such, the C(01)-Au-P bond angle is 180°. The Au-C_{Me} bond length is 2.083(14) Å, shorter, but not significantly so, than 1-Ph-2-{P(*o*-tol)$_3$Au}-1,2-*closo*-$C_2B_{10}H_{10}$ (2.046(8) Å). It is however, significantly shorter than for P(*o*-tol)$_3$AuCl (2.281(3) Å).[10] The Au-P bond length is 2.289(2) Å, which is typical for Au(I) bonded to phosphorous. The geometry of the phosphorous is approximately tetrahedral with the Au-P-C(11) and C(11)-P-C(11)′ bond angles of 113.99(22) and 104.60(26)°, respectively.

The *ortho*-methyl groups point towards the gold atom in a fashion similar to that described for **6** and P(*o*-tol)$_3$AuCl, with the shortest Au-H_{Me} contact being 2.73 Å.

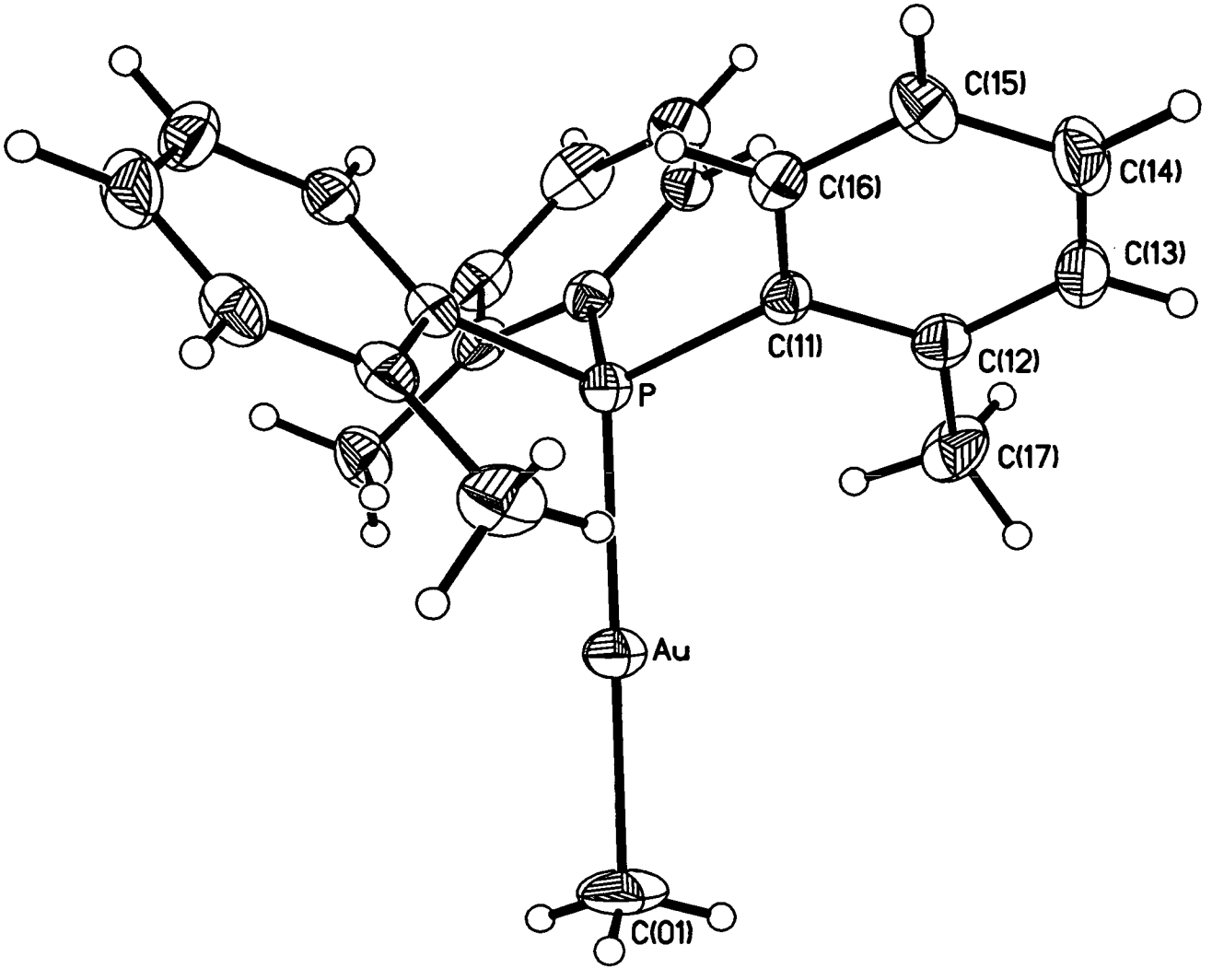

Figure 3.7 Perspective View of **6a**

Table 6aA Selected Bond Lengths (Å) and Angles (°) for **6a**

Au-C(01)	2.082(14)	Au-P	2.306(3)
P-C(11)	1.818(7)	C(11)-C(16)	1.393(10)
C(11)-C(12)	1.419(10)	C(12)-C(13)	1.391(10)
C(12)-C(17)	1.507(11)	C(13)-C(14)	1.390(13)
C(14)-C(15)	1.380(12)	C(15)-C(16)	1.373(10)

C(01)-Au-P	180.0	C(11)-P-C(11)#2	104.6(3)
C(11)-P-Au	114.0(2)	C(16)-C(11)-C(12)	117.9(7)
C(16)-C(11)-P	120.8(5)	C(12)-C(11)-P	121.2(6)
C(13)-C(12)-C(11)	118.6(7)	C(13)-C(12)-C(17)	119.6(8)
C(11)-C(12)-C(17)	121.7(7)	C(14)-C(13)-C(12)	122.2(8)
C(15)-C(14)-C(13)	118.7(8)	C(16)-C(15)-C(14)	120.2(8)
C(15)-C(16)-C(11)	122.3(7)		

Table 6aB Atomic Coordinates (x 10^4) and Equivalent Isotropic Thermal Parameters (Å^2 x 10^3) for **6a**

	x	y	z	U(eq)
Au	2045(1)	7045(1)	7955(1)	44(1)
C(01)	2810(5)	7810(5)	7190(5)	77(6)
P	1198(1)	6198(1)	8802(1)	32(1)
C(11)	814(4)	6724(4)	9759(5)	32(1)
C(12)	435(5)	7543(5)	9722(5)	40(2)
C(13)	193(5)	7933(6)	10479(5)	49(2)
C(14)	307(6)	7545(6)	11266(6)	59(2)
C(15)	672(5)	6747(5)	11294(5)	50(2)
C(16)	917(4)	6349(4)	10555(4)	37(2)
C(17)	263(5)	7982(5)	8887(6)	58(2)

Crystallographic Study of PCy_3AuMe (7a)

Colourless, diffraction quality *blocks* of **7a** were grown by diffusion of *i*-hexane and a CH_2Cl_2 solution at -30°C. Intensity data were measured on an Enraf-Nonius CAD4 diffractometer operating with Mo-K_α *X*-radiation (λ_{bar} = 0.71073 Å). The single crystal was mounted in a glass capillary and the experiment performed at 291(2) K.

Crystal data

$C_{19}H_{36}AuP$, M = 492.41, triclinic, *P*bar1, a = 9.241(4) Å, b = 10.125(5) Å, c = 10.883(4) Å, α = 88.99(3)°, β = 81.126(23)°, γ = 76.842(14)°, V = 979.4(8) Å^3, from least squares refinement of 25 reflections ($10 \leq \theta \leq 11°$) at 291(2) K, Z = 2, D_c = 1.670 gcm^{-3}, μ(Mo-K_α) = 7.59 mm^{-1}, F(0,0,0) = 488e.

Data collection and reduction

Intensity data collected in the range $2<2\theta<50°$ by the ω-2θ scan method; ω-scan width (0.8+0.34tanθ), ω-scan speeds in the range 0.92 to 2.35°min^{-1}. The intensities of 3423 unique reflections (h -10 to 10, k -11 to 12, l 0 to 12) were measured (DATCOL).

Structure solution and refinement

The structure was solved using Patterson methods (Au) (SHELX76) and ΔF syntheses (P, C) and developed by iterative, full-matrix least-squares refinement and further difference Fourier syntheses (SHELXTL). There are two molecules *per* unit cell. In the final model all non-H atoms were refined anisotropically. The cyclohexyl H atoms were set in idealised positions (C-H =0.93 Å) and allowed to refine on their respective carbon atoms with U(H) = 1.2 U(C/B). The methyl protons were also fixed in idealised positions and allowed to ride on their respective carbon atoms with U(H) = 1.5 U(C_{Me}).

Data were absorption corrected (DIFABS) and weighted such that $w^{-1} = [\sigma^2(F_o^2) + (0.0507P)^2 + 0.6775P]$ where $P = [\max.(F_o^2) + 2F_c^2]/3$. Using 3151 observed data ($F_o > 4.0\sigma(F_o)$), R = 0.0337, wR_2 = 0.0802 and S = 1.080 for 191 variable parameters. The maximum residue and minimum trough in

a final difference Fourier synthesis were 1.69 and -1.42 eÅ^{-3}, respectively. Atomic scattering factors were those inlaid in SHELXTL. Selected bond lengths (Å) and angles (°), fractional coordinates and equivalent isotropic thermal parameters of non-hydrogen atoms are in **Tables 7aA** and **7aB**, respectively.

The crystallographic study confirmed that the compound was PCy_3AuMe (**Fig 3.8**). The geometry about the gold atom is slightly, but significantly, deviated from linearity (176.04(23)°). The Au-C(01) bond length is significantly shorter than that in compound **7**, again suggesting that the carbaborane is acting as an efficient σ-donor. The conformation of the cyclohexyl rings is similar to that observed for **7** and PCy_3AuCl.[16a]

Previous to this thesis, there had been only two structural determinations of PR'_3AuMe species; PPh_3AuMe[18] and PMe_3AuMe[19] (electron-diffraction).

Table 3.9 presents some selected bond lengths and angles determined from these studies.

Table 3.9 Pertinent Bond Lengths (Å) and Angles (°) for PR'_3AuMe Species

Compound	**P(*o*-tol)$_3$AuMe**	**PCy$_3$AuMe**	**PPh$_3$AuMe**	**PMe$_3$AuMe**
Au-C$_{Me}$/(Å)	2.083(14)	2.065(6)	2.124(28)	2.034(12)
Au-P/(Å)	2.306(3)	2.292(2)	2.279(8)	2.280(5)
C$_{Me}$-Au-P/(°)	180	176.04(23)	179.1(8)	180
Au-P-C^1/(°)	113.99(22)	109.15(17)	112.3(7)	115.2(3)
Au-P-C^2/(°)	-	115.21(19)	114.4(7)	-
Au-P-C^3/(°)	-	112.37(18)	115.1(7)	-
P-C^1/(Å)	1.818(7)	1.841(5)	1.819(19)	1.829(6)
P-C^2/(Å)	-	1.844(5)	1.822(25)	-
P-C^3/(Å)	-	1.847(5)	1.833(20)	-

(NB: the model for PMe_3AuMe was fixed with a C_3 axis through P, Au and C_{Me})

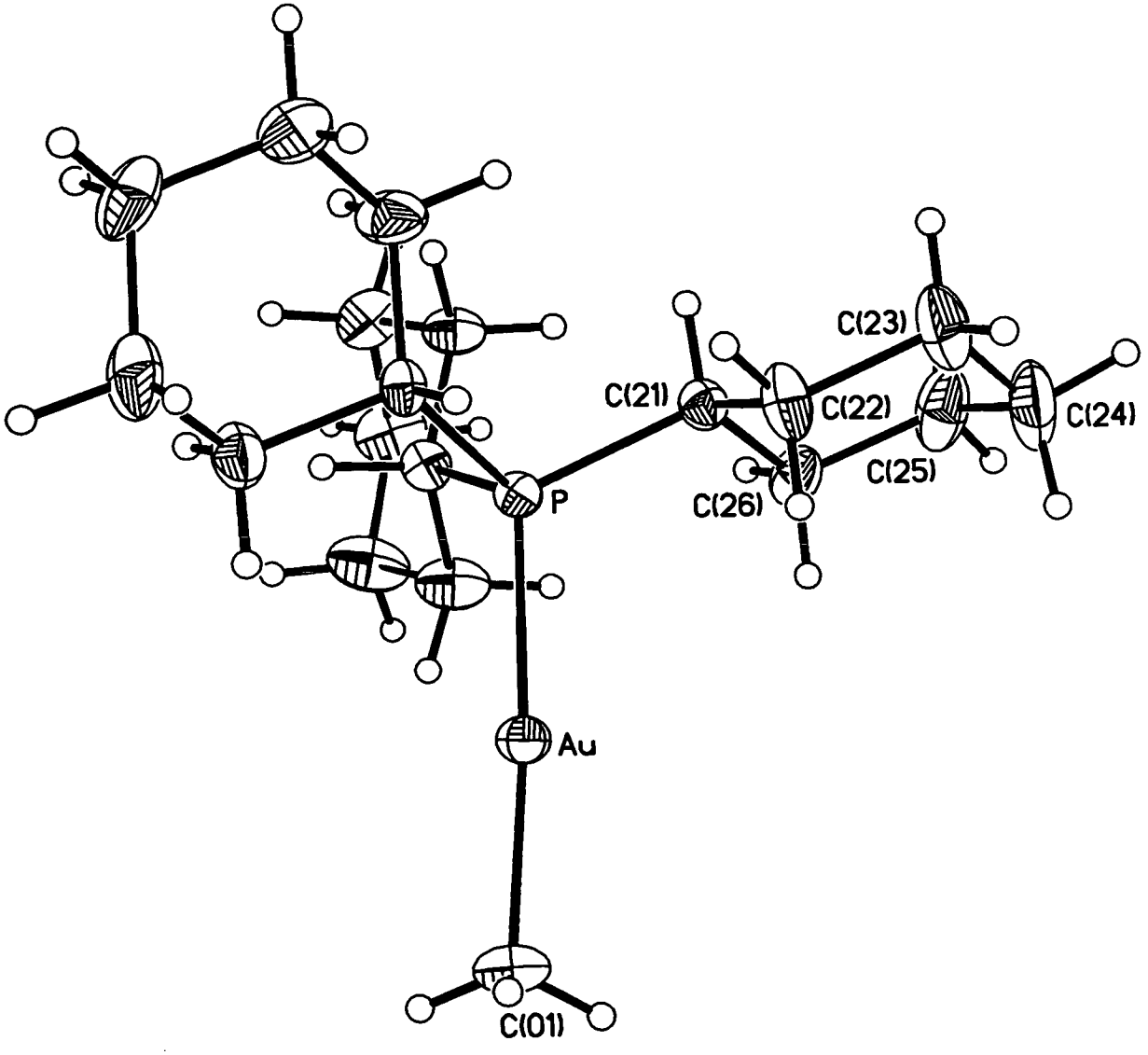

Figure 3.8 Perspective View of **7a**

The Au-P and Au-C_{Me} bond lengths are not significantly different from each other, respectively, except for Au-C_{Me} in PPh_3AuMe, which is a rather inaccurate determination. The geometries about the phosphorous atoms are all similar, with Au-P bond lengths that are significantly different, yet typical for phosphorous bound to Au(I). The P-C bond lengths are similarly typical.

In a recent paper,[11] Hawthorne disagreed with the view of the carbaborane as an efficient σ-donor, arguing that the unusually short Au-C_{cage} bond distance observed for class 3 carbaauraboranes was due to the hybridisation of the atomic orbitals on the cage carbon atom, where there was a greater degree of *s*-character associated with these atomic orbitals compared to the sp^3 orbitals of methyl and other alkyl groups, and not that the carbaborane is acting as a σ-donor, indeed that it is electron-withdrawing. Although we generally agree with this hypothesis, there are several points which can not be explained by this model, for example the EHMO calculations performed by Reid,[6] which demonstrated that there was a greater net charge on the gold atom when attached to the carbaborane compared to methyl. On balance, we do not, regard the carbaborane a strong electron-withdrawer, merely a weak σ-donor.

Table 7aA Selected Bond Lengths (Å) and Angles (°) for **7a**

Au-C(01)	2.065(6)	Au-P	2.292(2)
P-C(21)	1.841(5)	P-C(11)	1.844(5)
P-C(31)	1.847(5)	C(11)-C(16)	1.520(8)
C(11)-C(12)	1.525(7)	C(12)-C(13)	1.503(9)
C(13)-C(14)	1.521(12)	C(14)-C(15)	1.480(10)
C(15)-C(16)	1.536(8)	C(21)-C(26)	1.517(8)
C(21)-C(22)	1.519(8)	C(22)-C(23)	1.517(9)
C(23)-C(24)	1.545(13)	C(24)-C(25)	1.520(12)
C(25)-C(26)	1.512(9)	C(31)-C(32)	1.512(8)
C(31)-C(36)	1.540(8)	C(32)-C(33)	1.512(8)
C(33)-C(34)	1.505(9)	C(34)-C(35)	1.529(10)
C(35)-C(36)	1.517(10)		

C(01)-Au-P	176.0(2)	C(21)-P-C(11)	105.3(2)
C(21)-P-C(31)	108.1(2)	C(11)-P-C(31)	106.1(2)
C(21)-P-Au	115.2(2)	C(11)-P-Au	109.2(2)
C(31)-P-Au	112.4(2)	C(16)-C(11)-C(12)	110.0(5)
C(16)-C(11)-P	117.4(4)	C(12)-C(11)-P	111.1(4)
C(13)-C(12)-C(11)	112.4(5)	C(12)-C(13)-C(14)	111.8(6)
C(15)-C(14)-C(13)	111.3(6)	C(14)-C(15)-C(16)	111.1(6)
C(11)-C(16)-C(15)	110.6(5)	C(26)-C(21)-C(22)	110.3(5)
C(26)-C(21)-P	111.4(4)	C(22)-C(21)-P	110.2(4)
C(23)-C(22)-C(21)	111.8(5)	C(22)-C(23)-C(24)	110.9(7)
C(25)-C(24)-C(23)	110.8(7)	C(26)-C(25)-C(24)	111.4(6)
C(25)-C(26)-C(21)	112.4(6)	C(32)-C(31)-C(36)	110.3(4)
C(32)-C(31)-P	117.2(4)	C(36)-C(31)-P	112.3(4)
C(33)-C(32)-C(31)	112.3(5)	C(34)-C(33)-C(32)	111.8(6)
C(33)-C(34)-C(35)	111.5(5)	C(36)-C(35)-C(34)	112.8(6)
C(35)-C(36)-C(31)	110.7(6)		

Table 7aB Atomic Coordinates (x 10^4) and Equivalent Isotropic Thermal Parameters ($Å^2$ x 10^3) for **7a**

	x	y	z	U(eq)
Au	8817(1)	-449(1)	7776(1)	36(1)
C(01)	8375(9)	-2358(7)	7759(8)	64(2)
P	9137(2)	1725(1)	7854(1)	29(1)
C(11)	8340(5)	2462(6)	9417(5)	33(1)
C(12)	6704(7)	2366(8)	9767(6)	51(2)
C(13)	6070(8)	2823(9)	11087(7)	64(2)
C(14)	6272(8)	4234(8)	11351(6)	62(2)
C(15)	7868(9)	4310(9)	11040(6)	65(2)
C(16)	8490(9)	3891(7)	9677(6)	55(2)
C(21)	11105(6)	1886(6)	7601(5)	36(1)
C(22)	11929(6)	1155(8)	8611(6)	53(2)
C(23)	13563(8)	1249(10)	8426(9)	75(2)
C(24)	14372(8)	700(10)	7124(10)	82(3)
C(25)	13542(8)	1422(9)	6114(8)	72(2)
C(26)	11908(7)	1341(7)	6327(6)	49(1)
C(31)	8127(6)	2844(6)	6752(5)	35(1)
C(32)	8593(7)	4164(6)	6444(5)	43(1)
C(33)	7575(9)	5061(7)	5652(6)	54(2)
C(34)	7491(10)	4344(8)	4474(6)	62(2)
C(35)	7069(11)	2981(9)	4747(7)	70(2)
C(36)	8079(9)	2084(7)	5550(6)	56(2)

3.6.3 Crystallographic Studies of 1-R-2-{P(*o*-tol)$_3$Au}-1,2-*closo*-$C_2B_{10}H_{10}$

Crystallographic Study of 1-Ph-2-{P(*o*-tol)$_3$Au}-1,2-*closo*-$C_2B_{10}H_{10}$ (6)

See **Section 3.6.1.** for details of the structural study.

The main features of the structure, a perspective view of which is shown in **Figure 3.1**, are that the C(1)-C(2) distance (1.709(12) Å) is lengthened relative to compounds **1** and **11** (1.640(5) and 1.656(7) Å, respectively), the phenyl ring is twisted away from the conformation observed for **1** to one for which $\theta = 5.9^o$ and that the C(2)-Au-P bond angle (173.97(18)°) significantly deviates from linearity.

Crystallographic Study of 1-H-2-{P(*o*-tol)$_3$Au}-1,2-*closo*-$C_2B_{10}H_{10}$ (11)

Colourless, diffraction quality *blocks* of **11** were grown by diffusion of *i*-hexane and a CH_2Cl_2 solution at -30°C. Intensity data were measured on an Enraf-Nonius CAD4 diffractometer operating with Mo-K_α X-radiation (λ_{bar} = 0.71073 Å). The single crystal was mounted in a glass capillary and the experiment performed at 198(2) K.

Crystal data

$C_{23}H_{32}B_{10}AuP.\ CH_2Cl_2$, M = 729.50, triclinic, *P*bar1, a = 10.5037(12) Å, b = 10.8241(14) Å, c = 14.3665(15) Å, α = 75.412(7)°, β = 73.648(6)°, γ = 84.872(7)°, V = 1516.5(3) Å^3, from least squares refinement of 25 reflections ($11 \leq \theta \leq 13^o$) at 198(2) K, Z = 2, D_c = 1.597 gcm^{-3}, μ(Mo-K_α) = 5.09 mm^{-1}, F(0,0,0) = 712e.

Data collection and reduction

Intensity data collected in the range $0<2\theta<50^o$ by the ω-2θ scan method; ω-scan width (0.8+0.34tanθ), ω-scan speeds in the range 0.92 to 2.35°min^{-1}. The intensities of 5315 unique reflections (*h* -11 to 12, *k* -12 to 12, *l* 0 to 17) were measured (DATCOL).

Structure solution and refinement

The structure was solved using Patterson methods (Au) (SHELX76) and ΔF syntheses (P, C, B, Cl) and developed by iterative, full-matrix least-squares refinement and further difference Fourier syntheses (SHELXTL). There are two molecules of **11** and two of CH_2Cl_2 *per* unit cell. In the final model all non-H atoms were refined anisotropically. The solvent protons were fixed in idealised positions (C-H = 0.93 Å). The C_6 rings were treated as planar hexagons (C-C = 1.39 Å) with the 2-Me groups modelled as being rigid. The *o*-tolyl H atoms were also set in idealised positions (C-H = 0.93 Å). Cage H atoms were located from difference Fourier syntheses and allowed free positional refinement. All H atoms were given a common thermal parameter, which was 0.0549(33) at convergence.

Data were absorption corrected (DIFABS) and weighted such that $w^{-1} = [\sigma^2(F_o^2) + (0.1P)^2]$ where $P = [\text{max. } (F_o^2) + 2F_c^2]/3$. Using 4947 observed data ($F_o > 4.0\sigma(F_o)$), $R = 0.0294$, $wR_2 = 0.0993$ and $S = 0.913$ for 350 variable parameters. The maximum residue and minimum trough in a final difference Fourier synthesis were 1.29 and -0.91 eÅ^{-3}, respectively. Atomic scattering factors were those inlaid in SHELXTL. Selected bond lengths (Å) and angles (°), fractional coordinates and equivalent isotropic thermal parameters of non-hydrogen atoms are given in **Tables 11A** and **11B**, respectively.

The crystallographic study confirmed that the carbaborane cage had the expected icosahedral geometry, with the C(2)-Au-P sequence being essentially linear (178.44(13)°) (**Fig. 3.9**), reflecting the minimal steric crowding between the {P(*o*-tol)$_3$Au} fragment and the adjacent C(1) H atom. Moreover, the C(1)-C(2) distance (1.656(7) Å) is the shortest of the four compounds and not significantly different to that of *o*-$C_2B_{10}H_{12}$ (1.65(5) Å).[20] The B-C and B-B distances are in the range 1.706(11) to 1.729(12) Å and 1.756(13) to 1.786(14) Å, respectively, typical for *closo* C_2B_{10} cages.

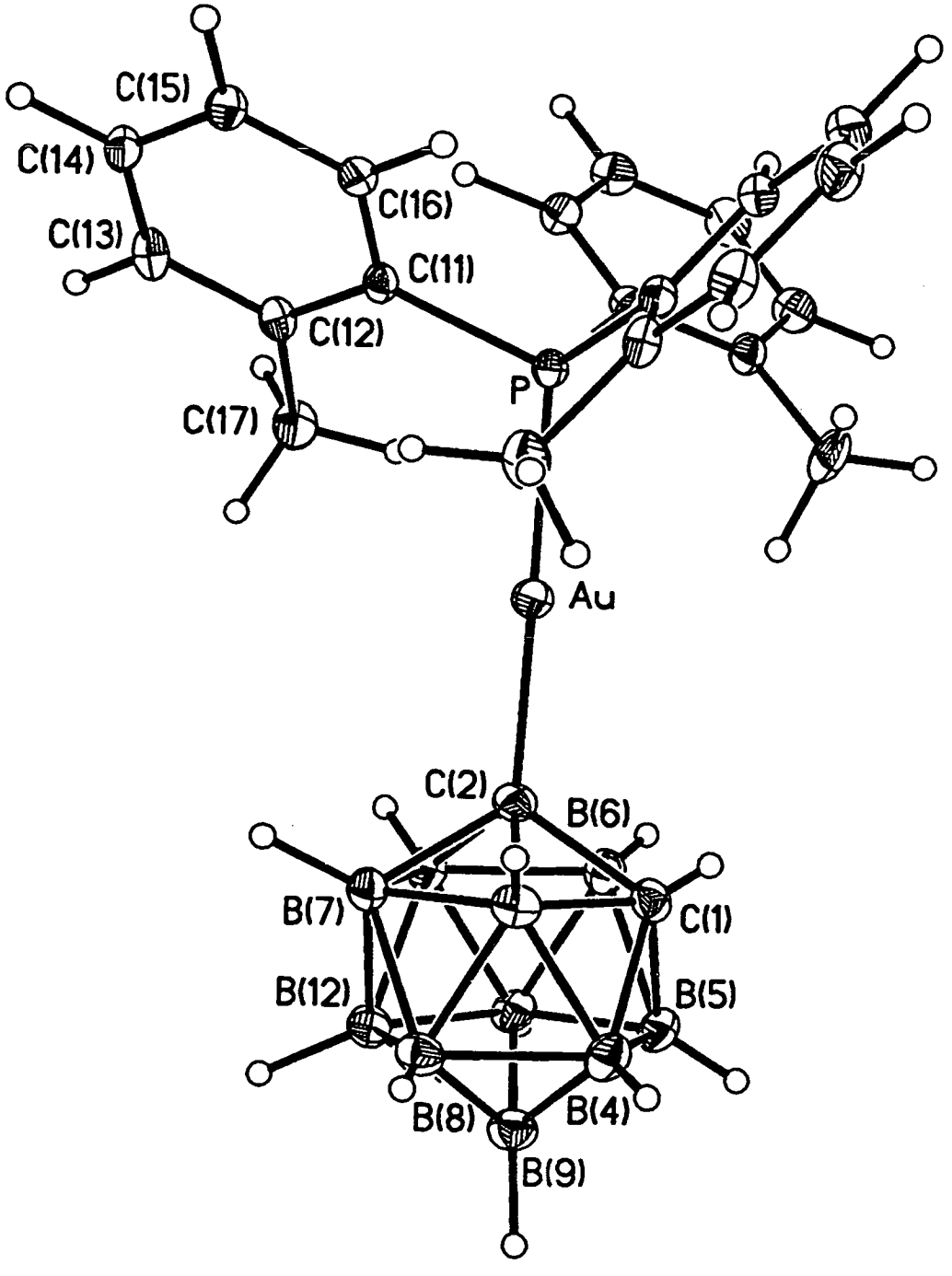

Figure 3.9 Perspective View of **11**

Table 11A Selected Bond Lengths (Å) and Angles (°) for **11**

Au-C(2)	2.053(5)	Au-P	2.2802(12)
C(1)-C(2)	1.655(7)	C(1)-B(3)	1.685(7)
C(1)-B(4)	1.682(8)	C(1)-B(5)	1.697(8)
C(1)-B(6)	1.702(8)	C(2)-B(11)	1.706(7)
C(2)-B(7)	1.710(8)	C(2)-B(3)	1.732(7)
C(2)-B(6)	1.728(8)	B(3)-B(4)	1.762(8)
B(3)-B(7)	1.769(9)	B(3)-B(8)	1.768(8)
B(4)-B(8)	1.761(9)	B(4)-B(9)	1.777(9)
B(4)-B(5)	1.775(8)	B(5)-B(10)	1.750(9)
B(5)-B(9)	1.767(9)	B(5)-B(6)	1.768(8)
B(6)-B(10)	1.758(8)	B(6)-B(11)	1.763(8)
B(7)-B(11)	1.768(8)	B(7)-B(12)	1.777(8)
B(7)-B(8)	1.766(9)	B(8)-B(12)	1.770(9)
B(8)-B(9)	1.785(8)	B(9)-B(12)	1.771(9)
B(9)-B(10)	1.780(9)	B(10)-B(11)	1.766(8)
B(10)-B(12)	1.765(8)	B(11)-B(12)	1.776(9)
P-C(31)	1.820(2)	P-C(11)	1.831(2)
P-C(21)	1.832(2)	C(12)-C(17)	1.516(5)
C(22)-C(27)	1.514(6)	C(32)-C(37)	1.532(5)
C(01)-Cl(01)	1.745(7)	C(01)-Cl(02)	1.741(6)

C(2)-Au-P	178.44(14)	C(2)-C(1)-B(3)	62.4(3)
B(3)-C(1)-B(4)	63.1(3)	B(4)-C(1)-B(5)	63.4(3)
C(2)-C(1)-B(6)	61.9(3)	B(5)-C(1)-B(6)	62.7(3)
B(11)-C(2)-B(7)	62.4(3)	C(1)-C(2)-B(3)	59.6(3)
B(7)-C(2)-B(3)	61.9(3)	C(1)-C(2)-B(6)	60.4(3)
B(11)-C(2)-B(6)	61.8(3)	C(1)-C(2)-Au	119.0(3)
B(11)-C(2)-Au	123.4(3)	B(7)-C(2)-Au	122.6(3)
B(3)-C(2)-Au	116.8(3)	B(6)-C(2)-Au	118.2(3)
C(1)-B(3)-C(2)	57.9(3)	C(1)-B(3)-B(4)	58.3(3)
C(2)-B(3)-B(7)	58.4(3)	B(4)-B(3)-B(8)	59.9(3)
B(7)-B(3)-B(8)	59.9(3)	C(1)-B(4)-B(3)	58.5(3)
B(8)-B(4)-B(3)	60.2(3)	B(8)-B(4)-B(9)	60.6(3)
C(1)-B(4)-B(5)	58.7(3)	B(9)-B(4)-B(5)	59.7(3)
B(10)-B(5)-B(9)	60.8(4)	C(1)-B(5)-B(6)	58.8(3)
B(10)-B(5)-B(6)	60.0(3)	C(1)-B(5)-B(4)	57.9(3)
B(9)-B(5)-B(4)	60.2(3)	C(1)-B(6)-C(2)	57.7(3)
C(2)-B(6)-B(11)	58.5(3)	C(1)-B(6)-B(5)	58.5(3)
B(10)-B(6)-B(5)	59.5(3)	C(2)-B(7)-B(11)	58.7(3)
C(2)-B(7)-B(3)	59.7(3)	B(11)-B(7)-B(12)	60.1(3)
B(3)-B(7)-B(8)	60.0(3)	B(12)-B(7)-B(8)	59.9(3)
B(4)-B(8)-B(3)	59.9(3)	B(3)-B(8)-B(7)	60.1(3)
B(12)-B(8)-B(7)	60.3(3)	B(4)-B(8)-B(9)	60.2(4)
B(12)-B(8)-B(9)	59.8(4)	B(4)-B(9)-B(5)	60.1(3)
B(4)-B(9)-B(8)	59.3(3)	B(12)-B(9)-B(8)	59.7(4)
B(5)-B(9)-B(10)	59.1(3)	B(12)-B(9)-B(10)	59.6(3)
B(6)-B(10)-B(5)	60.5(3)	B(6)-B(10)-B(11)	60.1(3)

B(11)-B(10)-B(12)	60.4(3)	B(5)-B(10)-B(9)	60.1(4)
B(12)-B(10)-B(9)	59.9(4)	C(2)-B(11)-B(6)	59.7(3)
B(6)-B(11)-B(10)	59.7(3)	C(2)-B(11)-B(7)	58.9(3)
B(10)-B(11)-B(12)	59.8(3)	B(7)-B(11)-B(12)	60.2(3)
B(7)-B(12)-B(8)	59.7(3)	B(8)-B(12)-B(9)	60.5(4)
B(9)-B(12)-B(10)	60.5(4)	B(7)-B(12)-B(11)	59.7(3)
B(10)-B(12)-B(11)	59.9(3)	C(31)-P-C(11)	105.2(2)
C(31)-P-C(21)	105.84(14)	C(11)-P-C(21)	106.26(14)
C(31)-P-Au	114.52(12)	C(11)-P-Au	112.92(11)
C(21)-P-Au	111.47(11)	C(16)-C(11)-P	118.9(2)
C(12)-C(11)-P	121.1(2)	C(11)-C(12)-C(17)	123.3(3)
C(13)-C(12)-C(17)	116.7(3)	C(26)-C(21)-P	119.0(2)
C(22)-C(21)-P	120.9(2)	C(21)-C(22)-C(27)	122.9(3)
C(23)-C(22)-C(27)	117.1(3)	C(36)-C(31)-P	117.9(2)
C(32)-C(31)-P	122.1(2)	C(31)-C(32)-C(37)	122.4(3)
C(33)-C(32)-C(37)	117.6(3)	Cl(01)-C(01)-Cl(02)	111.6(4)

Table 11B Atomic Coordinates (x 10^4) and Equivalent Isotropic Displacement Parameters ($Å^2$ x 10^3) for **11**

	x	y	z	U(eq)
Au	1274(1)	1364(1)	2130(1)	27(1)
C(1)	-59(5)	-896(5)	3980(4)	30(1)
C(2)	-109(5)	-25(5)	2863(4)	28(1)
B(3)	-1271(6)	230(5)	3926(4)	31(1)
B(4)	-1570(6)	-1284(6)	4758(4)	33(1)
B(5)	-531(6)	-2422(6)	4186(5)	34(1)
B(6)	417(6)	-1603(6)	2999(4)	32(1)
B(7)	-1735(6)	183(6)	2844(5)	31(1)
B(8)	-2677(6)	-632(6)	4033(5)	32(1)
B(9)	-2227(6)	-2287(6)	4207(5)	35(1)
B(10)	-983(6)	-2461(5)	3110(5)	31(1)
B(11)	-690(6)	-946(6)	2273(5)	30(1)
B(12)	-2321(6)	-1371(6)	3018(5)	34(1)
P	2820(1)	2888(1)	1276(1)	21(1)
C(13)	1313(3)	4728(3)	-1067(2)	32(1)
C(14)	1419(3)	6006(2)	-1089(2)	32(1)
C(15)	1950(3)	6338(2)	-404(2)	31(1)
C(16)	2375(3)	5391(2)	304(2)	25(1)
C(11)	2269(3)	4112(2)	326(2)	23(1)
C(12)	1738(3)	3781(2)	-359(2)	27(1)
C(17)	1569(6)	2410(5)	-375(4)	37(1)
C(23)	6142(3)	629(3)	600(2)	37(1)
C(24)	6641(2)	1105(3)	-422(2)	36(1)
C(25)	6001(3)	2127(3)	-924(2)	34(1)
C(26)	4862(3)	2672(2)	-403(2)	27(1)
C(21)	4362(2)	2195(3)	619(2)	25(1)
C(22)	5002(3)	1174(3)	1121(2)	28(1)
C(27)	4518(6)	609(6)	2234(4)	43(1)
C(33)	2772(3)	4920(3)	3344(2)	37(1)
C(34)	4118(3)	5077(3)	3204(2)	37(1)
C(35)	5052(2)	4576(3)	2488(2)	36(1)
C(36)	4640(2)	3919(3)	1911(2)	28(1)
C(31)	3294(3)	3762(3)	2051(2)	25(1)
C(32)	2361(2)	4263(3)	2768(2)	28(1)
C(37)	865(5)	4107(5)	2965(4)	37(1)
C(01)	6240(7)	2827(6)	-5402(6)	52(2)
Cl(01)	6428(2)	1961(2)	-4245(1)	67(1)
Cl(02)	7228(2)	4172(2)	4131(2)	73(1)

The conformation of the {P(*o*-tol)$_3$Au} fragment is similar to that observed for compounds **6, 6a, 12, 13** and P(*o*-tol)$_3$AuCl,[10] in which the *ortho*-methyl groups point towards their respective gold atoms. **Table 3.11** (below) details pertinent geometrical data for **11**, and is discussed further in relation to the other structures in this series.

Compounds **12** and **13** are structurally very similar to **6** and **11** (above). As such, they will not be described fully. Instead, pertinent bond lengths and angles are presented in **Table 3.10**, with only notable features and general structural trends discussed below.

Table 3.10 Pertinent Bond Lengths (Å) and Angles (°) for Compounds **6**, **11**, **12** and **13**

	6	**11**	**12**	**13**
C(1)-C(2)/(Å)	1.709(12)	1.656(7)	1.694(8)	1.680(10)
C(1)-C(X)/(Å)	1.492(8)	-	1.500(8)	1.573(12)
Au-C(2)/(Å)	2.046(8)	2.053(4)	2.053(6)	2.067(7)
Au-P/(Å)	2.289(2)	2.280(1)	2.283(2)	2.283(2)
C(2)-Au-P/(°)	173.97(18)	178.44(13)	176.65(16)	173.05(20)
Au-P-C(11)/(°)	116.03(19)	112.94(10)	109.72(14)	113.61(18)
Au-P-C(12)/(°)	112.25(18)	111.50(10)	115.48(13)	113.63(19)
Au-P-C(13)/(°)	111.34(18)	114.49(11)	114.17(15)	111.93(18)
mean Au-P-C/(°)	113.21	112.98	113.12	113.06
C-B min/(Å)	1.706(11)	1.685(7)	1.684(10)	1.695(11)
C-B max/(Å)	1.729(12)	1.730(7)	1.721(8)	1.746(13)
B-B min/(Å)	1.756(13)	1.700(7)	1.746(10)	1.737(14)
B-B max/(Å)	1.786(14)	1.784(8)	1.791(11)	1.797(15)

Crystallographic Study of 1-Me-2-{P(*o*-tol)$_3$Au}-1,2-*closo*-$C_2B_{10}H_{10}$ (12)

Colourless, diffraction quality *blocks* of **12** were grown by diffusion of *n*-hexane and a CH_2Cl_2 solution at -30°C. Intensity data were measured on an Enraf-Nonius CAD4 diffractometer operating with Mo-K_α X-radiation (λ_{bar} = 0.71073 Å). The single crystal was mounted in a glass capillary and the experiment performed at 291(2) K.

Crystal data

$C_{24}H_{34}B_{10}AuP$, M = 658.55, monoclinic, $P2_1/c$, a = 14.607(5) Å, b = 7.956(3) Å, c = 24.544(6) Å, β = 90.84(3)°, V = 2852.0(16) Å^3, from least squares refinement of 25 reflections ($9 \leq \theta \leq 11°$) at 291(2) K, Z = 4, D_c = 1.534 gcm^{-3}, μ(Mo-K_α) = 5.23 mm^{-1}, F(0,0,0) = 1288e.

Data collection and reduction

Intensity data collected in the range $0 < 2\theta < 50°$ by the ω-2θ scan method; ω-scan width (0.8+0.34tanθ), ω-scan speeds in the range 0.92 to 2.35°min^{-1}. The intensities of 5012 unique reflections (h -17 to 17, k 0 to 9, l 0 to 28) were measured (DATCOL).

Structure solution and refinement

The structure was solved using Patterson methods (Au) (SHELX76) and ΔF syntheses (P, C, B) and developed by iterative, full-matrix least-squares refinement and further difference Fourier syntheses (SHELXTL). There are 4 molecules *per* unit cell. In the final model all non-H atoms were refined anisotropically. The C_6 rings were treated as planar hexagons (C-C = 1.39 Å). The *o*-tolyl and methyl H atoms were set in idealised positions (C-H = 0.93 Å). Cage H atoms were also set in idealised positions, 1.10 Å from the carbon or boron atoms on a radial extension from the centre of the icosahedron. Methyl protons were allowed to ride on their respective carbon atoms with U(H) = 1.5 U(C_{Me}). All other fixed protons were similarly fixed with U(H) = 1.2 U(C/B).

Data were absorption corrected (DIFABS) and weighted such that $w^{-1} = [\sigma^2(F_o^2) + (0.0271P)^2 + 2.27P]$ where $P = [\max.(F_o^2) + 2F_c^2]/3$. Using

Data were absorption corrected (DIFABS) and weighted such that $w^{-1} = [\sigma^2(F_o^2) + (0.0271P)^2 + 2.27P]$ where $P = [\text{max.}\ (F_o^2) + 2F_c^2]/3$. Using 3672 observed data ($F_o > 4.0\sigma(F_o)$), $R = 0.0348$, $wR_2 = 0.0678$ and $S = 1.033$ for 299 variable parameters. The maximum residue and minimum trough in a final difference Fourier synthesis were 0.47 and -0.56 $eÅ^{-3}$, respectively. Atomic scattering factors were those inlaid in SHELXTL. Interatomic distances (Å) and selected interbond angles (°), fractional coordinates and anisotropic thermal parameters of non-hydrogen atoms are in tables **12A** and **12B**, respectively.

The crystallographic study confirmed compound to be 1-Me-2-{P(*o*-tol)$_3$Au}-1,2-*closo*-$C_2B_{10}H_{10}$ (**Fig. 3.10**), with the carbaborane cage had the expected icosahedral geometry with B-C and B-B connectivities in the ranges 1.684(10) to 1.721(8) Å and 1.746(10) to 1.791(11) Å, respectively. The Au-P-C(2) bond angle (176.65(16)°) is significantly deviated away from the linear geometry predicted for Au(I) species. The C(1)-C(2) and C(1)-C(01) distances are 1.694(8) and 1.500(8) Å, respectively

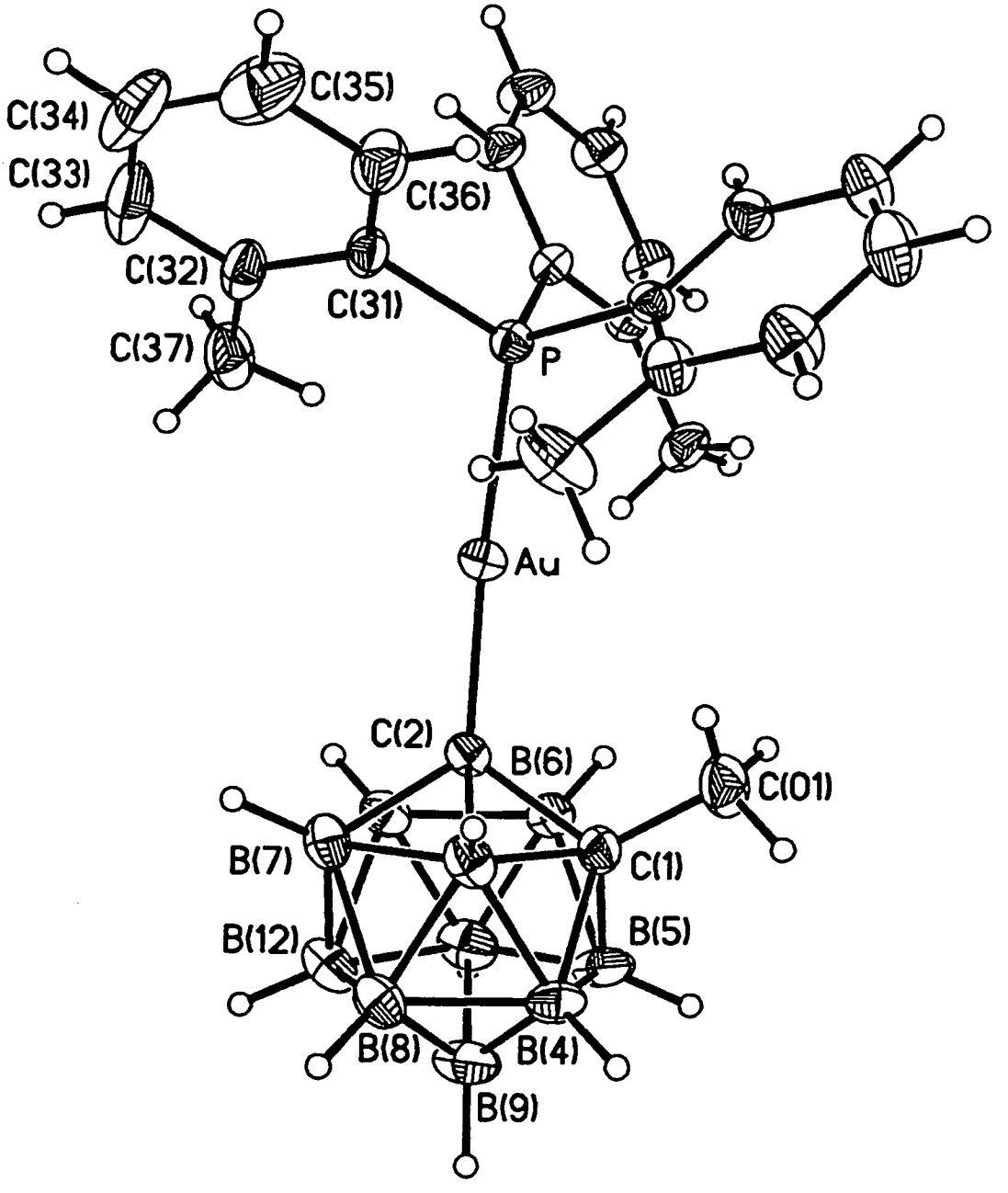

Figure 3.10 Perspective View of **12**

Table 12A Selected Bond Lengths (Å) and Angles (°) for **12**

Au-C(2)	2.053(6)	Au-P	2.283(2)
C(1)-C(01)	1.500(8)	C(1)-B(5)	1.684(9)
C(1)-B(4)	1.685(9)	C(1)-C(2)	1.694(8)
C(1)-B(3)	1.699(9)	C(1)-B(6)	1.704(9)
C(2)-B(11)	1.700(8)	C(2)-B(7)	1.716(9)
C(2)-B(3)	1.719(8)	C(2)-B(6)	1.721(8)
B(6)-B(10)	1.747(10)	B(6)-B(11)	1.747(10)
B(6)-B(5)	1.761(10)	B(5)-B(4)	1.755(11)
B(5)-B(9)	1.760(12)	B(5)-B(10)	1.765(12)
B(4)-B(9)	1.750(12)	B(4)-B(3)	1.764(11)
B(4)-B(8)	1.770(11)	B(3)-B(7)	1.761(10)
B(3)-B(8)	1.766(11)	B(11)-B(10)	1.760(10)
B(11)-B(7)	1.764(9)	B(11)-B(12)	1.769(10)
B(10)-B(12)	1.784(11)	B(10)-B(9)	1.791(11)
B(9)-B(8)	1.747(10)	B(9)-B(12)	1.760(12)
B(8)-B(12)	1.752(10)	B(8)-B(7)	1.758(11)
B(7)-B(12)	1.761(10)	P-C(31)	1.819(3)
P-C(11)	1.831(3)	P-C(21)	1.836(3)
C(12)-C(17)	1.531(7)	C(22)-C(27)	1.522(6)
C(32)-C(37)	1.515(7)		

C(2)-Au-P	176.6(2)	C(01)-C(1)-B(4)	121.2(5)
C(01)-C(1)-C(2)	117.4(5)	B(4)-C(1)-B(3)	62.8(4)
C(01)-C(1)-B(6)	116.8(5)	C(2)-C(1)-B(6)	60.9(3)
C(1)-C(2)-B(3)	59.7(4)	C(1)-C(2)-B(6)	59.8(4)
C(1)-C(2)-Au	119.9(4)	B(7)-C(2)-Au	123.6(4)
B(6)-C(2)-Au	116.5(4)	C(2)-B(6)-B(11)	58.7(3)
C(1)-B(6)-B(5)	58.1(4)	C(1)-B(5)-B(4)	58.6(4)
C(1)-B(5)-B(6)	59.2(4)	B(6)-B(5)-B(10)	59.4(4)
B(9)-B(4)-B(5)	60.3(5)	B(9)-B(4)-B(8)	59.5(5)
C(1)-B(3)-C(2)	59.4(3)	C(1)-B(3)-B(4)	58.2(4)
B(4)-B(3)-B(8)	60.2(5)	B(6)-B(11)-B(10)	59.7(4)
B(10)-B(11)-B(12)	60.7(4)	B(6)-B(10)-B(11)	59.8(4)
B(11)-B(10)-B(12)	59.9(4)	B(12)-B(10)-B(9)	59.0(4)
B(8)-B(9)-B(12)	59.9(4)	B(12)-B(9)-B(10)	60.3(5)
B(9)-B(8)-B(12)	60.4(4)	B(9)-B(8)-B(4)	59.7(5)
B(4)-B(8)-B(3)	59.9(4)	B(3)-B(7)-B(8)	60.3(4)
C(2)-B(7)-B(11)	58.5(3)	B(8)-B(12)-B(9)	59.7(5)
B(7)-B(12)-B(11)	60.0(4)	B(11)-B(12)-B(10)	59.4(4)
C(31)-P-C(21)	104.9(2)	C(31)-P-Au	114.2(2)
C(21)-P-Au	115.48(13)	C(16)-C(11)-P	117.9(2)
C(11)-C(12)-C(17)	123.1(3)	C(26)-C(21)-P	118.2(2)
C(23)-C(22)-C(27)	116.5(3)	C(36)-C(31)-P	119.3(3)
C(31)-C(32)-C(37)	122.1(4)	C(01)-C(1)-B(5)	120.7(6)
B(5)-C(1)-B(4)	62.8(4)	C(01)-C(1)-B(3)	117.8(5)
C(2)-C(1)-B(3)	60.9(3)	B(5)-C(1)-B(6)	62.6(4)
B(11)-C(2)-B(7)	62.2(4)	B(7)-C(2)-B(3)	61.7(4)

B(11)-C(2)-B(6)	61.4(4)	B(11)-C(2)-Au	120.9(4)
B(3)-C(2)-Au	120.7(4)	C(1)-B(6)-C(2)	59.3(3)
B(10)-B(6)-B(11)	60.5(4)	B(10)-B(6)-B(5)	60.4(5)
B(4)-B(5)-B(9)	59.7(5)	B(9)-B(5)-B(10)	61.1(5)
C(1)-B(4)-B(5)	58.6(4)	C(1)-B(4)-B(3)	58.9(4)
B(3)-B(4)-B(8)	60.0(4)	C(2)-B(3)-B(7)	59.1(4)
B(7)-B(3)-B(8)	59.8(4)	C(2)-B(11)-B(6)	59.9(4)
C(2)-B(11)-B(7)	59.3(3)	B(7)-B(11)-B(12)	59.8(4)
B(6)-B(10)-B(5)	60.2(4)	B(5)-B(10)-B(9)	59.3(5)
B(8)-B(9)-B(4)	60.8(5)	B(4)-B(9)-B(5)	60.0(5)
B(5)-B(9)-B(10)	59.6(5)	B(12)-B(8)-B(7)	60.2(4)
B(7)-B(8)-B(3)	60.0(4)	C(2)-B(7)-B(3)	59.2(4)
B(12)-B(7)-B(8)	59.7(4)	B(12)-B(7)-B(11)	60.3(4)
B(8)-B(12)-B(7)	60.1(4)	B(9)-B(12)-B(10)	60.7(5)
C(31)-P-C(11)	106.0(2)	C(11)-P-C(21)	105.8(2)
C(11)-P-Au	109.72(14)	C(12)-C(11)-P	121.9(2)
C(13)-C(12)-C(17)	116.7(3)	C(22)-C(21)-P	121.8(2)
C(21)-C(22)-C(27)	123.5(3)	C(32)-C(31)-P	120.7(3)
C(33)-C(32)-C(37)	117.8(4)		

Table 12B Atomic Coordinates (x 10^4) and Equivalent Isotropic Displacement Parameters ($Å^2$ x 10^3) for **12**

	x	y	z	U(eq)
Au	2337(1)	1493(1)	589(1)	37(1)
C(1)	2383(4)	1079(7)	-727(2)	43(2)
C(2)	2148(3)	167(7)	-122(2)	35(1)
B(6)	1270(4)	828(9)	-545(3)	40(2)
B(5)	1632(5)	481(12)	-1217(3)	58(2)
B(4)	2747(6)	-338(11)	-1186(3)	57(2)
B(3)	3070(5)	-493(10)	-493(3)	45(2)
B(11)	1224(4)	-1109(8)	-211(3)	42(2)
B(10)	881(5)	-942(10)	-900(3)	57(2)
B(9)	1818(6)	-1690(12)	-1296(3)	62(2)
B(8)	2699(5)	-2302(10)	-850(3)	48(2)
B(7)	2341(4)	-1952(9)	-178(3)	44(2)
B(12)	1558(5)	-2685(10)	-677(3)	53(2)
C(01)	2756(5)	2835(8)	-715(3)	62(2)
P	2570(1)	3099(2)	1349(1)	33(1)
C(11)	3421(2)	4728(4)	1210(2)	33(1)
C(12)	4222(2)	4378(4)	933(2)	45(2)
C(13)	4814(2)	5675(6)	796(2)	62(2)
C(14)	4605(3)	7322(5)	938(2)	65(2)
C(15)	3804(3)	7671(4)	1215(2)	56(2)
C(16)	3212(2)	6374(5)	1351(2)	43(1)
C(17)	4540(4)	2589(9)	805(3)	71(2)
C(21)	1558(2)	4215(5)	1597(1)	32(1)
C(22)	908(2)	4898(5)	1242(1)	36(1)
C(23)	145(2)	5712(5)	1447(1)	46(2)
C(24)	32(2)	5844(5)	2007(2)	52(2)
C(25)	682(3)	5162(5)	2362(1)	53(2)
C(26)	1445(2)	4348(5)	2157(1)	46(2)
C(27)	972(4)	4793(9)	624(2)	51(2)
C(31)	3007(3)	1939(5)	1936(2)	41(2)
C(32)	2562(3)	504(5)	2118(2)	52(2)
C(33)	2918(4)	-395(5)	2558(2)	86(3)
C(34)	3720(4)	140(8)	2816(2)	99(3)
C(35)	4165(3)	1575(8)	2635(2)	95(3)
C(36)	3808(3)	2474(5)	2195(2)	60(2)
C(37)	1674(4)	-109(9)	1860(3)	65(2)

Crystallographic Study of 1-^{t}Bu-2-{P(*o*-tol)$_3$Au}-1,2-*closo*-$C_2B_{10}H_{10}$ (13)

Colourless, diffraction quality *blocks* of **13** were grown by the slow evaporation of an *i*-hexane solution at room temperature. Intensity data were measured on an Enraf-Nonius CAD4 diffractometer operating with Mo-K_α *X*-radiation (λ_{bar} = 0.71073 Å). The single crystal was mounted in a glass capillary and the experiment performed at 198(2) K.

Crystal data

$C_{29}H_{36}B_{10}AuP$, M = 700.12, triclinic, *P*bar1, a = 10.214(3) Å, b = 10.724(3) Å, c = 15.124(3) Å, α = 74.23(2)°, β = 87.54(2)°, γ = 86.93(1)°, V = 1591.3(8) Å^3, from least squares refinement of 24 reflections ($9 \leq \theta \leq 14°$) at 291(2)K, Z = 2, D_c = 1.462 gcm^{-3}, μ(Mo-K_α) = 4.69 mm^{-1}, F(0,0,0) = 692e.

Data collection and reduction

Intensity data collected in the range $0<2\theta<50°$ by the ω-2θ scan method; ω-scan width (1.4+0.35tanθ), ω-scan speeds in the range 1.21 to 1.89°min^{-1}. The intensities of 5409 unique reflections (h -12 to 11, k -12 to 12, l 0 to 17) were measured (DATCOL).

Structure solution and refinement

The structure was solved using Patterson methods (Au) (SHELX76) and ΔF syntheses (P, C, B) and developed by iterative, full-matrix least-squares refinement and further difference Fourier syntheses (SHELXTL). There are 2 molecules *per* unit cell. In the final model all non-H atoms were refined anisotropically. The *o*-tolyl and cage *tert*-butyl H atoms were all set in idealised positions (C-H = 0.93 Å). Cage H atoms were also set in idealised positions, 1.10 Å from the carbon or boron atoms on a radial extension from the centre of the icosahedron. Methyl and *tert*-butyl protons were allowed to ride on their respective carbon atoms with U(H) = 1.5 U(C_{Me}). All other fixed protons were similarly fixed with U(H) = 1.2 U(C/B).

Data were absorption corrected (ψ-scans) and weighted such that $w^{-1} = [\sigma^2(F_o^2) + (0.01P)^2 + 7.79P]$ where P = [max. (F_o^2) + $2F_c^2]/3$. Using 5639

observed data, R = 0.038, wR_2 and S = 1.536 for 319 variable parameters. The maximum residue and minimum trough in a final difference Fourier synthesis were 1.03 and -0.76 eÅ^{-3}, respectively. Atomic scattering factors were those inlaid in SHELXTL. Interatomic distances (Å) and selected interbond angles (°), fractional coordinates and anisotropic thermal parameters of non-hydrogen atoms are in tables **13A** and **13B**, respectively.

The compound was confirmed as being 1-^{t}Bu-2-{P(*o*-tol)$_3$Au}-1,2-*closo*-$C_2B_{10}H_{10}$ (**Fig. 3.11**), with an icosahedral cage with B-C and B-B connectivities in the range 1.695(11) to 1.746(13) Å and 1.737 to 1.797(15) Å, respectively. The C(1)-C(2) distance is relatively large (1.680(10) Å) and the C(2)-Au-P sequence significantly less than 180° (173.05(20)°), reflecting the large steric bulk of the *tert*-butyl group. The Au-C(2) bond length (2.067(7) Å) is not significantly different to those in compounds **6, 11** and **12.** The closest Au···H$_{Me}$ distances are 2.515 Å (H(171) - *o*-tolyl) and 2.566 Å (H(113) - *tert*-butyl).

Structural studies on compounds **6, 11, 12** and **13** afforded the expected *closo,* icosahedral geometry for the carbaborane cage. The geometry of the gold atoms are all approximately linear with deviations from 180° being loosely related to the size of the adjacent C(1) substituent. As observed for other compounds containing the {P(*o*-tol)$_3$Au} fragment, the *ortho*-methyl groups point towards the gold atom. In addition to the phosphine groups adopting the same conformation, the Au-P-C and C-P-C angles are all similar. Pertinent data from these studies is presented in **Table 3.10**, above (page 196).

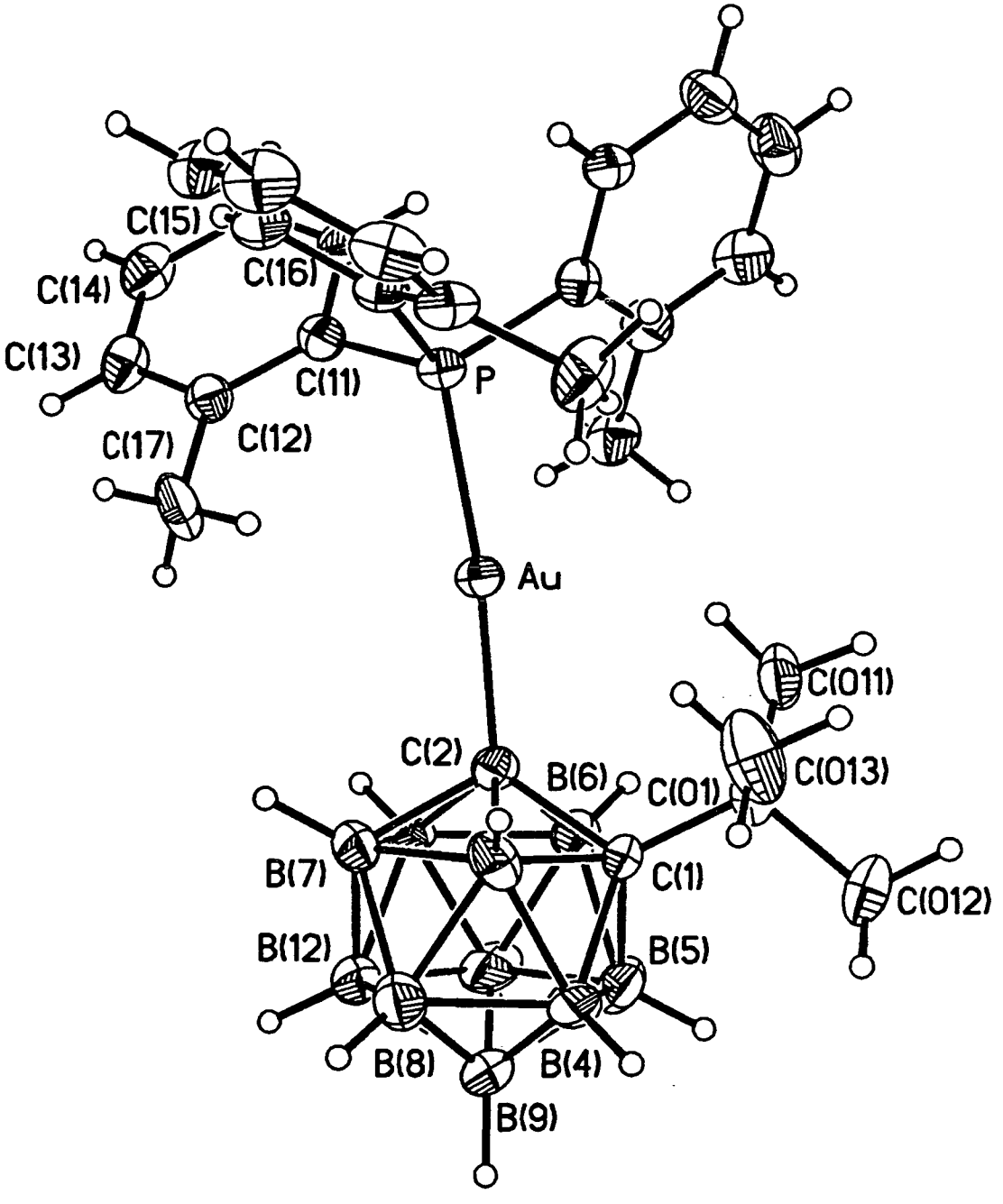

Figure 3.11 Perspective View of **13**

Structural studies of only two of the parent carbaboranes have so far been undertaken (1-Ph-1,2-*closo*-$C_2B_{10}H_{11}$ and 1,2-*closo*-$C_2B_{10}H_{12}$ (electron-diffraction)) and thus comparisons between compounds **6** and **11** and the unhindered parent carbaboranes can be made. Comparisons between **6** and its parent carbaborane, **1**, have already been detailed (**Section 3.6.1**), which indicate that the C(1)-C(2) connectivity is significantly lengthened and that the phenyl ring is forced to adopt a less favourable conformation. The electron-diffraction study of 1,2-*closo*-$C_2B_{10}H_{12}$, afforded a C(1)-C(2) distance of 1.65(5) Å, not significantly shorter than for **11** (1.656(7) Å). Comparison of **11** with the phenyl (**6**), methyl (**12**) and *tert*-butyl (**13**) substituted derivatives shows a significant increase in the C(1)-C(2) lengths (1.656(7) Å *vs* 1.709(12), 1.694(8) and 1.680(10) Å, respectively), as well as a decrease in the C(2)-Au-P bond angles (178.44(13)° *vs*. 173.97(18), 178.44(13) and 173.05(20)°, respectively).

Table 13A Selected Bond Lengths (Å) and Angles (°) for **13**

Au-C(2)	2.050(5)	Au-P	2.3100(14)
C(1)-C(01)	1.518(8)	C(1)-C(2)	1.688(8)
C(1)-B(6)	1.716(9)	C(1)-B(3)	1.716(8)
C(1)-B(4)	1.718(9)	C(1)-B(5)	1.734(9)
C(2)-B(7)	1.696(8)	C(2)-B(11)	1.714(8)
C(2)-B(6)	1.716(8)	C(2)-B(3)	1.713(8)
B(3)-B(7)	1.745(9)	B(3)-B(8)	1.759(10)
B(3)-B(4)	1.773(9)	B(4)-B(5)	1.770(11)
B(4)-B(8)	1.784(10)	B(4)-B(9)	1.797(11)
B(5)-B(9)	1.769(10)	B(5)-B(10)	1.767(11)
B(5)-B(6)	1.797(9)	B(6)-B(11)	1.767(9)
B(6)-B(10)	1.776(10)	B(7)-B(11)	1.746(9)
B(7)-B(12)	1.784(10)	B(7)-B(8)	1.781(9)
B(8)-B(12)	1.783(11)	B(8)-B(9)	1.796(11)
B(9)-B(10)	1.764(11)	B(9)-B(12)	1.770(10)
B(10)-B(11)	1.787(10)	B(10)-B(12)	1.791(11)
B(11)-B(12)	1.776(10)	C(01)-C(06)	1.370(8)
C(01)-C(02)	1.382(8)	C(02)-C(03)	1.397(9)
C(03)-C(04)	1.375(9)	C(04)-C(05)	1.353(9)
C(05)-C(06)	1.414(9)	P-C(31)	1.828(5)
P-C(21)	1.841(5)	P-C(11)	1.839(5)
C(11)-C(16)	1.404(7)	C(11)-C(12)	1.417(8)
C(12)-C(13)	1.399(8)	C(12)-C(17)	1.512(8)
C(13)-C(14)	1.378(8)	C(14)-C(15)	1.386(8)
C(14)-C(18)	1.500(8)	C(15)-C(16)	1.393(7)
C(16)-C(19)	1.515(8)	C(21)-C(22)	1.412(8)
C(21)-C(26)	1.415(7)	C(22)-C(23)	1.403(7)
C(22)-C(27)	1.498(7)	C(23)-C(24)	1.397(7)
C(24)-C(25)	1.363(8)	C(24)-C(28)	1.511(7)
C(25)-C(26)	1.388(8)	C(26)-C(29)	1.518(8)
C(31)-C(32)	1.409(7)	C(31)-C(36)	1.423(7)
C(32)-C(33)	1.391(8)	C(32)-C(37)	1.525(7)
C(33)-C(34)	1.383(8)	C(34)-C(35)	1.385(8)
C(34)-C(38)	1.493(8)	C(35)-C(36)	1.383(8)
C(36)-C(39)	1.520(7)		

C(2)-Au-P	179.0(2)	C(01)-C(1)-C(2)	119.7(4)
C(01)-C(1)-B(6)	120.1(5)	C(2)-C(1)-B(6)	60.5(3)
C(01)-C(1)-B(3)	117.4(5)	C(2)-C(1)-B(3)	60.4(3)
C(01)-C(1)-B(4)	119.1(5)	B(3)-C(1)-B(4)	62.2(4)
C(01)-C(1)-B(5)	121.4(5)	B(6)-C(1)-B(5)	62.7(4)
B(4)-C(1)-B(5)	61.7(4)	B(7)-C(2)-B(11)	61.6(4)
C(1)-C(2)-B(6)	60.5(3)	B(11)-C(2)-B(6)	62.0(4)
C(1)-C(2)-B(3)	60.6(3)	B(7)-C(2)-B(3)	61.6(4)
C(1)-C(2)-Au	118.4(4)	B(7)-C(2)-Au	122.9(4)
B(11)-C(2)-Au	121.6(4)	B(6)-C(2)-Au	116.9(4)
B(3)-C(2)-Au	119.7(4)	C(2)-B(3)-C(1)	59.0(3)

C(2)-B(3)-B(7)	58.8(4)	B(7)-B(3)-B(8)	61.1(4)
C(1)-B(3)-B(4)	59.0(4)	B(8)-B(3)-B(4)	60.7(4)
C(1)-B(4)-B(5)	59.6(4)	C(1)-B(4)-B(3)	58.9(4)
B(3)-B(4)-B(8)	59.3(4)	B(5)-B(4)-B(9)	59.5(4)
B(8)-B(4)-B(9)	60.2(4)	C(1)-B(5)-B(4)	58.7(4)
B(9)-B(5)-B(4)	61.0(4)	B(9)-B(5)-B(10)	59.8(4)
C(1)-B(5)-B(6)	58.1(4)	B(10)-B(5)-B(6)	59.8(4)
C(2)-B(6)-C(1)	58.9(3)	C(2)-B(6)-B(11)	58.9(3)
B(11)-B(6)-B(10)	60.6(4)	C(1)-B(6)-B(5)	59.1(4)
B(10)-B(6)-B(5)	59.3(4)	C(2)-B(7)-B(3)	59.7(4)
C(2)-B(7)-B(11)	59.7(4)	B(11)-B(7)-B(12)	60.4(4)
B(3)-B(7)-B(8)	59.9(4)	B(12)-B(7)-B(8)	60.0(4)
B(3)-B(8)-B(7)	59.0(4)	B(7)-B(8)-B(12)	60.1(4)
B(3)-B(8)-B(4)	60.0(4)	B(12)-B(8)-B(9)	59.3(4)
B(4)-B(8)-B(9)	60.2(4)	B(10)-B(9)-B(5)	60.0(4)
B(10)-B(9)-B(12)	60.9(4)	B(5)-B(9)-B(4)	59.5(4)
B(12)-B(9)-B(8)	60.0(4)	B(4)-B(9)-B(8)	59.6(4)
B(9)-B(10)-B(5)	60.1(4)	B(5)-B(10)-B(6)	60.9(4)
B(6)-B(10)-B(11)	59.4(4)	B(9)-B(10)-B(12)	59.7(4)
B(11)-B(10)-B(12)	59.5(4)	C(2)-B(11)-B(7)	58.7(3)
C(2)-B(11)-B(6)	59.1(3)	B(7)-B(11)-B(12)	60.9(4)
B(6)-B(11)-B(10)	60.0(4)	B(12)-B(11)-B(10)	60.3(4)
B(11)-B(12)-B(7)	58.7(4)	B(9)-B(12)-B(8)	60.7(4)
B(7)-B(12)-B(8)	59.9(4)	B(9)-B(12)-B(10)	59.4(4)
B(11)-B(12)-B(10)	60.1(4)	C(06)-C(01)-C(02)	119.1(6)
C(06)-C(01)-C(1)	121.7(6)	C(02)-C(01)-C(1)	119.2(5)
C(01)-C(02)-C(03)	120.6(6)	C(04)-C(03)-C(02)	119.4(7)
C(05)-C(04)-C(03)	121.0(7)	C(04)-C(05)-C(06)	119.5(7)
C(01)-C(06)-C(05)	120.4(6)	C(31)-P-C(21)	112.2(2)
C(31)-P-C(11)	110.6(2)	C(21)-P-C(11)	112.5(2)
C(31)-P-Au	107.2(2)	C(21)-P-Au	104.4(2)
C(11)-P-Au	109.6(2)	C(16)-C(11)-C(12)	119.4(5)
C(16)-C(11)-P	123.5(4)	C(12)-C(11)-P	117.0(4)
C(13)-C(12)-C(11)	118.7(5)	C(13)-C(12)-C(17)	116.8(5)
C(11)-C(12)-C(17)	124.5(5)	C(14)-C(13)-C(12)	122.7(6)
C(13)-C(14)-C(15)	117.0(5)	C(13)-C(14)-C(18)	121.7(6)
C(15)-C(14)-C(18)	121.3(5)	C(14)-C(15)-C(16)	123.5(5)
C(15)-C(16)-C(11)	118.3(5)	C(15)-C(16)-C(19)	116.3(5)
C(11)-C(16)-C(19)	125.4(5)	C(22)-C(21)-C(26)	119.9(5)
C(22)-C(21)-P	123.2(4)	C(26)-C(21)-P	116.1(4)
C(21)-C(22)-C(23)	117.2(5)	C(21)-C(22)-C(27)	124.8(5)
C(23)-C(22)-C(27)	117.9(5)	C(24)-C(23)-C(22)	123.6(5)
C(25)-C(24)-C(23)	116.5(5)	C(25)-C(24)-C(28)	122.7(5)
C(23)-C(24)-C(28)	120.8(5)	C(24)-C(25)-C(26)	123.9(5)
C(25)-C(26)-C(21)	118.4(5)	C(25)-C(26)-C(29)	117.3(5)
C(21)-C(26)-C(29)	124.3(5)	C(32)-C(31)-C(36)	118.1(5)
C(32)-C(31)-P	117.2(4)	C(36)-C(31)-P	124.6(4)
C(33)-C(32)-C(31)	120.0(5)	C(33)-C(32)-C(37)	116.7(5)
C(31)-C(32)-C(37)	123.2(5)	C(34)-C(33)-C(32)	122.3(5)

C(33)-C(34)-C(35)	116.9(5)	C(33)-C(34)-C(38)	121.1(5)
C(35)-C(34)-C(38)	122.1(5)	C(36)-C(35)-C(34)	123.7(5)
C(35)-C(36)-C(31)	118.6(5)	C(35)-C(36)-C(39)	117.3(5)
C(31)-C(36)-C(39)	124.1(5)		

Table 13B Atomic Coordinates (x 10^4) and Equivalent Isotropic Displacement Parameters ($Å^2$ x 10^3) for **13**

	x	y	z	U(eq)
Au	4164(1)	1417(1)	4089(1)	16(1)
C(1)	3617(4)	1275(3)	2771(2)	26(2)
C(2)	3585(3)	938(3)	3426(2)	21(1)
B(3)	4218(4)	596(3)	2907(3)	24(2)
B(4)	3655(5)	693(4)	2253(3)	33(2)
B(5)	2673(5)	1106(4)	2396(3)	37(2)
B(6)	2659(4)	1274(3)	3147(3)	26(2)
B(7)	3593(4)	126(3)	3366(3)	24(2)
B(8)	3628(5)	-55(4)	2625(3)	37(2)
B(9)	2649(5)	260(4)	2316(3)	42(2)
B(10)	2037(5)	630(4)	2861(3)	39(2)
B(11)	2626(4)	532(3)	3513(3)	25(2)
B(12)	2622(5)	-97(4)	3001(3)	35(2)
C(01)	4110(4)	1899(3)	2681(2)	24(1)
C(02)	4918(4)	1881(3)	2424(3)	34(2)
C(03)	5378(4)	2448(3)	2320(3)	42(2)
C(04)	5020(5)	3027(3)	2478(3)	45(2)
C(05)	4230(5)	3056(3)	2730(3)	47(2)
C(06)	3765(4)	2481(3)	2833(3)	34(2)
P	4831(1)	1967(1)	4824(1)	16(1)
C(11)	4189(3)	1876(3)	5480(2)	17(1)
C(12)	3851(3)	1256(3)	5598(2)	19(1)
C(13)	3247(3)	1187(3)	6040(2)	25(2)
C(14)	2972(3)	1696(3)	6369(2)	24(1)
C(15)	3359(3)	2287(3)	6267(2)	24(1)
C(16)	3975(3)	2391(3)	5841(2)	18(1)
C(17)	4121(4)	649(3)	5290(2)	25(1)
C(18)	2296(4)	1615(3)	6823(3)	38(2)
C(19)	4371(4)	3057(3)	5815(2)	23(1)
C(21)	5914(3)	1597(3)	4881(2)	18(1)
C(22)	6247(3)	1342(3)	5393(2)	17(1)
C(23)	6949(3)	914(3)	5350(2)	21(1)
C(24)	7360(3)	762(3)	4837(2)	22(1)
C(25)	7064(4)	1072(3)	4363(3)	27(1)
C(26)	6354(3)	1484(3)	4361(2)	20(1)
C(27)	5939(3)	1522(3)	5978(2)	20(1)
C(28)	8098(4)	284(3)	4819(3)	34(2)
C(29)	6122(3)	1804(3)	3799(2)	28(2)
C(31)	4887(3)	2812(3)	4613(2)	15(1)
C(32)	4127(3)	3090(3)	4385(2)	19(1)
C(33)	4164(4)	3691(3)	4126(2)	22(1)
C(34)	4917(4)	4054(3)	4114(2)	25(1)
C(35)	5645(4)	3791(3)	4372(3)	26(2)
C(36)	5655(3)	3193(3)	4629(2)	20(1)

C(37)	3239(3)	2766(3)	4409(3)	26(2)
C(38)	4934(4)	4700(3)	3837(3)	44(2)
C(39)	6490(3)	2992(3)	4926(3)	29(2)

3.6.4 Crystallographic study of $C_6F_5AuP(C_6F_5)Me_2$ (15)

Colourless, diffraction quality *needles* of **15** were grown by the slow diffusion of *n*hexane and a CH_2Cl_2 solution at -30°C. Intensity data were measured on an Siemens P4 diffractometer operating with Mo-K_α *X*-radiation (λ_{bar} = 0.71073 Å). The single crystal was mounted in a glass capillary and the experiment performed at 293(2) K.

Crystal data

$C_{14}H_6F_{10}AuP$, M = 592.12, monoclinic, $P2_1/n$, a = 6.9340(14) Å, b = 15.180(3) Å, c = 15.311(3) Å, β = 93.84(3)°, V = 1608.0(6) Å^3, from least squares refinement of 43 reflections ($9 \leq \theta \leq 25°$) at 291(2) K, Z = 4, D_c = 2.446 gcm^{-3}, μ(Mo-K_α) = 9.35 mm^{-1}, F(0,0,0) = 1096e.

Data collection and reduction

Intensity data collected in the range $4 < 2\theta < 50°$ by the ω-scan method; ω-scan width 1.0°, ω-scan speeds in the range 1 to 60°min^{-1}. The intensities of 2772 unique reflections (h -1 to 8, k -1 to 18, l -18 to 18) were measured (XSCANS).

Structure solution and refinement

The structure was solved using Patterson methods (Au) and ΔF syntheses (P, C, F) and developed by iterative, full-matrix least-squares refinement and further difference Fourier syntheses (SHELXTL). There are 4 molecules *per* unit cell. In the final model all non-H atoms were refined anisotropically. The methyl protons were fixed in idealised positions (C-H = 0.93 Å) and allowed to ride on their respective carbon atoms with U(H) = 1.5 U(C_{Me}).

Data were absorption corrected (ψ-scans) and weighted such that $w^{-1} = [\sigma^2(F_o^2) + (0.010P)^2 + 60.0P]$ where $P = [\text{max.}\ (F_o^2) + 2F_c^2]/3$. Using 2003 observed data ($F_o > 4.0\sigma(F_o)$), R = 0.0671, wR_2 = 0.3196 and S = 2.202 for 235 variable parameters. The maximum residue and minimum trough in a final Fourier synthesis were 1.69 and -1.15 eÅ^{-3}, respectively. Atomic scattering factors were those inlaid in SHELXTL. Selected bond lengths (Å)

and angles (°), fractional coordinates and equivalent isotropic thermal parameters of non-hydrogen atoms are given in **Tables 15A** and **15B**, respectively.

The main features of the structure of **15** (a perspective view of which is shown in **Figure 3.12**) is the conformation of the two C_6F_5 rings and the crystal packing of the molecule.

The individual rings are essentially planar (C(11)-F(16), σ = 0.019 Å; C(21)-F(26), σ = 0.076 Å), with an angle of 3.7° between the two planes. The mean plane for the whole molecule (excluding the two methyl groups) is 0.046 Å. The planarity of this portion of the molecule leads to some rather complicated packing within the crystal lattice, with many close intermolecular contacts (see **Figs. 3.13**, **3.14**, below).

The methyl groups are arranged in an approximately tetrahedral arrangement (Au-P-C(01/2) = 112.85(91) and 112.62(90)°, respectively) around the phosphorous atom. The C-P bond lengths are 1.821(24) (P-C(01)) and 1.812(27) Å (P-C(02)), typical of P-alkyl bond lengths.[21] The P-C_6F_5 bond length is slightly longer at 1.84(2) Å, again, typical of P-aryl bond lengths.[22] There is no significant deviation in the length of the C-F bonds, which have a mean value of 1.33 Å.

The geometry around the gold atom is slightly, but significantly deviated from linearity (C(11)-Au-P = 176.62(65)°). The Au-C(11) and Au-P bond lengths are 2.013(21) and 2.269(6) Å, respectively. There have been several structural determinations of molecules containing a {C_6F_5Au(I)P} fragment (**Table 3.11**).[23] Interestingly, the Au-C bond lengths in all of these species are consistently longer than that for **15**.

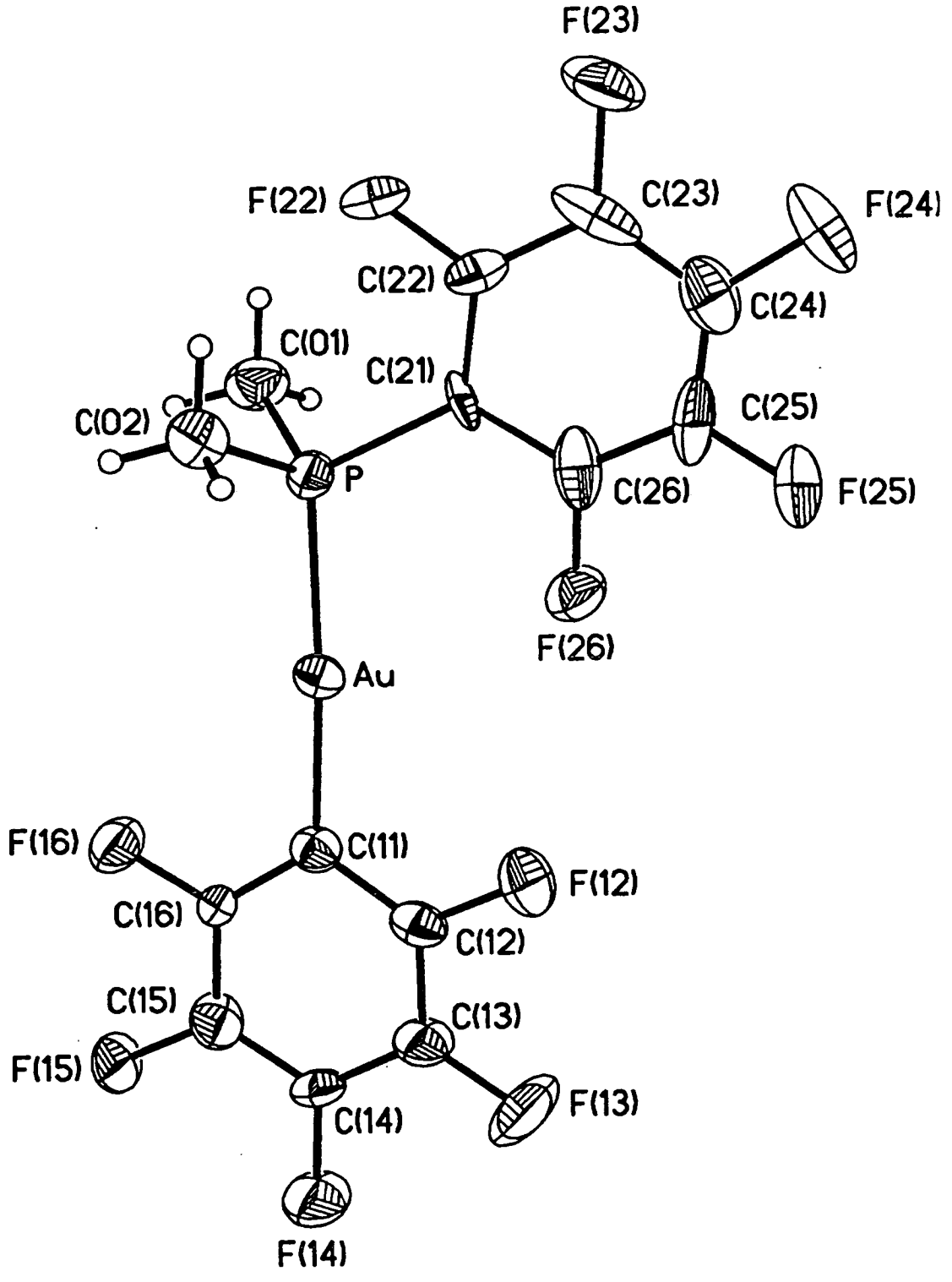

Figure 3.12 Perspective View of **15**

Table 3.11 Pertinent Bond Lengths (Å) and Angles (°) for Molecules Containing the {C_6F_5AuP} Fragment

Compound	Au-C/(Å)	Au-P/(Å)	C-Au-P/(°)	Ref.
$C_6F_5AuP(C_6F_5)Me_2$	2.013(21)	2.269(6)	176.6(7)	
$C_6F_5AuPPh_3$	2.07(2)	2.27(1)	178(1)	**23a**
$[C_6F_5Au(dppm)]_2Pd(C_6F_5)_2$	2.074(7)	2.266(4)	175.6(3)	**23b**
$C_6F_5AuPPh_2CH_2PPh_2Me$	2.057(6)	2.287(2)	174.8(2)	**23c**
$(C_6F_5)_2Au_2(dppm)$	2.063(12)	2.288(3)	176.6(3)	**23d**
	2.058(12)	2.279(3)	175.8(3)	

One reason for this could be that the conformation of the molecule allows the π-systems of the **two** C_6F_5 rings to overlap, which coupled with the highly electron-withdrawing nature of these groups affords the short Au-C distance, although in the related species, $C_6F_5AuPPh_3$, in which a C_6F_5 and phenyl ring (C(9)-C(14)) lie almost coplanar (the angle between the two rings is 11.6° and the mean plane for the two rings and Au and P atoms is 0.084 Å), a similar shortening of the Au-C bond is not observed. The Au-P-C(21) bond angle (116.2(8)°) is significantly larger than for Au-P-C_{Me}, reflecting the relative sizes of the C_6F_5 and Me groups. The angle at the *ipso* carbon of the C_6F_5 ring is 113.5(21)°, typical for all of the above structures.

The molecules pack in layers normal to the *a* direction, whilst in the *c* direction, there are close F(15)-F(23) contacts (2.872 Å). In the *b* direction, there are Au-F(13) contacts (3.623 Å). There are also close in-plane contacts as well as between the layers (**Figure 3.13a**), which are approximately 3.4 Å apart. Molecules are stacked in positions directly above other molecules in alternate layers, in an *ababab* fashion (**Figure 3.13b**). Molecules in adjacent layers are related to each other by an inversion centre. Each gold atom approaches the F(25) atom of the molecules above and below to a distance of 3.579 Å. The F(25)-Au-F(13) angle is 75°.

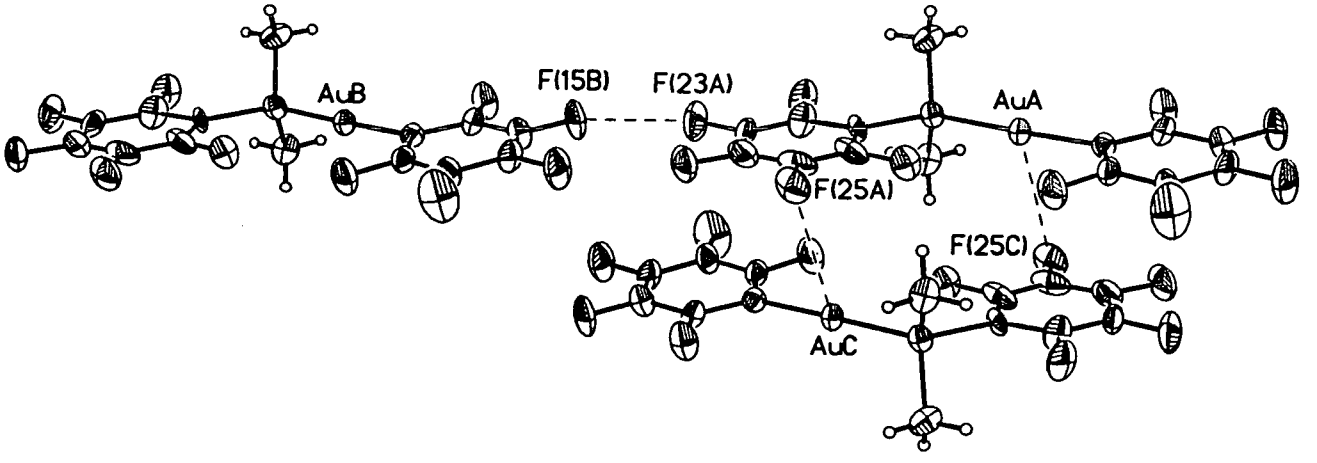

Figure 3.13a Some In-Plane and Inter-Layer Contacts for **15**

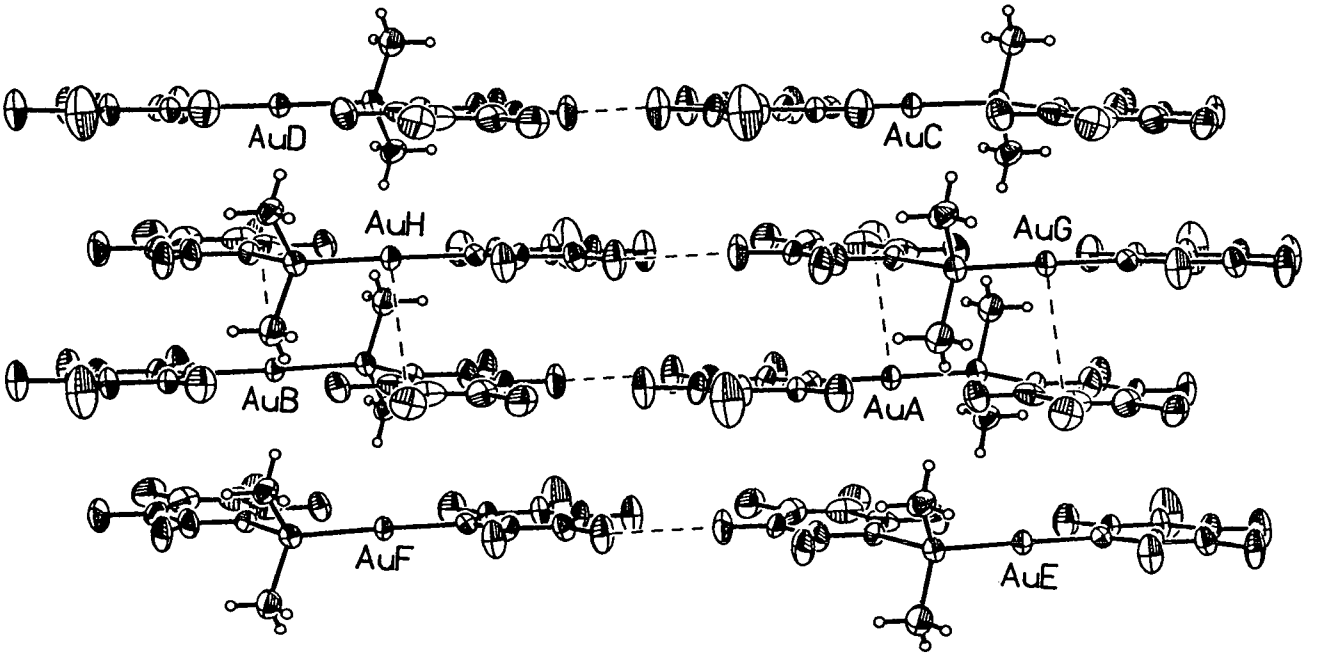

Figure 3.13b Packing Between Layers for **15**

Table 15A Selected Bond Lengths (Å) and Angles (°) for **15**

Au-C(11)	2.01(2)	Au-P	2.269(6)
P-C(02)	1.81(3)	P-C(01)	1.82(2)
P-C(21)	1.84(2)	F(12)-C(12)	1.37(3)
F(13)-C(13)	1.33(3)	F(14)-C(14)	1.33(3)
F(15)-C(15)	1.35(3)	F(16)-C(16)	1.31(2)
F(22)-C(22)	1.31(3)	F(23)-C(23)	1.32(3)
F(24)-C(24)	1.33(3)	F(25)-C(25)	1.28(3)
F(26)-C(26)	1.36(4)	C(11)-C(16)	1.40(3)
C(11)-C(12)	1.40(3)	C(12)-C(13)	1.38(3)
C(13)-C(14)	1.42(3)	C(14)-C(15)	1.35(3)
C(15)-C(16)	1.37(3)	C(21)-C(22)	1.38(3)
C(21)-C(26)	1.40(3)	C(22)-C(23)	1.39(4)
C(23)-C(24)	1.43(5)	C(24)-C(25)	1.33(4)
C(25)-C(26)	1.33(4)		

C(11)-Au-P	176.6(7)	C(02)-P-C(01)	105.5(13)
C(02)-P-C(21)	104.0(11)	C(01)-P-C(21)	104.7(11)
C(02)-P-Au	112.8(9)	C(01)-P-Au	112.6(9)
C(21)-P-Au	116.2(8)	C(16)-C(11)-C(12)	112(2)
C(16)-C(11)-Au	126(2)	C(12)-C(11)-Au	122(2)
F(12)-C(12)-C(13)	114(2)	F(12)-C(12)-C(11)	119(2)
C(13)-C(12)-C(11)	127(2)	F(13)-C(13)-C(12)	125(2)
F(13)-C(13)-C(14)	118(2)	C(12)-C(13)-C(14)	117(2)
F(14)-C(14)-C(15)	121(2)	F(14)-C(14)-C(13)	120(2)
C(15)-C(14)-C(13)	119(2)	F(15)-C(15)-C(14)	121(2)
F(15)-C(15)-C(16)	118(2)	C(14)-C(15)-C(16)	121(2)
F(16)-C(16)-C(15)	118(2)	F(16)-C(16)-C(11)	117(2)
C(15)-C(16)-C(11)	125(2)	C(22)-C(21)-C(26)	114(2)
C(22)-C(21)-P	124(2)	C(26)-C(21)-P	123(2)
F(22)-C(22)-C(21)	119(2)	F(22)-C(22)-C(23)	119(3)
C(21)-C(22)-C(23)	122(3)	F(23)-C(23)-C(22)	118(4)
F(23)-C(23)-C(24)	123(3)	C(22)-C(23)-C(24)	119(3)
C(25)-C(24)-F(24)	128(3)	C(25)-C(24)-C(23)	119(3)
F(24)-C(24)-C(23)	114(3)	F(25)-C(25)-C(24)	115(3)
F(25)-C(25)-C(26)	125(4)	C(24)-C(25)-C(26)	120(3)
C(25)-C(26)-F(26)	114(3)	C(25)-C(26)-C(21)	126(3)
F(26)-C(26)-C(21)	119(2)		

Table 15B Atomic Coordinates (x 10^4) and Equivalent Isotropic Thermal Parameters ($Å^2$ x 10^3) for **15**

	x	y	z	U(eq)
Au	2446(1)	5885(1)	1124(1)	51(1)
P	2352(9)	6527(4)	-217(4)	49(1)
F(12)	2976(27)	3923(11)	1828(11)	95(5)
F(13)	3074(43)	3219(12)	3455(14)	150(10)
F(14)	2852(30)	4296(12)	4864(10)	103(6)
F(15)	2368(28)	6062(9)	4632(9)	89(5)
F(16)	2182(28)	6723(9)	3037(10)	86(5)
F(22)	2098(27)	6900(10)	-2177(10)	88(5)
F(23)	2195(27)	5794(14)	-3517(9)	104(6)
F(24)	2456(25)	4055(14)	-3260(11)	108(6)
F(25)	2654(26)	3437(10)	-1607(12)	92(5)
F(26)	2607(23)	4495(9)	-253(10)	75(4)
C(11)	2541(30)	5388(15)	2345(14)	48(5)
C(12)	2755(34)	4484(17)	2512(15)	57(6)
C(13)	2910(39)	4085(19)	3323(15)	69(7)
C(14)	2683(42)	4633(16)	4064(15)	67(7)
C(15)	2507(41)	5514(17)	3943(17)	68(7)
C(16)	2359(32)	5866(14)	3114(13)	49(5)
C(21)	2352(30)	5774(13)	-1161(13)	47(5)
C(22)	2280(42)	6054(17)	-2017(17)	73(8)
C(23)	2320(38)	5468(29)	-2713(16)	90(11)
C(24)	2417(43)	4544(24)	-2541(24)	82(9)
C(25)	2525(38)	4274(17)	-1716(26)	81(9)
C(26)	2492(36)	4856(17)	-1070(22)	73(8)
C(01)	219(35)	7212(18)	-434(18)	72(7)
C(02)	4396(40)	7246(18)	-354(18)	78(8)

3.7 Conclusions

A series of σ-bonded carbaauraboranes, which conformed to two general types (1-Ph-2-{PR_3Au}-1,2-*closo*-$C_2B_{10}H_{10}$ (R = *o*-tol (**6**), Cy (**7**), Et (**8**), mes (**9**), C_6F_5 (**10**)) and 1-R-2-{$P(o\text{-tol})_3Au$}-1,2-*closo*-$C_2B_{10}H_{10}$ R = Ph (**6**), H (**11**), Me (**12**), ^{t}Bu (**13**)), have been synthesised and fully characterised by microanalysis, IR and nmr (^{1}H, ^{11}B-{^{1}H} and ^{31}P-{^{1}H}) spectroscopies and X-ray crystallography. A combination of the nmr spectroscopic and X-ray crystallographic data was shown to be not inconsistent with the carbaborane cage acting as a σ-donor, albeit a weak one.

The δ ^{31}P shifts of the the carbaauraboranes correlated well with the basicity of the phosphines (as described by Tolman), gradually shifting to lower field (deshielding) as the basicity of the phosphine increased.

The ^{11}B-{^{1}H} and ^{31}P-{^{1}H} nmr spectra were suggestive of the carbaborane was acting as an efficient σ-donor. The ^{11}B-{^{1}H} nmr spectra showed that substitution of the C_{cage} proton by {PR_3Au}$^+$ caused deshielding of the boron nuclei, indicating an apparent loss of electron density from the cage. The ^{31}P chemical shifts for a number of PR'_3AuX species (where X = carbaborane) were found to be between those of the respective methyl and chloride analogues (the δ ^{31}P shifts of the carbaboranes were lower than the methyl, but higher than the chloride species), suggesting intermediate donor ability of the carbaborane ligand

Crystallographic studies on compounds **6** and **7** and their methyl analogues, **6a** and **7a**, also suggested that the carbaborane ligand to be a good σ-donor. In both cases, the Au-C_{cage} bond length was shorter than the corresponding Au-C_{Me} distance in the related PR'_3AuMe species. Moreover, as the basicity of the phosphine increased, the difference in the Au-C_{cage} and Au-C_{Me} distances also decreased. This could be due to the carbaborane being more able to donate electron density to the metal than the methyl species to compensate a not very basic phosphine *trans* to itself.

A recent paper by Hawthorne suggested an alternative reason for the observed spectroscopic and crystallographic data, specifically that the C_{cage} carbon atoms were differently hybridised to CH_3 (sp^3) containing more *s*-character. Although we agree that carbaborane is not as efficient a

σ-donor as methyl, we do not agree that the carbaborane is strongly electron-withdrawing, merely a weak donor.

It was also shown that changing the C(1) substituent did not significantly affect the electronic properties of the cage, reflected by the similarity of the shifts of the ^{11}B-{^1H} and ^{31}P-{^1H} nmr spectra for compounds **6**, **11**, **12** and **13**. Substitution of the C_{cage} protons by {P(*o*-tol)$_3$Au}, although causing deshielding of the ^{11}B nuclei relative to the parent carbaboranes, had no marked effect on δ ^1H for the C(1) substituents. It was not possible to measure this for R = Ph (the only group capable of π-bonding), due to the overlap of resonances of the phenyl and *ortho*-tolyl protons.

Consistent with this view were the structural determinations of the above compounds, which showed slight or no change in Au-C_{cage} bond lengths with changing R. This was further investigated by EHMO calculations used to predict the energies of the HOMO's of a series of carbaborane anions of the type [1-R-1,2-*closo*-$C_2B_{10}H_{10}$]$^-$ and showing them to be extremely similar.

The novel compounds P(C_6F_5)$_3$AuCl, **14**, and C_6F_5AuP(C_6F_5)Me$_2$, **15**, were synthesised and characterised by microanalysis and nmr (^1H, ^{19}F-{^1H} and ^{31}P-{^1H}) spectroscopies. The latter compound was structurally characterised by a single crystal X-ray diffraction study, which showed the two C_6F_5 rings to be lying almost coplanar.

Chapter 3 References

1 E.g. (**a**) A. Stock, "*Hydrides of Boron and Silicon*," Cornell University Press, Ithaca, New York, 1936; (**b**) W.N. Lipscomb, "*Boron Hydrides*," Benjamin, New York, 1963; (**c**) E.L. Muetterties, "*Boron Hydrides*," Academic Press, New York, 1975; (**d**) K.F. Purcell and J.C. Kotz, "*Inorganic Chemistry*," Chapter 18, W.B. Saunders Company, Philadelphia, 1977.

2 D.A. Owen, J.C. Smart, P.M. Garrett and M.F. Hawthorne, *J. Am. Chem. Soc.*, 1971, **93**, 1362.

3 S. Bresadola and B. Longato, *Inorg. Chem.*, 1974, **13**, 539.

4 C.M. Mitchell and F.G.A. Stone, *J. Chem. Soc., Chem Commun.*, 1970, 1263.

5 D.G. Evans and D.M.P. Mingos, *J. Organomet. Chem.*, 1982, **232**, 171.

6 B.D. Reid and A.J. Welch, *J. Organomet. Chem.*, 1992, **438**, 371.

7 E.g. (**a**) K.F. Shaw and A.J. Welch, *Polyhedron*, 1992, **11**, 431; (**b**) P.T. Brain, J. Cowie, D.J. Donohoe, M. Hofmann D. Hnyk, D.W.H. Rankin, D. Reed, B.D. Reid, H.E. Robertson, P.v.R. Schleyer and A.J. Welch, *Inorg. Chem.*, 1996, **35**, 1701.

8 "*Spectroscopic Methods in Organic Chemistry*" (Third Edition), D.H. Williams and I. Fleming, McGraw-Hill Book Company (UK) Limited, 1980, pp 146.

9 C.A. Tolman, *Chem. Rev.*, 1977, 313 and references therein.

10 C.S.W. Harker and E.R.T. Tiekink, *Acta Cryst.*, 1990, **C46**, 1546.

11 D.E. Harwell, M.D. Mortimer, C.B. Knobler, F.A.L. Anet and M.F. Hawthorne, *J. Am. Chem. Soc.*, 1996, **118**, 2679.

12 K. Angermaier, E. Zeller and H. Schmidbaur, *J. Organomet. Chem.*, 1994, **472**, 371.

13 R.J. Puddephatt, in "*Comprehensive Organometallic Chemistry*," Eds. G. Wilkinson, F.G.A. Stone and E.W. Abel, Pergamon Press, 1981, Section 15.

14 E.C. Alyea, G. Ferguson, J.F. Gallagher and J. Malito, *Acta Cryst.*, 1993, **C49**, 1473.

15 T.V. Baukova, L.G. Kuz'mina, N.V. Dvortsova, M.A. Porai-Koshits, D.N. Kravtsov and E.G. Perevalova, *Metalorg. Khim*, 1989, **2**, 1098.

16 (**a**) J.A. Muir, M.M. Muir, and L.B. Pulgar, *Acta Cryst.*, 1985, **C41**, 1174;

(**b**) E.R.T. Tiekink, *Acta Cryst.*, 1989, **C45**, 1233; (**c**) Reference **14**; (**d**) Reference **18**.

17 P.G. Jones, *J. Organomet. Chem.*, 1988, **345**, 405.

18 P.D. Gavens, J.J. Guy, M.J. Mays and G.M. Sheldrick, *Acta Cryst.*, 1977, **B33**, 137.

19 A. Haaland, J. Hougen, H.V. Volden and R.J. Puddephatt, *J. Organomet. Chem.*, 1987, **325**, 311.

20 R.K. Bohn and R.D. Bohn, *Inorg. Chem.*, 1971, **10**, 350,

21 E.g. (**a**) Reference **21b**; (**b**) Reference **21d**; (**c**) Reference **16**.

22 E.g. (**a**) A. Karipdes and C.M. Cosio, *Acta Cryst.*, 1989, **C45**, 1743; (**b**) Reference **14**; (**c**) Reference **18**.

23 (**a**) R.W. Baker and P.J. Pauling, *J. Chem. Soc., Dalton Trans.*, 1972, 2264; (**b**) R. Uson, A. Laguna, J. Fornies, I. Valenzuela, P.G. Jones and G.M. Sheldrick *J. Organomet. Chem.*, 1984, **273**, 129; (**c**) R. Uson, A. Laguna, M. Laguna, A. Morata, P.G. Jones and G.M. Sheldrick, *J. Chem. Soc., Dalton Trans.*, 1986, 669; (**d**) P.G. Jones and C. Thone, *Acta Cryst.*, 1992, **C48**, 1312.

Chapter 4

Chemistry of the [7,8-Ph_2-7,8-*nido*-$C_2B_9H_{10}$]$^-$ Ligand

4.1 Introduction

Recent work by this group has focussed upon the systematic crowding of carba(metalla)boranes. Central to this has been the use of the [7,8-Ph_2-7,8-*nido*-$C_2B_9H_{10}$]$^-$ anion, which, with its two bulky phenyl groups, has given rise to three main types of deformation; **polyhedral distortion**, **polyhedral isomerisation** and **vertex extrusion**, described previously in **Section 1.5**. It would therefore be of value to determine the structure of the anion to provide a structural reference point for these systematic deformations to enable the comparison of structural parameters between series of compounds, in much the same way as for mono-phenylcarbaborane (**Section 2.2**).

In 1974, Hawthorne *et al* synthesised the *closo* carbarhodaborane, 3,3-$(PPh_3)_2$-3-H-3,1,2-*closo*-$RhC_2B_9H_{11}$, by heating to reflux $(PPh_3)_3RhCl$ and Cs[7,8-*nido*-7,8-$C_2B_9H_{12}$] in EtOH for 48 hours (**Fig. 4.1**).[1]

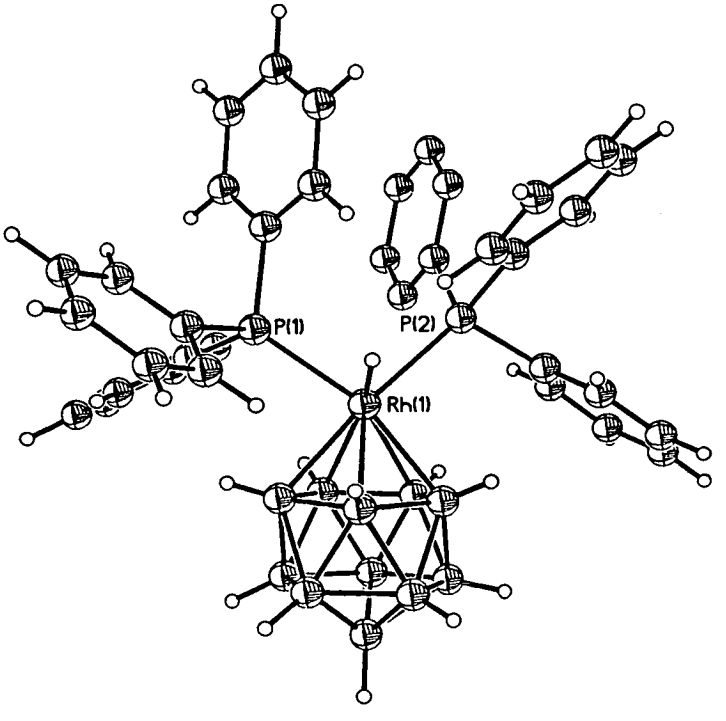

Figure 4.1 Perspective View of 3,3-$(PPh_3)_2$-3-H-3,1,2-*closo*-$RhC_2B_9H_{11}$

Rather surprisingly, in view of the fact that that the metal centre was both coordinatively (*pseudo*-octahedral geometry) and electronically (Rh(III), 18e$^-$) saturated, it showed catalytic activity, e.g. catalysis of the isomerisation of hex-1-ene to hex-2-ene.[2] After further work on a series of C-substituted analogues of the general type 1-R-2-R′-3,3-$(PPh_3)_2$-3-H-3,1,2-*closo*-$RhC_2B_9H_9$ (e.g. R = Ph, R′ = H, Me; R, R′ = *o*-phenylene), he hypothesised that there was another, tautomeric, form responsible for this activity (**Fig. 4.2**).[3]

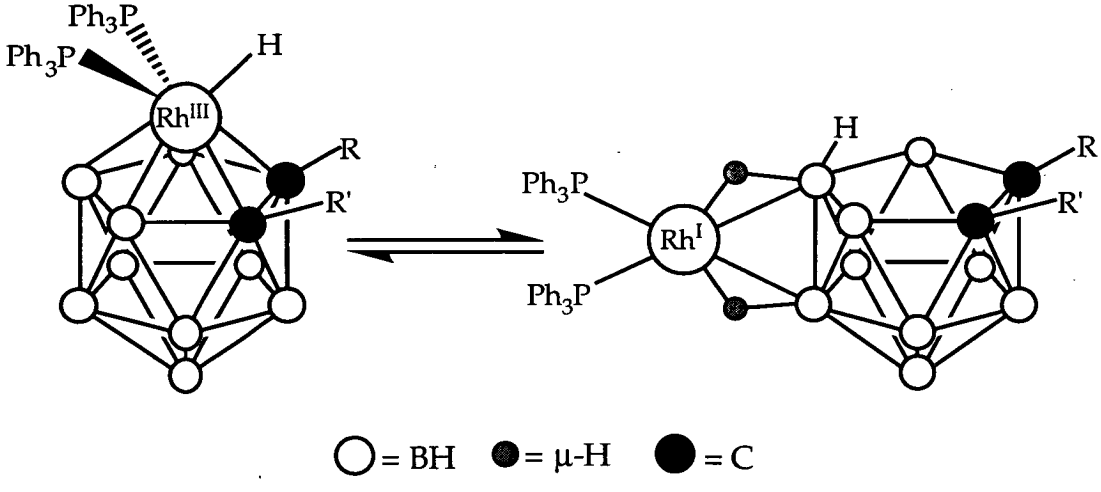

Figure 4.2 Representations of 1-R′-2-R-3,3-$(PPh_3)_2$-3-H-3,1,2-*closo*-$RhC_2B_9H_9$ and its *Exo-Nido* Tautomer (R = Alkyl, Aryl)

In this tautomer, termed *exo-nido*, the metal-ligand fragment is *exo* to the *nido* C_2B_9 cage. The rhodium is now unsaturated, both coordinatively (square planar c.f. $(PPh_3)_3RhCl$) and electronically (Rh(I), 16e$^-$). Hawthorne found that as the steric bulk of the R and R′ substituents increased, so too did the proportion of the *exo-nido* tautomer. For the original, unsubstituted compound, the equilibrium is far to the left and only the *closo* tautomer can be detected by nmr spectroscopy. For the phenyl, methyl/methyl and phenyl/methyl substituted examples, the products are *closo*, a mixture of *closo* and *exo-nido* and exclusively *exo-nido*, respectively. From steric arguments, an analogous reaction with the [7,8-Ph_2-7,8-*nido*-$C_2B_9H_{10}$]$^-$ anion should also afford the *exo-nido* species as the exclusive product. Moreover, due to the high steric bulk of the reacting species (a di-phenyl substituted,

nido carbaborane and a $\{(PPh_3)_2Rh\}$ fragment), other deformations in addition to the predicted vertex extrusion are possible.

The use of chelating ligands to stabilise metal centres is well documented.[4] It would be interesting, therefore, to synthesise *exo-nido* carbarhodaboranes where the two mono-dentate phosphines are replaced by a single, bi-dentate phosphine, such as bis(diphenylphosphino)ethane (dppe). If such a compound could be synthesised, would it be; a) more stable? b) more catalytically active?

Recent work by Stone has indicated that *exo-nido* species could possibly be synthesised via another route (**Fig. 4.3**).[5]

Treatment of the anion, $[1,2\text{-}Me_2\text{-}3\text{-}(1,5\text{-cod})\text{-}3,1,2\text{-}RhC_2B_9H_9]^-$, with acid ($CF_3CO_2H$) affords $1,2\text{-}Me_2\text{-}3\text{-}(\eta^3\text{-}C_8H_{13})\text{-}3,1,2\text{-}RhC_2B_9H_9$.[6] The latter compound is an extremely stable, 16-electron species, which unlike similar organometallic compounds is not stabilised by interaction of the metal centre with the σ-electrons of any proximal C-H bonds (hence affording the metal centre an 18-electron configuration).[7] Reaction of this compound with donor ligands such as CO affords 18-electron species. If the donor ligand used is a small phosphine and the reaction is performed using CH_2Cl_2 as the solvent, however, the cyclooctenyl ligand is displaced as (1,5-cod) and bis(phosphine)hydrido (PEt_3) and bis(phosphine)chloro (PMe_3) species are afforded.[5]

It would seem reasonable that similar chemistry would be observed for the diphenyl substituted analogues of the above carbametallaboranes with these small phosphines. Were this the case, analogous reactions with either PPh_3 or dppe, could possibly afford a new synthetic route to *exo-nido* carbametallaboranes.

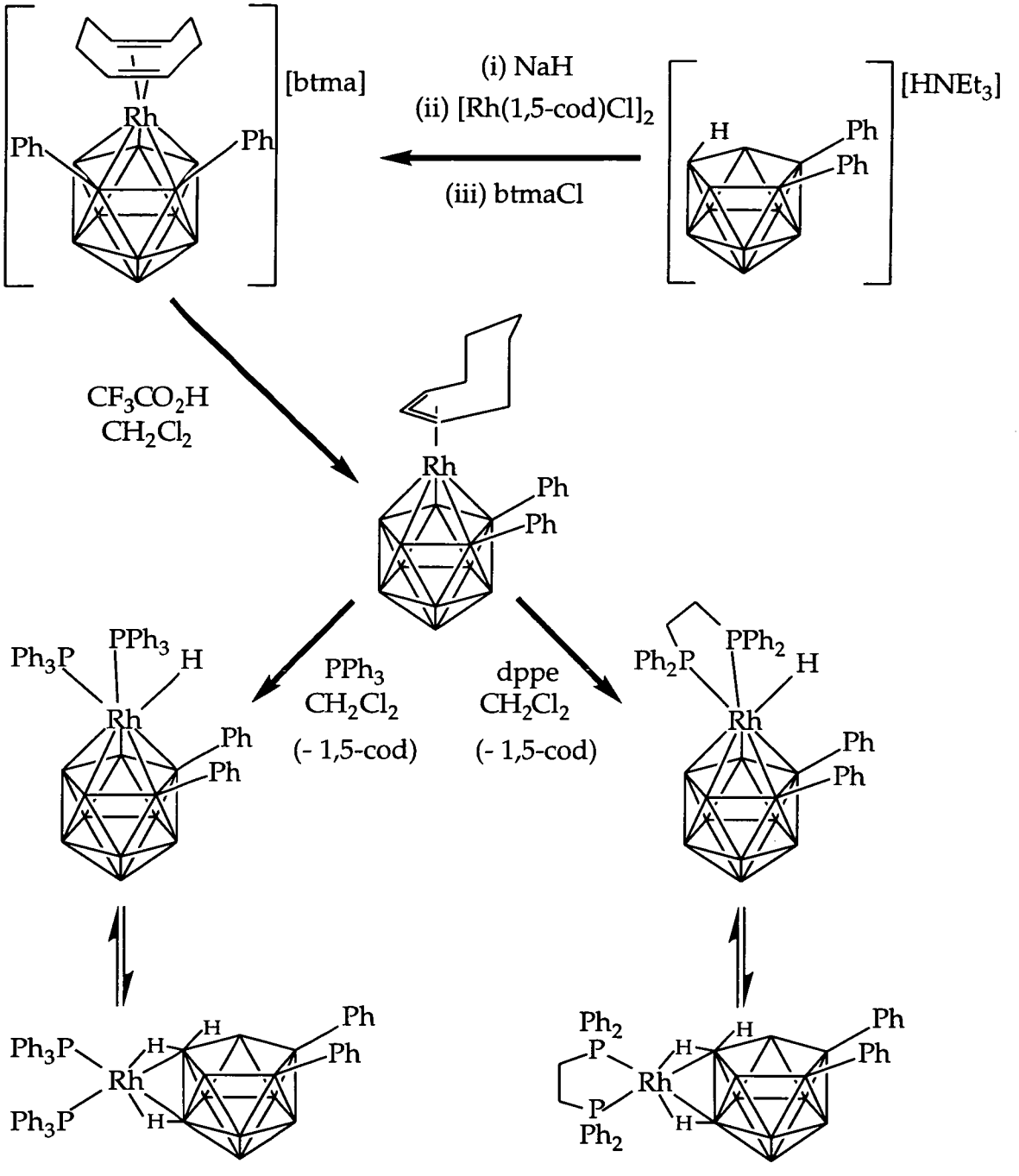

Figure 4.3 Representation of Possible Synthetic Routes to *Exo-Nido* Carbametallaboranes

4.2 $[HNEt_3][7,8\text{-}Ph_2\text{-}7,8\text{-}nido\text{-}C_2B_9H_{10}]$ (16)

4.2.1 Synthesis

The potassium salt of $[7,8\text{-}Ph_2\text{-}7,8\text{-}nido\text{-}C_2B_9H_{10}]^-$ was synthesised by heating to reflux for forty-eight hours an ethanolic solution of $1,2\text{-}Ph_2\text{-}1,2\text{-}closo\text{-}C_2B_{10}H_{10}$ in the presence of two equivalents of KOH. Removal of excess KOH was effected by its precipitation and then filtration as K_2CO_3 by bubbling CO_2 through the cooled reaction mixture. The solvent was removed and the potassium salt dissolved in water before being precipitated as the $[HNEt_3]^+$ salt by the addition of an aqueous solution of one equivalent of $HNEt_3Cl$ in the minimum amount of water. The precipitate was extracted three times into Et_2O. Removal of Et_2O from the combined washings afforded an oil, which was recrystallised from petroleum ether (60-80) to afford pure **16** in high yield (*ca.* 82%).

Previous syntheses had only heated the solution to reflux for 2-3 hours, which, although sufficient for the deboronation of $1,2\text{-}closo\text{-}C_2B_{10}H_{12}$, does not allow the reaction to go to completion in the case of $1,2\text{-}Ph_2\text{-}1,2\text{-}closo\text{-}C_2B_{10}H_{10}$. This is no doubt due to the presence of the sterically bulky phenyl groups on the two cage carbons, hindering nucleophilic attack by the ethoxide ion,[8] although the $^{11}B\text{-}\{^1H\}$ shifts of the B(3,6) atoms (the boron atoms, adjacent to the two cage-carbon atoms, that are removed to afford the $7,8\text{-}nido\text{-}C_2B_9$ species) become gradually more deshielded as the number of phenyl groups increases and should, therefore be easier to remove.

The precipitate afforded by the addition of the $HNEt_3Cl$ is often fine and filtration is an inefficient method of separation. Extraction into Et_2O, however, is essentially quantitative and easy to follow since the aqueous layer changes from white to colourless as the extraction progresses. The oil produced upon removal of the Et_2O is recrystallised by the addition of petroleum ether (60-80) to afford the product as a microcrystalline solid in 82% yield. The compound is readily soluble in chlorinated solvents, thf, acetone and Et_2O and insoluble in *n*-pentane and hexanes. As such,

colourless, diffraction quality needles were grown by the slow diffusion of *n*-hexane and a CH_2Cl_2 solution (4:1) at -30°C.

The mono-phenylcarbaborane analogue, **16a**, was synthesised according to the method of Hawthorne[8] by heating to reflux for 24 hours an ethanolic solution of the *closo* carbaborane in the presence of two equivalents of KOH. The work-up procedure was similar to that described above, and afforded the product as a white crystalline solid in 92% yield.

4.2.2 Characterisation

Characterisation of $[HNEt_3][7,8\text{-}Ph_2\text{-}7,8\text{-}nido\text{-}C_2B_9H_{10}]$, **16**, was carried out by microanalysis, IR and nmr (^1H, ^{11}B and $^{11}B\{^1H\}$) spectroscopies. Structural characterisation was by a single-crystal X-ray diffraction study.[9]

Initial characterisation was by IR spectroscopy, which showed a strong absorption band at 2530 cm^{-1}, due to B-H_{exo} stretches. Microanalysis figures were in excellent accordance with the calculated values.

The ^1H nmr spectrum (**Fig. 4.5**) shows that the product is a 1:1 salt. The resonances due to the C_6H_5 protons occur as a multiplet centred at 6.95 ppm and that due to the NH proton as a broad singlet at 3.65 ppm. The CH_2 and CH_3 resonances occur as a quartet and a triplet, centred at 3.40 and 1.41 ppm, respectively. From low- to high-field, the integrals of the resonances are in the ratio 10:1:6:9. Analysis of the high-field region showed a broad doublet at -1.9 ppm. This is due to an *endo*-proton on B(10), coupling to the $H(10)_{exo}$ proton (see below) and is similar to that observed for the unsubstituted analogue $[7,8\text{-}nido\text{-}C_2B_9H_{12}]^-$.[10]

The $^{11}B\{^1H\}$ nmr spectrum of **16** shows six resonances (**Figure 4.6** above). From low- to high-field, these occur at -6.49, (2B), -12.77 (1B), -14.80 (2B), -17.30 (2B), -31.49 (1B), -33.84 (1B) ppm. This shielding pattern, with two high-field integral-one resonances, is typical of a symmetrically substituted 7,8-*nido*-C_2B_9 carbaborane. **Figure 4.4** shows a plan view of such a cluster (for R = R'; protons are omitted for clarity), which shows that the molecule has C_s symmetry, with the mirror-plane bisecting the B(3), B(1) and B(10) atoms.

These three atoms are unique and are give rise to the three integral-one resonances. The resonances of relative integral-two are due to the three pairs of boron atoms, B(2,4), B(5,6) and B(9,11), each boron in the pair being related to the other one by reflection in the mirror-plane. The ^{11}B nmr spectrum (**Fig. 4.6**) shows the expected splitting of each resonance into doublets by the associated *exo*-H ($^1J_{B\text{-}Hexo}$ = 137-160 Hz).

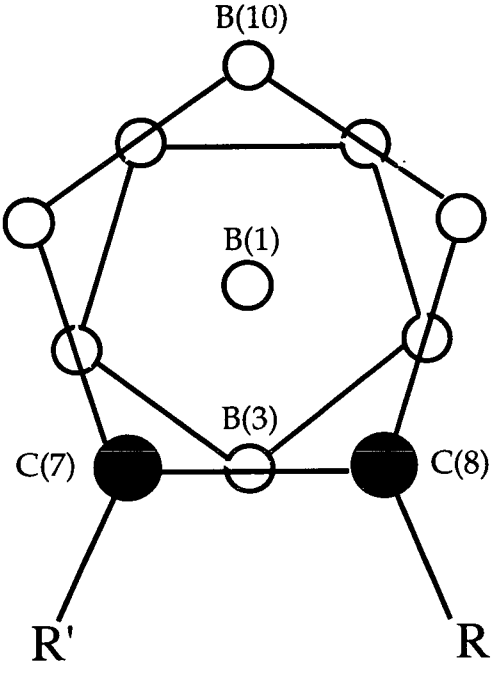

Figure 4.4 Plan View Representation of a 7,8-*Nido*-C_2B_9 Cage

The integral-one resonance at -31.49 ppm, however, is not a simple doublet, being further split ($^1J_{B\text{-}H}$ = 49.4 Hz) to give an unresolved doublet of doublets (the high-field half of the apparent quartet is masked by the overlapping doublet due to the resonance at -33.84 ppm (**Figure 4.6**)). This second splitting is due to the *endo*-proton attached to B(10) on the open C_2B_3 face. The coupling constant, 49.4 Hz, is typical for an *endo*-H, which must be associated with B(10), as this is the only integral-one boron in the open-face (the facial proton cannot be bridging as none of the other boron resonances are broadened). This assignment is in accordance with the structural determinations for the related anions, $[C_2B_9H_{12}]^-$ [10] and [7-CH_2OCH_3-7,8-*nido*-$C_2B_9H_{11}]^-$,[11] both of which show a B(10)-bound, *endo*-proton.

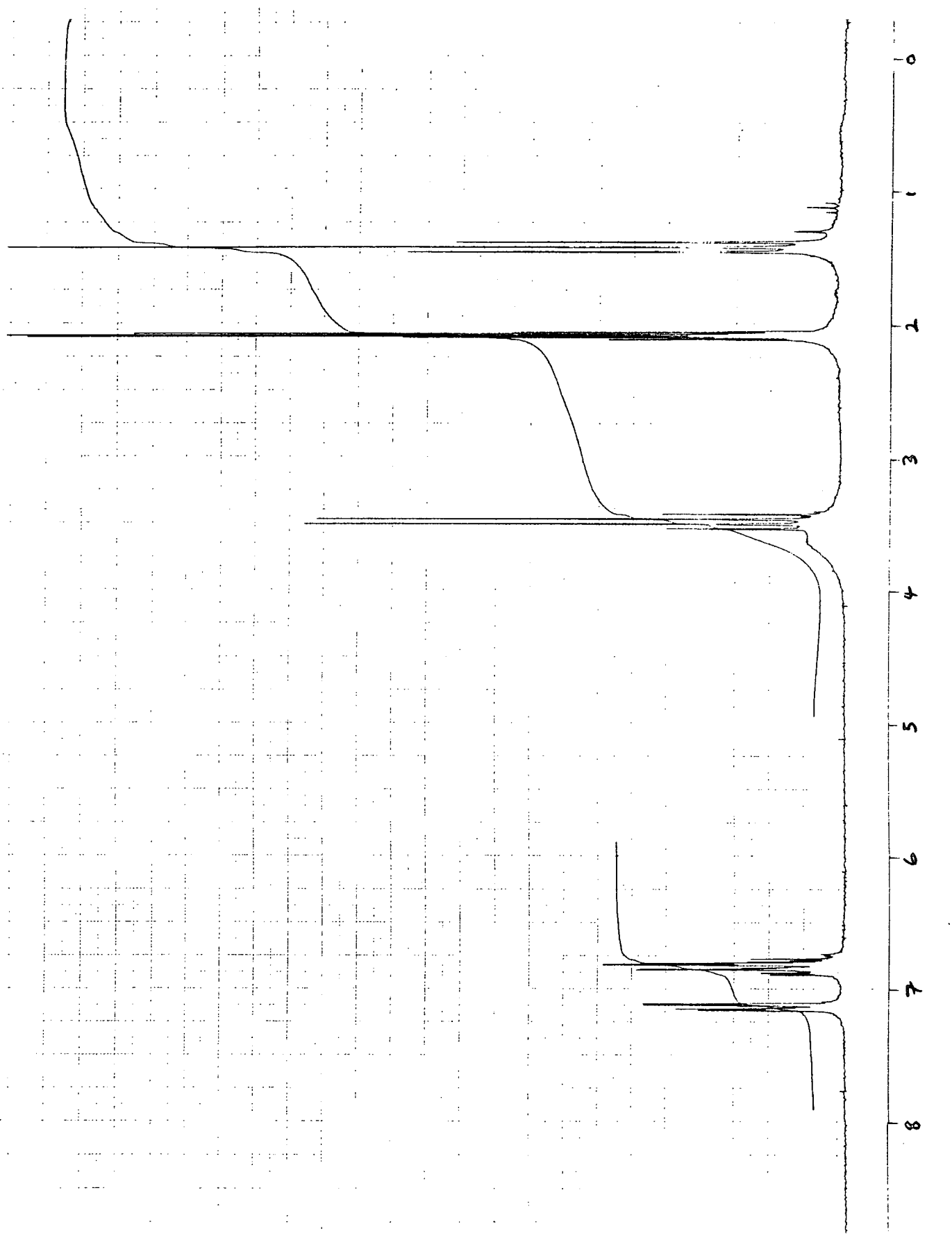

Figure 4.5 ^{1}H Nmr Spectrum of **16** (200.1 MHz)

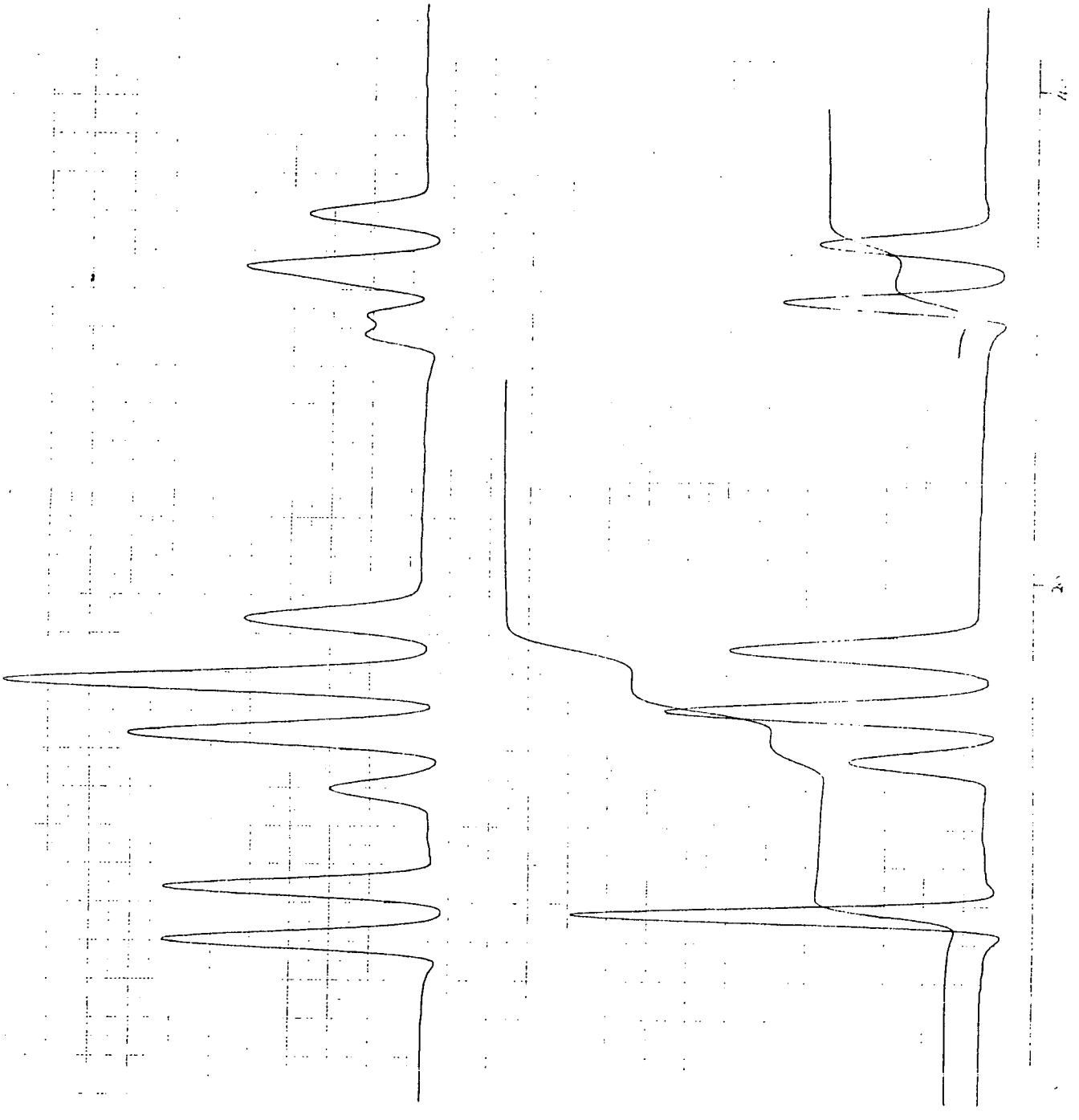

Figure 4.6 ^{11}B-{^{1}H} and ^{11}B Nmr Spectra of **16** (64.2 MHz)

The related compound, [$HNEt_3$][7-Ph-7,8-*nido*-$C_2B_9H_{11}$], **16a**, was also characterised by microanalysis and IR and nmr (^1H, ^{11}B and ^{11}B-{^1H}) spectroscopies.

IR spectroscopy showed that the absorption band due to B-H_{exo} stretching occurs at 2530 cm^{-1}. Again microanalysis figures are in excellent accordance with the calculated values.

The ^1H nmr spectrum shows the phenyl protons of the anion and the the methylene, N-H and methyl protons of the counter-ion, in the ratio 5:6:1:9, respectively. The C_{cage} proton is not observed. The *endo*-proton appears as a broad doublet at -2.3 ppm and is probably attached to the B(10) atom (see below).

The ^{11}B-{^1H} nmr spectrum shows nine boron resonances between -5.61 and -32.65 ppm. This is because the cage is unsymmetrically substituted and the plane of symmetry has been removed making all the boron atoms inequivalent. Again the two highest-field boron atoms are several ppm to lower frequency than the next highest-field resonance, at similar shifts to those observed for **16**. In the ^{11}B spectrum, there is slight broadening of the resonance at 29.56 ppm, due to the presence of an *endo*-proton ($^1J_{B\text{-}H endo}$ = *ca.* 50Hz). This extra coupling, however, was not as well resolved as for **16** and could not be measured accurately.

4.2.3 Crystallographic Study of 16

Colourless, diffraction quality *plates* of **16** were afforded by the slow diffusion of *n*-hexane and a CH_2Cl_2 solution at -30°C. Intensity data were measured on an Enraf-Nonius CAD4 diffractometer operating with Mo-K_α *X*-radiation (λ_{bar} = 0.71073 Å). The single crystal was mounted in a glass capillary and the experiment performed at 291(2) K.

Crystal data

$C_{20}H_{36}B_9N$, M = 387.79, triclinic, *P*bar1, a = 11.014(4) Å, b = 11.030(7) Å, c = 12.333(7) Å, α = 67.83(5)°, β = 80.78(4)°, γ = 60.20(5)°, V = 1203.3(11) Å^3, from least squares refinement of 25 reflections ($9 \leq \theta \leq 13°$) at 291(2) K, Z = 2 ion pairs, D_c = 1.070 gcm^{-3}, μ(Mo-K_α) = 0.06 mm^{-1}, F(0,0,0) = 416e.

Data collection and reduction

Intensity data collected in the range $2<2\theta<50°$ by the ω-2θ scan method; ω-scan width (0.8+0.34tanθ), ω-scan speeds in the range 0.87 to 2.35°min^{-1}. The intensities of 4462 unique reflections (h 0 to 13, k -13 to 13, l -14 to 14) were measured (DATCOL).

Structure solution and refinement

The structure was solved using direct methods (SHELX86) and developed by iterative, full-matrix least-squares refinement and difference Fourier syntheses (SHELX76, SHELXTL). The are two ion pairs *per* unit cell. The anion is slightly disordered with high residual electron density (0.78eÅ^{-3}) at the missing twelfth icosahedral vertex, which is due to it being partially occupied. Consequently, there is an equal depopulation of the B(3) position (the positions of the missing vertex and the B(3) atom are related by reflection in the plane which bisects C(7), C(8), B(5) and B(6)). This disorder prevented the B(10)-bound *endo*-H atom (observed by ^{11}B nmr spectroscopy) from being found from ΔF syntheses and it was, therefore, modelled (for the purposes of the **Figs. 4.7** and **4.8** alone) using CALC[12] with parameters taken from a previous structural determination of [7,8-*nido*-$C_2B_9H_{12}$]$^-$. The cage H_{exo}

atoms were located from ΔF syntheses and refined positionally with a group thermal parameter, which was 0.0809(27) at convergence. Phenyl H-atoms were fixed in idealised positions (C-H = 0.93 Å) and refined in a similar manner to the cage H_{exo} atoms. The cation is severely disordered, with all carbon atoms (except C(12), C(22) and C(31)) occupying two sites. The disordered non-H atoms were hence refined isotropically with 50% occupancies. The cation hydrogen atoms (attached to C(11), C(12), C(21), C(21A), C(32) and C(32A)) were fixed in idealised positions and modelled with 50% occupancies where appropriate.

Data were absorption corrected (DIFABS) and weighted such that $w^{-1} = [\sigma^2(F_o^2) + 0.1695P^2 = 0.27P]$ where $P = [\text{max. } (F_o^2 \text{ or } 0) + 2F_c^2]/3$. Using 3289 observed data ($F_o > 4.0\sigma(F_o)$), $R = 0.0956$, $wR_2 = 0.1943$ and $S = 1.154$ for 296 variable parameters. The maximum residue and minimum trough in a final difference Fourier synthesis were 0.78 and -0.28 eÅ^{-3}, respectively. Atomic scattering factors were those inlaid in SHELXTL. Selected bond lengths (Å) and angles (°), fractional coordinates and equivalent isotropic thermal parameters of non-hydrogen atoms are in **Tables 16A** and **16B**, respectively.

The compound was confirmed as being the title compound by the structural study and perspective and plan views of the anion are shown in **Figures 4.7 and 4.8**, respectively.

The anion has near C_s symmetry, with the *pseudo* mirror plane bisecting the B(1), B(3) and B(10) atoms (**Figures 4.6** and **4.8**) as described in **Section 4.2.2**. The lower B_5 pentagon is essentially planar ($\sigma = 0.003$, where $\sigma = (\Sigma z_i^2)^{1/2}$ and z_i is the the displacement of the i^{th} atom from the least squares plane). The upper C_2B_3 pentagon, however, is folded into an envelope conformation ($\sigma = 0.049$). The fold of 4.4° at the C(8)-B(10) vector is such that B(9) is below the approximate plane described by C(7), C(8), B(10) and B(11). The major deviation from C_s symmetry is the orientation of the two phenyl rings, described by θ (θ is defined in a similar manner to that described in **Section 2.1**, hence for the C(7)-bound phenyl ring, C(71-76), it is the modulus of the average of the C(8)-C(7)-C(71)-C(72) and C(8)-C(7)-C(71)-C(76) torsion angles. i.e. for $\theta = 90°$, the phenyl ring and two cage carbon atoms are

coplanar; for $\theta = 0^o$, the ring is twisted about C(7)-C(71) such that C(8) is the furthest distance from it). For C(71-76) $\theta = 5.60^o$ and for C(81-86) $\theta = 10.02^o$ and hence the two rings are almost parallel to each other.

The C(7)-C(8) distance is 1.590(5) Å, longer than in the unsubstituted anion [7,8-*nido*-$C_2B_9H_{12}$]$^-$ (1.542(3) Å),[10] which is as expected since there is a large mutual repulsion between the two adjacent phenyl groups. The equivalent (mean) distance in the parent *closo* carbaborane is 1.727(6) Å. C-B and B-B connectivities are in the range 1.631(7) to 1.758(7) and 1.735(8) to 1.839(8) Å, respectively. A previous determination of the anion as the [btma]$^+$ salt afforded a C(7)-C(8) distance of 1.602(3) Å.[9] Values of θ were also similar, with those for C(71-76) and C(81-86) calculated as being 17.9 and 20.0^o respectively. These two determinations of the anion are discussed further with respect to the anion in compound **18, Section 4.5.3.**

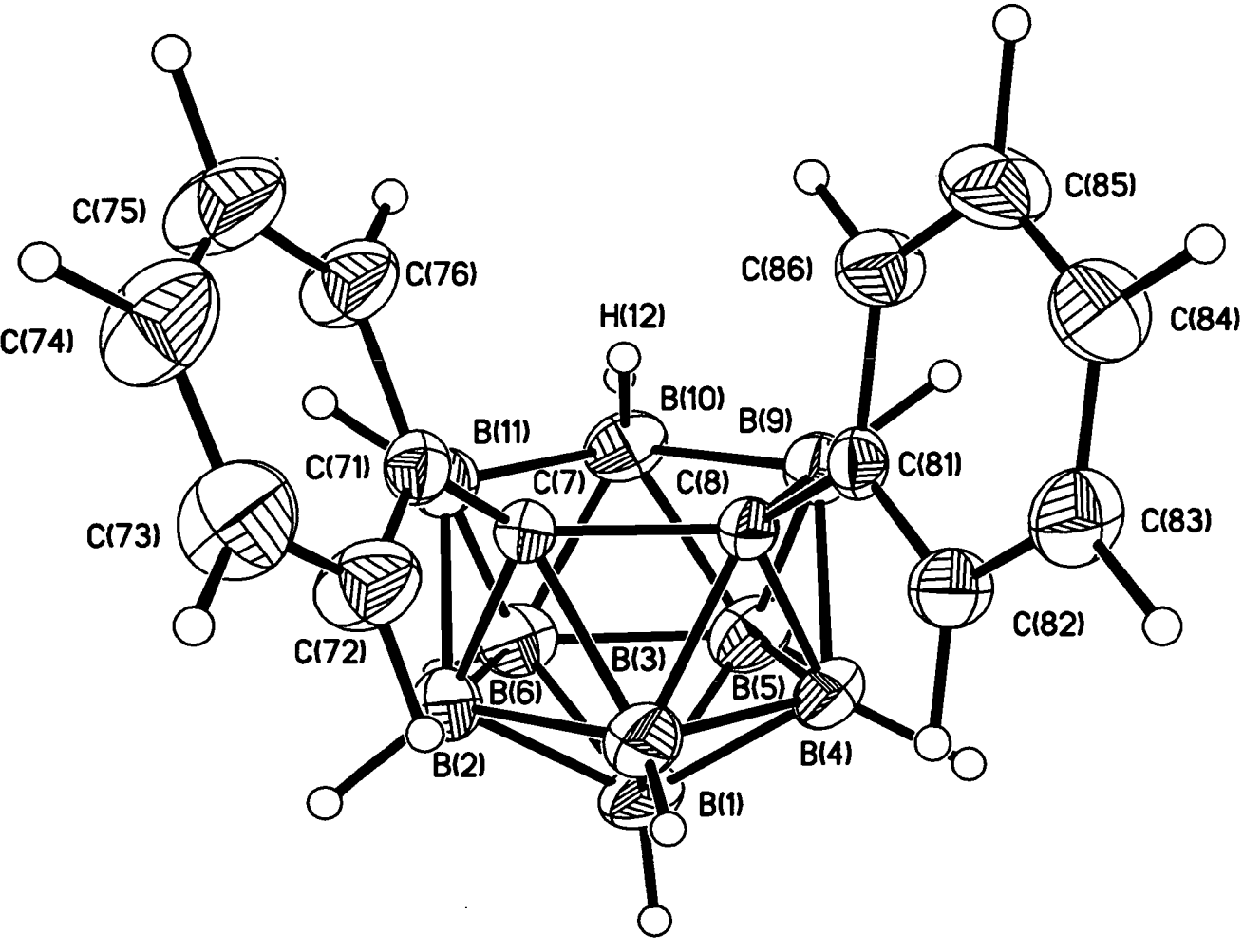

Figure 4.7 Perspective View of the Anion in **16**

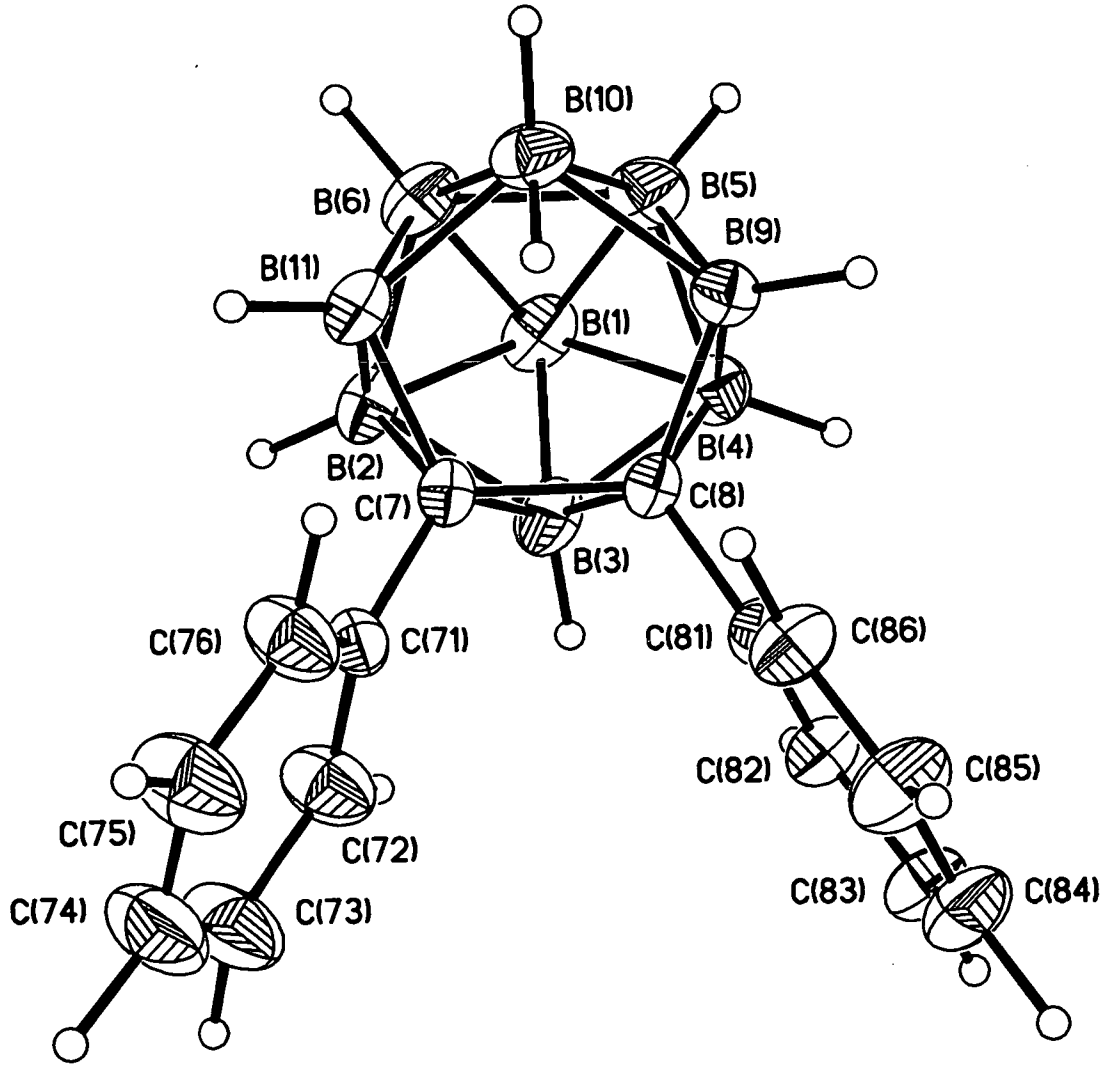

Figure 4.8 Plan View of the Anion in **16**

Table 16A Selected Bond Lengths (Å) and Angles (°) for **16**

B(1)-B(3)	1.750(6)	B(1)-B(4)	1.759(5)
B(1)-B(2)	1.769(6)	B(1)-B(5)	1.790(6)
B(1)-B(6)	1.801(5)	B(2)-C(7)	1.711(5)
B(2)-B(3)	1.742(5)	B(2)-B(6)	1.757(6)
B(2)-B(11)	1.779(5)	B(3)-C(8)	1.732(5)
B(3)-B(4)	1.740(6)	B(3)-C(7)	1.749(5)
B(4)-C(8)	1.698(4)	B(4)-B(5)	1.747(6)
B(4)-B(9)	1.799(5)	B(5)-B(9)	1.777(5)
B(5)-B(10)	1.783(5)	B(5)-B(6)	1.812(6)
B(6)-B(11)	1.746(5)	B(6)-B(10)	1.758(6)
C(7)-C(71)	1.498(4)	C(7)-C(8)	1.596(4)
C(7)-B(11)	1.632(4)	C(8)-C(81)	1.507(4)
C(8)-B(9)	1.637(4)	B(9)-B(10)	1.831(5)
B(10)-B(11)	1.795(6)	C(71)-C(72)	1.366(5)
C(71)-C(76)	1.385(4)	C(72)-C(73)	1.378(5)
C(73)-C(74)	1.355(6)	C(74)-C(75)	1.358(6)
C(75)-C(76)	1.376(5)	C(81)-C(86)	1.387(4)
C(81)-C(82)	1.390(4)	C(82)-C(83)	1.365(4)
C(83)-C(84)	1.382(5)	C(84)-C(85)	1.372(5)
C(85)-C(86)	1.367(5)	N-C(11A)	1.29(2)
N-C(21)	1.380(10)	N-C(31A)	1.52(2)
N-C(11)	1.624(11)	N-C(21A)	1.780(11)
C(11)-C(12)	1.272(11)	C(21)-C(22)	1.587(12)
C(21A)-C(22)	1.323(11)	C(31)-C(32)	1.22(2)
C(31)-C(32A)	1.32(2)		

B(3)-B(1)-B(4)	59.5(2)	B(3)-B(1)-B(2)	59.4(2)
B(4)-B(1)-B(5)	59.0(2)	B(2)-B(1)-B(6)	59.0(2)
B(5)-B(1)-B(6)	60.6(2)	C(7)-B(2)-B(3)	60.9(2)
B(3)-B(2)-B(1)	59.8(2)	B(6)-B(2)-B(1)	61.4(2)
C(7)-B(2)-B(11)	55.7(2)	B(6)-B(2)-B(11)	59.2(2)
C(8)-B(3)-B(4)	58.5(2)	C(8)-B(3)-C(7)	54.6(2)
B(2)-B(3)-C(7)	58.7(2)	B(4)-B(3)-B(1)	60.5(2)
B(2)-B(3)-B(1)	60.9(2)	C(8)-B(4)-B(3)	60.5(2)
B(3)-B(4)-B(1)	60.0(2)	B(5)-B(4)-B(1)	61.4(2)
C(8)-B(4)-B(9)	55.8(2)	B(5)-B(4)-B(9)	60.1(2)
B(4)-B(5)-B(9)	61.4(2)	B(9)-B(5)-B(10)	61.9(2)
B(4)-B(5)-B(1)	59.6(2)	B(10)-B(5)-B(6)	58.5(2)
B(1)-B(5)-B(6)	60.0(2)	B(11)-B(6)-B(2)	61.0(2)
B(11)-B(6)-B(10)	61.6(2)	B(2)-B(6)-B(1)	59.6(2)
B(10)-B(6)-B(5)	59.9(2)	B(1)-B(6)-B(5)	59.4(2)
C(71)-C(7)-C(8)	118.6(2)	C(71)-C(7)-B(11)	117.9(2)
C(71)-C(7)-B(2)	120.5(2)	B(11)-C(7)-B(2)	64.2(2)

C(71)-C(7)-B(3)	118.4(3)	C(8)-C(7)-B(3)	62.2(2)
B(2)-C(7)-B(3)	60.4(2)	C(81)-C(8)-C(7)	118.3(2)
C(81)-C(8)-B(9)	118.6(2)	C(81)-C(8)-B(4)	121.0(2)
B(9)-C(8)-B(4)	65.3(2)	C(81)-C(8)-B(3)	117.6(2)
C(7)-C(8)-B(3)	63.3(2)	B(4)-C(8)-B(3)	61.0(2)
C(8)-B(9)-B(4)	59.0(2)	B(5)-B(9)-B(4)	58.5(2)
B(5)-B(9)-B(10)	59.2(2)	B(6)-B(10)-B(5)	61.6(2)
B(6)-B(10)-B(11)	58.9(2)	B(5)-B(10)-B(9)	58.9(2)
C(7)-B(11)-B(2)	60.0(2)	B(6)-B(11)-B(2)	59.8(2)
B(6)-B(11)-B(10)	59.5(2)	C(72)-C(71)-C(76)	116.6(3)
C(72)-C(71)-C(7)	124.2(3)	C(76)-C(71)-C(7)	119.2(3)
C(71)-C(72)-C(73)	121.9(4)	C(74)-C(73)-C(72)	120.5(4)
C(73)-C(74)-C(75)	118.9(4)	C(74)-C(75)-C(76)	120.6(4)
C(75)-C(76)-C(71)	121.3(4)	C(86)-C(81)-C(82)	117.8(3)
C(86)-C(81)-C(8)	119.2(3)	C(82)-C(81)-C(8)	122.9(3)
C(83)-C(82)-C(81)	121.0(3)	C(82)-C(83)-C(84)	120.6(3)
C(85)-C(84)-C(83)	119.0(3)	C(86)-C(85)-C(84)	120.7(3)
C(85)-C(86)-C(81)	121.1(3)	C(11A)-N-C(21)	55.2(10)
C(11A)-N-C(31)	127.8(13)	C(21)-N-C(31)	103.9(9)
C(11A)-N-C(11)	55.6(10)	C(21)-N-C(11)	110.5(7)
C(31)-N-C(11)	112.2(8)	C(11A)-N-C(21A)	101.0(11)
C(21)-N-C(21A)	47.4(6)	C(31)-N-C(21A)	65.4(8)
C(11)-N-C(21A)	150.3(6)	C(12)-C(11)-N	117.0(8)
N-C(21)-C(22)	117.1(8)	C(22)-C(21A)-N	108.5(8)
C(21A)-C(22)-C(21)	53.1(6)	C(32)-C(31)-C(32A)	63.1(11)
C(32)-C(31)-N	97.3(14)	C(32A)-C(31)-N	109.8(13)

Table 16B Atomic Coordinates (x 10^4) and Equivalent Isotropic Thermal Parameters ($Å^2$ x 10^3) for **16**

	x	y	z	U(eq)
B(1)	2756(4)	10376(4)	6871(4)	60(1)
B(2)	2108(4)	9131(4)	7060(3)	54(1)
B(3)	3713(4)	8836(4)	6416(4)	58(1)
B(4)	4578(4)	9289(4)	7138(3)	52(1)
B(5)	3528(4)	9878(4)	8249(4)	63(1)
B(6)	1945(4)	9776(4)	8206(4)	64(1)
C(7)	3526(3)	7393(3)	7537(2)	40(1)
C(8)	4918(3)	7493(3)	7555(2)	39(1)
B(9)	4926(4)	8020(4)	8629(3)	50(1)
B(10)	3231(4)	8434(4)	9320(3)	56(1)
B(11)	2442(4)	7901(4)	8542(3)	51(1)
C(71)	3630(3)	6148(3)	7238(3)	47(1)
C(72)	3599(5)	6189(5)	6121(3)	78(1)
C(73)	3617(6)	5049(5)	5894(4)	96(1)
C(74)	3666(5)	3837(5)	6786(4)	96(2)
C(75)	3755(6)	3736(5)	7905(4)	97(2)
C(76)	3748(4)	4867(4)	8134(3)	73(1)
C(81)	6274(3)	6336(3)	7262(2)	42(1)
C(82)	6875(3)	6607(3)	6176(3)	53(1)
C(83)	8140(4)	5551(4)	5967(3)	66(1)
C(84)	8847(4)	4180(4)	6832(4)	74(1)
C(85)	8263(4)	3900(4)	7907(3)	78(1)
C(86)	6998(3)	4956(4)	8121(3)	62(1)
N	8920(5)	-1281(5)	7779(4)	109(1)
C(11)	8322(12)	-1472(11)	9091(9)	102(3)
C(12)	8936(8)	-2756(12)	9873(7)	195(4)
C(11A)	8615(22)	-2322(23)	8398(20)	194(7)
C(21)	8917(11)	-2294(11)	7381(10)	98(3)
C(21A)	8882(11)	-1298(12)	6348(9)	99(3)
C(22)	9869(8)	-2610(10)	6306(8)	173(3)
C(31)	7984(19)	221(19)	6891(15)	163(6)
C(32)	8130(9)	987(15)	7301(9)	249(6)
C(32A)	6903(15)	1002(15)	7415(12)	137(4)

4.3 *Exo-Nido*-Carbarhodaboranes

4.3.1 Synthesis

Initial attempts to synthesise μ_2-*exo*-{$(PPh_3)_2Rh$}-7,8-Ph_2-7,8-*nido*-$C_2B_9H_{10}$, **17**, were based upon the route used by Hawthorne to prepare 3,3-$(PPh_3)_2$-3-H-3,1,2-*closo*-$RhC_2B_9H_{11}$.[1] As such, Cs[7,8-Ph_2-7,8-*nido*-$C_2B_9H_{10}$] and $(PPh_3)_3RhCl$ were heated to reflux in EtOH for 48 hours. This approach, however, afforded only oils or intractable tars. Microanalyses of some of these products were inconclusive and ^{31}P-{^1H} nmr spectra showed only broad singlets, instead of the expected doublet ($^1J_{Rh-P}$ = 170-200 Hz), indicating that the metal was no longer attached to the phosphine ligands.

The title compound, **17**, and a related species, **17a**, were synthesised by short stirring (3 hours) of [$HNEt_3$][7,8-Ph_2-7,8-*nido*-$C_2B_9H_{10}$] and $(PPh_3)_3RhCl$ in CH_2Cl_2. This approach had several advantages: Firstly, shortening the reaction time should reduce the chances of the compound degrading. Secondly, in CH_2Cl_2, $(PPh_3)_3RhCl$ partially dissociates, losing a PPh_3 ligand.[13] Such a dissociation is clearly necessary to achieve the required stoichiometry and the fact that it is a facile process is naturally desirable. Moreover, the $[HNEt_3]^+$ cation is very halophilic and the resulting carbaborane salt very soluble in organic solvents, especially CH_2Cl_2. This avoids the use of EtOH as the solvent and precludes any possible nucleophilic attack of the cage or metal centre by $[EtO]^-$. Moreover, the $[HNEt_3]^+$ salt had been fully characterised (**Section 4.2**) and is easily purified by recrystallisation from petroleum ether (60-80) in high yield (*ca.* 80%). This is in contrast to the Cs^+ salt, which had only been characterised by IR spectroscopy (KBr disc, υ_{max} at 2569 cm^{-1}) and microanalysis (Calculated for $C_{14}H_{20}B_9Cs$: %C 40.18, %H 4.82; Found: %C 39.51, %H 4.65). Furthermore, yields of the caesium salt were poor, typically less than 20%, and low solubility in organic solvents made nmr spectroscopy difficult.

The reaction mixture was separated by colum chromatography into a red band, **17**, eluted with CH_2Cl_2, and a yellow band, **17a**, subsequently eluted with CH_2Cl_2:CH_3CN (3:1). On removal of solvents, red and orange solids

were afforded, respectively. Both compounds are extremely air-sensitive in solution (**17** goes from red to yellow; **17a** goes from orange to yellow).

The compounds are soluble in chlorinated solvents, thf, CH_3CN and acetone and insoluble in *n*-pentane and *n*-hexane. Red, diffraction quality blocks of **17** were grown in a Young's tube by the slow diffusion of *n*-hexane and a CH_2Cl_2 solution (1:4) at -30°C, using solvents that had been thoroughly degassed beforehand.

4.3.2 Characterisation

Compounds **17** and **17a** were initially characterised by IR spectroscopy as KBr discs, due to their high air-sensitivity in solution. Characteristic peaks were observed at 2540cm^{-1} and 2420cm^{-1}, respectively, due to B-H stretches.

The two compounds (**17a** values given in {parentheses}) were further characterised by nmr (^{1}H, ^{11}B, ^{11}B-{^{1}H } and ^{31}P-{^{1}H}) spectroscopy. The ^{1}H nmr spectrum shows the phenyl resonances as multiplets centred at 7.1 {7.2} ppm and a broad doublet due to an *endo*-H atom at -1.85 {-1.6} ppm in the ratio 40:1. This broad doublet is similar to that seen in the high-field region of the ^{1}H nmr spectrum of **16**. The expected signals due to the two bridging Rh-H-B protons are not, however, observed (although this is often the case). Inspection of the hydride region afforded no evidence of the *closo* species, in that the expected doublet of triplets, from coupling to rhodium and two equivalent phosphorous atoms, was not observed.

The ^{11}B-{^{1}H} spectrum (**Figure 4.9**, above), although much broadened with respect to that of **16**, still shows the same 2:1:2:2:1:1 shielding pattern, with the last two resonances at much higher field than the other four. Hence, the cage has retained the (*pseudo*) mirror symmetry of the anion. The resonances occur at -11.03 {-8.46}, -14.04 (2+1 coincidence) {-13.39, -16.94}, -15.53 {-18.04}, -32.76 {-32.95} and -35.95 {-35.40} ppm. Moreover, the second-highest-field resonances both show broadening, due to a second smaller coupling. However, since it was impossible to determine the coupling constants and coupling to other boron atoms cannot be observed, the source of this extra coupling cannot be absolutely shown to be an *endo*-proton bound to B(10). It

was entirely feasible that the extra proton is bridging and only when $^{1}H\text{-}\{^{11}B_{selective}\}$ nmr experiments were carried out could the nature of the extra proton be determined unequivocally. Irradiating the boron atoms (from low- to high-field) enhanced protons in the ratio 2:3:2:2:1 {2:1:2:2:2:1} (the underlined number accounts for an *endo*- and an *exo*-proton). Moreover, excitation of none of the other resonances enhanced the *endo*-proton signal. Hence, the extra facial proton is *endo*, the same as in the anion.

The $^{31}P\text{-}\{^{1}H\}$ nmr spectrum (**Fig. 4.10**) shows a doublet ($^{1}J_{Rh(I)\text{-}P}$ = 187.3 {186.9} Hz). This is typical for phosphorous coupling to a square-planar rhodium (I) centre, and is similar to that observed for similar *exo-nido* species.[3a, 3b]

The data, however, is apparently contrary to the solid state structure of **17** (**Section 4.3.3**), a plan view schematic of which is given in **Figure 4.11**. The $\{(PPh_3)_2Rh\}$ fragment is bonded to the side of the cage at the B(4) and B(9) positions by single Rh-H-B bridges. Since the mirror symmetry of the molecule has been destroyed, one would now expect to see nine unique boron environments instead of the six observed (the possibility that there are several coincidences, which would result in an apparently smaller number of environments can be discounted from the $^{1}H\text{-}\{^{11}B_{selective}\}$ experiments described previously). Furthermore, the two phosphorous atoms are now inequivalent, which would give two signals in the $^{31}P\text{-}\{^{1}H\}$ nmr spectrum, each a doublet of doublets. The higher symmetry of the spectra could be explained by the fluxionality within the compound, as observed by Hawthorne for previous *exo-nido* species.[3a, 3b] The $\{(PPh_3)_2Rh\}$ fragment presumably migrates rapidly around the sides of the cage, with concomitant rotation of the phosphine ligands about the P-Rh-P bisector. Thus the phosphorous atoms become equivalent and the cage has time-averaged mirror symmetry.

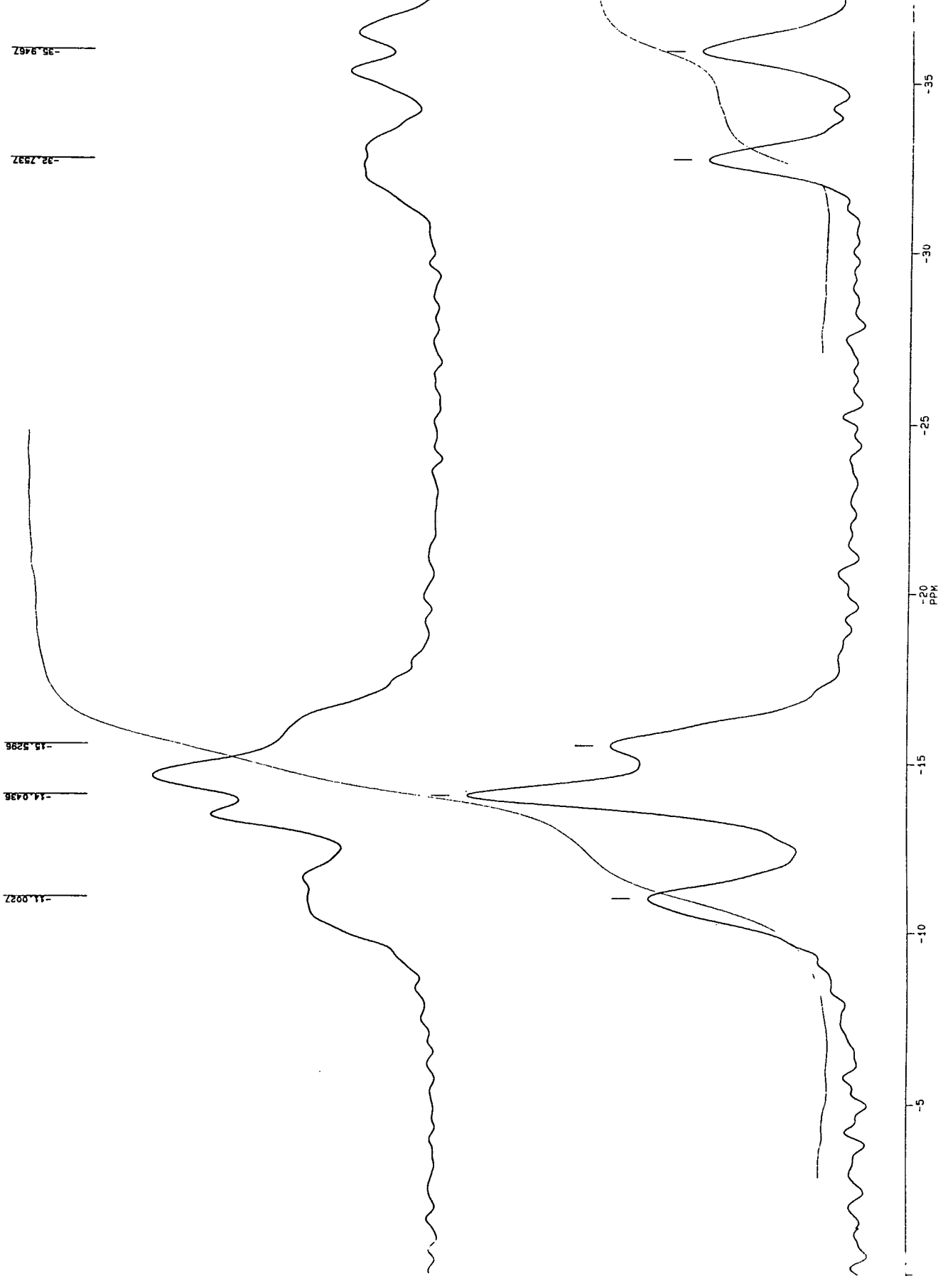

Figure 4.9 ^{11}B-{^{1}H} and ^{11}B Nmr Spectra of **17** (64.2 MHz)

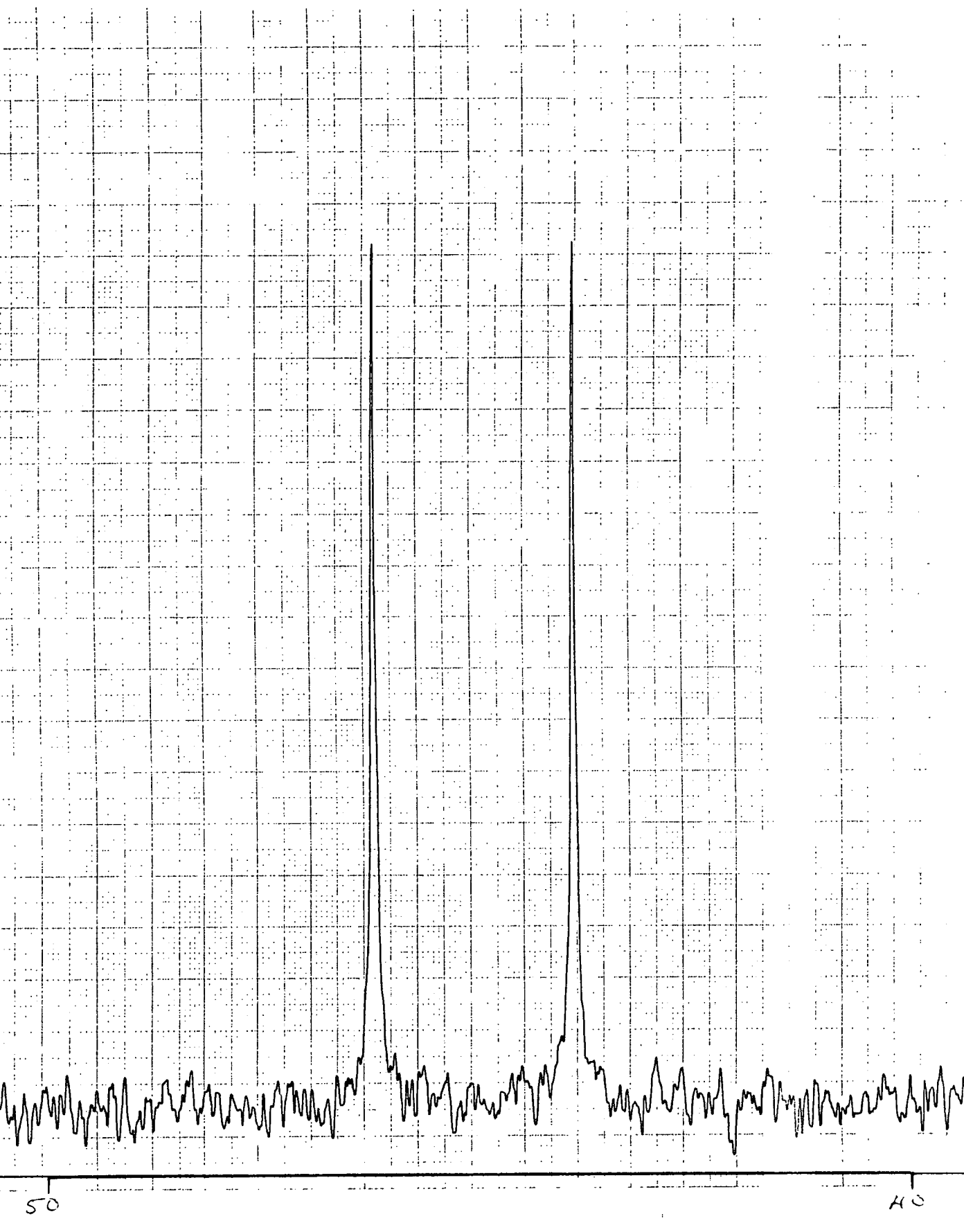

Figure 4.10 ^{31}P-{^{1}H} Nmr Spectrum of **17** (80.1 MHz)

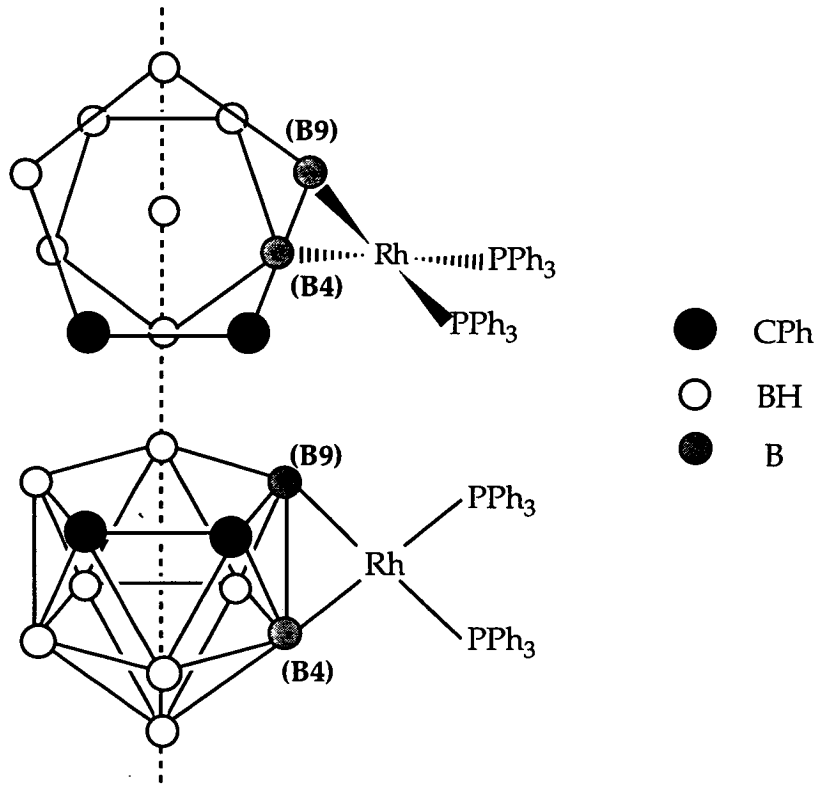

Figure 4.11 Representation of **17**

The absolute structure of **17a** could not be determined as suitable crystals could not be grown. However, there are several data that indicate a probable structure for the compound. The nmr data indicates that the molecule is similar to **17**, an *exo-nido* carbarhodaborane. The $^{31}P\text{-}\{^{1}H\}$ nmr spectrum is a doublet, with a coupling constant typical of phosphorous bound to Rh(I). The $^{11}B\text{-}\{^{1}H\}$ nmr spectrum indicates that the molecule possesses (time-averaged) C_s symmetry, similar to that observed for **17**. Compound **17a** cannot simply be a positional isomer of **17** (i.e. where the $\{(PPh_3)_2Rh\}$ fragment is bonded to boron atoms other than B(4) and B(9)) as the two compounds do not interchange in solution. We hypothesise, therefore, that **17a** is the **7,9-** analogue of **17**, i.e. the two cage carbon atoms are now separated on the open face (**both** of the two cage carbons must either be both located on the open face or, much less likely, in the lower B_5 pentagon, so as to preserve the observed mirror symmetry of the molecule). This structure is in accordance with the spectroscopic data, as well as being more thermodynamically stable due to the separation of the cage carbon atoms.

4.3.3 Crystallographic Study of $\mu_{(4,9)}$-*exo*-{$(PPh_3)_2Rh$}-7,8-Ph_2-7,8-*nido*-$C_2B_9H_{10}$ (17)

Red, diffraction quality *blocks* of **17** were grown in a Young's tube by the slow diffusion of *n*-hexane and a CH_2Cl_2 solution at -30°C, using thoroughly degassed solvents. Intensity data were measured on an Enraf-Nonius CAD4 diffractometer operating with Mo-K_α *X*-radiation (λ_{bar} = 0.71073 Å). The single crystal was mounted in a glass capillary and the experiment performed at 293(2) K.

Crystal data

$C_{50}H_{50}B_9RhP_2.CH_2Cl_2$, M = 998.03, triclinic, *P*bar1, a = 10.6178(23) Å, b = 12.534(4) Å, c = 20.461(4) Å, α = 102.82(2)°, β = 94.55(2)°, γ = 105.37(2)°, V = 2533.0(11) $Å^3$, from least squares refinement of 25 reflections ($11 \leq \theta \leq 13°$) at 291(2) K, Z = 2, D_c = 1.306 gcm^{-3}, μ(Mo-K_α) = 5.40 mm^{-1}, F(0,0,0) = 1020e.

Data collection and reduction

Intensity data collected in the range $0<2\theta<50°$ by the ω-2θ scan method; ω-scan width (0.8+0.34tanθ), ω-scan speeds in the range 0.9 to 2.35°min^{-1}. The intensities of 9427 unique reflections (h 0 to 7, k -9 to 9, l -14 to 14) were measured (DATCOL).

Structure solution and refinement

The structure was solved using Patterson methods (Rh) and ΔF syntheses (P, C, B) (SHELX76) and developed by iterative, diagonal, least-squares refinement and further difference Fourier syntheses (SHELXTL). There is one molecule of CH_2Cl_2 *per* molecule of **17**. All cage H-atoms were positionally refined except the *endo*-H atom, which could not be located due to disorder of the cage (see below). Phenyl rings were fixed as planar hexagons (C-C = 1.39 Å), with phenyl H-atoms fixed in idealised positions (C-H = 0.93 Å). All H atoms were refined isotropically; the cage-H atoms were given a group thermal parameter, which was 0.0809(27) at convergence, whilst phenyl H atoms were allowed to ride on their respective carbon atom with

U(H) = 1.2 U(C). Again, there was disorder at the 'missing' twelfth vertex, and hence the B(3) and B(12) sites were modelled as being 0.667B and 0.333B, respectively. Data were weighted such that $w^{-1} = [\sigma^2(F_o^2) + (0.1101P)]$ where $P = [\text{max.}\ (F_o^2) + 2F_c^2]/3$. For 6488 observed reflections ($F_o > 4.0\sigma(F_o)$), R = 0.0594, wR_2 = 0.1757 and S = 1.081 for 512 variable parameters. The maximum residue and minimum trough in a final difference Fourier synthesis were 1.48 and -0.91 eÅ^{-3}, respectively. Atomic scattering factors were those inlaid in SHELXTL. Selected bond lengths (Å) and angles (°), fractional coordinates and equivalent isotropic thermal parameters of non-hydrogen atoms are in **Tables 17A** and **17B**, respectively.

Plan and perspective views of compound **17** are given in **Figures 4.12** and **4.13**, respectively showing the geometry of the carbaborane cage and the metal atom, respectively. These figures show clearly that the molecule adopts the predicted *exo-nido* geometry, in agreement with spectroscopic data.

The metal centre has an approximate square planar geometry, typical of Rh(I) species. The P(1)-Rh-P(2) angle is 96.25(5)°, with Rh-P bond lengths of 2.214(2) and 2.238(2) Å, respectively. The P(1) and P(2) atoms are almost *trans* to B(4) and B(9), respectively (P(1)-Rh-B(4) = 151.85(19)°; P(2)-Rh-B(9) = 154.05(19)°) with the RhP_2B_2 plane not being totally planar (σ = 0.126 Å), similar to previously characterised *exo-nido* RhP_2[3b] species. The $\{(PPh_3)_2Rh\}$ fragment is attached to the carbaborane cage *via* bridging hydrogen atoms at B(4) and B(9) (Rh-B(4) = 2.368(8) Å; Rh-B(9) = 2.381(8) Å).

Although the majority of previous structural characterisations of *exo-nido* species have placed the *exo* metal fragment as far away as possible from the C_{cage} substituents at the B(10) and B(6) positions (e.g. $\mu_{(10,6)}$-*exo*-$\{(PPh_3)(PCy_3)Rh\}$-7,8-μ-(1'2'-$CH_2C_6H_4CH_2$)-7,8-*nido*-$C_2B_9H_{10}$),[3b] presumably to reduce interligand repulsions, coordination at the 4 and 9 positions has previously been observed for the (7)-methyl-(8)-phenyl analogue, where the $\{(PPh_3)_2Rh\}$ fragment is adjacent to the C(8)-bound phenyl group.[3b] Furthermore, the related (unsubstituted) species, $\mu_{(3,9)}$-*exo*-$\{(P(o\text{-tol})_3)_2Ir(H)_2\}$-7,8-*nido*-$C_2B_9H_{12}$[14] also coordinates at sites adjacent to the cage carbon atoms. There is a graphitic interaction in **17** between a pair of phenyl rings (one

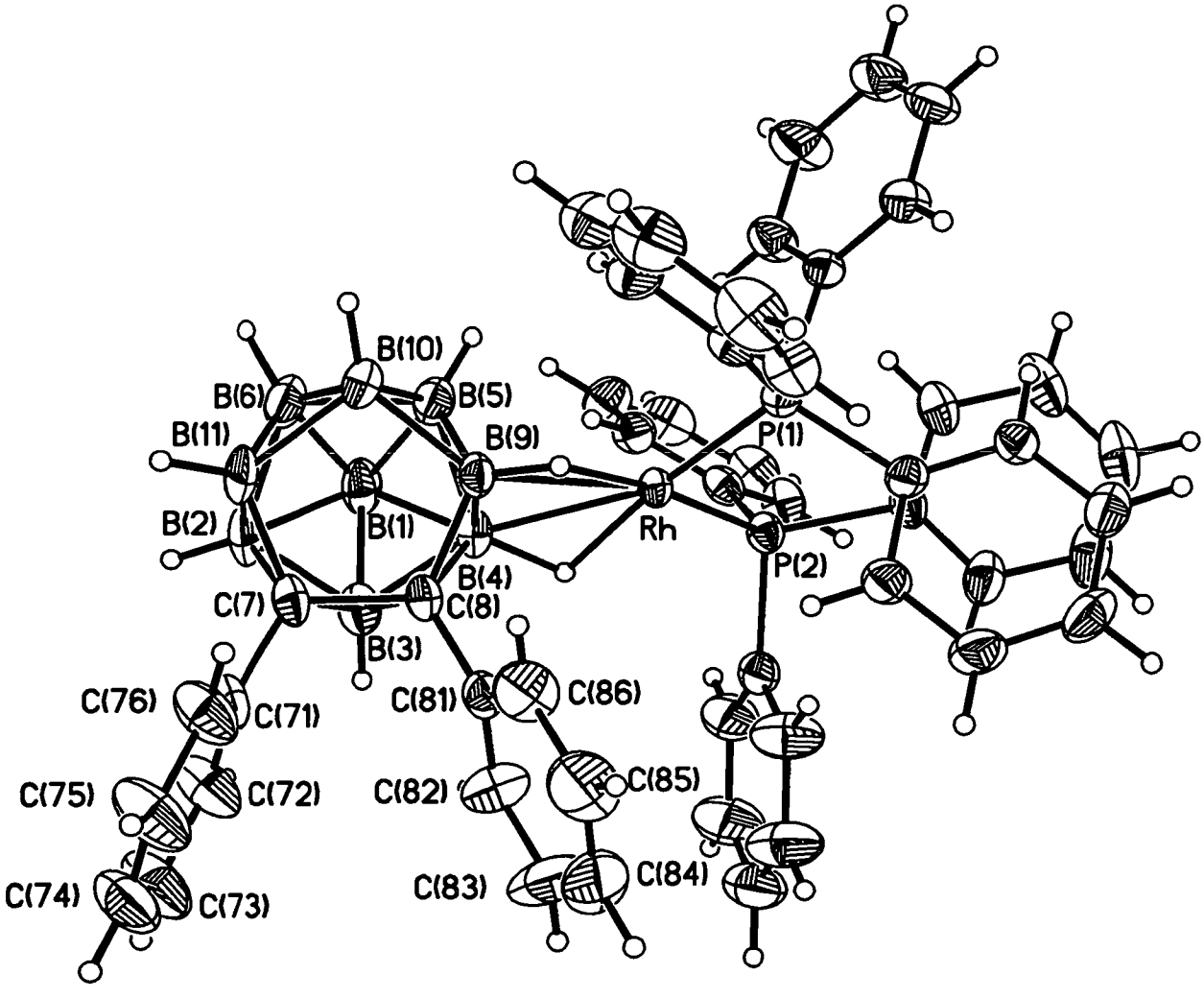

Figure 4.12 Plan View of **17**

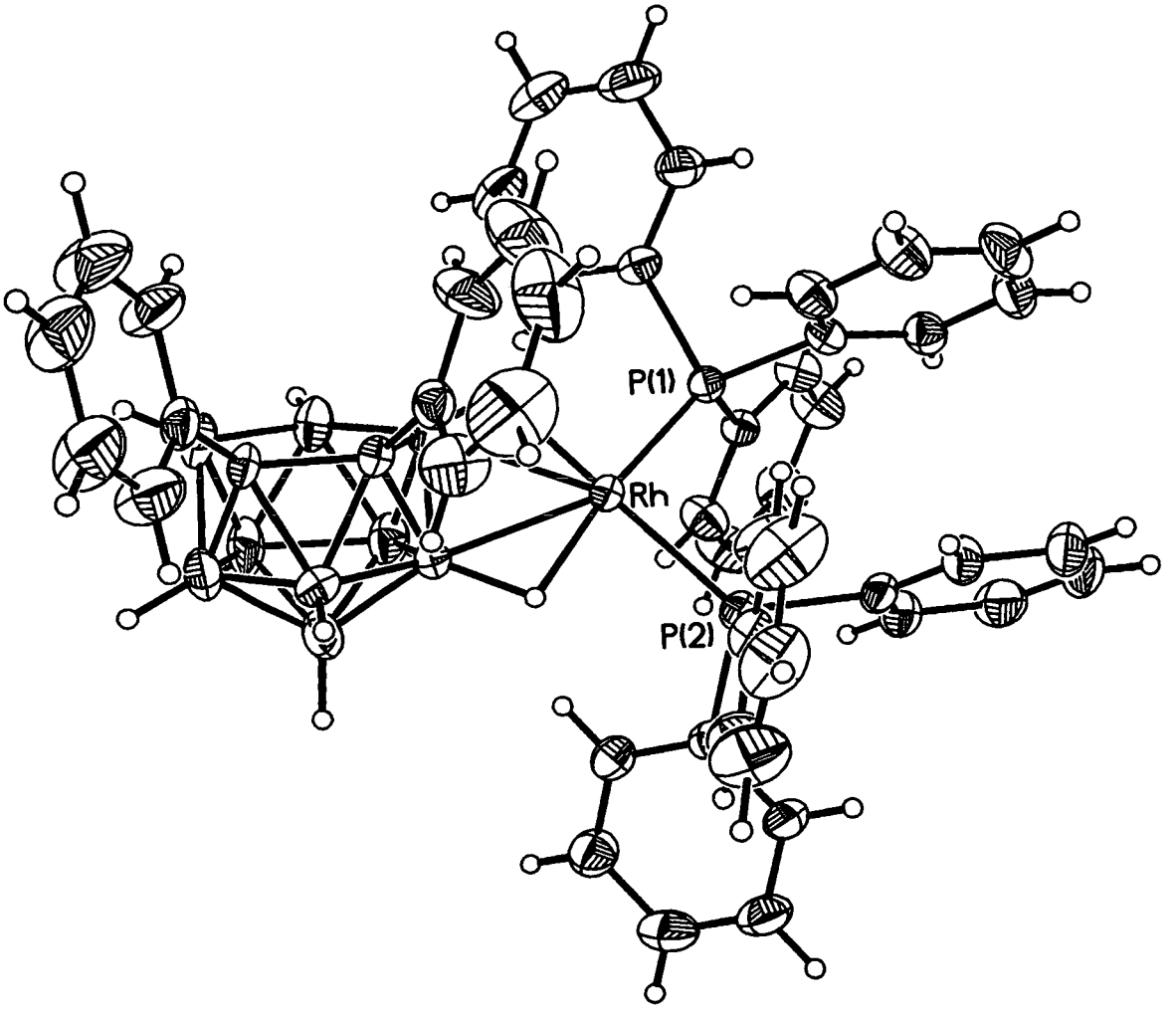

Figure 4.13 Perspective View of **17**

from each of the phosphine groups), which lie almost parallel, the distance between the two mean planes being 3.5 Å.

The carbaborane cage displays a *nido* geometry, similar to that observed for the anion of **16**, [7,8-Ph_2-7,8-*nido*-$C_2B_9H_{10}$]$^-$. The C(7)-C(8) distance is 1.580(9) Å, not significantly different to that found in **16**, as are the θ values of the two C-bound phenyl rings, C(71-76) (3.38°) and C(81-86) (9.85°). The open C_2B_3 and lower B_5 pentagons are essentially planar (σ = 0.044 and 0.034 Å, respectively). The rest of the cage, moreover, is not distorted either, with B-C and B-B distances in the normal ranges.

Table 17A Selected Bond Lengths (Å) and Angles (°) for **17**

Rh-P(1)	2.2141(14)	Rh-P(2)	2.237(2)
Rh-B(4)	2.370(6)	Rh-B(9)	2.379(6)
P(1)-C(111)	1.823(3)	P(1)-C(121)	1.826(3)
P(1)-C(131)	1.848(3)	P(2)-C(211)	1.835(3)
P(2)-C(231)	1.841(3)	P(2)-C(221)	1.846(3)
B(1)-B(3)	1.74(2)	B(1)-B(4)	1.767(9)
B(1)-B(5)	1.777(12)	B(1)-B(6)	1.786(13)
B(1)-B(2)	1.788(11)	B(2)-C(7)	1.673(10)
B(2)-B(3)	1.704(14)	B(2)-B(6)	1.772(13)
B(2)-B(11)	1.819(12)	B(3)-B(4)	1.712(13)
B(3)-C(7)	1.729(11)	B(3)-C(8)	1.743(12)
B(4)-C(8)	1.682(8)	B(4)-B(9)	1.746(9)
B(4)-B(5)	1.763(10)	B(5)-B(9)	1.745(10)
B(5)-B(10)	1.780(11)	B(5)-B(6)	1.795(10)
B(6)-B(11)	1.770(12)	B(6)-B(10)	1.809(13)
C(7)-C(71)	1.510(6)	C(7)-C(8)	1.575(7)
C(7)-B(11)	1.691(11)	C(7)-B(12)	1.82(2)
C(8)-C(81)	1.489(6)	C(8)-B(9)	1.658(8)
C(8)-B(12)	1.76(3)	B(9)-B(12)	1.69(2)
B(9)-B(10)	1.756(9)	B(10)-B(12)	1.69(3)
B(10)-B(11)	1.808(11)	B(11)-B(12)	1.71(3)
C(99)-Cl(98)	1.68(2)	C(99)-Cl(99)	1.71(2)
P(1)-Rh-P(2)	96.25(5)	P(1)-Rh-B(4)	151.9(2)
P(2)-Rh-B(4)	111.0(2)	P(1)-Rh-B(9)	109.5(2)
P(2)-Rh-B(9)	154.1(2)	B(4)-Rh-B(9)	43.1(2)
C(111)-P(1)-C(121)	109.7(2)	C(111)-P(1)-C(131)	102.2(2)
C(121)-P(1)-C(131)	98.7(2)	C(111)-P(1)-Rh	114.53(13)
C(121)-P(1)-Rh	115.69(12)	C(131)-P(1)-Rh	114.17(14)
1(16)-C(111)-P(1)	115.2(2)	C(112)-C(111)-P(1)	124.8(2)
C(126)-C(121)-P(1)	121.1(2)	C(122)-C(121)-P(1)	118.8(2)
C(136)-C(131)-P(1)	122.9(2)	C(132)-C(131)-P(1)	117.0(2)
2(11)-P(2)-C(231)	105.2(2)	2(11)-P(2)-C(221)	100.6(2)
C(231)-P(2)-C(221)	103.5(2)	2(11)-P(2)-Rh	114.01(13)
C(231)-P(2)-Rh	107.0(2)	C(221)-P(2)-Rh	124.72(14)
C(216)-2(11)-P(2)	119.6(2)	C(212)-2(11)-P(2)	120.4(2)
C(226)-C(221)-P(2)	121.8(2)	C(222)-C(221)-P(2)	118.2(2)
C(236)-C(231)-P(2)	122.3(3)	C(232)-C(231)-P(2)	117.7(3)
B(3)-B(1)-B(4)	58.5(5)	B(4)-B(1)-B(5)	59.7(4)
B(5)-B(1)-B(6)	60.5(5)	B(3)-B(1)-B(2)	57.9(5)
B(6)-B(1)-B(2)	59.5(5)	C(7)-B(2)-B(3)	61.6(5)
B(3)-B(2)-B(1)	59.5(5)	B(6)-B(2)-B(1)	60.2(5)
C(7)-B(2)-B(11)	57.7(4)	B(6)-B(2)-B(11)	59.0(5)

B(2)-B(3)-C(7)	58.3(5)	B(2)-B(3)-B(1)	62.6(6)
B(4)-B(3)-B(1)	61.7(5)	B(4)-B(3)-C(8)	58.3(4)
C(7)-B(3)-C(8)	54.0(4)	C(8)-B(4)-B(3)	61.8(4)
C(8)-B(4)-B(9)	57.8(3)	B(9)-B(4)-B(5)	59.7(4)
B(3)-B(4)-B(1)	59.8(5)	B(5)-B(4)-B(1)	60.5(4)
C(8)-B(4)-Rh	102.8(3)	B(3)-B(4)-Rh	157.9(6)
B(9)-B(4)-Rh	68.7(3)	B(5)-B(4)-Rh	89.8(4)
B(1)-B(4)-Rh	142.2(4)	B(9)-B(5)-B(4)	59.7(4)
B(4)-B(5)-B(1)	59.9(4)	B(9)-B(5)-B(10)	59.7(4)
B(1)-B(5)-B(6)	60.0(5)	B(10)-B(5)-B(6)	60.8(5)
B(11)-B(6)-B(2)	61.8(5)	B(2)-B(6)-B(1)	60.3(5)
B(1)-B(6)-B(5)	59.5(4)	B(11)-B(6)-B(10)	60.7(5)
B(5)-B(6)-B(10)	59.2(4)	C(71)-C(7)-C(8)	117.4(5)
C(71)-C(7)-B(2)	121.5(5)	C(71)-C(7)-B(11)	120.8(5)
B(2)-C(7)-B(11)	65.5(5)	C(71)-C(7)-B(3)	118.1(6)
C(8)-C(7)-B(3)	63.5(4)	B(2)-C(7)-B(3)	60.1(5)
C(71)-C(7)-B(12)	117.5(8)	C(8)-C(7)-B(12)	62.0(8)
B(11)-C(7)-B(12)	58.0(9)	C(81)-C(8)-C(7)	117.1(4)
C(81)-C(8)-B(9)	119.5(4)	C(81)-C(8)-B(4)	121.9(4)
B(9)-C(8)-B(4)	63.0(4)	C(81)-C(8)-B(3)	119.4(6)
C(7)-C(8)-B(3)	62.6(4)	B(4)-C(8)-B(3)	59.9(5)
C(81)-C(8)-B(12)	115.0(9)	C(7)-C(8)-B(12)	66.0(8)
B(9)-C(8)-B(12)	59.3(7)	C(8)-B(9)-B(12)	63.5(9)
C(8)-B(9)-B(4)	59.2(4)	B(5)-B(9)-B(4)	60.7(4)
B(12)-B(9)-B(10)	58.8(10)	B(5)-B(9)-B(10)	61.1(4)
C(8)-B(9)-Rh	103.2(3)	B(12)-B(9)-Rh	158.7(10)
B(5)-B(9)-Rh	89.9(3)	B(4)-B(9)-Rh	68.2(3)
B(10)-B(9)-Rh	142.1(4)	B(12)-B(10)-B(9)	58.8(9)
B(9)-B(10)-B(5)	59.1(4)	B(12)-B(10)-B(11)	58.3(9)
B(5)-B(10)-B(6)	60.0(4)	B(11)-B(10)-B(6)	58.6(5)
C(7)-B(11)-B(12)	64.9(9)	B(12)-B(11)-B(10)	57.6(8)
B(6)-B(11)-B(10)	60.8(5)	C(7)-B(11)-B(2)	56.8(4)
B(6)-B(11)-B(2)	59.2(5)	B(9)-B(12)-B(10)	62.4(8)
B(10)-B(12)-B(11)	64.2(10)	B(9)-B(12)-C(8)	57.3(8)
B(11)-B(12)-C(7)	57.1(8)	C(8)-B(12)-C(7)	52.0(7)
C(72)-C(71)-C(7)	120.8(4)	C(76)-C(71)-C(7)	119.1(4)
C(82)-C(81)-C(8)	120.9(4)	C(86)-C(81)-C(8)	119.1(4)
Cl(98)-C(99)-Cl(99)	110.8(10)		

Table 17B Atomic Coordinates (x 10^4) and Equivalent Isotropic Thermal Parameters ($Å^2$ x 10^3) for **17**

	x	y	z	U(eq)
Rh	3327(1)	508(1)	2436(1)	36(1)
P(1)	2152(1)	285(1)	1445(1)	38(1)
C(112)	280(3)	1427(3)	1124(2)	51(1)
C(113)	-886(4)	1715(3)	1204(2)	67(2)
C(114)	-1672(3)	1314(4)	1661(2)	77(2)
C(115)	-1293(4)	625(4)	2037(2)	73(2)
C(116)	-127(4)	337(3)	1957(2)	58(2)
C(111)	659(3)	738(3)	1501(2)	43(1)
C(122)	4420(3)	1398(4)	998(2)	62(2)
C(123)	5145(3)	1835(4)	531(2)	85(2)
C(124)	4517(4)	1754(4)	-108(2)	79(2)
C(125)	3164(4)	1235(4)	-280(1)	70(2)
C(126)	2440(3)	798(3)	187(2)	56(2)
C(121)	3067(3)	879(3)	826(2)	40(1)
C(132)	2408(3)	-1815(3)	788(2)	64(2)
C(133)	1991(5)	-2924(3)	377(2)	81(2)
C(134)	660(6)	-3436(3)	124(2)	84(2)
C(135)	-253(4)	-2839(4)	281(2)	91(3)
C(136)	164(3)	-1729(3)	691(2)	65(2)
C(131)	1495(4)	-1217(2)	944(2)	44(1)
P(2)	3597(1)	2384(1)	2809(1)	42(1)
C(212)	6341(4)	2748(2)	2940(2)	53(1)
C(213)	7650(3)	3419(3)	3090(2)	70(2)
C(214)	7948(3)	4602(3)	3300(2)	77(2)
C(215)	6936(4)	5114(2)	3361(2)	73(2)
C(216)	5627(4)	4443(3)	3212(2)	61(2)
C(211)	5329(3)	3260(3)	3001(2)	46(1)
C(222)	3495(4)	3616(4)	1838(2)	64(2)
C(223)	2983(5)	4272(4)	1485(2)	85(2)
C(224)	1840(5)	4549(4)	1643(2)	92(3)
C(225)	1209(4)	4169(4)	2154(3)	88(3)
C(226)	1720(4)	3512(4)	2507(2)	68(2)
C(221)	2863(4)	3236(3)	2349(2)	49(1)
C(232)	1647(4)	2020(4)	3629(2)	91(3)
C(233)	1111(5)	2162(5)	4229(3)	113(3)
C(234)	1885(6)	2882(5)	4824(2)	96(3)
C(235)	3196(6)	3459(5)	4819(2)	103(3)
C(236)	3732(4)	3317(4)	4219(2)	79(2)
C(231)	2958(4)	2598(4)	3624(2)	53(1)
B(1)	6182(7)	-302(7)	3359(5)	65(2)
B(2)	5863(8)	-1595(7)	3632(5)	71(2)

B(3)	4967(11)	-662(8)	3856(6)	58(3)
B(4)	4598(6)	-136(5)	3184(3)	46(1)
B(5)	5384(7)	-663(7)	2510(4)	61(2)
B(6)	6178(9)	-1612(8)	2793(5)	73(2)
C(7)	4220(6)	-2115(5)	3553(3)	52(1)
C(8)	3503(5)	-1306(4)	3291(3)	43(1)
B(9)	3697(7)	-1258(5)	2501(3)	46(1)
B(10)	4650(8)	-2166(7)	2208(4)	65(2)
B(11)	4911(9)	-2755(7)	2920(5)	69(2)
B(12)	3434(24)	-2556(19)	2671(12)	65(6)
C(72)	3880(5)	-2309(4)	4732(2)	96(3)
C(73)	3215(7)	-2887(5)	5167(2)	115(4)
C(74)	2241(6)	-3922(5)	4905(3)	106(3)
C(75)	1931(5)	-4378(4)	4209(3)	115(4)
C(76)	2596(5)	-3800(4)	3773(2)	84(2)
C(71)	3570(4)	-2765(3)	4035(2)	59(2)
C(82)	2187(5)	-607(4)	4167(2)	90(2)
C(83)	981(7)	-589(6)	4381(3)	140(5)
C(84)	-189(5)	-1230(7)	3957(4)	141(5)
C(85)	-154(3)	-1889(6)	3320(4)	132(4)
C(86)	1052(5)	-1907(4)	3105(2)	88(2)
C(81)	2223(3)	-1266(4)	3529(2)	54(1)
C(99)	3040(17)	4208(15)	8489(9)	202(7)
Cl(98)	3745(5)	4516(4)	9299(3)	206(2)
Cl(99)	1729(8)	4752(7)	8431(4)	303(3)

4.4. $[(dppe)_2Rh][7,8\text{-}Ph_2\text{-}7,8\text{-}nido\text{-}C_2B_9H_{10}]$ (18)

4.4.1 Synthesis

Compound **18** was initially afforded whilst attempting to synthesise the dppe analogue of compound **17**.

The metal-containing precursor of compound **18** was synthesised by the dropwise addition of a toluene solution of two equivalents of dppe to a toluene solution of $[Rh(C_2H_4)_2Cl]_2$.[15] This afforded a yellow precipitate of "$Rh(C_2H_4)(dppe)Cl$", which was collected by filtration. The precipitate was dissolved in CH_2Cl_2, causing loss of the labile ethene ligand, and cooled to 78 K. Two equivalents of solid compound **16** were added and the mixture warmed to room temperature, then stirred for one hour. During this time, a white precipitate (presumably $HNEt_3Cl$) was observed forming. The reaction mixture was reduced *in vacuo*, purified by column chromatography and recrystallised from CH_2Cl_2/petroleum ether (60-80) to afford a yellow, microcrystalline solid in *ca.* 50% yield.

The same compound was also synthesised by the reaction of 0.95 equivalents of dppe with compound **17**. It was hoped that this latter approach would afford the desired product *via* substitution of the two, mono-dentate phosphines with a single, bi-dentate phosphine to form the more stable chelated analogue of **17**. The phosphine was added as very dilute solution to a dilute solution of **17** with stirring to try and disfavour the formation of the bis-chelate cation. However, $^{31}P\text{-}\{^1H\}$ nmr spectroscopy showed the product to be compound **18**.

The compound was readily soluble in chlorinated solvents. Yellow, diffraction quality blocks and needles of **18** were grown by the slow diffusion of petroleum ether (60-80) and a CH_2Cl_2 solution at room temperature.

4.4.2 Characterisation

Initial characterisation of compound **18** was by IR spectroscopy. There was a broad absorption peak, characteristic of B-H stretching, at 2536 cm^{-1}. Microanalysis was not available when the experiment was initially performed.

The ^{1}H nmr spectrum (**Fig. 4.14**, below) shows multiplet resonances due to phenyl protons at 7.24 and 6.81 ppm and methylene protons at 2.12 ppm. Due to the broadness of the methylene resonances, as well as the fact that they overlap the broad hump due to B-H resonances, the measurement of integrals was rather inaccurate (this was also true of the broad doublet at -1.6 ppm due to the *endo*-proton). The ratio of C_6H_5 to CH_2 protons was calculated as being approximately 30:4, the expected ratio for the proposed, *exo-nido* structure. This data, together with that from the ^{11}B-{^{1}H} and ^{31}P-{^{1}H} nmr spectra, was fully consistent with the target compound, μ_2-*exo*-{(dppe)Rh}-7,8-Ph_2-7,8-*nido*-$C_2B_9H_{10}$.

The ^{11}B-{^{1}H} spectrum shows the same 2:1:2:2:1:1 shielding pattern observed for compounds **16, 17** and **17a**. The resonances are, however, much sharper than those for **17** and **17a**. The resonances are shifted relative to those in compound **16**, but this is not surprising since the samples were run in different solvents. Moreover, it was expected that the environments of the ^{11}B nuclei would be different. The second-highest-field resonance is also broadened, presumably by an extra, *endo*-proton attached to the B(10) atom, although it was not possible to measure the coupling constant accurately.

The ^{31}P-{^{1}H} nmr spectrum shows the expected doublet ($^{1}J_{Rh(I)-P}$ = 126.0 Hz) at 58.76 ppm. Although this coupling constant is smaller than for previous examples, this is explained by the fact that the phosphine is chelating and, as such, the phosphorous atoms are constrained as part of a five-membered ring, thus reducing the ($^{1}J_{Rh-P}$) coupling constant. There have been several synthetic studies on $[(dppe)_2Rh]^+$ species and similar Rh-P coupling constants to **18** are observed.[16]

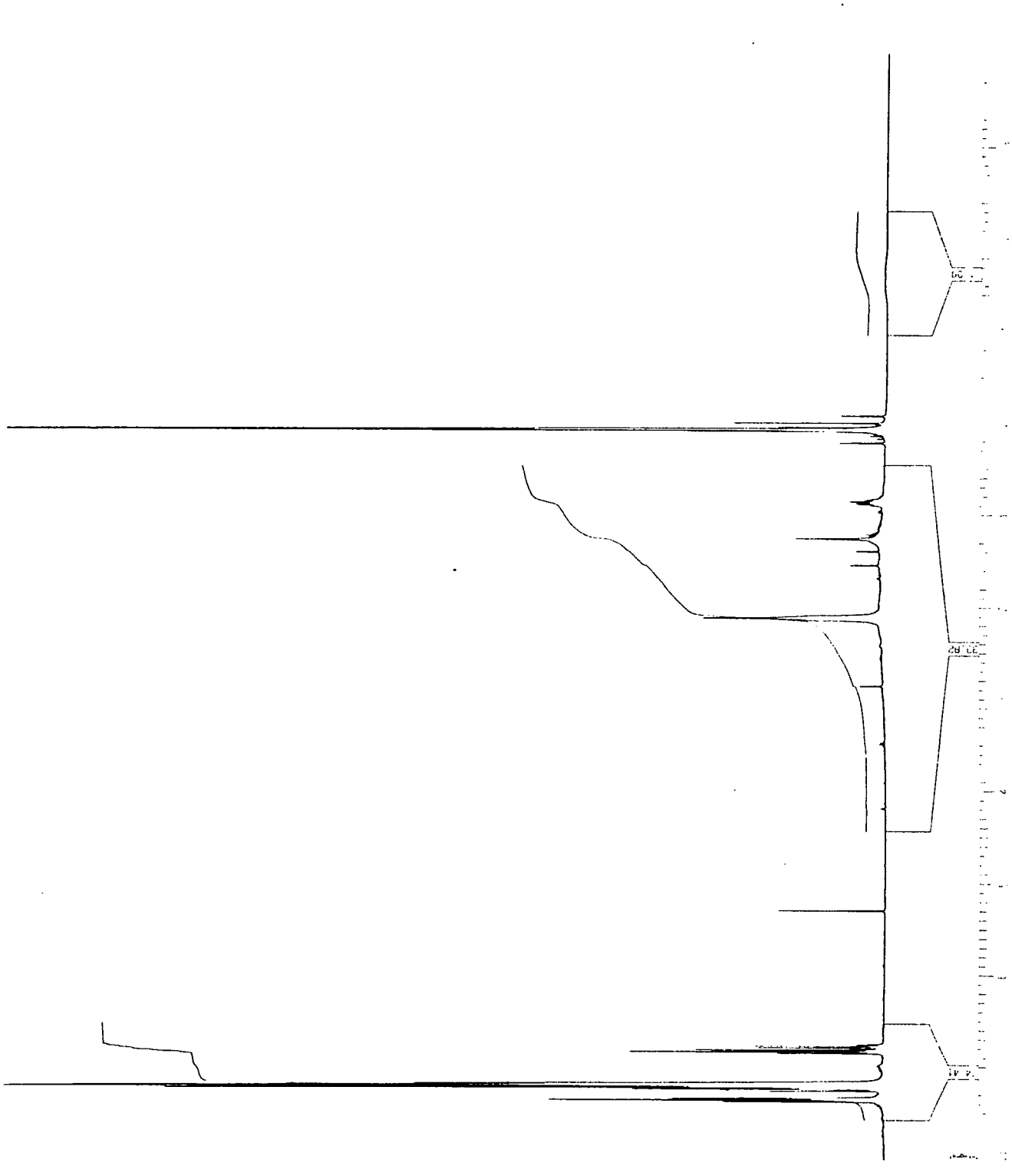

Figure 4.14 ^{1}H Nmr Spectrum of **18** (400 MHz)

Compound **18** was structurally characterised by an X-ray diffraction study on a single crystal grown by slow diffusion of petroleum ether (60-80) and a CH_2Cl_2 solution at room temperature, which showed the compound to be the ion-pair, $[(dppe)_2Rh][7,8\text{-}Ph_2\text{-}7,8\text{-}nido\text{-}C_2B_9H_{10}]$ (**Section 4.4.3**).

Microanalysis figures (available only after the crystallographic study) were in good accordance with the calculated figures for this compound. The nmr data was still consistent with the determined structure. In the ^1H nmr spectrum, the ratio of the integrals due to the phenyl and methylene protons was re-measured and found to be 50:8 (still close to the previous value of 30:4). Moreover, in compound **17**, coordination of the $\{(PPh_3)_2Rh\}$ fragment significantly broadened the $^{11}B\text{-}\{^1H\}$ resonances. This broadening relative to the starting material, **16**, was not observed in the $^{11}B\text{-}\{^1H\}$ nmr spectrum of **18**; again this was consistent with a mono-anionic cage. The $^{31}P\text{-}\{^1H\}$ nmr data were also consistent with the formulation of the product as all of the phosphorous atoms are equivalent. The chemical shift and coupling constant are very close to those reported for a similar series of compounds of the type $[Rh(diphos)_2]X$ (diphos = e.g. dppe, dppp; X = e.g. Cl, SbF_6, PF_6, BF_4, ClO_4).[16] For example, for $[(dppe)_2Rh][BF_4]$ in $CDCl_3$, δ $^{31}P\text{-}\{^1H\}$ = -57.22 ppm, $^1J_{Rh\text{-}P}$ = 132.7 Hz). Moreover, the colours of the compounds are also similar to that observed for **18** (X = ClO_4 - golden yellow, X = BPh_4, Cl - yellow). The ^1H nmr shifts of the phenyl and methylene resonances are also similar to the previously reported values (7.25 and 2.15 ppm for X = BF_4; 7.24 and 2.12 for **18**).

4.4.3 Crystallographic Study of [(dppe)$_2$Rh][7,8-Ph$_2$-7,8-*nido*-C$_2$B$_9$H$_{10}$] (18)

Yellow, diffraction quality *blocks* and *prisms* of **18** were grown by the slow diffusion of petroleum ether (60-80) and a CH_2Cl_2 solution at room temperature. Intensity data were measured on an Siemens P4 diffractometer operating with Mo-K_α *X*-radiation (λ_{bar} = 0.71073 Å). The single crystal (*block*) was mounted in a glass capillary and the experiment performed at 293(2) K.

Crystal data

$C_{66}H_{68}B_9RhP_4$, M = 1184.28, monoclinic, $P2_1/n$, a = 14.3190(10) Å, b = 27.015(2) Å, c = 16.3960(10) Å, β = 102.250(10)°, V = 6198.0(7) Å^3, from least squares refinement of 41 reflections ($9 \leq \theta \leq 25°$) at 291(2) K, Z = 4 ion-pairs, D_c = 1.269 gcm^{-3}, μ(Mo-K_α) = 0.42 mm^{-1}, F(0,0,0) = 2452e.

Data collection and reduction

Intensity data collected in the range $2<2\theta<50°$ by the ω-scan method; ω-scan width 0.78°, ω-scan speeds in the range 1.0 to 60.0 °min^{-1}. The intensities of 10766 unique reflections (*h* 0 to 17, *k* 0 to 32, *l* -20 to 19) were measured (XSCANS).

Structure solution and refinement

The structure was solved using Patterson methods (Rh) and developed by iterative, full-matrix least-squares refinement and difference Fourier syntheses (P, C, B) (SHELXTL). There are four ion-pairs per unit cell. The phenyl H atoms were fixed in idealised positions (C-H = 0.93 Å) and allowed to ride on their respective carbon atoms with U(H) = 1.2 U(C). Cage H atoms (except H(12)) were restrained (B-H = 1.10 Å), but allowed to refine freely. There was partial disorder of the *nido* cage, causing extra electron density (0.44 eÅ^{-3}) at the 'missing' twelfth vertex. The disorder was minimal, however as U_{eq} for B(3) is not anomalously large and was this atom was refined with full occupancy.

Data were absorption corrected (ψ-scans) and weighted such that $w^{-1} = [\sigma^2(F_o^2) + (0.0340P)^2 + 2.26P]$ where $P = [\text{max.}\ (F_o^2) + 2F_c^2]/3$. Using 7262 observed data ($F_o > 4.0\sigma(F_o)$), $R = 0.0456$, $wR_2 = 0.1273$, and $S = 1.205$ for 761 variable parameters. The maximum residue and minimum trough in a final difference Fourier synthesis were 0.34 and -0.32 $eÅ^{-3}$, respectively. Atomic scattering factors were those inlaid in SHELXTL. Selected bond lengths (Å) and angles (°), fractional coordinates and equivalent isotropic thermal parameters of non-hydrogen atoms are in **Tables 18A** and **18B**, respectively.

The X-ray crystallographic study characterised **18** as the ion-pair [(dppe)$_2$Rh][7,8-Ph$_2$-7,8-*nido*-$C_2B_9H_{10}$] (**Fig. 4.15**) and not the expected dppe analogue of compound **17**. The closest inter-ion contacts are between C(83) and H(116) (2.909 Å) and C(83) and H(123) (2.957 Å). The anion (with $[HNEt_3]^+$ and $[btma]^+$ [9]) and cation (with $[ClO_4]^-$ [16a]) have been determined previously by X-ray crystallography and this discussion will therefore focus upon comparing the present study to those above.

The anion was confirmed as having a *nido* geometry with an open C_2B_3 face (**Fig. 4.16**, above). The C(7)-C(8) distance is 1.594(5) Å, not significantly different from those of the the $[HNEt_3]^+$ and $[btma]^+$ salts **1.590(5)** and <u>1.602(3)</u> Å, respectively (values from these two studies will be given in **bold** and <u>underlined</u>, respectively), but, as noted before, significantly shorter than in the parent carbaborane, 1,2-Ph$_2$-1,2-*closo* $C_2B_{10}H_{10}$ (1.727(6) Å).[17] The conformations of the phenyl rings are θ = 20.6 and 14.6° for C(71-76) and C(81-86), respectively, giving the anion *pseudo* mirror symmetry. These values are significantly larger than for the $[HNEt_3]^+$ and $[btma]^+$ salts (**5.6** and **10.0** and <u>17.9</u> and <u>20.0</u>°, respectively), although extended Hückel calculations suggest that the energies required for such twists are well within the range of crystal packing forces.[17] The B-C and B-B connectivities are in the range 1.628(6) to 1.733(6) and 1.742(7) to 1.830(7) Å, respectively, similar to those for the previous crystallographic determinations.

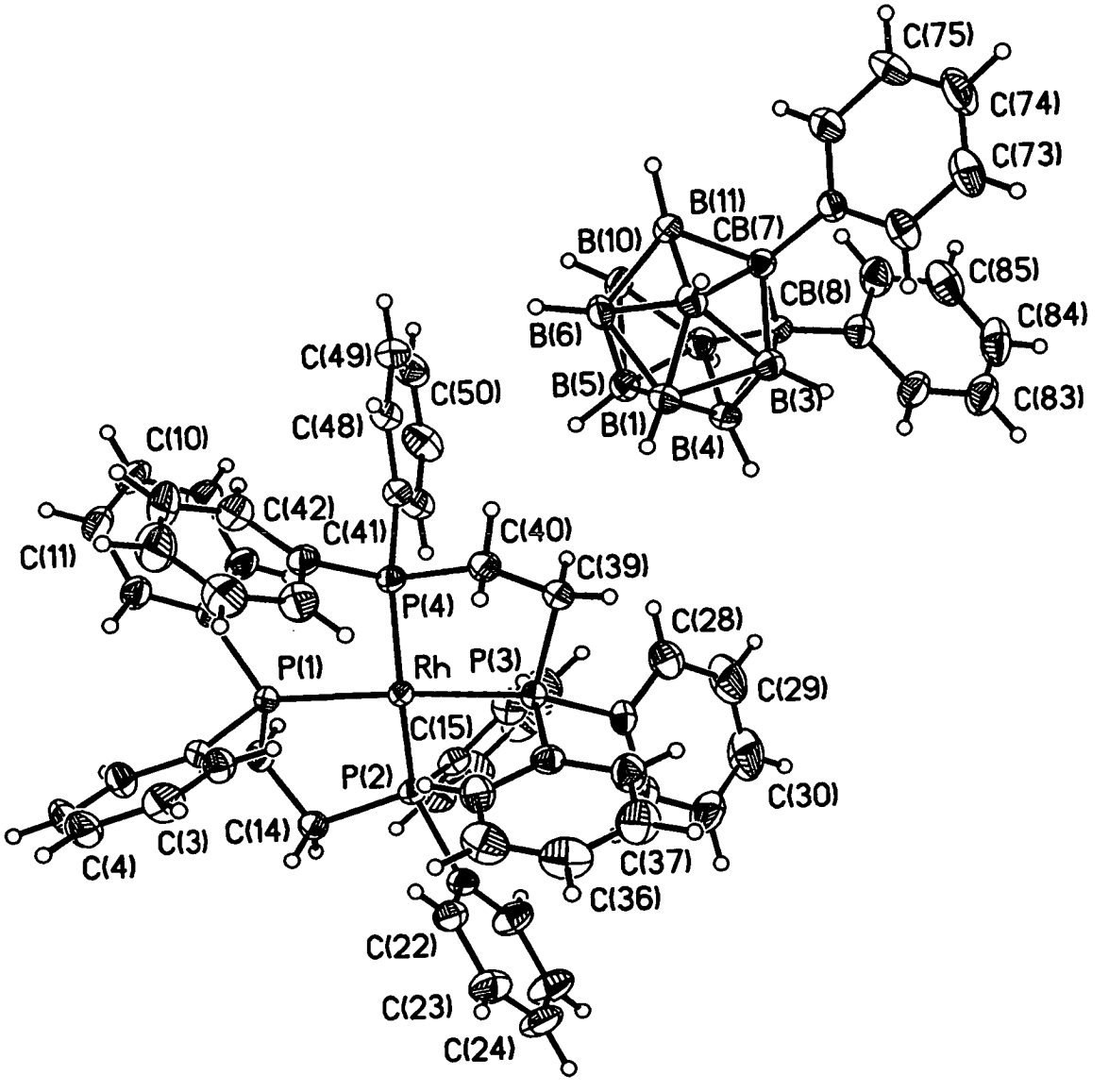

Figure 4.15 Perspective View of **18**

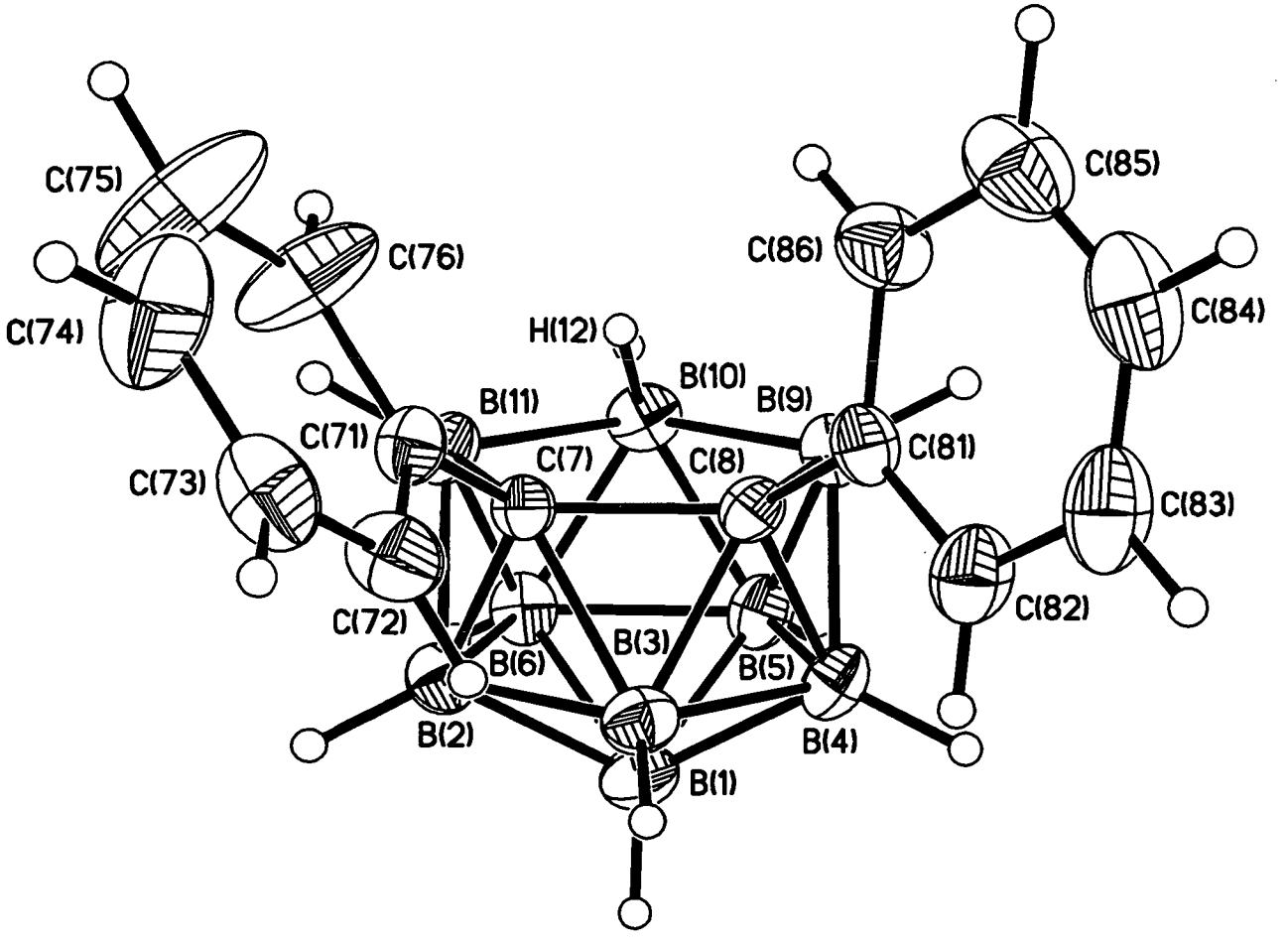

Figure 4.16 Perspective View of the Anion in **18**

As for the $[HNEt_3]^+$ and $[btma]^+$ salts, the lower B_5 pentagon of **18** is essentially planar, whilst the upper C_2B_3 face is slightly buckled (σ = 0.013 and 0.018 Å, respectively), although the differences between them are small (see **Table 4.1**, which lists pertinent structural data from the three crystallographic determinations of the anion).

Table 4.1 Geometrical Data for the [7,8-Ph_2-7,8-*nido*-$C_2B_9H_{10}$]$^-$ Anion

Counter-ion	**$[(dppe)_2Rh]^+$**	**$[HNEt_3]^+$**	**$[btma]^+$**
C(7)-C(8)/(Å)	1.594(5)	1.590(5)	1.602(3)
θ C(71-76)/(°)	20.6	5.6	17.9
θ C(81-76)/(°)	14.6	10.0	20.0
B-C min./(Å)	1.628(6)	1.631(7)	1.630(4)
B-C max./(Å)	1.733(6)	1.758(7)	1.728(4)
B-B min./(Å)	1.742(7)	1.729(8)	1.753(4)
B-B max./(Å)	1.830(7)	1.839(8)	1.843(4)
σ C_2B_3/(Å)	0.018	0.049	0.050
σ B_5/(Å)	0.013	0.003	0.016

Figure 4.17 (below) shows a perspective view of the cation, $[(dppe)_2Rh]^+$, the rhodium centre of which was found to adopt an essentially square planar geometry, typical of Rh(I) complexes. The four Rh-P bond lengths are detailed below in **Figure 4.18** and are not significantly different (except for Rh-P(3) , which is ca. 0.02 Å longer than the other three), with a mean bond length is 2.308 Å. These values compare well with a previous determination of the perchlorate salt. There is a slight deviation from the expected planar geometry (σ = 0.125 Å), with the phosphorous atoms which are mutually trans to each other either above or below the mean plane by 0.150 Å. The rhodium atom lies to the same side of the plane as P(1) and P(3) by 0.067 Å. The P(1)-Rh-P(2) and P(3)-Rh-P(4) angles (83.59(4) and 83.79(4)°, respectively) are less than the expected 90°, due to the fact that the phosphine is bidentate and forms a (slightly strained) five-membered ring. The cations of **18** and $[(dppe)_2Rh][ClO_4]$[16a] are compared in **Figure 4.18** (**a** and **b**, respectively).

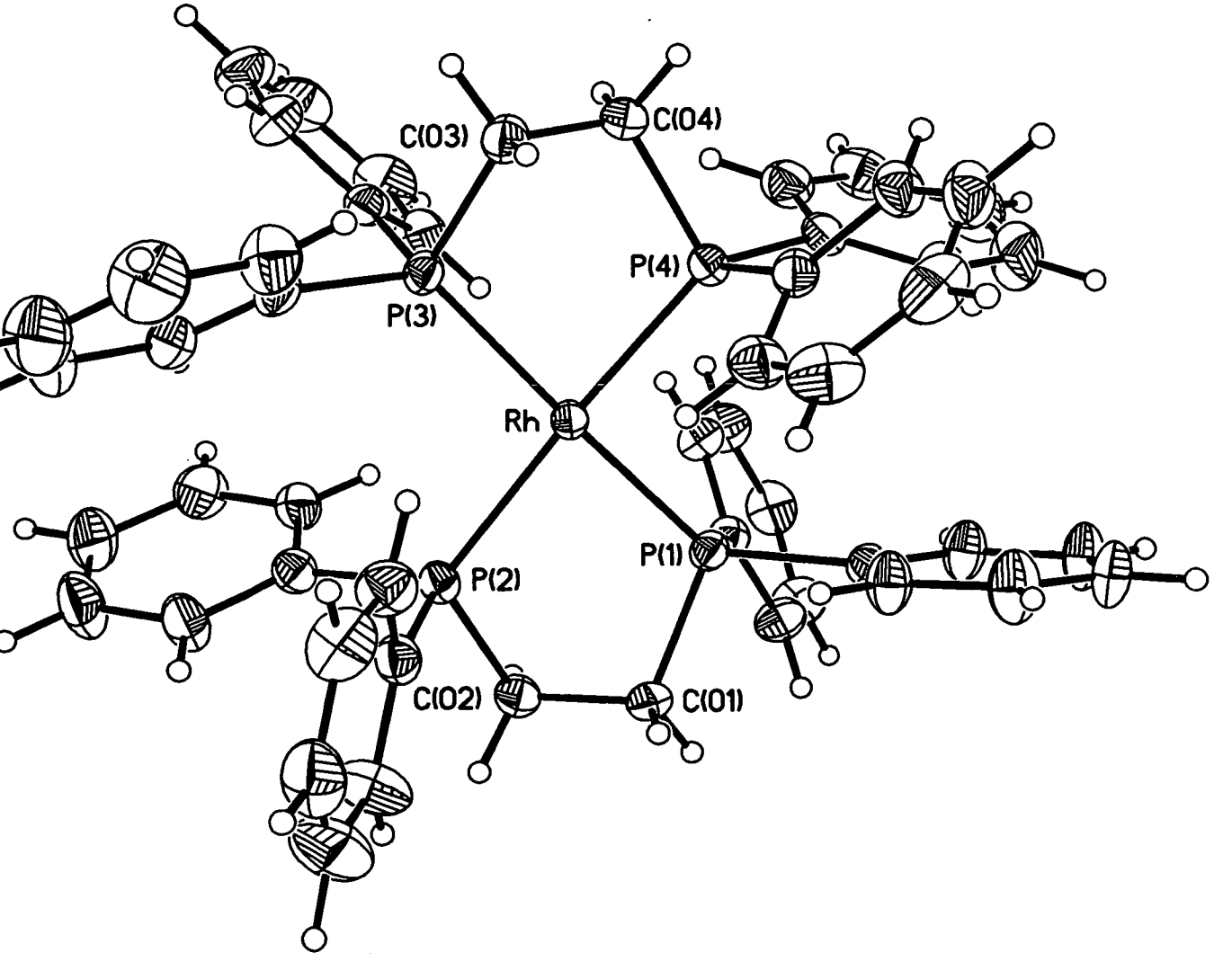

Figure 4.17 Perspective View of the Cation in **18**

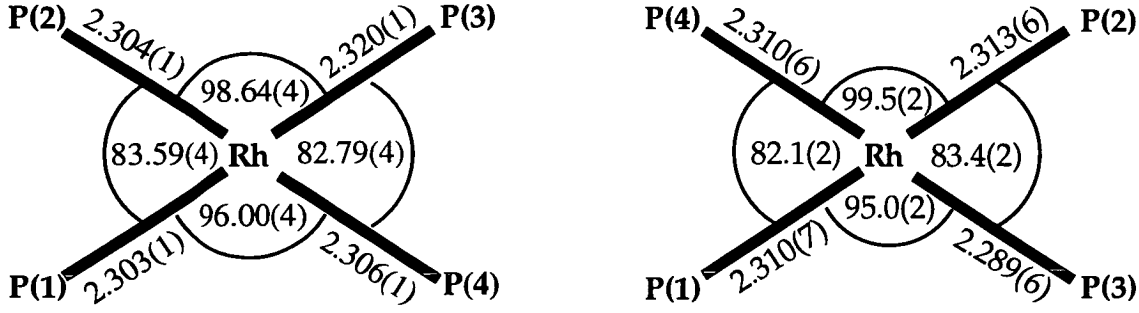

Figure 4.18 Bond Lengths (Å) and Angles (°) for the $[(dppe)_2Rh]^+$ Cations in (**a**) **18** and (**b**) $[(dppe)_2Rh][ClO_4]$

The conformation of the methylene bridges of **18** with respect to the mean RhP_4 plane are shown in **Figure 4.19** (**a**), different to those observed for the perchlorate salt where the methylene bridges are unsymmetrically positioned relative to each other (**Fig. 4.19** (**b, c**)). As such, the torsion angles in the five-membered rings are significantly different from those in $[(dppe)_2Rh][ClO_4]$.

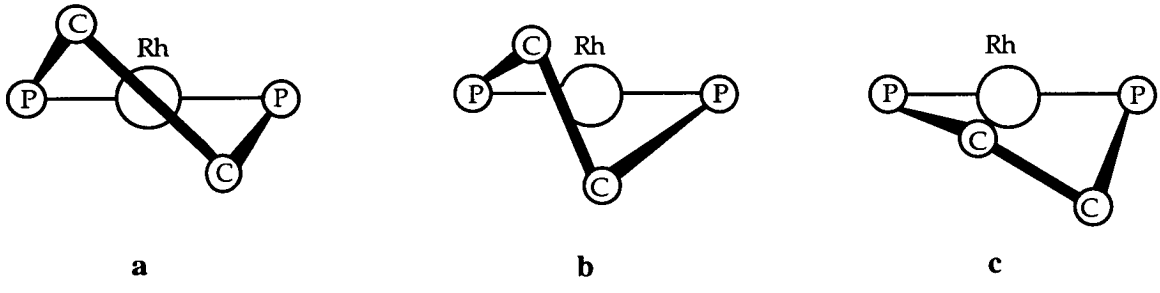

Figure 4.19 Representations of the Conformations of the Methylene Bridges in (**a**) **18** and (**b, c**) $[(dppe)_2Rh][ClO_4]$

Table 18A Selected Bond Lengths (Å) and Angles (°) for **18**

Rh-P(1)	2.3033(10)	Rh-P(2)	2.3045(11)
Rh-P(4)	2.3058(11)	Rh-P(3)	2.3200(11)
P(1)-C(111)	1.825(4)	P(1)-C(121)	1.829(4)
P(1)-C(01)	1.844(4)	P(2)-C(221)	1.819(4)
P(2)-C(211)	1.827(4)	P(2)-C(02)	1.844(4)
P(3)-C(321)	1.831(4)	P(3)-C(311)	1.836(4)
P(3)-C(03)	1.844(4)	P(4)-C(421)	1.823(4)
P(4)-C(411)	1.822(4)	P(4)-C(04)	1.843(4)
C(111)-C(112)	1.379(6)	C(111)-C(116)	1.396(6)
C(112)-C(113)	1.387(6)	C(113)-C(114)	1.366(7)
C(114)-C(115)	1.368(7)	C(115)-C(116)	1.381(6)
C(121)-C(122)	1.371(6)	C(121)-C(126)	1.381(6)
C(122)-C(123)	1.385(6)	C(123)-C(124)	1.367(6)
C(124)-C(125)	1.348(6)	C(125)-C(126)	1.384(6)
C(01)-C(02)	1.517(6)	C(211)-C(212)	1.377(6)
C(211)-C(216)	1.390(6)	C(212)-C(213)	1.384(7)
C(213)-C(214)	1.368(8)	C(214)-C(215)	1.354(8)
C(215)-C(216)	1.378(8)	C(221)-C(222)	1.386(6)
C(221)-C(226)	1.387(6)	C(222)-C(223)	1.388(6)
C(223)-C(224)	1.375(7)	C(224)-C(225)	1.358(8)
C(225)-C(226)	1.386(7)	C(311)-C(312)	1.378(6)
C(311)-C(316)	1.390(6)	C(312)-C(313)	1.393(8)
C(313)-C(314)	1.365(9)	C(314)-C(315)	1.362(8)
C(315)-C(316)	1.383(7)	C(321)-C(322)	1.381(6)
C(321)-C(326)	1.392(6)	C(322)-C(323)	1.384(7)
C(323)-C(324)	1.360(8)	C(324)-C(325)	1.374(8)
C(325)-C(326)	1.390(7)	C(03)-C(04)	1.517(6)
C(411)-C(412)	1.371(6)	C(411)-C(416)	1.392(6)
C(412)-C(413)	1.383(7)	C(413)-C(414)	1.375(8)
C(414)-C(415)	1.365(8)	C(415)-C(416)	1.379(7)
C(421)-C(426)	1.382(6)	C(421)-C(422)	1.396(6)
C(422)-C(423)	1.377(7)	C(423)-C(424)	1.367(8)
C(424)-C(425)	1.366(8)	C(425)-C(426)	1.385(7)
B(1)-B(2)	1.752(7)	B(1)-B(4)	1.753(8)
B(1)-B(3)	1.762(7)	B(1)-B(6)	1.789(7)
B(1)-B(5)	1.792(7)	B(2)-C(7)	1.725(6)
B(2)-B(6)	1.754(7)	B(2)-B(3)	1.765(7)
B(2)-B(11)	1.782(7)	B(3)-C(8)	1.712(6)
B(3)-C(7)	1.735(6)	B(3)-B(4)	1.743(7)
B(4)-C(8)	1.725(6)	B(4)-B(5)	1.748(7)
B(4)-B(9)	1.793(7)	B(5)-B(9)	1.757(7)
B(5)-B(10)	1.767(7)	B(5)-B(6)	1.805(7)
B(6)-B(10)	1.758(7)	B(6)-B(11)	1.763(7)

B(9)-C(8)	1.632(6)	B(9)-B(10)	1.812(7)
B(10)-B(11)	1.843(7)	B(11)-C(7)	1.631(6)
C(7)-C(71)	1.500(5)	C(7)-C(8)	1.595(5)
C(8)-C(81)	1.500(5)	C(71)-C(76)	1.351(6)
C(71)-C(72)	1.377(6)	C(72)-C(73)	1.386(6)
C(73)-C(74)	1.328(8)	C(74)-C(75)	1.349(9)
C(75)-C(76)	1.388(8)	C(81)-C(86)	1.373(6)
C(81)-C(82)	1.382(6)	C(82)-C(83)	1.359(7)
C(83)-C(84)	1.346(8)	C(84)-C(85)	1.364(8)
C(85)-C(86)	1.405(7)		

P(1)-Rh-P(2)	83.58(4)	P(1)-Rh-P(4)	95.99(4)
P(2)-Rh-P(4)	171.81(4)	P(1)-Rh-P(3)	172.57(4)
P(2)-Rh-P(3)	98.64(4)	P(4)-Rh-P(3)	82.82(4)
C(111)-P(1)-C(121)	103.2(2)	C(111)-P(1)-C(01)	103.0(2)
C(121)-P(1)-C(01)	102.9(2)	C(111)-P(1)-Rh	114.87(14)
C(121)-P(1)-Rh	122.23(13)	C(01)-P(1)-Rh	108.38(13)
C(221)-P(2)-C(211)	104.3(2)	C(221)-P(2)-C(02)	102.1(2)
C(211)-P(2)-C(02)	104.2(2)	C(221)-P(2)-Rh	120.87(14)
C(211)-P(2)-Rh	115.01(14)	C(02)-P(2)-Rh	108.42(14)
C(321)-P(3)-C(311)	103.4(2)	C(321)-P(3)-C(03)	100.9(2)
C(311)-P(3)-C(03)	103.1(2)	C(321)-P(3)-Rh	112.57(14)
C(311)-P(3)-Rh	125.65(14)	C(03)-P(3)-Rh	108.26(14)
C(421)-P(4)-C(411)	105.9(2)	C(421)-P(4)-C(04)	101.9(2)
C(411)-P(4)-C(04)	103.5(2)	C(421)-P(4)-Rh	111.67(14)
C(411)-P(4)-Rh	121.85(14)	C(04)-P(4)-Rh	109.94(14)
C(112)-C(111)-C(116)	118.4(4)	C(112)-C(111)-P(1)	119.9(3)
C(116)-C(111)-P(1)	121.4(3)	C(111)-C(112)-C(113)	120.7(4)
C(114)-C(113)-C(112)	120.3(5)	C(115)-C(114)-C(113)	119.8(5)
C(114)-C(115)-C(116)	120.7(4)	C(115)-C(116)-C(111)	120.1(4)
C(122)-C(121)-C(126)	118.5(4)	C(122)-C(121)-P(1)	117.8(3)
C(126)-C(121)-P(1)	123.6(3)	C(121)-C(122)-C(123)	120.4(4)
C(124)-C(123)-C(122)	120.6(4)	C(125)-C(124)-C(123)	119.3(4)
C(124)-C(125)-C(126)	121.0(4)	C(121)-C(126)-C(125)	120.2(4)
C(02)-C(01)-P(1)	107.3(3)	C(01)-C(02)-P(2)	108.1(3)
C(212)-C(211)-C(216)	117.6(5)	C(212)-C(211)-P(2)	118.8(4)
C(216)-C(211)-P(2)	123.6(4)	C(211)-C(212)-C(213)	121.0(5)
C(214)-C(213)-C(212)	120.0(6)	C(215)-C(214)-C(213)	120.0(6)
C(214)-C(215)-C(216)	120.4(6)	C(215)-C(216)-C(211)	121.0(6)
C(222)-C(221)-C(226)	118.7(4)	C(222)-C(221)-P(2)	116.5(3)
C(226)-C(221)-P(2)	124.7(4)	C(223)-C(222)-C(221)	120.5(4)
C(224)-C(223)-C(222)	119.9(5)	C(225)-C(224)-C(223)	120.1(5)
C(224)-C(225)-C(226)	120.8(5)	C(221)-C(226)-C(225)	120.1(5)
C(312)-C(311)-C(316)	118.7(4)	C(312)-C(311)-P(3)	121.7(4)
C(316)-C(311)-P(3)	119.5(3)	C(311)-C(312)-C(313)	119.9(6)
C(314)-C(313)-C(312)	120.3(6)	C(315)-C(314)-C(313)	120.6(6)

C(314)-C(315)-C(316)	119.6(6)	C(315)-C(316)-C(311)	120.8(5)
C(322)-C(321)-C(326)	118.5(4)	C(322)-C(321)-P(3)	119.8(3)
C(326)-C(321)-P(3)	121.6(3)	C(323)-C(322)-C(321)	120.6(5)
C(324)-C(323)-C(322)	120.8(5)	C(323)-C(324)-C(325)	119.5(5)
C(324)-C(325)-C(326)	120.6(5)	C(325)-C(326)-C(321)	119.9(5)
C(04)-C(03)-P(3)	107.9(3)	C(03)-C(04)-P(4)	107.7(3)
C(412)-C(411)-C(416)	118.1(4)	C(412)-C(411)-P(4)	122.4(4)
C(416)-C(411)-P(4)	119.3(3)	C(411)-C(412)-C(413)	121.1(5)
C(414)-C(413)-C(412)	120.1(6)	C(415)-C(414)-C(413)	119.6(5)
C(414)-C(415)-C(416)	120.3(6)	C(415)-C(416)-C(411)	120.8(5)
C(426)-C(421)-C(422)	118.6(4)	C(426)-C(421)-P(4)	119.4(3)
C(422)-C(421)-P(4)	122.0(4)	C(423)-C(422)-C(421)	120.3(5)
C(424)-C(423)-C(422)	119.7(5)	C(425)-C(424)-C(423)	121.3(5)
C(424)-C(425)-C(426)	119.2(5)	C(421)-C(426)-C(425)	120.9(5)
B(2)-B(1)-B(3)	60.3(3)	B(4)-B(1)-B(3)	59.5(3)
B(2)-B(1)-B(6)	59.4(3)	B(4)-B(1)-B(5)	59.1(3)
B(6)-B(1)-B(5)	60.5(3)	B(6)-B(2)-B(1)	61.4(3)
C(7)-B(2)-B(3)	59.6(3)	B(1)-B(2)-B(3)	60.1(3)
C(7)-B(2)-B(11)	55.4(2)	B(6)-B(2)-B(11)	59.8(3)
C(8)-B(3)-C(7)	55.1(2)	C(8)-B(3)-B(4)	59.9(3)
B(4)-B(3)-B(1)	60.0(3)	C(7)-B(3)-B(2)	59.0(3)
B(1)-B(3)-B(2)	59.6(3)	C(8)-B(4)-B(3)	59.1(3)
B(3)-B(4)-B(1)	60.5(3)	B(5)-B(4)-B(1)	61.6(3)
C(8)-B(4)-B(9)	55.2(3)	B(5)-B(4)-B(9)	59.5(3)
B(4)-B(5)-B(9)	61.5(3)	B(9)-B(5)-B(10)	61.9(3)
B(4)-B(5)-B(1)	59.4(3)	B(10)-B(5)-B(6)	58.9(3)
B(1)-B(5)-B(6)	59.7(3)	B(2)-B(6)-B(11)	60.9(3)
B(10)-B(6)-B(11)	63.1(3)	B(2)-B(6)-B(1)	59.3(3)
B(10)-B(6)-B(5)	59.5(3)	B(1)-B(6)-B(5)	59.8(3)
C(8)-B(9)-B(4)	60.3(3)	B(5)-B(9)-B(4)	59.0(3)
B(5)-B(9)-B(10)	59.3(3)	B(6)-B(10)-B(5)	61.6(3)
B(5)-B(10)-B(9)	58.8(3)	B(6)-B(10)-B(11)	58.6(3)
C(7)-B(11)-B(2)	60.5(3)	B(6)-B(11)-B(2)	59.3(3)
B(6)-B(11)-B(10)	58.3(3)	C(71)-C(7)-C(8)	118.6(3)
C(71)-C(7)-B(11)	119.3(3)	C(71)-C(7)-B(2)	121.2(3)
B(11)-C(7)-B(2)	64.1(3)	C(71)-C(7)-B(3)	117.5(3)
C(8)-C(7)-B(3)	61.7(3)	B(2)-C(7)-B(3)	61.4(3)
C(81)-C(8)-C(7)	118.7(3)	C(81)-C(8)-B(9)	117.1(3)
C(81)-C(8)-B(3)	118.3(3)	C(7)-C(8)-B(3)	63.2(3)
C(81)-C(8)-B(4)	120.2(3)	B(9)-C(8)-B(4)	64.5(3)
B(3)-C(8)-B(4)	61.0(3)	C(76)-C(71)-C(72)	116.8(4)
C(76)-C(71)-C(7)	119.3(4)	C(72)-C(71)-C(7)	123.8(4)
C(71)-C(72)-C(73)	121.7(5)	C(74)-C(73)-C(72)	120.0(6)
C(73)-C(74)-C(75)	119.7(5)	C(74)-C(75)-C(76)	120.7(6)
C(71)-C(76)-C(75)	121.1(6)	C(86)-C(81)-C(82)	117.8(4)
C(86)-C(81)-C(8)	119.2(4)	C(82)-C(81)-C(8)	122.9(4)

C(83)-C(82)-C(81)	122.1(5)	C(84)-C(83)-C(82)	120.1(6)
C(83)-C(84)-C(85)	120.2(5)	C(84)-C(85)-C(86)	120.1(6)
C(81)-C(86)-C(85)	119.7(5)		

Table 18B Atomic Coordinates (x 10^4) and Equivalent Isotropic Displacement Parameters ($Å^2$ x 10^3) for **18**

	x	y	z	U(eq)
Rh	2154(1)	394(1)	2778(1)	33(1)
P(1)	3155(1)	-216(1)	3446(1)	35(1)
P(2)	2232(1)	681(1)	4115(1)	39(1)
P(3)	993(1)	931(1)	2072(1)	38(1)
P(4)	2268(1)	174(1)	1444(1)	40(1)
C(111)	2569(3)	-802(2)	3571(2)	39(1)
C(112)	1703(3)	-916(2)	3055(3)	48(1)
C(113)	1288(4)	-1377(2)	3093(3)	65(1)
C(114)	1730(4)	-1724(2)	3649(3)	62(1)
C(115)	2582(4)	-1615(2)	4174(3)	62(1)
C(116)	3012(3)	-1160(2)	4137(3)	52(1)
C(121)	4232(3)	-406(2)	3097(2)	37(1)
C(122)	4857(3)	-44(2)	2973(3)	54(1)
C(123)	5652(4)	-162(2)	2656(4)	68(2)
C(124)	5834(3)	-641(2)	2477(3)	63(1)
C(125)	5220(4)	-1000(2)	2595(3)	64(1)
C(126)	4413(3)	-888(2)	2898(3)	54(1)
C(01)	3625(3)	-18(2)	4532(2)	43(1)
C(02)	2798(3)	200(2)	4856(2)	47(1)
C(211)	2985(3)	1226(2)	4401(3)	47(1)
C(212)	3041(3)	1571(2)	3795(3)	62(1)
C(213)	3542(4)	2009(2)	3993(4)	78(2)
C(214)	4026(4)	2094(2)	4793(5)	85(2)
C(215)	4003(5)	1753(3)	5395(4)	96(2)
C(216)	3490(4)	1322(2)	5208(3)	80(2)
C(221)	1150(3)	819(2)	4485(3)	44(1)
C(222)	392(3)	494(2)	4245(3)	51(1)
C(223)	-472(4)	579(2)	4477(3)	67(1)
C(224)	-577(4)	987(2)	4950(4)	81(2)
C(225)	167(4)	1302(2)	5202(4)	83(2)
C(226)	1032(4)	1225(2)	4971(3)	64(1)
C(311)	832(3)	1578(2)	2356(3)	47(1)
C(312)	1244(4)	1963(2)	2008(3)	71(2)
C(313)	1142(5)	2446(2)	2269(5)	101(2)
C(314)	631(6)	2541(2)	2867(5)	101(2)
C(315)	208(4)	2166(2)	3210(4)	77(2)
C(316)	315(3)	1684(2)	2962(3)	57(1)
C(321)	-214(3)	672(2)	1923(2)	42(1)
C(322)	-336(4)	185(2)	2136(3)	56(1)
C(323)	-1238(4)	-25(2)	1987(3)	74(2)
C(324)	-2023(4)	243(2)	1632(4)	76(2)

C(325)	-1915(4)	727(2)	1410(3)	78(2)
C(326)	-1016(3)	945(2)	1553(3)	57(1)
C(03)	1132(3)	977(2)	981(3)	50(1)
C(04)	1285(3)	459(2)	678(2)	50(1)
C(411)	2247(3)	-470(2)	1115(2)	46(1)
C(412)	3063(4)	-727(2)	1076(3)	63(1)
C(413)	3036(5)	-1228(2)	905(4)	87(2)
C(414)	2183(5)	-1480(2)	776(4)	89(2)
C(415)	1361(5)	-1230(2)	805(3)	74(2)
C(416)	1386(4)	-729(2)	967(3)	61(1)
C(421)	3317(3)	447(2)	1156(3)	44(1)
C(422)	3577(3)	335(2)	404(3)	55(1)
C(423)	4364(4)	555(2)	201(4)	69(2)
C(424)	4891(4)	888(2)	739(4)	76(2)
C(425)	4639(4)	1015(2)	1470(4)	74(2)
C(426)	3847(4)	795(2)	1676(3)	57(1)
B(1)	1439(4)	1502(2)	-1023(3)	48(1)
B(2)	1476(4)	1524(2)	-2083(3)	44(1)
B(3)	1019(4)	2032(2)	-1614(3)	46(1)
B(4)	1692(4)	2095(2)	-601(3)	48(1)
B(5)	2604(4)	1654(2)	-430(3)	48(1)
B(6)	2472(4)	1292(2)	-1373(3)	45(1)
B(9)	2877(4)	2259(2)	-698(3)	45(1)
B(10)	3398(4)	1729(2)	-1113(3)	45(1)
B(11)	2653(4)	1692(2)	-2176(3)	43(1)
C(7)	1834(3)	2119(1)	-2248(2)	36(1)
C(8)	1962(3)	2436(1)	-1411(2)	37(1)
C(71)	1486(3)	2375(2)	-3068(2)	42(1)
C(72)	568(3)	2548(2)	-3336(3)	58(1)
C(73)	272(4)	2770(2)	-4110(3)	72(2)
C(74)	878(6)	2816(2)	-4617(4)	101(2)
C(75)	1785(6)	2655(3)	-4368(5)	142(4)
C(76)	2087(5)	2431(3)	-3595(4)	102(2)
C(81)	1753(3)	2980(2)	-1476(3)	44(1)
C(82)	948(4)	3186(2)	-1275(3)	60(1)
C(83)	815(5)	3684(2)	-1258(3)	76(2)
C(84)	1475(5)	3993(2)	-1447(4)	82(2)
C(85)	2271(5)	3809(2)	-1670(4)	81(2)
C(86)	2412(4)	3295(2)	-1693(3)	64(1)

4.5 1,2-Ph_2-3-(η^3-C_8H_{13})-3,1,2-*pseudocloso*-$RhC_2B_9H_9$ (19) and 1-Ph-3-(η^3-C_8H_{13})-3,1,2-*closo*-$RhC_2B_9H_{10}$ (19a)

4.5.1 Synthesis

Compound **19** was synthesised in good yield (67%) by heating to reflux $[Rh(1,5\text{-cod})Cl]_2$ with two equivalents of compound **16** in CH_2Cl_2 for 72 hours. The reaction was monitored by spot tlc, which showed the presence of a mobile orange band (solvent and eluant CH_2Cl_2; R_f = 1.0) and a broad yellow band (R_f = 0.7) due to unreacted $[Rh(1,5\text{-cod})Cl]_2$. During the reaction, the solution gradually turned from a yellow to a dark orange colour and heating was discontinued when this latter band disappeared. Although initially isolated using preparative tlc (conditions as above), later, larger scale syntheses used column chromatography to purify the compound. The product was collected as an orange band and recrystallised in bulk from CH_2Cl_2/petroleum ether (60-80) to afford dark orange microcrystals. The compound was air-stable as a solid and in solution and was especially soluble in chlorinated solvents. It was also slightly soluble in petroleum ethers (40-60 and 60-80), and attempts to grow diffraction quality crystals by solvent diffusion were unsuccessful. This was also partly due to the relatively small amounts of compound involved in these initial attempts. Thick, red, diffraction quality plates were eventually grown by cooling a saturated CH_2Cl_2/petroleum ether (60-80) to -4°C.

Compound **19a** was synthesised by the reaction of compound **16a** and $[Rh(1,5\text{-cod})Cl]_2$, in a similar manner to that described for **19**, except that the reaction time was reduced from 72 to 30 hours, since the reaction proceeded much more quickly. Indeed, within several minutes, the reaction mixture had turned markedly darker. Again the compound was isolated by column chromatography, but attempts at recrystallisation were unsuccessful affording only oily solids. Attempts to grow diffraction quality crystals were also unsuccessful. This was due to the compound being relatively soluble in petroleum ethers as well as there being only a small amount of compound available.

4.5.2 Characterisation

Compound **19** was initially characterised by IR spectroscopy, which showed the expected absorption band due to B-H streching at 2565 cm^{-1}. Microanalysis of crystalline samples was in excellent accordance with the calculated values.

The ^{1}H nmr spectrum (**Fig. 4.20**) shows a quartet at 5.34, which integrates to two protons. This quartet is due to coupling of the equivalent allylic protons, H(31) and H(51) to the unique allylic proton, H(41), one pair of the adjacent methylene protons and one other nucleus (either Rh or the other methylene proton). The coupling between H(31) and H(51) and these nuclei are all close to 8.3 Hz, causing overlap of the doublets. There is also a triplet at 4.72 ppm ($^{3}J_{H-H}$ = 8.3 Hz), which integrates to one proton and is due H(41) coupling to H(31) and H(51). The remaining methylene protons (10H) occur as broad, unresolved multiplet resonances between 1.8 and 0.6 ppm. The phenyl protons (10H) also occur as a multiplet, which is centred at 7.53 ppm.

The ^{11}B-{^{1}H} nmr spectrum (**Fig. 4.21**, above) shows resonances in the ratio 1:1:2:2:2:1, indicating that the molecule has a *closo* geometry with C_s symmetry. Although the the shielding pattern is typical for a *closo* species, the mean ^{11}B-{^{1}H} shift (5.79 ppm) is much higher than one would expect, being over 10 ppm to higher frequency than **19a**. This shift to higher frequency is typical of *pseudocloso* species, such as 1,2-Ph_2-3-(η-C_9Me_7)-3,1,2-*pseudocloso*-$RuC_2B_9H_9$ compared to its mono-phenyl substituted analogue, 1-Ph-3-(η-C_9Me_7)-3,1,2-*closo*-$RuC_2B_9H_{10}$.[18]

The metal-ligand fragment in compound **19** is identical to that in 1,2-Me_2-3-{η^3-C_8H_{13}}-3,1,2-*closo*-$RhC_2B_9H_9$, synthesised by protonation of [PPN][3,3-(1,5-cod)-1,2-Me_2-3,1,2-*closo*-$RhC_2B_9H_9$] with an excess of CF_3CO_2H in CH_2Cl_2, with protonation probably occuring at one of the olefinic carbon atoms, followed by a series of 1,2-hydrogen shifts.[6] The mechanism for the formation of **19** is unclear, as protonation could be effected by either the *endo*-H or, less likely, by the ammonium proton in $[HNEt_3]^+$. One possibility is that the reaction proceeds via an *exo-nido* intermediate, whereby a {Rh(1,5-cod)}

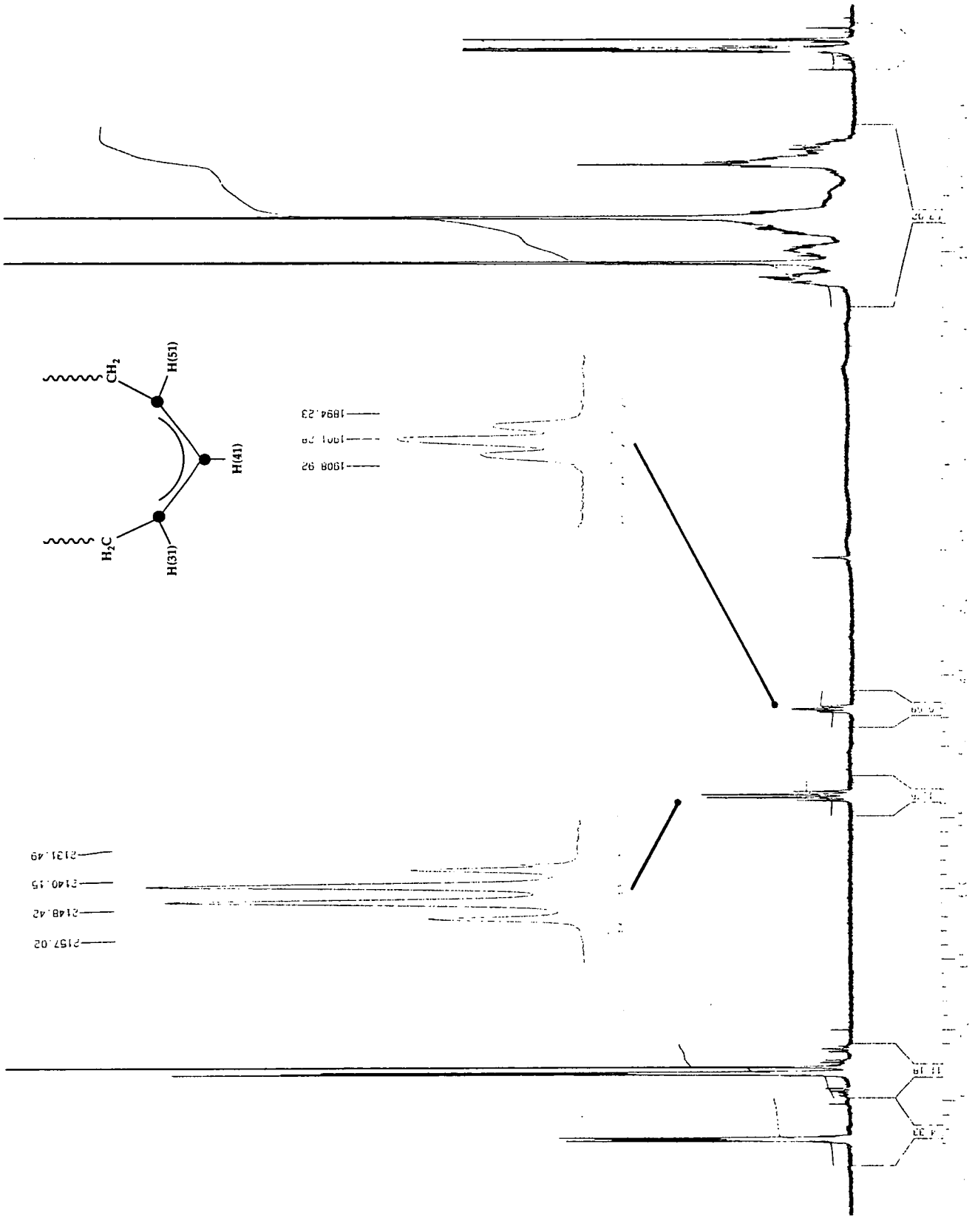

Figure 4.20 ^{1}H Nmr Spectrum of **19** (400 MHz)

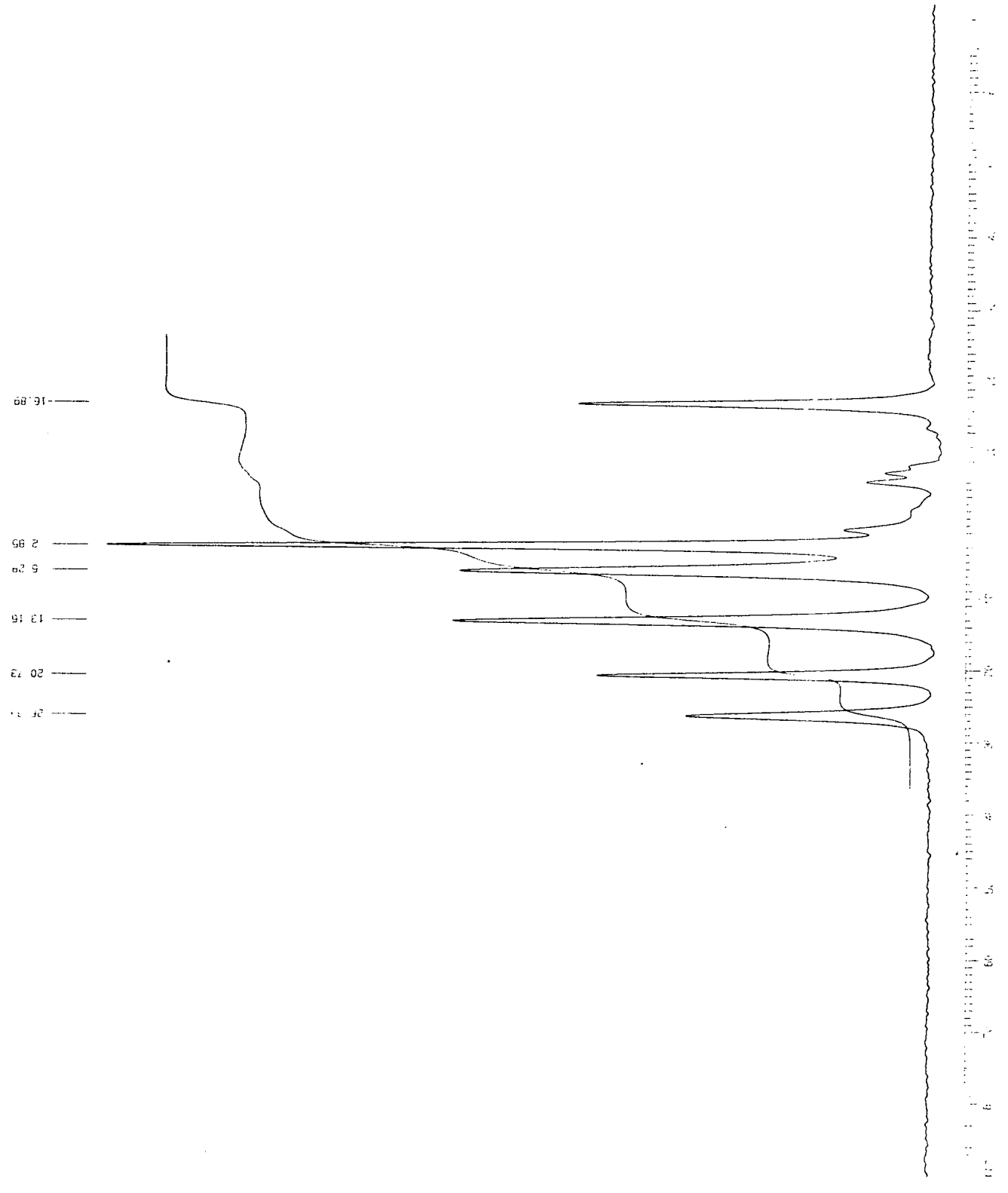

Figure 4.21 ^{11}B-{^{1}H} Nmr Spectrum of **19** (128.4 MHz)

fragment is attached to the side of the cage. Protonation of the 1,5-cod group, followed by a series of 1,2-hydrogen shifts, similar to those postulated for the di-methyl analogue, would afford the cyclooctenyl ring, which would presumably lower the steric requirements of the fragment, enabling it to assume a capping position above the C_2B_3 face.

Compound **19a** was similarly characterised by IR spectroscopy with a broad absorption band observed at 2565 cm^{-1}. Attempts to recrystallise the compound were unsuccessful and hence microanalysis was not possible.

The ^1H nmr spectrum of **19a** showed the C_{cage} proton as a broad singlet at 4.63 ppm and the phenyl protons as a multiplet at 7.20 ppm, with integrals in the ratio 1:5. There are two low-field doublets of doublets, which occur at 6.02 and 5.84 ppm. These are due to the no longer equivalent H(31) and H(51) allylic protons, coupling to H(31) and one of the adjacent methylene protons. There is also an apparent triplet at 4.48 ppm, due to H(51) coupling to the two (non-equivalent) allylic protons to afford two doublets, which overlap to give the appearance of being a triplet. The remaining methylene protons (10H) resonate between 2.43 and 0.20 ppm and are much more distinct from each other relative to **19**, reflecting the asymmetry of the molecule.

As there is no mirror plane in the molecule (cf. **19**), all of the boron nuclei are unique and hence the ^{11}B-{^1H} nmr spectrum (**Fig. 4.22**) shows eight resonances, with that at -2.09 ppm presumably being a (1+1) coincidence. As described previously, the mean shift of the undistorted *closo* species is significantly less than that of the *pseudocloso* analogue (-5.96 and 5.79 ppm, respectively).

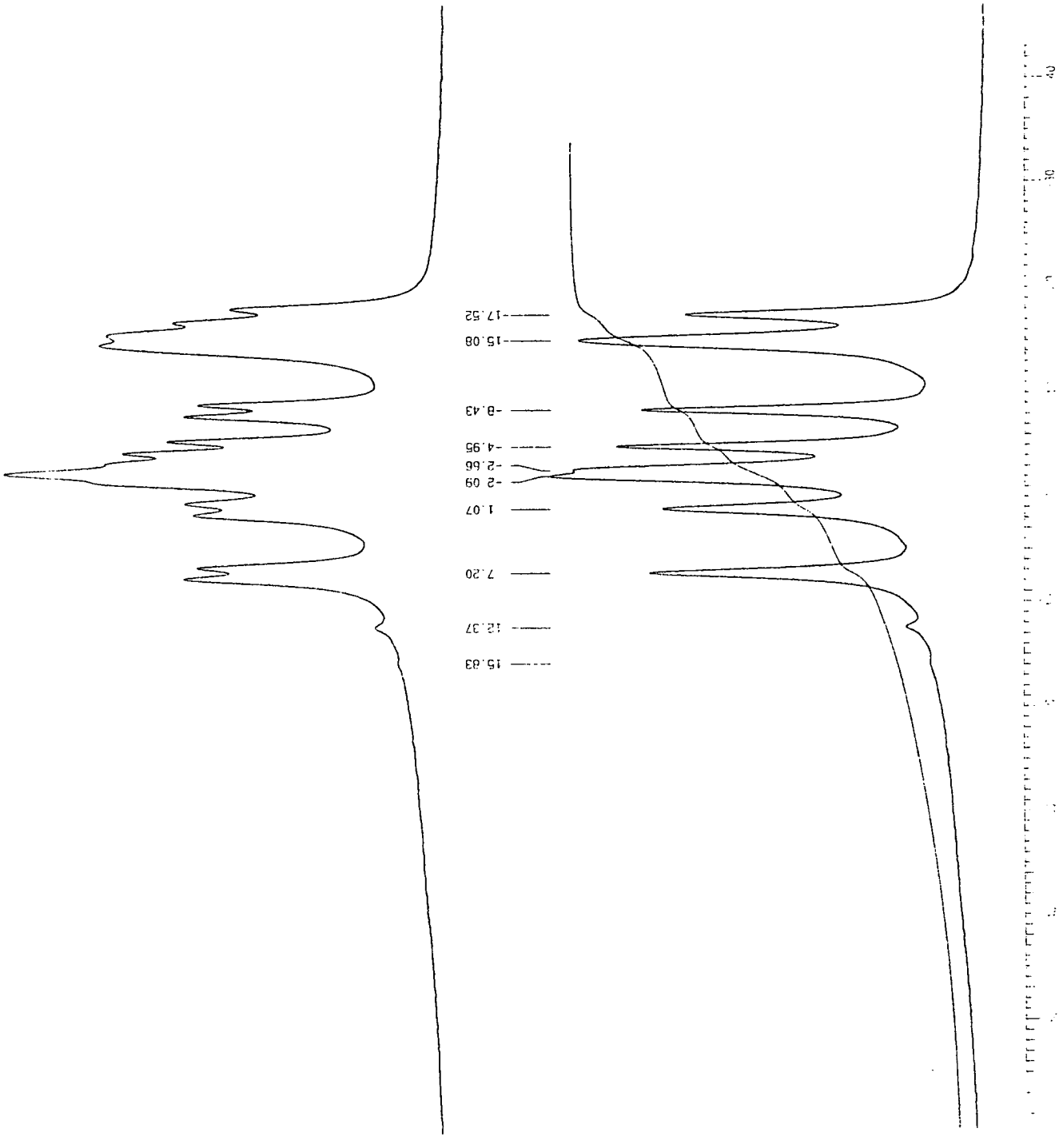

Figure 4.22 ^{11}B-{^{1}H} and ^{11}B Nmr Spectra of **19a** (128.4 MHz)

4.5.3 Crystallographic Study 1,2-Ph_2-3-{η^3-C_8H_{13}}-3,1,2-*pseudocloso*-$RhC_2B_9H_9$ (19)

Scarlet, diffraction quality *plates* of **19** were grown by cooling a saturated petroleum ether (60-80)/CH_2Cl_2 solution to -4°C. Intensity data were measured on an Siemens P4 diffractometer operating with Mo-K_α X-radiation (λ_{bar} = 0.71073 Å). The single crystal was mounted in a glass capillary and the experiment performed at 293(2) K.

Crystal data

$C_{22}H_{32}B_9Rh$, M = 496.68, monoclinic, $P2_1/n$, a = 11.028(3) Å, b = 14.535(6) Å, c = 15.228(3) Å, β = 95.671(19)°, V = 2429.0(14) Å^3, from a random search of a single hemisphere at 291(2) K, Z = 4, D_c = 1.358 gcm^{-3}, μ(Mo-K_α) = 0.71 mm^{-1}, F(0,0,0) = 1016e.

Data collection and reduction

Intensity data collected in the range 4<2θ<50° by the ω-scan method; ω-scan width 1.2°, ω-scan speeds in the range 1.5 to 60°min^{-1}. The intensities of 4217 unique reflections (h -1 to 13, k -1 to 17, l -18 to 18) were measured (XSCANS[23]).

Structure solution and refinement

The structure was solved using Patterson methods (Rh) and developed by iterative, full-matrix least-squares refinement and difference Fourier syntheses (C,B) (SHELXTL). There are four molecules *per* unit cell. In the final model, all non-H atoms were refined anisotropically. The phenyl and cyclooctenyl H atoms were fixed in idealised positions (C-H = 0.93 Å) riding on their respective carbon atoms with U(H) = 1.2 U(C). Cage H atoms were restrained (B-H = 1.10 Å), but allowed to refine freely.

Data were absorption corrected (ψ-scans) and weighted such that w^{-1} = $[\sigma^2(F_o^2) + (0.0483P)^2 + 1.21P]$ where P = [max. (F_o^2) + $2F_c^2]/3$. Using 3324

observed data ($F_o > 4.0\sigma(F_o)$), R = 0.0373, wR_2 = 0.0947 and S = 1.040 for 315 variable parameters. The maximum residue and minimum trough in a final difference Fourier synthesis were 0.64 and -0.43 eÅ^{-3}, respectively. Atomic scattering factors were those inlaid in SHELXTL. Selected bond lengths (Å) and angles (°), fractional coordinates and equivalent isotropic thermal parameters of non-hydrogen atoms are in **Tables 19A** and **19B**, respectively.

Figure 4.23 shows a perspective view of the molecule, which confirms that the molecule has the predicted (^{11}B-{^{1}H} nmr spectroscopy) *pseudocloso* geometry, with a C(1)···C(2) distance of 2.409(5) Å.

This distance is slightly shorter than those previously determined for similar *pseudocloso* structures (**Table 4.2**), which are in the range 2.485(8) to 2.51(3) Å, reflecting the relatively smaller steric requirements of the cyclooctenyl ring (in particular the η-bonded C(3)-C(4)-C(5) sequence), compared to the other capping ligands. Moreover, the Rh-B(6) distance is slightly greater (3.015(4) Å) than the equivalent distances in these structures, again indicating that the degree of deformation is not as great as that afforded by other capping ligands, e.g. Cp*[19], Indy*[18], [9]aneS$_3$[20]. The lower B$_5$ pentagon is distorted, with B(6) pulled 0.32 Å out of the mean plane defined by B(5), B(9), B(11) and B(12). Analogous distortions are listed below in **Table 4.2** and are in the range of 0.29 to 0.34 Å. The rest of the polyhedron is relatively undistorted, with remaining B-C and B–B connectivities in the expected ranges (1.617(6) to 1.749(6) and 1.746(7) to 1.885(7), respectively). The Rh-C/B distances are almost identical to those observed in similar *pseudocloso* species, being in the range 2.12 to 2.20 Å. These and other pertinent data are compared with previously determined structures in **Table 4.2** (below).

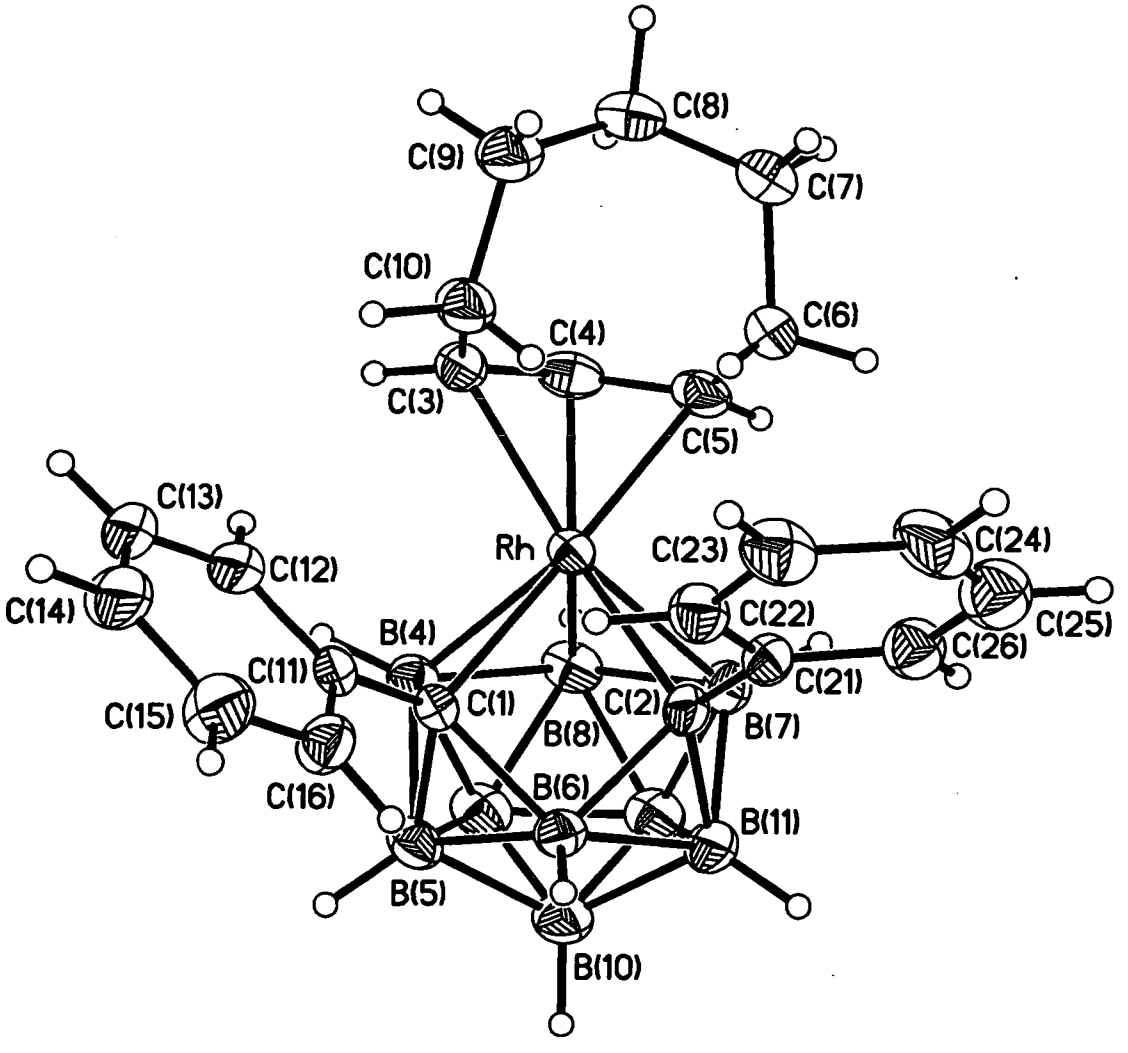

Figure 4.23 Perspective View of **19**

Table 4.2 Pertinent Geometrical Data (Å, °) For **19** and Other *Pseudocloso* Compounds

M	Rh	Rh ‡	Rh	Ru	Ru	Ru
L	C_8H_{13}	Cp*[26]	Indy*[25]	C_6H_6[21]	*p*-cym[28]	[9]aneS_3[27]
C(1)-C(2)	**2.409(5)**	2.51(3)	2.491(6)	2.485(8)	2.453(5)	2.504(7)
M-B(6)	**3.015(4)**	2.92(2)	2.960(5)	2.946(7)	2.987(5)	2.960(6)
θ (C11-6)	**31.9**	78	92.2	61.6	65.9	53.4
θ (C21-6)	**89.5**	87	72.2	61.6	43.9	53.9
C1-M-C2	**68.03**	70.3(8)	70.3(2)	71.1(2)	69.5(2)	70.5(2)
C1-B6-C2	**87.6(3)**	94.4(15)	91.7(3)	91.0(4)	89.5(3)	92.3(4)
B6-C1-M	**99.10**	-	99.3(3)	98.4(2)	100.4(2)	98.4(3)
B6-C2-M	**103.06**	-	97.2(3)	98.4(2)	98.9(2)	97.6(3)
M-C(1)	**2.195(3)**	2.185(20)	2.133(4)	2.136(4)	2.144(4)	2.163(5)
M-C(2)	**2.108(4)**	2.167(21)	2.191(5)	2.136(4)	2.161(4)	2.175(5)
B(6)-C(1)	**1.749(6)**	1.67(3)	1.737(7)	1.742(6)	1.729(6)	1.730(8)
B(6)-C(2)	**1.731(5)**	1.74(3)	1.735(7)	1.742(6)	1.755(6)	1.741(7)
Δ B(6)	**0.32**	-	0.33	0.34	0.29	-

(‡ Molecule A)

The C(1)···C(2) distance is nevertheless greatly lengthened relative to **16**, the compound from which it was synthesised (the crystallographic study of this anion as the $[HNEt_3]^+$ salt determined the C-C distance to be 1.590(5) Å). The 'closing' of the structure by the {Rh(C_8H_{13})} fragment also markedly affects the θ values of the phenyl rings. In the anion, the values for C(71-76) and C(81-86) are 5.6 and 10.0°, respectively. This compares with θ values of 31.9 and 85.9° for C(11-16) and C(21-26) (where C(11-16) and C(21-26) are equivalent to C(71-76) and C(81-86), respectively). Perspective views of the anion in **16** and the carbaborane portion of the molecule are shown in **Figure 4.24**, to illustrate how capping by {Rh(C_8H_{13})} has distorted the di-phenyl substituted C_2B_9 cage.

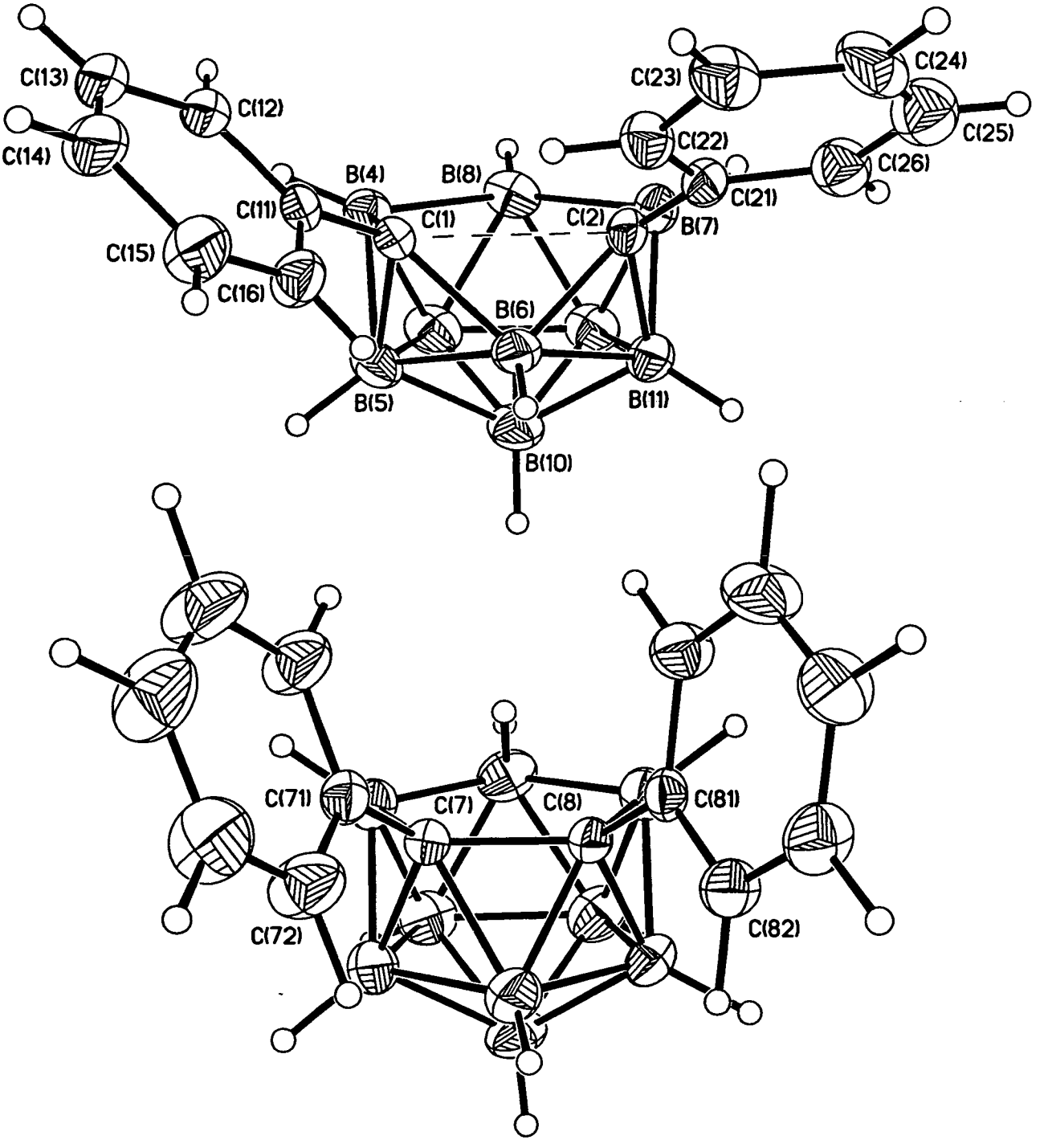

Figure 4.24 Perspective Views of **19** (Capping Fragment Removed) and the Anion in **16**

It can be seen that there is a significant difference (> 50°) in the θ values of the two phenyl rings of **19**. Since the ^{11}B-{^{1}H} nmr spectrum (**Section 4.5.2**) indicates that the molecule has C_s symmetry, it would appear that the molecule is fluxional in solution. This is typically the case for di-phenyl C_2B_9 and C_2B_{10} species, which only requires slight libration of the phenyl rings to confer time-averaged symmetry upon the molecule. The difference in the conformations of the phenyl rings in the solid state are the greatest thus far observed (the next greatest difference is for M(η-L) = Ru(η-*p*-cym),[21] where θ = 65.9° for C(11-16) and 43.9° for C(21-26)). This dramatic asymmetry is reflected in both the open RhC_2B face and the capping cyclooctenyl ligand. The connectivities from C(1) to Rh and B(6) are significantly longer than those from C(2), with a slight decrease of the Rh-C(1)-B(6) angle compared to the analogous angle at C(2) (**Figure 4.23**).

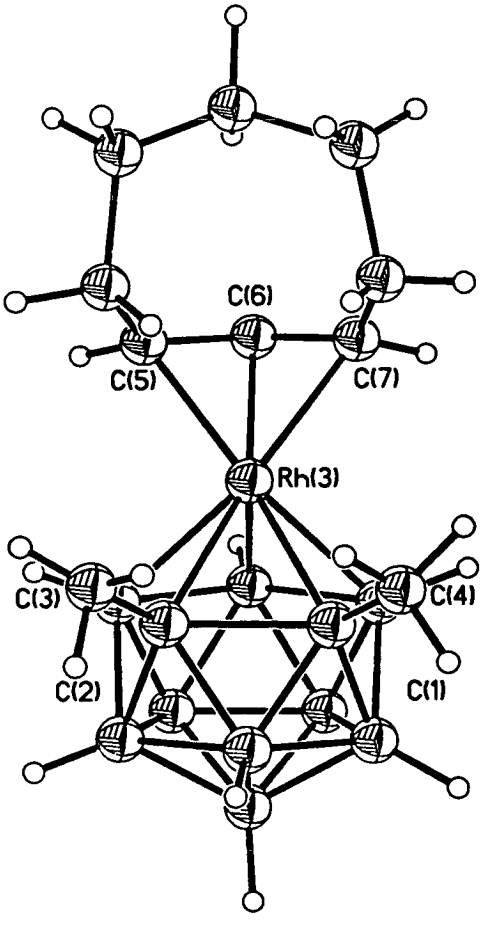

Figure 4.25 Perspective View of 1,2-Me_2-3-{η^3-C_8H_{13}}-3,1,2-*closo*-$RhC_2B_9H_9$

The capping allyl fragment (i.e C(3)-C(4)-C(5)) is almost symmetrically bound to the rhodium atom, with distances to C(3), C(4) and C(5) of 2.210(4), 2.144(4) and 2.181(4) Å, respectively. This contributes to a tilt of the allyl fragment, relative to the η^5-C_2B_3 face of the carbaborane, of 8.1°, towards B(8) and B(7). The allyl fragment is *trans* to the two cage carbon atoms, which is a similar conformation to that observed by Hawthorne for 1,2-Me_2-3-{η^3-C_8H_{13}}-3,1,2-*closo*-$RhC_2B_9H_9$ (**Fig. 4.25**, above).[6]

The cyclooctenyl ring of the molecule, adopts a *pseudo* boat conformation, similar to that observed for the di-methyl analogue. In the case of **19**, however, the saturated portion (C6)-C(10)) displays an exaggerated lean away from the C(1)-bound phenyl ring; indeed, the C(8) atom is 0.48 Å out of the (*pseudo*) mirror plane (Rh, B(8), B(6), B(10)). The pairs of atoms, C(9,7) and C(6,10) are also unsymmetrically positioned with respect to this (*pseudo*) mirror plane. As previously mentioned, the steric requirements of the cyclooctenyl ring are not as large as those of other capping ligands, thus the cage carbon atoms are not forced as far apart and only one of the phenyl rings can adopt a conformation for which $\theta = 90°$. A slightly lower θ value for the C(11-16) ring is therefore observed, which leads to the observed asymmetry of the cyclooctenyl ring with respect to the carbaborane cage.

The bonding mode of the allyl fragment is typical for a delocalised system, with C(3)-C(4) and C(4)-C(5) bond lengths determined as 1.391(6) and 1.404(6) Å, respectively with a C(3)-C(4)-C(5) angle of 127.7(4)°, similar to those of the less crowded di-methyl analogue (1.405 and 1.392 Å and 123.33°, respectively).[6] **Figure 4.26** gives details of distances (Å) and angles (°) between Rh, C(1), C(2) and B(6) for the two molecules. The C(1)-C(2) distance for the di-methyl analogue is relatively long (1.851 Å), indicating the beginnings of cage deformation due to steric strain between the two C-bound methyl groups and the capping ligand. However, it is still considerably shorter than the 2.409(5) Å observed for **19**. The bond lengths and angles for the rest of the molecule are essentially the same as for the di-methyl substituted analogue.

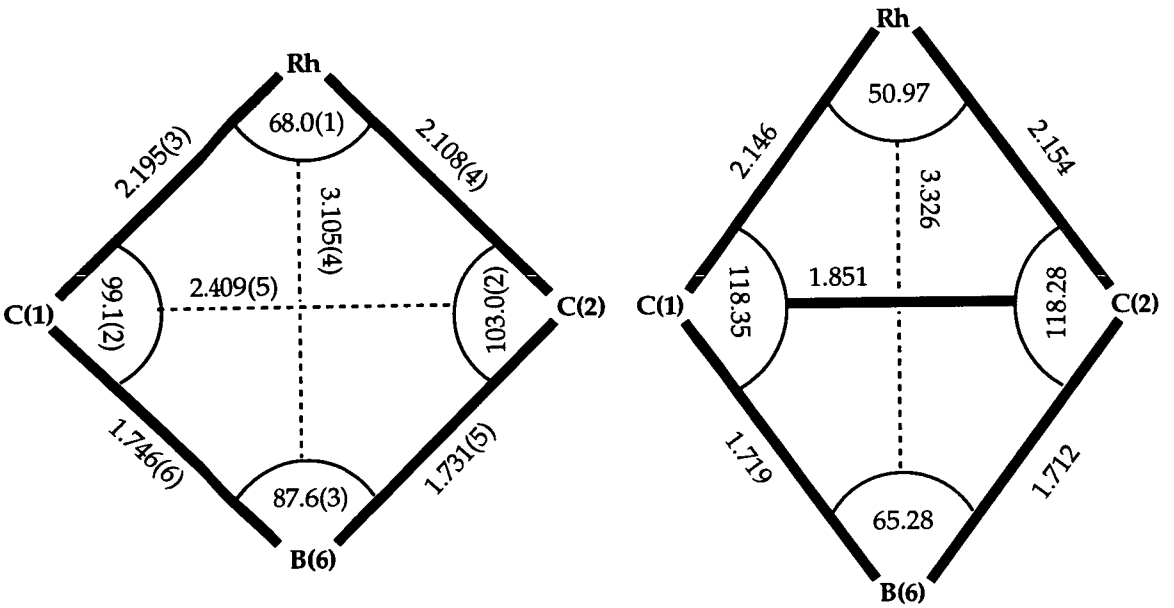

19 **1,2-Me_2-3-{η^3-C_8H_{13}}-3,1,2-*closo*-$RhC_2B_9H_9$

Figure 4.26 Selected Bond Lengths (Å) and Angles (°) Between Rh, C(1), C(2) and B(6) for **19** and 1,2-Me_2-3-{η^3-C_8H_{13}}-3,1,2-*closo*-$RhC_2B_9H_9$

Table 19A Selected Bond Lengths (Å) and Angles (°) for **19**

Rh-C(2)	2.109(4)	Rh-B(8)	2.117(5)
Rh-C(4)	2.144(4)	Rh-C(5)	2.181(4)
Rh-C(1)	2.195(4)	Rh-B(4)	2.203(5)
Rh-C(3)	2.210(4)	Rh-B(7)	2.219(5)
C(1)-C(11)	1.495(5)	C(1)-B(4)	1.620(6)
C(1)-B(5)	1.630(6)	C(1)-B(6)	1.749(6)
C(2)-C(21)	1.486(6)	C(2)-B(7)	1.617(6)
C(2)-B(11)	1.626(6)	C(2)-B(6)	1.731(6)
B(4)-B(9)	1.796(7)	B(4)-B(5)	1.818(7)
B(4)-B(8)	1.886(7)	B(5)-B(10)	1.747(7)
B(5)-B(9)	1.778(7)	B(5)-B(6)	1.811(7)
B(6)-B(11)	1.821(7)	B(6)-B(10)	1.863(7)
B(7)-B(12)	1.792(7)	B(7)-B(11)	1.798(7)
B(7)-B(8)	1.870(8)	B(8)-B(12)	1.795(8)
B(8)-B(9)	1.789(7)	B(9)-B(12)	1.782(8)
B(9)-B(10)	1.766(8)	B(10)-B(11)	1.747(8)
B(10)-B(12)	1.773(7)	B(11)-B(12)	1.775(8)
C(11)-C(12)	1.391(6)	C(11)-C(16)	1.388(6)
C(12)-C(13)	1.377(6)	C(13)-C(14)	1.372(7)
C(14)-C(15)	1.370(7)	C(15)-C(16)	1.384(6)
C(21)-C(26)	1.391(6)	C(21)-C(22)	1.392(6)
C(22)-C(23)	1.386(6)	C(23)-C(24)	1.381(8)
C(24)-C(25)	1.342(8)	C(25)-C(26)	1.383(7)
C(3)-C(4)	1.391(6)	C(3)-C(10)	1.506(6)
C(4)-C(5)	1.404(7)	C(5)-C(6)	1.491(7)
C(6)-C(7)	1.548(6)	C(7)-C(8)	1.477(7)
C(8)-C(9)	1.483(7)	C(9)-C(10)	1.544(6)

C(2)-Rh-B(8)	83.4(2)	C(2)-Rh-C(4)	148.6(2)
B(8)-Rh-C(4)	95.8(2)	C(2)-Rh-C(5)	111.4(2)
B(8)-Rh-C(5)	102.0(2)	C(4)-Rh-C(5)	37.9(2)
C(2)-Rh-C(1)	68.03(14)	B(8)-Rh-C(1)	84.4(2)
C(4)-Rh-C(1)	143.3(2)	C(5)-Rh-C(1)	173.5(2)
C(2)-Rh-B(4)	93.5(2)	B(8)-Rh-B(4)	51.7(2)
C(4)-Rh-B(4)	110.7(2)	C(5)-Rh-B(4)	142.4(2)
C(1)-Rh-B(4)	43.2(2)	C(2)-Rh-C(3)	161.0(2)
B(8)-Rh-C(3)	115.5(2)	C(4)-Rh-C(3)	37.2(2)
C(5)-Rh-C(3)	67.8(2)	C(1)-Rh-C(3)	110.5(2)
B(4)-Rh-C(3)	97.4(2)	C(2)-Rh-B(7)	43.8(2)
B(8)-Rh-B(7)	51.0(2)	C(4)-Rh-B(7)	113.6(2)
C(5)-Rh-B(7)	88.4(2)	C(1)-Rh-B(7)	95.1(2)
B(4)-Rh-B(7)	91.3(2)	C(3)-Rh-B(7)	150.6(2)
C(11)-C(1)-B(4)	125.4(3)	C(11)-C(1)-B(5)	120.2(3)

B(4)-C(1)-B(5)	68.1(3)	C(11)-C(1)-B(6)	118.7(3)
B(5)-C(1)-B(6)	64.7(3)	C(11)-C(1)-Rh	117.1(2)
B(4)-C(1)-Rh	68.6(2)	B(5)-C(1)-Rh	121.0(3)
B(6)-C(1)-Rh	99.1(2)	C(21)-C(2)-B(7)	125.2(3)
C(21)-C(2)-B(11)	126.0(4)	B(7)-C(2)-B(11)	67.3(3)
C(21)-C(2)-B(6)	117.4(3)	B(11)-C(2)-B(6)	65.6(3)
C(21)-C(2)-Rh	107.8(3)	B(7)-C(2)-Rh	71.7(2)
B(11)-C(2)-Rh	124.6(3)	B(6)-C(2)-Rh	103.0(2)
C(1)-B(4)-B(5)	56.2(3)	B(9)-B(4)-B(5)	58.9(3)
B(9)-B(4)-B(8)	58.1(3)	C(1)-B(4)-Rh	68.1(2)
B(9)-B(4)-Rh	111.5(3)	B(5)-B(4)-Rh	112.0(3)
B(8)-B(4)-Rh	61.8(2)	B(10)-B(5)-B(9)	60.1(3)
C(1)-B(5)-B(6)	60.8(3)	B(10)-B(5)-B(6)	63.1(3)
C(1)-B(5)-B(4)	55.7(3)	B(9)-B(5)-B(4)	59.9(3)
C(2)-B(6)-C(1)	87.6(3)	C(1)-B(6)-B(5)	54.5(2)
C(2)-B(6)-B(11)	54.4(2)	B(5)-B(6)-B(10)	56.8(3)
B(11)-B(6)-B(10)	56.6(3)	C(2)-B(7)-B(11)	56.6(3)
B(12)-B(7)-B(11)	59.3(3)	B(12)-B(7)-B(8)	58.7(3)
C(2)-B(7)-Rh	64.5(2)	B(12)-B(7)-Rh	111.8(3)
B(11)-B(7)-Rh	110.7(3)	B(8)-B(7)-Rh	61.6(2)
B(12)-B(8)-B(9)	59.6(3)	B(12)-B(8)-B(7)	58.5(3)
B(9)-B(8)-B(4)	58.4(3)	B(12)-B(8)-Rh	116.5(3)
B(9)-B(8)-Rh	115.8(3)	B(7)-B(8)-Rh	67.3(2)
B(4)-B(8)-Rh	66.5(2)	B(12)-B(9)-B(10)	60.0(3)
B(10)-B(9)-B(5)	59.1(3)	B(12)-B(9)-B(8)	60.4(3)
B(5)-B(9)-B(4)	61.2(3)	B(8)-B(9)-B(4)	63.5(3)
B(11)-B(10)-B(12)	60.6(3)	B(5)-B(10)-B(9)	60.8(3)
B(12)-B(10)-B(9)	60.4(3)	B(11)-B(10)-B(6)	60.5(3)
B(5)-B(10)-B(6)	60.1(3)	B(10)-B(11)-B(12)	60.4(3)
C(2)-B(11)-B(7)	56.1(3)	B(12)-B(11)-B(7)	60.2(3)
C(2)-B(11)-B(6)	60.0(2)	B(10)-B(11)-B(6)	62.9(3)
B(9)-B(12)-B(8)	60.0(3)	B(9)-B(12)-B(10)	59.6(3)
B(10)-B(12)-B(11)	59.0(3)	B(8)-B(12)-B(7)	62.8(3)
B(11)-B(12)-B(7)	60.5(3)	C(12)-C(11)-C(16)	117.5(4)
C(12)-C(11)-C(1)	119.7(4)	C(16)-C(11)-C(1)	122.7(3)
C(11)-C(12)-C(13)	121.2(4)	C(14)-C(13)-C(12)	120.2(4)
C(15)-C(14)-C(13)	119.8(4)	C(14)-C(15)-C(16)	120.0(5)
C(15)-C(16)-C(11)	121.2(4)	C(26)-C(21)-C(22)	118.2(4)
C(26)-C(21)-C(2)	120.9(4)	C(22)-C(21)-C(2)	120.9(3)
C(23)-C(22)-C(21)	121.4(4)	C(24)-C(23)-C(22)	118.7(5)
C(25)-C(24)-C(23)	120.6(5)	C(24)-C(25)-C(26)	121.7(5)
C(25)-C(26)-C(21)	119.4(5)	C(4)-C(3)-C(10)	123.3(4)
C(4)-C(3)-Rh	68.8(2)	C(10)-C(3)-Rh	101.0(3)
C(3)-C(4)-C(5)	122.3(4)	C(3)-C(4)-Rh	74.0(2)
C(5)-C(4)-Rh	72.5(2)	C(4)-C(5)-C(6)	127.7(4)
C(4)-C(5)-Rh	69.6(2)	C(6)-C(5)-Rh	108.2(3)

C(5)-C(6)-C(7)	113.9(4)	C(8)-C(7)-C(6)	116.8(4)
C(7)-C(8)-C(9)	120.1(5)	C(8)-C(9)-C(10)	118.6(4)
C(3)-C(10)-C(9)	114.5(4)		

Table 19B Atomic Coordinates (x 10^4) and Equivalent Isotropic Displacement Parameters ($Å^2$ x 10^3) for **19**

	x	y	z	U(eq)
Rh	84(1)	6465(1)	8195(1)	37(1)
C(1)	467(3)	6288(3)	6818(2)	39(1)
C(2)	-1021(4)	5439(3)	7545(2)	42(1)
B(4)	1675(4)	6116(4)	7493(3)	47(1)
B(5)	1259(5)	5415(4)	6521(3)	53(1)
B(6)	-365(5)	5281(3)	6569(3)	45(1)
B(7)	-296(5)	4988(3)	8415(3)	50(1)
B(8)	1329(5)	5366(4)	8447(3)	54(1)
B(9)	1955(5)	4898(4)	7503(4)	59(1)
B(10)	756(5)	4343(4)	6855(4)	59(1)
B(11)	-580(5)	4391(3)	7381(3)	53(1)
B(12)	845(5)	4260(4)	8021(4)	59(1)
C(11)	252(3)	7100(3)	6220(2)	40(1)
C(12)	882(4)	7915(3)	6415(3)	51(1)
C(13)	749(5)	8661(3)	5857(3)	60(1)
C(14)	-43(6)	8621(3)	5104(3)	70(1)
C(15)	-658(5)	7821(3)	4886(3)	71(1)
C(16)	-505(4)	7064(3)	5436(3)	55(1)
C(21)	-2302(4)	5768(3)	7480(3)	46(1)
C(22)	-2661(4)	6538(3)	6976(3)	53(1)
C(23)	-3834(4)	6885(4)	6950(3)	67(1)
C(24)	-4665(4)	6435(5)	7419(4)	89(2)
C(25)	-4337(5)	5684(4)	7898(4)	76(2)
C(26)	-3162(4)	5343(3)	7953(3)	61(1)
C(3)	728(4)	7824(3)	8698(3)	52(1)
C(4)	633(4)	7206(3)	9385(3)	55(1)
C(5)	-460(5)	6749(3)	9507(3)	57(1)
C(6)	-1719(4)	7134(3)	9405(4)	69(1)
C(7)	-1877(5)	8007(4)	9965(4)	74(2)
C(8)	-995(5)	8760(4)	9886(3)	72(1)
C(9)	-765(6)	9111(3)	9003(3)	75(2)
C(10)	-304(5)	8433(3)	8330(3)	61(1)

4.6 Conclusions

The compound $[HNEt_3][7,8\text{-}Ph_2\text{-}7,8\text{-}nido\text{-}C_2B_9H_{10}]$, **16**, has been successfully synthesised and characterised by microanalysis, IR and nmr (^1H, ^{11}B, $^{11}B\text{-}\{^1H\}$) spectroscopies and ultimately by an X-ray diffraction study. The nature of the extra facial proton was determined as being *endo* to the open face by nmr spectroscopy. The X-ray diffraction study confirmed the molecule as having the expected *nido* geometry, with the phenyl rings orientated so as to be almost parallel to each other. The *pseudo* mirror symmetry of the anion was consistent with the $^{11}B\text{-}\{^1H\}$ nmr spectrum.

The compound $\mu_{(4,9)}\text{-}exo\text{-}\{(PPh_3)_2Rh\}\text{-}7,8\text{-}Ph_2\text{-}7,8\text{-}nido\text{-}C_2B_9H_{10}$, **17**, was successfully synthesised by the reaction of **16** with $(PPh_3)_3RhCl$ in CH_2Cl_2. A crystallographic study confirmed that the molecule, due to the extreme steric requirements of the compound, was forced to tautomerise, with the $\{(PPh_3)_2Rh\}$ fragment adopting a position on the side of the *nido* carbaborane cage, attached to B(4) and B(9) by Rh-H-B bridges. The $^{11}B\text{-}\{^1H\}$ and $^{31}P\text{-}\{^1H\}$ nmr spectra indicated that cage possessed C_s symmetry and that the phosphorous atoms were equivalent, respectively. Hence, the fragment was demonstrated to migrate around the surface of the cage, with concomitant rotarion of the phosphine groups. The related compound **17a** is hypothesised to be the 7,9-isomer of **17** on the basis of spectroscopic and physical data.

Attempts to synthesise the dppe analogue of **17** were unsuccessful, affording instead the ion-pair $[(dppe)_2Rh][7,8\text{-}Ph_2\text{-}7,8\text{-}nido\text{-}C_2B_9H_{10}]$, **18**. The compound was characterised by microanalysis, IR and nmr (^1H, $^{11}B\text{-}\{^1H\}$) spectroscopies. An X-ray diffraction study confirmed the anion to be similar to that in **16**, with the only real difference being the orientation of the phenyl rings. The geometry of the rhodium atom for the cation was approximately square planar, typical for d^8 Rh (I) and not significantly different to that observed for $[(dppe)_2Rh][ClO_4]$.

The heating to reflux of **16** and $[Rh(1,5\text{-}cod)Cl]_2$ in CH_2Cl_2 afforded the compound $1,2\text{-}Ph_2\text{-}3\text{-}\{\eta^3\text{-}C_8H_{13}\}\text{-}3,1,2\text{-}pseudocloso\text{-}RhC_2B_9H_9$, **19**, which was characterised by microanalysis, IR and nmr (^1H, $^{11}B\text{-}\{^1H\}$) spectroscopies. The compound was shown to possess a *pseudocloso* geometry by high frequency

resonances in the ^{11}B-{^{1}H} nmr spectrum and an X-ray diffraction study, which showed that the C(1)-C(2) connectivity had been broken as a result of the steric crowding between the two cage-phenyl groups and the cyclooctenyl ring. The C(1)-C(2) distance was 2.409(5) Å, slightly shorter than for other *pseudocloso* compounds, reflecting the relatively small size of the allyl fragment. The phenyl rings display very different conformations (θ C(11-16) = 31.9°; θ C(21-26) = 85.9°) and the asymmetry of the molecule is further emphasised by the cyclooctenyl ring, which leans away from the C(1)-bound phenyl ring. An analogous reaction, substituting the less crowded **16a** for **16** afforded a *closo* species, **19a**, (^{11}B-{^{1}H} nmr spectroscopy).

Chapter 4 References

1 T.E. Paxson and M.F. Hawthorne, *J. Am. Chem. Soc.*, 1974, **96**, 4674.

2 (**a**) P.E. Behnken, J.A. Belmont, D.C. Busby, M.S. Delaney, R.E. King, C.W. Kreimendahl, T.B. Marder, J.J. Wilczynski and M.F. Hawthorne, *J. Am. Chem. Soc.*, 1984, **106**, 3011; (**b**) P.E. Behnken, D.C. Busby, M.S. Delaney, R.E. King, C.W. Kreimendahl, T.B. Marder, J.J. Wilczynski and M.F. Hawthorne, *J. Am. Chem. Soc.*, 1984, **106**, 7444.

3 (**a**) J.A. Long, T.B. Marder, P.E. Behnken and M.F. Hawthorne, *J. Am. Chem. Soc.*, 1984, **106**, 2979; (**b**) C.B. Knobler, T.B. Marder, E.A. Mizusawa, R.G. Teller, J.A. Long, P.E. Behnken and M.F. Hawthorne, *J. Am. Chem. Soc.*, 1984, **106**, 2990; (**c**) J.A. Long, T.B. Marder and M.F. Hawthorne, *J. Am. Chem. Soc.*, 1984, **106**, 3004.

4 K.F. Purcell and J.C. Kotz, "*Inorganic Chemistry*," Chapter 18, W.B. Saunders Company, Philadelphia, 1977.

5 J.C. Jeffery, F.G.A. Stone, and I. Topaloglu, *Polyhedron*, 1993, **12**, 319.

6 D.M. Speckman, C.B. Knobler and M.F. Hawthorne, *Organometallics*, 1985, **4**, 426.

7 M. Brookhart and M.L.H. Green, *J. Organomet. Chem.*, 1983, **250**, 395, and references therein.

8 M.F. Hawthorne, D.C. Young, P.M. Garrett, D.A. Owen, S.G. Schwerin, F.N. Tebbe and P.A. Wegner, *J. Am. Chem. Soc.*, 1968, **90**, 862.

9 J. Cowie, D.J. Donohoe, N.L. Douek and A.J. Welch, *Acta Cryst.*, 1993, **C49**, 710.

10 J. Buchanan, E.J.M. Hamilton, D. Reed and A.J. Welch, *J. Chem. Soc., Dalton Trans.*, 1990, 677.

11 K.F. Shaw and A.J. Welch, *Polyhedron*, 1992, **11**, 157.

12 CALC: R.O. Gould and P. Taylor, University of Edinburgh, 1986.

13 J.A. Osborn and G. Wilkinson, *Inorg. Synth.*, 1966, **8**, 211.

14 J.A. Doi, R.G. Teller and M.F. Hawthorne, *J. Chem. Soc., Chem. Commun.*, 1980, 80.

15 D.P. Fairlie and B. Bosnich, *Organometallics*, 1988, **7**, 936.

16 (**a**) M.C. Hall, B.T. Kilbourn and K.A. Taylor, *J. Chem. Soc. (A)*, 1970, 2539; (**b**) B.R. James and D. Mahan, *Can. J. Chem.*, 1979, **57**, 180.

17 Z.G. Lewis and A.J. Welch, *Acta Cryst.*, 1993, **C49**, 705.

18 U. Grädler, A.S. Weller, A.J. Welch and D. Reed, *J. Chem. Soc., Dalton Trans.*, 1996, 335.

19 Z.G. Lewis and A.J. Welch, *J. Organomet. Chem.*, 1992, **430**, C45.

20 A.S. Weller and A.J. Welch, *Inorg. Chem.*, In Press.

21 P.T. Brain, M. Bühl, J. Cowie, Z.G. Lewis and A.J. Welch, *J. Chem. Soc., Dalton Trans.*, 1996, 231.

Chapter 5

5.1 Introduction

This chapter details the synthesis and characterisation of the compounds previously described in **Chapters 2, 3** and **4** and is divided into two sections.

Section 5.2 describes syntheses of all compounds **1 - 19a**, together with their characterisation by spectroscopic and analytical techniques, where applicable.

Section 5.3 describes crystallographic techniques used to determine the structures of compounds **1 - 19**.

5.2 Synthetic Methods

5.2.1 General Techniques

All reactions were carried out under dry, oxygen-free conditions using standard Schlenk-line techniques, with some subsequent manipulation in air. Dichloromethane (dried over CaH_2 or P_2O_5), acetonitrile (P_2O_5), *n*-hexane, *i*-hexane, petroleum ether (60-80 and 40-60), tetrahydrofuran, diethyl ether, toluene (sodium wire), methanol and ethanol (Mg/I_2) were freshly distilled before use. Parent carbaboranes were dried over $MgSO_4$ as Et_2O solutions prior to use. Preparative tlc was performed using glass plates coated with Kieselgel F_{254} (0.2mm thick), prewashed with eluant prior to use. Infra-red spectra were recorded as dichloromethane solutions, unless otherwise stated, in CaF_2 cells on a Perkin-Elmer 598 spectrophotometer or a Nicolet Impact 400 FTIR spectrophotometer. Mass spectrometry was carried out on a Vacuum Generators MS9 double sector machine operating under FAB conditions (NOBA matrix, room temperature, 10^{-6}mm Hg, Ar as the fast atom gas). Nmr spectra were recorded as $CDCl_3$ solutions, unless otherwise stated, on Varian VXR600S (^1H, ^1H-$\{^{11}B\}$, ^1H-$\{^{11}B\}\backslash^1H$-$\{^{11}B\}$ COSY, ^{11}B, ^{11}B-$\{^1H\}$, and ^{11}B-$\{^1H\}\backslash^{11}B$-$\{^1H\}$ COSY), Bruker DPX400 (^1H, ^{11}B, ^{11}B-$\{^1H\}$, ^{19}F-$\{^1H\}$, ^{31}P-$\{^1H\}$), Bruker WH360 (^1H, ^1H-$\{^{11}B_{selective}\}$, ^{11}B, $^{11}B\{^1H\}$ and ^{31}P-$\{^1H\}$) and Bruker WP200SY (^1H, ^{11}B, ^{11}B-$\{^1H\}$ and ^{31}P-$\{^1H\}$) spectrometers. Chemical shifts are quoted relative to $SiMe_4$ (^1H), $BF_3.OEt_2$, (^{11}B), CF_3CO_2H (^{19}F) and 80% H_3PO_4 (^{31}P), with positive shifts to high frequency. Techniques for recording ^1H-$\{^{11}B\}\backslash^1H$-$\{^{11}B\}$[1] and ^{11}B-$\{^1H\}\backslash^{11}B$-$\{^1H\}$[2] COSY spectra have been reported previously. Microanalyses (C, H and N) were performed by the departmental service.

5.2.2 Starting Materials

The starting materials 1-Ph-1,2-*closo*-$C_2B_{10}H_{11}$,[3] 1,2-Ph_2-1,2-*closo*-$C_2B_{10}H_{10}$,[4] 1-CH_2OCH_3-1,2-*closo*-$C_2B_{10}H_{11}$,[5] 1-Me-1,2-*closo*-$C_2B_{10}H_{11}$,[6] 1-^{t}Bu-1,2-*closo*-$C_2B_{10}H_{11}$,[7] $[HNEt_3][7,8\text{-}Ph_2\text{-}7,8\text{-}nido\text{-}C_2B_9H_{10}]$, $[HNEt_3][7\text{-}Ph\text{-}7,8\text{-}nido\text{-}C_2B_9H_{11}]$,[8] PR'_3AuCl,[9] (R' = *o*-tol, Cy, Et, mes, C_6F_5), PR'_3AuMe, (R' = *o*-tol, Cy, Et),[10] $[Me_2GaCl]_2$,[11] $(PPh_3)_3RhCl$,[12] $[Rh(C_2H_4)_2Cl]_2$[13] and $[Rh(1,5\text{-cod})Cl]_2$[14] were prepared by previously published literature methods, or slight variations thereof. All other starting materials were available commercially, and were used as received.

5.2.3 Synthesis of 1-Ph-1,2-*closo*-$C_2B_{10}H_{11}$ (1)

Compound **1** was synthesised according to the method of Reid.[15] Typically, $B_{10}H_{14}$ (3.91g, 31.99mmol), CH_3CN (0.14g, 3.20mmol) and PhC_2H (3.27g, 32.00mmol), were stirred for one hour in benzene (*ca.* 45ml) before being heated to reflux for 72 hours. After cooling, volatiles were removed *in vacuo* and the product extracted into *n*-pentane (1 x 40ml, 4 x 20ml). The filtered pentane extract was reduced *in vacuo* to afford a yellow, waxy solid, which was recrystallised by slow diffusion of a very dilute methanolic solution and water (1:5) at 0°C (the water layer was overlaid with a thin layer (*ca.* 1cm) of methanol before the methanolic solution was added). The colourless needles afforded were dissolved in Et_2O (*ca.* 40ml) and dried over $MgSO_4$ for 18 hours. The suspension was filtered and the Et_2O removed *in vacuo* to afford **1-Ph-1,2-*closo*-$C_2B_{10}H_{11}$**, **1**, as a white *solid* in 62.5% (4.41g) yield. Diffraction quality, colourless *blocks* were grown by very slow cooling of a hot-filtered, ethanolic solution.

Microanalysis: Calculated (for $C_8H_{16}B_{10}$): %C 43.61, %H 7.32; Found: %C 43.9, %H 7.38.

IR: ν_{max}: 2595 (s, br) (B-H) cm^{-1}.

NMR: ^1H-{^{11}B} (δ/ppm): 7.58-7.33 (5H, m $C_6\boldsymbol{H}_5$), 3.97 (1H, s, br, C_{cage}-***H***), 2.62 (2H, s, B***H***), 2.53 (2H, s, B***H***), 2.46 (1H, s, B***H***), 2.35 (3H [2+1 coincidence], s, B***H***), 2.30 (2H, s, B***H***).

^{11}B-{^1H} (δ/ppm): -1.19 (1B, ***B***(9)), -3.49 (1B, ***B***(12)), -8.06 (2B, ***B***(8,10)), -9.88 (2B, ***B***(4,5)), -10.32 (2B, ***B***(3,6)), -11.85 (2B, ***B***(7,11)).

5.2.4 Synthesis of Li[1,2-*closo*-$C_2B_{10}H_{11}$]

According to the method of Zakharkin and Grebennikov,[16] 1,2-*closo*-$C_2B_{10}H_{12}$ in benzene (*ca.* 30ml) was heated to 75°C. 1.1 equivalents of *n*-BuLi were added dropwise *via* a dropping funnel as a benzene solution over a period of several minutes, affording an instant white precipitate of **Li[1,2-*closo*-$C_2B_{10}H_{11}$]**. The suspension was cooled to room temperature and Et_2O (*ca.* 10ml) was added to dissolve the precipitate. The resulting cloudy solution was then used immediately.

5.2.5 Synthesis of Li[1-R-1,2-*closo*-$C_2B_{10}H_{10}$]

According to the method of Reid,[15] 1.1 equivalents of MeLi was added (dropwise as an Et_2O solution) to a stirring solution of 1-R-1,2-*closo*-$C_2B_{10}H_{11}$ (R = Ph, CH_2OCH_3, ^tBu, Me) in Et_2O (*ca.* 10-15ml) at 0°C, upon which the solutions generally became pale yellow and cloudy and effervescence was sometimes observed. The solutions of **Li[1-R-1,2-*closo*-$C_2B_{10}H_{10}$]** were allowed to warm to room temperature and then used immediately.

5.2.6 Synthesis of 1-CO_2H-1,2-*closo*-$C_2B_{10}H_{11}$ (2)

In a slight variation of Zakharkin and Grebennikov's method, CO_2 was bubbled through a stirring C_6H_6/Et_2O solution of Li[1,2-*closo*-$C_2B_{10}H_{11}$] (5.42mmol) at room temperature for thirty minutes to afford a milky solution. The solvents were removed *in vacuo* and the resulting white solid redissolved in Et_2O. The Et_2O solution was hydrolysed with an excess (*ca.* 20ml) of 2M HCl and transferred to a separating funnel, where the ethereal layer was removed. The aqueous layer was extracted with Et_2O (2 x 20ml) and the Et_2O extractions combined and dried over $MgSO_4$ for 18 hours. The suspension was filtered and the filtrate reduced *in vacuo* to afford an off-white, microcrystalline *solid* of **1-CO_2H-1,2-*closo*-$C_2B_{10}H_{11}$, 2**, in 73% yield.

Microanalysis: Calculated (for $C_3H_{12}B_{10}O_2$): %C 19.14, %H 6.43; Found: %C 18.33, %H 6.90.

IR: ν_{max}: 2592 (s, br) (B-H), 1736.6, 1761.2 (s) (C=O) cm^{-1}.

NMR: ^1H (δ/ppm): 10.40 (1H, s, br, O***H***), 4.00 (1H, s, C_{cage}-***H***).

^{11}B-{^1H} (δ/ppm): 0.77 (2B), -5.97 (2B), -8.79 (2B), -10.52 (2B), -11.65 (2B).

5.2.7 Synthesis of 1-CO_2H-2-R-1,2-*closo*-$C_2B_{10}H_{10}$

According to the method of Grafstein, gaseous CO_2 was bubbled through an ethereal solution of Li[1-Me-1,2-*closo*-$C_2B_{10}H_{10}$] (5.42mmol) at room temperature for twenty minutes to afford a milky solution. This was hydrolysed with 2M HCl (*ca.* 20ml) and transferred to a separating funnel, where the ethereal layer was removed and the aqueous layer washed with

Et_2O (2 x 20ml). The Et_2O extractions were combined and dried over $MgSO_4$ for 18 hours. The suspension was filtered and the filtrate reduced *in vacuo* to afford an off-white, microcrystalline *solid* of **1-CO_2H-2-Me-1,2-*closo*-$C_2B_{10}H_{10}$**, **3**, in 67% yield.

Microanalysis: Calculated (for $C_4H_{14}B_{10}O_2$): %C 23.75, %H 6.98; Found: %C 24.00, %H 7.17.

IR: ν_{max}: 2594.1 (s, br) (B-H), 1730.4, 1761,5 (s) (C=O) cm^{-1}.

NMR: ^1H (δ/ppm): 8.81 (1H, s, br, O***H***), 2.22 (3H, s, CH_3).

^{11}B-{^1H} (δ/ppm): 2.66 (1B), -2.36 (1B), -6.34 (8B).

Similarly, the following colourless compound was prepared:

1-CO_2H-2-CH_2OCH_3-1,2-*closo*-$C_2B_{10}H_{10}$, **4**, in 74% yield.

Microanalysis: Calculated (for $C_5H_{16}B_{10}O_3$): %C 25.86, %H 6.94; Found: %C 26.37, %H 7.08.

IR: ν_{max}: 2584.2 (br) (B-H), 1732.2, 1764.3 (C=O) cm^{-1}.

NMR: ^1H (δ/ppm): 6.55 (1H, s, br, O***H***), 4.05 (2H, s, C$H_2$$OCH_3$), 3.37 (3H, s, CH_2OCH_3).

^{11}B-{^1H} (δ/ppm): 1.65 (1B), -0.78 (1B), -7.55(8B).

5.2.8 Synthesis of [$HNEt_3$][1-CO_2-2-R-1,2-*closo*-$C_2B_{10}H_{10}$]

To a stirring ethereal solution (*ca.* 5ml) of **2** was added excess NEt_3 to afford **[$HNEt_3$][1-CO_2-1,2-*closo*-$C_2B_{10}H_{11}$]**, (**2a**), as an immediate fine, white precipitate. The solvent was removed *in vacuo* and the product recrystallised from *n*-hexane to give a white crystalline solid in 67% yield. All attempts to grow diffraction quality crystals of **2a** were unsuccessful, but colourless, diffraction quality *blocks* were grown in very low yield (<5%) by slow diffusion of *n*-hexane and a thf solution (1:5) of **[$HNMe_2Et$][1-CO_2-1,2-*closo*-**

$C_2B_{10}H_{11}$], **2b**, at -30°C, which had been synthesised by an analogous method to that given above.

Microanalysis: Calculated (for $C_9H_{27}B_{10}NO_2$): %C 37.35, %H 9.40, %N 4.84; Found: %C 37.75, %H 9.67, %N 4.96.

IR: ν_{max}: 2593.4 (s, br) (B-H), 1656.4, 1336.7 (C=O) cm^{-1}.

NMR: ^1H (δ/ppm): 4.07 (1H, s, br, C_{Cage}-***H***), 3.65 (1H, s, br, N***H***), 2.99 (6H, q, $^3J_{H-H}$ = 7.3Hz, C***H***$_2$CH$_3$), 1.23, (9H, t, $^3J_{H-H}$ = 7.3Hz, CH$_2$C***H***$_3$).

^{11}B-{^1H} (δ/ppm): 0.46 (1B), -2.08 (1B), -6.35 (2B), -8.82 (2B), -10.57 (2B), -11.52 (2B).

Similarly, the following colourless crystalline compounds were prepared:

[HNEt$_3$][1-CO$_2$-2-Me-1,2-*closo*-$C_2B_{10}H_{10}$], **3a**, in 66% yield.

Colourless, diffraction quality *needles* were grown by slow diffusion of *n*-hexane and a CH_2Cl_2 solution (1:4) at -30°C.

Microanalysis: Calculated (for $C_{10}H_{29}B_{10}NO_2$): %C 39.61, %H 9.64, %N 4.60; Found: %C 40.03, %H 9.74, %N 4.55.

IR: ν_{max}: 2583.2 (s, br) (B-H), 1652.7, 1326.7 (C=O) cm^{-1}.

NMR : ^1H (δ/ppm): 3.71 (1H, s, br N***H***), 3.06 (6H, q, $^3J_{H-H}$ = 7.3Hz, C***H***$_2$CH$_3$), 2.15 (3H, s, C***H***$_3$), 1.28 (9H, t, $^3J_{H-H}$ = 7.3Hz, CH$_2$C***H***$_3$).

^{11}B-{^1H} (δ/ppm): -0.84 (1B), -3.41 (1B), -7.44 (8B).

[HNEt$_3$][1-CO$_2$-2-CH$_2$OCH$_3$-1,2-*closo*-$C_2B_{10}H_{10}$], **4a**, in 44% yield.

Colourless diffraction quality *needles* were grown by slow diffusion of *n*-hexane and a CH_2Cl_2 solution (1:4) at -30°C.

Microanalysis: Calculated (for $C_{11}H_{31}B_{10}NO_3$): %C 39.62, %H 9.37, %N 4.20; Found: %C 39.32, %H 9.29, %N 4.16.

IR: ν_{max}: 2594.4 (s, br) (B-H), 1650.3, 1331.7 (C=O) cm^{-1}.

NMR : ^1H (δ/ppm): 4.10 (2H, s, CH_2OCH_3), 3.67 (1H, s, br, N*H*), 3.32 (3H, s, CH_2OCH_3), 3.00 (6H, q, $^3J_{H-H}$ = 7.3Hz, CH_2CH_3), 1.23 (9H, t, $^3J_{H-H}$ = 7.3Hz, CH_2CH_3).

$^{11}B-\{^1H\}$ (δ/ppm): -1.52 (2B), -7.98 (8B).

5.2.9 Synthesis of 1-CH_2OCH_3-2-{Me_2Ga}-1,2-*closo*-$C_2B_{10}H_{10}$ (5)

A solution of Li[1-CH_2OCH_3-1,2-*closo*-$C_2B_{10}H_{10}$] (5.30mmol) in Et_2O (*ca.* 20ml) was reduced *in vacuo* to afford a dry off-white solid. Toluene (*ca.* 25ml) was added and the resulting fine suspension added to a stirring solution of $[Me_2GaCl]_2$ (0.64g, 2.65mmol) in toluene (*ca.* 15ml) *via* a cannula to afford a white precipitate, which was stirred for 18 hours. Stirring was discontinued, the precipitate was allowed to settle and the supernatant decanted off. The product was washed with toluene (2 x 5ml), and the supernatant and washings reduced *in vacuo* to afford **1-CH_2OCH_3-2-{Me_2Ga}-1,2-*closo*-$C_2B_{10}H_{10}$, 5**, as a dry, off-white solid. Some of the product was further purified by sublimation to afford a white, microcrystalline *solid.*

Microanalysis: Calculated (for $C_6H_{21}B_{10}OGa$): %C 25.10, %H 7.37; Found: %C 25.46, %H 7.74.

IR (KBr disc): ν_{max}: 2565.2 (s, br) (B-H), 1476.3, 1387.6, 1198.6 (CH_2OCH_3) cm^{-1}.

NMR (*d*-8 toluene): ^1H (δ/ppm): 2.84 (2H, s, CH_2OCH_3), 2.19 (3H, s, CH_2OCH_3), -0.39 (6H, s, CH_3).

$^{11}B-\{^1H\}$ (δ/ppm): -0.72 (1B), -1.16 (1B), -4.27 (2B), -8.74 (2B), -9.57 (4B).

FAB MS: Molecular ion-peak at 287 amu.

5.2.10 Synthesis of 1-R-2-{PR'$_3$Au}-1,2-*closo*-$C_2B_{10}H_{10}$

Following the method of Reid,[17] a solution of Li[1-Ph-1,2-*closo*-$C_2B_{10}H_{10}$] (1.09mmol) was added *via* a cannula to a stirring suspension of P(*o*-tol)$_3$AuCl (0.591g, 1.10mmol) in Et_2O (*ca.* 10ml). The resulting suspension was stirred for two hours and solvents removed *in vacuo* to afford a peachy white solid. The product was extracted into CH_2Cl_2 by stirring for 30 minutes before being filtered. Spot tlc showed the presence of a mobile, colourless band. Solvent was removed *in vacuo* to afford a golden brown solid, which was purified by preparative tlc (solvent and eluent CH_2Cl_2; R_f = 0.70) to afford **1-Ph-2-{P(*o*-tol)$_3$Au}-1,2-*closo*-$C_2B_{10}H_{10}$, 6**, as a dry, white solid in 45% yield. Colourless, diffraction quality *blocks* were grown by diffusion of *n*-hexane and a CH_2Cl_2 solution at -30°C.

Microanalysis: Calculated (for $C_{29}H_{36}B_{10}PAu$): %C 48.33, %H 5.04; Found: %C 47.65, %H 4.91.

IR: ν_{max}: 2580 (s, br) (B-H) cm^{-1}.

NMR: ^{1}H (δ/ppm): 7.17 (17H, m, $C_6\boldsymbol{H}_5$, 2-CH_3-$C_6\boldsymbol{H}_4$), 2.35 (9H, s, 2-$C\boldsymbol{H}_3$-C_6H_4)

^{11}B-{^{1}H} (δ/ppm): 1.63 (2B), -1.00 (2B), -4.65 to -5.98 (6B).

^{31}P-{^{1}H} (δ/ppm): 17.50 (s).

Similarly, the following colourless, crystalline compounds were prepared:

1-Ph-2-{PCy$_3$Au}-1,2-*closo*-$C_2B_{10}H_{10}$, 7, in 44% yield.

Colourless, diffraction quality *blocks* and *needles* were grown by diffusion of *n*-hexane and a CH_2Cl_2 (4:1) solution at -30°C.

Microanalysis: Calculated (for $C_{26}H_{48}B_{10}PAu$): %C 44.82, %H 6.94; Found: %C 44.71, %H 7.09.

IR: ν_{max}: 2590 (s, br) (B-H) cm^{-1}.

NMR: ^{1}H (δ/ppm): 7.45 (5H, m, $C_6\boldsymbol{H}_5$), 1.96-0.99 (33H, m, $C_6\boldsymbol{H}_{11}$).

^{11}B-{^1H} (δ/ppm): 1.72 (1B), 1.01 (1B), -4.65 (4B), -5.59 (4B).

^{31}P-{^1H} (δ/ppm): 56.11 (s).

1-Ph-2-{PEt_3Au}-1,2-*closo*-$C_2B_{10}H_{10}$, 8, in 37% yield.

Colourless, diffraction quality *blocks* were grown by diffusion of petroleum ether (60-80) and a CH_2Cl_2 solution (4:1) at -30°C.

Microanalysis: Calculated (for $C_{14}H_{30}B_{10}PAu$): %C 31.46, %H 5.66; Found: %C 30.84, %H 5.49.

IR: ν_{max}: 2583.4 (s, br) (B-H) cm^{-1}.

NMR: ^1H (δ/ppm): 7.81, 7.39 (5H, m, $C_6\boldsymbol{H}_5$), 1.57 (6H, d of q ,$^3J_{H-H}$ = 7.4Hz, $^2J_{P-H}$ = 10.0Hz, $C\boldsymbol{H}_2CH_3$), 1.17 (9H, d of t ,$^3J_{H-H}$ = 7.4Hz, $^3J_{P-H}$ = 18.4Hz, $CH_2C\boldsymbol{H}_3$).

^{11}B-{^1H} (δ/ppm): 1.74 (2B), 1.05 (2B), -4.58 to -5.80 (6B).

^{31}P-{^1H} (δ/ppm): 37.37 (s).

1-Ph-2-{$Pmes_3Au$}-1,2-*closo*-$C_2B_{10}H_{10}$, 9, in 23% yield.

Compound was isolated as a mobile, colourless band by preparative tlc (solvent CH_2Cl_2; eluent CH_2Cl_2/petroleum ether (60-80) (1:9); R_f = 0.17). Colourless, diffraction quality *blocks* were grown by diffusion of petroleum ether (60-80) and a CH_2Cl_2 solution (4:1) at room temperature.

Microanalysis: Calculated (for $C_{35}H_{48}B_{10}PAu$): %C 52.23, %H 6.01; Found: %C 52.28, %H 6.01.

IR: ν_{max}: 2590 (s, br) (B-H) cm^{-1}.

NMR: ^1H (δ/ppm): 7.20 (11H, m, $C_6\boldsymbol{H}_5$, 2,4,6-$(CH_3)_3$-$C_6\boldsymbol{H}_2$), 2.32 (18H, s, 2,4,6-$(C\boldsymbol{H}_3)_3$-C_6H_2), 1.58, (9H, s, 2,4,6-$(C\boldsymbol{H}_3)_3$-C_6H_2).

^{11}B-{^1H} (δ/ppm): 1.27 (2B), -0.95 (2B), -4.83 (6B).

^{31}P-{^{1}H} (δ/ppm): 5.54 (s).

1-Ph-2-{P(C_6F_5)$_3$Au}-1,2-*closo*-$C_2B_{10}H_{10}$, 10, in 15% yield.

The compound was purified by preparative TLC (solvent and eluent CH_2Cl_2; R_f = 0.46). Colourless, diffraction quality *plates* were grown by diffusion of *n*-hexane and a CH_2Cl_2 solution (4:1) at -30°C.

Microanalysis: Calculated (for $C_{26}H_{15}B_{10}F_{15}PAu$): %C 32.93, %H 1.59; Found: %C 33.21, %H 1.71.

IR: ν_{max}: 2575.6 (s, br) (B-H) cm^{-1}.

NMR: ^{1}H (δ/ppm): 7.52, 7.04 (m, $C_6\boldsymbol{H}_5$).

^{11}B-{^{1}H} (δ/ppm): 2.55 (1B), 1.01 (1B), -4.47 (4B), -5.74 (4B).

^{31}P-{^{1}H} (δ/ppm): -19.35 (unresolved multiplet).

1-H-2-{P(*o*-tol)$_3$Au}-1,2-*closo*-$C_2B_{10}H_{10}$, 11, in 43% yield.

The compound was purified by preparative tlc (solvent CH_2Cl_2; eluent CH_2Cl_2/*i*-hexane (1:1); R_f = 0.86). Colourless, diffraction quality *needles* (containing one molecule of CH_2Cl_2 of crystallisation *per* molecule of **11**) were grown by diffusion of *i*-hexane and a CH_2Cl_2 solution (5:1) at -30°C.

Microanalysis: Calculated (for $C_{23}H_{32}B_{10}PAu$): %C 42.86, %H 5.00; Found: %C 42.63, %H 5.22.

IR: ν_{max}: 2605 (s, br) (B-H) cm^{-1}.

NMR: ^{1}H (δ/ppm): 7.21 (12H, m, 2-CH_3-$C_6\boldsymbol{H}_4$), 3.37 (1H, s, br, C_{cage}-***H***), 2.50 (9H, s, 2-$C\boldsymbol{H}_3$-C_6H_4).

^{11}B-{^{1}H} (δ/ppm): 0.26 (2B), -5.39 (2B), -6.51 (2B), -8.69 (2B), -9.34 (2B).

^{31}P-{^{1}H} (δ/ppm): 16.51 (s).

1-Me-2-{P(*o*-tol)$_3$Au}-1,2-*closo*-$C_2B_{10}H_{10}$, 12, in 60% yield.

Colourless, diffraction quality *blocks* were grown by diffusion of *n*-hexane and a CH_2Cl_2 solution (6:1) at -30°C.

Microanalysis: Calculated (for $C_{24}H_{34}B_{10}PAu$): %C 43.77, %H 5.20; Found: %C 43.69, %H 5.42.

IR: ν_{max}: 2585 (s, br) (B-H) cm^{-1}.

NMR: ^{1}H (δ/ppm): 7.13 (12H, m, 2-CH_3-$C_6\boldsymbol{H}_4$), 2.69 (9H, s, 2-C$\boldsymbol{H}_3$-C_6H_4), 1.98 (3H, s, C$\boldsymbol{H}_3$).

^{11}B-{^{1}H} (δ/ppm): 1.12 (1B), -4.45 (5B), -5.58 (4B).

^{31}P-{^{1}H} (δ/ppm): 17.47 (s).

1-^{t}Bu-2-{P(*o*-tol)$_3$Au}-1,2-*closo*-$C_2B_{10}H_{10}$, 13, in 56% yield.

Compound was purified by preparative tlc (solvent CH_2Cl_2; eluent CH_2Cl_2/*i*-hexane (50%); R_f = 0.75). Colourless, diffraction quality *plates* were grown by slow evaporation of an *i*-hexane solution at room temperature. A further set of diffraction quality *needles* and *blocks* were grown by slow diffusion of *i*-hexane and a CH_2Cl_2 solution (4:1) at -30°C, but these slowly lost solvent in air becoming opaque.

Microanalysis: Calculated (for $C_{27}H_{40}B_{10}PAu$): %C 46.26, %H 5.76; Found: %C 46.32, %H 5.68.

IR: ν_{max}: 2590 (s, br) (B-H) cm^{-1}.

NMR: ^{1}H (δ/ppm): 7.09 (12H, m, 2-CH_3-$C_6\boldsymbol{H}_4$), 2.60 (9H, s, 2-C$\boldsymbol{H}_3$-C_6H_4), 1.28 (9H, s, C$\boldsymbol{H}_3$).

^{11}B-{^{1}H} (δ/ppm): 1.28 (1B), -0.53 (1B), -5.72 (8B).

^{31}P-{^{1}H} (δ/ppm): 17.21 (s).

5.2.11 Synthesis of PR'_3AuMe

According to the method of Reid,[15] 1.4M MeLi (0.29ml, 0.41mmol) (1.1 equivalents) was added dropwise to a stirring solution of $P(o\text{-tol})_3AuCl$ (0.20g, 0.37mmol) in Et_2O (*ca.* 15ml) at 0°C. The resulting cloudy solution was allowed to warm to room temperature and degassed, distilled water (*ca.* 10ml) added dropwise. The Et_2O layer was removed and the aqueous phase extracted twice more (2 x 10ml). The combined extracts were then dried over $MgSO_4$ for 18 hours. The suspension was filtered and solvent removed in vacuo to afford **$P(o\text{-tol})_3AuMe$, 6a**, as a white solid in 54% yield. Colourless, diffraction quality *blocks* and *octahedra* were grown by slow diffusion of *i*-hexane and a CH_2Cl_2 solution at -30°C.

NMR: $^{31}P\text{-}\{^1H\}$ (δ/ppm): 37.02 (s).

Similarly, the following colourless compounds were prepared:

PCy_3AuMe, 7a, in 45% yield.

Colourless, diffraction quality *blocks* were grown by slow diffusion of *i*-hexane and a CH_2Cl_2 solution at -30°C.

NMR: $^{31}P\text{-}\{^1H\}$ (δ/ppm): 60.02 (s).

PEt_3AuMe, 8a, in 52% yield.

NMR: $^{31}P\text{-}\{^1H\}$ (δ/ppm): 46.52 (s).

5.2.12 Synthesis of $P(C_6F_5)_3AuCl$ (14)

To a stirring solution of $HAuCl_4.3H_2O$ (0.16g, 0.41mmol) in EtOH (*ca.* 10ml) was added two equivalents of $P(C_6F_5)_3$ (0.44g, 0.83mmol). The orange solution went colourless over a period of approximately ten minutes, with occasional warming. The solvent was removed *in vacuo* to afford the product as a white solid, which was recrystallised from CH_2Cl_2/i-hexane in 75% yield. Diffraction quality *blocks* were grown by diffusion of *i*-hexane and a CH_2Cl_2 solution (4:1) at -30°C.

Microanalysis: Calculated (for $C_{18}F_{15}PAuCl$): %C 28.28; Found: %C 28.14.

NMR: $^{31}P-\{^1H\}$ (δ/ppm): -32.02 (unresolved multiplet).

$^{19}F-\{^1H\}$ (δ/ppm): -128.00 (2F, t, br, $^3J_{F-F}$ = 20.4Hz, *meta-**F***), -141.20 (1F, s, br, *para-**F***), -156.47 (2F, unresolved multiplet, *ortho-**F***).

5.2.13 Synthesis of $C_6F_5AuP(C_6F_5)Me_2$ (15)

To a stirring suspension of **14** (0.29g, 0.38mmol) in Et_2O (*ca.* 10ml) was added 1.1 equivalents of 1.4M MeLi (0.30ml, 0.42mmol) dropwise, affording an immediate purple solution. The solution was transferred to a separating funnel and distilled, degassed water (*ca.* 15ml) added. The Et_2O layer was removed and the aqueous layer washed twice more with Et_2O (2 x 10ml). The combined washings were reduced *in vacuo* to afford a light purple solid. The compound was purified by preparative tlc (solvent and eluent CH_2Cl_2: R_f = 1.0) and colourless, diffraction quality needles were afforded by slow diffusion of *n*-hexane and a CH_2Cl_2 solution at -30°C in 34% yield.

Microanalysis: Calculated (for $C_{14}H_6F_{10}PAu$): %C 28.40, %H 1.02; Found: %C 28.52, %H 0.98.

NMR: ^1H (δ/ppm): 2.05 (6H, d of t, $^2J_{P-H}$ = 9.2Hz, $^5J_{F-H}$ = 1.5Hz, C***H***$_3$).

$^{31}P-\{^1H\}$ (δ/ppm): 10.98 (d of t (apparent quintet), $^3J_{P-F}$ = 10Hz).

$^{19}F-\{^1H\}$ (δ/ppm): -116.50 (2F, m), -129.38 (2F, m), -146.23 (1F, t, br, $^3J_{F-F}$ = 21.5Hz,*para-**F***), -158.19 (1F, t, $^3J_{F-F}$ = 20Hz, *para-**F***), -158.35 (2F, m), -162.58 (2F, d of t, $^3J_{F-X}$ = 8Hz, $^3J_{F-F}$ = 20Hz).

5.2.14 Synthesis of [$HNEt_3$][7,8-Ph_2-7,8-*nido*-$C_2B_9H_{10}$] (16)

In a variation of the method of Hawthorne *et al.*,[8] 1,2-Ph_2-1,2-*closo*-$C_2B_{10}H_{10}$ (0.656g, 2.21mmol) and KOH (0.268g, 4.77mmol) in EtOH (*ca.* 30ml) were stirred for 45 minutes before being heated to reflux for 48 hours. Excess KOH was removed by bubbling CO_2 through the cooled solution and the resultant white precipitate of K_2CO_3 filtered off. The EtOH was removed *in vacuo* and the resulting white solid, K[7,8-Ph_2-7,8-*nido*-$C_2B_9H_{10}$], dissolved in distilled degassed water (*ca.* 40ml). The milky solution was filtered and $HNEt_3Cl$ (0.304g, 2.21mmol), dissolved in the minimum amount of water, was added to the filtrate to afford a white precipitate, which was left for several minutes, before being extracted into Et_2O (3 x 50ml). The combined extracts were reduced *in vacuo* to afford an oil, which was recrystallised from petroleum ether (60-80) (*ca* 50ml). The product was dried *in vacuo* to afford **[$HNEt_3$][7,8-Ph_2-7,8-*nido*-$C_2B_9H_{10}$], 16,** in 82% yield. Diffraction quality, colourless *plates* were grown by slow diffusion of *n*-hexane and a CH_2Cl_2 solution (4:1) at -30°C.

Microanalysis: Calculated (for $C_{20}H_{36}B_9N$): %C 61.91, %H 9.37, %N 3.61; Found: %C 61.06, %H 9.36, %N 3.87.

IR: ν_{max}: 2530 (s, br) (B-H) cm^{-1}.

NMR (*d*-6 acetone): ^1H (δ/ppm): 6.95 (10H, m, $C_6\boldsymbol{H}_5$), 3.65 (1H, s, br, N***H***), 3.40 (6H, q, $^3J_{H-H}$ = 7.3Hz, $C\boldsymbol{H}_2CH_3$), 1.41, (9H, t, $^3J_{H-H}$ = 7.3Hz, $CH_2C\boldsymbol{H}_3$), -1.9 (1H, br, d, *endo-**H***).

^{11}B-{^1H} (δ/ppm): -6.49 (2B), -12.77 (1B), -14.80 (2B), -17.30 (2B), -31.49 (1B), -33.84 (1B).

The ^{11}B spectrum showed all ^{11}B nuclei coupling to one *exo*-hydrogen atom, $^1J_{B\text{-}H\textit{exo}}$ 137.0 - 160.1Hz, except for the resonance at -31.49ppm, which also couples to an *endo* proton, $^1J_{B\text{-}H\textit{endo}}$ = 49.4Hz

Similarly, **[HNEt$_3$][7-Ph-7,8-*nido*-$C_2B_9H_{11}$]**, **16a**, was synthesised and isolated as a white microcrystalline *solid* in 92% yield.

Microanalysis: Calculated (for $C_{14}H_{32}B_9N$): %C 53.94, %H 10.35, %N 4.49; Found: %C 54.08, %H 10.80, %N 4.33.

IR: ν_{max}: 2530 (s, br) (B-H) cm^{-1}.

NMR (*d*-6 acetone): ^{1}H (δ/ppm): 7.29-6.99 (5H, m, $C_6\boldsymbol{H}_5$), 3.22 (6H, q, $^3J_{H-H}$ = 7.3Hz, $C\boldsymbol{H}_2CH_3$), 2.45 (1H, s, br, N***H***), 1.46, (9H, t, $^3J_{H-H}$ = 7.3Hz, $CH_2C\boldsymbol{H}_3$), -2.3 (1H, br, d, *endo* -***H***). C_{cage}-***H*** not observed.

^{11}B-{^{1}H} (δ/ppm): -5.61 (1B), -7.09 (1B), -10.51 (1B), -13.24 (1B), -14.93 (1B), -16.40 (1B), -19.70 (1B), -29.56 (1B) -32.65 (1B)

5.2.15 Reactions of 16 with $(PPh_3)_3RhCl$ (17 and 17a)

Compound **16** (0.11g, 0.55mmol) and (0.42g, 0.55mmol) were stirred in CH_2Cl_2 for 2 $^1/_2$ hours. A column (Florisil® 100-200 mesh, 8 x 2cm, CH_2Cl_2 solvent) was used to separate, firstly a red band, **17**, by elution with CH_2Cl_2 and then a lesser, yellow band, **17a**, with CH_2Cl_2/CH_3CN (3:1). Removal of solvents *in vacuo* afforded dry, red and yellow solids, respectively. Red, diffraction quality *blocks* of **$\mu_{(4,9)}$-*exo*-{$(PPh_3)_2Rh$}-7,8-Ph_2-7,8-*nido*-$C_2B_9H_{10}$**, **17**, were grown by slow diffusion of *n*-hexane and a CH_2Cl_2 solution at -30°C.

17:

Microanalysis: Calculated (for $C_{50}H_{50}B_9P_2Rh.CH_2Cl_2$): %C 61.37, %H 5.25; Found: %C 62.6, %H 5.4.

IR (KBr disc): ν_{max}: 2540 (s, br) (B-H) cm^{-1}.

NMR: ^{1}H (δ/ppm): 7.12 (40H, m, $C_6\boldsymbol{H}_5$), -1.95 (1H, d,$^2J_{H-H}$ = *ca.* 60Hz, br, *endo*-***H***).

^{11}B-{^{1}H} (δ/ppm): -11.03 (2B), -14.04 to -15.53 (5B), -32.75 (1B), -35.95 (1B).

^{31}P-{^{1}H} (δ/ppm): 45.07 (d, $^1J_{Rh-P}$ = 187.3 Hz).

17a:

Microanalysis: Not available.

IR (KBr disc): ν_{max}: 2420 (s, br) (B-H) cm^{-1}.

NMR: ^1H (δ/ppm): 7.2 (40H, m, $C_6\boldsymbol{H}_5$), -1.65 (1H, d,$^2J_{H-H}$ = *ca.* 70Hz, br, *endo-**H***)

^{11}B-{^1H} (δ/ppm): -8.46 (2B), -13.91 (1B), -16,94 (4B), -32.95 (1B), -35.40 (1B).

^{31}P-{^1H} (δ/ppm): 44.72 (d, $^1J_{Rh-P}$ = 186.9 Hz).

5.2.16 Synthesis of [(dppe)$_2$Rh][7,8-Ph$_2$-7,8-nido-C$_2$B$_9$H$_{10}$] (18)

Method 1

A toluene solution (*ca.* 6ml) of dppe (0.115g, 0.28mmol) was added to a stirring, clear, yellow, toluene solution (*ca.* 10ml) of $[Rh(C_2H_4)_2Cl]_2$ (0.05g, 0.13mmol) to afford an immediate, yellow precipitate. This was allowed to settle, the supernatant decanted off and the solid washed with more toluene (2 x 5ml), before being dried *in vacuo*. The yellow solid was dissolved in CH_2Cl_2 (*ca.* 10ml) and frozen to 78K. Compound **16** (0.10g, 0.26mmol) was added and the mixture allowed to warm to room temperature, before being storred for one hour, during which time a fine white precipitate formed. The mixture was reduced *in vacuo* to afford a yellow oil, which was purified by column chromatography under N_2 (Sorbsil C60 40/60H silica, 2 x 10cm, CH_2Cl_2 solvent and eluent). A mobile yellow band was collected and recrystallised from CH_2Cl_2/petroleum ether (60-80) to afford yellow microcrystals of **[(dppe)$_2$Rh][7,8-Ph$_2$-7,8-nido-C$_2$B$_9$H$_{10}$]**, **18**. X-ray diffraction quality *blocks* and *needles* were grown by slow diffusion of petroleum ether (60-80) and a CH_2Cl_2 solution at room temperature.

Method 2

To a stirring solution of compound **17** (0.14g, 0.15mmol) in CH_2Cl_2 (*ca.* 40ml) was added dropwise 0.95 equivalents of dppe (0.06g, 0.14mmol) in CH_2Cl_2 (*ca.* 40ml) over a period of twenty minutes. The solution gradually

turned from red to yellow. The solvent was reduced *in vacuo* to *ca.* 3ml and separated by column chromatography as for method 1. A mobile, yellow band was collected and recrystallised from CH_2Cl_2/petroleum ether (60-80) to afford yellow microcrystals. The compound was confirmed as [(dppe)$_2$Rh][7,8-Ph_2-7,8-*nido*-$C_2B_9H_{10}$] by ^{31}P-{^1H} nmr.

Microanalysis: Calculated (for $C_{66}H_{68}B_9P_4Rh$): %C 66.88, %H 5.78; Found: %C 65.80, %H 5.53.

IR: ν_{max}: 2536 (s, br) (B-H) cm^{-1}.

NMR: ^1H (δ/ppm): 7.24, 6.81 (50H, m, $C_6\boldsymbol{H}_5$), 2.12 (8H, m, br, $C\boldsymbol{H}_2$), -1.58 (1H, d, $^2J_{H-H}$ = *ca.* 70 Hz, br, *endo-**H***).

^{11}B-{^1H} (δ/ppm): -8.94 (2B), -14.72 (1B), -16.83 (2B), -18.66 (2B), -33.36 (1B), -35.79 (1B).

^{31}P-{^1H} (δ/ppm): 58.76 (d, $^1J_{Rh-P}$ = 126.0 Hz).

5.2.17 Synthesis of 1,2-Ph_2-3-(η^3-C_8H_{13})-3,1,2-*pseudocloso*-$RhC_2B_9H_9$ (19)

Compound **16** (0.85g, 0.22mmol) and [Rh(1,5-cod)Cl]$_2$ (0.54g, 0.11mmol) were heated to reflux in CH_2Cl_2 for 72 hours, after which time the yellow solution had turned orange. The reaction was monitored by tlc, the product appearing as a mobile orange band (CH_2Cl_2 solvent and eluent; R_f = 1.0). The product was separated by column chromatography (Florisil® 100-200 mesh, 2 x 10cm, CH_2Cl_2 solvent and eluent), the orange band collected and the solvent removed *in vacuo* to afford a dark orange solid, which was recrystallised from CH_2Cl_2/petroleum ether (60-80) to afford orange microcrystals of **1,2-Ph_2-3-(η^3-C_8H_{13})-3,1,2-*pseudocloso*-$RhC_2B_9H_9$, 19**, in 67% yield. Red, diffraction quality *plates* were grown by cooling a saturated CH_2Cl_2/petroleum ether (60-80) solution to -4°C.

Microanalysis: Calculated (for $C_{22}H_{32}B_9Rh$): %C 53.17, %H 6.49; Found: %C 53.24, %H 6.39.

IR: ν_{max}: 2564.9 (s, br) (B-H) cm^{-1}.

NMR: ^{1}H (δ/ppm): 7.82-7.23 (10H, m, $C_6\boldsymbol{H}_5$) 5.34 (2H, q, $^{3}J_{H\text{-}H}$ = 8.3Hz, allylic-***H***), 4.72 (1H, t, $^{3}J_{H\text{-}H}$ = 8.3Hz, allylic-***H***), 1.80-1.14 (8H, m, $C\boldsymbol{H}_2$), 0.89-0.62 (2H, m, $C\boldsymbol{H}_2$).

$^{11}B\text{-}\{^{1}H\}$ (δ/ppm): 26.33 (1B), 20.73 (1B), 13.16 (2B), 6.28 (2B), 2.85 (2B), -16.89 (2B).

5.2.18 Synthesis of 1-Ph-3-(η^3-C_8H_{13})-3,1,2-*closo*-$RhC_2B_9H_{10}$ (19a)

Compound **16a** (0.034g, 0.10mmol) and $[Rh(1,5\text{-cod})Cl]_2$ (0.027g, 0.05mmol) were heated to reflux in CH_2Cl_2 for 30 hours, after which time, the yellow solution had turned orange. The reaction was monitored by tlc, the product appearing as a mobile, dark orange band (CH_2Cl_2 solvent and eluent; R_f = 0.9). The product was separated by column chromatography (Florisil® 100-200 mesh, 2 x 10cm, CH_2Cl_2 solvent and eluent), the dark orange band collected and the solvent removed *in vacuo* to afford a dark orange solid, which was recrystallised from CH_2Cl_2/petroleum ether (60-80) to afford **1-Ph-3-(η^3-C_8H_{13})-3,1,2-*closo*-$RhC_2B_9H_{10}$** as a dark orange *powder*.

Microanalysis: Not available.

IR: ν_{max}: 2565.3 (s) (B-H) cm^{-1}.

NMR: ^{1}H (δ/ppm): 7.20 (5H, m, $C_6\boldsymbol{H}_5$), 6.01 (1H, q, $^{3}J_{H\text{-}H}$ = 8.3Hz, allylic-***H***), 5.87 (1H, d of d (apparent quartet), $^{3}J_{H\text{-}H}$ = 8.1Hz, allylic-***H***) 4.63 (1H, s, br, C_{cage}-***H***), 4.48 (1H, d of d (apparent triplet), $^{1}J_{H\text{-}H}$ = 8.1Hz, allylic-***H***), 1.90-0.20 (10H, unresolved multiplets, $C\boldsymbol{H}_2$).

$^{11}B\text{-}\{^{1}H\}$ (δ/ppm): 7.20 (1B), 1.07 (1B), -2.09 (2B), -2.66 (1B), -4.95 (1B), -8.43 (1B), -15.08 (2B), -17.52 (1B).

5.3 Crystallographic Techniques

This Section describes the general crystallographic techniques used to determine the solid state structures of the compounds described above in **Chapter 2, 3** and **4** (individual experimentals can be found in the relevant Chapters).

Crystallographic measurements were made using Enraf-Nonius CAD4 (λ_{bar} = 0.71069 Å), Enraf-Nonius FAST and Siemens P4 diffractometers (both λ_{bar} = 0.71073 Å) The two Enraf-Nonius diffractometers are equipped with a ULT-1 device for data collection at 199 K.

Crystals were mounted within Lindemann tubes, using vacuum grease to hold them in place and, if necessary, to reduce possible solvent loss. Several of the experiments were performed at 199 K, which also had the effect of slowing any solvent loss. The crystal was optically centred before determination of the unit cell parameters and orientation matrix by least squares analysis of (usually 25) strong, high-angle reflections.

The minimum number of data were generally collected by the ω-2θ (DATCOL[18] - Enraf-Nonius CAD4) or ω-scan methods (MADNES[19] - Enraf-Nonius FAST; XSCANS[20] - Siemens P4) and corrected for Lorentz and polarisation effects and any crystal decay (CADABS[21] - Enraf-Nonius CAD4; XSCANS - Siemens P4). Absorption correction was performed by DIFABS[22] (on a post-isotropic model - Enraf-Nonius CAD4) or ψ-scans (XSCANS - Siemens P4). In the final stages of refinement, data were weighted according to w -1 = $[\sigma^2(F_o^2) + P^2 + P]$, where P = [max. $(F_o^2) + 2\,F_c^2]/3$.

Scattering factors (Au, Rh) were either obtained from International Tables[23] (for SHELX76[24]) or were inlaid in SHELXTL.[25] In the case of compounds containing heavy atoms (Au, Rh), initial structure solution was by Patterson methods (SHELX76, SHELXTL), otherwise direct methods were used (SHELX86,[26] SHELXTL). Structure refinement was accomplished using iterative, full-matrix least squares refinement and difference Fourier syntheses (SHELX76, SHELXTL). Figures and tables were produced using XP and XCIF, respectively (both SHELXTL). Molecular geometry calculations were performed using CALC.[27]

Isotropic thermal parameters take the form:

$$\exp[-8\pi^2 U(\sin^2\theta)/\lambda^2]$$

The general anisotropic thermal parameter, U_{ij}, is given by:

$$U_{ij} = [-2\pi^2(U_{11}a^{*2}h^2 + U_{22}b^{*2}k^2 + U_{33}c^{*2}l^2 + 2U_{23}b^*c^*kl + 2U_{13}a^*c^*hl + 2U_{12}a^*b^*hk)]$$

The equivalent isotropic thermal parameter, U_{eq}, is given by:

$$U_{eq} = [\Sigma_i\Sigma_j U_{ij}a_i^*a_j^*a_ia_j]/3$$

The residuals *R* and w*R*2 and a goodness of fit, *S*, are defined by:

$$R = \Sigma\,|\,|F_o| - |F_c|\,|\,/\Sigma|F_o|$$

$$wR2 = (\Sigma w\,|\,|F_o| - |F_c|\,|\,/\,\Sigma w\,|F_o|)^{1/2}$$

$$S = [\Sigma\{|\,|F_o| - |F_c|\,|/\sigma^2(F_o)\}^2/(N - P)]$$

(where N = number of variable parameters)

1 (a) T.L. Venable, W.C. Hutton, R.N. Grimes, *J. Am. Chem Soc.*, 1984, **106**, 29; (b) G.B. Jacobsen, D.G. Meina, J.H. Morris, C. Thomson, S.J. Andrews, D. Reed, A.J. Welch and D.F. Gaines, *J. Chem. Soc., Dalton Trans.*, 1985, 1645.

2 X.L.R. Fontaine and J.D. Kennedy, *J. Chem Soc., Chem. Commun.*, 1986, 779.

3 B.D. Reid and A.J. Welch, *J. Organomet. Chem.*, 1992, **438**, 371.

4 M.M. Fein, J. Bobinski, N. Myers, N. Schwartz and M.S. Cohen, *Inorg. Chem.*, 1963, **2**, 1111.

5 K.F. Shaw and A.J.Welch, *Polyhedron*, 1992, **11**, 157.

6 D. Grafstein and J. Dvorak, *Inorg. Chem.*, **2**, 1963, 1128.

7 T.D. McGrath, Ph.D. Thesis, University of Edinburgh, 1995.

8 M.F. Hawthorne, D.C. Young, P.M. Garrett, D.A. Owen, S.G. Schwerin, F.N. Tebbe and P.A. Wegner, *J. Am. Chem. Soc.*, 1968, **90**, 862.

9 M.I. Bruce, B.K. Nicholson and O. Bin Shawkataly, *Inorg. Synth.*, 1989, **26**, 324.

10 H. Schmidbaur, T. Pollock, R. Herr, F.E. Wagner, R. Bau, J. Reide and G. Muller, *Organometallics*, 1986, **5**, 566.

11 G.E. Coates and K. Wade, "*Organometallic Compounds*," Volume 1 (Main Group Elements), Third Edition, Methuen, 1967, p355.

12 J.A. Osborne and G. Wilkinson, *Inorg. Synth.*, 1967, **10**, 67.

13 D.P. Fairlie and B. Bosnich, *Organometallics*, 1988, **7**, 936.

14 G.Giordiano and R.H. Crabtree, *Inorg. Synth.*, 1979, **19**, 218.

15 Bruce Reid, Ph.D. Thesis, University of Edinburgh, 1992.

16 L.I. Zakharkin and A.V Grebennikov, *Isz. Akad. Nauk. SSR. Ser Khim.*, 1967, **6**, 1376.

17 B.D. Reid and A.J. Welch, *Polyhedron*, 1992, **438**, 371.

18 DATCOL: Program for data collection, Enraf-Nonius CAD4 manual.

19 MADNES: Cell refinement program, J.W. Pflugrath and A. Messerschmidt, Munich Area Detector, Enraf-Nonius, Delft, The Netherlands, 1991.

20 XSCANS: Program for data collection, Version 2.2, Siemens Analytical X-ray Instruments Inc., Madison, Wisconsin, USA, 1993.

21 CADABS: Program for data reduction, R.O. Gould and D.E. Smith, University of Edinburgh, Scotland, 1986.

22 DIFABS: Absorption correction program, N. Walker and D. Stuart, *Acta Cryst.*, 1983, **A39**, 158.

23 *"International Tables for Crystallography,"* Volume 4, Kynoch Press, Birmingham, 1974.

24 SHELX76: Program for crystal structure solution and refinement, G.M. Sheldrick, University of Cambridge, England, 1976.

25 SHELXTL (PC Version): Program for crystal structure solution and refinement, Siemens Analytical X-ray Instruments Inc., Madison, Wisconsin, USA, 1994.

26 SHELX86: Program for crystal structure solution, G.M. Sheldrick, University of Göttingen, 1986.

27 CALC: Program for crystallographic calculations, R.O. Gould and P. Taylor, University of Edinburgh, 1986.

Appendix A

Courses, Lectures and Meetings Attended

"Inorganic Medicinal Chemistry" By Drs. S.K. Chapman and A.J. Welch
"Industrial Chemistry" by Dr. I. Gosney
"EPR Spectroscopy" by Dr. R.E.P. Winpenny

Inorganic Section Meetings, 1992-1995*
Firbush Meetings, 1994 and 1995*
Departmental Postgraduate Lectures, Research seminars and Colloquia, 1992-1995

Imeboron 8, Knoxville, Tennessee, 1993**
Intraboron 13, Manchester Metropolitan University, 1993
Intraboron 14, Strathclyde University, 1994*
Intraboron 15, University of Leeds, 1995*
USIC '93, '94 and '95*
RSC, Scottish Dalton Meetings:

- Heriot-Watt University, 1993
- Strathclyde University, 1994
- Paisley University, 1995

BCA Residential Crystallography School, Aston University, 1995

(* paper presented; ** co-author of presented paper)

Appendix B

Certain of these results have been published. The references for these papers are:

J.Cowie, D.J. Donohoe, N.L. Douek and A.J. Welch, *Acta Cryst.*, **C49**, 1993, 710.

D.J. Donohoe, D. Reed and A.J. Welch, *Polyhedron*, 1995, **14**, 961.

P.T. Brain, J. Cowie, D.J. Donohoe, M. Hofmann D. Hnyk, D.W.H. Rankin, D. Reed, B.D. Reid, H.E. Robertson, P.v.R. Schleyer and A.J. Welch, *Inorg. Chem.*, 1996, **35**, 1701.

Reprints are included in this appendix.

Acta Cryst. (1993). C**49**, 710–714

Structures of $[HNEt_3]^+$ and $[Me_3NCH_2C_6H_5]^+$ Salts of $[7,8\text{-}Ph_2\text{-}7,8\text{-}nido\text{-}C_2B_9H_{10}]^-$

BY JILL COWIE, DAVID J. DONOHOE, NATALIA L. DOUEK AND ALAN J. WELCH

Department of Chemistry, University of Edinburgh, Edinburgh EH9 3JJ, Scotland

(*Received* 24 *August* 1992; *accepted* 17 *November* 1992)

Abstract. Triethylammonium 7,8-diphenyl-7,8-dicarba-*nido*-decahydroundecaborate(1−), $C_6H_{16}N^+.C_{14}H_{20}B_9^-$, $M_r = 387.80$, triclinic, $P\bar{1}$, $a = 11.014$ (4), $b = 11.030$ (7), $c = 12.333$ (6) Å, $\alpha = 67.83$ (5), $\beta = 80.78$ (4), $\gamma = 60.20$ (5)°, $V = 1203.3$ Å^3, $Z = 2$, $D_x = 1.070$ Mg m^{-3}, λ(Mo $K\alpha$) = 0.71069 Å, $\mu = 0.052$ mm^{-1}, $F(000) = 416$, $T = 291$ (1) K, $R = 0.1074$ for 3289 independent observed reflections. Benzyltrimethylammonium 7,8-diphenyl-7,8-dicarba-*nido*-decahydroundecaborate(1−), $C_{10}H_{16}N^+.C_{14}H_{20}B_9^-$, $M_r = 435.85$, monoclinic, $P2_1/n$, $a = 10.751$ (4), $b = 21.662$ (4), $c = 11.9745$ (25) Å, $\beta = 106.592$ (23)°, $V = 2672.5$ Å^3, $Z = 4$, $D_x = 1.083$ Mg m^{-3}, λ(Mo $K\alpha$) = 0.71069 Å, $\mu = 0.053$ mm^{-1}, $F(000) = 928$, $T = 185$ (1) K, $R = 0.0637$ for 3857 independent observed reflections. In both determinations, the phenyl substituents lie very roughly orthogonal to the open C_2B_3 face of the anion, pairs of rings being twisted (in a conrotatory manner) by an average of 7.8° for the $[HNEt_3]^+$ salt, and 19.0° for the $[Me_3NCH_2C_6H_5]^-$ salt, from this extreme. In the latter case, this twist is traced to interion contacts. The C(cage)—C(cage) distances, 1.590 (5) and 1.602 (3) Å, respectively, and the mean facial B—B and facial B—C distances are discussed in relation to the equivalent distances in 1,2-Ph_2-1,2-*closo*-$C_2B_{10}H_{10}$.

Introduction. The preceding paper (Lewis & Welch, 1993*a*) reports the molecular structure of 1,2-Ph_2-1,2-*closo*-$C_2B_{10}H_{10}$, noting the relatively long C(1)—C(2) connectivity [1.727 (6) Å averaged over the two crystallographically independent molecules] and the low θ values [θ is the average difference between 90° and the moduli of the C(cage)—C(cage)—C—C torsion angles] that describe the molecular conformation.

Our interest in diphenylcarbaborane rests primarily in its use as a ligand to *d*- and *f*-block metals, predominantly in the partially degraded form $[7,8\text{-}Ph_2\text{-}7,8\text{-}nido\text{-}C_2B_9H_9]^{2-}$ [note the change in conventional numbering between related *closo* and *nido* polyhedra (Casey, Evans & Powell, 1983)]. We have already shown (Lewis & Welch, 1992) that unusual structure deformation can arise when the phenyl

0108-2701/93/040710-05$06.00

rings are twisted into positions described by high θ values on ligation to a sterically demanding metal fragment such as Rh(η-C_5Me_5).

In this context, we considered it important to have full stereochemical information on diphenylcarbaborane in its ligand form. As is the case with the parent compound [7,8-*nido*-$C_2B_9H_{11}$]$^{2-}$ and related derivatives, it is convenient to study such species as the partially protonated monoanion, in which the additional H atom occupies an *endo* position on B(10) (Buchanan, Hamilton, Reed & Welch, 1990; Shaw & Welch, 1992). Thus the present studies were undertaken.

Experimental. K[7,8-Ph_2-7,8-*nido*-$C_2B_9H_{10}$], a light yellow solid, was prepared from 1,2-Ph_2-1,2-*closo*-$C_2B_{10}H_{10}$ by an analogous method to that which affords K[7,8-*nido*-$C_2B_9H_{12}$] from $C_2B_{10}H_{12}$ (Hawthorne, Young, Garrett, Owen, Schwerin, Tebbe & Wegner, 1968). The title salts were each isolated as fine white precipitates by addition of aqueous solutions of excess [$HNEt_3$]Cl or [$Me_3NCH_2C_6H_5$]Br to an aqueous solution of K[7,8-Ph_2-7,8-*nido*-$C_2B_9H_{10}$], and recrystallized from CH_2Cl_2–*n*-hexane (1/3) at 243 K. ^{1}H NMR spectroscopy in $(CD_3)_2CO$ showed each to be a 1:1 salt and ^{11}B and ^{11}B-{^{1}H} NMR spectroscopies revealed signals very similar to those (fully assigned) of 7,8-*nido*-$C_2B_9H_{12}$]$^-$ (Buchanan, Hamilton, Reed & Welch, 1990). Thus, for the [$HNEt_3$]$^+$ salt, ^{11}B-{^{1}H} δ −6.49 (2B), −12.77 (1B), −14.80 (2B), −17.30 (2B), −31.49 (1B) and −33.84 p.p.m. (1B), all signals showing doublet coupling [$^1J_{BH(exo)}$ 137–160 Hz] with that at −31.49 showing additional doublet coupling [$^1J_{BH(endo)}$ 49.5 Hz] in the ^{11}B spectrum. Crystals of both salts were mounted on an Enraf–Nonius CAD-4 diffractometer (graphite monochromator). Experimental details in curly brackets, {}, represent differences in respect of the [$Me_3NCH_2C_6H_5$]$^+$ salt. Crystal size 0.3 × 0.2 × 0.2 mm {0.2 × 0.15 × 0.15 mm}; cell parameters and orientation matrix from least-squares refinement of the setting angles (9{12} < θ < 13°) of 25 centred reflections; data collection by ω–2θ scans in 96 steps with ω-scan width (0.8 + 0.34tanθ)°; data (h 0 to 13, k −13 to 13, l −14 to 14 {h 0 to 12, k 0 to 25, l −13 to 13}) measured for $1 \le \theta \le 25°$ at room temperature {185 (1) K, ULT-1 low-temperature attachment} over 96 {115} X-ray hours with *ca* 2% decay subsequently corrected {no appreciable decay or movement}; corrections for Lorentz and polarization effects applied (Gould & Smith, 1986); of 4462 {5118} data measured, 3289 {3857} [$F \ge 2.0\sigma(F)$] used to solve [direct methods for most non-H atoms (Sheldrick, 1986), difference Fourier syntheses for all others (Sheldrick, 1976)] and refine (least squares on F) the structure.

In the case of the [$HNEt_3$]$^+$ salt, the ethyl groups of the cation were found to be involved in disorder, the best model of which involves six methylene C atoms and four methyl C atoms with 0.5 occupancy, only one methyl C atom, C(12), being essentially ordered; all cation atoms were refined with isotropic thermal parameters and no cation H atoms were included; cage H atoms were allowed positional refinement [except H(12), the *endo* H atom bound to B(10), which was included in an idealized position (Buchanan, Hamilton, Reed & Welch, 1990) but not thereafter refined] and phenyl H atoms were set in idealized positions (C—H 1.08 Å); non-H atoms of the anion were refined with anisotropic thermal parameters but cage and phenyl H atoms were refined with a single group isotropic thermal parameter, 0.085 (3) Å^2 at convergence; weights were assigned according to $w^{-1} = [\sigma^2(F) + 0.000306F^2]$; R = 0.1074, wR = 0.1206, S = 2.165; max. shift/e.s.d. in final cycle < 0.15; max. and min. residues in final ΔF synthesis 0.64 and −0.42 e Å^{-3}, respectively; the former of these essentially caps the *nido* polyhedral face, 1.73–1.80 Å from atoms C(7)—B(11), and is presumably due to partial boron disorder. Such a phenomenon is fairly frequently met in structural studies of *nido* icosahedral (hetero)boranes; scattering factors for N, C, B and H inlaid in *SHELX*76; Fig. 1 drawn using *EASYORTEP* (Mallinson & Muir, 1985); molecular geometry calculations *via CALC* (Gould & Taylor, 1986); we ascribe the relatively high residuals to the crystallographic disorder in both anion and cation, and to the relatively poor quality of the crystal used.

In the case of the [$Me_3NCH_2C_6H_5$]$^+$ salt, the cation is ordered but the same disorder is apparent in the anion; all non-H atoms were refined with anisotropic thermal parameters, and all H atoms [except that *endo* to B(10), which was treated similarly as above] were located from ΔF maps and freely refined, albeit with an overall isotropic thermal parameter, 0.0510 (13) Å^2 at convergence; weights were assigned according to $w^{-1} = [\sigma^2(F) + 0.002546F^2]$; R = 0.0637, wR = 0.0930, S = 1.084; max. shift/e.s.d. in final cycle < 0.01; max. and min. residues in final ΔF synthesis 0.94 and −0.30 e Å^{-3}, respectively; the former 1.59–1.84 Å from the facial C or B atoms.

Discussion. Table 1* lists coordinates of refined non-H atoms and equivalent isotropic thermal

* Lists of structure factors, anisotropic thermal parameters, H-atom parameters and complete geometry have been deposited with the British Library Document Supply Centre as Supplementary Publication No. SUP 55795 (56 pp.). Copies may be obtained through The Technical Editor, International Union of Crystallography, 5 Abbey Square, Chester CH1 2HU, England. [CIF reference: MU1027]

Table 1. *Fractional coordinates and equivalent isotropic thermal parameters* ($Å^2$) *for non-*H *atoms in* $[HN(C_2H_5)_3][7,8\text{-}Ph_2\text{-}7,8\text{-}nido\text{-}C_2B_9H_{10}]$

$U_{eq} = (1/3)\sum_i\sum_j U_{ij}a_i^*a_j^*\mathbf{a}_i.\mathbf{a}_j.$

	x	y	z	U_{eq}
B(1)	0.2764 (5)	1.0369 (5)	0.6872 (4)	0.064 (4)
B(2)	0.2111 (5)	0.9131 (5)	0.7057 (4)	0.064 (4)
B(3)	0.3716 (5)	0.8841 (5)	0.6418 (5)	0.070 (4)
B(4)	0.4574 (5)	0.9292 (5)	0.7136 (4)	0.064 (4)
B(5)	0.3532 (6)	0.9879 (5)	0.8239 (5)	0.075 (5)
B(6)	0.1933 (6)	0.9790 (5)	0.8204 (4)	0.071 (4)
C(7)	0.3530 (4)	0.7386 (4)	0.7539 (3)	0.048 (3)
C(8)	0.4916 (4)	0.7489 (4)	0.7557 (3)	0.045 (3)
B(9)	0.4926 (5)	0.8022 (5)	0.8627 (4)	0.061 (4)
B(10)	0.3227 (5)	0.8435 (5)	0.9324 (4)	0.069 (4)
B(11)	0.2444 (5)	0.7905 (5)	0.8539 (4)	0.059 (4)
C(71)	0.3635 (4)	0.6146 (4)	0.7246 (3)	0.054 (3)
C(72)	0.3595 (5)	0.6205 (5)	0.6114 (4)	0.094 (5)
C(73)	0.3601 (7)	0.5063 (7)	0.5881 (5)	0.127 (6)
C(74)	0.3662 (7)	0.3832 (6)	0.6783 (5)	0.128 (6)
C(75)	0.3751 (7)	0.3738 (5)	0.7913 (5)	0.117 (6)
C(76)	0.3744 (5)	0.4878 (5)	0.8137 (4)	0.090 (4)
C(81)	0.6275 (4)	0.6341 (4)	0.7262 (3)	0.048 (3)
C(82)	0.6866 (4)	0.6612 (4)	0.6178 (3)	0.061 (3)
C(83)	0.8148 (5)	0.5542 (5)	0.5969 (4)	0.077 (4)
C(84)	0.8847 (5)	0.4181 (5)	0.6819 (4)	0.083 (4)
C(85)	0.8260 (5)	0.3894 (5)	0.7909 (4)	0.081 (4)
C(86)	0.6997 (4)	0.4954 (4)	0.8126 (4)	0.067 (4)
N	0.1087 (6)	1.1281 (6)	1.2206 (5)	0.1194 (17)
C(11*A*)	0.1076 (13)	1.2369 (13)	1.2586 (12)	0.109 (4)
C(11*B*)	0.1150 (14)	1.1252 (14)	1.3724 (11)	0.112 (4)
C(12)	0.0109 (10)	1.2626 (10)	1.3697 (8)	0.177 (3)
C(21*B*)	0.136 (3)	1.244 (3)	1.129 (3)	0.259 (11)
C(21*A*)	0.1769 (13)	1.1357 (14)	1.0901 (12)	0.101 (4)
C(22*B*)	0.1199 (17)	1.2309 (20)	1.0170 (14)	0.123 (5)
C(22*A*)	0.0947 (14)	1.3151 (15)	1.0018 (11)	0.104 (4)
C(31*A*)	0.214 (3)	0.966 (3)	1.3061 (20)	0.214 (9)
C(31*B*)	0.1687 (18)	0.9453 (20)	1.2417 (14)	0.140 (5)
C(32*A*)	0.2042 (14)	0.8458 (15)	1.2973 (12)	0.107 (4)
C(32*B*)	0.3185 (18)	0.8887 (17)	1.2571 (14)	0.142 (5)

Table 2. *Interatomic distances* (Å) *and interbond angles* (°) *in* $[HN(C_2H_5)_3][7,8\text{-}Ph_2\text{-}7,8\text{-}nido\text{-}C_2B_9H_{10}]$

B(1)—B(2)	1.766 (8)	B(10)—B(11)	1.795 (8)
B(1)—B(3)	1.738 (8)	C(71)—C(72)	1.379 (7)
B(1)—B(4)	1.747 (8)	C(71)—C(76)	1.376 (7)
B(1)—B(5)	1.779 (8)	C(72)—C(73)	1.391 (9)
B(1)—B(6)	1.802 (8)	C(73)—C(74)	1.373 (10)
B(2)—B(3)	1.741 (8)	C(74)—C(75)	1.374 (10)
B(2)—B(6)	1.764 (8)	C(75)—C(76)	1.381 (8)
B(2)—C(7)	1.716 (7)	C(81)—C(82)	1.383 (6)
B(2)—B(11)	1.778 (8)	C(81)—C(86)	1.394 (6)
B(3)—B(4)	1.729 (8)	C(82)—C(83)	1.382 (7)
B(3)—C(7)	1.758 (7)	C(83)—C(84)	1.367 (8)
B(3)—C(8)	1.731 (7)	C(84)—C(85)	1.389 (8)
B(4)—B(5)	1.735 (8)	C(85)—C(86)	1.369 (7)
B(4)—C(8)	1.704 (7)	N—C(11*A*)	1.437 (16)
B(4)—B(9)	1.799 (8)	N—C(11*B*)	1.873 (16)
B(5)—B(6)	1.820 (8)	N—C(21*B*)	1.48 (3)
B(5)—B(9)	1.775 (8)	N—C(21*A*)	1.654 (16)
B(5)—B(10)	1.794 (8)	N—C(31*A*)	1.60 (3)
B(6)—B(10)	1.769 (8)	N—C(31*B*)	1.704 (21)
B(6)—B(11)	1.753 (8)	C(11*A*)—C(12)	1.618 (18)
C(7)—C(8)	1.590 (5)	C(11*B*)—C(12)	1.363 (19)
C(7)—B(11)	1.631 (7)	C(21*B*)—C(22*B*)	1.49 (4)
C(7)—C(71)	1.489 (6)	C(21*A*)—C(22*A*)	1.682 (22)
C(8)—B(9)	1.638 (7)	C(31*A*)—C(32*A*)	1.43 (3)
C(8)—C(81)	1.505 (5)	C(31*B*)—C(32*B*)	1.46 (3)
B(9)—B(10)	1.839 (8)		

B(2)—B(1)—B(3)	59.6 (3)	B(4)—C(8)—C(81)	120.6 (3)
B(2)—B(1)—B(6)	59.2 (3)	C(7)—C(8)—C(81)	118.6 (3)
B(3)—B(1)—B(4)	59.5 (3)	B(9)—C(8)—C(81)	118.4 (3)
B(4)—B(1)—B(5)	58.9 (3)	B(4)—B(9)—B(5)	58.1 (3)
B(5)—B(1)—B(6)	61.1 (3)	B(4)—B(9)—C(8)	59.2 (3)
B(1)—B(2)—B(3)	59.4 (3)	B(5)—B(9)—B(10)	59.5 (3)
B(1)—B(2)—B(6)	61.4 (3)	B(5)—B(10)—B(6)	61.4 (3)
B(3)—B(2)—C(7)	61.1 (3)	B(5)—B(10)—B(9)	58.5 (3)
B(6)—B(2)—B(11)	59.3 (3)	B(6)—B(10)—B(11)	58.9 (3)
C(7)—B(2)—B(11)	55.6 (3)	B(2)—B(11)—B(6)	60.0 (3)
B(1)—B(3)—B(2)	61.0 (3)	B(2)—B(11)—C(7)	60.3 (3)
B(1)—B(3)—B(4)	60.5 (3)	B(6)—B(11)—B(10)	59.8 (3)
B(2)—B(3)—C(7)	58.8 (3)	C(7)—C(71)—C(72)	123.4 (4)
B(4)—B(3)—C(8)	59.0 (3)	C(7)—C(71)—C(76)	119.3 (4)
C(7)—B(3)—C(8)	54.2 (3)	C(72)—C(71)—C(76)	117.2 (4)
B(1)—B(4)—B(3)	60.0 (3)	C(71)—C(72)—C(73)	121.6 (5)
B(1)—B(4)—B(5)	61.4 (3)	C(72)—C(73)—C(74)	120.2 (6)
B(3)—B(4)—C(8)	60.6 (3)	C(73)—C(74)—C(75)	118.7 (6)
B(5)—B(4)—B(9)	60.3 (3)	C(74)—C(75)—C(76)	120.7 (6)
C(8)—B(4)—B(9)	55.7 (3)	C(71)—C(76)—C(75)	121.6 (5)
B(1)—B(5)—B(4)	59.6 (3)	C(8)—C(81)—C(82)	123.0 (4)
B(1)—B(5)—B(6)	60.1 (3)	C(8)—C(81)—C(86)	118.8 (4)
B(4)—B(5)—B(9)	61.7 (3)	C(82)—C(81)—C(86)	118.1 (4)
B(6)—B(5)—B(10)	58.6 (3)	C(81)—C(82)—C(83)	120.7 (4)
B(9)—B(5)—B(10)	62.0 (3)	C(82)—C(83)—C(84)	120.8 (5)
B(1)—B(6)—B(2)	59.4 (3)	C(83)—C(84)—C(85)	118.9 (5)
B(1)—B(6)—B(5)	58.8 (3)	C(84)—C(85)—C(86)	120.6 (5)
B(2)—B(6)—B(11)	60.7 (3)	C(81)—C(86)—C(85)	120.8 (4)
B(5)—B(6)—B(10)	60.0 (3)	C(11*A*)—N—C(21*A*)	111.5 (9)
B(10)—B(6)—B(11)	61.3 (3)	C(11*A*)—N—C(31*A*)	108.2 (12)
B(2)—C(7)—B(3)	60.1 (3)	C(11*B*)—N—C(21*B*)	113.3 (14)
B(2)—C(7)—B(11)	64.1 (3)	C(11*B*)—N—C(31*B*)	102.8 (9)
B(2)—C(7)—C(71)	120.6 (3)	C(21*B*)—N—C(31*B*)	131.7 (15)
B(3)—C(7)—C(8)	62.0 (3)	C(21*A*)—N—C(31*A*)	104.1 (12)
B(3)—C(7)—C(71)	118.8 (3)	N—C(11*A*)—C(12)	114.0 (10)
C(8)—C(7)—C(71)	118.6 (3)	N—C(11*B*)—C(12)	103.7 (10)
B(11)—C(7)—C(71)	118.1 (4)	N—C(21*B*)—C(22*B*)	104.3 (21)
B(3)—C(8)—B(4)	60.4 (3)	N—C(21*A*)—C(22*A*)	106.8 (10)
B(3)—C(8)—C(7)	63.7 (3)	N—C(31*A*)—C(32*A*)	115.1 (20)
B(3)—C(8)—C(81)	117.6 (3)	N—C(31*B*)—C(32*B*)	99.8 (13)
B(4)—C(8)—B(9)	65.1 (3)		

parameters, and Table 2 details internuclear distances not involving H atoms and selected interbond angles thereby derived for the $[HNEt_3]^+$ salt. Equivalent information for the $[Me_3NCH_2C_6H_5]^+$ salt is contained in Tables 3 and 4, respectively. Fig. 1 shows a perspective view of a single molecule of the anion (that actually plotted is the $[HNEt_3]^+$ salt, but the anion in both determinations appears practically identical) and gives the atomic numbering scheme. Note that H(*endo*) appears as H(12) in the determination of the $[HNEt_3]^+$ salt and H(10*B*) in the determination of the $[Me_3NCH_2C_6H_5]^+$ salt.

These structural studies confirm the identity of the anion as $[7,8\text{-}Ph_2\text{-}7,8\text{-}nido\text{-}C_2B_9H_{10}]^-$. As expected (Wade, 1971), the anion geometry is that of a *nido* fragment of an icosahedron. In both determinations the anion suffers partial disorder, manifested by the appearance of electron density (0.64 e $Å^{-3}$ in the case of the $[HNEt_3]^+$ salt; 0.94 e $Å^{-3}$ in the case of the $[Me_3NCH_2C_6H_5]^+$ salt) in the 12th icosahedral position. As each of the anion's phenyl substituents appear ordered it is likely that in both cases this residual electron density arises from incomplete occupation of the B(3) cage position, but the degree of disorder is clearly small and in neither case is the refined U_{eq} value of B(3) anomalously large when this atom is refined with full occupancy. Most of the triethylammonium cation is also disordered.

The anions have near C_s symmetry about a plane passing through B(1), B(3) and B(10). The lower pentagonal rings [B(2), B(3), B(4), B(5), B(6)] are essentially planar [$\sigma = 0.003$ and 0.016 Å for $[HNEt_3]^+$ and $[Me_3NCH_2C_6H_5]^+$ salts, respectively $[\sigma = (\sum z_i^2)^{1/2}$, where z_i is the displacement of the ith atom from the least-squares plane]}, but the upper C_2B_3 rings are not ($\sigma = 0.049$ and 0.050 Å, respectively), each being folded into an envelope conformation. In the case of the $[HNEt_3]^+$ salt, this fold (4.4°)

Table 3. *Fractional coordinates and equivalent isotropic thermal parameters* ($Å^2$) *for non-*H *atoms in* $[(CH_3)_3NCH_2Ph][7,8\text{-}Ph_2\text{-}7,8\text{-}nido\text{-}C_2B_9H_{10}]$

$U_{eq} = (1/3)\sum_i \sum_j U_{ij} a_i^* a_j^* \mathbf{a}_i . \mathbf{a}_j$.

	x	y	z	U_{eq}
B(1)	0.5435 (3)	−0.68272 (14)	−0.30457 (22)	0.0367 (15)
B(2)	0.54174 (25)	−0.60240 (13)	−0.27735 (22)	0.0343 (14)
B(3)	0.3969 (3)	−0.63991 (14)	−0.35050 (25)	0.0424 (17)
B(4)	0.39660 (25)	−0.71428 (12)	−0.28893 (23)	0.0342 (14)
B(5)	0.54012 (24)	−0.72280 (13)	−0.17422 (22)	0.0343 (14)
B(6)	0.63337 (25)	−0.65163 (13)	−0.16668 (23)	0.0356 (15)
C(7)	0.40440 (20)	−0.59031 (10)	−0.23629 (18)	0.0277 (12)
C(8)	0.32363 (20)	−0.65294 (10)	−0.24159 (18)	0.0276 (12)
B(9)	0.39669 (24)	−0.70195 (12)	−0.14091 (22)	0.0324 (14)
B(10)	0.54984 (24)	−0.66878 (13)	−0.06127 (22)	0.0327 (14)
B(11)	0.53948 (25)	−0.59203 (12)	−0.12985 (22)	0.0334 (14)
C(71)	0.32655 (21)	−0.53165 (10)	−0.26517 (19)	0.0316 (12)
C(72)	0.2476 (3)	−0.51717 (12)	−0.37649 (22)	0.0436 (15)
C(73)	0.1721 (3)	−0.46427 (14)	−0.3961 (3)	0.0516 (17)
C(74)	0.1727 (3)	−0.42440 (13)	−0.3068 (3)	0.0526 (18)
C(75)	0.25170 (25)	−0.43740 (13)	−0.1963 (3)	0.0469 (16)
C(76)	0.32641 (23)	−0.49036 (11)	−0.17596 (22)	0.0367 (14)
C(81)	0.17885 (20)	−0.64790 (10)	−0.27410 (18)	0.0278 (11)
C(82)	0.09892 (23)	−0.66809 (11)	−0.38085 (21)	0.0363 (13)
C(83)	−0.03526 (23)	−0.66437 (12)	−0.40560 (23)	0.0414 (15)
C(84)	−0.09154 (24)	−0.64015 (13)	−0.3252 (3)	0.0474 (16)
C(85)	−0.01311 (23)	−0.61965 (12)	−0.21893 (24)	0.0434 (15)
C(86)	0.12052 (21)	−0.62343 (11)	−0.19342 (22)	0.0350 (13)
N	−0.02785 (17)	−0.82683 (9)	−0.18356 (16)	0.0327 (11)
C(1)	0.0961 (3)	−0.79193 (14)	−0.1679 (3)	0.0498 (17)
C(2)	−0.1174 (3)	−0.78885 (13)	−0.13586 (23)	0.0422 (15)
C(3)	0.0022 (3)	−0.88648 (12)	−0.11812 (25)	0.0426 (15)
C(4)	−0.08716 (25)	−0.83870 (13)	−0.31385 (20)	0.0411 (15)
C(41)	−0.21154 (24)	−0.87444 (12)	−0.34244 (21)	0.0402 (14)
C(42)	−0.3309 (3)	−0.84562 (15)	−0.36198 (25)	0.0512 (17)
C(43)	−0.4436 (3)	−0.87970 (18)	−0.3839 (3)	0.0662 (22)
C(44)	−0.4363 (3)	−0.94263 (20)	−0.3873 (4)	0.082 (3)
C(45)	−0.3207 (3)	−0.97157 (17)	−0.3727 (4)	0.0785 (25)
C(46)	−0.2090 (3)	−0.93769 (14)	−0.3493 (3)	0.0571 (19)

Table 4. *Interatomic distances* (Å) *and interbond angles* (°) *in* $[(CH_3)_3NCH_2Ph][7,8\text{-}Ph_2\text{-}7,8\text{-}nido\text{-}C_2B_9H_{10}]$

B(1)—B(2)	1.771 (4)	B(9)—B(10)	1.800 (4)
B(1)—B(3)	1.775 (4)	B(10)—B(11)	1.843 (4)
B(1)—B(4)	1.779 (4)	C(71)—C(72)	1.396 (4)
B(1)—B(5)	1.795 (4)	C(71)—C(76)	1.393 (3)
B(1)—B(6)	1.789 (4)	C(72)—C(73)	1.385 (4)
B(2)—B(3)	1.753 (4)	C(73)—C(74)	1.373 (4)
B(2)—B(6)	1.765 (4)	C(74)—C(75)	1.381 (4)
B(2)—C(7)	1.704 (4)	C(75)—C(76)	1.381 (4)
B(2)—B(11)	1.787 (4)	C(81)—C(82)	1.391 (3)
B(3)—B(4)	1.772 (4)	C(81)—C(86)	1.398 (3)
B(3)—C(7)	1.722 (4)	C(82)—C(83)	1.390 (4)
B(3)—C(8)	1.728 (4)	C(83)—C(84)	1.378 (4)
B(4)—B(5)	1.758 (4)	C(84)—C(85)	1.383 (4)
B(4)—C(8)	1.719 (3)	C(85)—C(86)	1.383 (4)
B(4)—B(9)	1.792 (4)	N—C(1)	1.497 (4)
B(5)—B(6)	1.827 (4)	N—C(2)	1.498 (3)
B(5)—B(9)	1.758 (4)	N—C(3)	1.497 (3)
B(5)—B(10)	1.768 (4)	N—C(4)	1.529 (3)
B(6)—B(10)	1.784 (4)	C(4)—C(41)	1.497 (4)
B(6)—B(11)	1.770 (4)	C(41)—C(42)	1.386 (4)
C(7)—C(8)	1.602 (3)	C(41)—C(46)	1.373 (4)
C(7)—B(11)	1.636 (3)	C(42)—C(43)	1.378 (5)
C(7)—C(71)	1.506 (3)	C(43)—C(44)	1.366 (5)
C(8)—B(9)	1.630 (3)	C(44)—C(45)	1.358 (6)
C(8)—C(81)	1.497 (3)	C(45)—C(46)	1.365 (5)

B(2)—B(1)—B(3)	59.25 (16)	C(7)—C(8)—C(81)	117.40 (18)
B(2)—B(1)—B(6)	59.46 (15)	B(9)—C(8)—C(81)	119.05 (18)
B(3)—B(1)—B(4)	59.80 (16)	B(4)—B(9)—B(5)	59.35 (15)
B(4)—B(1)—B(5)	58.92 (15)	B(4)—B(9)—C(8)	60.10 (14)
B(5)—B(1)—B(6)	61.28 (15)	B(5)—B(9)—B(10)	59.60 (15)
B(1)—B(2)—B(3)	60.49 (16)	B(5)—B(10)—B(6)	61.88 (15)
B(1)—B(2)—B(6)	60.79 (16)	B(5)—B(10)—B(9)	59.03 (15)
B(3)—B(2)—C(7)	59.75 (15)	B(6)—B(10)—B(11)	58.39 (15)
B(6)—B(2)—B(11)	59.76 (15)	B(2)—B(11)—B(6)	59.51 (15)
C(7)—B(2)—B(11)	55.83 (14)	B(2)—B(11)—C(7)	59.52 (14)
B(1)—B(3)—B(2)	60.26 (16)	B(6)—B(11)—B(10)	59.15 (15)
B(1)—B(3)—B(4)	60.21 (16)	C(7)—C(71)—C(72)	123.71 (21)
B(2)—B(3)—C(7)	58.72 (15)	C(7)—C(71)—C(76)	119.18 (20)
B(4)—B(3)—C(8)	58.82 (15)	C(72)—C(71)—C(76)	117.02 (22)
C(7)—B(3)—C(8)	55.32 (14)	C(71)—C(72)—C(73)	121.00 (25)
B(1)—B(4)—B(3)	59.99 (16)	C(72)—C(73)—C(74)	121.0 (3)
B(1)—B(4)—B(5)	61.00 (15)	C(73)—C(74)—C(75)	118.9 (3)
B(3)—B(4)—C(8)	59.33 (15)	C(74)—C(75)—C(76)	120.4 (3)
B(5)—B(4)—B(9)	59.37 (15)	C(71)—C(76)—C(75)	121.69 (23)
C(8)—B(4)—B(9)	55.26 (14)	C(8)—C(81)—C(82)	122.65 (20)
B(1)—B(5)—B(4)	60.08 (15)	C(8)—C(81)—C(86)	119.11 (20)
B(1)—B(5)—B(6)	59.20 (15)	C(82)—C(81)—C(86)	118.22 (21)
B(4)—B(5)—B(9)	61.28 (15)	C(81)—C(82)—C(83)	120.59 (22)
B(6)—B(5)—B(10)	59.49 (15)	C(82)—C(83)—C(84)	120.60 (24)
B(9)—B(5)—B(10)	61.37 (15)	C(83)—C(84)—C(85)	119.4 (3)
B(1)—B(6)—B(2)	59.75 (15)	C(84)—C(85)—C(86)	120.39 (25)
B(1)—B(6)—B(5)	59.52 (15)	C(81)—C(86)—C(85)	120.83 (22)
B(2)—B(6)—B(11)	60.73 (15)	C(1)—N—C(2)	108.75 (20)
B(5)—B(6)—B(10)	58.63 (15)	C(1)—N—C(3)	108.60 (20)
B(10)—B(6)—B(11)	62.47 (15)	C(1)—N—C(4)	108.02 (19)
B(2)—C(7)—B(3)	61.53 (16)	C(2)—N—C(3)	109.90 (19)
B(2)—C(7)—B(11)	64.65 (15)	C(2)—N—C(4)	110.80 (19)
B(2)—C(7)—C(71)	122.25 (18)	C(3)—N—C(4)	110.70 (19)
B(3)—C(7)—C(8)	62.52 (15)	N—C(4)—C(41)	113.89 (21)
B(3)—C(7)—C(71)	116.54 (19)	C(4)—C(41)—C(42)	121.96 (24)
C(8)—C(7)—C(71)	116.47 (18)	C(4)—C(41)—C(46)	119.86 (24)
B(11)—C(7)—C(71)	120.62 (19)	C(42)—C(41)—C(46)	118.2 (3)
B(3)—C(8)—B(4)	61.85 (15)	C(41)—C(42)—C(43)	120.8 (3)
B(3)—C(8)—C(7)	62.16 (15)	C(42)—C(43)—C(44)	119.0 (3)
B(3)—C(8)—C(81)	117.13 (19)	C(43)—C(44)—C(45)	121.0 (4)
B(4)—C(8)—B(9)	64.64 (15)	C(44)—C(45)—C(46)	119.8 (4)
B(4)—C(8)—C(81)	120.61 (18)	C(41)—C(46)—C(45)	121.2 (3)

is convex about the C(8)···B(10) vector, whereas for the $[Me_3NCH_2C_6H_5]^+$ salt the fold (4.2°) is concave about the B(9)···B(11) vector. However, these structural differences are slight, as is demonstrated by the calculation of an overall root-mean-square misfit (Macgregor, Wynd, Gould, Moulden, Taylor, Yellowlees & Welch, 1991) of only 0.024 Å between the C_2B_9 portions of both anions.

The major deviation form C_s symmetry of the anions in the solid state, indeed the major structural difference between the anions in the two crystallographic determinations, resides in the twists of the phenyl substituents about their C(cage)—C(aryl) bonds. As previously noted (Lewis & Welch, 1993*a*), it is convenient to describe these twists by the parameter θ. In both salts of $[7,8\text{-}Ph_2\text{-}7,8\text{-}nido\text{-}C_2B_9H_{10}]^-$ studied herein, θ values are generally low, so that in a broad sense both phenyl groups can be described as lying essentially orthogonal to the open C_2B_3 carbaborane face. In detail, however, both phenyl rings in each salt are measurably twisted from this extreme position in a conrotatory manner, recording θ values of 5.6 [ring C(71)–C(76)] and 10.0° [ring C(81)–C(86)] in the $[HNEt_3]^+$ salt, and 17.9 [C(71)–C(76)] and 20.0° [C(81)–C(86)] in the $[Me_3NCH_2C_6H_5]^+$ salt. Molecular-orbital (MO) calculations at the extended Hückel level on 1,2-Ph_2-1,2-*closo*-$C_2B_{10}H_{10}$ (Lewis & Welch, 1993*a*) imply that the energies required for twists of these magnitudes are well within the range of crystal packing forces, and it may be significant in this respect that, in the crystal of the $[Me_3NCH_2C_6H_5]^+$ salt, ring C(81)–C(86) is proximal to the C(1)H_3 methyl group of the cation [shortest contacts H(14)···C(81) 2.75 (3), H(14)···C(82) 2.84 (3), H(14)···C(86) 2.82 (3) Å]. Were these contacts to be responsible for the twist of the C(81)–

C(86) ring it would be likely that the C(71)–C(76) ring would twist in the same sense by roughly the same amount as a consequence of interphenyl intramolecular crowding. In the following paper (Lewis & Welch, 1993*b*), a further example of this structural cooperation between the adjacent phenyl rings of carbaboranes is described.

Inclusion of one or both phenyl rings in the misfit calculations has the expected results; the $\{C_2B_{10}$[C(81)–C(86)]$\}$ fragments have an r.m.s. misfit of 0.086 Å and the $\{C_2B_{10}$[C(71)–C(76)]$\}$ fragments an r.m.s. misfit of 0.160 Å, the greatest individual misfits occurring for the *ortho* and *meta* C atoms. For $\{C_2B_{10}[C_6]_2\}$ fragments the r.m.s. misfit is 0.184 Å.

The C(7)—C(8) distance, 1.590 (5) Å in the $[HNEt_3]^+$ salt and 1.602 (3) Å in the $[Me_3NCH_2C_6H_5]^+$ salt, is substantially less than the C(cage)—C(cage) distance in 1,2-Ph_2-1,2-*closo*-$C_2B_{10}H_{10}$ (Lewis & Welch, 1993*a*). This is an important result since it shows that aryl-bearing cage C atoms can approach to within reasonably short distances [for comparison, C—C in [7,8-*nido*-$C_2B_9H_{12}]^-$ is 1.542 (4) Å (Buchanan, Hamilton, Reed & Welch, 1990)] and it supports the conclusion (Lewis & Welch, 1993*a*) that there is an electronic contribution to the long C(cage)—C(cage) connectivity in 1,2-Ph_2-1,2-*closo*-$C_2B_{10}H_{10}$ at low θ values. In fact, the change in the C(cage)—C(cage) length is only one of three measurable structural differences between 1,2-Ph_2-1,2-*closo*-$C_2B_{10}H_{10}$ and [7,8-Ph_2-7,8-*nido*-$C_2B_9H_{10}]^-$, the others being ⟨facial B—B⟩ and ⟨facial B—C⟩, where facial refers to the open C_2B_3 face of the *nido* polyhedron as a capping $\{BH\}^{2+}$ fragment is replaced by an *endo* [to B(10)] proton. Table 5 summarizes the relevant parameters and shows that from 1,2-Ph_2-1,2-*closo*-$C_2B_{10}H_{10}$ to [7,8-Ph_2-7,8-*nido*-$C_2B_9H_{10}]^-$, ⟨facial B—B⟩ lengthens, ⟨facial B—C⟩ shortens and, as previously noted, C—C shortens.

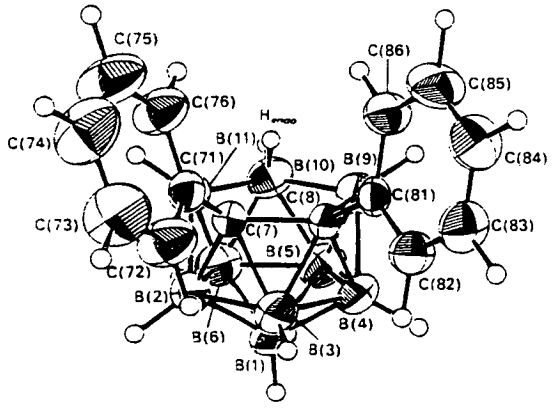

Fig. 1. Perspective view of [7,8-Ph_2-7,8-*nido*-$C_2B_9H_{10}]^-$ ($[HNEt_3]^+$ salt, 50% thermal ellipsoids, except for H atoms which have artificial radii of 0.1 Å for clarity).

Table 5. *Comparison of key molecular parameters* (Å) *in* 1,2-Ph_2-1,2-*closo*-$C_2B_{10}H_{10}$ *and* [7,8-Ph_2-7,8-*nido*-$C_2B_9H_{10}]^-$

	1,2-Ph_2-1,2-*closo*-$C_2B_{10}H_{10}$	[7,8-Ph_2-7,8-*nido*-$C_2B_9H_{10}]^-$
⟨Facial B—B⟩	1.767 (8)[a,g]	1.819 (25)[a,g]
⟨Facial B—C⟩	1.710 (5)[b,g]	1.634 (3)[e,g]
⟨C—C⟩	1.727 (4)[c,g]	1.596 (4)[f,g]

Notes: (*a*) average of 8 measurements over 2 molecules, range 1.754 (6)–1.781 (6) Å; (*b*) average of 4 measurements over 2 molecules, range 1.795 (8)–1.843 (4) Å; (*c*) 8 measurements, 1.700 (5)–1.715 (5) Å; (*d*) 4 measurements, 1.630 (3)–1.638 (7) Å; (*e*) 2 measurements, 1.720 (4) and 1.733 (4) Å; (*f*) 2 measurements, 1.590 (5) and 1.602 (3) Å; (*g*) e.s.d. of mean from (e.s.d.)$^2 = [\Sigma(\kappa_i - \kappa_{bar})^2]/(N - 1)$ where κ_i is the ith e.s.d. and κ_{bar} the mean of N similar types; (*h*) e.s.d. of mean is mean e.s.d.

These changes are fully analogous to those previously identified in the comparison of [3-PPh_3-3,1,2-*closo*-$CuC_2B_9H_{11}]^-$ (Do, Kang, Knobler & Hawthorne, 1987) and [7,8-*nido*-$C_2B_9H_{12}]^-$ (Buchanan, Hamilton, Reed & Welch, 1990), and have been traced (Hamilton & Welch, 1990) to differing degrees of depopulation of the filled π MO's of $[7,8\text{-}nido\text{-}C_2B_9H_{11}]^{2-}$ by zero-electron three-orbital ($\{R_3PCu\}^+$ or $\{BH\}^{2+}$) and zero-electron one-orbital (H^+) units.

We thank the University of Edinburgh for support in the form of a Demonstratorship and Watt Studentship (JC) and a Dewar Research Studentship (NLD), and the Callery Chemical Company for a generous gift of $B_{10}H_{14}$.

References

BUCHANAN, J., HAMILTON, E. J. M., REED, D. & WELCH, A. J. (1990). *J. Chem. Soc. Dalton Trans.* pp. 677–680.

CASEY, J. B., EVANS, W. J. & POWELL, W. H. (1983). *Inorg. Chem.* **22**, 2228–2235.

DO, Y., KANG, H. C., KNOBLER, C. B. & HAWTHORNE, M. F. (1987). *Inorg. Chem.* **26**, 2348–2350.

GOULD, R. O. & SMITH, D. E. (1986). *CADABS*. Program for data reduction. Univ. of Edinburgh, Scotland.

GOULD, R. O. & TAYLOR, P. (1986). *CALC*. Program for crystallographic calculations. Univ. of Edinburgh, Scotland.

HAMILTON, E. J. M. & WELCH, A. J. (1990). *Polyhedron*, **9**, 2407–2412.

HAWTHORNE, M. F., YOUNG, D. C., GARRETT, P. M., OWEN, D. A., SCHWERIN, S. G., TEBBE, F. N. & WEGNER, P. A. (1968). *J. Am. Chem. Soc.* **90**, 862–868.

LEWIS, Z. G. & WELCH, A. J. (1992). *J. Organomet. Chem.* **430**, C45–C50.

LEWIS, Z. G. & WELCH, A. J. (1993*a*). *Acta Cryst.* C**49**, 705–710.

LEWIS, Z. G. & WELCH, A. J. (1993*b*). *Acta Cryst.* C**49**, 715–718.

MACGREGOR, S. A., WYND, A. J., GOULD, R. O., MOULDEN, N., TAYLOR, P., YELLOWLEES, L. J. & WELCH, A. J. (1991). *J. Chem. Soc. Dalton Trans.* pp. 3317–3324.

MALLINSON, P. & MUIR, K. W. (1985). *J. Appl. Cryst.* **18**, 51–53.

SHAW, K. F. & WELCH, A. J. (1992). *Polyhedron*, **11**, 157–167.

SHELDRICK, G. M. (1976). *SHELX76*. Program for crystal structure determination. Univ. of Cambridge, England.

SHELDRICK, G. M. (1986). *SHELXS86*. Program for the solution of crystal structures. Univ. of Göttingen, Germany.

WADE, K. (1971). *J. Chem. Soc. Chem. Commun.* pp. 792–793.

Pergamon

0277-5387(94)00485-4

Polyhedron Vol. 14, No. 7, pp. 961-965, 1995
Elsevier Science Ltd
Printed in Great Britain
0277-5387/95 $9.50+0.00

COMMUNICATION

THE APPLICATION OF TOCSY TO BORON CHEMISTRY

DAVID J. DONOHOE, DAVID REED* and ALAN J. WELCH

Department of Chemistry, University of Edinburgh, West Mains Road, Edinburgh EH9 3JJ, U.K.

(*Received* 30 *September* 1994; *accepted* 21 *November* 1994)

Abstract—The use of the two-dimensional TOCSY experiment in the NMR analysis of boron hydrides is demonstrated. Both the ^{11}B and the ^{1}H nuclei have been shown to provide potentially useful results with this technique. The results are compared with those obtained using the well established COSY experiments.

During the last decade the use of two-dimensional techniques in the NMR analysis of boron compounds has progressed rapidly, to the point where such experiments are applied routinely in many laboratories. Both homonuclear ($^{11}B/^{11}B$ and $^{1}H/^{1}H$ COSY) and heteronuclear ($^{11}B/^{1}H$ HETCOR) correlation experiments have been applied successfully to such systems, though there are limitations imposed by the efficient nature of the relaxation of the boron nuclei.[1,2] In general, it has been observed that ^{11}B homonuclear COSY experiments only show correlations (cross peaks) between adjacent boron nuclei, with ^{1}H COSY experiments yielding cross peaks primarily between H nuclei separated by three bonds, though longer range connectivities can be detected. One major problem with ^{11}B COSY experiments is that often cross peaks that would be expected to show are not observed.[1-3] For ^{1}H COSY experiments, possible difficulties are incomplete ^{11}B decoupling, and a narrow chemical shift range for ^{1}H, leading to a high possibility of signal overlap.[4]

In an effort to extend the range of techniques available, the use of the TOCSY (Total Correlation Spectroscopy) sequence in the study of such systems was investigated, looking at results from both the ^{11}B and ^{1}H nuclei. The TOCSY sequence has already been widely used in ^{1}H NMR analyses, particularly in the study of polypeptides/proteins, and is designed to show cross peaks linking all the members of a given spin system.[5] Thus it would be expected that all the proton signals arising from a particular amino acid in a peptide sequence would be correlated to one another. Extending this approach to boranes, one would expect all the ^{11}B signals deriving from a specific borane cluster to exhibit cross peaks to each other in an ^{11}B TOCSY experiment, and similarly all the ^{1}H signals in a ^{1}H TOCSY experiment.

RESULTS AND DISCUSSION

The ^{11}B TOCSY experiment has been performed on both the *closo*-carbaborane 1-Ph-1,2-$C_2B_{10}H_{11}$ and the *nido*-selenaborane 7,9-$Se_2B_9H_9$, the structures of which are shown in Fig. 1, and the results compared with corresponding ^{11}B COSY experiments as shown in Figs 2 (for the carbaborane) and 3 (for the selenaborane). The full analyses of the ^{11}B and ^{1}H spectra of these compounds are reported elsewhere,[3,6] with the results of these assignments being used here to help us to carry out the comparison between the COSY and TOCSY experiments. Tables 1 and 2 show the assignments for these compounds.

Comparison of the ^{11}B TOCSY and COSY results on the carbaborane (Fig. 2), highlight two major features which show up on examination of the spectra. Firstly, the TOCSY experiment shows cross peaks between all the different signals in the

* Author to whom correspondence should be addressed.

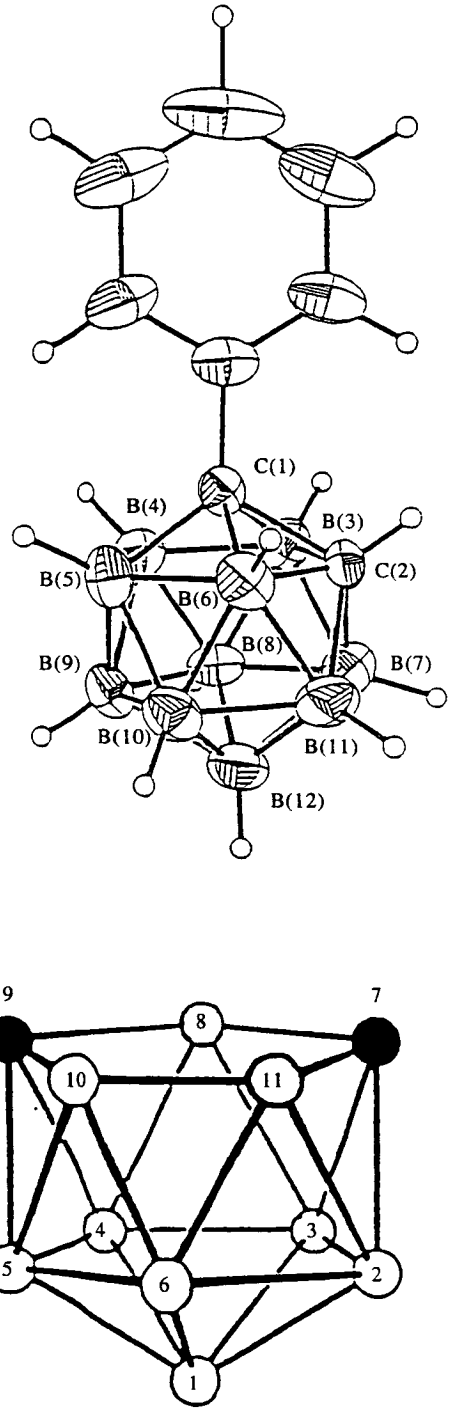

Fig. 1. The structures of *closo*-1-Ph-1,2-$C_2B_{10}H_{11}$ (top) and *nido*-7,9-$Se_2B_9H_9$ (bottom). The selenium atoms are indicated by the filled circles.

spectrum, whereas the COSY shows cross peaks only between signals arising from adjacent boron atoms, as alluded to earlier. The TOCSY experiment has, in this case, provided an ideal result, in that it has provided cross peaks for the complete spin system, for all the signals, in keeping with the

Table 1. Assignments for the ^{11}B and ^1H spectra of *closo*-1-Ph-1,2-$C_2B_{10}H_{11}$

B/H Site	$\delta(^{11}B)^a$	$\delta(^1H)^b$
9	−1.1	2.45
12	−3.4	2.36
8, 10	−7.9	2.36
4, 5	−9.7	2.54
3, 6	−10.2	2.62
7, 11	−11.8	2.30

[a] Chemical shifts of ^{11}B referenced to external $BF_3 \cdot OEt_2$ at 0 ppm.
[b] Chemical shifts of ^1H referenced to internal TMS at 0 ppm: $\delta(^1H)$ for cluster CH is 3.99 ppm.

Table 2. Assignments for the ^{11}B and ^1H spectra of *nido*-7,9-$Se_2B_9H_9$

B/H Site	$\delta(^{11}B)^a$	$\delta(^1H)^b$
6	2.1	3.68
2, 5	1.6	3.43
10, 11	−0.6	3.02
3, 4	−1.0	3.24
8	−8.6	2.64
1	−34.6	2.32

[a] Chemical shifts of ^{11}B referenced to external $BF_3 \cdot OEt_2$ at 0 ppm.
[b] Chemical shifts of ^1H referenced to internal TMS at 0 ppm.

results often obtained in proton NMR experiments. The second feature shown up by these experiments is that the cross peaks are more compact in the TOCSY experiment than in the COSY experiment. This is because TOCSY experiments are carried out in the phase sensitive mode, whilst COSY experiments on borane systems are carried out in the absolute value (magnitude) mode. Thus the TOCSY method gives rise to much better resolved two-dimensional results than the COSY techniques adopted for such systems.

The ^{11}B TOCSY experiment performed on the selenaborane produced results which were less comprehensive than those for the carbaborane, but which still extracted several additional correlations compared to the COSY experiment (Fig. 3). The COSY plot, which was used to elucidate the structure of the selenaborane previously,[3] nonetheless had several cross peaks missing which would be expected to show on the basis that adjacent borons are likely to be coupled: these "missing" cross peaks being those between signals B and C, and

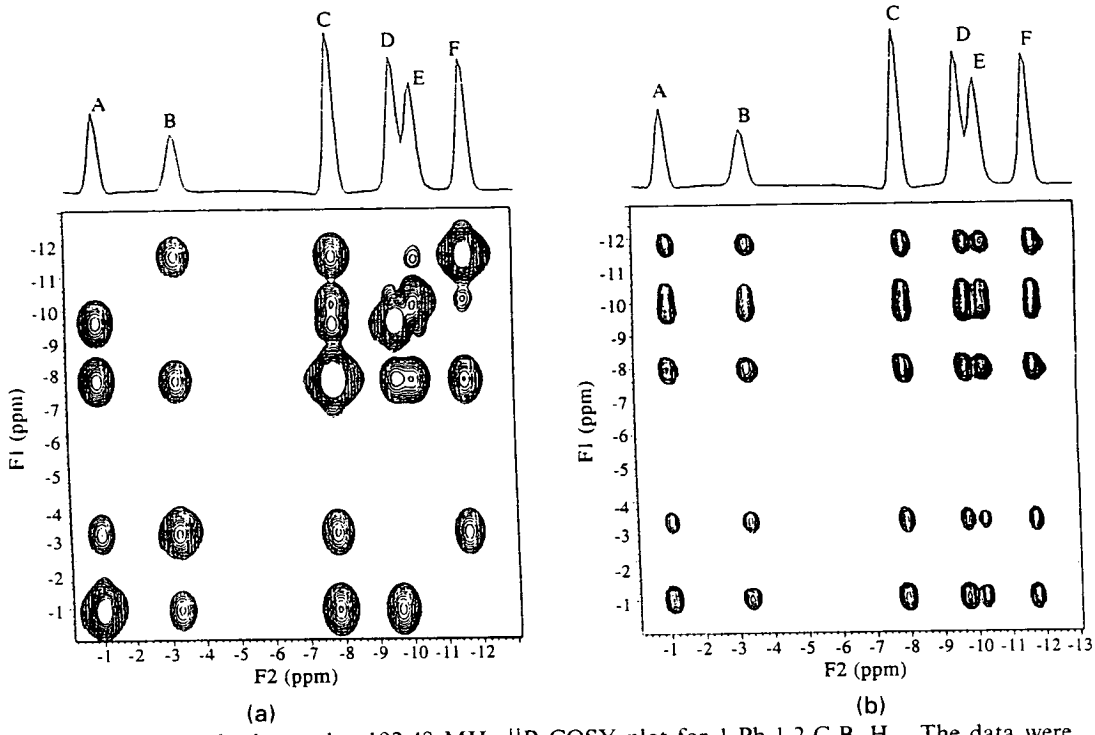

Fig. 2. (a) The absolute value 192.48 MHz ^{11}B COSY plot for 1-Ph-1,2-$C_2B_{10}H_{11}$. The data were acquired using a spectral width of 9363 Hz in both dimensions. There were 128 fids collected, each of 512 data points, which were zero filled to 1024 data points on Fourier transformation. The f1 dimension was also zero filled to 1024 data points. Proton decoupling was applied throughout the experiment. The 90° pulse was 45 μs, and a relaxation delay of 300 ms was used. Data processing involved pseudo echo multiplication in each dimension prior to Fourier transformation. (b) The 192.48 MHz ^{11}B TOCSY plot for 1-Ph-1,2-$C_2B_{10}H_{11}$. The data were acquired using the States–Haberkorn–Ruben method, with 128 t_1 increments. Each fid was of 576 data points and they were zero filled to 2048 points on Fourier transformation. The f1 dimension was zero filled to 1024 data points. Proton decoupling was applied throughout the experiment. The 90° pulse was 45 μs. and a relaxation delay of 300 ms was used. The spin lock mixing time employed was 20 ms.

signals B and D. The TOCSY experiment has brought out these cross peaks, and has also shown a number of other correlations which do not relate to adjacent boron nuclei, namely the cross peaks linking signals E and F, signals D and F, and signals A and D. Most importantly, signal F (from B(1)) displays cross peaks to all other signals in the spectrum, consistent with the signals all deriving from a single spin system.

The two examples discussed thus far highlight some of the types of information that can be obtained using ^{11}B TOCSY experiments. It is clear however that the selenaborane has produced a rather less complete result than did the carbaborane. Possible reasons for this are:

(i) The spectrum width is much larger for the selenaborane, and this will result in the signals at the outside edges of the spectrum receiving pulses which are less than specified in the sequence.

(ii) The COSY experiment for the carbaborane contained all the expected cross peaks, whereas that for the selenaborane did not. It was not surprising therefore to get similar behaviour from the TOCSY.

To further look into TOCSY as a mode of study of boranes, the ^{1}H nucleus was also used, and Fig. 4 shows the comparison between the TOCSY and COSY results for *nido*-7,9-$Se_2B_9H_9$. The COSY experiment shows all the cross peaks arising from ^3J(H,H), and also some correlations from longer range couplings, as evidenced by cross peaks between signals A and E, and between signals C and D. The TOCSY experiment yielded results which showed all the ^{1}H resonances in the spectrum displaying cross peaks to all the others, confirming the potential of this experimental technique for these systems. Again the cross peak areas are much smaller in this experiment than in the corresponding COSY, due to the phase sensitive nature of TOCSY.

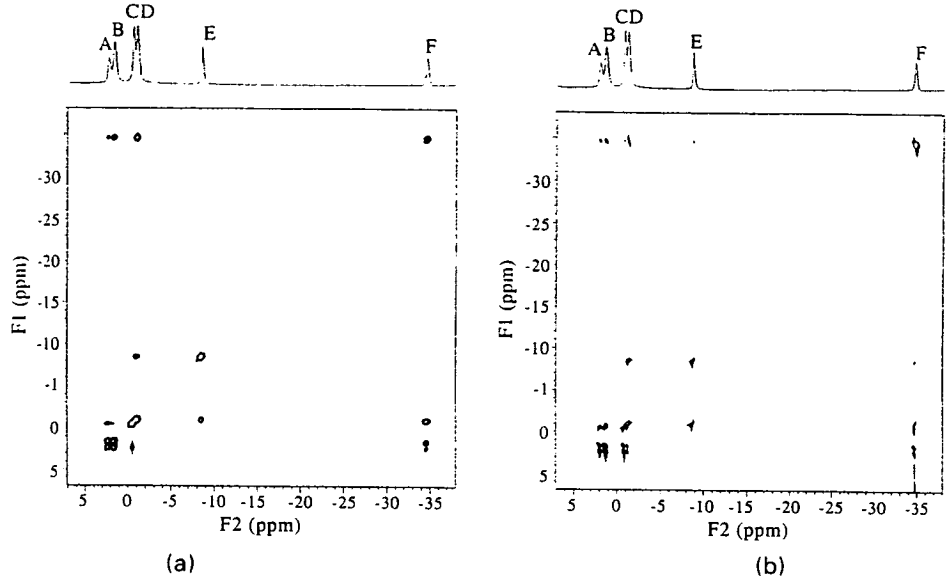

Fig. 3. (a) The absolute value 192.48 MHz ^{11}B COSY plot for 7,9-$Se_2B_9H_9$. The data were acquired using a spectral width of 10,500 Hz in both dimensions. There were 512 fids collected, each of 1280 data points, which were zero filled to 2048 data points on Fourier transformation. The f1 dimension was zero filled to 2048 data points. Proton decoupling was applied throughout the experiment. Data processing involved pseudo-echo multiplication in each dimension prior to Fourier transformation. (b) The 192.48 MHz ^{11}B TOCSY plot for 7,9-$Se_2B_9H_9$. The data were acquired using a spectral width of 10,500 Hz in both dimensions, using the States–Haberkorn–Ruben method, with 256 t_1 increments. Each fid was of 1280 data points, which were zero filled to 2048 data points on Fourier transformation. The f1 dimension was zero filled to 2048 data points. Proton decoupling was applied throughout the experiment. The 90° pulse was 43 μs, and a relaxation delay of 300 ms was used. The spin lock mixing time employed was 30 ms.

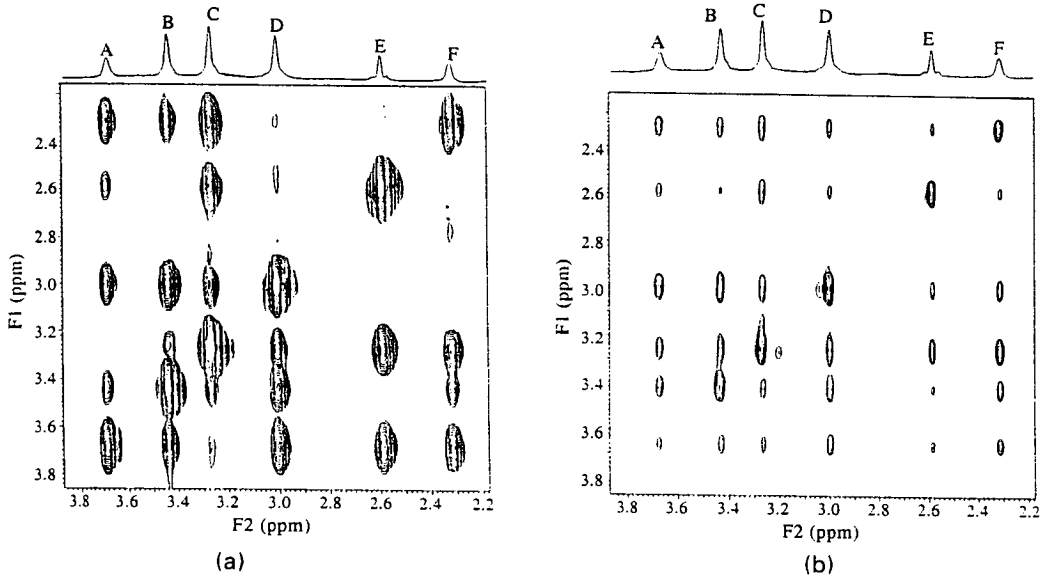

Fig. 4. (a) The absolute value 600 MHz ^{1}H COSY plot for 7,9-$Se_2B_9H_9$. The data were acquired using a spectral width of 4000 Hz in both dimensions. Each fid was of 1024 data points, which were zero filled to 2048 data points on Fourier transformation. The f1 dimension was zero filled to 512 data points. ^{11}B decoupling was applied throughout the experiment. The 90° pulse was 31.7 μs, and a relaxation delay of 1.5 s was used. Data processing involved pseudo-echo multiplication in each dimension prior to Fourier transformation. (b) The 600 MHz ^{1}H TOCSY plot for 7,9-$Se_2B_9H_9$. The data were acquired using a spectral width of 4000 Hz in both dimensions, using the States–Haberkorn–Ruben method, with 128 t_1 increments. Each fid was of 1024 data points, which were zero filled to 2048 data points on Fourier transformation. The f1 dimension was zero filled to 1024 data points. ^{11}B decoupling was applied throughout the experiment. The 90° pulse was 31.7 μs, and a relaxation delay of 1.5 s was used. The spin lock mixing time employed was 50 ms.

CONCLUSIONS

It has been shown that the TOCSY experiment can be successfully applied to boron hydride derivatives, using either ^{11}B and ^{1}H as the observe nuclei. It is likely that the use of ^{11}B as the observe nucleus may be inhibited by its relaxation properties and, in some instances, by its wide chemical shift range, whereas the most probable limiting factors in the use of ^{1}H are likely to be its relatively narrow chemical shift range (with the consequent signal overlap that may result) and the difficulties in getting complete ^{11}B decoupling, though the latter problem is somewhat offset by improvements in decoupling techniques (e.g. GARP[7] etc.). These problems are, of course, equally evident for the COSY experiments. It is most likely that TOCSY will find most use in supplementing results using the COSY sequence, along with heteronuclear correlation experiments. It is also likely that more complex systems (e.g. those with more than one borane cage) will be more readily studied as a result of the increased degree of resolution afforded by this technique. Further investigations are currently in progress to examine the potentials of the various correlation techniques across a wide range of systems containing borane clusters.

Acknowledgement—We wish to thank the EPSRC for the provision of the Ultra High Field NMR facility.

REFERENCES

1. D. Reed, *Chem. Soc. Rev.* 1993, **22**, 109.
2. S. Hermanek, *Chem. Rev.* 1992, **92**, 325.
3. O. Ni Dhubhghaill, D. Reed and T. R. Spalding, *Polyhedron* 1993, **12**, 1977; D. Reed, G. Ferguson, B. L. Ruhl, O. Ni Dhubhghaill and T. R. Spalding, *Polyhedron* 1988, **7**, 117.
4. X. L. R. Fontaine and J. D. Kennedy, *J. Chem. Soc., Chem. Commun.* 1986, 779.
5. L. Braunschweiler and R. R. Ernst, *J. Magn. Reson.* 1983, **53**, 521; A. Bax and D. G. Davis, *J. Magn. Reson.* 1985, **65**, 355.
6. P. T. Brain, D. J. Donohoe, D. Hynk, M. Buhl, D. W. H. Rankin, D. Reed, B. D. Reid, H. E. Robertson and A. J. Welch, in preparation.
7. A. J. Shaka, P. B. Barker and R. Freeman, *J. Magn. Reson.* 1985, **64**, 547.

1-Phenyl-1,2-dicarba-*closo*-dodecaborane, 1-Ph-1,2-*closo*-$C_2B_{10}H_{11}$. Synthesis, Characterization, and Structure As Determined in the Gas Phase by Electron Diffraction, in the Crystalline Phase at 199 K by X-ray Diffraction, and by *ab Initio* Computations

Paul T. Brain, Jill Cowie, David J. Donohoe, Drahomír Hnyk,† David W. H. Rankin, David Reed, Bruce D. Reid, Heather E. Robertson, and Alan J. Welch*

Department of Chemistry, University of Edinburgh, West Mains Road, Edinburgh EH9 3JJ, U.K.

Matthias Hofmann and Paul von Ragué Schleyer

Computer-Chemie-Centrum des Instituts für Organische Chemie, Universität Erlangen-Nürnberg, Nägelbachstrasse 25, D-91052 Erlangen, Germany

Received August 24, 1995[⊗]

The compound 1-phenyl-1,2-dicarba-*closo*-dodecaborane(12), 1-C_6H_5-1,2-*closo*-$C_2B_{10}H_{11}$ (**1**), has been synthesized and characterized by a complete assignment of its ^{11}B NMR spectrum *via* ^{11}B{^{1}H}/^{11}B{^{1}H} (COSY), ^{1}H{^{11}B$_{selective}$} and ^{1}H{^{11}B}/^{1}H{^{11}B} (COSY) spectroscopy. An electron- and X-ray diffraction investigation of **1**, complemented by *ab initio* calculations, has been undertaken. The gas-phase electron-diffraction (GED) data can be fitted by several models describing conformations which differ in the position of the phenyl ring with respect to the carborane cage. Local symmetries of C_{2v} and D_{6h} for the 1,2-C_2B_{10} and C_6 moieties, respectively, were adopted in the GED model in order to simplify the problem. In addition, constraints among the close-lying C−C and B−B bonds were employed. However, even though such simplifications led to satisfactory refinements (R_G = 0.069−0.071), a unique, definitive solution could not be gained. The $(C-C)_{mean}$, $(C-B)_{mean}$ and $(B-B)_{mean}$ bond lengths, r_a, are *ca.* 1.44, 1.72, and 1.78 Å, respectively. The C_6 hexagon, with $r_a(C-C)$ = *ca.* 1.394 Å, either eclipses the C(1)−C(2) vector (overall C_s symmetry) or more or less eclipses the C(1)−B(4) cluster bond (overall C_1 symmetry). In contrast, in the solid at 199 K, the ring lies at a position intermediate between the two GED positions, as determined by X-ray crystallography [$C_8H_{16}B_{10}$, monoclinic $P2_1/a$: a = 12.047(3) Å, b = 18.627(4) Å, c = 12.332(5) Å, β = 110.09(4)°, Z = 8]. The C−B distances span the range 1.681(6)−1.743(5) Å, and B−B lengths lie between 1.756(6) and 1.795(6) Å. A similar conformation was found for the theoretical (RHF/6-31G* level) structure which was fully optimized in C_1 symmetry. The r_e distances are consistent with the dimensions derived in the experimental studies. IGLO calculations of the ^{11}B chemical shifts, in addition to SCF single-point energies of the GED structures, further support these observations.

Introduction

1-Ph-1,2-*closo*-$C_2B_{10}H_{11}$ (henceforth referred to as monophenylcarborane, **1**) was one of the first carbon-substituted analogues of 1,2-*closo*-$C_2B_{10}H_{12}$ to be reported, more than 30 years ago.[1] Surprisingly, however, even though it can be regarded as the fusion of two fragments (phenyl and *closo*-carborane) each of which has an extensive chemistry, relatively little work on it or its derivatives has since been published. There are a few reports of derivatives of 1-Ph-2-X-1,2-*closo*-$C_2B_{10}H_{10}$, where X is an organic group,[2] an inorganic group,[3] or a transition metal fragment;[4] also, monophenylcarborane is readily deboronated [losing B(3) or B(6)] to afford the anion [7-Ph-7,8-*nido*-$C_2B_9H_{10}$]$^{2-}$ which can function as an η-ligand to a variety of metal-based fragments.[5]

In considering the structural chemistry of monophenylcarborane and its various derivatives, one important feature is the orientation of the phenyl ring relative to the C(1)−C(2) vector. This is described in terms of the angle θ', where θ' = 90° − [C(2)−C(1)−C(11)−C(16)], such that (a) when θ' = 90°, C(2) lies in the plane of the phenyl ring (Figure 1a), and (b) when θ'

* Author to whom correspondence should be addressed.
† On leave from the Institute of Inorganic Chemistry of the Academy of Sciences of the Czech Republic, 250 68 Řež near Prague, Czech Republic.
⊗ Abstract published in *Advance ACS Abstracts,* February 15, 1996.

(1) Heying, T. L.; Ager, J. W.; Clark, S. L.; Mangold, D. J.; Goldstein, H. L.; Hillman, M.; Polak, R. J.; Szymanski, J. W. *Inorg. Chem.* **1963**, *2*, 1089.
(2) (a) Lewis, Z. G.; Welch, A. J. *Acta Crystallogr.* **1993**. *C49*, 705. (b) Murphy, D. M.; Mingos, D. M. P.; Forward, J. M. *J. Mater. Chem.* **1993**, *3*, 67. (c) Murphy, D. M.; Mingos, D. M. P.; Haggitt, J. L.; Powell, H. R.; Westcott, S. A.; Marder, T. B.; Taylor, N. J.; Kanis, D. R. *J. Mater. Chem.* **1993**, *3*, 139. (d) Clegg, W.; Coult, R.; Fox, M. A.; Gill, W. R.; MacBride, J. A. H.; Wade, K. *Polyhedron* **1993**, *12*, 2711. (e) McGrath, T. D.; Welch, A. J. *Acta Cryst.* **1995**. *C51*, 646.
(3) (a) Zakharkin, L. I.; Podvistotskaya, L. S. *Izv. Akad. Nauk SSSR, Ser. Khim.* **1965**, *8*, 1464. (b) Zakharkin, L. I.; Bregadze, V. I.; Okhlobytsin, O. Yu. *J. Organomet. Chem.* **1965**, *4*, 211. (c) McGrath, T. D.; Welch, A. J. *Acta Crystallogr.* **1995**. *C51*, 649. (d) McGrath, T. D.; Welch, A. J. *Acta Crystallogr.* **1995**. *C51*, 651. (e) McGrath, T. D.; Welch, A. J. *Acta Crystallogr.* **1995**. *C51*, 654.
(4) (a) Garrett, P. M.; Hawthorne, M. F.; Owen, D. A.; Smart, J. C. *J. Am. Chem. Soc.* **1971**, *93*, 1362. (b) Bresadola, S.; Frigo, A.; Longato, B.; Rigatti, G. *Inorg. Chem.* **1973**, *12*, 2788. (c) Reid, B. D.; Welch, A. J. *J. Organomet. Chem.* **1992**, *438*, 371.
(5) (a) Doi, J. A.; Mizusawa, E. A.; Knobler, C. B.; Hawthorne, M. F. *Inorg. Chem.* **1984**. *23*, 1482. (b) Knobler, C. B.; Marder, T. B.; Mizusawa, E. A.; Teller, R. G.; Long, J. A.; Behnken, P. E.; Hawthorne, M. F. *J. Am. Chem. Soc.* **1984**, *106*, 2990. (c) Lewis, Z. G.; Reed, D.; Welch, A. J. *J. Chem. Soc., Dalton Trans.* **1992**, 731. (d) Lewis, Z. G.; Welch, A. J. *J. Organomet. Chem.* **1992**, *438*, 353. (e) Baghurst, D. R.; Copley, R. C. B.; Fleischer, H.; Mingos, D. M. P.; Kyd, G. O.; Yellowlees, L. J.; Welch, A. J.; Spalding, T. R.; O'Connell, D. *J. Organomet. Chem.* **1993**, *C14*, 447. (f) Cowie, J.; Reid, B. D.; Watmough, J. M. S.; Welch, A. J. *J. Organomet. Chem.* **1994**, *481*, 283. (g) Kyd, G. O.; Yellowlees, L. J.; Welch, A. J. *J. Chem. Soc., Dalton Trans.* **1994**, 3129.

0020-1669/96/1335-1701$12.00/0

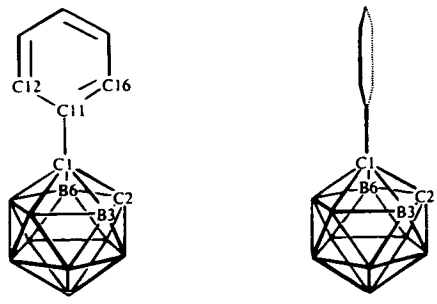

(a) θ' = 90° (b) θ' = 0°

Figure 1. (a) When $\theta' = 90°$, C(2) lies in the plane of the phenyl ring. (b) When $\theta' = 0°$, the ring is twisted about C(1)−C(11) such that C(2) lies in a plane perpendicular to it.

$= 0°$, the ring is twisted about C(1)−C(11) such that C(2) lies in a plane perpendicular to it (Figure 1b).[6]

Recently, extended Hückel molecular orbital (EHMO) calculations on an idealized model of monophenylcarborane have been reported.[2(a)] These suggested that the conformation with $\theta' = 90°$ occurred at the minimum on the potential energy surface, *ca.* 22 kJ mol^{-1} lower in energy than the conformation with $\theta' = 0°$. Interestingly, these calculations further suggested that both the C(1)−C(2) and C(1)−C(11) interactions should be strongest at $\theta' = 90°$, with, moreover, C(1)−C(2) stronger in this conformation (and weaker at $\theta' = 0°$) than in the parent compound $C_2B_{10}H_{12}$. However, as far as we are aware, the optimum conformation of monophenylcarborane, and the strength of preference for that conformation, have been explored neither experimentally nor by *ab initio* MO calculations.

The molecular structures of other large heteroboranes, *e.g.* 1,7-Cl_2-1,7-*closo*-$C_2B_{10}H_{10}$ and 1,2-*closo*-$C_2B_8H_{10}$,[7,8] have been determined recently in the gas-phase. In these studies, electron-diffraction data and *ab initio* geometry optimizations (MP2/6-31G* level) have been combined with ^{11}B IGLO (individual gauge for localized orbitals)[9] chemical-shift calculations in the so-called *ab initio*/IGLO/NMR/GED approach.[10] In such studies, constraints derived from geometries optimized *ab initio* are used in the GED refinements for parameters describing the boron cage. Such parameters, defining small differences in interatomic B−B and B-C distances, generally cannot be refined due to the effects of correlation between parameters.

In this paper, we report the results of studies of the molecular structure and the conformation of monophenylcarborane in both the gas phase (by electron diffraction) and the solid phase (by X-ray crystallography). In addition, the results of a theoretical study of the structure by *ab initio* and ^{11}B IGLO NMR[9] calculations are presented. Finally, we report the experimental ^{11}B NMR spectrum of monophenylcarborane and its complete assignment *via* ^{11}B{^{1}H}/^{11}B{^{1}H} (COSY), ^{1}H{^{11}B$_{selective}$} and ^{1}H{^{11}B}/^{1}H{^{11}B} (COSY) spectroscopy. These complement results of an ^{11}B{^{1}H}/^{11}B{^{1}H} (TOCSY; total correlation spectroscopy) experiment on 1-Ph-1,2-*closo*-$C_2B_{10}H_{11}$ reported recently.[11]

Table 1. Nozzle-to-Plate Distances, Weighting Functions, Correlation Parameters, Scale Factors, and Electron Wavelengths Used in the Electron-Diffraction Study of **1**

Nozzle-to-plate dist/mm	weighting functions/nm^{-1}					corrln param	scale factor, k[a]	electron wavelength[b]/pm
	Δs	s_{min}	sw_1	sw_2	s_{max}			
258.7	2	30	50	140	164	0.489	0.655(8)	5.701
93.8	4	92	112	232	272	0.131	0.538(11)	5.698

[a] Figures in parentheses are the estimated standard deviations. [b] Determined by reference to the scattering pattern of benzene vapor.

Experimental Section

General Procedures. The synthesis of 1-Ph-1,2-*closo*-$C_2B_{10}H_{11}$ was performed using standard Schlenk techniques with subsequent manipulation in the open atmosphere. Benzene, chloroform and pentane were dried over sodium wire prior to use. Acetonitrile, *N,N*-dimethylaniline, and $CDCl_3$ were predried over 4 Å molecular sieves. $B_{10}H_{14}$ (Callery) was recrystallized from Et_2O before use. PhCCH (Aldrich) was used as supplied. The IR spectrum was recorded from a $CHCl_3$ solution on a Perkin-Elmer 598 spectrophotometer using matched CaF_2 cells. NMR spectra (^{1}H at 600 MHz, ^{11}B at 192.5 MHz) were recorded from $CDCl_3$ solutions at 291 K on a Varian VXR600S spectrometer. Chemical shifts are referenced to external $SiMe_4$ (^{1}H) or BF_3·OEt_2 (^{11}B) with positive shifts to high frequency. Techniques for recording ^{11}B{^{1}H}/^{11}B{^{1}H}[12] and ^{1}H{^{11}B}/^{1}H{^{11}B}[13] spectra have been reported previously.

Improved Synthesis of 1-Ph-1,2-*closo*-$C_2B_{10}H_{11}$. $B_{10}H_{14}$ (3.91 g, 32.1 mmol), PhCCH (3.47 g, 34.0 mmol), and MeCN (2.78 g, 67.8 mmol) were stirred for 1 h at room temperature in 45 mL of C_6H_6, and the reaction mixture heated subsequently to reflux for 72 h. After cooling, volatiles were removed *in vacuo*, leaving a yellow oil. The product was extracted into *n*-pentane (5 × 20 mL) and filtered, and the pentane was removed *in vacuo* to afford the crude product as a white, waxy solid. Crystallization from MeOH/H_2O (1:6) at room temperature produced 3.65 g (52% yield) of colorless needles of 1-Ph-1,2-*closo*-$C_2B_{10}H_{11}$ which were analytically pure. Using *N,N*-dimethylaniline instead of MeCN afforded yields at least as high (60−65%). ^{1}H{^{11}B} NMR: δ 7.58−7.33 (5H, m, C_6H_5), 3.97 (1H, s, $C_{cage}H$), 2.62 (2H, s, B*H*), 2.53 (2H, s, B*H*), 2.46 (1H, s, B*H*), 2.35 (3H [2 + 1 coincidence], s, B*H*), 2.30 ppm (2H, s, B*H*). ^{11}B{^{1}H} NMR: δ −1.19 (1B, s), −3.49 (1B, s), −8.06 (2B, s), −9.88 (2B, s), −10.32 (2B, s), −11.85 ppm (2B, s). IR: 2595 cm^{-1} (broad, ν_{B-H}). Anal. Calcd for $C_8H_{16}B_{10}$: C, 43.6; H, 7.32. Found: C, 43.6; H, 7.44.

Electron Diffraction. Electron-scattering intensities were recorded on Kodak electron image plates using the Edinburgh gas-diffraction apparatus operating at *ca.* 44.5 kV (electron wavelength *ca.* 5.7 pm).[14] Nozzle-to-plate distances for the stainless steel inlet nozzle employed were *ca.* 94 and 259 mm, yielding data in the *s* range 30−272 nm^{-1}. The sample and nozzle were held at *ca.* 468 and 488 K respectively during the exposures.

The scattering patterns of benzene were also recorded for the purpose of calibration; these were analyzed in exactly the same way as those of the carborane so as to minimize systematic errors in the wavelengths and camera distances. Nozzle-to-plate distances, weighting functions used to set up the off-diagonal weight matrix, correlation parameters, final scale factors, and electron wavelengths for the measurements are collected together in Table 1.

(6) This is slightly different from the definition θ = the modulus of the average $C_{cage}-C_{cage}-C_{ring}-C_{ring}$ used previously. See: Cowie, J.; Reid, B. D.; Watmough, J. M. S.; Welch, A. J. *J. Organomet. Chem.* **1994**, *481*, 283.

(7) Hnyk, D.; Brain, P. T.; Robertson, H. E.; Rankin, D. W. H.; Hofmann, M.; Schleyer, P.v.R.; Bühl, M. *J. Chem. Soc., Dalton Trans.* **1994**, 2885.

(8) Hnyk, D.; Rankin D. W. H.; Robertson, H. E.; Hofmann, M.; Schleyer, P.v.R.; Bühl, M. *Inorg. Chem.* **1994**, *33*, 4781.

(9) (a) Kutzelnigg, W. *Isr. J. Chem.* **1980**, *19*, 193. (b) Schindler, M.; Kutzelnigg, W. *J. Chem. Phys.* **1982**, *76*, 1919. (c) Kutzelnigg, W.; Schindler, M.; Fleischer, U. *NMR, Basic Principles and Progress*; Springer Verlag: Berlin, New York, 1990; Vol. 23, p 165. (d) Meier, U.; van Wüllen Ch.; Schindler, M. *J. Comput. Chem.* **1992**, *13*, 551.

(10) See, for example: Hnyk, D.; Bühl, M.; Volden, H. V.; Gundersen, S.; Müller, J.; Paetzold, P. *Inorg. Chem.* **1993**, *32*, 2442.

(11) Donohoe, D. J.; Reed, D.; Welch, A. J. *Polyhedron* **1995**, *14*, 961.

(12) (a) Venable, T. L.; Hutton, W. C.; Grimes, R. N. *J. Am. Chem. Soc.* **1984**, *106*, 29. (b) Jacobsen, G. B.; Meina, D. G.; Morris, J. H.; Thomson, C.; Andrews, S. J.; Reed, D.; Welch, A. J.; Gaines, D. F. *J. Chem. Soc., Dalton Trans.* **1985**, 1645.

(13) Fontaine, X. L. R.; Kennedy, J. D. *J. Chem. Soc., Chem. Commun.* **1986**, 779.

(14) Huntley, C. M.; Laurenson, G. S.; Rankin, D. W. H. *J. Chem. Soc., Dalton Trans.* **1980**, 954.

Table 2. Crystallographic Data for 1-Ph-1,2-*closo*-$C_2B_{10}H_{11}$

$C_8H_{16}B_{10}$	fw = 220.23
a = 12.047(3) Å	space group: $P2_1/a$ (monoclinic)
b = 18.627(4) Å	T = 199 K
c = 12.332(5) Å	λ_{bar} = 0.71069 Å
β = 110.09(4)°	D_{calc} = 1.128 g cm^{-3}
V = 2595.3(14) Å^3	μ(Mo K_α) = 0.49 cm^{-1}
Z = 8	R^a = 0.0831
	S^b = 1.073

^{a} $R = \Sigma||F_o| - |F_c||/\Sigma F_o$. ^{b} $S = [\Sigma w(|F_o| - |F_c|)^2/(n_o - n_v)]^{1/2}$.

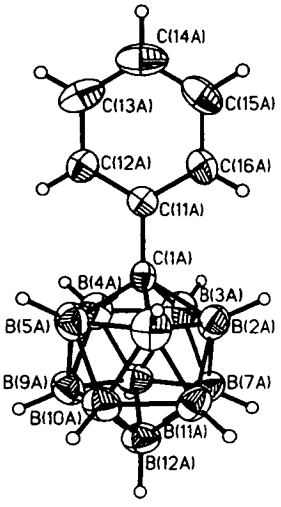

Figure 2. Perspective view of molecule A refined from the X-ray data (30% ellipsoids except for H atoms which have an artificial radius of 0.1 Å for clarity).

The electron-scattering patterns were converted into digital form using a computer-controlled Joyce-Loebl MDM6 microdensitometer with a scanning program described elsewhere.[15] The programs used for data reduction[15] and least-squares refinement[16] have been described previously; the complex scattering factors employed were those listed by Ross *et al.*[17]

X-ray Diffraction. Crystals suitable for X-ray diffraction were grown by very slow cooling (to room temperature) of a warm, concentrated, ethanolic solution. Crystallographic data were collected on an Enraf-Nonius CAD4 diffractometer operating with Mo-K_α X-radiation (λ_{bar} = 0.71069 Å), with the glass capillary containing the crystal held in a stream of nitrogen gas at 199 K. The unit cell was determined by the least-squares refinement of the setting angles of 25 reflections in the range 16 < 2θ < 22°. Intensity data in the range 2 < 2θ < 50° were collected by the ω-2θ scan technique; ω-scan width (0.8 + 0.34 tan θ), ω-scan speeds in the range 0.235 to 0.782° min^{-1}. The intensities of 4572 unique reflections were measured (h, −14 to +14; k, 0 to 22; l, 0 to 14); of these, 2592 reflections had $F > 4\sigma(F)$. There was no decay or crystal movement during the 158 h of data collection (CADABS[18]). Crystallographic data are summarized in Table 2.

The structure was solved using direct methods (SHELXS86)[19] and developed by iterative full matrix least-squares refinement and difference Fourier syntheses (SHELXTL).[20] In molecule A (Figure 2), the cage carbon not carrying the phenyl substituent could not be unambiguously identified and consequently a disordered model was adopted in which all five boron atoms adjacent to C(1A) were given an occupancy of 1.04. In contrast, molecule B (Figures 3 and 4) was fully ordered and the position of C(2B) was clear. Phenyl rings were treated as planar hexagons (C−C = 1.390 Å) with phenyl-H atoms set in idealized positions (C−H = 0.93 Å). In the final stages of refinement, all non-H atoms were refined with anisotropic thermal parameters. Cage-H atoms were set 1.10 Å from C or B on a radial extension. All H atoms were

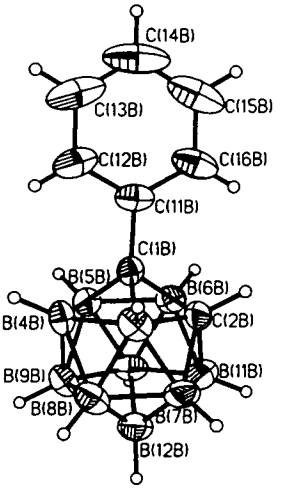

Figure 3. Perspective view of molecule B refined from the X-ray data (30% ellipsoids except for H atoms which have an artificial radius of 0.1 Å for clarity).

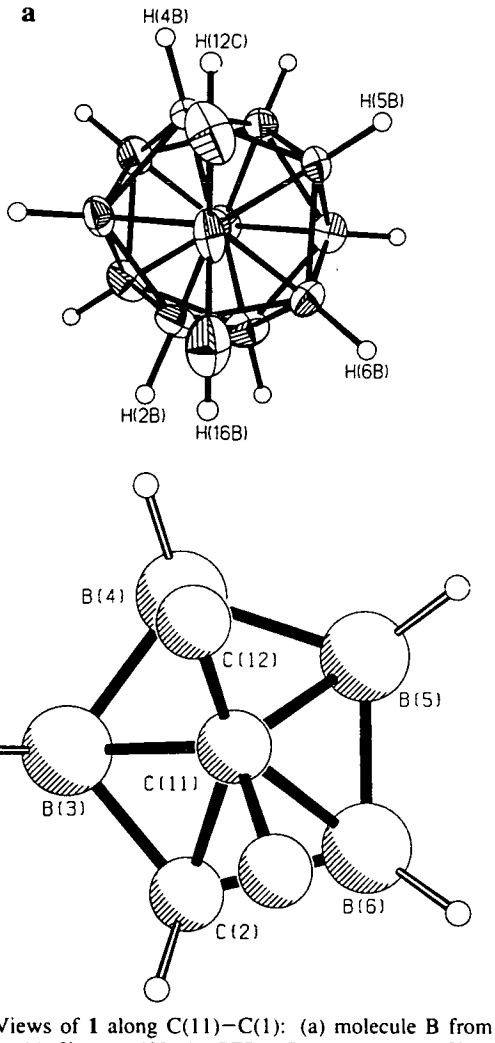

Figure 4. Views of **1** along C(11)−C(1): (a) molecule B from the X-ray study, with θ' = *ca.* 68°; (b) GED refinement B, with θ' = 54°. Parts of the phenyl ring and carborane cage are omitted for clarity.

(15) Cradock, S.; Koprowski, J.; Rankin, D. W. H. *J. Mol. Struct.* **1981**, *77*, 113.
(16) Boyd, A. S. F.; Laurenson, G. S.; Rankin, D. W. H. *J. Mol. Struct.* **1981**, *71*, 217.
(17) Ross, A. W.; Fink, M.; Hilderbrandt, R. In *International Tables for Crystallography*; Wilson, A. J. C., Ed.; Kluwer Academic Publishers: Dordrecht, The Netherlands, Boston, MA, and London, 1992; Vol. C, p 245.
(18) Gould, R. O.; Smith, D. E. CADABS. Program for data reduction. University of Edinburgh, U.K., 1986.
(19) Sheldrick, G. M. SHELXS86. Program for crystal structure solution. University of Göttingen, Germany, 1986.
(20) SHELXTL PC version 5.0. Siemens Analytical Intruments Inc., Madison, WI, 1994.

Table 3. Fractional Coordinates ($\times 10^4$) and Equivalent Isotropic Displacement Parameters[a] ($Å^2 \times 10^3$) in 1-Ph-1,2-*closo*-$C_2B_{10}H_{11}$

	x	*y*	*z*	U_{eq}
C(12A)	462(2)	−45(1)	6913(2)	43(1)
C(13A)	1091(2)	−401(1)	6321(2)	58(1)
C(14A)	1758(2)	−13(2)	5803(2)	62(1)
C(15A)	1795(2)	732(2)	5877(2)	59(1)
C(16A)	1166(2)	1089(1)	6468(2)	43(1)
C(11A)	499(2)	700(1)	6986(?)	31(1)
C(1A)	−197(3)	1083(2)	7610(3)	30(1)
B(2A)	−160(3)	1985(2)	7745(3)	48(1)
B(3A)	560(4)	1458(2)	8944(3)	53(1)
B(4A)	−348(4)	712(2)	8787(3)	51(1)
B(5A)	−1557(3)	754(2)	7511(4)	53(1)
B(6A)	−1437(4)	1566(2)	6846(4)	56(1)
B(8A)	−422(4)	1390(3)	9734(4)	46(1)
B(9A)	−1720(4)	947(3)	8846(4)	49(1)
B(10A)	−2412(4)	1492(3)	7623(4)	51(1)
B(11A)	−1524(4)	2279(2)	7752(4)	50(1)
B(7A)	−298(4)	2209(2)	9059(4)	47(1)
B(12A)	−1713(4)	1893(3)	9001(4)	51(1)
C(12B)	−63(2)	5150(1)	2294(2)	60(1)
C(13B)	445(3)	5680(1)	1825(3)	85(2)
C(14B)	1213(3)	5493(2)	1252(3)	86(2)
C(15B)	1473(2)	4775(2)	1148(2)	79(2)
C(16B)	965(2)	4244(1)	1617(2)	59(1)
C(11B)	197(2)	4431(1)	2190(2)	41(1)
C(1B)	−406(3)	3872(2)	2669(3)	32(1)
C(2B)	175(3)	3067(2)	2949(3)	42(1)
B(3B)	274(4)	3605(2)	4102(3)	42(1)
B(4B)	−1081(3)	4069(2)	3650(3)	37(1)
B(5B)	−1911(3)	3813(2)	2199(3)	34(1)
B(6B)	−1073(4)	3177(2)	1757(3)	38(1)
B(10B)	−2225(4)	2872(2)	2210(4)	42(1)
B(9B)	−2234(4)	3431(2)	3377(4)	41(1)
B(8B)	−879(4)	3305(3)	4553(4)	46(1)
B(7B)	−36(4)	2678(3)	4094(4)	50(1)
B(11B)	−852(5)	2415(3)	2662(4)	53(1)
B(12B)	−1586(4)	2567(2)	3651(4)	47(1)

[a] $U_{eq} = \sum_i \sum_j U_{ij} a_i^* a_j^* \mathbf{a}_i \cdot \mathbf{a}_j$.

given isotropic displacement parameters riding at 1.2 times the equivalent isotropic parameter of their attached atom. Data were weighted such that $w^{-1} = [\sigma^2(F_o^2) + (0.1189P)^2 + 1.05P]$ where $P = [\max.(F_o^2 \text{ or } 0) + 2F_c^2]/3$. Using 2592 observed data, $R = 0.0831$ and $S = 1.073$ for 301 variable parameters. The maximum residue and minimum trough in a final Fourier synthesis were +0.34 and −0.26 e $Å^{-3}$, respectively. Atomic scattering factors were those inlaid in SHELXTL. The atomic fractional coordinates and equivalent isotropic thermal parameters for non-hydrogen atoms are listed in Table 3. Hydrogen atom fractional coordinates, non-hydrogen anisotropic thermal parameters, and a full listing of bond lengths and bond angles are available as Supporting Information.

***Ab Initio* Calculations.** The geometry was fully optimized in C_s and C_1 symmetry by standard *ab initio* methods[21] at the RHF/6-31G* level using the Gaussian 92[22] program package. Computations at a correlated level (*e.g.* MP2) were not possible due to the demands on CPU time and disk space for such a large, low symmetry molecule. ^{11}B chemical shieldings were computed with the IGLO (individual gauge for localized orbitals) program[9] using Huzinaga basis sets:[23] DZ: (7s3p) contracted to [4111, 21] for C,B and (3s) contracted to [21] for H: II″, (9s5p1d) contracted to [51111, 2111, 1] for C,B (cage atoms and C(11)), (7s3p) contracted to [4111, 21] for C(12−16) and (3s) contracted to [21] for H. Computations employing the DZ basis were obtained with an IGLO lobe version, while for the II″ basis the direct IGLO program (DIGLO)[9d] was used.

Table 4. Molecular Parameters (r_a/Å or ∠/deg)[a] for the GED Study of **1**

		refinement[c]	
parameter[b]		A	B
p_1	r(C−C)$_{av.}$ $^1/_8$[(1−2) + 6(C−C)$_{ring}$ + (1−11)]	1.440(2)	1.436(2)
p_2	r(C−B)$_{av.}$ $^1/_2$[(1−3) + (1−4)]	1.711(5)	1.720(6)
p_3	r(B−B)$_{av.}$ $^1/_{15}$[4(3−4) + 4(4−8) + 2(7−11) + (9−12) + 4(8−12)]	1.788(4)	1.784(5)
p_4	r(C−H)	1.113(10)	1.120(12)
p_5	r(B−H)	1.179(8)	1.176(13)
p_6	C(2)C(1)B(4)	111.1(4)	110.6(4)
p_7	C(2)C(1)C(11)	126.3(7)	119.6(17)
p_8	BBH	120.0(f)	120.0(f)
p_9	C(1)C(2)H(2)	117.0(f)	117.0(f)
p_{10}	θ' [90° − C(2)C(1)C(11)C(16)]	90.0(f)	54.0(f)
p_{11}	Δ [C(1)−C(2)]−[(C−C)$_{ring}$]	0.238(7)	0.233(7)
p_{12}	Δ [C(1)−C(2)]−[C(1)−C(11)]	0.121(8)	0.126(8)
p_{13}	Δ [C(1)−B(3)]−[C(1)−B(4)]	−0.006(9)	−0.004(9)
p_{14}	Δ [B(3)−B(4)]−[B(4)−B(8)]	−0.004(8)	−0.001(9)
p_{15}	Δ [B(3)−B(4)]−[B(7)−B(11)]	0.005(8)	0.002(8)
p_{16}	Δ [B(3)−B(4)]−[B(9)−B(12)]	−0.007(10)	−0.008(10)
p_{17}	Δ [B(3)−B(4)]−[B(8)−B(12)]	−0.047(7)	−0.045(7)

[a] Figures in parentheses are the estimated standard deviations of the last digits: f = fixed. [b] For definitions, see text; for atom numbering see Figures 3 and 4. [c] For method of refinement, see text.

Molecular Model for the GED Refinement. Since 1-phenyl-1,2-dicarba-*closo*-dodecaborane(12), 1-Ph-1,2-*closo*-$C_2B_{10}H_{11}$, has either C_1 or, at most, C_s symmetry and a large number of different interatomic distances, it is a difficult system for investigation by electron-diffraction. Thus, in order to reduce the problem to a manageable dimension, local symmetries of C_{2v} and D_{6h} for the 1,2-C_2B_{10} cage and the C_6 hexagonal ring, respectively, were assumed. Such assumptions were based on the theoretically optimized geometry (HF/6-31G* level) in C_1 symmetry which predicted only small deviations from the idealized symmetries for these moieties (see below). However, even for this simplified model, in which only the weighted mean values of the C−C (p_1), C−B (p_2), and B−B (p_3) bonds were considered (see Table 4), seven parameters (p_{11}−p_{17}) defining differences between the close-lying C−B, B−B and C−C distances were also necessary. The initial values of such differences were derived from the HF/6-31G* optimization in C_1 symmetry. To complete the description of the C_2B_{10} framework, the C(2)C(1)B(4) bond angle (p_6) was used. The position of the phenyl ring with respect to the cage was defined by both the C(2)−C(1)−C(11) bond angle (p_7) and by the torsion angle, $\theta' = 90° - [C(2)-C(1)-C(11)-C(16)]$,($p_{10}$). The B−H bonds were assumed to be all of equal length (p_5), as were the six C−H bonds [five (C−H)$_{ring}$ and C(2)−H(2)] (p_4). For the angle parameters, the cluster hydrogens were located assuming a single value for the BBH angles (p_8) and the angle C(1)C(2)H(2) (p_9). Thus, the structure was defined by 17 refinable parameters in this model as listed in Table 4.

Results

Electron Diffraction. Electron-diffraction refinements for structures with a range of fixed θ' values were undertaken. The fit of data for the C_s structure with $\theta' = 0°$ was poorer ($R_G > 0.09$) than for either the C_s structure with $\theta' = 90°$ (refinement A, $R_G = 0.069$) or the optimum refinement in C_1 symmetry with $\theta' = 54°$, *i.e.* B(4)−C(1)−C(11)−C(12) = *ca.* 1° (refinement B, $R_G = 0.071$). In the original refinements, it was possible to refine five of the geometrical parameters (Table 4), *viz.* p_1−p_4 and p_7. Attempts to refine other parameters led to either unreasonable values or an unstable refinement. Consequently, the esd's for some of the independent and dependent parameters were likely to be underestimated, *e.g.* r[C(1)−C(2)] = 1.629(2) Å. Subsequent refinements were therefore undertaken using the method of flexible parameter constraints.[24]

(21) See: (a) Hehre, W.; Radom, L.; Schleyer, P. v.R.; Pople, J. A. *Ab Initio Molecular Orbital Theory*; Wiley: New York, 1986. (b) Foresman, J. B.; Frisch, Æ. *Exploring Chemistry with Electronic Structure Methods*; Gaussian Inc.: Pittsburgh PA, 1993.

(22) Frisch, M. J.; Trucks, G. W.; Head-Gordon, M.; Gill, P. M. W.; Wong, M. W.; Foresman, J. B.; Schlegal, H. B.; Raghavachari, K.; Robb, M. A.; Replogle, E. S.; Gomperts, R.; Andres, J. L.; Binkley, J. S.; Gonzalez, C.; Martin, R.; Fox, D. J.; DeFrees, D. J.; Baker, J.; Stewart, J. J. P.; Pople, J. A. Gaussian Inc., Pittsburgh, PA, 1992.

(23) Huzinaga, S. *Approximate Atomic Wavefunctions*; University of Alberta: Edmonton, Canada, 1971.

Flexible parameter constraints may allow the refinement of rameters which would usually have to be fixed. Estimates the values of these parameters and their uncertainties are used additional observations in a combined analysis similar to those utinely carried out for electron-diffraction data combined with ation constants and/or dipolar coupling constants. The rting values and uncertainties for the extra observations are rived from another method such as X-ray diffraction or oretical computations. *All* parameters are then included in refinements. Upon refinement, if the intensity pattern ntains useful information concerning one of these parameters, will refine with an esd less than the uncertainty in the rresponding additional observation. However, if there is little no relevant information, the parameter will refine with an l equal to the uncertainty of the extra observation. In this se, the parameter can simply be fixed, in the knowledge that ing this does not influence either the magnitudes or the esd's other parameters. In some cases, increasing the number of ining parameters allows all effects of correlation to be nsidered, and so some esd's may actually increase. Overall, s approach utilizes all available data as fully as possible and urns more realistic esd's for parameters, *e.g.* r[C(1)−C(2)] 1.627(8) Å.

Using the method of flexible constraints, it was possible to ine simultaneously 14 geometrical parameters (Table 4). eavy-atom distance differences (p_{11}−p_{17}) were constrained th an uncertainty of 0.01 Å and r(B−H) with 0.02 Å. ldditionally, eight amplitudes of vibration were refined simulneously in the final refinements while the dependence of the al structure on other fixed amplitudes was also explored.

The parameters for refinements A and B are summarized in ble 4. Interatomic distances, vibrational amplitudes and gles as obtained in refinement B are listed in Table 5 and the ost important elements of the least-squares correlation matrix e given in Table 6. Atomic coordinates of the HF/6-31G* d GED (refinement B) C_1 geometries are included as part of e Supporting Information. The radial-distribution curves and olecular-scattering intensities are shown in Figures 5 and 6, spectively.

***Ab Initio* and IGLO Computations.** IGLO ^{11}B chemical-ift calculations, performed for various HF/6-31G* optimized uctures differing mainly in the phenyl ring position, indicated at the $\delta(^{11}B)$ values are sensitive to the phenyl-ring orientation, only to a small degree. The HF/6-31G* level energy mputations favor the structures in which the ring eclipses the 1)-C(2) bond (C_s symmetry, $\theta' = 90°$), or more or less lipses the C(1)-B(4) bond (C_1 symmetry, $\theta' = 65°$, B(4)−1)−C(11)−C(12) = *ca.* 14°), the latter being found as the inimum on the potential energy (p.e.) hypersurface, relative the structure with the phenyl ring "perpendicular" to the 1)−C(2) bond (C_s symmetry, $\theta' = 0°$). Selected geometrical rameters from the *ab initio* study are given in Table 7, and e results of the IGLO computations are shown in Table 8.

X-ray. There are two crystallographically-independent molcules of 1-Ph-1,2-*closo*-$C_2B_{10}H_{11}$ (molecules A and B) in the ymmetric fraction of the unit cell, and these are drawn in gures 2 and 3, respectively. There are no significant contacts etween molecules. Interatomic distances and selected interond angles are given in Table 8; a full listing of geometrical rameters is included in the Supporting Information. In olecule A, the cage carbon atom not carrying the phenyl bstituent, C(2), could not be distinguished with a sufficient degree of certainty [C(1A)−cage atom distances = 1.674(5)−1.728(5) Å], whereas in molecule B its location (based on a combination of interatomic distances and refined [as B] isotropic thermal parameters) was unambiguously established. Since the key feature of the structure of monophenylcarborane is the twist angle θ' which describes the conformation of the phenyl ring with respect to C(1)−C(2), only parameters for molecule B will be discussed.

Table 5. Final Interatomic Distances (r_a/Å)[a−c] and Mean Amplitudes of Vibration (u/Å) from the GED Refinement B of **1**

	distance	r_a	u
r_1	C(1)−C(2)	1.627(8)	0.045(f)
r_2	C(1)−B(3)	1.718(8)	0.054(f)
r_3	C(1)−B(4)	1.722(7)	0.054(f)
r_4	B(3)−B(4)	1.771(6)	
r_5	B(4)−B(5)	1.770(9)	
r_6	B(8)−B(12)	1.816(5)	
r_7	B(4)−B(8)	1.772(9)	0.062(4)
r_8	B(9)−B(12)	1.779(12)	
r_9	B(7)−B(12)	1.806(14)	
r_{10}	B(3)−B(8)	1.788(18)	
r_{11}	C(1)−C(11)	1.500(8)	0.042(f)
r_{12}	$(C-C)_{ring}$	1.394(2)	0.042(f)
r_{13}	B−H	1.176(13)	0.108(f)
r_{14}	$(C-H)_{ring}$	1.120(12)	0.078(f)
r_{15}	C(2)−H(2)	1.120(12)	0.085(f)
r_{16}	(C···B) [two bond]	2.752−2.831	0.075(5)
r_{17}	(B···B) [two bond]	2.837−2.925	
r_{18}	(C···B)[d]	3.302(18)	0.084(f)
r_{19}	(B···B)[d]	3.343−3.418	0.093(f)
r_{20}	C(12)···C(16)	2.414(3)	0.067(4)
r_{21}	C(11)···C(14)	2.788(3)	0.068(7)
r_{22}	$(C_{ring}$···B) [four/five bond]	4.470−5.071	0.152(30)
r_{23}	$(C_{ring}$···B) [four/five bond]	4.678−5.370	0.185(26)

[a] Values in parentheses are the estimated standard deviations of the final digits: f = fixed. [b] For atom numbering scheme, see Figures 3 and 4. [c] All C(x)···C(1,2) and C(x)···B(N) distances (x = 11, 14, 15, 16; N = 3, ..., 12) with multiplicity 1 were included in the refinement but most are not shown here. Similarly, all the B···H, C···H, and H···H distances (cage and ring), with amplitudes fixed in the range 0.090−0.180 Å, were also included. [d] Cage body diagonals.

Table 6. Least Squares Correlation Matrix (×100) for GED Refinement B[a]

p_6	p_{11}	p_{12}	u_7	u_{21}	u_{23}	
	65					p_1
			75			p_2
72						p_3
				66		p_7
		50				p_{11}
					55	u_{22}

[a] Only elements with absolute values ≥ 50 are shown.

NMR. The $^{11}B\{^1H\}$ NMR spectrum of monophenylcarborane (Figure 7) reveals 6 resonances of relative integral 1:1:2:2:2:2 at −1.19, −3.49, −8.06, −9.88, −10.32, and −11.85 ppm respectively, all of which appear as doublets ($^1J_{BH}$ = 148−170 Hz) in the proton-coupled spectrum.

In the $^{11}B\{^1H\}/^{11}B\{^1H\}$ COSY spectrum (Figure 8) the only integral-2 peak which couples to all other ^{11}B resonances is that at −8.06 ppm and is therefore assigned to B(8,10). The two highest frequency resonances (each integral-1) must be due to B(9) and B(12). They show, as expected, coupling to each other and to B(8,10). In addition, each couples to one other integral-2 resonance. The integral-2 resonance that does *not* couple to

4) Blake, A. J.; Brain, P. T.; McNab, H.; Miller, J.; Morrison, C. A.; Parsons, S.; Rankin, D. W. H.; Robertson, H. E.; Smart, B. A. *J. Phys. Chem.*, in press.

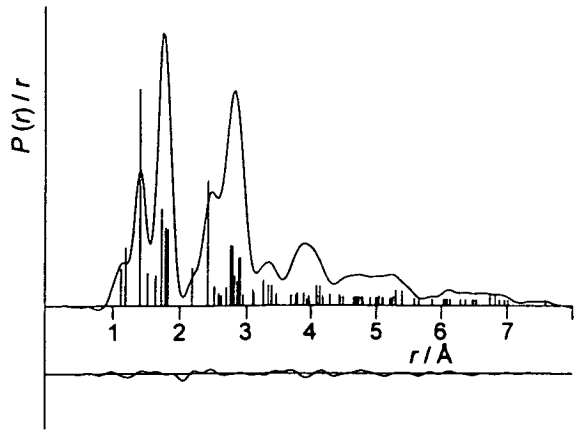

Figure 5. Observed and final weighted difference radial-distribution curves for the GED study of **1**. Before Fourier inversion the data were multiplied by $s \exp[(-0.00002s^2)/(Z_B - f_B)(Z_C - f_C)]$.

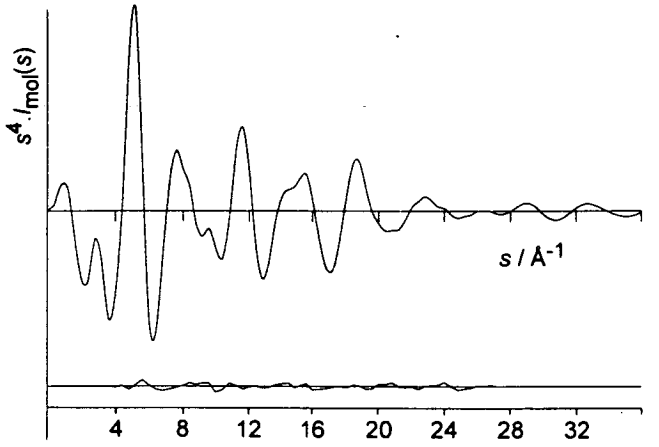

Figure 6. Observed and final weighted difference combined molecular-scattering intensity curves for the GED study of **1**. Theoretical data are shown for the regions 0–30 and 272–360 nm^{-1} for which no experimental data are available.

either B(9) or B(12) is that at −10.32 ppm, which must therefore arise from B(3,6).

In the $^1H\{^{11}B\}$ spectrum (Figure 9) there are five peaks in the B*H* region, of relative integral 2:2:1:3:2 (high frequency to low frequency) the underlined resonance representing a 2 + 1 coincidence. In addition, the C(2)*H* proton (integral-1) resonates at a much higher frequency, 3.97 ppm. A series of $^1H\{^{11}B_{selective}\}$ experiments, following the order of the ^{11}B resonances, revealed enhancement of the proton signals at 2.46, 2.35, 2.35, 2.53, 2.62 and 2.30 ppm, respectively. Clearly H(8,10) resonates at 2.35 ppm and H(3,6) at 2.62 ppm.

The ambiguities in the ^{11}B and ^1H assignments were resolved by a $^1H\{^{11}B\}/^1H\{^{11}B\}$ COSY spectrum (Figure 10). C(2)*H* showed two couplings, to the highest (2.62 ppm) and lowest (2.30 ppm) frequency B*H* resonances, and the last must therefore be due to H(7,11). Therefore B(7,11) resonates at −11.85 ppm. From the $^{11}B\{^1H\}/^{11}B\{^1H\}$ COSY spectrum the resonance at −3.49 ppm is now assigned to B(12), that at −1.19 ppm to B(9), and that at −9.88 ppm to B(4,5); from these, the remaining ^1H assignments were easily made.

Discussion

At the HF/6-31G* level, a conformation with the phenyl twist (θ') of *ca.* 65° is computed to be a minimum on the potential-energy hypersurface (Table 8). However, a conformation with C_s symmetry in which the phenyl ring eclipses the C−C cluster bond ($\theta' = 90°$) is predicted to lie only 0.3 kJ mol^{-1} higher in energy.

Table 7. Comparison of Theoretical and Experimental Geometrical Parameters for **1**[a–c]

distance/angle	theoretical[d] $\theta' = 65°$	GED[e] $\theta' = 54°$(f)	X-ray[f] $\theta' = 67.7(3)°$
C(1)−C(2)	1.626	1.627(8)	1.640(5)
C(1)−B(3)	1.733		1.743(5)
C(1)−B(6)	1.739	1.718(8)	1.719(5)
C(2)−B(3)	1.713		1.709(6)
C(2)−B(6)	1.708		1.711(6)
C(1)−B(4)	1.720		1.716(5)
C(1)−B(5)	1.722	1.722(7)	1.705(5)
C(2)−B(7)	1.701		1.683(5)
C(2)−B(11)	1.702		1.681(6)
B(3)−B(4)	1.780		1.758(6)
B(6)−B(5)	1.779	1.771(6)	1.761(6)
B(3)−B(7)	1.782		1.766(7)
B(6)−B(11)	1.785		1.768(6)
B(4)−B(8)	1.792		1.771(6)
B(5)−B(10)	1.785	1.772(9)	1.795(6)
B(7)−B(8)	1.787		1.764(7)
B(10)−B(11)	1.782		1.770(7)
B(4)−B(5)	1.785	1.770(9)	1.784(5)
B(7)−B(11)	1.785		1.767(7)
B(8)−B(12)	1.803		1.787(7)
B(10)−B(12)	1.803	1.816(5)	1.767(6)
B(8)−B(9)	1.799		1.783(6)
B(9)−B(10)	1.802		1.780(6)
B(9)−B(12)	1.791	1.779(12)	1.769(6)
B(7)−B(12)	1.784		1.766(6)
B(11)−B(12)	1.783	1.806(14)	1.761(7)
B(4)−B(9)	1.785		1.769(6)
B(5)−B(9)	1.781		1.778(6)
B(3)−B(8)	1.766	1.788(18)	1.756(6)
B(6)−B(10)	1.770		1.761(6)
C(1)−C(11)	1.516	1.500(8)	1.503(4)
$(C-C)_{ring}$	1.386[g]	1.394(2)	1.39(f)
C(2)C(1)C(11)	118.3	119.6(17)	119.2(3)
C(2)C(1)B(4)	109.9	110.6(4)	108.6(3)
C(1)C(2)B(7)	113.5	110.6(4)	113.1(3)

[a] For atom numbering scheme, see Figures 3 and 4. [b] $\theta' = 90° - [C(2)C(1)C(11)C(16)]$. [c] Figures in parentheses are the estimated standard deviations of the last digits: f = fixed. [d] HF/6-31G* level. [e] Model B, C_{2v} cage geometry. [f] Molecule B. [g] A mean value is given.

Refinements of the electron-diffraction data, assuming local C_{2v} symmetry for the C_2B_{10} cage and D_{6h} symmetry for the phenyl ring, are consistent equally with conformations in which $\theta' = 90°$ (refinement A) or $\theta' = 54°$ (refinement B). Both conformations exhibit geometrical parameters similar to those found in the *ab initio* optimization in C_1 symmetry (Table 7) with the exception of the bond angle C(2)C(1)C(11), which is considerably larger in refinement A [126.3(7)°] than in B [119.6(17)°], *cf.* HF/6-31G* 118.3°. Theoretical single-point SCF energies are computed lower for refinement B than for A, both with the DZ and II″ basis sets. Thus, considered in conjunction with the *ab initio* study, GED refinement B, with $\theta' = 54°$, is favored over refinement A.

At 488 K, the temperature of the vapor in the GED experiment, $RT = 4.1$ kJ mol^{-1}. The potential-energy barrier to rotation of the phenyl ring about C(1−C(11), assuming that the conformation with $\theta' = 90°$ lies at the maximum on the p.e. hypersurface (Table 8), is predicted to be 2.1 kJ mol^{-1} at the HF/6-31G* level. It thus seems likely that the gas-phase geometry of **1** is defined by almost unrestricted rotation of the phenyl ring, although the complexity of the GED analysis of such a dynamic motion precludes the possibility of confirming this experimentally.

Table 8. IGLO results for 1-Ph-1,2-$C_2B_{10}H_{11}$

level of theory//geometry	$\delta(^{11}B)^a$ B(3,6)	B(4,5)	B(7,11)	B(8,10)	B(9)	B(12)	relative energy[b]
DZ//HF/6-31G* (C_1, $\theta' = 65°$)	−11.9	−14.9	−16.9	−16.2	−3.8	−3.6	0.0
DZ//HF/6-31G* (C_s, $\theta' = 90°$)	−11.8	−14.5	−17.3	−16.0	−3.9	−3.7	0.3
DZ//HF/6-31G* (C_s, $\theta' = 0°$)	−14.5	−13.7	−16.4	−17.1	−2.1	−3.5	2.1
DZ//HF/6-31G* ("C_{2v}", $\theta' = 65°$)[c]	−12.2	−15.6	−16.7	−15.9	−2.9	−2.9	5.8
DZ//GED (C_s, $\theta' = 90°$)	−12.4	−11.4	−15.0	−12.6	4.7	2.1	60.7[d]
DZ//GED (C_1, $\theta' = 54°$)	−12.2	−13.9	−14.1	−13.1	3.8	1.8	53.1[d]
II″//HF/6-31G* (C_1, $\theta' = 65°$)	−11.4	−12.5	−15.0	−12.0	−2.2	−2.7	0.0
II″//GED (C_s, $\theta' = 90°$)	−11.8	−8.8	−13.2	−7.9	6.7	3.6	57.7[e]
II″//GED (C_1, $\theta' = 54°$)	−11.6	−11.4	−12.0	−8.4	5.7	3.3	50.6[e]
experimental[f]	−10.3	−9.9	−11.9	−8.1	−1.2	−3.5	

[a] Relative to $BF_3{\cdot}OEt_2$ (ppm); average values for effective C_s symmetry. [b] Energy (kJ mol^{-1}) of the structure relative to the HF/6-31G* fully optimized C_1 structure ($\theta' = 65°$, potential energy minimum). [c] C_{2v} symmetry for the C_2B_{10} cage is used. [d] HF/6-31G* single-point energy with respect to the HF/6-31G* fully optimized C_1 structure. [e] Relative energies at the HF/II″ level. [f] This work.

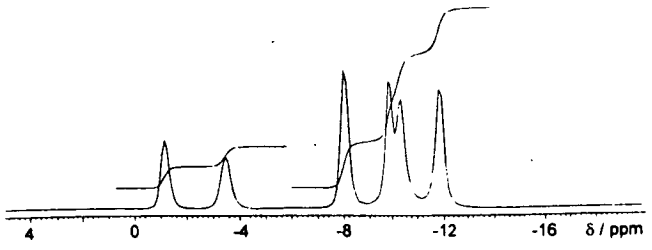

Figure 7. $^{11}B\{^1H\}$ NMR spectrum of **1**.

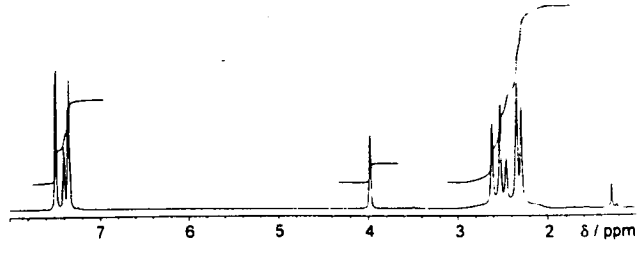

Figure 9. $^1H\{^{11}B\}$ NMR spectrum of **1**.

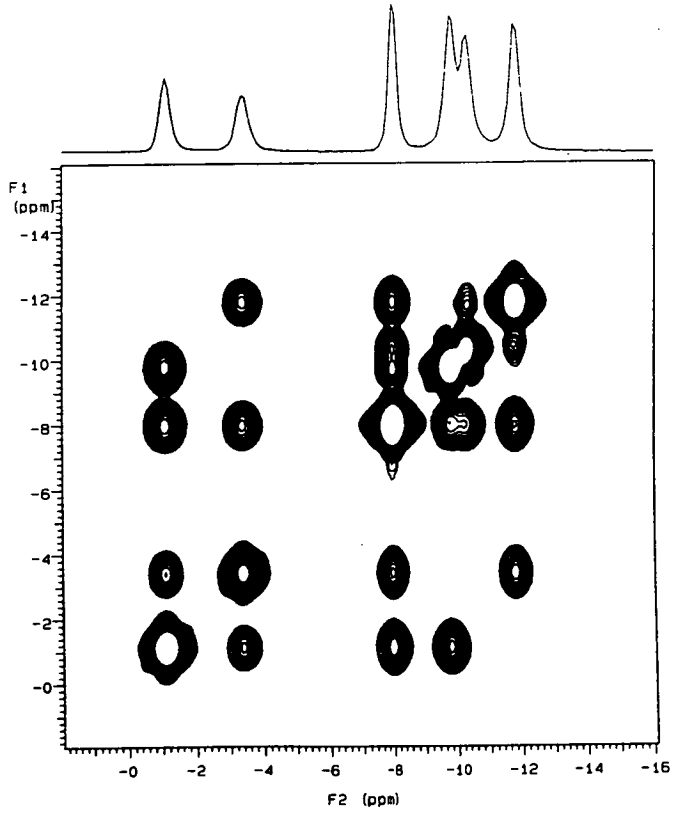

Figure 8. $^{11}B\{^1H\}/^{11}B\{^1H\}$ NMR COSY spectrum of **1**.

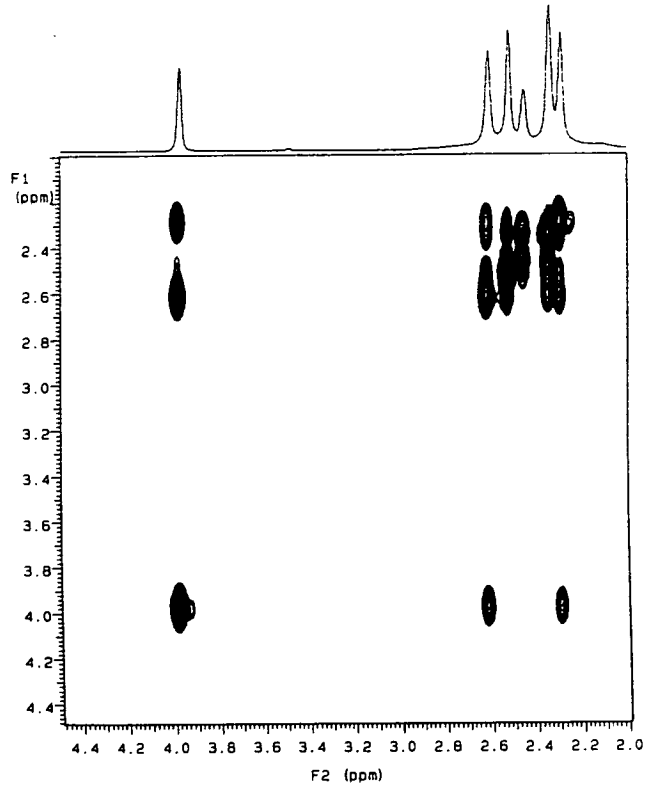

Figure 10. $^1H\{^{11}B\}/^1H\{^{11}B\}$ NMR COSY spectrum of **1**.

The fully assigned ^1H and ^{11}B chemical shifts for monophenylcarborane are listed in Table 9. Comparing the ^{11}B chemical shifts with those of the ubiquitous parent species 1,2-*closo*-$C_2B_{10}H_{12}$,[25] we note (a) a significant shift to high frequency of the resonances due to B(3,6) ($\Delta\delta$ = *ca.* 4 ppm) and B(4,5) ($\Delta\delta$ = *ca.* 3 ppm), atoms adjacent to C(1), the site of substitution, (b) relatively little difference ($\Delta\delta = 0-1$ ppm) in the chemical shifts of B(9,8,10,7,11), and (c) a marked shift to low frequency ($\Delta\delta$ = *ca.* 2.7 ppm) of the resonance due to the antipodal atom B(12). Overall the pattern and values of ^{11}B resonances in monophenylcarborane are very similar to those recently reported[25] for the ether-substituted species 1-(CH_2OCH_3)-1,2-*closo*-$C_2B_{10}H_{11}$.

The experimental ^{11}B chemical shifts are reproduced well by the IGLO calculations, (see Table 8), with the exception of the $\delta(^{11}B)$ IGLO values of B(9) and B(12), antipodally coupled with C(2) and C(1), which are slightly overestimated (with both the

(25) Shaw, K. F.; Welch, A. J. *Polyhedron* **1992**, *11*, 157.

Table 9. Assignment of the Experimental ^{11}B and ^{1}H NMR Chemical Shifts in 1-Ph-1,2-*closo*-$C_2B_{10}H_{11}$

position	$\delta(^1H)$	$\delta(^{11}B)$	$\delta(^{11}B, 1,2\text{-}C_2B_{10}H_{12})$[25]
9	2.46	−1.19	−1.78
12	2.35	−3.49	−1.78
8, 10	2.35	−8.06	−8.59
4, 5	2.53	−9.88	−12.99
3, 6	2.62	−10.32	−14.10
7, 11	2.30	−11.85	−12.99

DZ and II″ basis sets) when employing the GED structures. For refinement B, the final experimental geometry of **1** is computed to lie 53.1 kJ mol^{-1} (6-31G* basis set) and 50.6 kJ mol^{-1} (II″ basis set) above the theoretical C_1 fully optimized structure. Such values are somewhat larger than usually observed for "excess energies" of GED structures.[7,8,10] However, considering the large number of relatively poorly defined geometrical parameters (including 16 hydrogen atoms), these values are not unreasonable.

In the solid-phase molecular structure, the angle θ' in molecule B is 67.7(3)°. The distance C(1B)−C(2B) is 1.640(5) Å (*cf.* GED 1.627(8) Å, *ab initio* 1.626 Å), significantly shorter than any other connectivity on the surface of the pseudoicosahedral carborane polyhedron including others to C(2B), 1.681(6)−1.711(6) Å.[26] We have already noted[2a] that a contribution to the short C(1)−C(2) connectivity derives from the orientation of the phenyl substituent. Thus, in derivatives 1-Ph-2-X-1,2-*closo*-$C_2B_{10}H_{10}$ (X = Me, Br), the 2-substituent is sufficiently bulky to ensure a conformation near $\theta' = 0°$ (experimentally 16.7 and 2.2°, respectively)[2e,3c] and results in C(1)-C(2) distances of 1.695(5) Å and 1.692(8) Å. Bulkier X groups, such as Ph,[2a] CCCPh,[2e] $SiMe_3$,[3d] and $SiMe_2{}^tBu$[3e] maintain or extend C(1)−C(2) and can additionally result in bending back of substituents and/or deformation of the cage.

In molecule B of 1-Ph-1,2-*closo*-$C_2B_{10}H_{11}$, C−B distances span the range 1.681(6)−1.743(5) Å, and B−B lengths lie between 1.756(6) and 1.795(6) Å. Inspection of the C(11B)−C(1B)−C/B angles reveals that the phenyl substituent is slightly tilted away from B(4B) and B(5B); however, there is a compensatory asymmetry in C(1B)−C(11B)−C angles, with that to C(12B) being measureably narrower than that to C(16B).

The conformation of molecule B is in excellent agreement with that determined by *ab initio* MO calculations (Table 7), as discussed above. We believe that this conformation is measureably different from that ($\theta' = 90°$) predicted by the earlier EHMO calculations[2a] because of steric crowding between cage- and *ortho*-phenyl-H atoms, poorly modeled in the former, low-level, calculation. In molecule B determined crystallographically, H(16B)···H(2B) = 2.21 Å, H(16B)···H(6B) = 2.81 Å, H(12B)···H(4B) = 2.30 Å and H(12B)···H(5B) = 3.03 Å.

(26) Since submission of this manuscript, the crystal structure of a second polymorph of monophenylcarborane has been determined. In this new modification, $\theta' = 71.2(2)°$ and r[C(1)−C(2)] = 1.649(2) Å. See: Thomas. R. Ll.; Rosair. G. M.; Welch, A. J. *Acta Crystallogr.*, C, in press.

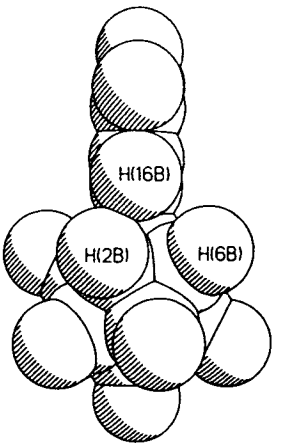

Figure 11. Space-filling plot of molecule B from the X-ray study. Sphere radii are proportional to the respective van der Waals' radii.

Figure 4 shows a view of the molecule from above (top half of the phenyl ring omitted for clarity), showing that the H(16B)···H(2B) repulsion would be more pronounced if the $\theta' = 90°$ conformation were adopted. Figure 11, a side view of the molecule, confirms that there are touching van der Waals' spheres on H(16B) and H(2B).

Acknowledgment. We acknowledge the Science and Engineering Research Council (now EPSRC) for support of the Edinburgh Electron-Diffraction Service (Grant No. GR/J59258), including provision of microdensitometer facilities at the Daresbury laboratory, the award of research fellowships to D.H., P.T.B., and H.E.R, and the award of research studentships to D.J.D. and B.D.R. We also thank the University of Edinburgh for the award of a studentship to J.C. D.H. thanks the Academy of Sciences of the Czech Republic (Grant No. 432402) and the Grant Agency of the Czech Republic (Grant No. 203/94/0984) for financial support. We thank Dr. M. Bühl for performing the IGLO calculations employing the II″ basis set. The calculations in Erlangen were performed on a Convex C220S computer and were supported by the Deutsche Forschungsgemeinschaft and the Fonds der Chemischen Industrie. Computer time was granted on a Cray YMP-8 of the Höchstleistungsrechenzentrum Jülich. We thank Professor W. Kutzelnigg, Dr. M. Schindler, Dr. U. Fleischer, and Dr. Ch. van Wüllen for the IGLO and DIGLO programs. A.J.W. acknowledges the Callery Chemical Co. for a generous gift of $B_{10}H_{14}$.

Supporting Information Available: Listings of (a) data pertinent to the crystal structure analysis, including (i) all bond distances and angles, (ii) fractional atomic coordinates and isotropic displacement parameters for the hydrogen atoms, and (iii) fractional atomic coordinates and anisotropic displacement parameters for the non-hydrogen atoms, and (b) atomic coordinates for the GED and theoretically optimized geometries is available (9 pages). Ordering information is given on any current masthead page.

IC9511128